AGARD-CP-592

AGARD

ADVISORY GROUP FOR AEROSPACE RESEARCH & DEVELOPMENT
7 RUE ANCELLE, 92200 NEUILLY-SUR-SEINE, FRANCE

AGARD CONFERENCE PROCEEDINGS 592

Advances in Rotorcraft Technology

(les Avancées en technologies pour aéronefs à voilure tournante)

Papers presented at the Flight Vehicle Integration Panel Symposium held in Ottawa, Canada, 27-30 May 1996.

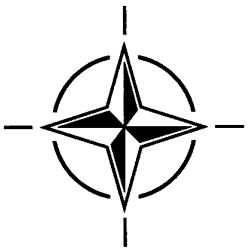

NORTH ATLANTIC TREATY ORGANIZATION

DISTRIBUTION STATEMENT A
Approved for public release;
Distribution Unlimited

Published April 1997

Distribution and Availability on Back Cover

DISCLAIMER NOTICE

THIS DOCUMENT IS BEST QUALITY AVAILABLE. THE COPY FURNISHED TO DTIC CONTAINED A SIGNIFICANT NUMBER OF PAGES WHICH DO NOT REPRODUCE LEGIBLY.

AGARD-CP-592

AGARD

ADVISORY GROUP FOR AEROSPACE RESEARCH & DEVELOPMENT
7 RUE ANCELLE, 92200 NEUILLY-SUR-SEINE, FRANCE

AGARD CONFERENCE PROCEEDINGS 592

Advances in Rotorcraft Technology

(les Avancées en technologies pour aéronefs à voilure tournante)

Papers presented at the Flight Vehicle Integration Panel Symposium held in Ottawa, Canada, 27-30 May 1996.

DTIC QUALITY INSPECTED 2

North Atlantic Treaty Organization
Organisation du Traité de l'Atlantique Nord

19970501 102

The Mission of AGARD

According to its Charter, the mission of AGARD is to bring together the leading personalities of the NATO nations in the fields of science and technology relating to aerospace for the following purposes:

- Recommending effective ways for the member nations to use their research and development capabilities for the common benefit of the NATO community;
- Providing scientific and technical advice and assistance to the Military Committee in the field of aerospace research and development (with particular regard to its military application);
- Continuously stimulating advances in the aerospace sciences relevant to strengthening the common defence posture;
- Improving the co-operation among member nations in aerospace research and development;
- Exchange of scientific and technical information;
- Providing assistance to member nations for the purpose of increasing their scientific and technical potential;
- Rendering scientific and technical assistance, as requested, to other NATO bodies and to member nations in connection with research and development problems in the aerospace field.

The highest authority within AGARD is the National Delegates Board consisting of officially appointed senior representatives from each member nation. The mission of AGARD is carried out through the Panels which are composed of experts appointed by the National Delegates, the Consultant and Exchange Programme and the Aerospace Applications Studies Programme. The results of AGARD work are reported to the member nations and the NATO Authorities through the AGARD series of publications of which this is one.

Participation in AGARD activities is by invitation only and is normally limited to citizens of the NATO nations.

The content of this publication has been reproduced
directly from material supplied by AGARD or the authors.

Published April 1997

Copyright © AGARD 1997
All Rights Reserved

ISBN 92-836-0038-X

Printed by Canada Communication Group
45 Sacré-Cœur Blvd., Hull (Québec), Canada K1A 0S7

Advances in Rotorcraft Technology

(AGARD CP-592)

Executive Summary

The last half of the twentieth century has seen the rotorcraft come in to prominence as a combat system. Rotorcraft have proven their worth in all environments and in all domains of conflict. They will continue to provide essential military capabilities for the Alliance well into the next century. The objective of this symposium was to capture the current situation in the rapidly changing field of rotorcraft technology.

The symposium met its objective. Different parts of this Conference Proceedings should be valuable to anyone currently designing or developing rotorcraft, or doing basic research in rotorcraft technology. Special emphasis in the programme was placed upon the following subjects:

— the impact of the increasing use of commercial off-the-shelf technology in military helicopter development and use;

— the increasing acceptance and expanded use of Aeronautical Design Standard ADS-33;

— the issue of rotorcraft flight safety.

This symposium provided an excellent forum for a varied program of technical presentations. It specifically provided information on the Bell 230, the Tiger, Eurocopter EC 135, the V-22 and the RAH Comanche. The knowledge gained and exchanged at this symposium should assist the attendees in helping to provide NATO with the future affordable combat rotorcraft it will need to maintain our current technological lead.

Les avancées en technologies pour aéronefs à voilure tournante

(AGARD CP-592)

Synthèse

La deuxième moitié du vingtième siècle a vu arriver les aéronefs à voilure tournante à un rang proéminent en tant que systèmes de combat. Leurs mérites ont été clairement démontrés dans tout environnement et dans tout domaine de conflit. Ils continueront à assurer des capacités militaires essentielles pour l'Alliance jusqu'au milieu du siècle prochain. Ce symposium a eu pour objectif de saisir la situation actuelle dans le domaine des technologies des aéronefs à voilure tournante, qui est en évolution constante et rapide.

Cet objectif a été atteint. Les différents chapitres de ce compte rendu seront précieux pour tous ceux qui sont impliqués dans la conception et le développement des aéronefs à voilure tournante, ainsi que pour les chercheurs travaillant dans ce domaine. Un accent particulier à été mis sur les sujets suivants dans le cadre de ce programme:

— l'impact de l'utilisation accrue de technologies sur étagère pour le développement et l'exploitation des hélicoptères;

— l'acceptation accrue et l'utilisation étendue de la norme de conception aéronautique ADS-33;

— la question de la sécurité de vol des aéronefs à voilure tournante.

Ce symposium a été un excellent forum pour un programme varié de présentations techniques. Il a permis en particulier de communiquer des informations sur le Bell 230, le Tiger, l'Eurocopter EC 135 et le RAH Comanche. Les connaissances acquises et l'information échangée lors de ce symposium doivent permettre d'aider aux participants pour fournir à l'OTAN le futur hélicoptère de combat au coût abordable dont elle a besoin pour maintenir notre avance technologique.

Contents

	Page
Executive Summary	iii
Synthèse	iv
Theme/Thème	viii
Flight Vehicle Integration Panel	ix
Acknowledgements	x
	Reference
Technical Evaluation Report by M. Sinclair	T
Keynote Address 1 by B.Gen. K.R. Pennie	K1
Keynote Address 2 by Gen. C. Batllo	K2
Certification of Model 230 Helicopter for Category 'A Elevated Helipad Operations by J. Goldenberg, L. Meslin, M. Blondino and D. Williams	1
Paper 2 cancelled	
The Use of Simulation to Develop an Improved Understanding of Helicopter Tail Rotor Failures and Develop Aircrew Emergency Advice by A.W. Martyn, P. Phipps and E. Mustard	3
Optimal Trajectories for the Helicopter in One-Engine-Inoperative Terminal-Area Operations by R.T.N. Chen and Y. Zhao	4
No written version is available for Paper 5	
An Investigation of Primary Flight Control Failure in a Piloted Helicopter by S.R. Gibbard and L.D. Reid	6
Simulation de mission pour le TIGRE (Version Appui Protection) by J.F. Rigal and G. Colas	7
Modular Roll-on / Roll-off Design Concept of a Rotorcraft Simulation Center by K. Niessen	8
Evaluation de la pilotabilité des hélicoptères de transport en utilisant les essais en vol de type ADS-33C Formalisation de la méthodologie et de l'instrumentation d'essais by D. Fournier and D. Papillier	9

ADS-33 Flight Testing - Lessons Learned 10
by C.J. Ockier and V. Gollnick

ONERA & DLR Cooperation on the 'Smart Helicopter Concept'
- Handling Qualities Data Base for Hover and Low Speed Flight - 11
by G. Bouwer, A. Taghizad and H. Mödden

Development of a Tactical Helicopter Infrared Signature Suppression (IRSS) System 12
by P.R. Sully, D. VanDam, J. Bird and D. Luisi

Model 412 Composite Tailboom 13
by G. Mussett and R. Fews

Crash Resistant Composite Subfloor Structures for Helicopters 14
by A.F. Johnson, C.M. Kindervater, H.G.S.J. Thuis and J.F.M. Wiggenraad

Paper 15 cancelled

Introduction of Beryllium Aluminum Castings in the RAH-66 Comanche EOSS Program 16
by J.P. Seinberg, D.P. Tetz and K.R. Raftery

Reduction of the Noise Signature of the EUROCOPTER EC 135 17
by G. Niesl and G. Arnaud

Ducted Tail Rotor Designs for Rotorcraft and their Low Noise Features 18
by B. Edwards, J. Andrews and C. Rahnke

Mesures en vol et prévision du bruit interne d'un hélicoptère ECUREUIL 19
by A. Morvan and J-M. David

Upgrading of Classical Lifting-Line Theory to obtain Accurate Flight Mechanical
Helicopter Models: Improved Correction for Sweep Effects 20
by Th. van Holten

Rotorcraft - Pilot Coupling
A Critical Issue for Highly Augmented Helicopters? 21
by P.G. Hamel

An Empirical Correction Method for Improving Off-Axes Response Prediction
in Component Type Flight Mechanics Helicopter Models 22
by M.H. Mansur and M.B. Tischler

Effect of Propulsion System Dynamics on Rotorcraft Aeromechanical Stability
in Straight and Turning Flight 23
by G. Guglieri, R. Celi and F. Quagliotti

Aerodynamic and Acoustics of Rotorcraft
A Survey of the 75th Fluid Dynamics Panel Symposium - Berlin 24
by H. Körner and K. Pahlke

The Integrated Development of a Medium Lift Military/Civil Helicopter 25
by J.P. Graham

Compound Interest - A Dividend for the Future? 26
by D.V. Humpherson

RAH-66 Comanche Program Status 27
by A.W. Linden and M.H. Stieglitz

The Application of Helicopter Mission Simulation to System Trade-Off Issues 28
by N. Tatlock, C. Silvester and P. Birkett

V-22 Technical Challenges 29
by S.I. Glusman, R.A. Hyland and R.L. Marr

Cockpit Technologies Research at the Flight Research Laboratory of the National Research Council of Canada 30
by J.M. Morgan and S.W. Baillie

Advances in Helicopter Carefree Handling and Control Augmentation 31
by C.P. Massey and J. Howitt

Active Control of Aeromechanical Stability 32
by T. Krysinski

Helicopters and Night Vision Goggles: A Synopsis of Current Research on Helicopter Handling Qualities during Flight in Degraded Visual Environments 33
by S.W. Baillie and J.M. Morgan

The Solid State Adaptive Rotor Design, Development and Implications for Future Rotorcraft 34
by R. Barrett and J. Stutts

Theme

Rotorcraft is one of the major topics for regular FVP Symposia. Since the last FVP Symposium on this subject, there have been many significant developments in both the design and operational aspects of rotorcraft. Several new rotorcraft have been designed, tested or introduced into service. These include the Agusta 129, the AH-1W Super Cobra, the EH101, the Eurocopter Tiger and Panther, the MBB BO-108, the McDonnell Douglas MD520, the Boeing-Sikorsky Comanche and the Bell-Boeing V-22. These aircraft utilize a variety of new technologies such as extensive use of composites, use of fly-by-wire flight controls and advanced mission avionics. Several of them also use new rotor designs to reduce maintenance requirements while improving performance, vibration and noise characteristics.

From an operational standpoint, the experience with rotorcraft in the Gulf War and in some of the ongoing United Nations activities should offer insight into future rotorcraft design requirements and operational developments.

This Symposium will cover several sessions on Flight Safety, Handling Qualities and Simulation, Vehicle Technology, Methodology, Programs, and Advanced Control.

Thème

"Les aéronefs à voilure tournante" est l'un des grands sujets à être examiné régulièrement lors des symposia FVP. De nombreux développements importants se sont produits au niveau de la conception et de l'exploitation des aéronefs à voilure tournante depuis le dernier symposium FVP sur ce sujet. Plusieurs nouveaux aéronefs à voilure tournante ont été développés, essayés et mis en service et notamment: l'Agusta 129, l'AH-1W Super Cobra, l'EH 101, l'Eurocopter Tiger et Panther, le MBB BO-108, le McDonnell Douglas MD 520, le Boeing-Sikorsky Comanche et le Bell-Boeing V-22. Ces aéronefs font appel à toute la gamme des nouvelles technologies comme en témoigne l'emploi généralisé de nouveaux matériaux composites, la mise en œuvre de commandes de vol électriques et l'utilisation d'une avionique de mission avancée. Certains d'entre eux intègrent de nouveaux types de rotors, conçus pour une maintenance réduite, tout en permettant d'améliorer les caractéristiques de performance, de vibration et de bruit.

Du point de vue opérationnel, l'expérience acquise sur les aéronefs à voilure tournante pendant la guerre du golfe, conjuguée à celle résultant des différentes opérations menées par les Nations-Unies, devrait permettre de mieux apprécier les cahiers de charges des aéronefs à voilure tournante futurs, ainsi que les développements opérationnels.

Le symposium est organisé en différentes sessions couvrant: la sécurité du vol, la manœuvrabilité, la simulation, les technologies des structures, les méthodologies, les programmes, et les systèmes de pilotage avancés.

Flight Vehicle Integration Panel

Chairman: Dipl.-Ing. Horst WÜNNENBERG
Mgr. of Flight Physics & Predesign
DORNIER Luftfahrt GmbH
P.O. Box 1103
D-82230 Wessling
Germany

Deputy Chairman: Mr Barry TOMLINSON
Flight Dynamics & Simulation Dept.
Flight Systems Department
Defence Research Agency
Bedford, MK41 6AE
United Kingdom

TECHNICAL PROGRAMME COMMITTEE

Mr. B. BLAKE
Director, Research & Technology
BOEING Defense & Space Group
Helicopters Division
P.O. Box 16858
Mail Stop P3-10
Philadelphia, PA 19142-0858
U.S.A.

Mr. J. d'AUTUME
Sous Directeur
Recherche & Développement/DCT/T
Société AEROSPATIALE
37, blvd de Montmorency
75781 Paris Cedex 16
FRANCE

HOST NATION COORDINATOR

Mr. Stewart W. BAILLIE
Flight Research Laboratory
Institute for Aerospace Research
National Research Council
Montreal Road
Ottawa, Ontario K1A 0R6
CANADA

PANEL EXECUTIVE

John B. WHEATLEY, LTC, USA

Mail from Europe:
LTC J.B. WHEATLEY
AGARD-OTAN/FVP
7, rue Ancelle
92200 Neuilly-sur-Seine
France

Mail from USA and Canada:
AGARD-NATO/FVP
PSC 116
APO AE 09777

Acknowledgements

The Flight Vehicle Integration Panel wishes to express its thanks to the National Authorities of Canada for the invitation to hold this symposium in their country.

TECHNICAL EVALUATION REPORT FOR THE SYMPOSIUM ON "ADVANCES IN ROTORCRAFT TECHNOLOGY"

(Ottawa, Canada, 27 - 30 April, 1996)

by

M. Sinclair
124 Withrow Avenue
Nepean, Ontario K2G 2S7
Canada

INTRODUCTION

Background

The Flight Vehicle Integration Panel regularly addresses rotorcraft issues within the various subject areas and activities of the Panel's technical program, along side those of the other aviation modes. From time to time, however, the Panel dedicates a symposium exclusively to rotorcraft, for the purpose of taking stock in a more focused way of the expanding operational role of military rotorcraft and the evolution of the vehicle, its systems and technologies.

In planning this latest in the series of dedicated rotorcraft symposia, the Panel could look back over almost a decade of progress and change since the 1986 symposium on "Rotorcraft Design for Operations". In that time, new rotorcraft have been designed and tested; others have been introduced into operational service; and on all sides, so-called new technologies have become commonplace in applications. The Gulf War put rotorcraft to the test in new war-fighting conditions, redefining terms such as "degraded visual environment" and "situational awareness" in a complex digital war in the desert. And finally, the defining event of this last decade, the end to the Cold War, has dramatically changed the posture of all of the western world militaries; it is widely accepted, however, that the new world that is emerging in place of the old will demand expanded use of rotorcraft.

Theme

The subject of the meeting, "Advances in Rotorcraft Technology", is very broad and encompassing. Rotorcraft capabilities continue to expand rapidly and a very large, active international rotorcraft R&D community continues to develop new technologies and methods for improving the vehicle and its flight and fighting systems. Two professional societies dedicated to the advancement of rotorcraft technology produce a rich variety of high quality technical and scientific communications each year, most of which would fit under this symposium title.

With this wealth of information and activities to draw upon, the program committee constrained the scope of the meeting by establishing themes for a series of program sessions. In a somewhat abbreviated form, these were:

- the expanding role of the rotorcraft - present and future operational roles, with emphasis on design requirements that are mission driven
- advanced control concepts and visionics, addressing integration of flight, engine and fire control system - looking at their impact on survivability, environmental effects, mission reliability, availability and life cycle cost
- structural design for producibility, low-cost operation and survivability - addressing as well, maintainability, cost of production and crash-survivable characteristics
- advances in rotorcraft design methodologies and tools - presenting the latest techniques in modeling, CFD, parameter identification as they are applied in flight performance, handling qualities and aerodynamic loads
- applications of simulation to rotorcraft - examining use of simulation for requirements definition, system integration, pilot-aircraft interface studies, operational test and training
- current programs and projects - describing current rotorcraft development and research programs

The final program retained the core of this ambitious outline, compressed and reorganized to accommodate the specific input from invited authors. Certainly, all of the themes implied here did not appear prominently at the meeting or in the papers, but most did and several additional *global* themes emerged, largely because they are common concerns of the rotorcraft community at this time. These included:

- the impact of the increasing use of commercial off-the-shelf (COTS) technology in military helicopter development and use, and the consequent dependence on civil standards in place of military standards and specifications;
- the increasing acceptance and expanded use of Aeronautical Design Standard ADS-33;
- and of course, flight safety, which you will see was the title of Session I in the final version of the program.

The result was an interesting and varied program of good technical presentations, emphasizing the core flight mechanics technology areas, but providing insights, as well, into progress in rotorcraft aerodynamics, structures and materials and propulsion technologies.

Keynote Addresses

The technical proceedings were opened with two excellent keynote addresses. The first, by Brigadier General Pennie, Commander of Canadian Tactical Aviation was direct, specific and immediate in its focus on current problems. This was followed by an elegant global presentation by Le Général Battlo, Commander of French Army Aviation, describing the growth of the helicopter as an element of the French land-fighting forces, specifically as an anti-tank warrior - and its recent adaptation to the post-Cold War world.

General Pennie related the circumstances that have led the Canadian Forces to undertake their full-range of tactical helicopter roles with a single type, the new Bell 412 Griffon. This difficult task is further complicated by the fact that the Griffon is a commercial off-the-shelf (COTS) helicopter which is to be maintained, spared and modified as though it were a civil aircraft. The presentation had a particularly Canadian flavour, but it describes a predicament that is faced by more and more military operators, as budgets shrink and the economies of commercial practices attract military buyers and operators.

General Pennie laid out a spectrum of problems that face his forces in adapting the "civil" Griffon to its military environment and missions. Some of these, such as the incompatibility between the cockpit lighting needs for military NVG operations and the civil requirement for aviation red warning lights, will simply be solved by implementing a safe solution *that does not comply with civil rules:* even in the COTS environment, military operators are still free to do this, since the result will not affect the lifing or warranties of major systems or parts.

Other challenges associated with the proliferation of mission systems and system CDU's in the civil cockpit space are similar in kind to the general military cockpit challenge. Here, General Pennie pleaded with the R&D community to make good on the promise of modern systems such as HMD's, direct voice input systems and cognitive aids, to bring order to the cockpit and workload relief to the pilot.

But the "sleeper" in the business of adapting civil aircraft to military use - *while retaining civil maintenance programs and all of the conveniences and savings that flow from this* - arises in the area of use rather than modification. This point was raised at the end of General Pennie's speech and was left open. Military forces *will* operate outside the normal civil envelopes and use-spectra. How this will be managed and what it will "cost" are still open questions in the case of the Griffon - and I am sure they preoccupy other forces that are similarly involved in the use of civil off-the-shelf aircraft.

The technical subjects that are linked to these questions are not new, but neither are they all resolved. They cross the panel boundaries of AGARD, dealing with integrated health and usage monitoring systems, structural design philosophies and lifing of components and parts, control systems and autopilot design. The larger question remains - "Can fleet safety be managed economically by following civil maintenance programs while flying (real) military mission profiles?"

General Battlo traced the history of military doctrine and technology advancement that established the helicopter as "un véritable engin principal de combat" within the French Army, from primitive origins in the technologies of the early 1950's to the dominant role of the helicopter as an anti-tank weapon system by the end of the Cold War era. It was his descriptions of the transition to a new aeromobility doctrine and concept in the current post Cold War period, however, that provided an important backdrop for the symposium.

In the specific French/European context, the dominant role for the new aeromobility forces has shifted from anti-tank combat to an airborne protection/support role. But in a more general sense, the hallmarks of the post Cold War roles and missions for military helicopters will be flexibility, change and even ambiguity. This most "polyvalente" of all flying machines must add peace making, peace keeping and support for other humanitarian and diplomatic activities to its more traditional roles of troop support, protection, transport, reconnaissance and battle fighting, further complicating "Rotorcraft Design for Operations".

ANALYSIS AND COMMENTS

Session I: Flight Safety

Three of the six presentations in the session (papers #1,4 and 5) addressed safety and performance issues relating to helicopter operation under civil transport Category "A" rules. Category "A" certification applies to multi-engine helicopters with independent engine systems and requires that the helicopter be able to make a safe "landback" to the takeoff area or a safe continuation of flight out of the terminal area following an engine failure. These rather simply stated restrictions can have a profound influence on payload and the required size and preparation of landing and takeoff areas.

This is a very active area of research and testing and the three papers presented complementary examples across the spectrum of these activities. The discussion of the M230 certification program illustrated how demanding the Category "A" requirements can be in an already hostile operational environment of an off-shore elevated helipad - and demonstrated the value of high quality simulation in support of the certification process. Presentation #4 summarized optimal control analytical studies that provide the means for introducing performance and operational variables and constraints - in some optimal ways - into the complex Cat "A" flight control tasks. And, finally, the display studies described in presentation #5 addressed the need to assist the pilot, both in analyzing the situation and flying the emergency recoveries precisely. Category "A" could be seen in these presentations as a work in progress, challenging the operators and the research communities alike, and demanding integrated application of new guidance, display and control technologies.

The question of the *military* relevance of civil Category "A" operations might have been raised, since AGARD serves a military client. (In fact, I do not believe it was noted at all at the meeting.) Military operators do not use Category "A" rules and they are unlikely to do so formally, even where their flight vehicles and operations are similar to the civil Cat "A" case. Clearly, militaries work in a different operational safety framework than the civil authorities do. But the trade-offs of safety, performance, control, handling, pilot information and workload are similar in both environments. The underlying problems, and the methods being used by the Cat "A" community to tackle these problems, should provide useful new knowledge for military as well as civil operators. This possibility, however, may not be immediately evident to the military community.

Presentation #3 addressed tail rotor failure, one of the fundamental issues in helicopter flight safety. The British project that is the basis for this study was initiated in 1993 by the RAF Handling Squadron at Boscombe Downs, and the FVP paper picks up the project very near the end of the study but far from the end of the story. The inspiration for the work grew from knowledge of the disturbingly high frequency of these failures - and a desire to develop better "advice" for pilots on appropriate action following tail rotor failure. The scope of study is far broader than this, however, touching on fundamental elements of vehicle and safety system design. The paper is thorough and detailed, as are its conclusions and recommendations, but it does not close the book on such a complex problem. In fact, while much of the work described has generic value, much is type specific to the Lynx helicopter. Nevertheless, this is important and exemplary work that could perhaps be the basis for a wider exchange of information among the NATO/AGARD partners.

The session was leavened by a presentation from Auburn University on the use of solid state piezoelectric actuators to provide the primary control inputs to a helicopter rotor. In the smart structures community, the Auburn University team is one of several groups pursuing feasibility studies on solid state actuation systems suitable for integrating as control elements in individual rotor blades. The objectives of the studies and model tests range from modest attempts at vibration suppression and load tailoring to full control of a model helicopter. The Auburn group has laid a substantial foundation of research and component testing for its intended flight of a model piezoelectric adaptive rotor in the near future. Clearly, there is potential in this approach for improving flight safety, when vulnerable mechanical control rods and swash plates are replaced by electrically activated solid state components in the rotor. Furthermore, techniques such as higher-harmonic control and individual blade control would be very easily implemented with this type of actuation system. There is still a long path to tread, however, before the the new

solid state systems could be considered for rotor applications in an operational context, since their potential benefits are accompanied by a new set of vulnerabilities that must be overcome in a very hostile environment.

The final presentation of the session looked at a specific class of catastrophic failures in an advanced fly-by-wire system. In the case study, the control system automatically adjusted to the failure state - circumventing the problem area to provide the necessary control for continued flight to a landing. The specific failures and fixes considered in the study present the pilot with the task of flying pitch attitude control - that is, longitudinal cyclic pitch control - with pedals. It is the ability of the pilot to adapt to this unconventional control configuration that formed the kernel of the study. This would appear to be a somewhat "benign-catastrophic" event if it were to occur in a sophisticated FBW environment, since all of the primary actuation systems continue to respond to control signals and the control computers continue to operate. With these functions available, there would appear to be other FBW design options that might be exercised for circumventing the failure before settling on a pedals-for-pitch control mode. (I had the impression that the FVP audience would have appreciated more elaboration on the rationale for this specific case.) Nevertheless, the study demonstrated the inherent safety and robustness that come with FBW system design, where built-in automated adjustments can "work around" certain classes of system failures. In the case studied, pilots successfully adapted to the unconventional post-failure control mode and had little difficulty recovering to a safe landing.

Session II: Handling Qualities and Simulation

Presentations in this session were evenly divided between handling qualities and simulation topics. In the simulation portion, two of the three presentations provided complementary detailed descriptions of the use of high fidelity simulation for mission system studies. The presentation from the Centre d'essais en vol (CEV) on the mission system simulator for the Tiger helicopter focused on an evaluation and validation of the technical performance of the basic Tiger mission systems along with its support-protection mission system suite. Here, the simulation process is deeply imbedded in the development stream, timed, in fact, to evaluate the integrated systems at a specific stage in the airborne software suite development. This use of simulation to integrate systems and evaluate the integrated package in realistic operational environments with representative crew workload, has become an indispensable element in military helicopter programs, extending throughout the development cycle. It is indispensable and, as the authors emphasize, economical - by some estimations, saving as much as the cost of one prototype.

At the other end of the spectrum, the DRA presentation on their HOVERS generic mission simulator illustrated the use of simulation as a tool for system trade-off studies for *the next generation* of fighting helicopters. Again, there is strong emphasis on high fidelity simulation of aircraft systems and the operational environment - including, in this case, the rich information environment of the future battle-field. The HOVERS studies envision, for example, a tactical data network linked to the cockpit, which will provide the crew with an abundance of information on the tactical situation - from various sources and in various stages of interpretation. This will necessitate the development of an onboard Information Management System to sift and sort, prioritize and present relevant usable information to the crew. The studies clearly show that factually correct and appropriately presented tactical information increases survivability; however they also raise the spectre of information latency and inaccuracy that could present the crew with a compelling *but false* view of the immediate situation. Both of these aspects of the future operational situation can be effectively captured and analyzed in mission simulation systems.

The third simulation presentation, paper #8, described a modular approach to the commercial development of a suite of twelve training simulators for the German army aviation corps. The simulators will be outfitted in three configurations to represent three helicopter types in the current training fleet of the corps. Development plans aim to define common modules, to the degree possible, and by this means to reap the benefits of commonality both in manufacturing and sparing of the suite.

Presentations 9,10 and 11 shared two common themes, first, the general subject of helicopter handling qualities and secondly, Aeronautical Design Standard ADS-33, the recently published standard on Handling Qualities Requirements for Military Rotorcraft. ADS-33 has been developed by the US Army Aeroflightdynamics Directorate (AFDD) to replace the venerable Military Specification Mil-H-8501A. This monumental undertaking, initiated by the US Army in the early 1980's and led by AFDD, was also supported by collaborative participation from the national aeronautical research agencies of Canada, Germany and the United Kingdom.

The new mission-oriented standard emphasizes active controls and advanced display systems, frequency domain specifications and testing, use of Cooper-Harper handling qualities ratings, characterization of degraded visual environments and precisely defined test manoeuvres for both day and degraded visual conditions. As we see in the papers of this session, ADS-33 is an effective engineering tool with growing influence and acceptance in the rotorcraft community.

Presentation #9 from the CEV focused on the proposed use of the ADS-33 handling qualities *test manoeuvres* in the NH 90 helicopter development program. Using a Super Puma helicopter, the CEV performed manoeuvres of the type called up in ADS-33, to refine the test methods and gain experience with the new standard in advance of its application in the NH 90 program. This was followed by a description of a recent wide-ranging evaluation of ADS-33 by DLR and the German Armed Forces Flight Test Center, in which they assessed applicability and repeatability of criteria, and consistency between quantitative and qualitative criteria. In the final presentation of the session, ONERA and DLR described a special evaluation of ADS-33, with an eye to using it in their collaborative "Smart Helicopter Concept" study.

Each of these activities identified what they would characterize as minor shortcomings in the standard, generally dealing with issues of detail. In the specific case of the "Smart Helicopter Concept" study, the use of ADS-33 is being extended somewhat beyond its intended military application. In this case, therefore, it would be necessary to develop special new background data to accommodate the proposed civil task and civil mission cases. Nevertheless, in all of these assessments, the user agencies have found the general framework of the criteria and methods of ADS-33 to be sound, consistent and repeatable.

Session III: Vehicle Technology

Session III comprised a series of technology development and technology application presentations that are improving rotorcraft at the individual system level. We began to hear, in this session and the following one, concern and consideration for *system engineering* concepts such as producibility, maintainability, survivability and life cycle cost. As a first example, a film-cooled tailpipe design for infra-red signature suppression in the Bell 412 engine exhaust, will reduce detectability and improve survivability in an operational environment threatened by IR guided missiles. An advanced composite tailboom, soon to be certified for the 412, will be stronger, lighter, simpler to produce and maintain and resistant to corrosion and fatigue. We saw elegant structural design techniques that are being developed for use in composite structures where there is a requirement for high strength during normal loading and good energy absorption in the crash design case: techniques involving sine-wave beam web designs and imbedded failure "triggers" promise producible, crash resistant and crash survivable composite structures.

Two presentations addressed the subject of external noise signatures of rotorcraft, both from a detectability and from a community acceptance standpoint. In a presentation from Eurocopter, the successful design evolutions of the main and tail rotors of the EC-135 were described, emphasizing design for reduced noise. The presentation that followed, from Bell Helicopter, described the development and testing of Bell's new ducted tail rotor design. Both cases have demonstrated that a major improvement can be achieved in the overall external noise signature by *detuning* some of the interference aerodynamic noise sources generated by interaction of the tail rotor with the main rotor wake. In each case, the technique involves use of an uneven angular spacing of tail rotor blades or tail fan blades. This has the effect of spreading out the noise spectrum and reducing the amplitudes of imbedded tones. The result is a substantially reduced perceived noise level.

The session clearly touched on a very diverse range of subjects. If there is an underlying message, however, it may simply be that helicopter designers continue to be among the most creative users of each new stream of aeronautical technology.

Session IV: Methodology

I will defer comment on presentation #21 on Rotorcraft-Pilot Coupling, which was delivered in Session IV, to consider it with the other control system presentations of Session VI. With this change, the predominant subject of the Methodology Session was the state of progress in rotorcraft aerodynamics and acoustics. From the standpoint of a non-specialist in these areas, the presentations underlined the degree to which improvements in rotorcraft performance and simulation still depend upon better understanding of very fundamental aspects of rotor aerodynamics. Rotors and rotorcraft still present serious challenges for the aerodynamics disciplines and survey presentation #24 at the end of the session confirmed this point. Summarizing the proceedings of a recent Fluid

Mechanics Panel symposium on Aerodynamics and Acoustics, the presentation emphasized that dynamic stall phenomena are still not fully understood; that rotor solutions based on comprehensive 3-D CFD analysis codes do not yet correlate satisfactorily with experimental results; and that the weakest points in aeroacoustic modeling are difficulties in predicting aerodynamic flow fields.

While the aerodynamicists work to improve their rotorcraft modeling techniques, flight mechanics engineers are using empirical means to improve the aerodynamic force representations in their current flight dynamics models. A presentation from the US Army AFDD provided a good illustration of the empirical approach. The AFDD study was based on a blade-element model of the Apache helicopter, which does not adequately reproduce the roll response of the helicopter to pitch control inputs or the pitch response to roll control inputs, that is, the cyclic control cross-coupling effects. It was found that the deficiency is largely overcome by applying simple first-order low-pass filters to the calculated elemental lift and drag forces. This time-lagging of the force calculations may well be capturing one specific physical effect that is absent from the base model: several candidate effects are in fact proposed in the paper. Or it may just be a good "fitting factor" for the accumulated error from several sources. In either event, the "aerodynamic phase lag", as the correction is being called, improves the fidelity of the model for flight mechanics applications.

In a theoretically-based aerodynamics presentation from Delft University, an improved "sweep effect" correction was proposed for rotor modeling applications that are based on the lifting-line approach. This is an extension of some much earlier work on classical unsteady lifting-line theory for fixed-wing aircraft. The proposed correction could have a significant impact on rotorcraft modeling, since lifting-line theory is still the basis for many helicopter models used for flight dynamics analysis.

Two additional presentations provided snapshots of particular *methodologies.* Presentation #19 from ONERA dealt with prediction of internal cabin noise in a helicopter, using Statistical Energy Analysis (SEA) methods and correlation with measured noise characteristics. Studies based on the Ecureuil show good results for the SEA method and followup work is being extended to the more complex and challenging Dauphin medium helicopter case.

A presentation on the effects of propulsive system dynamics on aeromechanical stability of a hingeless rotor helicopter completed the session. Recently, there has been considerable interest in the subject of engine-governor-rotor dynamic interactions that introduce oscillatory modes into the frequency range of concern for helicopter handling qualities. The presentation provided a report on numerical simulation studies of a hingeless rotor helicopter, looking at a range of propulsion system characteristics in straight and level and coordinated turning flight cases. For the test points investigated, propulsion system dynamics did not materially affect pitch or roll handling qualities. In some elevated-g (turning) cases, degraded heave-axis handling qualities were predicted.

Session V: Programs

The Program Session provided overview presentations on three well-known development and production programs, EH101, Comanche and V-22 - and a review of a compound helicopter concept study. As context for some general observations on the session, the following paragraphs will summarize one or two of the main themes of each presentation.

The EH101 presentation emphasized the impact of the decision to produce a single design able to satisfy the operational and regulatory requirements of both civil and military customers. This has been a pioneering effort, successful in an overall sense - and one that will undoubtedly be repeated to various degrees in the future. The EH101 experience illustrates that the principle of a common civil/military design is feasible and that the cost and performance penalties are manageable and generally come with a bonus of added safety. The author is clear, however, in stating that the process would be greatly simplified if the impetus for merged requirements came from the civil and military regulatory authorities, rather than from the manufacturers. In fact, the future appears to be unfolding along these lines.

A wide ranging description of Comanche followed. It is difficult to write anything new about this much heralded helicopter. While it will field an array of revolutionary new technologies and capabilities, these are all realizations of systems that have been in AGARD's "sights" for some time. In the context of the themes for this meeting however, less well-known supportability and maintainability projections for the Comanche are of particular interest. If design levels are achieved in these areas - reductions by a factor of four in maintenance hours per flight hour and greatly reduced in-the-field infrastructure - the impact on operations on the battle field will be dramatic.

The presentation on the V-22 began by describing the current Engineering Manufacturing Development phase of the program, but moved on to a discussion of engineering problems or "technical challenges" that surfaced in the earlier full-scale development flight tests. The challenges ranged from empennage buffet in certain areas of the manoeuvring envelope to the need for structural load limiting control laws. There was special interest, however, in a series of three pilot-induced oscillation cases, two of which were solved by implementing notch filters and the third by lateral stick mass balancing. (The general issue of rotorcraft-pilot coupling was singled out for special emphasis in presentation #21.)

Common threads in all of these programs are their long gestation periods and their highly political development histories. The significant improvements in technology and increases in effectiveness that they unquestionably deliver will come at a very high cost in each case.

They are also, all, extremely large and complex programs which present major challenges at every level of program management. It is interesting to note that the Comanche and the EH101 programs appear to have incorporated "systems engineering" practices and computer aided systems engineering (CASE) tools, in a formal way, into their program management structures. This is likely to be a prevalent trend as computer-based program planning and program management systems meet up with common engineering design data bases and concurrent engineering. The resulting integrated process is developing a new and formalized systems engineering (SE) culture. SE in this recently defined sense, as formalized for example in IEEE Standard P 1220 or Draft MIL-STD-499B, has spawned a new international society and an active research and academic publication stream. In the AGARD universe, this new subject may well be within the domain of interest of the FVP.

The fourth presentation in the session described a concept configuration study. There appears to be little appetite right now within the rotorcraft community for revolutionary design experimentation. It was interesting, therefore, to see a strong case for reconsidering compound helicopter configurations presented by Westlands. The author contends that conditions are ripe for exploring lift or thrust compounding or a combination of the two, since recent technology improvements in rotor design and engines will substantially improve the efficiency of compound configurations. Encouraged by initial analytical studies, a Lynx-based demonstrator program is now being contemplated. Detractors may say that a compound rotary wing solution is an inherently complex and inelegant VSTOL solution; on the other hand, the Cheyenne that was cancelled 24 years ago would be an impressive flying machine if it incorporated the relevant technology advances of the intervening years.

Session VI: Advanced Controls

The presentations of this final session covered a wide area of interests including subjects outside the general domain of flight control. The initial presentation of the session summarized research that is being conducted at the NRC (Canada) on three specific cockpit technologies, using helicopter in-flight simulation facilities as the research environment. There was an underlying message here that a large gap separates the promise held out by the new technologies and the ability to apply them in integrated functions that help the pilot. The three examples cited - high-performance full-field-of-view helmet mounted displays, direct voice input systems and 3-D head-down displays - are all relatively mature physical systems, but they all continue to present significant challenges in areas of pilot-aircraft integration.

Two presentations directed our attention back to the capabilities and needs of the current generation of military helicopters. There is general agreement in the helicopter research and development community that we could make better use of the standard control system architectures that are installed in the current operational fleet. These systems usually combine relatively capable limited-authority automatic flight control systems (AFCS) in combination with conventional full-authority mechanical controls.

A presentation by Westlands and DRA described a generic research program that would use limited-authority stability and control augmentation systems to improve operational capability in three specific areas: to improve the quickness of changes in engine torque in response to rapid manoeuvring rotor load changes; secondly, to conserve rotor speed following engine failure; and finally, to implement a "carefree handling" feature for aggressive collective/vertical manoeuvring, providing torque limit protection. Studies indicate that substantial enhancements of performance and safety could be achieved by implementing these system adaptations using the current standard control hardware.

This same theme was addressed in the final presentation of the symposium, from NRC, within a general discussion of handling qualities requirements for flight in degraded visual environments. Background research

for Aeronautical Design Standard ADS-33 has defined relationships between control mode stabilization requirements and the level of visual cues available to the pilot. More recent studies are showing that the levels of attitude and speed stabilization that are required for flight in degraded visual environments can be achieved using limited-authority control augmentation systems. This will require the implementation of new control laws - and, presumably, new digital processing systems. But the standard limited-authority electro-hydraulic control hardware in the current helicopter designs should do the job.

It seems clear that, in a variety of ways, the good "old" AFCS hardware, driven by new mission-adapted control laws, could greatly enhance flight safety and operational capability for this current generation of helicopters - particularly when they must operate in degraded visual environments. It is also clear that modifications of this type to the operational fleets would carry a substantial price tag associated with proof of compliance or certification. In some cases, however, the mission performance and safety gains should be a bargain.

Presentation #32 from Eurocopter described simulation design studies and flight validation experiments for active control of helicopter aeromechanical stability. The specific aims of the work are to improve air and ground resonance stability and overall drive train stability of modern rotors, and to simplify the design of lead-lag dampers for soft in-plane rotors. Relatively simple ACT implementations, easily integrated into a conventional flight control system, have proven to be highly effective in simulation and are being validated in flight tests on a Super Puma Mk2.

Finally, to return to presentation #21 from DLR on rotorcraft-pilot coupling: this was a call for caution directed at the emerging community of developers and operators of highly-augmented helicopters. The challenge is to learn about - *and learn from* - the experiences of the fixed wing community with high-gain high-performance control systems - and to avoid repeating the major errors that have cost lives and programs.

No one will disagree. It could be said that helicopters do things differently, that unlike fixed-wing aircraft they may experience and resolve many serious problems while in hovering flight or in the very low and very slow flight regime. But in many ways, the control forces being commanded and the dynamic systems that respond are less well understood for helicopters than they are for fixed-wing aircraft. PIO or adverse pilot-helicopter coupling is frequently encountered in the helicopter business. The paper should be an inspiration, directing attention and future work toward an understanding of the underlying phenomena.

CLOSING DISCUSSIONS

The symposium ended with a discussion around three questions posed by the program committee and animated by a head table of prominent participants. The questions were the following:

- What are the two most important technologies needed for future rotorcraft?
- Does our research effectively influence rotorcraft affordability and safety?
- Will use of common standards in place of military specifications and standards result in lower cost for the same effectiveness?

No radically new ideas were advanced during the discussions. Regarding technology needs, there was strong support for highly integrated active control technologies and unspecified " technologies that will improve existing helicopters" - for more advanced flight aids to improve all-environment operations, for reduced acoustic signatures and for a good, inexpensive low-speed airspeed system.

Concerning the links between research and affordability, there appeared to be agreement that design for affordability and low life-cycle cost have not been prime drivers in our research programs - and that these elements must be brought more directly into the equation in the future. On the other hand, research has been very effective in improving flight safety and operational effectiveness. Two additional statements were made on the subject of research, dealing more generally with the way rotorcraft research is done. First, while the research community has undoubtedly become much more customer-oriented in recent years, researchers acknowledge that they still need to get out into the field more often to experience the operatoral environment. As a final point, there was a plea for a "strategic policy" on research to avoid having all research centres doing similar things.

The issue of common standards raised in the third question was a significant theme of the meeting. The discussion around the question repeated and underlined points made during the earlier presentations, but extended those arguments as well. The main comments are listed here in abbreviated form:

- Common standards will reduce effectiveness of military aircraft.

- We must be careful in deciding which military specifications get eliminated. In some areas there are no commercial alternatives. Ignoring the military standards in these areas can be costly.

- In this new environment, the developer must have a clear understanding with the customer regarding requirements versus cost.

- ADS-33 is an example of a standard that must be kept, since there is no civil equivalent. Handling qualities define "goodness", something that is more difficult to quantify than hard objective structural requirements, for example. ADS-33 has given handling qualities the necessary objective framework.

- An important point is being missed: specifications and standards are not the problem. The cost of demonstrating compliance with the specifications and standards is the problem. We need to reduce the cost of the compliance process.

These uncontested views were "left on the table" as the meeting was closed.

SUGGESTIONS FOR CONSIDERATION BY THE PANEL

1. Military use of commercial off-the-shelf equipment and development of new military equipment using common standards present immediate and longer term challenges to the rotorcraft community. Within AGARD these are issues that cross the panel boundaries, but they concern FVP in particular way, since they have a large impact on operations, vehicle design and integration. The impact of COTS and common standards on operations and costs deserves immediate focused attention by the Panels.

2. The tail rotor failure issues raised in paper #3 could be considered the basis for a broader exchange of data and information among the NATO partners, facilitated by the FVP.

3. There is an acknowledged need to extend the operational life and improve the operational effectiveness of the current aging fleets of military helicopters, and to do this *affordably*. AGARD program initiatives addressing this need would be timely. (Within the scope of the FVP mandate there are many candidate technology applications that qualify for consideration in such an effort, beginning with the implementation of new control laws for current limited-authority automatic control systems, as suggested in papers 31 and 33 of these proceedings.)

4. I assume that the Panel will discuss Dr. Peter Hamel's plea for attention to the potential dangers of adverse pilot-aircraft coupling in highly augmented helicopter designs, as described in paper #21 in the proceedings. I would endorse and encourage a measured series of initiatives in this area.

5. I would encourage the FVP to present symposia dedicated to rotorcraft issues at four or five year intervals, rather than the 10 years gap that separated the last two. I would also encourage organizers to focus the meeting presentations on two or at most three well defined themes that reflect the unique mission and objectives of the FVP.

6. The meeting demonstrated the value of the thorough instructions that AGARD provides to authors on the essential elements of preparation and delivery of good technical presentations: in general, the quality of the presentations was high. There were a few exceptions, however, that confirm the need for continuing reminders to presenters that they should heed this good advice.

POSTCRIPT

I wish to thank the Flight Vehicle Integration Panel for inviting me to participate in the Ottawa meeting in this special way.

Keynote Address AGARD FVP Symposium

"Advances in Rotorcraft Technology"

Brigadier General K. Pennie
OMM, CD
Commander, 10 Tactical Air Group
CFB Montreal
St. Hubert, H3Y 5T4, Québec

Good morning, on behalf of LGen DeQuetteville, the Commander of the Canadian Air Force, I would like to welcome you to Ottawa for this AGARD conference on rotorcraft technology.

As the Commander of Canadian Tactical Aviation, I have a vested interest in this topic; particularly during these times we are all experiencing, and I thank you for inviting me to open this year's conference.

As you are aware, and many of you are likely experiencing, we, in the Canadian military are going through a period of downsizing, defence spending cutbacks, and very slow economic recovery. We in the Canadian Tactical aviation community are lucky enough to be introducing a new helicopter fleet into our inventory to support the Army. It is very important to keep in mind, however, that although we are implementing a new aircraft, we can only afford one fleet of helicopters and it is a compromise. We have retired our observation fleet, the CH136 Kiowa, and our medium lift fleet, the CH147 Chinook. We are replacing our Utility transport fleet, the CH135 Twin Huey, with the new Bell 412, a commercial off-the-shelf helicopter which we have named the Griffon.

It is also important to remember that the Army doctrinal requirement to cover the full spectrum of helicopter operations actually still demands four fleets of combat capable helicopters: ATTACK (AH types e.g. AH-64), RECONNAISSANCE (LH types e.g. OH58 D), UTILITY (UTTH types e.g. UH 60), MEDIUM (MTH types e.g. CHINOOK). In fact, operations such as Desert Storm, Restore Hope, and the like, continue to confirm and justify this requirement. The reality however is such that NATO countries are facing fiscal pressures and have to adjust accordingly. In our case it has forced us away from full Mil Spec to commercial off-the-shelf (COTS).

I now come back to my position as the commander of tactical aviation with the requirement to meet the Army's expectations with a single fleet of commercial

Bonjour. Au nom du lgén DeQuetteville, commandant des Forces aériennes du Canada, je vous souhaite la bienvenue à Ottawa dans le cadre de la conférence AGARD sur la technologie des aéronefs à voilure tournante.

Comme je commande l'Aviation tactique du Canada, cette question m'intéresse, tout particulièrement dans le contexte actuel. Je vous remercie de m'avoir invité à ouvrir la conférence de cette année.

Comme vous le savez - et bon nombre d'entre vous le vivent - l'Armée canadienne est soumise actuellement à des diminutions d'effectifs. En outre, les dépenses allouées à la défense sont réduites, et la reprise économique est très lente. Toutefois, il y a une lueur d'espoir pour l'Aviation tactique du Canada, car une nouvelle flotte d'hélicoptères destinée à appuyer l'Armée est introduite dans les stocks de la défense. Il est très important de se rappeler cependant qu'une seule flotte d'hélicoptères nous a été autorisée, et ce, au terme d'un compromis. Nous avons retiré notre flotte d'hélicoptères d'observation CH136 Kiowa et notre flotte d'hélicoptères de transport moyen CH147 Chinook. Nous remplaçons nos hélicoptères polyvalents CH135 Twin Huey par le nouveau Bell 412. Il s'agit d'un hélicoptère commercial standard baptisé Griffon.

Il est tout aussi important de ne pas perdre de vue qu'en vertu de la doctrine de l'Armée, il faut être en mesure de mener toute la gamme des opérations héliportées. Pour ce faire, il faut quatre flottes d'hélicoptères au potentiel de combat: ATTAQUE (types AH, p. ex. AH-64), OBSERVATION (types LH, p. ex. OH58 D), POLYVALENT (types UTTH, p. ex. UH 60), TRANSPORT MOYEN (types MTH, p. ex. CHINOOK). En fait, les opérations du type Tempête du désert et Rendre l'espoir continuent de confirmer et de justifier cette exigence. Toutefois, dans l'état actuel des choses, les pays de l'OTAN sont soumis à des pressions financières et doivent s'adapter en conséquence. Dans notre cas, nous avons été obligés de nous écarter des spécifications militaires intégrales pour des raisons de coûts.

En tant que commandant de l'Aviation tactique, je me dois de répondre aux attentes de l'Armée à l'aide d'une seule flotte d'hélicoptères commerciaux polyvalents.

Paper presented at the FVP Symposium on "Advances in Rotorcraft Technology", held in Ottawa, Canada, 27-30 May 1996, and published in CP-592.

utility lift helicopters. I don't need to tell you the difficult position I am placed in.

Inutile de vous dire que je me trouve dans une position difficile.

This is where AGARD and conferences such as this one demonstrate their importance and how, perhaps over time, you can assist countries with reducing military budgets to cope better with this dilemma. I will use a few examples of current problems we face as we introduce the new helicopter, to point out how the technical/industrial community can help to provide workable and, just as important, affordable solutions to countries like Canada, that cannot afford large investments in military technology.

Voilà donc pourquoi ce type de conférence est important et comment, peut-être, vous pourrez éventuellement m'aider à résoudre mon problème. Je vous donnerai quelques exemples des problèmes que nous cause l'introduction du nouvel hélicoptère. Ces exemples serviront à illustrer comment la communauté technologique industrielle peut nous aider à trouver des solutions possibles qui - ce qui est tout aussi important - sont économiquement réalisables dans un pays qui, comme le Canada, ne peut pas se permettre d'investir beaucoup d'argent dans la technologie militaire.

The Bell 412 is a civilian pattern, medium transport aircraft that our crews must employ on the moderm battlefield to support our Army. Something as simple as NVG flight is taken for granted by military helicopter users because it has been a way of life for many years. The civilian community is, however, quite different, and has not endorsed the requirement for NVG compatible cockpits. For example, you are aware that the FAA in USA and MOT in Canada will not certify cockpits with other than aviation red warning lights. Herein lies our first challenge: how can you satisfy the NVG compatibility requirement while meeting the civilian certification requirements as well. I can say that there are ways to manage this problem, but we have yet to find a fully functional technical solution.

Le Bell 412 est un hélicoptère polyvalent de modèle civil que nos équipages de vol doivent utiliser sur le champ de bataille moderne en appui de l'Armée. Pour les pilotes d'hélicoptères militaires, un simple vol effectué à l'aide de lunettes de vision nocturne va de soi, car, pour eux, depuis de nombreuses années, l'utilisation de ce dispositif est chose courante. Par contre, dans le milieu civil, il en va tout autrement, car l'aviation civile n'a pas cru bon d'exiger que les postes de pilotage des hélicoptères soient adaptables pour la vision nocturne. Par exemple, vous savez sans doute que la FAA aux États-Unis et Transports Canada ne certifieront pas les postes de pilotage dotés d'un dispositif autre que des feux rouges d'aviation. Voilà notre premier défi: comment concilier notre besoin d'un dispositif de vision nocturne et les exigences de certification civile. Il y a des façons de solutionner le problème, mais il nous reste encore à trouver une solution technique tout à fait fonctionnelle.

The issue of communications and avionics equipment in military helicopters is an interesting one. It seems we just can't seem to get enough radios and equipment in the cockpit to everybody's liking, except for maybe the engineers. Civilian aircraft tend not to have the same requirement for extensive systems such as defensive electronic warfare suites with radar warning and missile approach warning, and extensive communication packages with two or three multi-band radios for UHF, VHF/AM, VHF FM and police band, not to mention HF for long range communications.

La question de l'équipement de communication et de l'avionique dans les hélicoptères militaires est intéressante. Il semble tout simplement qu'il nous soit impossible d'obtenir sans que quelqu'un s'objecte - sauf les ingénieurs peut-être - tous les postes radio et tout l'équipement de communication dont nous avons besoin dans le poste de pilotage des hélicoptères. En général, les aéronefs civils n'ont pas à être dotés de tous les systèmes dont l'Armée a besoin, notamment des systèmes de guerre électronique défensive munis de dispositifs d'avertissement radar et d'avertissement d'approche missile et des groupes d'appareils de communication perfectionnés dotés de deux ou trois postes radio multi-bandes UHF, VHF/AM, VHF FM, bande radio-police, sans mentionner les bandes HF pour les communications longue distance.

One of the problems we have been faced with as we introduce the 412 is how to manage all these systems from the cockpit, while still ensuring that the pilots can safely fly the aircraft in the low level tactical environment. We have taken the 412 cockpit and modified it such that we have installed dual cockpit display units (called CDUs) to serve as the control head for many of the aircraft systems remotely placed throughout the airframe. The solution however has created two new problems: a single point of failure problem and a cockpit resource management problem. Again we are managing to find workable solutions but they are nonetheless not ideal solutions.

Un des problèmes soulevés par l'introduction du Bell 412 est le suivant: comment les pilotes peuvent-ils arriver à gérer tous ces systèmes à partir du poste de pilotage tout en pilotant l'appareil de façon sûre au cours de vols tactiques basse altitude. Nous avons modifié le poste de pilotage du Bell 412 en y installant des panneaux de commande et d'affichage doubles (communément appelés «CDU») servant de centres de contrôle pour bon nombre des systèmes dispersés dans toute la cellule. Toutefois, cette solution a soulevé deux nouveaux problèmes: un problème de point de panne unique et un problème de gestion des ressources du poste de pilotage. Encore une fois, nous essayons de trouver des solutions réalisables, lesquelles néanmoins demeurent imparfaites.

The challenge here is how best to provide the crew the means to effectively employ the aircraft's systems to successfully complete their mission, while also providing them a means to manage those systems without compromising safety. Technologies such as day-HUDs, helmet-mounted displays, voice-activated systems control, or even pilot's associate systems provide potential solutions; some of which you are likely going to discuss in the next few days.

Le défi est de taille: comment fournir à l'équipage le meilleur moyen d'utiliser efficacement les systèmes de l'appareil qui lui permettent de mener à bien sa mission tout en lui donnant la possibilité de gérer ces mêmes systèmes sans nuire à la sécurité du vol. Des technologies comme les visualisations tête haute - jour (HUD), les dispositifs d'affichage montés sur casques, les systèmes de contrôle à commande vocale ou même des systèmes connexes du pilote offrent des éléments de solution. Nous discuterons probablement d'un certain nombre d'entre elles au cours des prochains jours.

Ideally these operational systems would be designed into a combat helicopter, but increasingly a retrofit of a COTS helicopter may be the solution for countries with reducing military budgets.

Idéalement, ces systèmes devraient être conçus en fonction des hélicoptères de combat; mais, la remise en état de plus en plus fréquente d'hélicoptères COTS peut s'avérer une solution intérressante pour les pays dont les budgets militaires sont restreints.

Another case in point, with respect to employing a modified civilian airframe in a military operational role, is that with respect to mission equipment. As you are aware, we recently sent several helicopters to Haiti to support ongoing UN operations there. Although we are currently employing the Twin Huey there, we are conducting the detailed staff planning to deploy our Bell 412's (GRIFFONS) to Haiti, once we can resolve some planning issues. One such issue is that of mission equipment; some examples are self-protection door guns, armour protection from small arms rounds, searchlights, FLIR systems, and a plethora of other ancillary equipment associated with these systems.

L'équipement de mission est un autre bon exemple de l'utilisation des cellules d'aéronefs civils modifiées dans un contexte opérationnel militaire. Comme vous le savez, nous avons envoyé récemment en Haïti des hélicoptères en appui des opérations de l'ONU. Nous utilisons à l'heure actuelle des Twin Huey en Haïti, mais une planification d'état-major détaillée en cours prévoit le déploiement de nos hélicoptères Bell 412 (GRIFFON) dans ce pays, une fois certaines questions de planification résolues. Une de ces questions est celle de l'équipement de mission, p. ex. des armes de porte d'autodéfense, un blindage contre les armes de petit calibre, des projecteurs, des détecteurs infrarouges avant (FLIR) et un important équipement auxiliaire à ces systèmes.

You can see that as we continue to load up with these systems we now get to the point where the aircraft can survive in the theatre, but we can't do what we are tasked to do because the helicopter is already overweight. So what I need to do is provide the same capability but use systems and equipment that do not have the same weight and space penalty. The challenge is to provide button- and strap-on mission kits that are fully capable but are lighter and smaller. This issue of button- and strap-on equipment is not likely one that is going to go away for the foreseeable future; and it is very real. Many of the smaller military users are facing this every day as they introduce commercial off-the-shelf products into their inventory and modify them for use in operational environments.

Comme vous pouvez le constater, à force d'ajouter des systèmes, nous en sommes arrivés au point où l'appareil est maintenant en mesure de survivre dans le théâtre des opérations. Mais, nous ne pouvons pas faire ce qu'on nous demande de faire parce que l'hélicoptère est trop lourd. Donc, il me faut obtenir le même potentiel, mais en utilisant des systèmes et de l'équipement qui sont moins lourds et qui occupent moins d'espace. Les accessoires d'installation des ensembles de mission doivent être plus légers et plus petits tout en demeurant tout aussi performants. Cette question ne semble pas en voie d'être résolue dans un proche avenir. Toutefois, elle demeure très réelle. Bon nombre de petits utilisateurs militaires font face à ce problème tous les jours lorsqu'ils ajoutent des produits commerciaux standard à leurs stocks et doivent les modifier pour les adapter aux environnements opérationnels.

As I have previously alluded, the Canadian Army requirement for four combat helicopter fleets continues to be justified and supported, at least in doctrinal terms but not necessarily in fiscal terms. The requirement for a reconnaissance and surveillance capability is well recognized as a critical requirement for a land force commander to ensure successful operations on the battlefield. With a single fleet of utility aircraft, this becomes a rather daunting task for me. How could my unit commanders employ their aircraft so as to meet the Army commander's reconnaissance and surveillance requirements.

Comme je l'ai mentionné au début, le besoin qu'a l'Armée canadienne d'avoir quatre flottes d'hélicoptères de combat continue à être justifié au plan de la doctrine, sans nécessairement l'être au plan financier. La nécessité de posséder un potentiel de reconnaissance et de surveillance est admise comme étant un élément essentiel à un commandant d'une force terrestre pour que le succès des opérations soit assuré sur le champ de bataille. Cela devient un défi de taille pour moi si je ne possède qu'une seule flotte d'aéronefs polyvalents. Comment, en effet, mes commandants d'unité pourraient-ils utiliser leurs aéronefs de manière à répondre aux exigences du commandant de l'Armée en matière de reconnaissance et de surveillance?

Well, the first thing I would need to address is survivability. In my opinion, this equates to stand-off and self-protection. If we intend to use the GRIFFON airframe for reconnaissance and surveillance missions we will need to provide the crew with effective optical enhancement systems to ensure they can achieve the stand-off distances required to remain outside the lethal envelope of the threat's capability. The system will also need to be multi-spectral including the near- and mid-IR as well as visual ranges of the electromagnetic spectrum.

Le point que je devrai considérer, c'est la surviabilité. À mon avis, cette surviabilité s'obtient par le maintien d'une distance de sécurité et l'autoprotection. Si nous envisageons d'utiliser la cellule du GRIFFON pour des missions de reconnaissance et de surveillance, nous devons fournir aux équipages des systèmes optiques efficaces pour qu'ils puissent demeurer à distance de sécurité des armes ennemies. Le système devra également être à spectres multiples et englober l'IR proche et moyen ainsi que la gamme des radiations visibles du spectre électromagnétique.

Now, I am aware that all the systems that meet this requirement have been manufactured for many years and are not necessarily new technology. Notwithstanding this, I do have some very specific challenges. The system must be readily available when I deploy and must be capable of being installed and removed from the aircraft at will, within reasonable time frames, and without extensive support requirements. On top of all that, the system must be light-weight so as not to adversely affect the aircraft C of G. This is most important because, remember, my aircraft is already close to being overweight.

Je sais que tous les systèmes qui répondent à ce besoin sont fabriqués depuis de nombreuses années, et qu'il ne s'agit pas nécessairement d'une nouvelle technologie. Quoi qu'il en soit, je fais face à des problèmes très particuliers. En effet, le système doit être disponible au moment où je déciderai de déployer mes appareils, et il doit pouvoir être installé et enlevé à volonté, et ce, dans des délais raisonnables et sans qu'il soit nécessaire de faire appel à un soutien élaboré. En plus de tout cela, le système doit être léger afin de ne pas déplacer le centre de gravité des appareils, surtout parce que - rappelez-vous - ceux-ci sont déjà surchargés.

Finally, and not nearly least, is the ability to provide training to the crew to effectively use the equipment. This aspect is often overlooked when looking at button- and strap-on mission kits. Again it leads to the cockpit resource management and workload problem. As the strap-on systems add up, so too does the man-machine-interface problem of effectively operating the systems while safely managing them and continuing to fly the aircraft.

Finalement, il y a un autre problème et non le moindre: il faut pouvoir montrer aux équipages comment utiliser efficacement l'équipement. Cette question est souvent négligée lorsqu'il est question des accessoires d'installation des ensembles de mission. Encore une fois, nous faisons face au problème de gestion des ressources du poste de pilotage et de charge de travail pour l'équipage. Les systèmes d'appoint compliquent la situation et posent un problème d'interface homme-machine. En effet, on demande aux équipages non seulement d'utiliser efficacement les systèmes, mais de les gérer de façon sûre, et ce, tout en continuant de piloter l'aéronef.

These are only a few of current challenges I am faced with as the new aircraft is bought into our inventory. If you sit and think for a minute of how you, as an operator, would employ a civilian aircraft in a military environment, you will begin to see many other issues that need to be resolved. As you continue the conference throughout the remainder of the week, I would like you to keep in mind the issues I have highlighted, so as to determine if any of the current, developing or enabling technologies can be applied to the challenges I've presented. I sincerely hope you enjoy the conference and your stay in Ottawa, and again thank you very much for the opportunity to speak with you today. I will be happy to address any questions or comments you have.

Il ne s'agit là que d'un certain nombre de problèmes auxquels je suis confronté depuis l'introduction du nouvel aéronef. Si vous réfléchissez quelques instants à la façon dont vous utiliseriez un aéronef civil dans un environnement militaire, vous entreverriez déjà beaucoup d'autres problèmes. Pendant le restant de la semaine au cours de la conférence, j'aimerais que vous vous rappeliez les questions que j'ai soulevées afin de déterminer si une des technologies actuelles, en développement ou habilitantes, peut répondre aux problèmes que j'ai exposés. J'espère sincèrement que vous apprécierez la conférence et votre séjour à Ottawa. Je vous remercie encore une fois de m'avoir donné l'occasion de vous adresser la parole aujourd'hui. Il me fera plaisir maintenant de répondre à vos questions ou d'entendre vos commentaires.

EVOLUTION DU CONCEPT D'EMPLOI DES FORMATIONS AEROMOBILES DE L'ARMEE DE TERRE FRANCAISE

Général de division BATLLO
Commandant l'Aviation Légère de l'Armée de Terre
Zone Aéronautique Louis Breguet
Porte No. 5, 78129 Villacoublay-Air, France

Très vite, l'hélicoptère s'est imposé dans les armées parce qu'il portait en lui des possibilités indiscutables et prometteuses.

Certes, il a eu, et il a toujours des détracteurs - les pessimistes - qui ne mettent en avant que son apparente fragilité. Heureusement, les optimistes ont raison de lui faire confiance et, aujourd'hui, toute armée moderne se forge son aéromobilité, c'est à dire un "mode d'emploi" de son parc d'hélicoptères.

Je vous propose de parcourir, en quelques minutes, "l'aéromobilité française" en examinant plus particulièrement :
- les 3 faits majeurs qui, aux années 60, ont fait de l'hélicoptère un engin de combat à part entière,
- notre concept d'emploi des hélicoptères à l'époque de la "guerre froide",
- notre concept actuel, porteur de vastes potentialités pour l'avenir.

Les temps ont changé, les matériels ont évolué, l'hélicoptère, lui, reste un véritable engin de combat qui, ces dernières années, s'est affirmé comme un outil de projection privilégié pour la gestion des crises.

xx
x

1. LE TOURNANT DES ANNEES 60

L'aviation légère de l'armée de terre française, l'ALAT, a vu le jour en 1944.

A cette époque, elle n'était constituée que d'avions légers, des PIPER, destinés essentiellement aux réglages des tirs d'artillerie. Dés le début des années 50, elle s'est dotée d'hélicoptères pour l'aide au commandement et aux armes, le renseignement, le transport de commandos et de matériel et les évacuations sanitaires.

Ce sont des appareils à moteur à pistons, ils permettent de s'affranchir des obstacles du terrain et de gagner du temps. Ils sont employés isolés ou par petites formations, éparpillées au sein des grandes unités de l'armée de terre, travaillant toujours à leur profit direct et souvent à leur rythme.

A la fin des années 50 et au tout début des années 60 apparaissent en France les premiers hélicoptères à moteur à turbine, le DJINN, mais surtout l'Alouette II et l'Alouette III.

Le moteur à turbine donnant à l'hélicoptère
- puissance,
- fiabilité,
- maniabilité,

il lui permet :
- de transporter de l'armement,
- et, surtout, de pratiquer le VOL TACTIQUE, type de vol qui se conduit au ras du sol, dans le micro-relief, qui assure une protection indiscutable et garantit la surprise. C'est un véritable "vol de combat" qui obéit à l'une des règles de base du fantassin : voir sans être vu, tirer sans être tiré.

A peu près à la même époque, apparaît le missile antichar filoguidé. Ce missile se monte très facilement sur les hélicoptères, il est précis, performant et permet d'atteindre les objectifs au-delà de la portée des armes à tir tendu de l'ennemi.

Ainsi, ces trois facteurs :
- le moteur à turbine,
- le vol tactique,
- le missile

ont fait de l'hélicoptère un véritable "engin principal de combat".

A partir de cette innovation, l'armée de terre française va réorganiser son aviation légère en regroupant les petites unités dans des groupes divisionnaires et de corps d'armée de 40 à 50 appareils pour donner à la manoeuvre aéromobile puissance et cohérence. Par ailleurs, ces regroupements faciliteront le commandement, la coordination et le soutien.

2. L'AEROMOBILITE DE COMBAT A L'EPOQUE DE LA "GUERRE FROIDE"

Jusqu'au début des années 90, la menace majeure en Europe a été constituée par les dizaines de milliers de chars et de blindés du Pacte de Varsovie. Or, l'accession de l'hélicoptère au rang des engins de combat ne peut pas laisser les stratèges indifférents. Un avenir se présente pour l'hélicoptère antichar. Il faut l'utiliser. Et la mission principale confiée à l'aviation légère

Paper presented at the FVP Symposium on "Advances in Rotorcraft Technology", held in Ottawa, Canada, 27-30 May 1996, and published in CP-592.

française tout au long de cette période de la "Guerre froide" devient la lutte antichar.

L' ALAT possède un système d'arme adapté à la menace. A elle de mettre au point le mode d'emploi, c'est à dire le "concept aéromobile". L'idée est d'employer les hélicoptères en formations massives et autonomes pour tirer le meilleur parti de la vitesse, de la souplesse, de la furtivité et de la capacité à s'affranchir du terrain de cet aéronef.

Le pion de base du combat aéromobile, l'outil principal c'est le "régiment d'hélicoptères de combat" à 60 appareils, régiment qui possède en son sein tous les moyens lui permettant de mener le combat :
- une escadrille de 10 hélicoptères de reconnaissance équipés de lunettes gyrostabilisées à fort grossissement,
- une escadrille d'appui-protection à 10 Gazelle canon,
- trois escadrilles antichars, soit 30 Gazelle armées chacune de 4 missiles HOT,
- une escadrille de 10 hélicoptères de transport tactique.

Ce régiment est "polyvalent" dans ses moyens mais prioritairement voué au combat antichar.

Les différentes escadrilles sont en permanence entraînées à travailler ensemble,dans le même but : repérer les colonnes de chars, les ralentir et les détruire.

Ainsi, de l'appui rapproché des unités au sol, à leur rythme, dans leur petit volume d'action, par des patrouilles de 2, 3 ou 4 appareils, on est passé à l'engagement autonome de grandes formations, loin en avant, sur les flancs, dans les intervalles des unités au sol, pour aller attaquer les groupements blindés adverses lorsqu'ils sont en mouvement.

De l'éparpillement des moyens, il a fallu passer à leur concentration pour produire un effet significatif et rapide sur l'ennemi.

Et l'aboutissement de ce concept a donné naissance, en 1985, à la division aéromobile, grande unité regroupant 240 appareils en 4 régiments d'hélicoptères, un régiment de soutien aéromobile et un régiment d'infanterie spécialisée (pour l'Histoire, notons que ce régiment, le 1er régiment d'infanterie, est "le plus vieux régiment de la chrétienté". Il a été fondé en 1479 et, aujourd'hui, il est le plus moderne et le plus polyvalent de l'armée française).

La 4ème division aéromobile, dont 2/3 des hélicoptères sont dédiés au combat antichar, travaille selon les règles classiques du combat terrestre.

Par une manoeuvre coordonnée, intégrée à l'action d'ensemble du théâtre d'opérations, elle a pour "contrat" de neutraliser en 48 heures une division blindée renforcée.

Pour ce faire,
- avec ses hélicoptères de reconnaissance, elle va chercher le renseignement sur l'ennemi, en s'infiltrant tout au long des itinéraires routiers, pour déterminer son contour et son axe d'effort ;
- puis, avec ses GAZELLE missile, elle attaque les colonnes de chars, de préférence par actions "coup de poing" rapides et successives, en s'infiltrant en vol tactique intégral dans le terrain et en changeant en permanence les itinéraires et les positions de tir.

Une logistique de l'avant, très mobile, entièrement assurée par les hélicoptères de transport tactique (80 PUMA au total pour la division), afin de ne pas ralentir le rythme de la manoeuvre aéromobile, permet d'engager les moyens de renseignement, d'appui et d'attaque jusqu'à 100/120 kilomètres en avant des lignes amies.

Pour les mêmes raisons, les moyens de commandement sont toujours installés à bord d'hélicoptères spécialement équipés.

La nuit, les compagnies antichars du 1er régiment d'infanterie gardent le contact avec l'ennemi et préparent le réengagement des hélicoptères.

Au fil des ans, les procédés de combat sont améliorés, les matériels se perfectionnent et, en particulier, les moyens de vision nocturne élargissent le champ d'action des formations aéromobiles au combat de nuit et par visibilité réduite.

Cette forme de combat aéromobile, difficile, exigeant une conjugaison permanente des moyens, des renseignements précis et toujours réactualisés, une coordination minutieuse avec l'artillerie et l'armée de l'air, une grande maîtrise du pilotage et un sens du terrain "très fantassin" nous a permis de donner à nos équipages une aisance, un professionnalisme et une polyvalence qui les a aidés à s'adapter très vite à un nouveau concept du combat aéromobile qui nous est imposé par la nouvelle donne stratégique et la prolifération des "crises".

3. APRES LE GRAND TOURNANT DES ANNEES 1989-1991, UN NOUVEAU CONCEPT AEROMOBILE S'IMPOSE

1989, c'est la chute du mur de BERLIN, suivie par l'éclatement du Pacte de VARSOVIE et la Guerre du Golfe en 1991. Puis ,c'est le drame de l'ex-Yougoslavie et les crises humanitaires de SOMALIE et du RWANDA, pour ne citer que ces faits majeurs.

L'aviation légère de l'armée de terre française participe directement à tous ces conflits, elle doit s'adapter et, face à l'avenir qui se dessine, elle met au point, progressivement, un nouveau concept d'emploi de ses formations aéromobiles. Initialement adapté à l'hypothèse d'un conflit majeur en Europe, moins probable aujourd'hui, notre concept d'emploi, qui préconisait un engagement tous moyens réunis, s'oriente maintenant vers des engagements plus limités, en contact direct avec les unités au sol, pour le rétablissement ou le maintien de la paix, pour l'assistance et le soutien humanitaire.

De la priorité à la lutte antichar, nous passons à la priorité à l'appui protection. Au lieu de 2/3 d'appareils dédiés au combat antichar, nous aurons très bientôt 2/3 d'appareils dédiés à l'appui-protection.

Paradoxalement, nous retrouvons "un peu" les missions, le concept de notre aviation légère des années 50, mais avec d'autres appareils, tellement plus performants que les méthodes sont différentes et les possibilités décuplées.

La nécessité d'agir au contact direct des populations, au milieu desquelles, hélas, viennent s'imbriquer l'ennemi ou des combattants de tous les camps, cette nécessité implique l'engagement d'unités modulables, de volume limité, travaillant en étroite coopération avec les amis au sol et rassemblant toutes les fonctions du combat aéromobile au sein même de chaque formation, constituée à la demande, et dont la taille ne doit pas être une entrave à la projection à longue distance, qu'elle se fasse par transport aérien, par bateau ou en vol autonome.

Ainsi, à partir d'un régiment d'hélicoptères, on construit un ou plusieurs détachements aéromobiles mixtes comprenant, suivant le cas, autour des appareils d'appui-protection ou des appareils de transport tactique,
- des hélicoptères de reconnaissance,
- des hélicoptères d'attaque,
- des hélicoptères de commandement et de logistique.

Bien sûr, cette mixité, ce mélange des genres, impose à nos équipages un effort permanent d'adaptation aux changements de structures. Par exemple, un commandant d'escadrille de transport tactique doit savoir engerber dans son unité des appareils de reconnaissance et d'attaque en intégrant dans sa manoeuvre les possibilités et les contraintes des appareils de renfort.

Le logisticien doit prévoir toutes les composantes de l'unité mixte ainsi constituée. Et les autres commandants d'escadrille doivent savoir travailler avec une unité amputée provisoirement d'une partie de ses moyens.

Cette nouvelle forme d'aéromobilité, par la réponse rapide qu'elle peut apporter à une menace, ou au risque de menace, par l'effet spectaculaire et significatif de l'aéronef, par sa capacité à la réversibilité, c'est à dire son aptitude à changer de zone ou à quitter le terrain si la diplomatie l'exige, par sa polyvalence enfin, qui lui permet d'enchaîner missions militaires et missions humanitaires ou d'assistance, cette nouvelle aéromobilité offre au politique et au militaire un outil idéal de projection et de gestion des crises.

Notre concept a toujours visé à exploiter l'hélicoptère dans toutes ses possibilités. Certes, nous gardons en vue l'aptitude au combat antichar de cet engin, nous entretenons nos savoir-faire dans ce domaine, mais nous nous orientons maintenant beaucoup plus vers des missions
- de renseignement (renseignement sur le terrain, les voies de communication, leur encombrement, les mouvements de population, l'écoulement des courants logistiques ...)
- d'accompagnement de convois, qu'il faut protéger, renseigner, ravitailler,
- de neutralisation de tous types d'objectifs, et non plus seulement des chars, en priorité pour "retenir" la force avant qu'elle ne se déchaîne et, s'il s'agit de missions humanitaires, pour garantir la libre distribution des secours,
- de transport de troupes, de blessés, de réfugiés, de vivres, etc ...,
- enfin, missions à caractère "spécial" telles que la récupération par coups de main d'otages ou d'agents et la SAR (Search And Rescue) au profit de nos équipages.

Bref, des missions plus ponctuelles, plus différenciées, qui s'effectuent, non plus par grandes masses d'hélicoptères, mais par petits groupes d'appareils dont les capacités s'ajoutent et se complètent pour obtenir la polyvalence. Missions qui, par le contexte, s'inscrivent dans la durée, dans la permanence sur le terrain, à l'inverse des opérations "coups de poing".

Pourtant, il reste une constante, fondamentale, à laquelle nous tenons beaucoup. Pour nous, l'hélicoptère reste un engin de combat qui s'emploie "au sol", comme le reste de l'armée de terre, parce qu'en utilisant tous les avantages du terrain, il est à l'abri des vues, des tirs et des radars, il joue la discrétion et garantit la surprise.

De même, nous conservons notre concept logistique de l'avant, fondé sur l'emploi d'hélicoptères de transport tactique, pour livrer du carburant par bacs souples, réparer nos appareils sur le terrain, le jour, la nuit, et évacuer les blessés directement sur les hôpitaux de campagne à l'aide de nos appareils "médicalisés".

Par ailleurs, nous conduisons des études à la fois tactiques et techniques pour améliorer toujours notre aptitude à la permanence sur le terrain, quelles que soient les conditions de visibilité, ainsi que la protection des appareils : survivabilité, furtivité, contre-mesures, pour ne citer que ces axes d'efforts.

XX
X

Aujourd'hui, l'aviation légère de l'armée de terre française, l'ALAT, utilise des GAZELLE, des PUMA et des COUGAR, flotte qui se modernise progressivement avec l'arrivée des caméras thermiques et des missiles air-air, mais, bien sûr, nous attendons beaucoup du TIGRE et du NH 90 qui, troisième grand tournant dans l'histoire de notre aéromobilité, nous imposeront, une nouvelle fois, de réviser de fond en comble notre concept pour l'adapter à cette nouvelle donne technologique ... en espérant que la paix ne soit plus un souhait mais une réalité.

Toute armée moderne a sa propre forme de concept aéromobile, adapté à ses appareils, à leurs performances, à la politique de défense du pays et à sa culture militaire. Ce qui compte, ce n'est pas telle ou telle forme d'aéromobilité. L'important c'est de tirer le meilleur parti de cet engin de combat remarquable qui, au-delà de ses puissantes capacités de destruction, s'impose aujourd'hui plus qu'autrefois comme un instrument de secours, d'assistance humanitaire et de contrôle des crises.

Enfin, si un concept se construit pour faire face à une menace, autour d'un système d'arme mis au point par des ingénieurs et des opérationnels, il ne faut pas oublier celui qui le mettra en oeuvre dans toutes les conditions météo, face au danger, sur un terrain qu'il ne connait pas. Il ne faut pas oublier que la valeur d'un concept aéromobile sera d'abord celle des hommes qui auront pour mission d'en tirer toutes les possibilités.

CERTIFICATION OF MODEL 230 HELICOPTER FOR CATEGORY 'A' ELEVATED HELIPAD OPERATIONS

Joachim Goldenberg, L. Meslin

Bell Helicopter Textron Canada, Inc
12800 rue de l'Avenir
Mirabel, Quebec J7J 1R4
Canada

M. Blondino, D. Williams

Bell Helicopter Textron, Inc
P.O. Box 482
Fort Worth, Texas 76101-0482
USA

ABSTRACT

A flight test program leading to the certification of Model 230 helicopter for Category A elevated heliport operations was conducted. This paper discusses the development of the TakeOff and Landing profiles for Transport Helicopters operating from elevated helipads. The development included simulation, ground level helipad tests and elevated helipad testing. Also presented are the demonstrated helicopter performances for this type of operations. The developed procedures will enable operators to plan for Category A operations from elevated heliports.

ABBREVIATIONS

ADAS = Airborne Data Acquisition System
AGL = Above Ground Level
CDP = Critical decision Point
DP = Decision Point
FAA = Federal Aviation Administration
FP = Flying Pilot
ICU = Instrumentation Control Unit
KCAS = Calibrated Airspeed
KIAS = Indicated Airspeed
LCD = Liquid Crystal Display
LCP = Landing Decision Point
NFP = Non Flying Pilot
N_r = Main Rotor Speed
OEI = One Engine Inoperative
PMU = Programable Master Unit
PCM = Pulse Code Modulation
RPM = Rotation Per Minute
TCA = Transport Canada Aviation
TDP = Takeoff Decision Point
V_r = Rotation Speed
V_y = Climb Speed
V_{toss} = Takeoff Safety Speed
WAT = Weight-Altitude -Temperature

INTRODUCTION

Transport category helicopters certificated to Category A, in the event of a single engine failure during the takeoff or the landing profile, have the ability to either safely land on the helipad or continue flying.

The flight profiles provide added safety of operation, but allowable weights may be limited in order to achieve the required performance of the takeoff and landing.

The objectives of the Model 230 development and qualification flight test program undertaken were to develop Category 'A' Takeoff and Landing procedures that will provide safe and repeatable operations from elevated heliports while maximizing allowable gross weights and complying with FAR regulations.

The methodology used to develop the flight profiles is discussed. Detailed explanation of the flight profiles is provided.

Paper presented at the FVP Symposium on "Advances in Rotorcraft Technology", held in Ottawa, Canada, 27-30 May 1996, and published in CP-592.

Methodology

The development of the flight profiles for the Model 230 Category 'A' elevated helipad operations was conducted in four phases:

I. Procedure development using the BHTI Flight Simulator at BHTI, Fort Worth, Texas (US).

II. Procedure development using a painted ground level helipad at the BHTI Flight Research Centre, Arlington,Texas (US).

III. Procedure development and performance verification on an off-shore oil rig elevated helipad at Cameron, Louisiana (US).

IV. Qualification flight tests by TCA and FAA test pilots on an off-shore elevated helipad.

Both the TCA and FAA test pilots participated in each phase of the test program to evaluate the takeoff and landing procedures being developed and tested. Each phase of the test program evaluated procedures and performances for the following Category A Takeoff and Landing conditions: Rejected Takeoff, Completed Takeoff, Completed Landing and Balked Landing

The data obtained during the test program was used to establish aircraft operating limitations, aircraft performance, and clear space requirements for the above takeoff and landing conditions.

TEST HARDWARE

TEST HELICOPTER

The Model 230 Helicopter prototype (Figure 1) is powered by two Allison Gas Turbine 250-C30G/2 turboshaft engines. The Model 230 Helicopter is certificated to transport canada and U.S. Federal Aviation Administration Category A and B operation with a maximum Gross Weight of 8400 lb. The test aircraft was in skid landing gear configuration considered more critical then wheels. A float kit was incorporated for over water operation during the certification program. Power management of Single Engine operations featured a specially modified, electrically powered linear actuator in the #2 engine control system. This enabled the pilot to preset remaining engine power available on the #2 engine to predetermined test conditions. The aircraft was rigged to allow main rotor operation at 103% during Takeoff and Landings.

INSTRUMENTATION

The test aircraft utilized a Pulse Code Modulation (PCM) Airborne Data Acquisition System(ADAS) to sample and record the test parameters and a Canadian Marconi CMA-2012 Doppler Velocity Sensor to record aircraft position.

The BHTC Airborne Data Acquisition System was built around a Programmable Master Unit (PMU), Instrumentation Control Unit (ICU), and Analysis Package. PCM output from the PMU was received and distributed to a magnetic digital tape recorder by the ICU. The DATaRec-D2 digital tape deck recorded all instrumentation parameters on magnetic tape during each test.

The ADAS was maintained and monitored with the Analysis Package. The Analysis Package provided data in either raw form or Engineering Units for system evaluation. Furthermore, the Analysis Package was coupled to a Liquid Crystal Display (LCD) located in the cockpit to provide the flight crew real time instrumentation data in Engineering Units for evaluation during test flights.

A Canadian Marconi CMA-2012 Doppler Velocity Sensor was used to identify aircraft position along the trajectory during performed manoeuvres. The Marconi Doppler consisted of a Doppler Velocity Sensor, a "ruggedised" PC computer, control box, and analysis software. The Marconi Doppler Velocity Sensor measured and recorded the aircraft velocity in the pitch, roll, and yaw axis at an eight Hertz frequency using four microwave beams. Aircraft pitch and roll attitude was provided to the Marconi Doppler instrumentation from the BHTC ADAS for aircraft attitude correction. All Marconi Doppler information was stored on the "ruggedised" PC for post processing. Synchronization between the BHTC ADAS and Marconi Doppler Velocity Sensor was achieved when the flight crew activated the ADAS "Prime Data" switch.

Figure 1: Model 230 Helicopter

The Marconi supplied software integrated the velocity information to provide distance and course in all three flight axis. From the distance and course information, the aircraft flight trajectory was then reconstructed.

FLIGHT SIMULATOR

The BHTI Dome Flight Simulator included an equivalent M230 cockpit and a sophisticated mathematical model of the aircraft to provide realistic cues for piloted simulations. The visual image was projected as a continous view 240 degrees wide and 60 degrees high on a 30 ft dome. The equivalent Model 230 cockpit included an instrument panel providing the same visibility as the model 230 cockpit. Control forces matching those of the model 230 were provided. Cockpit instrumentation provided to the pilot included airspeed, rate of climb, altitude, radar altitude, aircraft attitude, heading, rotor and engine speed and rotor and engine torque.

HELIPADS

A ground level helipad was used at the BHTI Flight Test Research Center at Arlington , Texas for the initial evaluation of the techniques and the development of the flight profiles. Simulations were conducted on a 65 ft diameter elevated helipad painted on the ramp.

The elevated helipad (Figure 2) an oil rig landing platform was owned by Glomar Marine, Inc and was located 5 miles off the coast of Cameron, Louisiana. The elevated helipad was 65 ft in diameter and suspended 105 ft above the surface.

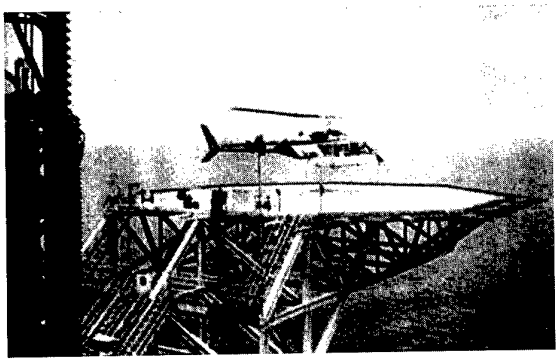

Figure 2: Elevated Helipad Test Site

TECHNIQUES DEVELOPMENT

Phase I and II of the test program emphasized the development of a repeatable and safe Category 'A' elevated heliport takeoff and landing technique that offered operational usability and maximized allowable gross weights.. Once a technique had been selected and adequate procedure developed, the test program proceeded with Phase III and Phase IV for procedures verification, performance evaluation and certification testing.

Various techniques for Category A takeoff and landings for elevated helipads have been investigated

The techniques evaluated included the Vertical Takeoff, the Straight-in Landing and the Static Sideways maneuver.

VERTICAL TAKEOFF

The Vertical Takeoff from an elevated helipad begins with a hover and a ascent to a Takeoff Decision Point (TDP) (Figure 3). The TDP is the point where in the event of a single engine failure, combinations of airspeed , height and OEI helicopter performance is sufficient to either enable a safe return to the takeoff helipad or to accelerate to a Takeoff Safety Speed and a safe flyaway.. Prior to reaching the TDP in the event of a single engine failure the pilot is capable to safely return to the helipad while maintaining continous sight of the helipad.

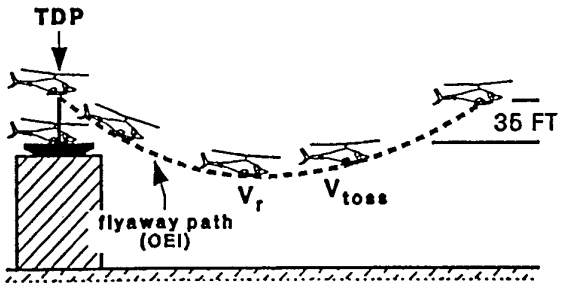

Figure 3: Vertical Takeoff Profile

If the failure occurs immediate beyond the TDP, the pilot while managing engine power will accelerate to V_{TOSS} and initiate a climb and continous flyaway.. Regulations require

the TDP to be located to enable the helicopter to achieve V_{TOSS} and a climb of at least 100 ft/min by no more then 35 ft above the takeoff surface. During this maneuver regulations allow loss of altitude and the aircraft may descend below the surface of the helipad.

STRAIGHT-IN LANDING

A Straight-in Landing (Figure 4) will begin with an approach to a Landing Decision Point, Figure 4. The LDP is the point where in the event of a single engine failure, combination of airspeed, height and OEI helicopter performance is sufficient to either abort the landing and continue flying or to perform a safe landing.

Prior to reaching the LDP, if one engine fails, the pilot, while managing remaining power will accelerate to V_{toss} and initiate a climb and continue the flyaway. If an engine fails after LDP the pilot will perform a safe landing while maintaining continuous sight of the helipad.

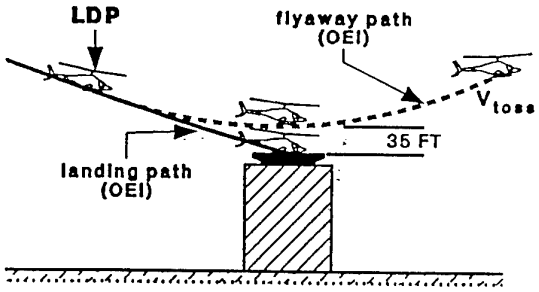

Figure 4: Straight -in Landing Path

STATIC SIDEWAYS MANEUVER

The Category 'A' elevated helipad Takeoff and Landing procedures developed feature a sideways ascent to and a sideways descent from the same space located Decision Point (DP). The DP is a point located 35 feet above the elevated helipad and laterally of its edge so that the Flying Pilot (FP) is in continuous view of the elevated helipad out of the crew door window. The Takeoffs and the Landings are executable from either the left or right crew seat depending on Takeoff and Landing directions (Figure 5).

For the Completed Takeoff, the flight crew is Go oriented if and engine failure occurs at or after the Decision Point (DP).

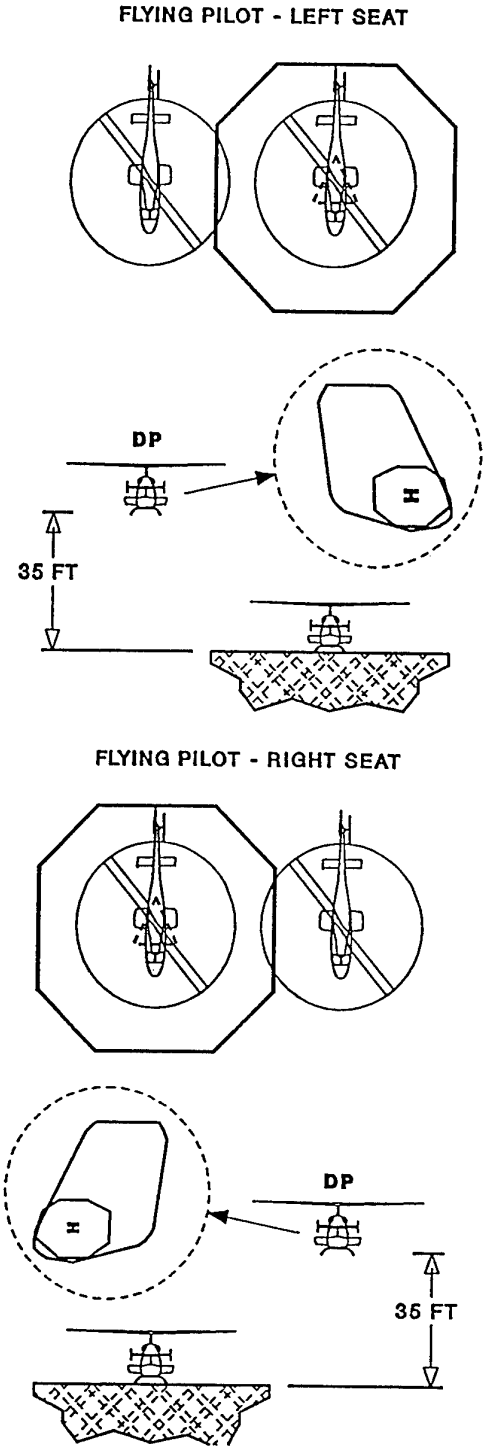

Figure 5: Static Sideways Decision Point

For the Takeoff the Flying Pilot (FP) will smoothly apply collective to obtain a slow lateral climb to a point 35 feet above and alongside the helipad with the proper sight picture of the helipad through the crew door window. At the DP the FP will apply collective, rotate to a 10 degree nose down pitch attitude and accelerate to V_{toss}, 35 knots. The Non -Flying-Pilot (NFP) will call airspeed and positive rate-of-climb. The NFP will monitor engine parameters.

If an engine failure occurs at or after DP, the FP will maintain safe clearances from the helipad and accelerate the aircraft to 35 knots ,V_r, while descending below the level of the helipad. At 35 knots indicated airspeed, the FP will rotate, continue to accelerate to V_{toss} and begin climbing. The 2.5 minute OEI power will be maintained while accelerating to V_y , 60 knots, and maintaining N_r at no less than 100%. At V_y the engine power will be decreased to 30 minute OEI power,(Figure 6).

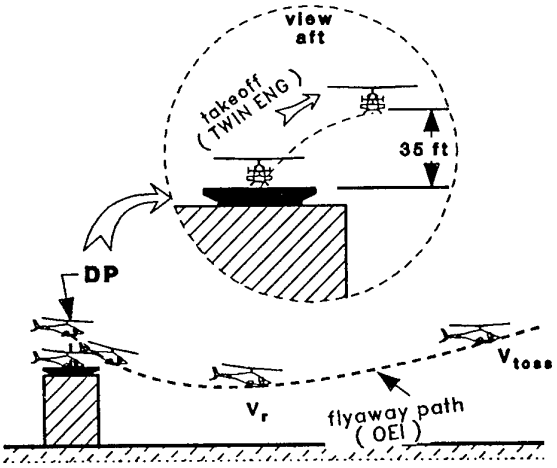

Figure 6: Completed TakeOff

If an engine failure occurs prior to or at DP, the FP will return to the landing surface using the remaining engine power available to land. The NFP will monitor engine parameters , N_r and alert the FP if any limitations are reached (Figure 7).

For Landing the FP will conduct a normal approach to a hover point 35 feet above and alongside the elevated helipad with the proper sight picture of the helipad through the crew door window.

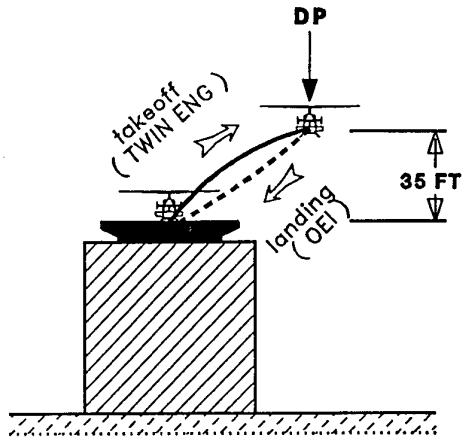

Figure 7: Rejected TakeOff Profile

If an engine failure occurs prior to or at DP, the FP will maintain safe clearances from the helipad, accelerate the aircraft to 35 knots, rotate, accelerate to V_{toss}, and begin climbing. OEI power will be maintained for 2.5 minutes while accelerating to V_y, 60 knots, and maintaining N_r at no less than 100%. At V_y the engine power will be decreased to 30 minute OEI power (Figure 8).

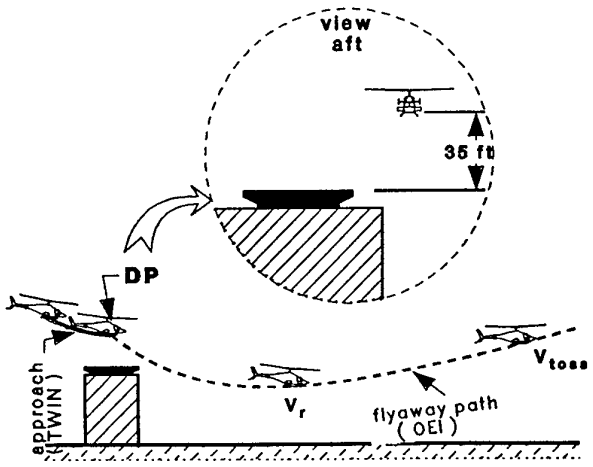

Figure 8: Balked Landing Profile

If an engine failure occurs at or after the DP, the FP will land on the helipad using the remaining engine power available. The NFP will monitor engine parameters and N_r and alert the FP if any limitations are reached (Figure 9).

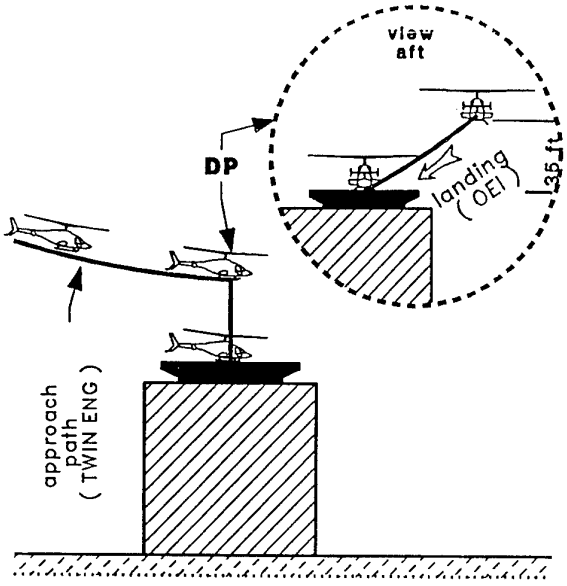

Figure 9: Completed Landing Profile

SIMULATOR RESULTS

Technique evaluation was conducted in the simulator using initially the Vertical Takeoff procedure and Straight-in Landing. Pilots from BHTI, BHTC, TCA and FAA participated in the simulation.

The Vertical Takeoff simulated consisted of a rapid vertical climb from a low hover point to a Takeoff Decision Point 25 feet vertically above the helipad, followed by a nose down pitch of 15 deg and acceleration to V_{toss} while allowing the helicopter to descent below the helipad takeoff surface.

The Simulated Straight-in Landing consisted of a continuous descent and deceleration to a Landing Decision Point located 50 feet above the helipad within a 5 deg descent slope at 30 Kias.

Simulation results indicated that while the Vertical Takeoff was repetitively performed variation in the ability to land was observed between the pilots. The main reason considered was the variation in the visual cues provided to the pilot.

The Straight-in Landing was thus considered as the most critical manoeuvre for determining the maximum weight to be evaluated during Phase II on a ground helipad.

GROUND HELIPAD RESULTS

The Straight-in Landing being considered as the critical landing maneuver was initially evaluated on the ground helipad.

A very precise approach and coordinated technique was required in order not to slide out of the 65 ft diameter helipad. The helicopter also had a tendency to accelerate forward as being levelled for touchdown following the flare. This procedure proved not to be simple and repeatable.

To improve the repeatability the sideways lateral maneuver was evaluated. The maneuver was relatively simple to execute and landings resulted in little or no sliding on the helipad.

This technique provided the necessary combination of repeatability, simple and safe operation and adequate performance.

Repeatability was achieved by eliminating the timing aspect of the vertical takeoff and straight in landing. Safety of operation was enhanced by enabling the crew to maintain continuous sight of the helipad during takeoff and landing. Simplicity of operation has been achieved by similarity of takeoff and landing techniques and designation of a single Decision Point for all manoeuvres.

This technique was selected for demonstration in Phase III and IV , on a 65 feet by 65 feet oil rig elevated helipad located in the Gulf of Mexico, Cameron, La, leading to qualification tests conducted by TCA and FAA flight test representatives.

PERFORMANCE RESULTS

Once the lateral takeoff and lateral landing technique selected, performance and qualification testing was conducted on an off shore oil rig elevated helipad to evaluate the validity of the operational procedures and to establish aircraft performances and operating limitations. The required performance testing was significantly reduced due to similarity in the procedure between the Takeoff and the Landing.

Performance data was determined at aircraft gross weights from the minimum practicable to maximum achievable at forward, aft and lateral CG extremes. Test day densities ranged from 1400 feet to 2000 feet.

Performance data was determined with manoeuvres conducted from left and right crew seats.

Following simulated engine failure, pilot recognition time was utilized prior to initiate recovery with primary controls. The Single Engine performances were evaluated with left engine at idle and right engine at a preset power available. The power available was based on a 2000 feet H_D and 35 deg Celsius day with standard temperature lapse and 100% turbine RPM. The right engine power was preset to the power available at the pressure altitude corresponding to the test day density altitude and standard temperature lapse rate.

WAT CURVE DEVELOPMENT

OEI climb performance at 2.5 min power for a Takeoff Safety Speed of 45 KTS have been computed to establish gross weights restrictions for all ambient conditions up to 4000 ft density altitude to comply with FAR 29.67 minimum OEI climb performance required for Category 'A'. Flight Tests indicated that the limiting conditions predicted for 100 ft/min OEI climb at 2.5 min power were less restrictive then the limitation in gross weight imposed by the Rejected Takeoff and Completed Landing manoeuvres. The WAT curve for zero wind was established based on maximum achievable gross weights resulting from these manoeuvres, Figure 10.

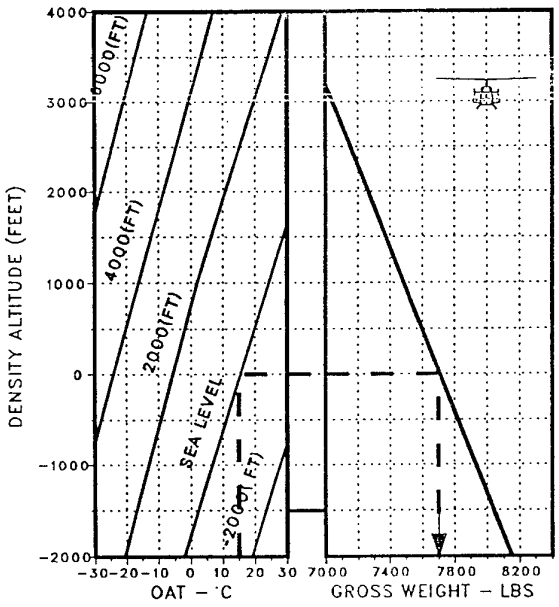

Figure 10: WAT Chart

REJECTED TAKEOFF / COMPLETED LANDING PERFORMANCE

Data obtained during Rejected Takeoff and Completed Landings performance testing allowed the establishment of the WAT curve and wind azimuth limitations. The Rejected Takeoff distance and the Landing distance are not applicable since the procedure developed provides for a lateral ascent to hover at Decision Point or a lateral descent from a hover at the same Decision Point. Simulated engine failures were demonstrated at five foot vertical height increments along the lateral climb/descent path to/from the 35 feet Decision Point. Simulated engine failures were executed from hover and during climb/descent to/from Decision Point with rotor RPM adjusted to 103% to maximize rotor performance at the end of landing profile. Flying parameters were recorded with the ADAS instrumentation system while trajectories were recorded through the Doppler system.

A typical trajectory for the Rejected Takeoff / Completed Landing trajectory manoeuvre with simulated engine occurring at Decision Point in shown in Figure 11.

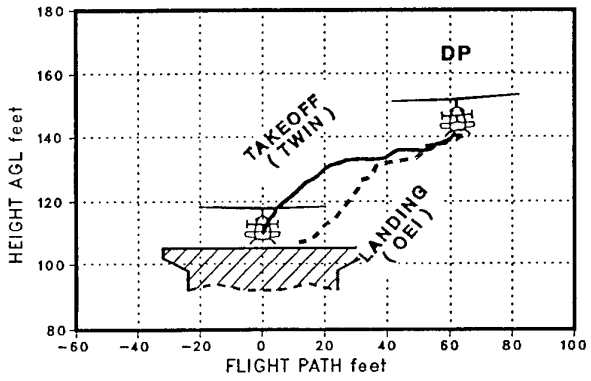

Figure 11: Rejected TakeOff / Completed Landing Trajectory

A typical time history for the Rejected Takeoff / Completed Landing trajectory manoeuvre with simulated engine occurring at Decision Point in shown in Figure 12.

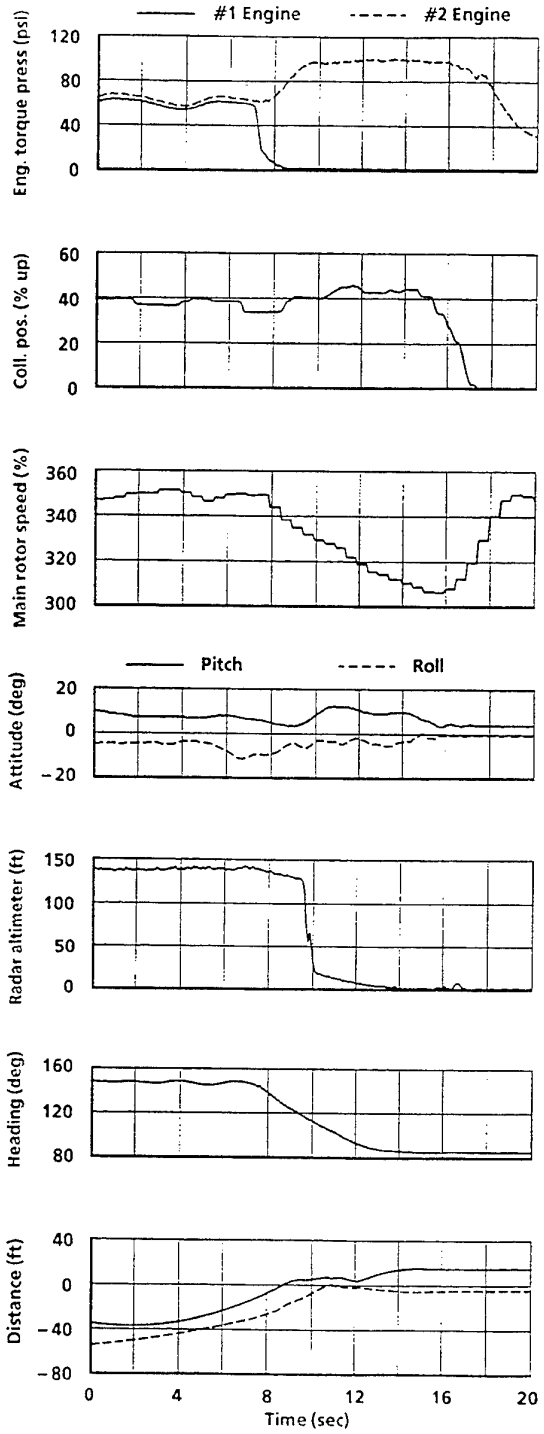

Figure 12: Rejected TakeOff / Completed Landing Time Histories

Since the Rejected Takeoff / Completed Landing is a lateral descent to the helipad, wind azimuth restriction were imposed to assure aircraft performance. For landings to the right, the allowable wind azimuth is from 345 to 90 degree relative to the nose of the aircraft. For Landing to the left, the allowable wind azimuth is from 270 to 15 degree relative to the nose of the aircraft, (Figure 13).

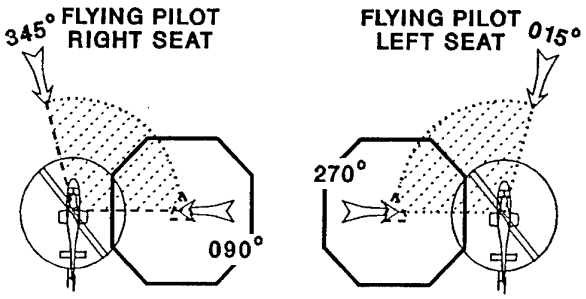

Figure 13: Wind Azimuth

COMPLETED TAKEOFF / BALKED LANDINGS PERFORMANCE

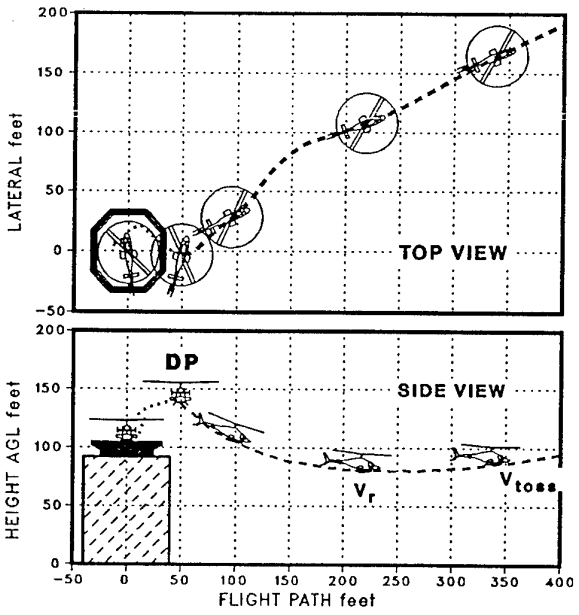

Figure 14: Completed TakeOff / Balked Landing Trajectory

OEI data collected during the Completed Takeoff and Balked Landings performance were used to establish the horizontal takeoff distance and altitude loss. The Completed Takeoff / Balked Landing manoeuvres were executed with simulated engine failure occurring at Decision Point. A typical Completed Takeoff / Balked Landing trajectory and time history is shown in Figure 14.and Figure 15.

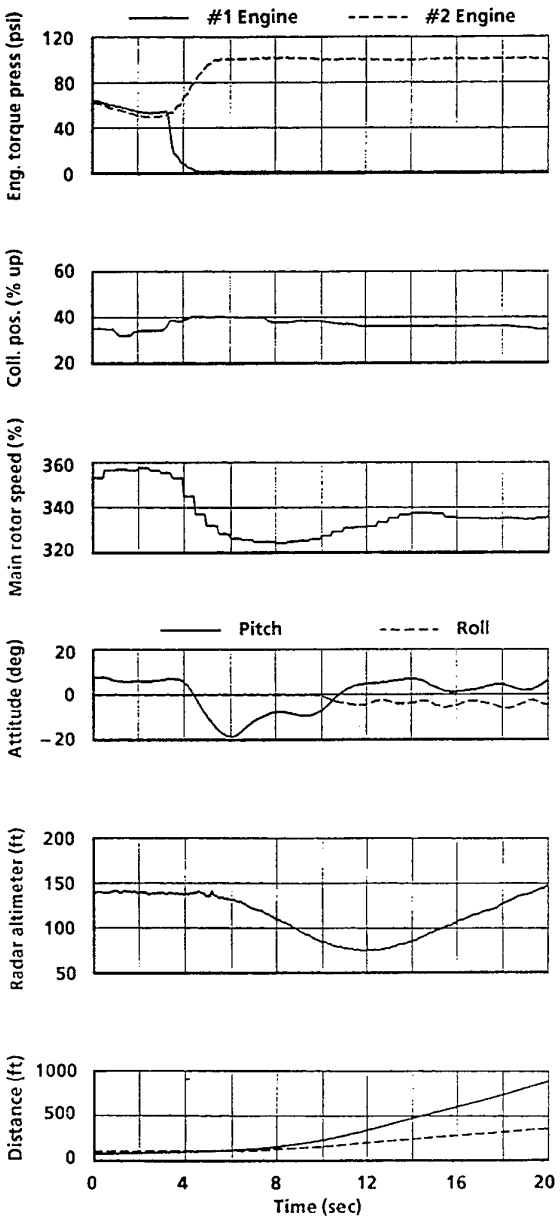

Figure 15: Completed TakeOff / Balked Landing Time Histories

The Completed Takeoff / Balked Landing distance is defined as the total flight path distance from the DP to the point at which the aircraft has attained V_{toss} and a positive rate of climb. V_{toss} was established at 45 KTS to minimize the Completed Takeoff and Balked Landing distance while maintaining FAR 29.67 climb performance requirements at WAT limiting conditions. Tests indicated that the distance to reach V_{toss} established at 45 Kts and a positive rate of climb varied from 350 ft to 550 ft. The distance to reach V_{toss} and positive rate of climb at 35 feet above landing surface varied from 500 ft to 1000 ft.

The distance depends on the pilot way of flying the helicopter, electing altitude over airspeed or airspeed over altitude.

During Completed Takeoff / Balked Landing while in OEI conditions, the aircraft descends below the level of the landing surface while accelerating to V_r and V_{toss}. Since the helicopter descends below the landing surface a minimum heliport height had to be established for all WAT conditions. To minimize aircraft height loss and heliport AGL height, V_r was established at 35 KTS. Test indicated that the height loss is a function of V_r and pilot technique to achieve this speed. Based on test results , height loss following a simulated engine failure at DP was 80 feet for all WAT conditions. For a Decision Point at 35 feet above helipad surface and a hight loss of 80 feet, the minimum heliport AGL elevation was set at 60 feet allowing 15 feet clearance from ground / water surface.(Figure 16)

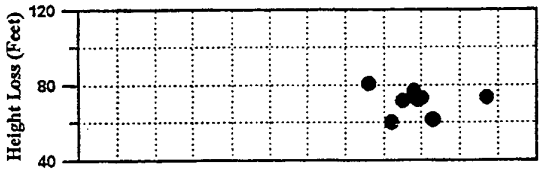

Figure 16: Hight loss during OEI flyaway

Additional tests were conducted to evaluate wind benefit while operating from an elevated helipad. A reduction in hover from a presence of headwind allows an increase in weight while maintaining same takeoff and landing capability. A Headwind Benefit chart with a 50% fact wind as presented in the Flight manual is shown in Figuret 16.

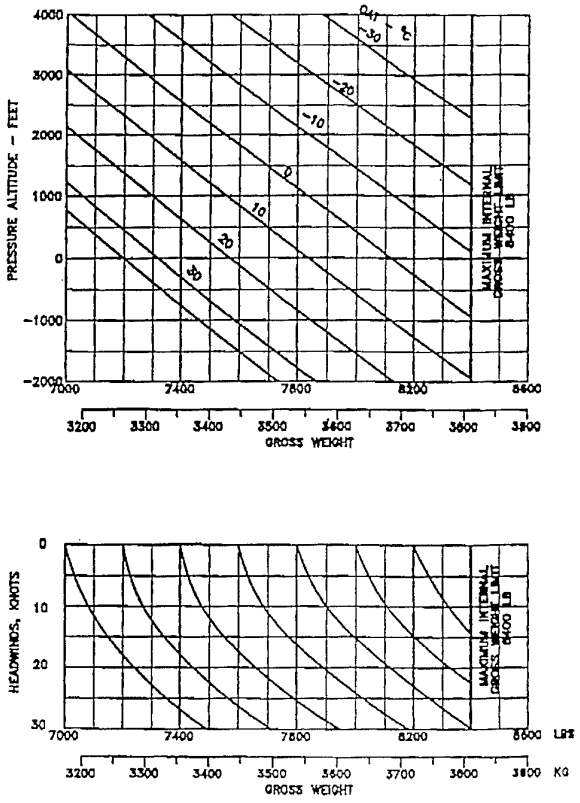

Figure 17: Headwind benefit

CONCLUSIONS

The Category 'A' elevated helipad Takeoff and Landing procedures developed for the Model 230, using a lateral Takeoff and Landing technique offers the desired combination of repeatability, operational usability and performance.

Single Decision Point, similarity in takeoff and landing techniques, continuous sight of the helipad , operations from left and right seat , 65 ft X 65 ft minimum helipad size , minimum clear space requirements and operational gross weight limitation, all these factors considered should enable operators to plan for Category 'A' operation from elevated heliports using a safe and reliable Takeoff and Landing procedure.

ACKNOWLEDGEMENTS

The authors wish to thank all those whom invaluable assistance contributed to the success of the program: Mr Leo Meslin and Mr. Dwaine Williams for their vision , persistence and daring skills. Mr. Dave Simmonds and his staff from PHI station in Cameron, La, for providing the link with the off shore test site and the necessary ground support, Mr Keith Mesker and the oil rig crews from Glomar Marine Inc for their hospitality and Mr. Chris Little and his rescue team from Oceaneering Inc for their reassuring presence. And finally to all Bell Helicopter Textron crew that kept the flight plans marching, instrumentation working, spent hours reducing data, documented the flying events and all of the mechanics and others who kept the helicopter performing so well.

REFERENCES

1. Federal Aviation Administration FAR29-Airworthiness Standards Transport Category Rotorcraft, CFR 14, Aeronautics and Space, January 1992.

2. Bell Model 230 - Rotorcraft Flight Manual, BHT-230-FM-1 Revision 0, Bell Helicopter Textron, July 1992

3. Bell Model 212 Rotorcraft Flight Manual BHT-212-FMS-7, Bell Helicopter Textron, Inc, August 1972.

4. T.L.Wood, M.Blondino, D.Williams "M230 Helcopter Performance for Cat A Elevated Helipad Operations", Nineteenth European Rotorcraft Forum, Cernobbio, Italy, September 1993.

THE USE OF SIMULATION TO DEVELOP AN IMPROVED UNDERSTANDING OF HELICOPTER TAIL ROTOR FAILURES AND DEVELOP AIRCREW EMERGENCY ADVICE

Lt Cdr A. W. Martyn, RN
Flight Dynamics and Simulation Department
Defence Research Agency
Bedford, MK41 6AE
United Kingdom

Mr P Phipps
Principal Aerodynamicist
&
Mr E Mustard
Test Pilot
Westland Helicopters Ltd, Box 231
Yeovil, Somerset, BA20 2YB
United Kingdom

Abstract

This paper reviews the use of simulation in recent UK programmes to improve our understanding of helicopter tail rotor failures, and develop the handling advice for aircrew following a tail rotor (TR) malfunction. The paper discusses the original motivation for the work and in particular the research work that has been carried out by the Defence Research Agency (DRA) and Westland Helicopters Ltd (WHL) under UK Ministry of Defence (MOD) funded programmes. This research has included flight trials conducted on the DRA Aeromechanics Lynx Control and Agility Testbed (ALYCAT) to develop Lynx TR control failure handling advice, and simulation trials on the DRA Bedford Advanced Flight Simulator (AFS) to develop Lynx TR drive failure handling advice. The AFS was also used to investigate the influence of helicopter design parameters on a pilot's ability to recover from a TR failure. Also described are off-line simulation and model development activities. The paper concludes with a review of lessons learnt.

Introduction

Motivation & TRAC

A tail rotor failure is arguably the most critical helicopter malfunction. Our individual experience, shocking video footage or a glance down published accident statistics in aviation magazines have perhaps given us all some evidence of the problem and its regularity. It is also clear from feedback and regular articles in Service flight safety magazines, that in operational crew rooms tail rotor failures continue to be a source of great interest and concern. But what are the failure statistics?, what is the nature of these failures?, what can be done to reduce these statistics in new aircraft?, and in particular what is the best advice that can be offered to aircrew in manuals? and can the advice be validated?.

Prompted by many of these issues, in January 1993 the Royal Air Force (RAF) Handling Squadron at Boscombe Down (the group in the UK responsible for publishing aircrew manual and flip-card advice) convened a meeting to discuss the issue of TR failures. This group included representatives from the 3 Services, MOD(Procurement Executive), DRA and the Civil Aviation Authority (CAA). This group was later to be given the title Tail Rotor Action Committee (TRAC). The group's aim was to investigate the problems associated with helicopter tail rotor drive and control failures and to make appropriate recommendations. The group defined four primary tasks:

a. To conduct an analysis of current UK military and civil helicopter safety records to establish the nature and extent of the problem.

b. To review the current advice to aircrew and identify shortcomings.

c. To assess the reliability and failure characteristics of current designs.

d. To make recommendations with respect to handling advice to aircrew,

© British Crown copyright 1996/DRA - published with the permission of Her Majesty's Stationary Office.

Paper presented at the FVP Symposium on "Advances in Rotorcraft Technology", held in Ottawa, Canada, 27-30 May 1996, and published in CP-592.

simulation and training, airworthiness requirements and future research.

TRAC Observations

TRAC observations included:

a. Tail rotor drive failures continue to occur at an unacceptably high rate in the UK helicopter fleets. MOD statistics between 1976-1993 show a technical failure rate of 11.2 per million flying hours. The UK design requirement for rotorcraft transmission systems (Ref 1) requires the probability of a transmission/TR drive failure that would prevent a subsequent controlled landing to be very remote ($<1x10^6$).

b. Tail rotor drive failures are more prevalent than control failures (UK military ratio 3:2).

c. Without a normally functioning tail rotor, many helicopter designs lack directional stability and some appear to be uncontrollable.

d. Although the reasons for tail rotor failures are always investigated and if possible remedied, not enough is known about the behaviour of individual helicopter types following tail rotor failure.

e. There are significant differences in the handling characteristics, post tail rotor malfunction, between helicopter types.

f. Improved handling advice for current helicopters is believed to be achievable if the necessary work is put in hand. Better handling advice would enhance survivability in what is always likely to be a difficult malfunction regime.

This paper describes the research activity conducted to support TRAC. The paper describes 3 activities, these are:

a. Flight trials to develop Lynx control failure advice.

b. Activities to develop the DRA HELSIM (Ref 2) simulation model for tail rotor drive failure trials, and the use of non-piloted simulation tools to develop control strategies.

c. AFS trials to develop Lynx drive failure advice.

Advice Validation & Test Facilities

Validation

The requirement set by the Lynx Project Office was to develop and where possible validate the advice given to aircrew in the event of a tail rotor malfunction. During early meetings levels of advice validation were allocated and detailed by WHL (Ref 3). These were:

a. Full/demonstrated in flight (Level 1).

b. Demonstration with best calculation and piloted simulation (Level 2).

c. Engineering Judgements (Level 3).

The tail rotor malfunctions were also placed in two broad categories;

- control failures, where control of tail rotor blade pitch is lost but the rotor continues to rotate and produce aerodynamic forces.

- drive failures where all power is lost to the tail rotor.

After some discussion, it was concluded that the programme would seek to provide level 1 validation of control failure advice, and level 2 validation of drive failure advice. It should be noted that the feasibility of declutching a tail rotor gearbox , in order to conduct level 1 trials, was discussed but it was concluded that:

a. Advanced simulation would be an essential step before in-flight testing.

b. The development of such a system was outside the financial scope of the programme.

It must also be said that there was some scepticism over the safety and wisdom of any such flight trial.

Facilities/Assets

The programme would use two important facilities the DRA Bedford Advanced Flight Simulator and the ALYCAT Lynx aircraft.

Advanced Flight Simulator

The AFS constitutes the DRA flight simulation facility at the Bedford site. It is a general purpose research tool which retains a high degree of flexibility to enable tailoring for a wide range of fixed and rotary wing applications. The simulation can be configured to meet the needs of a particular task by selecting hardware and software options. Briefly the various elements of the facility are summarised below: a more detailed description can be found in Reference 4.

a. Motion System - Platform motion cues are generated by the 5 degree-of-freedom Large Motion System (LMS). The system provides motion in roll, pitch, yaw and heave axes and, depending on cockpit orientation when mounted on the motion platform, in either sway or surge axes. Figure 1 shows the general arrangement of the motion system together with its performance characteristics. This is one of the highest performance systems in the world and provides excellent stimulation of the pilot's motion sensory mechanisms (Reference 5).

b. Visual System - A photo-textured computer generated image system is employed to provide visual cuing through 5 monitors.

c. Cockpit and controls - The cockpit has a generic layout based on pilot's station of the Lynx helicopter. This gives conventional controls and instrument arrangements. Control feel is provided by an electrically activated digital system. Vibration cues in the vertical axis are applied through an 'active' seat at a simulated 4R frequency and modulated by airspeed and normal acceleration effects.

d. Model - The AFS can be adapted to take any model (fixed, rotary wing etc). The primary model used for this work would be a development of the HELSIM model (Ref 2). Developments are discussed later in this paper.

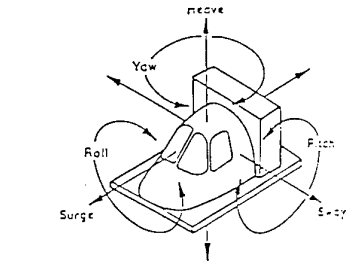

PERFORMANCE ENVELOPE

Axis	Displacement	Velocity	Acceleration
Pitch	± 0·5 Rad	± 0·5 Rad/s	± 2 Rad/s²
Roll	0·5 Rad	1·0 Rad/s	3 Rad/s²
Yaw	0·5 Rad	0·5 Rad/s	1·5 Rad/s²
Sway (Surge)	4m	2·5 m/s	5 m/s²(0·5g)
Heave	5m	3 m/s	10 m/s²(1·0g)

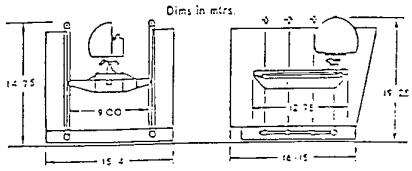

Fig 1 - AFS Motion System

ALYCAT Lynx

The aircraft used for the trials was the DRA Lynx Mk7 (ZD559) (also known by the acronym ALYCAT for Aeromechanics LYnx Control and Agility Testbed), Figure 2. The ALYCAT is extensively instrumented. Figure 3 shows a schematic of the instrumentation system with main rotor, tail rotor, airframe, body motion and control position data all routing through the Modular Data Acquisition System (MODAS), and/or to a recorder or via the telemetry link to the ground station. The MODAS system has a sampling rate of 256 K samples/sec, which enables the large amount of rotor data, in particular, to be handled during main rotor testing.

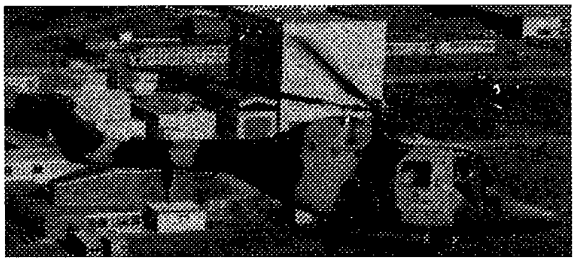

Fig 2 - ALYCAT Lynx over the AFS

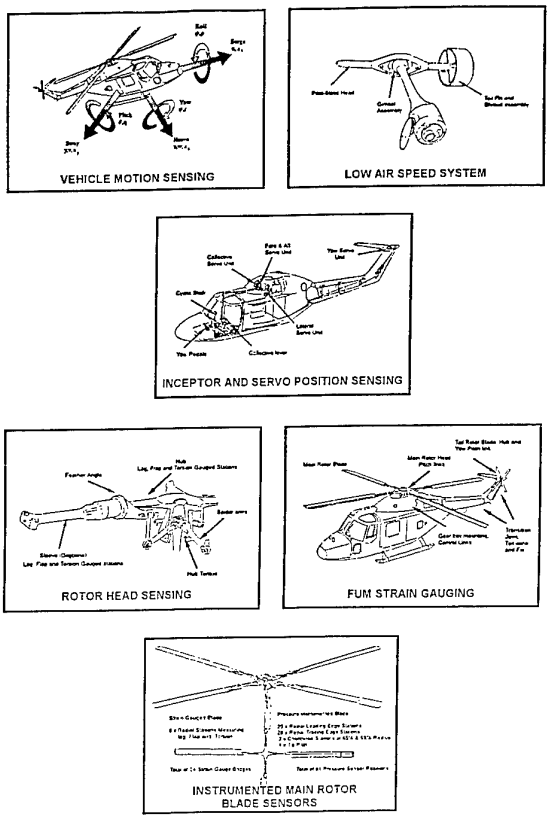

Fig 3- ALYCAT Instrumentation

For the tail rotor failure work the multi-channel telemetry transmitter and FUMS (Fatigue and Usage Monitoring System) were essential to provide real time safety monitoring via telemetry. In addition, test instrumentation gave in-cockpit feedback of precise tail rotor pitch angles and pedal positions. Finally, accurate low airspeed measurement was provided by the Helicopter Air Data System (HADS).

Flight Trials to Develop and Validate Lynx Control Failure Advice

Control Failure - Initial Work

The starting point prior to any flight trial planning was to review the current Lynx control failure advice and the tail rotor control system Failure Modes Effect Criticality Analysis (FMECA) for the Lynx. This work identified the failure modes and defined the flight conditions to be investigated in the flight trial. It also started the process to develop the Lynx advice beyond the often generic broad advice that was found to be prevalent in UK types during the TRAC study.

Control Failure - Aims & Objectives

The aims of the flight trial were to:

a. characterise and investigate handling and controllability of the Lynx post tail rotor control failure from various initial conditions.

b. develop and where possible validate advice to aircrew post a tail rotor control failure.

c. investigate handling and controllability of the Lynx with the tail rotor held at an angle of 3.5° (Note: 3.5° is associated with the Lynx Spring Bias Unit (SBU)).

The objectives of the work were to:

a. increase post-failure survivability.

b. reduce post-failure vehicle attrition/ damage.

c. ensure that the best advice was available to aircrew faced with tail rotor malfunctions.

Control Failure - Current Lynx Advice

A summary of key points from the current Lynx control failure advice are detailed below:

- Establish power and airspeed for level flight.

- Make an engine-off landing into wind or a running landing as appropriate.

Control Failure - Flight Trial Procedure, Special Fit & Conduct

Key points from the DRA Flight Trials Instruction (FTI) (Ref 6) for the work were:

a. The flight programme was divided into two parts, the first being to investigate and develop post control failure recovery techniques, and the second was to gather data

to validate the HELISIM simulation model in tail rotor failure recovery flight regimes (i.e. Autorotations).

b. The aircraft used for the flight trials was the DRA ALYCAT Lynx.

c. The, so-called, tail rotor failure phase of the programme was to be flown with the yaw/collective interlink removed.

The in-flight (Level 1) procedure developed to investigate control failures involved the removal of the yaw collective interlink, pedal positions being set and held by the Flight Test Engineer (these equated to the control "failure" positions), and the test pilot flying recoveries using only the available controls i.e. collective, cyclic and engine controls. The removal of the interlink precluded a change in tail rotor pitch with collective.

To enable this procedure, an amendment to the ALYCAT research flight clearance was issued by WHL. This amendment detailed the side slip limits for the flight trial, the requirements for on-line telemetry monitoring and referenced the WHL procedure to remove the yaw collective interlink and fit a pin within the control system.

Prior to the flight trial, work-up flights were conducted. The aim of these flights was to develop the in-flight procedures to establish the "failure" condition. This was achieved by the project pilot establishing the trimmed initial condition (0-120kn), the limiting side slip condition would then be set and the percentage pedal displacement noted from the in-cockpit flight test instrument. It should be noted that during this phase a fatigue limit exceedence on the tail cone lateral bending strain gauge was observed. This led to the 30 ° side slip limit (120 kn) being reduced to 20 °

Two types of control failure were investigated; control jams and control disconnects. The first three test points flown looked at control jams, the fourth looked at the control disconnect:

a. Recovery from tail rotor control failures in hover.

b. Recovery from tail rotor control failures in straight and level flight (80-120kn) with a resulting high tail rotor pitch setting.

c. Recovery from tail rotor control failures in straight and level flight (80-120kn) with a resulting low tail rotor pitch setting.

d. Handling and control with the tail rotor pitch set to 3.5° pitch (the Lynx SBU setting angle).

During the test flights the percentage pedal displacements recorded at each initial condition during work-up were then used by the Flight Test Engineer to establish the *failure* condition. The project test pilot then recovered the vehicle using the available controls i.e. No pedal.

Control Failure - Failure Classification

A failure resulting in a fixed pitch being applied to the tail rotor can be classified in one of three ways. A failure that predominantly produces left side slip (LSS) (ball out to the left) throughout the speed range, caused by the tail rotor pitch freezing at a setting commensurate with low power operations, Fig 4.

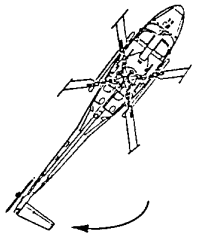

Fig 4 - Low Power Failure

A failure that predominantly produces right side slip (RSS) (ball out to the right) throughout the speed range, caused by the tail rotor pitch freezing at a setting commensurate with high power operations, Fig 5 .

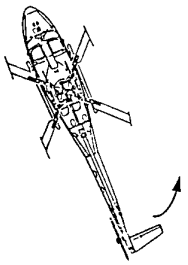

Fig 5 - High Power Failure

Finally, a failure that freezes tail rotor pitch at an intermediate setting allowing the aircraft to be flown throughout the vast majority of its speed range with little or any side slip. A failure that results in operation of the Spring Bias Unit (SBU) can be considered as the last case.

Diagnosing the type of failure present was found to be easier the greater the severity of the problem, and is achieved by reference to the slip ball in straight and level flight. Right ball means right side slip (high power), left ball means left side slip (low power). A failure that is hard to categorise due to only slight ball displacement or changes in direction of the side slip will generally be an intermediate failure.

Simple analysis predicted that an aircraft suffering a high power failure (RSS) would be more controllable at higher collective settings (e.g. low speed, high speed or in the climb). Similarly, a low power failure (LSS) would be more controllable at low collective settings (e.g. operation in the low power region of the power curve or during descent). This conjecture was borne out by flight test, although what was not envisaged beforehand was that the containment and recovery from tail rotor control failure would consist of two very definite and separate phases, the recovery and the approach to land.

a. Recovery Phase - The recovery phase included the recognition and diagnosis of a tail rotor control failure, followed by appropriate actions to bring the aircraft under sufficient control to allow positioning for an approach. The positioning included recovering, climbing and descending.

b. The Approach to Land - The approach to land was generally a short straight-in approach to either a hover or running landing.

Note: In order to protect the skids on the ALYCAT Lynx no running landings were completed during the flight trial, the vehicle was recovered 0-5 ft before touch-down.

By reference to Figures 6 and 7, the general characteristics of a LSS, RSS or intermediate (including Spring Bias Unit) failure can be appreciated.

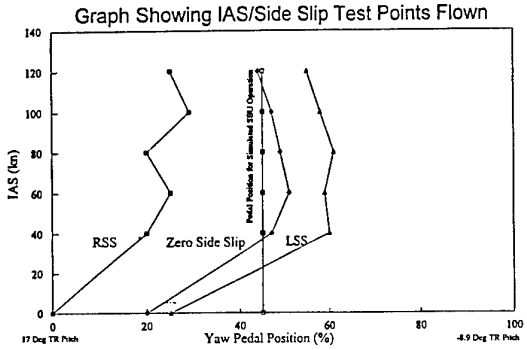

Fig 6 - IFS/Side Slip Test Point Flown

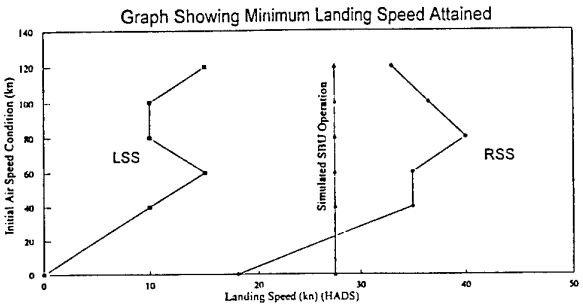

Fig 7 - Landing Speed Attained

These were:

a. LSS failure was characterised by being easy to control in the recovery phase the proximity to the zero side slip yaw control position line, Figure 6) with a high landing speed, Figure 7.

b. RSS failure case was very difficult to control at high speeds but would give a low landing speed.

c. Simulated SBU flying gave flight conditions close to trim for most of the flight envelope with a high landing speed.

The flight techniques developed during the flight trial varied depending upon whether the failure was

diagnosed as an intermediate (Spring Bias Unit) failure, a High Power (RSS) or Low Power (LSS) failure.

Control Failure - Simulated SBU Operation

The Lynx tail rotor control loads have been tuned to ensure a steep load pitch gradient, with a zero load condition occurring at approximately 3.5° . However, because the Lynx only has a simplex hydraulic system to the tail servo jack a No 1 hydraulics failure would result in excessive loads at the pilots feet. In order to enable safe manual reversion characteristics a spring bias unit (SBU) has been included in the control circuit close to the jack. On failure of the No 1 hydraulics the SBU becomes active and carries a large proportion of the tail rotor control load, enabling the pilot to operate the tail rotor pitch manually over its full pitch range. In the event of a control circuit disconnect between the jack and the tail rotor, the tail rotor pitch reverts to approximately 3.5° . If a control circuit disconnect occurs between the pedals and the SBU the tail rotor pitch will remain where the jack holds it, within the limits of the AFCS inputs. However, by switching out the No1 hydraulics the SBU becomes active and the combination of SBU forces and tail rotor control loads ensure that the tail rotor pitch once again migrates back to approximately 3.5° . The system used in the Lynx is understood to be a unique safety feature, not currently available on other aircraft.

During the trial the yaw pedals were held in a position to give a tail rotor pitch of 3.5 ° , and handling was assessed.

Recovery Phase - Recovery flying was easily achieved with the aircraft remaining close to trim in straight and level flight from 30 to 120 kn. Turns, climbing and descending were also carried out with little side slip.

Approach to Land - The minimum air speed achieved for a running landing was 28 kn (HADS). Both the approach to land and landing were easily controllable and safe provided the speed was not reduced below the minimum.

Failure in the Hover - A failure in the hover resulting in the operation of the SBU would result in a rapid yaw to the right. This case was not attempted, since it would have resulted in an exceedance of the spot turn limits detailed in the trial flight clearance. Experience gained during the flight trial would indicate that the onset and stabilised yaw rate would be very rapid and conjecture makes it hard to imagine that anything other than shutting down the engines and cushioning the landing would be possible.

Control Failure - Left Side Slip/Nose Right (Low Power Failure)

In general, this failure case was similar to that detailed above under simulated SBU operation, which is perhaps not surprising if the pedal positions are considered, Figure 6.

Recovery Phase - Recovery flying was easily achieved. Turns, climbing and descending were carried out successfully.

Approach to Land (Considerations) - The following sub-paragraphs detail considerations for the approach to landing.

a. As an LSS failure is associated with trimmed flight in the low power envelope, the high power requirements of a hover landing would clearly be problematic.

b. With fixed yaw pedals, as the collective is raised, the nose yaws from the left to the right.

c. As the undercarriage should be parallel to the flight path of the aircraft for a successful running landing, in still air there is therefore only one collective position for a selected airspeed, rotor RPM and AUW which gives the correct alignment of the undercarriage.

d. If on the final approach the nose is pointing to the left of the flight path, the application of more collective will align the nose and therefore the undercarriage with the flight path.

e. If the nose is to the right of the flight path, the lever must be lowered or the airspeed increased to align the nose.

f. The problem with the approach to landing phase of the LSS failure therefore is that reducing speed too much or easing descent rate with collective will result in the nose stabilising to the right of the aircraft flight path. In addition lowering the collective

will result in large rates of descent building up.

Approach to Land (Strategy) - The following sub-paragraphs detail the strategy for recovery:

a. The technique developed during the flight trial to overcome this problem was to fly towards the landing point at an altitude of approximately 100 ft, carrying out a level deceleration until the aircraft nose was coincident with the flight path.

b. At this speed the aircraft is at minimum landing speed (a conservative value since close to the ground, ground effect will reduce power requirements).

c. On approaching the landing point a positive check down on the collective initiated a rate of descent and yawed the nose left of aircraft flight path.

d. The landing was completed by pulling in power to align the nose once again with the flight path.

e. This technique was used to achieve comfortable running landings at air speeds between 18 and 40 kn, Figure 8.

Failure in the Hover - Failures in the hover were tested from the maximum yaw rate condition of 60 °/sec (nose right). It should be noted that it was found to be quite difficult to maintain orientation at this rotational rate. Although it was not tested it was considered doubtful that a conversion to forward flight could be achieved from this initial condition. During the flight trial it was found that by advancing the Speed Select Lever to increase the rotor RPM to maximum, rotational rate slowed dramatically, transition to forward flight could then be achieved and a running landing subsequently carried out.

The reason advancing the rotor RPM reduced the low power failure yaw rate, was because as main rotor RPM was increased, so was the tail rotor RPM, due to the gearing between the two. The increase tail rotor RPM, made the fixed pitch angle more effective, and the rate of rotation was slowed. In addition, as the main rotor RPM was increased, so the main rotor torque was reduced, and the anti-torque required from the tail rotor to balance main rotor torque was reduced. Thus advancing the main rotor RPM had a dual effect of reducing main rotor torque and increasing tail rotor speed to reduce the rate of rotation. The inverse was true in the high power case.

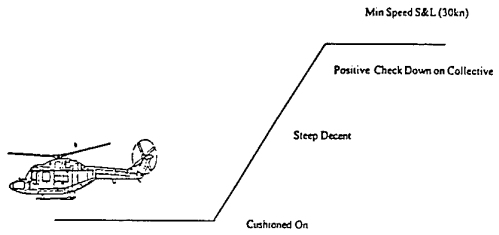

LOW POWER (LSS) RECOVERY STRATEGY

Fig 8 - Low Power (LSS) Recovery Strategy

Control Failure - Right Side Slip/Nose Left (High Power Failure)

In general the high power failure conditions, RSS, was the most difficult to control and, in turn, develop a strategy to enable recovery.

Recovery Phase - The main problem with an RSS failure was how to decelerate through the low power region of the power curve to the low speed, high power region. Initial attempts at relatively gentle decelerations resulted in very marginal levels of control as the aircraft attempted to 'swop ends'. The problem was solved by carrying out an aggressive left hand climbing cyclic turn, Figure 9, with the aim of establishing the aircraft at the top of the climb below 40 kn. At this point the aircraft could be held at low air speed to the final approach position. Care had to be taken, however, to avoid vortex ring.

Approach to Land - Due to the higher power condition of this failure, the landing was less problematic and generally resulted in lower landing speeds. The technique developed was to carry out a slow approach with the nose well to the left of the flight path, as the landing point was reached the nose could be aligned with the flight path by application of collective and a slow running landing carried out.

Failure in the Hover - By retarding the SSL to reduce rotor RPM to the minimum in- flight value, all rotation from a 60 °/sec (nose left) spot turn was arrested and a landing carried out with the failure pedal condition still set on the controls.

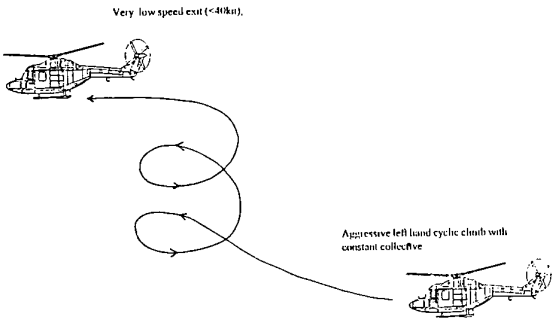

Fig 9 - High Power (RSS) Recovery Strategy

Control Failure - Use of Rotor RPM and the AFCS

A limited evaluation of the benefits of varying the rotor RPM and engaging/disengaging the FCS was carried out throughout the flight trial.

Varying Rotor RPM - As has already been reported, varying RPM had a significant effect in the hover. However, above approximately 20 kn, the benefits were minimal, any changes in RPM having only a transient effect on side slip. Above 40 kn there were no benefits at all.

Use of the AFCS - Should a failure mode allow AFCS inputs to the tail rotor, it was felt that the yaw damping effect in recovery flying should provide some directional stability. However, during the flight trial the reduction of yaw control power that the damping gave in the landing phase was considered detrimental.

Lynx Control Failure - Summary & General Advice

Figure 6 shows that only a small amount of available tail rotor pitch was used during the flight trial. This was due to the side slip restrictions placed on the flight trial. However, it is considered inconceivable that, during normal operational flying the, side slip achieved during the trial would be equalled. Therefore, assuming correct operation of the SBU, the likelihood of a worst case tail rotor control failure might be considered small. (However, it was thought possible that a rotor might 'fly' to an angle post failure and then freeze). Should a failure occur within the envelope tested, the following guidelines should be followed:

a. If flight post failure is uncomfortable due to side slip, bank away from the slip ball and 'drag' the ball into the centre, this will provide time to diagnose and manage the problem.

b. LSS cases will be reasonably comfortable in forward flight but, generally, require fast running landings; RSS cases will be most uncomfortable in forward flight and may require a left cyclic climbing turn.

c. On the approach, the aircraft nose should always be to the left of the flight path to allow collective to be applied to cushion the landing. In the latter stages, should the nose migrate to the right of the flight path OVERSHOOT IMMEDIATELY by lowering the nose, increasing speed then raising the collective.

d. Once on the ground DON'T RELAX, power should be taken from the rotor with great care.

Lynx Simulation Off Line Model and Strategy Development

Introduction

Prior to using the AFS to develop drive failure recovery strategies it was decided to enhance the Lynx simulation fuselage aerodynamics.

Aerodynamic Testing of a Lynx Fuselage

Helicopter computer simulations, whether carried out using a desktop system or through a large motion simulator, rely on a good fuselage aerodynamic data to ensure an accurate representation of the real vehicle. This is particularly important when simulating flight conditions which could quite possibly result in the aircraft operating outside of its normal trimmed flight condition. In order to satisfy this requirement and to achieve the large pitch and yaw angles required, a new small 1/7 scale Lynx model was constructed and tested in Westlands 12ft x 10ft wind tunnel. The model incorporated the main features of a utility Lynx fuselage, tail boom, fin and tailplane. It also included the main and tail rotor hubs but did not include the undercarriage.

Measurements of fuselage forces and moments were achieved in increments of pitch between +90° to -85°

and between 0° and +170° of yaw. The forces and moments measured were in tunnel axes and therefore to enable this data to be utilised within the DRA HELISM simulation it had to be converted into the body axes. Because it was not practical, in terms of time and physical constraints of the wind tunnel balance, to measure aerodynamic loads at every possible combination of fuselage pitch and yaw angle, a comprehensive look up table of aerodynamic data could not be generated. Therefore another method of incorporating the new aerodynamic data into the HELISM aircraft model was required. This was accomplished by fitting sets of polynomial equations to the data. Lift, drag, side force and pitching moment were plotted against pitch angle for each of the yaw angles tested and 10th order polynomial equations were fitted to the data. Rolling moment and yawing moments were plotted against yaw angle for each of the pitch angles tested and 6th order polynomial equations were fitted to the data. The polynomial coefficients were then used in new aerodynamic routines written for the simulation and enabled by interpolation, the fuselage steady state aerodynamic forces and moments to be calculated at any desired fuselage incidence and side slip.

Under tail rotor failure conditions fuselage yaw rate terms become important. In order to incorporate these effects into the HELISIM aircraft model, a fuselage strip analysis routine was also developed. This calculated the rate dependent fuselage yawing moments and enhanced the HELSIM yaw rate damping terms.

One remaining area of concern post this work, was the current absence of interactional aerodynamics in the model. Of particular concern in the tail rotor failure problem is the main rotor wake (MRW)/empennage interaction, where the MRW/tail plane interaction can lead to a change in pitching moment as the tail yaws through the wake, post failure. Large changes in pitching moment might have a significant impact on post failure control strategy.

Although the flight test data has yet to be fully analysed, validation flight trials on the ALYCAT showed no apparent tendency for the Lynx to change pitch attitude from a steady heading side slip entry to an autorotation.

Whilst this might be a small effect on the Lynx it is understood to a recognised dominant effect on aircraft with large horizontal tail-planes. This, combined with the influence of fin and tail boom area on the severity of the initial yaw post failure, and later the restoring moment, are examples of why the different aerodynamic characteristics of each type are expected to make type specific handling advice important.

It should be noted that the modelling of these interactional effects is currently the subject of research at DRA Bedford.

Strategy Development - Desktop Computer Simulation

To aid the development of the tail rotor drive failure piloting techniques and to reduce the time required to integrate the new wind tunnel data into HELSIM, a desktop simulation was undertaken at Westlands. The desktop simulation involved incorporating the Westlands HELMSMAN (Ref 7) pilot model with the HELSIM aircraft model. The use of a pilot model has several advantages when developing piloting strategies. It enables the engineer to replicate pilot actions and repeat these in a consistent manner while making parametric changes to the aircraft model. This approach is used frequently at Westlands when developing new piloting techniques. The HELMSMAN model also has the ability to use flight measured data to replay actual pilot control strategies and is an invaluable tool for both engineer and pilot when developing new techniques.

Once the validity of the combined models had been established and the integration of the new aerodynamics routines accomplished, desktop simulation was undertaken to investigate tail rotor drive failures in forward flight and hover. During the desktop simulation study, the pilot model intervened to control the aircraft following the drive failure, once a preset minimum pedal margin had been exceeded. Pilot intervention times were not studied during this phase of the investigation. The outcome from the desktop simulation indicated, as would be expected, that a drive failure in hover resulted in rotation rate building up rapidly. Cutting the engines reduced the rotation rate, but left only inertia in the rotor to cushion the landing. It was evident from the simulation that the landing could only be achieved with the aircraft still rotating. In forward flight, a tail drive failure resulted in the aircraft's sideslip building up. Once the pilot model reacted and removed the main rotor torque, maintaining an aircraft heading still became difficult. This is because, like most current helicopters without large tail fins, the Lynx fuselage without the tail rotor has low weathercock stability (or

yaw stiffness) at low pitch attitudes between +/- 25 ° of sideslip, Figure 10.

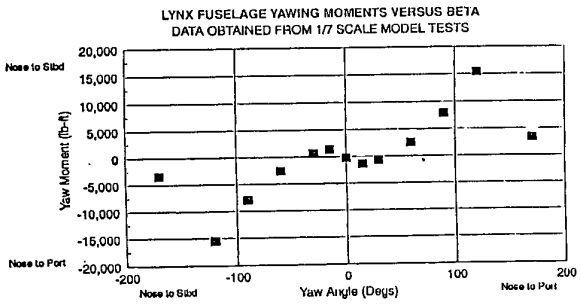

Fig 10 - Lynx Fuselage Yawing Moment versus Yaw Angle

However, as the sideslip builds up the weathercock stability increases and the yawing motion stops. The side force and drag also increase with increased side slip, and this results in a decay of speed. The simulation showed that initially the yaw motion oscillated from nose right to nose left, with the yaw angle increasing on each swing as the speed reduces. This situation would continue, eventually resulting in full rotations of the aircraft. Using the knowledge gained from the desktop simulation, the trials pilot was able to modify the control strategy, by introducing a nose down attitude post failure, to achieve a safe landing in the motion simulator at Bedford. Another advantage of the desktop simulation was that it was used to develop a parachute model that was later successfully tested in the AFS.

AFS Trials to Develop Lynx Drive Failure Advice

Drive Failure - Introduction

A handling assessment of Tail Rotor Drive Failures (TRDF) was carried out in the Large Motion Simulator (LMS), configured as a Lynx AH Mk7 with metal rotor blades. The simulation trial was conducted at DRA Bedford in November 1995. It should be noted that the AFS exhibits some key advantages over a training simulator for this work. These were:

a. The high fidelity motion cueing offered by the LMS.

b. A highly developed Lynx simulation with a known fidelity and validation level.

c. The ability to record data for post simulation trial analysis.

Drive Failure - Aim

The aim of the assessment was to support development of new Flight Reference Card (FRC) Emergency Drills for Lynx users in the event of a TRDF.

Drive Failure - Conditions Relevant

The LMS cockpit was a single-seat cockpit configured as the right hand seat of a Lynx with representative flight instruments N_R and N_F gauges and torque meter. There was a separate slip ball below the main Attitude Indicator. In addition a g-meter was fitted.
Representative Lynx flying controls were fitted, including a functioning four-way cyclic trimmer. For the simulation trial, a button on the collective lever handgrip could be pressed to shut down both engines simultaneously; the FIRE button on the cyclic handgrip could be pressed to deploy a notional drag parachute (modelled in HELSIM) which was intended to increase the model's yaw stiffness in forward flight and yaw rate damping in low speed flight.

The pilots seat was pulsed hydraulically at 4R to provide kinaesthetic cues and there was audio cueing of transmission noise.

The HELSIM model incorporated the WHL supplied aerodynamic routines obtained from wind-tunnel tests of a Lynx fuselage, detailed above. The model replicated a Lynx with AFCS engaged, less the heading hold. The simulation all up mass (AUM) was 10750 lbs and the atmosphere was ISA with nil wind or turbulence. The tail rotor elements of this model could be "failed" and the "run down" time varied.

The assessment test pilot had flown the LMS previously as a fixed base simulator for 8 hours, and with motion for 4 hours. He had flown 550 hrs of test flying in Lynx of all marks, but had no operational experience in Lynx.

Drive Failure - Assessment Criteria

Although Cooper-Harper (Ref 8) was briefly considered as the assessment criteria for the simulation trial it was rejected because it was felt that pilots ratings would fall in the HQR 9/10 bracket. Cooper-Harper simply was not refined enough at the poor end of the ratings scale for this simulation trial. Instead,

the success of a control strategy was assessed by noting the vehicle terminal conditions i.e. Maximum Vertical Velocity Touch Down (VVTD), Drift Angle +/- 5° and a Forward Velocity on touch down (UTD).

Clearly, however, there is an absence of criteria for handling characteristics following tail rotor failure. One can now envisage criteria being developed for the two phases of post failure handling (recovery and landing); perhaps the acceptable and desired criteria could be set by the ease with which each of the phases can be achieved, and the terminal conditions of the landing (side slip angle, vertical velocity and landing speed). These criteria currently do not exist.

Drive Failure - Current Advice

Key points from the current advice within the Lynx manual for a drive failure are summarised below:

Drive Failure - Hover Failure

- Reduce collective pitch.
- Cushion touchdown using collective pitch whilst attempting to maintain level attitude using cyclic control.
- Select both engines to off on touchdown.

Drive Failure - Forward Flight Failure

- Reduce collective pitch.
- Establish power and airspeed to minimise yaw.
- Make Engine off landing into wind.

Drive Failure - Structure of Simulation Trial

The simulation trial was divided into four phases. These were:

a. Phase 1 - Handling assessment and subjective comparison of the simulation model with flight tests flown on metal rotor blade Lynx at WHL & Empire Test Pilots School (ETPS) Boscombe Down.

b. Phase 2 - Handling assessment following TRDF's in autorotation.

c. Phase 3 - Strategy development following TRDF's in level forward flight (at two initial heights) throughout the speed range and in the hover, with first a dual engine shut-down using the Engine Shut Down Button (ESDB), then a time delay before using the ESDB to simulate the time taken for a Lynx crew to shut down both engines.

d. Phase 4 - Handling assessment following TRDF's with subsequent use of notional drag parachute.

Drive Failure - Phase 1 - Handling Assessment

The pilots initial assessment of the directional stability and control of the simulation was that he found the model to be more stable than the Lynx. Clearly, for a drive failure simulation trial this is potentially a significant point, since if the basic simulation is more directionally stable, post failure, the response of the vehicle could be more benign than the aircraft. The control strategies developed might then be inappropriate. Despite these comments, it was decided to proceed with the simulation trial since the pilot did not consider the problem was severe enough to negate the worth of the simulation trial.

Other important comments were:

a. Motion system and visual cues both proved particularly beneficial during the simulation. However, the relatively simplistic audio cues in the AFS were thought to be a weakness of the simulation. This point became particularly important in later phases when during high workload element, post failure, the pilot would normally be reliant on audio cues to control N_R.

b. Engine-Off landings (EOL) were flown using a variable flare initiated at 150 ft AGL and 80 kn. These EOLs were considered very realistic and reminiscent of real life EOLs flown in the Lynx. It was also noted that full right pedal was required to hold heading on landing as in the real aircraft. In addition, the LMS heave axis produced "fearsome" vertical g on ground contact which added greatly to the realism.

Drive Failure - Phase 2 - Handling assessment following TRDF's in autorotation

Phase 2 was introduced to the simulation trials programme post the difficulties the HELMSMAN pilot model had experienced recovering after failure. Here

the pilot established an autorotation before he was given the tail rotor failure. In all cases the pilot was able to recover the vehicle. Note-worthy points were:

a. From the stable autorotation, with a tail rotor failure, the pilot was able to conduct gentle left and right hand turns.

b. From the stable autorotation the pilot was able to conduct EOL. On all occasions touch down velocities were, however, very close to the Lynx undercarriage limits. This was caused by the tendency to keep the speed up, to overcome the nose left yaw (with the rotor) on flare.

Drive Failure - Phase 3 - Strategy development following TRDF's

The procedure adopted for this work was to start with fairly benign initial conditions and gradually present the pilot with more difficult conditions. Therefore, on the first run, the pilot was initiated high and fast (3000 ft, 140 kn); the tail rotor run down time was 30 seconds and the pilot was told of failure immediately. As the pilot developed a strategy to recover the vehicle, these conditions were constrained. In particular the following aspects were addressed:

a. Tail rotor run down time - For the majority of the simulation trial this was set to 2 seconds. It should be noted that an earlier simulation trial (Ref 9) had highlighted the benefits of a slow tail rotor decay time to recovering a vehicle at low altitude.

b. Initial speed - A range of initial speeds was selected (Hover, 50 kn, 80 kn, 140 kn). The aim was to capture data points along the speed axis of the speed/ power curve.

c. Initial height - Two heights were investigated 3000 ft and 500 ft. An additional 50 ft point was investigated for the hover case.

d. Pilot reaction time - In order to maintain consistency in this research simulation trial, the pilot was told that the tail rotor had failed 2 seconds after the failure. Again, an earlier simulation trial (Ref 9) had highlighted the importance of pilot reaction time to success, with a 1 second delay before response to failure considered unrealistically short, and a 4 second delay unrealistically long. 2 seconds, whilst perhaps a little faster than a pilot might be able to react in reality gave the pilot a chance to develop a recovery strategy.

The issue of pilot reaction time is linked to two major problems with simulation of failures. First, the pilot knows the failure is coming, and second, in a simulation trial of this nature, the pilot is asked to recover from so many failures, he becomes trained to the problem. Whilst these are both true the aim of the simulation trial should be recalled - to develop the best possible advice. This is only possible if these inherent problems are withheld.

One additional point from the simulation trial was that, it was decided that the Engine Shut Down Button (ESDB), that was being used by the pilot, was unrepresentative of the Lynx and indeed was having an impact on his control strategy and potential for success. This was proven when, in the later part of the simulation trial a time delay of 10 seconds between calling the dual engine shut down and removing the power was built into the strategy. This 10 second delay was intended to account for the time it would take for a second crew member to react to the call to shut down both engines and carry out the action. (10 seconds was later validated in a Lynx procedural simulator trainer). The recommendations that are going forward for inclusion in the aircrew advice are based on the strategies developed post the inclusion of a 10 second delay.

Drive Failure - Phase 3 TRDF Emergency Drill - Initial Recommendations

Although, at the time of print, the results from the simulation trial are still being reviewed prior to going forward for inclusion within Lynx Aircrew Manual and Flight Reference Cards, the following initial points were noted from the simulation trial:

a. If there is any indication of impending TRDF, such as high 1T to 4T vibration or increasing amount of left pedal being required to hold heading, the pilot should alter pitch attitude to achieve a speed of between 80-100 kn or land the aircraft if in a low hover.

b. When a TRDF occurs in any condition other than a low power descent, the

aircraft may yaw violently to the right through up to 270^0 before the pilot has time to lower the collective.

c. On sensing the failure, the pilot should lower the collective lever to reduce the torque to zero. Maintaining the torque below zero is more important than controlling N_R.

d. The yawing motion will increase drag and reduce total airspeed. A rate of descent is required to balance the excess main rotor torque with side slip post failure. (Ref 10)

Note: Up to 1500 to 2000 ft of height may be lost until controlled flight is achieved.

e. Once yawing stops, adjust pitch attitude to achieve 80 kn. 80 kn was found to be the optimum speed for autorotation since it gave a margin above 65 kn. During the trial the Lynx simulation was occasionally found to be unstable in a tail failed autorotation at approximately 65 kn, with the vehicle breaking away from a stable descent. This was particularly true when turns were initiated at this speed. It should be noted that the pilot could consistently decelerate through 65 kn during the variable flare landing without undue difficulty.

f. DO NOT ATTEMPT TO FIND A POWER/SPEED COMBINATION FOR CONTINUED FLIGHT; this will result in a yaw break-away to the right when the torque reaches 5 to 10 %. The aircraft then enters a flat yawing descent at zero IAS which could not be broken out of even with sustained full forward cyclic stick. Attempts to break out of the descent with lateral cyclic may cause the aircraft to invert.

g. Once yawing stops shut down engines whilst in a stable condition. Shutting down engines during the vehicle's initial response to failure had an adverse effect on the pilot's ability to recover the vehicle. After engine shut down, control the N_R with collective lever.

Note: The penalty associated with not shutting down the engines was highlighted when the simulation trials pilot omitted to shut down the engines during the procedure and he lost control of the vehicle for a second time as he tried to control NR, or as he flared for landing.

h. Once in autorotation at 80 kn, gentle left and right turns may be attempted, turns with the rotor (left turns) being more stable.

i. For the landing, a gentle stepped application of collective (variable flare) engine-off landing/ditching should be attempted reducing the speed from the autorotation speed (80kn) to approximately 40 kn. From a stable (engine off) autorotation, the tendency of the vehicle to yaw left (with the rotor) on application of collective was found to be minimal in the simulation. However, this was dependent on maintaining a high (40 kn) run-on landing speed.

j. If a TRDF occurs when the aircraft is in the hover, maintain the aircraft in a level attitude and cushion the touch down with collective lever. If time permits, shut down engines. It should be noted that up to 2000 ft height was found to be required before the vehicle could be 'flown out' of a hover TRDF.

When these points have been reviewed they will go forward to assist with the definition of new advice that will be agreed with RAF Handling Squadron, WHL, DRA and the Service training authorities.

Drive Failure - Phase 3 - Additional Observations

Several other points were noted during the phase 3 Lynx tail rotor drive failure simulation trial. These included:

a. Even from high altitude (3000 ft) initial conditions, and with an 'Apache like' chop collar, landing speed and vertical velocity were always marginal for vehicle/undercarriage survival.

b. Typically, height loss of 1500-2000 ft occurred before the pilot could regain control of the vehicle post failure. The availability of a chop switch had a significant impact on the control strategy; it also saved about 500 ft in recovery.

c. When the initial height was lowered from 3000 ft to 500 ft, the pilot had a major problem recovering the vehicle and failed to complete any landing/ditching within the Lynx undercarriage limits from an initial speed above 60 kts. Landings/ditching were achieved using the standard (collective, engines, attitude, cushion) strategy from initial condition below 60 kts but the pilot observed that, on the best of these, achieving success took all his attention and ability and were only just within the undercarriage design limits.

d. All hover failures at 50 ft resulted in vertical velocities at touch down (VVTD) in excess of 23 ft/s.

e. Two strategies were investigated for a high hover failure. The first was to " fly out" of the problem. Although the pilot attempted to keep the cyclic pointing at one point on the ground, this strategy resulted in a loss of control and inverted crash. The second strategy attempted was to lower the nose and chop engines. The latter was the more successful but still resulted in a landing in excess of the undercarriage limits.

Drive Failure - Phase 4 - Emergency Systems

The final phase of the simulation trial looked at the use of an emergency drag parachute. In an earlier simulation trial the benefits of a larger fin (Ref 9) had been noted and it had been postulated that a deployable fin might assist recovery. For this simulation trial a parachute was modelled and tested off-line using the HELMSMAN/HELISIM combination. Again it was tested from various initial conditions (height, speed) being "deployed" by the pilot from a switch on the cyclic.

This parachute had a significant impact on the pilot's success, in particular:

a. The chute allowed the pilot to recover the vehicle within undercarriage limits on all occasions, the only exception being the hover failure cases.

b. The chute allowed the vehicle to be recovered consistently within limits from below 500ft.

c. The chute allowed the pilot to handle the aircraft more freely in turns and in particular, allowed the pilot to fly the vehicle on, post failure.

The emergency chute system is thought to merit further consideration, despite the immediate problems associated with such a system of weight and uncommanded deployment.

Tail Rotor Failure Future Requirements and Designs

Based on results from Lynx TR trials, when future requirements, design standards and designs are considered, several points come to the fore;

a. There is an absence of criteria for handling characteristics following tail rotor failures. Since these criteria might be the basis for any future military design it is recommended that this should be one of the focus areas for development to ensure future types have more benign handling qualities post failure.

b. Procurement agencies should always be made aware of the impact on post failure handling of reducing fuselage/fin directional stability to achieve large low speed wind envelopes.

c. The advantages of a suitably protected power chop device operated from a control on the collective should be considered.

d. As was highlighted in an earlier study (Ref 9), pilot reaction time is a key to survival. Pilot reaction time is also increasingly important as aircraft height is reduced. The introduction of a tail rotor drive failure warning "caption" in cockpits, might reduce initial reaction times (even the smallest reduction would be important), and remove uncertainty e.g. a caption combined with the often quoted "bang from the rear of the aircraft" might allow the pilot to make the correct first action more promptly. It might also allow the pilot to make the sometimes important distinction between a control failure

and a drive failure. With the introduction of HUM systems, this is perhaps now more readily technically achievable and economically justifiable.

e. Particular consideration should be given to enhancing current designs which have weak fuselage/fin directional stability with:

(1) Health and Usage Monitoring Systems (HUMS) for at least the TR drive train.

(2) Emergency devices deployable to improve post failure recovery.

f. The control failure work highlighted the importance of a Spring Bias Unit (SBU) or similar device in the TR controls.

g. That undercarriage design limits are currently marginal, if not too low, to withstand post tail rotor failure landing conditions.

h. Further in the future the use of Active Control Technology (ACT) systems and perhaps cyclic control of tail rotor pitch might allow the available energy on failure to be harnessed and maintained by autorotating the tail rotor.

Conclusions & Recommendations

A research activity has been conducted by the DRA and WHL for the UK MOD Lynx Project Office, to improve the understanding of helicopter tail rotor failures, and develop handling advice for aircrew following a Lynx tail rotor (TR) malfunction.

Conclusions from the work include:

a. Tail rotor drive failures continue to occur at an unacceptably high rate (can be as high as 12 times UK requirement) in the UK MOD helicopter fleets.

b. The tail rotor malfunction can be separated in two broad categories;

- control failures, where control of tail rotor blade pitch is lost but the rotor continues to rotate and produce aerodynamic forces.

- drive failures where all power is lost to the tail rotor.

c. Tail rotor drive failures are more prevalent than control failures (UK military ratio 3:2).

d. Without a normally functioning tail rotor, many helicopter designs exhibit low directional stability.

e. Although the reasons for tail rotor failures are always investigated and if possible remedied, not enough is known about the behaviour of individual helicopter types following tail rotor failure. As a result, existing handling advice is inadequate and largely unsubstantiated.

f. Improved handling advice for current helicopters is believed to be achievable if the necessary work is put in hand. Better handling advice would enhance survivability in what is always likely to be a difficult malfunction regime.

g. Tail rotor failure aircrew emergency drill advice can often be weak and based on generic previous advice.

h. The programme used three important facilities the DRA Bedford Advanced Flight Simulator, the ALYCAT Lynx aircraft and the WHL HELMSMAN pilot model.

i. A useful procedure to develop and validate control failure advice is to remove the yaw collective interlink and fly recoveries, from various initial conditions, with the tail rotor pitch fixed from the co-pilots seat.

j. This (in-flight) control failure advice validation technique requires that:

(1) The design authority define the flight test envelop for the trials and any requirement for test instrumentation. e.g. Multi-channel telemetry

transmitter and FUMS (Fatigue and Usage Monitoring System). The design authority must also define the stress/strain limits for in-flight telemetry monitoring.

(2) The design authority must give permission to fly without the interlink and define the method for its removal and gagging.

k. Tail rotor control failure flight trials have been conducted and recommendations for amendments to Lynx aircrew failure emergency drills have been developed.

l. The DRA HELSIM Lynx simulation was developed, by included new aerodynamic fuselage data at high angles of attack and high yaw angles, for the AFS trials.

m. The different dynamic characteristics (aerodynamic, transmission, dynamic response) of helicopter types are expected to make type specific handling advice important in this key area.

n. Future work to develop interactional effects (MRW/ empennage) is required to improve confidence when using simulation to define post failure handling advice.

o. Tail rotor drive failure simulation trials have been conducted on the DRA AFS and recommendations for amendments to Lynx aircrew failure emergency drills have been developed.

It is recommended that:

a. Procurement agencies should be reminded of the penalty to post failure survivability of reduced fuselage/fin directional stability to achieve large low speed wind enevelopes.

b. Consideration should be given to the provision of a suitable protected power chop device operated from a control on the collective.

c. Particular consideration should be given to enhancing current designs which have weak fuselage/fin directional stability with HUMS.

d. The advantages of post failure emergency devices (parachutes, deployable fins) might outweigh the penalty and risk of their installation.

e. All future designs should include, and all current designs should be modified to include, an SBU (or similar device) in the TR controls.

f. Where possible, type-specific tail rotor failure advice should always be developed.

g. The use of a tail rotor drive failure cockpit warning "captions" should be considered for future designs.

h. In the absence of criteria, post failure handling characteristics are likely to remain poor. In particular, standards like ADS-33 (Ref 11), should be developed to provide criteria for post failure handling characteristics.

Figures

Fig 1 AFS Motion System

Fig 2 ALYCAT Over the AFS

Fig 3 ALYCAT Instrumentation

Fig 4 Low Power Freeze

Fig 5 High Power Freeze

Fig 6 Graph Showing IFS/Side Slip Test Points Flown

Fig 7 Graph Showing Landing Speed Attained.

Fig 8 Low Power (LSS) Recovery Strategy.

Fig 9 High Power (RSS) Recovery Strategy.

Fig 10 Lynx Fuselage Yawing Moments versus Yaw Angle.

References

1. UK Defence Standard 00-970, Design and Airworthiness Requirement For Service Aircraft, Chapter 705 para 3.2.

2. Padfield G D, " A theoretical model of helicopter flight mechanics for application to piloted simulation", RAE TR 81048, 1981.

3. Perry F J, Phipps P D, "Technical proposal for the work required to validate and qualify the Lynx aircrew manual advice", Unpublished WHL Aero Technical Note Lynx/267, 1993.

4. Padfield G. D, Charlton M. T, Kimberley A M, " Helicopter flying qualities in critical mission task elements. Initial experience with the DRA Bedford Large Motion Simulator"; Eighteenth European Rotorcraft Forum, Avignon, France, September 1992.

5. Tomlinson B. N, " Simulator motion characteristics and perceptual fidelity"; AGARD CP408 Flight Simulation, 1985.

6. Martyn, Lt Cdr A.W, ALYCAT Lynx Tail Rotor Control Failure Flight Trial Report, Unpublished DRA Report, 1995.

7. Hamm J. C, "The development of helicopter pilot models to control engineering simulations", RAeS Rotorcraft Simulation Conference , London, UK, 18-19 May 1994.

8. Cooper G. E, Harper R. P, " The use of pilot rating in the evaluation of aircraft handling qualities"; NASA TN D-5153, April 1969.

9. Martyn, Lt Cdr A.W, Improved Yaw Control for Helicopters, Unpublished DRA Report, May 1995.

10. O' Rouke M.J, A simulation model for tail rotor failures, AIAA-92-4633-CP, dated 1992.

11. Aeronautical Design Standard 33D, Handling Qualities Requirements for Military Rotorcraft United States Army Aviation Systems Command, St Louis, MO, July 1994.

Acknowledgment

The authors would like to acknowledge the assistance of Dr G D Padfield, Mr F J Perry, Mr J Hamm, Mr A McCallum, Lt Cdr S Cheyne and Mr A Kimberley with the compilation of this paper and the conduct of the trials programme.

© British Crown Copyright 1996/DRA Published with the permission of the Controller of Her Britannic Majesty's Stationery Office.

Optimal Trajectories for the Helicopter in One-Engine-Inoperative Terminal-Area Operations

Robert T. N. Chen
NASA Ames Research Center, M/S 211-2
Moffett Field, CA 94035-1000, USA

Yiyuan Zhao
University of Minnesota, 107 Akerman Hall
Minneapolis, MN 55455, USA

SUMMARY

This paper presents a summary of a series of recent analytical studies conducted to investigate one-engine-inoperative (OEI) optimal control strategies and the associated optimal trajectories for a twin engine helicopter in Category-A terminal-area operations. These studies also examine the associated heliport size requirements and the maximum gross weight capability of the helicopter. Using an eight states, two controls, augmented point-mass model representative of the study helicopter, continued takeoff (CTO), rejected takeoff (RTO), balked landing (BL), and continued landing (CL) are investigated for both vertical-takeoff-and-landing (VTOL) and short-takeoff-and-landing (STOL) terminal-area operations. The formulation of the non-linear optimal control problems with considerations for realistic constraints, solution methods for the two-point boundary-value problem, a new real-time generation method for the optimal OEI trajectories, and the main results of this series of trajectory optimization studies are presented. In particular, a new balanced-weight concept for determining the takeoff decision point for VTOL Category-A operations is proposed, extending the balanced-field length concept used for STOL operations.

NOMENCLATURE

C_P	power coefficient
C_T	thrust coefficient
(C_x, C_z)	(horizontal, vertical) component of thrust coefficient
c_d	mean profile drag coefficient of rotor blades
D_f	parasite drag of the fuselage
f_e	equivalent flat plate area for fuselage
f_G	ground effect factor
g	gravitational acceleration
(h, x)	(vertical, horizontal) position
H_R	rotor hub height when the helicopter is on the ground
I_R	polar moment of inertia of the main rotor
K_{ind}	induced power factor
m	helicopter mass
m_o	reference mass
P_{OEI}	maximum OEI power available
P_{pr}	main rotor profile power
P_{req}	helicopter power required
P_s	available shaft power
P_{TO}	one engine maximum normal takeoff power
R	main rotor radius
T	main rotor thrust
$(\overline{U}_c, \overline{U}_t)$	normalized climb and tangential flow components at the main rotor
U_2	horizontal component of V_{TOSS} or V_{BLSS}
(u, w)	(horizontal, vertical) velocity components
u_x, u_z	normalized control variables
V	airspeed
V_{TOSS}	takeoff safety speed
V_{BLSS}	balked landing safety speed
V_Y	airspeed at best rate of climb

Paper presented at the FVP Symposium on "Advances in Rotorcraft Technology", held in Ottawa, Canada, 27-30 May 1996, and published in CP-592.

v	induced velocity in ground effect
$\bar{v}_i$	normalized uniform induced velocity of the rotor
(X_{CTO}, X_{RTO})	total runway length in (continued takeoff, rejected takeoff)
$(x_{f\cdot cto}, x_{f\cdot rto})$	airborne runway required from optimization in (continued takeoff, rejected takeoff)
β	thrust vector inclination
γ	takeoff glide slope/approach angle
η	helicopter power efficient factor
ρ	air density
σ	rotor solidity ratio
τ_p	turboshaft engine time constant
θ_w	angle between rotor wake and a vertical reference line
Ω	main rotor angular speed
( )0	initial values at engine failure
( )max	maximum value allowed
( )min	minimum value allowed

Acronyms

AEO	all engine operating
BL	balked landing
CL	continued landing
CTO	continued takeoff
FAA	Federal Aviation Administration
JAA	Joint Aviation Authority
LDP	landing decision point
OEI	one engine inoperative
RTO	rejected takeoff
TDP	takeoff decision point

1. INTRODUCTION

Engine failure represents a major safety concern to helicopter operations, especially in the critical flight phases of takeoff and landing to or from small, confined areas. As a result, the JAA and the FAA both certificate a transport helicopter with a gross weight of 2720 kg (6000 lb) or more as either Category-A or Category-B according to the ability to continue its operations following engine failures (Refs. 1 and 2). The Category-B certification applies to either single engine or multiengine helicopters with gross weight less than 9070 kg (20,000 lb), and requires that a safe landing be possible in the event that one or all engines become inoperative. There is no requirement, however, for continued flight capability.

In contrast, Category-A certification, which applies to multi-engine transport helicopters with independent engine systems, requires that they have the capability to continue the flight with one engine inoperative (OEI). These stringent requirements, while permitting operations from rooftops and oil rigs, and flight to areas where no emergency landing sites are available, significantly restrict the payload of a Category-A transport helicopter to a value safe for continued flight as well as for landing with one engine inoperative. Typical Category-A helicopter takeoff and landing procedures are shown in Figs. 1 and 2, respectively, for short takeoff and landing (STOL) to or from a clear heliport and for vertical takeoff and landing (VTOL) to or from an elevated helipad. Specifically, in a takeoff flight (Figs. 1(a) and 2(a)), the pilot must continue the takeoff (CTO) if an engine failure occurs at or after passing the takeoff decision point (TDP), and should land, or reject the takeoff (RTO), if an engine failure occurs at or before reaching the TDP. In a landing flight (Figs. 1(b) and 2(b)), the pilot must continue the landing (CL) if an engine fails after the helicopter has passed the Landing Decision Point (LDP). The pilot may either continue or balk the landing (BL) if an engine failure occurs at or before reaching the LDP. If no engine fails, the helicopter simply proceeds with the all-engine-operating (AEO) normal takeoff or landing. In VTOL operations, confined helipads require that the helicopter land back to the original takeoff point.

The current certification process involves extensive flight tests, which are potentially dangerous, costly, and time consuming. These tests require the pilot to simulate engine failures at increasingly critical conditions. Flight manuals based on these tests tend to provide very conservative recommendations with regard to maximum takeoff weight or required runway length. Usually, a single TDP or LDP is recommended for all flight conditions. As a result, the pilot cannot trade favorable ambient conditions or less takeoff weight for a shorter runway length.

Recently, efforts were made to address these important issues. For Category-A VTOL operations, Lande (Ref. 3) experimentally investigated various takeoff and landing procedures to or from oil rigs in the North Sea, including static takeoff, dynamic takeoff, straight-in landing, and sideway ascent/descent. Stevens and Vodegel (Refs. 4 and 5) developed a computer program for the certification of Category-A helicopter VTOL operation. Goldenberg, Meslin, Blondino, and Williams (Ref. 6), and Wood, Blondino, and Williams (Ref. 7) investigated further the use of the sideway procedure initiated previously by Lande (Ref. 3), for the M230 helicopter on an elevated helipad. Some theoretical investigations have also been performed. Okuno and Kawachi (Ref. 8) studied VTOL OEI optimal trajectories by minimizing the touchdown impact speed in RTO, and by maximizing the minimum altitude in CTO flyout. Sharma, Zhao, and Chen (Ref. 9) conducted an OEI trajectory optimization study for the sideway Category-A operation previously investigated experimentally by Lande (Ref. 3), Goldenberg (Ref. 6), and Wood (Ref. 7). Optimal Category-A VTOL operation, including a backup takeoff

procedure, was also recently investigated by Zhao, Jhemi, and Chen (Ref. 10).

Research efforts were also made to better understand Category-A STOL operations. Saal and Cole (Ref. 11) conducted an extensive flight test with the S76B to investigate the merit of variable TDP and V_{TOSS}. Cerbe and Reichert (Ref. 12) conducted an analytical study to investigate optimal Category-A takeoff flight for the BO-105 helicopter using a static power-required field model. Okuno and Kawachi (Ref. 8) studied choices of the TDP velocity and takeoff slope for runway length reduction using nonlinear optimal control theory. Zhao and Chen (Ref. 13) determined Category-A takeoff trajectories of a UH-60A helicopter to minimize runway length and to maximize gross weight. Sharma (Ref. 14), and Sharma, Zhao, Chen, and Hindson (Ref. 15) examined optimal OEI trajectories associated with runway landing for the UH-60A helicopter. Optimal control theories have also been used to study landing procedures in autorotation after all engines fail (Refs. 16–19). In addition, a new method for real-time generation of optimal trajectories was recently developed by Jhemi, Zhao, and Chen (Ref. 20) for providing timely display guidance to assist the pilot in reducing his workload and to enhance the safety of Category-A operations.

The main objective of this paper is to summarize the key results of Refs. 10, 13, 14, 15, and 20. These efforts were made to enhance the understanding of the effects of fundamental parameters associated with Category-A VTOL and STOL operations. There are four primary concerns in these studies: (1) safety, (2) payload capability, (3) heliport size, and (4) real-time generation of optimal trajectories. In the sections that follow, the helicopter modeling, the formulation of the nonlinear optimal control problems with realistic constraints considered, the solution methods for the two-point-boundary-value problem thus formulated, and the new real-time generation method for the optimal OEI trajectories are discussed. Finally, the main results of this series of trajectory optimization studies are summarized.

2. HELICOPTER MODEL AND EQUATIONS OF MOTION

An augmented two-dimensional, point-mass model for the UH-60A helicopter, as schematically depicted in Fig. 3, is used for this series of trajectory optimization studies (Refs. 10 and 13–15). The governing equations are summarized below:

$$m\dot{w} = mg - \rho\left(\pi R^2\right)(\Omega R)^2 C_z - \frac{1}{2}\rho f_e w\sqrt{u^2+w^2} \tag{1}$$

$$m\dot{u} = \rho\left(\pi R^2\right)(\Omega R)^2 C_x - \frac{1}{2}\rho f_e u\sqrt{u^2+w^2} \tag{2}$$

$$I_R\Omega\dot{\Omega} = P_s - \frac{1}{\eta}\rho\left(\pi R^2\right)(\Omega R)^3 C_P \tag{3}$$

$$\dot{h} = -w \tag{4}$$

$$\dot{x} = u \tag{5}$$

where the thrust coefficients are defined as

$$C_T = T/\rho\left(\pi R^2\right)(\Omega R)^2 \tag{6}$$

$$C_x = C_T \sin\beta \tag{7}$$

$$C_z = C_T \cos\beta \tag{8}$$

The airspeed and flightpath angle are

$$V = \sqrt{u^2+w^2} \tag{9}$$

$$\sin\gamma = -\frac{w}{V} \tag{10}$$

Time derivatives of C_x and C_z, instead of C_x and C_z themselves, are used as control variables to avoid discontinuity at the point of engine failure. Also, first order response dynamics for the contingency power available are assumed for turboshaft engines.

$$\dot{C}_x = u_x \tag{11}$$

$$\dot{C}_z = u_z \tag{12}$$

$$\dot{P}_s = \frac{1}{\tau_p}\left(P_{OEI} - P_s\right) \tag{13}$$

Thus, in this augmented point-mass model, there are eight state variables: $u, w, h, x, C_x, C_z, \Omega$, and P_s, and two control variables: u_x and u_z, with helicopter mass, m, and OEI power available, P_{OEI}, playing the role of control parameters. The initial OEI conditions for the state variables are determined from the AEO takeoff or landing path immediately prior to the engine failure.

The required power coefficient, C_P, in Eq. (3) is calculated from the following equation:

$$C_P = C_T\sqrt{\frac{C_T}{2}}\left(K_{ind} f_G \bar{v}_i + \bar{U}_c\right) + \frac{1}{8}\sigma c_d \tag{14}$$

where

$$\bar{U}_c = \frac{u\sin\beta - w\cos\beta}{\Omega R\sqrt{C_T/2}} \tag{15}$$

$$\bar{U}_t = \frac{u\cos\beta + w\sin\beta}{\Omega R\sqrt{C_T/2}} \tag{16}$$

and the normalized, induced velocity of the rotor, i.e., normalized with the hover mean induced velocity, is computed using

$$\bar{v}_i = 1\Big/\sqrt{\bar{U}_t^2 + \left(\bar{U}_c + \bar{v}_i\right)^2}, \qquad \left(2\bar{U}_c + 3\right)^2 + \bar{U}t^2 > 1 \tag{17a}$$

$$= \bar{U}_c\left(0.373\bar{U}_c^2 + 0.598\bar{U}_t^2 - 1.991\right), \qquad \text{otherwise} \tag{17b}$$

Note that the rotor speed dynamics, Eq. (3), in the above set of equations is based on Ref. 21. The efficiency factor, η, in Eq. (3) accounts for the power losses associated with tail rotor and transmission (Ref. 22). Equation (17b) from Johnson (Ref. 17) is an empirical approximation to the induced velocity in the vortex-ring state. The momentum theory for the rotor induced velocity, Eq. (17a), and the power-required coefficient in Eq. (14) are discussed in detail in Refs. 23 and 24. Also, in Eq. (14), the term f_G accounts for the decrease in induced velocity due to ground effect. In general, benefits of ground effect are most pronounced at hover and decrease gradually as the horizontal speed increases (Ref. 25). The simple source model of Cheeseman and Benett (Ref. 26) to account for ground effect in forward flight was used in this study for simplicity, although there are some refinements (Refs. 27–29) to that model to include the effect of recirculation. From Ref. 26,

$$f_G = 1 - \frac{R^2 \cos^2 \theta_w}{16(h + H_R)^2} \tag{18}$$

where

$$\cos^2 \theta_w = \frac{(-wC_T + vC_z)^2}{(-wC_T + vC_z)^2 + (uC_T + vC_x)^2} \tag{19}$$

$$v = K_{ind} v_h \bar{v}_i f_G \tag{20}$$

The time constant associated with induced velocity dynamics is ignored because it is much smaller compared to the flight time associated with the critical phases of takeoff and landing (see, for example, Ref. 25).

The aerodynamic and structural limitations of the rotor blades result in constraints on the rotor speed, the rotor thrust, and the thrust angle.

$$\Omega_{\min} \le \Omega \le \Omega_{\max} \tag{21}$$

$$C_{T_{\min}} \le C_T \le C_{T_{\max}} \tag{22}$$

$$\beta_{\min} \le \beta \le \beta_{\max} \tag{23}$$

The OEI contingency power ratings are defined in terms of the level and the duration. In lieu of the 30-sec/2-min ratings, i.e., a 30-sec contingency power followed by a 2-min contingency power, which were proposed in Ref. 30 and recently applied in Ref. 31, the more traditional 2.5-min/30-min power ratings were used. In this paper, we assume that the 2.5 min OEI power rating is 110% of the AEO takeoff power rating, and the 30-min OEI power rating is 105% of the AEO takeoff power. These are typical values based on existing engine data. Therefore, upon a single engine failure, the maximum available power from the operating engine is the 2.5-min power rating assumed at 1656 hp, followed by the 30-min power at 1580 hp.

In this series of studies, the UH-60A helicopter (Refs. 32 and 33) was used as the example helicopter. This single rotor helicopter is powered by two T-700-GE-700 turboshaft engines. Some important parameters of this helicopter, compiled from Refs. 27 and 33 as well as the parameters used in the optimization studies, are listed in the Appendix.

3. ENERGY CONSIDERATIONS

Before discussing the formulation of the OEI trajectory optimization problem for Category-A STOL and VTOL operations using the helicopter model and equations of motion described above, it is instructive to consider first the problem from an energy perspective.

Category-A operations involve energy management to cope with the power deficiency resulting from loss of an engine, trading various energy sources, and controlling the rate of transfer among the levels of those energy sources. Unlike fixed-wing aircraft, the helicopter has the additional rotor rotational energy source to be utilized, in addition to the usual kinetic and potential energy sources. The total energy of the helicopter is therefore given by

$$E = mgh + \frac{1}{2} m V^2 + \frac{1}{2} I_R \Omega^2 + \frac{1}{2} I_{yy} q^2 \tag{24}$$

The last term in the above equation accounts for the energy associated with the rotation of the aircraft for the two-dimensional case considered.

The power deficiency in an OEI situation, i.e., the power available from the remaining engine(s) minus the helicopter power required, may be supplemented by a reduction in the total energy to yield

$$P_s - P_{req} = mg\dot{h} + mV\dot{V} + I_R \Omega \dot{\Omega} + I_{yy} q \dot{q} \tag{25}$$

Conversely, in a flight condition where the available OEI power exceeds the helicopter power required, the excess power may be used to gain altitude, to increase speed, to increase the rotor speed, or to change the flight direction.

Combining Eq. (25) with Eqs. (1) and (2), and noting that the power required is the sum of the power required for the main rotor, tail rotor/transmission, and the helicopter parasite-drag power, which is $(1/2)\rho f_e V^3$, i.e.,

$$P_{req} = P_{mr} + P_{tr} + P_{para}$$

the following equation for the OEI power balance is obtained.

$$\begin{aligned} P_s = {} & (P_{mr} + P_{tr}) + \rho \pi R^2 (\Omega R)^2 (uC_x - wC_z) \\ & + I_R \Omega \dot{\Omega} + I_{yy} q \dot{q} \end{aligned} \tag{26}$$

Equation (26), which provides a more complete alternative to Eq. (3) by including the power associated with the change in flight direction, may be appropriate when a complete six-degree-of-freedom rigid-body helicopter model is employed in the optimization analysis.

The helicopter power-required values for level flight at sea level standard atmospheric conditions for the study helicopter with a nominal gross weight of 16,500 lb are shown in Fig. 4, along with the OEI contingency power available. The power-required values were calculated from the augmented point-mass model,

as described in the previous section. They are compared with those from a comprehensive blade-element simulation model (Ref. 33), which have previously been partially validated with flight test data of the UH-60A helicopter (Ref. 34). Despite its simplicity, the augmented point-mass model matches fairly well with the blade-element model, especially in the critical low-speed region in which the OEI contingency power is deficient. The power required exhibits the familiar shape with the minimum power point located in the 70–80 kt region for the two models at the flight conditions considered. Note that the OEI contingency power becomes deficient when the airspeed is below approximately 25 kt.

The power deficiency in this critical low-speed region may be supplemented by drawing from the helicopter potential and rotor rotational energy sources as shown in the lower portion of Fig. 4. Shown in the figure are three average power components: a 9% drop in rotor RPM, a 25-ft drop in altitude, and a 10-kt decrease in airspeed from various speed levels for a representative 5-sec maneuver. It is interesting to note that the first two power components are roughly equivalent, and they are approximately equal to the third component at an airspeed of 35 kt. Note also that the power deficiency near hover flight conditions may be supplemented by the combined use of the drop in the rotor RPM and in altitude. Part of the energy from these two sources may also be utilized to accelerate the helicopter towards the power-excess region which begins at an airspeed of about 25 kt. The first two sources of energy may then be replenished as the airspeed increases further.

Obtaining the precise control strategy to effect the energy management, which involves the control of the level and rate of those energy sources in consonance with the available OEI power and the required power, is the purpose of the trajectory optimization as formulated in the next section.

4. FORMULATION OF THE OEI TRAJECTORY OPTIMIZATION PROBLEM

The OEI trajectory optimization problem will be formulated below for both VTOL and STOL operations, and will involve the four elements of takeoff and landing, i.e., rejected takeoff, continued takeoff, balked landing, and continued landing. For simplicity, a representative set of nominal AEO takeoff and landing paths was first assumed. Although the choice of the AEO takeoff or landing paths can affect the optimal OEI trajectories, the method allows us to be concerned with only OEI portion of the trajectories, not with the optimization of combined AEO and OEI trajectories.

4.1 Nominal AEO Takeoff and Landing Flightpaths

A. VTOL Case

The nominal AEO takeoff and landing flightpaths are shown in Figs. 2(a) and 2(b), respectively. These nominal AEO paths are selected based on recommended procedures for the UH-60A and the Super Puma helicopter. In the nominal AEO takeoff path, the helicopter begins with a 5-ft hover in ground effect. This is then followed by a steady linear backup climb ($\gamma = 150°$, $V_0 = 5$ kt, $\dot{V} = 0$) to the takeoff decision point. At any point before the TDP, the horizontal location is therefore given by

$$x_0 = -\sqrt{3}(h_0 - 5) \tag{27}$$

Around the TDP, the helicopter flies vertically up briefly before climbing out.

In the nominal AEO landing, the helicopter approaches the helipad with a constant glide path angle of –6°, and a constant deceleration of –0.075 g. It has a speed of 35 kt at $h = 100$ ft and reaches zero speed at $h = 25$ ft. At 25 ft above the surface of the helipad, the helicopter starts to descend and lands vertically. The horizontal location is therefore given by

$$x_0 = -\frac{h_0 - 25}{\tan 6°} \tag{28}$$

B. STOL Case

The nominal AEO STOL takeoff and landing paths are shown in Figs. 1(a) and 1(b). For takeoff flight, use is made of Schmitz's procedure (Ref. 16) for a heavily loaded helicopter. The helicopter begins with a hover in ground effect at 5 ft. It then accelerates horizontally at a constant $0.2g$ to an airspeed V_0. At V_0, the helicopter starts a climb at a constant flightpath angle, γ_0, while maintaining the constant airspeed. During climb, the horizontal location at any point before the TDP is thus given by

$$x_0 = \frac{V_0^2}{0.4g} + \frac{h_0 - 5}{\tan\gamma_0} \tag{29}$$

For the nominal AEO STOL landing path, it is assumed, for simplicity, that the flightpath consists of steady flight at constant airspeed, constant approach flightpath angle, and 100% rotor speed.

4.2 Rejected Takeoff Flight and Continued Landing

A. VTOL

During a successful RTO, the helicopter must return to the helipad and land safely. Therefore, the optimal control problem is formulated to minimize the dispersion of touchdown points, subject to specified touchdown speed limits. With the takeoff point taken as the origin, the following performance index is to be minimized through the use of an optimal control strategy for the two control variables, u_x, u_z, in the equations of motion and state path-constraints (Eqs. (1) to (23)),

$$\min \quad J = x^2(t_f) \tag{30}$$

subject to the terminal constraints:

$$h(t_f) = 0 \tag{31}$$

$$u(t_f) \le u_{\max} \tag{32}$$

$$w(t_f) \le w_{\max} \tag{33}$$

where t_f is the time at touchdown, which is to be determined. The values of the touchdown safety speeds, $u_{\max}, w_{\max}$, chosen for the study are 15 and 5 ft/sec, respectively. With a deceleration level of –0.2 g assumed, the stopping distance after touchdown amounts to no more than 17.5 ft.

Preliminary calculations indicate that Eq. (33) can be either active or inactive, depending on helicopter gross weight and initial conditions. Therefore, for consistency, Eq. (33) is enforced as an equality.

B. STOL Cases

Two different performance indices are considered for the rejected takeoff optimization in STOL operations. They are (1) minimum runway length, and (2) maximum takeoff weight, i.e.,

$$\min \quad J = x(t_f) \tag{34}$$

$$\min \quad J = W_0/W \tag{35}$$

where W_0 is a fixed, reference takeoff weight.

Again, the associated optimization problems are to find the control strategies for u_x, u_z, that minimize either the performance index (Eqs. (34) or (35)), subject to the equations of motion (Eqs. (1)–(20)), the state path-constraints (Eqs. (21)–(23)), and the terminal constraints (Eqs. (31)–(33)) to achieve reasonable touchdown speeds. For the STOL cases, the safe touchdown speeds, $u_{\max}, w_{\max}$, are chosen to be 40 ft/sec, and 5 ft/sec, respectively.

The trajectory optimization problems for the continued-landing transition flight are formulated for VTOL and STOL operations similar to those for the transition flight during the rejected takeoff described above.

4.3 Continued Takeoff and Balked Landing Flight

A. VTOL

A continued OEI takeoff must be possible after the failure of an engine at any point on or after the TDP. FAA regulations specify that at the end of a CTO transition flight, the helicopter achieves (1) a minimum of 35 ft above the takeoff surface (or above the sea level in the case of oil rig operations), (2) a minimum climb rate of 100 fpm, and (3) a pre-selected takeoff safety speed, V_{TOSS}. The required terminal constraints are therefore

$$h(t_f) \geq 35 \text{ ft} \tag{36}$$

$$-w(t_f) \geq 100 \text{ fpm} \tag{37}$$

$$u(t_f) \geq U_2(W) \tag{38}$$

$$\dot{w}(t_f) = 0 \tag{39}$$

$$\dot{u}(t_f) = 0 \tag{40}$$

$$\dot{\Omega}(t_f) = 0 \tag{41}$$

Equations (39) to (41) above are added to assure that a steady-state flight condition is attained at the end of the CTO transition. Note that U_2 in Eq. (38) is the horizontal component of V_{TOSS}, and they are approximately equal, since the vertical velocity component $w(t_f)$ as shown in Eq. (37) is very small in comparison. Eq. (38) is included as a terminal constraint to assure consistency between the OEI transition flight and the steady OEI climb, which is a function of gross weight and is obtained from the steady-state solution of Eqs. (1) to (3). Table 1 lists the relationship between U_2 and the maximum gross weight in steady OEI climb at the rate of 100 fpm, at the nominal rotor speed, and with P_{OEI} = 1656 hp. Further details will be discussed later.

In a continued takeoff, tradeoff exists among payload capability, heliport adjacent space requirement, and minimum altitude drop during the OEI transition flight to a steady climb. For a given gross weight, two optimization problems are therefore formulated for CTO transition flight to minimize (1) the required runway length, and (2) the altitude drop, both subject to the equations of motion (Eqs. (1)–(20)), the state path-constraints (Eqs. (21)–(23)), and the terminal constraints (Eqs. (36)–(41)). The two performance indices are, respectively, Eqs. (34) and (42a) shown below.

$$\max \ \min \ h(t) \tag{42a}$$

To simplify numerical solutions, the performance index (Eq. (42a)) will be replaced by an approximate form given by Johnson (Ref. 36):

$$\min \quad J = \int_{t_0}^{t_f} \left(H_{ref} - h\right)^q dt \tag{42b}$$

where q is an even integer and H_{ref} is a reference altitude, well above the altitude trajectory. In this paper, the values for these two parameters are: $q = 6$ (or 8), and $H_{ref} = h_0 + 100$ ft.

The optimization problems for balked landing (BL) are formulated in the same way as those for CTO cases; the balked landing safety speed, V_{BLSS}, is assumed to be identical to V_{TOSS}.

B. STOL

Two optimization problems are considered for the STOL continued takeoff flight. The first is the *minimum runway -length problem* using the performance index of Eq. (34). The second one is the *maximum takeoff weight* in transition flight, using the performance index (Eq. (35)). The minimum runway-length problem involves finding the control strategies for u_x and u_z that minimize Eq. (34), subject to the equations of motion (Eqs. (1)–(20)), the state path-constraints (Eqs. (21)–(23)), and the terminal constraints (Eqs. (36)–(41)). The maximum takeoff weight problem involves minimizing the performance index (Eq. (35)), subject to Eqs. (1)–(23), Eqs. (36)–(41), and the specified runway length, i.e.,

$$x(t_f) = X_{specified} \tag{43}$$

Again, the optimization problems for the balked landing flight are formulated identically to those for the CTO case assuming $V_{BLSS} = V_{TOSS}$.

5. METHODS OF SOLUTION AND NUMERICAL RESULTS

Obtaining the optimal flight trajectories for the OEI transition flight from the point of engine failure to the establishment of a steady climb or touchdown, as formulated in the preceding

section, requires that two steady-state analyses are first performed to establish initial conditions and the maximum gross weight that would permit a continued flight.

As described previously, the helicopter states at the point of engine failure on a nominal AEO takeoff or landing path are used as initial conditions for trajectory optimizations for the OEI transition flight. An assumption is made that an engine failure occurs during a steady climb or descent portion of the nominal AEO takeoff and landing flightpaths which are described in section 4.1. The maximum weight in a steady OEI climb is discussed below.

5.1 Maximum Weight in Steady OEI Climb

The OEI climb requirements determine the maximum takeoff weight which is meaningful for the whole Category-A operation. Therefore, maximum takeoff weights in the OEI climbout are examined using the steady-state equations of Eqs. (1)–(3). There are two segments in OEI climbout as shown in Fig. 1. In the first segment, from an altitude of 35 ft to at least 100 ft, the helicopter must be able to maintain a minimum climb rate of 100 fpm at V_{TOSS} or V_{BLSS} with the 2.5 min OEI power. For the second segment, from 100 to 1000 ft, the helicopter must be able to accelerate from V_{TOSS} or V_{BLSS} to V_Y and achieve a minimum rate of climb of 150 fpm at V_Y with the 30-min OEI power.

Figure 5, which is obtained from the steady-state solution of Eqs. (1) through (3), shows the maximum weight as a function of the horizontal velocity component of V_{TOSS} (or V_{BLSS}) in a steady climb. Three sets of conditions are included: (1) P_{OEI} = 110% AEO takeoff power (1656 hp), 100 fpm climb rate, 100% rotor RPM; (2) P_{OEI} = 110%, 100 fpm climb rate, 91% RPM; and (3) P_{OEI} = 105% (1580 hp), 150 fpm climb rate, and 100% RPM. Note that the maximum weight increases as U_2 increases and reaches a peak value at V_Y, in a manner consistent with the helicopter power required curve shown in Fig. 3. Clearly, the helicopter must attain a higher V_{TOSS} (or V_{BLSS}) in order to be capable of carrying a larger payload in the OEI climbout. In this series of studies, the value of U_2 examined ranges from 55 to 100 ft/sec. As shown in Fig. 5, the helicopter flying in this range of U_2 is capable of carrying less weight with 110% power than flying at V_Y with 105% power. Therefore, the first climb segment, which is more restrictive than the second segment, determines the maximum gross weight capability in OEI climbout as listed in Table 1 for a range of U_2 values.

5.2 Numerical Solution Techniques for Trajectory Optimization

The OEI trajectory optimization problems formulated in section 4 are solved numerically using the Sequential Gradient Restoration Algorithm (SGRA) developed by Miele et al. (Ref. 37), and coded by Zhao (Ref. 38). This algorithm provides a numerical technique to solve a general nonlinear optimal control problem subject to terminal and path constraints on states, controls, and parameters. Since the SGRA only treats equality constraints, all the inequality constraints, Eqs. (32), (33), and (36) to (38), are transformed to equality constraints using a slack variable method (Ref. 39) by adding a positive quantity on the appropriate side of the inequality.

Proper choice of normalization and scaling of variables are vital to the computational efficiency of the numerical methods and to a successful convergence of the optimization problem. A well-scaled problem is one in which a given order of magnitude change in any variable results in the same order of magnitude change in the performance index. The following normalization and scaling were found to be satisfactory: all distances are normalized by 10R, and time by $100/\Omega_0$, where Ω_0 is the nominal rotor speed. Details of the scaled helicopter-dynamic equations and constraints can be found in Refs. 13 and 14.

Extensive trajectory optimization was conducted using different initial guesses for states, controls, and parameters. In this paper, the results shown are for the following initial guesses: all state variables are constant and equal to their initial-time values; all control variables are also constant at the point of engine failure. Convergence criteria are selected such that further iterations will not change the performance indices by more than 0.5%.

5.3 Numerical Results – Rejected Takeoff

A. VTOL

Typical control strategies and the associated optimal trajectories for several rejected-takeoff transition flights from a backup takeoff are shown in Figs. 6 and 7. These are solutions with the performance index of Eq. (30). The backup AEO takeoff conditions are: γ_0 = 150°, V_0 = 5 kt; and P_{OEI} = 1656 hp. Figure 6 shows the effect of altitude at which the OEI occurs for gross weight at 16,000 lb. At these conditions and for the range of altitudes examined, the helicopter can always achieve successful RTOs to a close proximity of the original takeoff point, within the safe touchdown speeds of 5 ft/sec vertically and 15 ft/sec horizontally. This is consistent with the OEI H-V diagram for the helicopter at 16,000 lb. However, the touchdown point was found to deviate the most from the original takeoff point when an engine failure occurs at an altitude of 40–60 ft.

Immediately after engine failure, the optimal control strategy is to rapidly tilt the thrust vector forward to its 10° limit to accelerate the aircraft. At the same time, the thrust coefficient is increased to reduce the rotor speed to its lower limit. These maneuvers reduce the power requirement significantly to accommodate the OEI power available. When engine failure occurs at a lower altitude, the vertical descent rate and airspeed both reach the safety limit values at the touchdown point. When an engine fails at a higher altitude, the helicopter has more time to develop a higher descent rate before touchdown, and the airspeed reaches its peak during the RTO transition flight. In this case, the thrust inclination is reversed (aircraft pitched up) to reduce the airspeed and sink rate to meet their safety limits at touchdown. The maneuver time ranges from about 5 seconds to 15 seconds, depending on the altitude at which the engine failure occurs.

The effect of engine-failure altitude on the variation of rotor speed is also interesting. For higher engine-failure altitudes, the helicopter can build up airspeed to reduce the power requirement. This permits the rotor speed to increase, after the initial reduction, to replenish the rotational energy in the rotor. This energy is then used toward the end of the RTO transition flight to cushion the landing. For lower failure altitudes, the helicopter does not have enough altitude range to develop sufficient airspeed for any significant reduction in power required; the rotor speed therefore has to stay at the lower limit to reduce

profile power. The thrust coefficient increases gradually until at the end of the transition flight where it decreases, and the rotor speed increases owing to the ground effect. In reality, however, the pilot would likely increase collective pitch in the final seconds before landing, deleting the rotor speed below its calculated value.

Ground effect plays an important role in low speed landing, especially for helicopters with large rotors such as the study helicopter. In fact, calculations of the optimal RTO trajectories are also made without including the ground effect. Results indicate that there is no feasible solution for gross weight of 16,000 lb; a much lower weight has to be used. Therefore, one should consider the presence of ground effect in estimating the maximum payload capability. For VTOL operations from a ground-level confined heliport, ground effect is usually present. On building-top helipads, however, the ground effect is not always as pronounced, depending on the wind conditions. For consistency, all optimal trajectories of RTO and CL in this paper are computed with ground effect included.

Figure 7 shows the effect of helicopter gross weight on the optimal RTO trajectories for P_{OEI} = 1656 hp, V_0 = 5 kt, h_0 = 40 ft, γ_0 = 150°, and with several gross weight values ranging from 15,000 to 16,300 lb. Examinations of rotor-speed time histories in these optimal RTO solutions reveal the gross weight capability of the helicopter for a given OEI power level. For a larger gross weight, the rotor speed stays at the lower limit for a longer portion of the flight, and the final rotor speed is lower. Also, both the airspeed and descent rate reach higher peak values during the flight. No feasible solutions can be obtained if the gross weight is increased further. It was found that the maximum gross weight is defined by a rotor speed history that stays at the lower limit to the end of RTO transition flight.

Investigations were also made using higher OEI power levels and formulating the problem with an alternative performance index to Eq. (30) to minimize touchdown speeds with a constraint on touchdown point location. As expected, the results indicate that a larger limit of vertical descent rate or horizontal velocity component at touchdown allows the helicopter to carry more payload. However, the most effective way of increasing gross weight capability is by increasing the OEI contingency power available.

B. STOL

Minimum Runway Problem– Optimal trajectories that minimize the runway length required (Eq. (34)) are shown in Fig. 8 for the OEI initial conditions of h_0 = 20 ft, γ_0 = 6°, and V_0 = 60 ft/sec. The safe touchdown vertical and horizontal speed limits are 5 ft/sec and 40 ft/sec, respectively, and the gross weight ranges from 18,500 to 19,500 lb. The most interesting feature of the minimum runway RTO is that the optimal trajectories are relatively insensitive to the variation in gross weight. This general characteristic was also observed previously in the flight test with the S76B helicopter reported in Ref. 11.

Upon an engine failure, the thrust coefficient is decreased to reduce the power required; and at the same time, the thrust vector is tilted backward to the specified maximum limit of 10° to slow down the helicopter in the horizontal direction. After an initial droop in the rotor speed due to the OEI power transient, the rotor speed peaks to reach near its upper limit. As the helicopter approaches the ground, the rotor rotational energy is utilized, through an increase in the thrust coefficient, to arrest the sink rate to meet the safe touchdown speed limits. For the cases shown with initial altitude of 20 ft, the maneuver time is on the order of 4 sec, slightly shorter for a lighter weight configuration. The corresponding minimum airborne runway-length required in a rejected takeoff is on the order of 200 ft (a total runway length of 324 ft including the ground run). The rejected takeoff length increases as the initial altitude (at which an engine failure occurs) increases as discussed in Ref. 13.

Notice that the gross weight capability for STOL RTO transition flight is considerably higher than the maximum weight in a steady OEI climb shown in Table 1. Therefore, the gross weight capability in STOL operations is determined by the CTO segment of the flight, rather than the RTO segment. Because of a much lower speed region in which the VTOL RTO segment operates, compared with its STOL counterpart, the attendant higher power required dictates a considerably lower gross weight capability for the VTOL operation. This can be seen in Figs. 7 and 8. In fact, in contrast to the STOL case, it is the RTO segment of the flight, not the CTO, which limits the gross weight capability in VTOL operations, as will be discussed subsequently in the paper.

Maximum Takeoff Weight in STOL RTO– Numerical optimization to maximize the RTO gross weight using the performance index of Eq. (35) was conducted (Ref. 13). Extensive numerical runs using a range of h_0, V_0, and γ_0 indicated that the maximum RTO weights are between 21,000–23,000 lb. Therefore, the maximum takeoff weight in a Category-A runway (or STOL) takeoff is determined by continued takeoff and climbout (Table 1).

5.4 Continued Takeoff Flight

A. VTOL

Two optimization problems are investigated for CTO transition flight: (1) minimization of the runway length (Eq. (34)), and the minimization of the maximum altitude loss (Eq. (42b)). The main characteristics of the results are depicted in Figs. 9 and 10.

Figure 9 compares the optimal trajectories for the above two different performance indices. The flight conditions are W = 16,572 lb, V_0 = 2 ft/sec, γ_0 = 90, and U_2 = 46 ft/sec, with three values of the initial altitude, h_0, at 100, 120, and 140 ft. For minimizing the maximum altitude drop, the optimal trajectories have the identical shape for all three different altitudes at which an engine failure occurs. The control strategy is to rapidly tilt the thrust vector forward to its 10° limit to increase the forward speed, and to increase the collective (or thrust coefficient) to decrease the rotor speed down to its lower limit, trading all possible rotor rotational energy to gain altitude and airspeed. As the power deficiency diminishes with the increase in airspeed around 22 kt, the thrust vector can be rotated backward, somewhat gradually, to reduce the rate of descent and to initiate a climb.

Optimal trajectories that minimize the runway length behave differently for different initial altitude, as expected. As the initial altitude increases, the tradeoff between the potential energy and the rotor speed, and thus the control strategy for the thrust coefficient, is more apparent. The peak descent rate increases

and the rotor speed reaches higher values in the middle of the transition flight. Toward the end of the CTO transition flight, the thrust coefficient is increased more rapidly, thereby using the rotational energy reserve of the rotor to arrest the sink rate and then to meet the climb conditions. The control strategy for the thrust inclination remains essentially the same as that for the case of minimization of the maximum altitude drop when the initial altitude changes, resulting in almost identical behavior in airspeed. For all three initial altitudes, the final altitude reaches the same value at 35 ft. However, there is a slight reduction in both the maneuver time and the horizontal distance from those of minimization of the maximum altitude-loss case. The maneuver time for these CTO transition flights is on the order of 14 sec.

The effect of gross weight on the optimal CTO trajectories generated from the two performance indices is also evaluated, and the results are summarized in Fig. 10. It illustrates the tradeoff between gross weight and the vertical and horizontal space requirements. The OEI conditions are the same as those shown in Fig. 9, except that the initial altitude is fixed at 100 ft, with three values of gross weight set at 15,856, 16,209, and 16,572 lb (with corresponding U_2 = 38.75, 42.25, 45.75 ft/sec). For a lighter weight, the helicopter can minimize the horizontal distance required to achieve the desired steady OEI climb at the expense of a bigger altitude drop, or the altitude drop can be minimized at the expense of requiring a larger horizontal space. As the gross weight increases, the requirement for achieving the desired OEI climb conditions dominates the solution, and the difference between the optimal trajectories generated from the two performance indices becomes smaller and eventually yields identical solutions as the maximum gross weight is reached. Further increase in gross weight capability is possible through the use of a higher OEI power level, a larger initial airspeed, or a higher initial altitude and thus a larger altitude drop range. Similarly, a lower permissible altitude to clear in a CTO, e.g., the 15 ft recently recommended by the JAA instead of the 35 ft used in this paper to meet the FAA rules, should increase somewhat the gross weight capability, as far as CTO is concerned.

Note that the above results are obtained using the initial flightpath angle, $\gamma_0 = 90°$ starting from the added small vertical climb segment near the TDP in the backup takeoff procedure (see Fig. 2(a)). Without the addition of this vertical segment, the initial condition for the glideslope would be $\gamma_0 = 150°$. If this initial condition is used, optimal CTO trajectories will start with a rearward motion, similar to those shown in Figs. 6 and 7. The pilot usually prefers to fly forward immediately following an engine failure in the CTO transition flight, thus a brief vertical climb segment around the TDP is included in the nominal AEO takeoff path. When $\gamma_0 = 150°$ is used, the above conclusions are still valid, since the initial flightpath angle does not have significant effect on the CTO paths at low speed.

B. STOL

Minimum Runway-Length Problem– Extensive trajectory optimization runs were made to investigate the effects of initial states, V_0, h_0, γ_0, and gross weight. These represent the energy state and the power-required level at the moment when an engine failure occurs. Figure 11 shows the effect of the initial airspeed on the optimal CTO trajectories that minimize the runway length (Eq. (34)) for h_0 = 20 ft, $\gamma_0 = 6°$, Ω_0 = 100%, with U_2 = 70 ft/sec and W = 19,123 lb (see Table 1). Upon an engine failure, the optimal control strategy is to rapidly tilt the thrust vector forward about 5° to initiate an acceleration, and at the same time gradually increase the thrust coefficient to reduce the rotor RPM to its lower limit, hence reducing the power required to match the available OEI power. In all but the largest initial-airspeed case, which has a higher associated initial energy level, the rotor speed stays at the lower limit for the entire CTO transition flight. As the airspeed increases to within about 3 to 4 ft/sec of the desired final airspeed, the thrust vector is gradually rotated back to initiate a climbout and to meet the desired final conditions. The maneuver time for the entire CTO transition flight lasts for about 7 to 12 sec, and the horizontal distance ranges from about 480 to 840 ft, with the lowest initial-airspeed case taking the longest time and covering the longest distance.

Thus, for a given initial airspeed, V_0, the higher the value of V_{TOSS}, the longer the runway length is required for the CTO transition flight, although a higher speed provides a higher gross weight capability in steady OEI climbout (see Table 1). To determine a suitable value of V_{TOSS} for a given value of V_0, numerical experiments were conducted by varying their differences with values ranging from 5 to 20 ft/sec and with various initial conditions. Results show that a value of about 10 to 15 ft/sec provides a good compromise between the required runway length and the gross weight capability. Figure 12 shows a sample set of results using the initial conditions of V_0 = 50 ft/sec, h_0 = 20 ft, and $\gamma_0 = 5°$. The suitable range of $\Delta V = V_{TOSS} - V_0$ = 10 to 15 ft/sec, thus determined, appears to be consistent with the flight manual instructions of the Super Puma (Ref. 40). Based on flight test results of the S76-B, Ref. 11 also suggested that a 10-kt difference between V_{TOSS} and V_0 is appropriate for achieving balanced field length.

Thus, an alternative way of minimizing the runway length can be formulated with a fixed value of $V_{TOSS} - V_0$, such as $V_{TOSS} = V_0 + 15$ ft/sec, and minimizing the runway length for various weights. This approach offers consistency since the pilot does not have to adjust V_{TOSS} when the takeoff weight changes, as is required in the preceding formulation. Results from this alternative formulation are discussed in Ref. 13.

Maximum Takeoff Weight for CTO– The maximum takeoff weight problem to maximize the performance index (Eq. (35)) subject to the specified length (Eq. (43)) turns out to be a dual of the minimum runway problem for a given takeoff weight discussed above. The specified takeoff weight in the minimum runway-length problem is, in fact, the same as the solution to the maximum weight problem if the minimum runway length obtained from the first problem is specified for the second problem. Numerical solution of the optimal trajectories from the two problems was found to be almost identical in Ref. 13.

As the specified runway length decreases, the maximum weight attainable for the OEI CTO transition flight also decreases. As a result, the maximum takeoff weight in CTO is determined by the steady OEI climb requirements if the runway length is sufficient, and is otherwise determined by the available runway length.

5.5 Balked Landing

Regulations require that a balked landing must be possible for an engine failure occurring at and prior to the landing decision point along the nominal AEO landing path. The terminal

conditions for a BL transition flight are the same as for the CTO transition flight described earlier, except for the use of the balked landing safety speed, V_{BLSS}, instead of the takeoff safety speed, V_{TOSS}. However, the two safety speeds are often selected to be the same.

A. VTOL

The results of balked landing optimal trajectories are generally similar to those of continued takeoff. However, balked landing results have some unique characteristics. Due to a higher initial airspeed and a lower power required in a descent, a balked landing for an engine failure occurring at a higher altitude provides a larger gross weight capability compared with its continued takeoff counterpart. Also, since the airspeed decreases along the nominal AEO landing path, the maximum gross weight possible in a balked landing reduces significantly as the altitude decreases.

B. STOL

The optimal trajectories for the STOL balked landing transition flights are again generally similar to those of STOL continued takeoff. Figure 13 shows the effect of the initial airspeed on the minimum runway-length optimal BL trajectories for $W = 19{,}123$ lb, $U_2 = 70$ ft/sec, with the initial OEI flight conditions of $h_0 = 125$ ft and $\gamma_0 = -3°$. Upon an engine failure, the optimal control strategy is to rapidly tilt the thrust vector forward, some 7° to 9° depending on the initial airspeed, to accelerate the aircraft and reduce the power required. At the same time, the thrust coefficient is increased to reduce the rotor RPM to its lower limit, further reducing the power required to accommodate the power loss. As the airspeed increases, and thus the power required decreases, the thrust vector is rotated back to initiate a climbout and to meet the specified final conditions. The transitional flight time is on the order of 8 sec. The horizontal distance covered is about 530 ft.

This optimal control strategy is very similar to that used in the CTO case shown in Fig. 11. However, because of the higher initial altitude and the attendant higher potential energy for the BL case, the rotor rotational energy is partially replenished during the ensuing transition flight, and is then used to assist the climb. At the end of the transition flight the rotor speed reaches the lower limit, and the power required matches the power available, thus establishing the desired steady OEI climb.

5.6 Continued Landing Flight

A. VTOL

Optimal trajectories that minimize the heliport size requirement (Eq. (30)) are calculated for OEI-CL transition flight with various initial conditions. Results show some features are significantly different from those of the RTO counterpart in VTOL operations, which are generated from the same performance index as discussed previously.

Figure 14 shows a set of sample results with $W = 16{,}000$ lb, $P_{OEI} = 1656$ hp, and $\gamma_0 = -6°$. Because of a higher initial velocity associated with a higher initial altitude along the AEO landing path, the optimal OEI-CL trajectories are considerably different for an engine failure occurring at different altitudes. This is a result of the difference not only in the initial energy state (such as the case of RTO shown in Fig. 6), but also in the power required at the moment when an engine loses its power. For example, at $h_0 = 100$ ft with the associated initial airspeed, $V_0 = 59$ ft/sec (or 35 kt), the power required on the AEO landing path with a 6° glideslope is less than the OEI power available for the gross weight of 16,000 lb. Since the OEI available power is assumed to automatically increase to its maximum after an engine failure, the helicopter experiences a power excess and has to increase its power required to match the power available. As a result, the rotor speed increases. As shown in the figure, a similar situation also occurs for the initial conditions of $h_0 = 80$ ft and $V_0 = 50.6$ ft/sec. As the initial altitude and airspeed decrease along the nominal AEO landing path, the power required increases, and the optimal OEI CL trajectories are gradually characterized by a power deficiency, resembling those of the RTO shown in Fig. 6. Thus, for the lower altitude and lower airspeed cases, the rotor speed reduces to and stays at its lower limit until near touchdown, where it increases due to the ground effect. In actuality, however, the pilot would likely increase the collective in the final seconds before touchdown and reduce the rotor speed to below the calculated value.

The maximum gross weight is limited by continued landing at lower initial altitudes along the nominal AEO landing path that was considered. In fact, no feasible solutions can be obtained when the gross weight is increased to 16,500 lb or higher for continued landing starting at $h_0 = 25$ ft and $V_0 = 0$. Gross weight capability increases as the initial altitude and the associated initial airspeed increase. This limitation is consistent with the typical H-V diagram of a helicopter.

B. STOL

The landing decision point (LDP) is usually chosen such that its necessary energy level, together with its limited decreasing rate, permits a successful OEI-BL flight. As a result, the LDP altitude is typically 100 ft or higher, airspeed at LDP is usually a moderate 40 kt or so, and rate of descent is limited to about 400 fpm or lower. Because of the higher initial altitude together with a lower power required in a descent, the OEI-CL trajectories that minimize the runway length (Eq. (34)) have characteristics distinctively different from its RTO counterpart.

Figure 15 shows a family of minimum runway OEI-CL trajectories calculated for a range of gross weights with the initial conditions, $h_0 = 125$ ft, $\gamma_0 = -3°$, and $V_0 = 55$ ft/sec. Compared with its RTO counterpart as shown in Fig. 8, it is seen that, while the control strategy for the thrust coefficient and thus the resulting descent rate and rotor speed are generally similar, the control strategy for the thrust inclination and the resulting horizontal speed response are considerably different. Because of the lower power required in a descent together with a higher energy level at the moment when an engine failure occurs in the case of OEI CL, there is more exchange taking place among the helicopter potential, kinetic and rotor rotational energy sources. This is reflected in the control reversals, especially in the thrust inclination. Unlike the RTO case, the change in gross weight does alter significantly the time histories of the control inclination and the attendant speed. The helicopter has to maintain a higher airspeed during the transition flight to carry a heavier load. For the conditions shown, the CL transition flight time is slightly over 8 sec, depending on the gross weight, and is about twice as long as that of the RTO transition flight. It also covers a longer horizontal distance, some 340 ft, and is about 70% longer than that required for the RTO.

5.7 Conditions of the Decision Points

Definition of specific conditions of the takeoff decision point and landing decision point requires a comprehensive evaluation of the effects of weight, altitude, temperature and wind conditions using a high-fidelity mathematical model of the helicopter. While the augmented point mass model used in this paper falls short of meeting the requirements, it is useful, nevertheless, for exploring the basic tradeoffs in Category-A terminal area operations. Two concepts related to the choice of the takeoff decision point for STOL and VTOL Category-A operations are discussed in the following paragraphs.

Takeoff Decision Point – STOL

By combining the results of CTO and RTO, some insights into the choice of the takeoff decision point can be obtained. Figure 16 shows such a combined plot, indicating the minimum runway field lengths required for both the RTO and CTO for the flight conditions at $V_0 = 50$ ft/sec, $W = 18{,}610$ lb, and $\gamma_0 = 5°$, 7°, and 9°. The total runway lengths required are calculated by combining the airborne segments (the AEO segment and the OEI transition flight segment) and ground run in the case of RTO.

$$X_{CTO} = \frac{V_0^2}{0.4g} + \frac{h_0 - 5}{\tan\gamma_0} + x_{f\cdot cto} \quad \text{(ft)} \quad (44)$$

$$X_{RTO} = \frac{V_0^2 + u_{\max}^2}{0.4g} + \frac{h_0 - 5}{\tan\gamma_0} + x_{f\cdot rto} \quad \text{(ft)} \quad (45)$$

The choice of decision height can now be made with the aid of Fig. 16. For example, if one opts to use the criterion of balanced field length (BFL), whereby the RTO and CTO require the same runway length, TDP altitude will be 23.5 ft for an initial flightpath angle of 5°. As the initial flightpath angle increases, the TDP altitude and the corresponding BFL decrease. This figure can also be used to determine the best TDP altitude for unbalanced field length, if heliport configurations so dictate.

The choice of the TDP velocity affects both the runway length and the gross weight capability. Since the CTO flight segment determines the maximum takeoff weight capability, a higher TDP velocity results in a higher payload capability. However, this requires a longer runway length.

Balanced-Weight Concept for TDP Altitude– VTOL

For a given OEI power and the specified AEO VTOL flightpath, the gross weight capability is determined by the rejected takeoff and the continued landing flight phases. The maximum gross weight possible in a RTO or a CL is limited by the high power required at low speeds and by the shape of the OEI H-V diagram. To land safely on the helipad, the airspeed has to be low. As discussed earlier, rejected takeoffs are most difficult for engine failures occurring at a certain band of altitudes reflective of the OEI H-V diagram. Once above this critical altitude band, there is no advantage in locating the TDP altitude very high, since it must be possible to achieve a safe RTO at any point up to the TDP. However, from the perspective of the CTO or BL, gross weight capability is increased with the increase in the TDP altitude. Since the takeoff gross weight capability is limited by the lower of the maximum gross weights possible in the RTO or in the CTO, it is proposed to use a "balanced-weight" criterion for determining the TDP altitude. At this altitude, the maximum gross weight in CTO is about the same as that in RTO.

5.8 Real-Time Generation of Optimal Trajectories

As discussed in the preceding section, the optimal control strategies and the associated optimal trajectories are sensitive to the initial conditions. It is a challenge, therefore, to convey these optimal control strategies to assist the pilot, in a timely fashion, to cope with the situation when an engine failure occurs. Due to the large number of states and constraints, numerical solutions usually take a long time, even on a mainframe computer. The capability to provide a reliable real-time generation of optimal trajectories on board the aircraft with limited computing power and memory is extremely challenging.

A technique for real-time generation of *approximate* optimal trajectories has recently been proposed (Ref. 20) based on curve-fitting and interpolation. First, the optimal trajectories are solved off-line in a manner similar to that described in this paper. These off-line computed optimal trajectories are then approximated with a Fourier series. Finally, the Fourier coefficients are interpolated with multi-dimensional polynomials of initial conditions (i.e., $h_0, V_0, \gamma_0, \Omega_0$) and the control parameters, W, P_{OEI}. To facilitate this difficult interpolation process, a special scheme was devised to reduce the multi-dimensional fitting problem into several smaller independent problems in a nested fashion. Details are discussed in Ref. 20.

6. CONCLUSIONS

This paper summarizes some key results of a series of trajectory optimization studies conducted to examine basic characteristics of a twin engine helicopter in Category-A, one-engine-inoperative, takeoff and landing operations. Using an eight state, two controls, augmented point-mass model representative of the study helicopter, rejected takeoff, continued takeoff, balked landing, and continued landing are investigated for both vertical takeoff and landing to or from a helipad and short takeoff and landing to or from a clear heliport. For VTOL operations, a linear backup procedure is assumed for normal all-engine-operating takeoff, and a straight-in procedure for normal landing. In rejected takeoff and continued landing, optimal trajectories are calculated to minimize the deviations of the touchdown point from the original takeoff point, subject to safe touchdown speed limits. For continued takeoff and balked landing, two performance indices are considered: one minimizes the horizontal distance, and the other minimizes the maximum altitude drop. Both are subject to terminal constraints corresponding to the steady OEI climb required by the FAA regulations. In STOL operations, which use a typical normal AEO takeoff and landing procedure, two trajectory optimization problems are formulated for OEI transitional flight: one to minimize the runway length requirements and another to maximize the takeoff weight. Both are subject to appropriately specified terminal conditions. The major results from these extensive optimization studies show that:

1. The rejected takeoff and continued landing flight phases determine the maximum gross weight capability for VTOL Category-A operations. For STOL operations, it is the continued takeoff and balked landing flight phases that limit the gross weight capability.

2. In an OEI transitional flight, the optimal control strategies are such that they maneuver the helicopter to match the power required to the level of the OEI contingency power available, along the way trading among the helicopter's potential, kinetic, and rotor rotational energy sources.

3. For a VTOL rejected takeoff, the typical optimal control strategy after an engine failure is to tilt the thrust vector forward initially to increase the airspeed and to increase the thrust coefficient to reduce the rotor speed, thereby reducing the power required. Subsequently, the thrust vector is tilted backward to arrest the sink rate and reduce airspeed to satisfy the safe touchdown speeds. In contrast, for a STOL RTO transitional flight, the thrust vector is tilted backward to its specified limit to reduce the horizontal speed, and at the same time the collective is reduced to increase the rotor speed. Collective is then increased to arrest the sink rate and to make use of the rotor rotational energy for cushioning the landing. The STOL RTO trajectories are relatively insensitive to gross weight variation. The RTO transitional flight is typically very short, on the order of only 4 sec.

4. Upon an engine failure in a VTOL continued takeoff, the optimal control strategy is to tilt the thrust vector forward to its specified limit to accelerate the helicopter toward V_{TOSS}, and to increase the collective to reduce the rotor speed to its lower limit, trading the rotor rotational energy to gain airspeed and altitude. Depending on how the collective is used and the rotor speed is managed, one can trade off the horizontal distance required with the maximum allowable altitude drop. Optimal control strategies for STOL CTO are generally similar to those for the VTOL counterpart; however, because of a higher initial airspeed, the thrust vector is tilted forward less than in the VTOL CTO case.

5. The balked landing and continued landing are generally similar to CTO and RTO, respectively. However, because of the lower power required associated with a descent, coupled with a higher energy level at the moment when an engine failure occurs, more energy exchange takes place for a typical BL or CL, reflecting in more control reversals, especially in the thrust inclination.

6. A balanced field length concept can be used for determining the takeoff-decision-point altitude for STOL operations. Similarly, a balanced-weight concept can serve as a means of determining the TDP altitude for VTOL operations. These concepts are described in section 5.7.

7. The differential between V_{TOSS} and the TDP airspeed of 10 to 15 ft/sec is shown to be a desirable range from the optimization studies, which is consistent with the flight test results of the S76B and flight manual of the Super Puma.

8. Ground effect is found to be important in trajectory optimization for VTOL RTO and CL transitional flight phases, especially in the determination of the maximum gross weight capability.

REFERENCES

1. FAA Advisory Circular, Certification of Transport Category Rotorcraft, AC-29A, 1987.

2. Draft JAR 29 Subpart B Performance Requirements, NPA 29-2, Preliminary Issue 1, undated.

3. Lande, K.: New Offshore Helicopter Rig Takeoff and Landing Procedures. Proceedings of Society of Experimental Test Pilots 33rd Symposium, Sept. 1989, pp. 179–204.

4. Stevens, J.M.G.F. and Vodegel, H.J.G.C.: S-76B Certification for Vertical Take- Off and Landing Operations from Confined Areas. 16th European Rotorcraft Forum, Glasgow, UK, Sept. 1990.

5. Vodegel, H.J.G.C. and Stevens, J.M.G.F.: A Computer Program for the Certification of Helicopter Vertical Takeoff and Landing Operations and an Application to the S-76B Helicopter. Proc. AHS Annual Forum, May 1991, pp. 721–731.

6. Goldenberg, J., Meslin, L., Blondino, M., and Williams, D.: Certification of Model 230 Helicopter for Category 'A' Elevated Helipad Operations. Proc. AHS Annual Forum, May 1993, pp. 1497–1505.

7. Wood, T. L., Blondino, M., and Williams, D.: M 230 Helicopter Performance for Category A Elevated Helipad Operation. 19th European Rotorcraft Forum, Cernobbio, Italy, Sept. 1993.

8. Okuno, Y. and Kawachi, K.: Optimal Takeoff of a Helicopter for Category A STOL/VTOL Operations. Journal of Aircraft, Vol. 30, No. 2, March–April, 1993, pp. 235–240.

9. Sharma, V., Zhao, Y., and Chen, R.T.N.: Optimal Sideway Operation of a Category-A Helicopter from an Elevated Helipad. AHS Annual Forum, June 4–6, 1996.

10. Zhao, Y., Jhemi, A. A., and Chen, R.T.N.: Optimal VTOL Operation of a Multiengine Helicopter in the Event of One Engine Failure. AIAA Paper 95-3178, Aug. 1995.

11. Saal, K. W. and Cole, J. L.: Category 'A' Certification of S-76B Featuring Variable CDP and V2 Speeds. J. AHS, July 1990, pp. 12–21.

12. Cerbe, T. and Reichert, G.: Optimization of Helicopter Takeoff and Landing. J. Aircraft, Vol. 26, No. 10, Oct. 1989, pp. 925–931.

13. Zhao, Y. and Chen, R.T.N.: Critical Considerations for Helicopters During Runway Takeoffs. J. Aircraft, Vol. 32, No. 4, July–August 1995, pp. 773–781.

14. Sharma, V.: Optimal Helicopter Operation from a Clear Heliport in the Event of One Engine Failure. Ph.D. Dissertation, Dept. of Aerospace Engr. and Mechanics, University of Minnesota, Nov. 1994.

15. Sharma, V., Zhao, Y., Chen, R.T.N., and Hindson, W. S.: Optimal OEI Clear Heliport Operation of a Multiengine Helicopter. Proc. AHS Annual Forum, May 1995.

16. Schmitz, F. H.: Optimal Takeoff Trajectories of a Heavily Loaded Helicopter. J. Aircraft, Vol. 8, No. 9, Sept. 1971, pp. 717–723.

17. Johnson, W.: Helicopter Optimal Descent and Landing After Power Loss. NASA TM-73244, May 1977.

18. Lee, A. L., Bryson, A. E., and Hindson, W. S.: Optimal Landing of a Helicopter in Autorotation. J. Guidance, Control, and Dynamics, Vol. 11, No. 1, Jan.–Feb. 1988, pp. 7–12.

19. Okuno, Y., Kawachi, K., Azuma, A. and Saito, A.: Analytical Prediction of Height- Velocity Diagram of a Helicopter Using Optimal Control Theory. J. Guidance, Control, and Dynamics, Vol. 14, No.2, Mar.–Apr. 1991, pp. 453–459.

20. Jhemi, A. A., Zhao, Y., and Chen, R.T.N.: Real-Time Generation of Optimal Helicopter Trajectories for Cockpit Display. AIAA Paper 96-0792, AIAA Aerospace Sciences Meeting, Reno, NV, Jan. 1996.

21. Talbot, P. D., Tinling, B. E., Decker, W. A., and Chen, R.T.N.: A Mathematical Model of a Single Main Rotor Helicopter for Piloted Simulation. NASA TM-84281, Sept. 1982.

22. Johnson, W.: Helicopter Theory. Princeton University Press, 1980, pp. 282–283.

23. Gessow A. and Myers, G. C., Jr.: Aerodynamics of the Helicopter, Frederick Ungar Publishing Co., New York, 1952.

24. Stepniewski, W. Z. and Keys, C. N.: Rotary-Wing Aerodynamics, Dover Publications, Inc., 1984.

25. Chen, R.T.N.: A Survey of Nonuniform Inflow Models for Rotorcraft Flight Dynamics and Control Applications. NASA TM-102219, Nov. 1989.

26. Cheeseman, I. C. and Bennett, N. E.: The Effect of the Ground on a Helicopter Rotor in Forward Flight. British R&M, No. 3021, Sept. 1955.

27. Prouty, R. W.: Helicopter Performance, Stability, and Control, Krieger Publishing Co., 1990, p. 698.

28. Curtiss, H. C., Jr., Sun, M., Putman, W. F., and Hanker, E. J.: Rotor Aerodynamics in Ground Effect at Low Advance Ratios. J. AHS, Vol. 29, No. 1, Jan. 1984.

29. Cerbe, T., Reichert, G., and Curtiss, H. C., Jr.: Influence of Ground Effect on Helicopter Takeoff and Landing Performance. Paper No. 70, 14th European Rotorcraft Forum, Milano, Italy, Sept. 20–23, 1988, pp. 70-1 to 70-17.

30. Hirschkron, E., Martin E., and Samanich, N.: Powerplant Design for One Engine Inoperative Operation. Vertiflite, Vol. 30, No.5, July/August 1984, pp. 34–38.

31. Trivier, D. and Bosqui, O.: 30-Second/2-Minute One Engine Inoperative Certification for the AS 332 Super Puma MK II. Proc. 18th European Rotorcraft Forum, Sept. 1992, pp. 129-1 to 129-15.

32. Dept. of the Army: Operator's Manual: UH-60A and EH-60A Helicopters. TM 55-1520-237-10, Jan. 1988.

33. Ballin, M. G. and Dalang-Secretan, M. A.: Validation of the Dynamic Response of a Blade-Element UH-60 Simulation Model in Hovering Flight. J. AHS, Vol. 36, No. 4, Oct. 1991, pp. 77–88.

34. Howlett, J. J.: UH-60A Black Hawk Engineering Simulation Program. Vol. 1, NASA CR-166309, Dec. 1981.

35. Hilbert, K. B.: A Mathematical Model of the UH-60 Helicopter. NASA TM-85890, April 1984.

36. Johnson, C. D.: Optimal Control with Chebyshev Minimax Performance Index. J. Basic Engineering, June 1967, pp. 251–262.

37. Miele, A., Lamoulakis, J. N., Cloutier, J. R., and Tietze, J. L.: Sequential Gradient Restoration Algorithm for Optimal Control Problems with Non-differential Constraints. J. of Optimization Theory and Applications, Vol. 13, No. 2, Feb. 1974, pp. 218–255.

38. Zhao, Y.: Several Trajectory Optimization Problems. Dept. of Aerospace Engineering and Mechanics, University of Minnesota, 1989.

39. Jacobson, D. H. and Lele, M. M.: A Transformation Technique for Optimal Control Problems with a State Variable Inequality Constraint. IEEE Trans. Automatic Control, Vol. AC-14, No. 5, Oct. 1969, pp. 457–464.

40. Super Puma MK2 Supplement for Category A Operations. Undated Flight Manual.

APPENDIX: HELICOPTER PARAMETERS USED FOR OPTIMIZATION STUDIES

The study helicopter has a maximum takeoff weight of 22,000 lb and a maximum takeoff power of 3,086 shp. Other related parameters are: R = 26.83 ft, σ = 0.0821, Ω_0 = 27 rad/sec, $C_{T_{max}}$ = 0.01846, and I_R = 7,060 slug ft^2. Parameter values used in the optimization studies are: f_e = 30 ft^2, ρ = 0.002377 slug/ft^2, g = 32.2 ft/sec^2, $c_{\bar{d}}$ = 0.012, η = 0.9, K_{ind} = 1.15, β_{max} = 10°, β_{min} = −10°, Ω_{max} = 107%, Ω_{min} = 91%, w_{max} = 5 ft/sec, u_{max} = 15 ft/sec for VTOL and 40 ft/sec for STOL, τ_p = 1.5 sec, P_a = 47.3 hp, $P_{OEI,110\%}$ = 1656 hp, and $P_{OEI,105\%}$ = 1580 hp. The thrust constraints used in the optimizations are: $C_{T_{min}}$ = 0.002 and $C_{T_{max}}$ = 0.025; these limits are not encountered in the optimization process.

Table 1: Maximum weight in steady OEI climb (P_{OEI} = 1656 hp; SLS; climb rate = 100 fpm; 100% RPM)

U_2, fps	W, lb
55	17,554
60	18,086
65	18,610
70	19,123
75	19,621
80	20,101
85	20,561
90	20,999
95	21,413
100	21,802

(a)

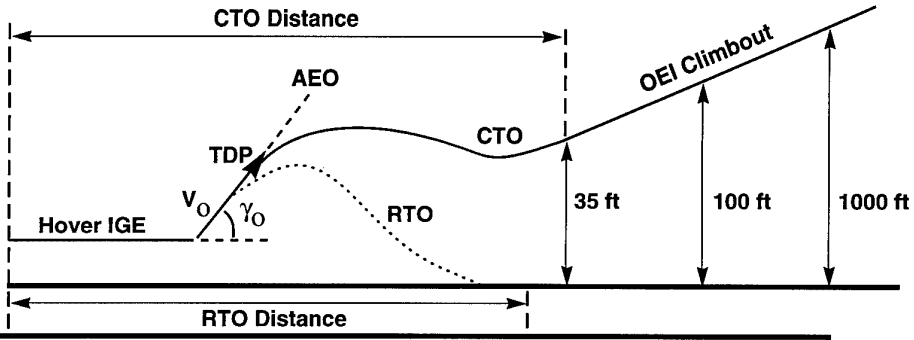

FAA OEI STOL Takeoff Requirements				
Rating	AEO TOP*	2.5 min	2.5 min	30 min
Airspeed	0 → V_{TDP}	V_{TDP} → V_{TOSS}	V_{TOSS}	V_Y
R/C, fpm	N/A	N/A	100	150
Rotor rpm	N/A	N/A	N/A	100%

*TOP = Takeoff Power

(b)

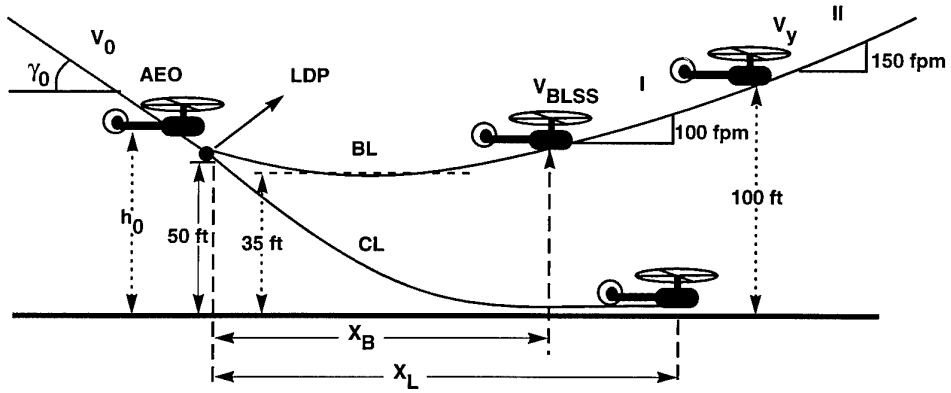

Fig. 1: Category-A clear heliport (or STOL) operation: (a) takeoff, (b) landing.

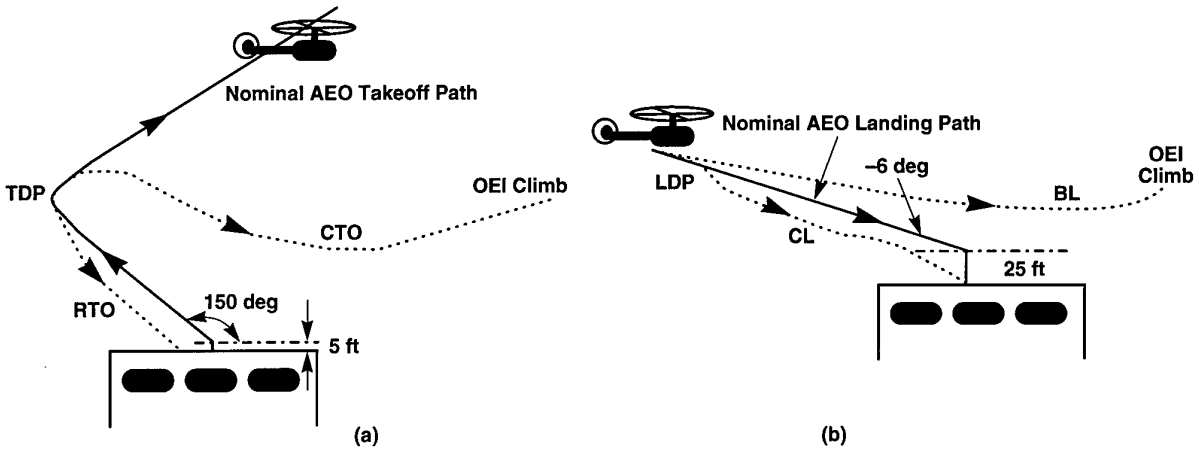

Fig. 2: Example VTOL Category-A operation: (a) backup takeoff, (b) landing.

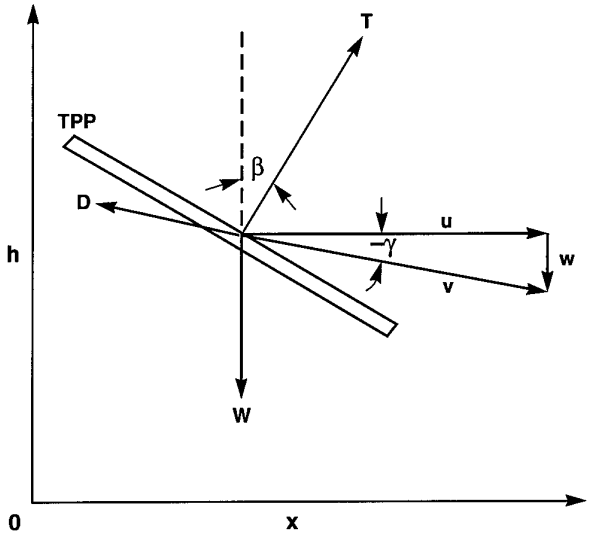

Fig. 3: Point-mass helicopter model.

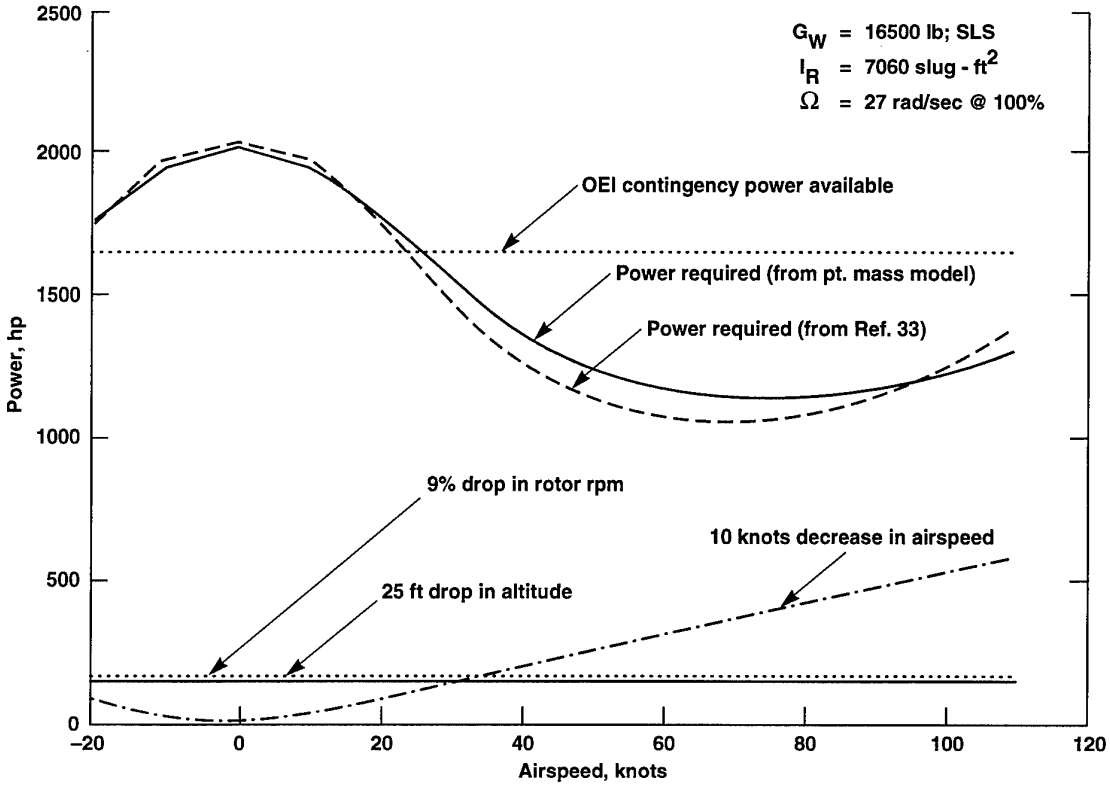

Fig. 4: Power components available for tradeoff in OEI maneuver – 5-sec average.

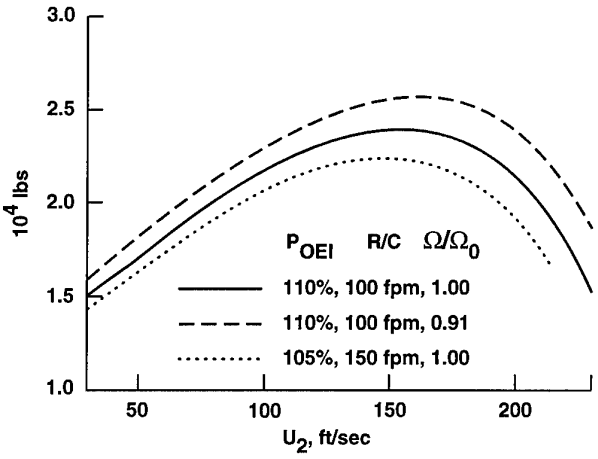

Fig. 5: Maximum weight in steady OEI climb.

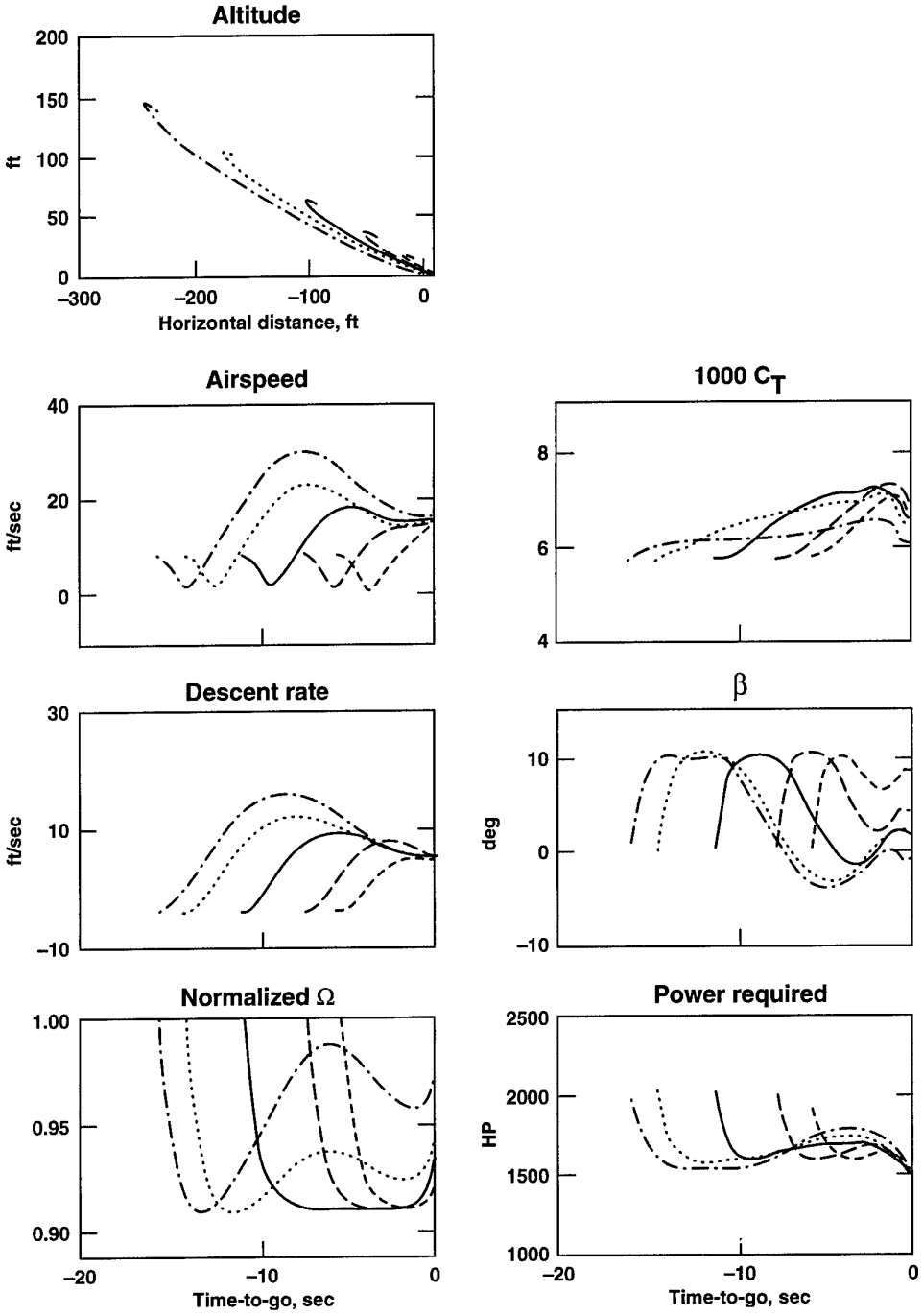

Fig. 6: Optimal VTOL- RTO trajectories: $W = 16{,}000$ lb, $P_{OEI} = 1656$ hp, $V_0 = 8.4$ ft/sec, and $\gamma_0 = 150°$.

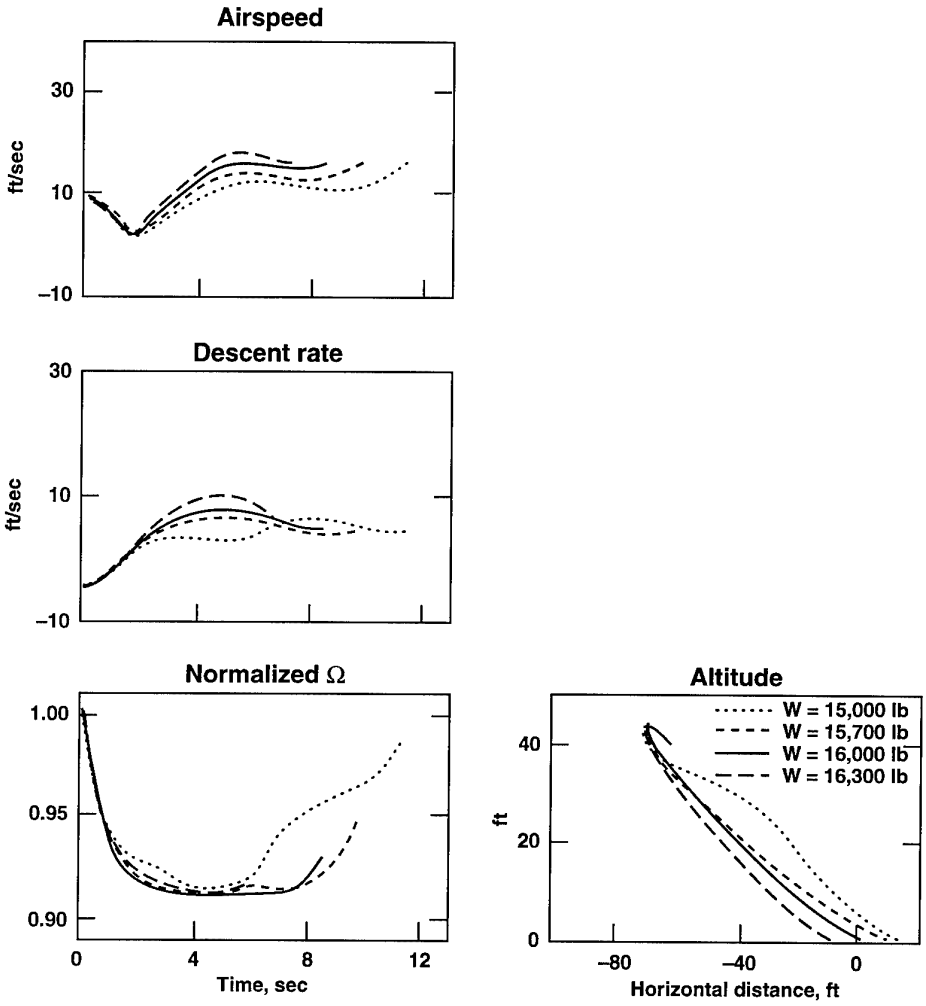

Fig. 7: Effect of helicopter gross weight on optimal VTOL- RTO trajectories: P_{OEI} = 1656 hp, h_0 = 40 ft, V_0 = 8.4 ft/sec, and γ_0 = 150°.

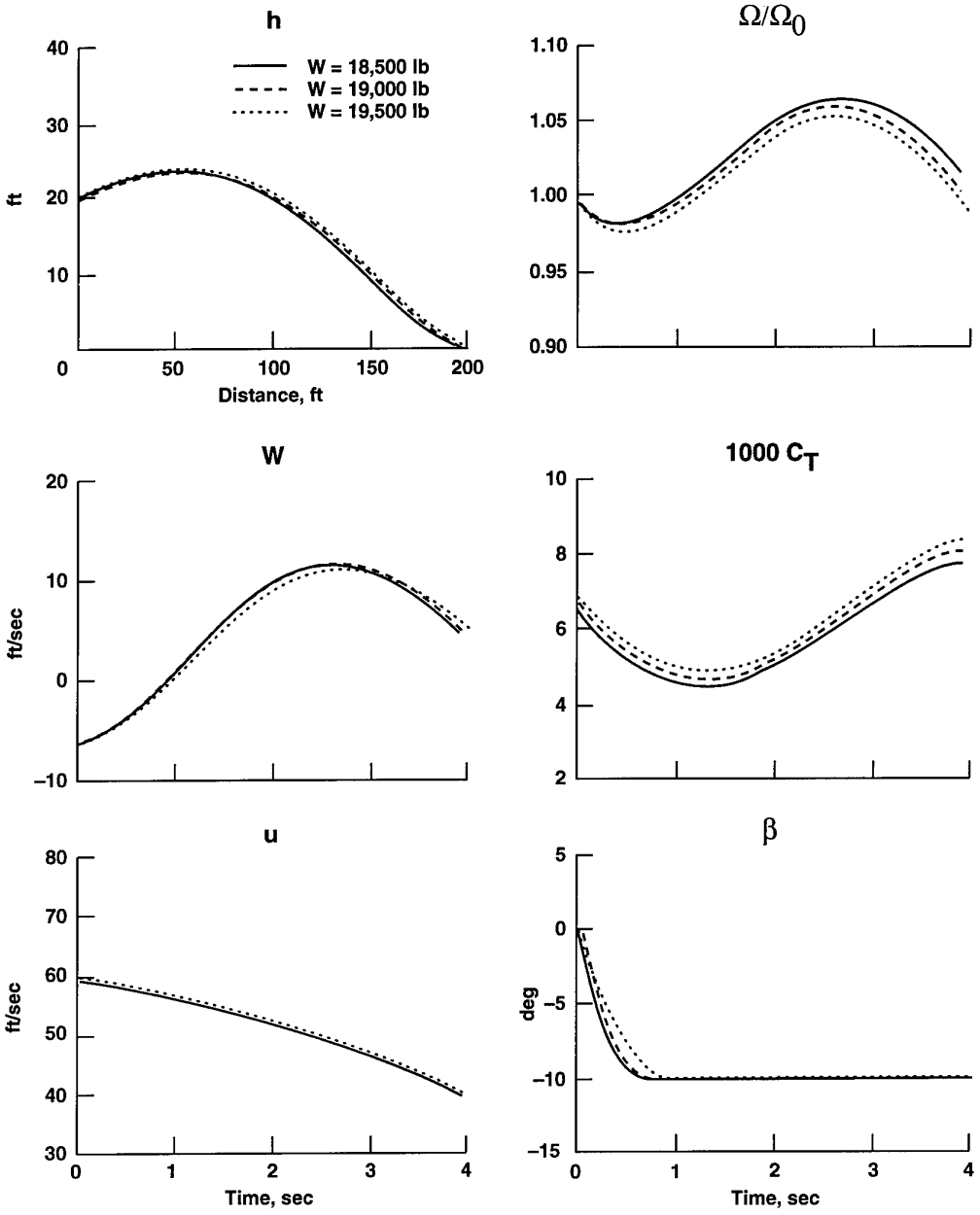

Fig. 8: Effect of helicopter gross weight on optimal STOL - RTO trajectories: P_{OEI} = 1656 hp, h_0 = 20 ft, V_0 = 60 ft/sec, and $\gamma_0 = 6°$.

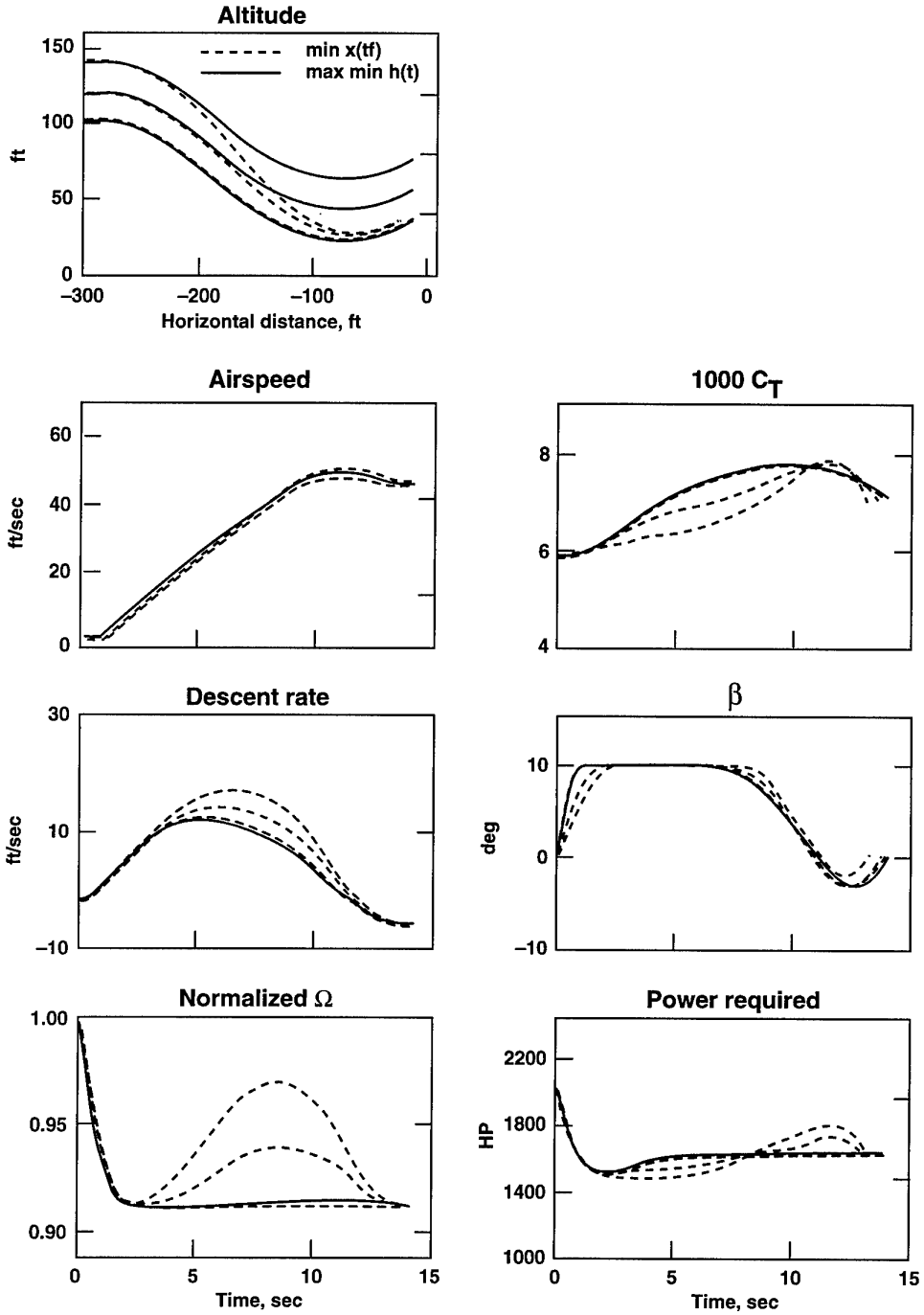

Fig. 9: Optimal VTOL- CTO trajectories: $W = 16{,}572$ lb, $U_2 = 46$ ft/sec, $P_{OEI} = 1656$ hp, $\gamma_0 = 90°$, and $V_0 = 2$ ft/sec.

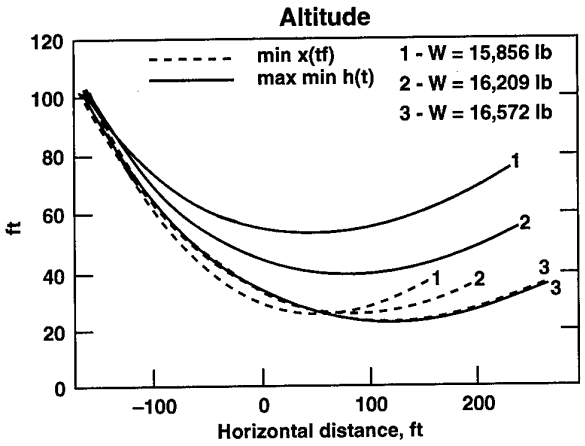

Fig. 10: Effect of gross weight and performance indices on VTOL- CTO trajectories: P_{OEI} = 1656 hp, h_0 = 100 ft, V_0 = 2 ft/sec, and $\gamma_0 = 90°$.

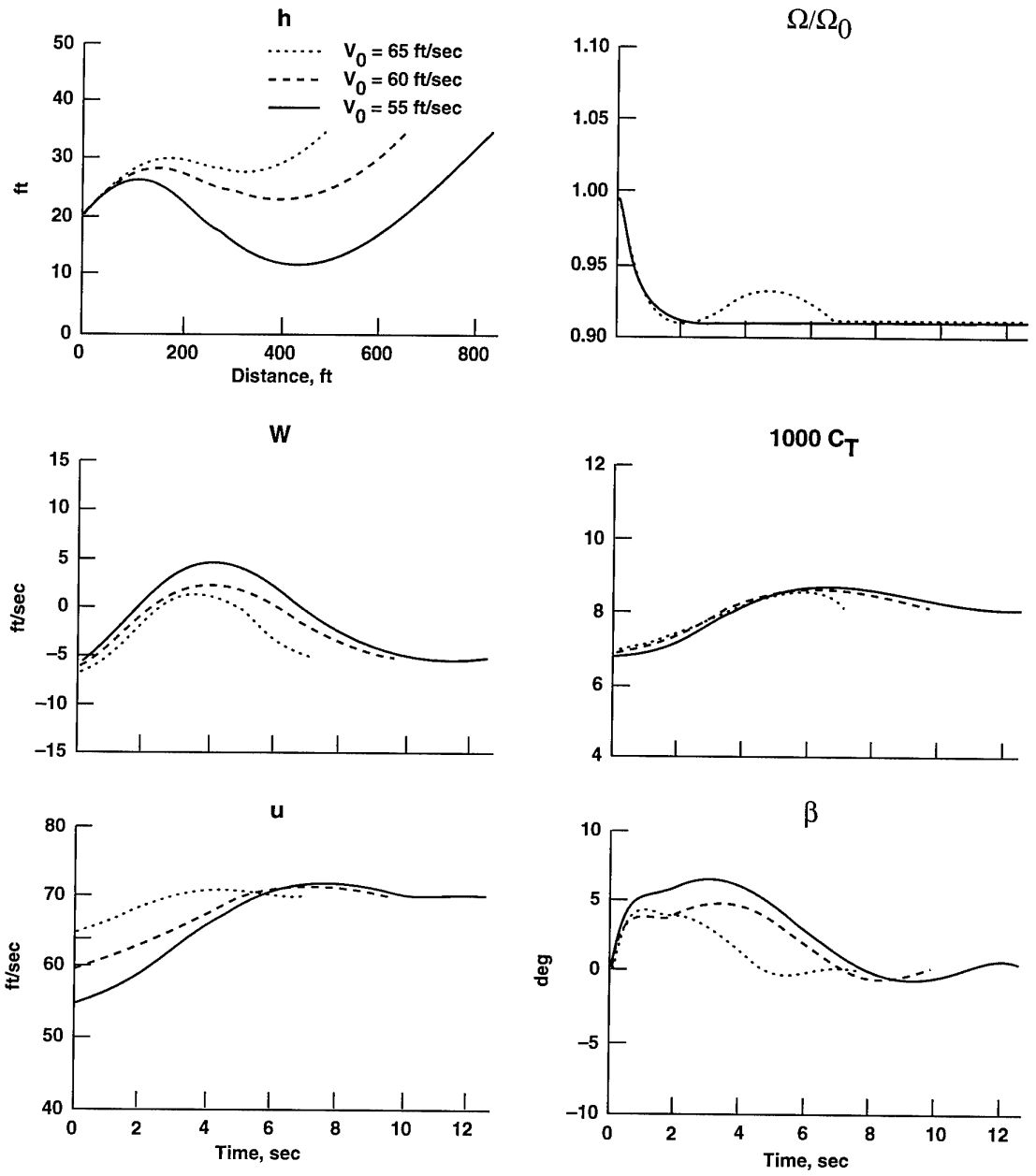

Fig. 11: Minimum runway STOL- CTO with different initial airspeeds: $h_0 = 20$ ft, $\gamma_0 = 6°$, $W = 19{,}123$ lb, and $U_2 = 70$ ft/sec.

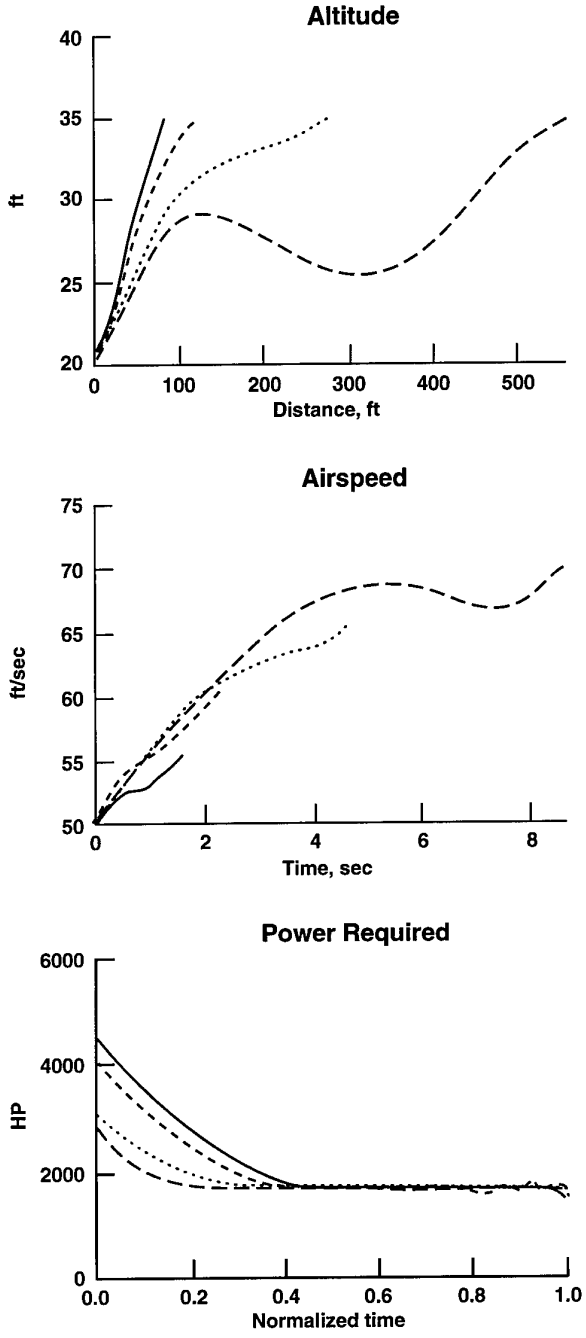

Fig. 12: Effect of U_2 in OEI minimum runway-length STOL- CTO (gross weight varied with U_2 shown in Table 1).

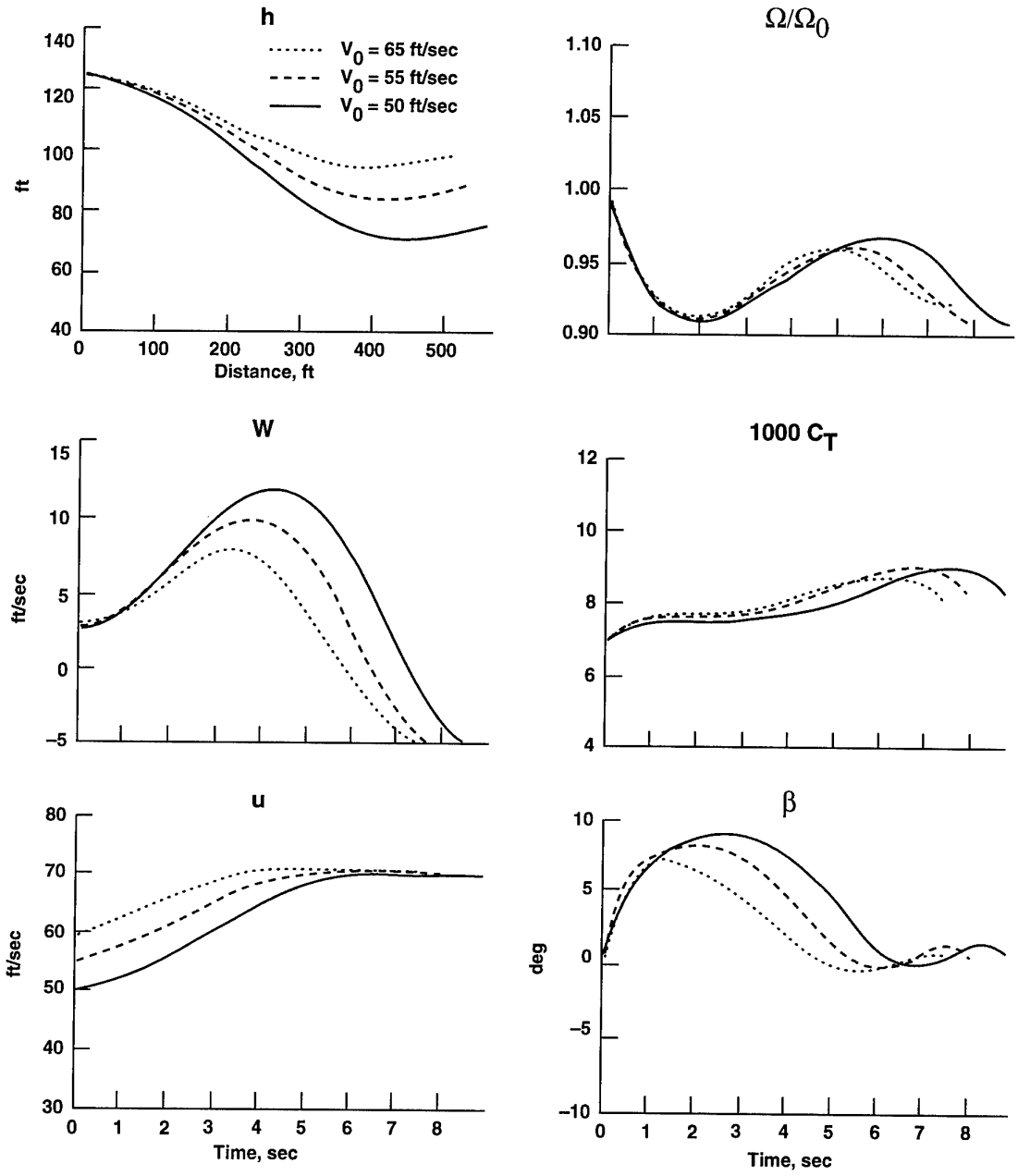

Fig. 13: Minimum runway BL with different initial airspeeds: W = 19,123 lb, U_2 = 70 ft/sec, h_0 = 125 ft, and γ_0 = –3°.

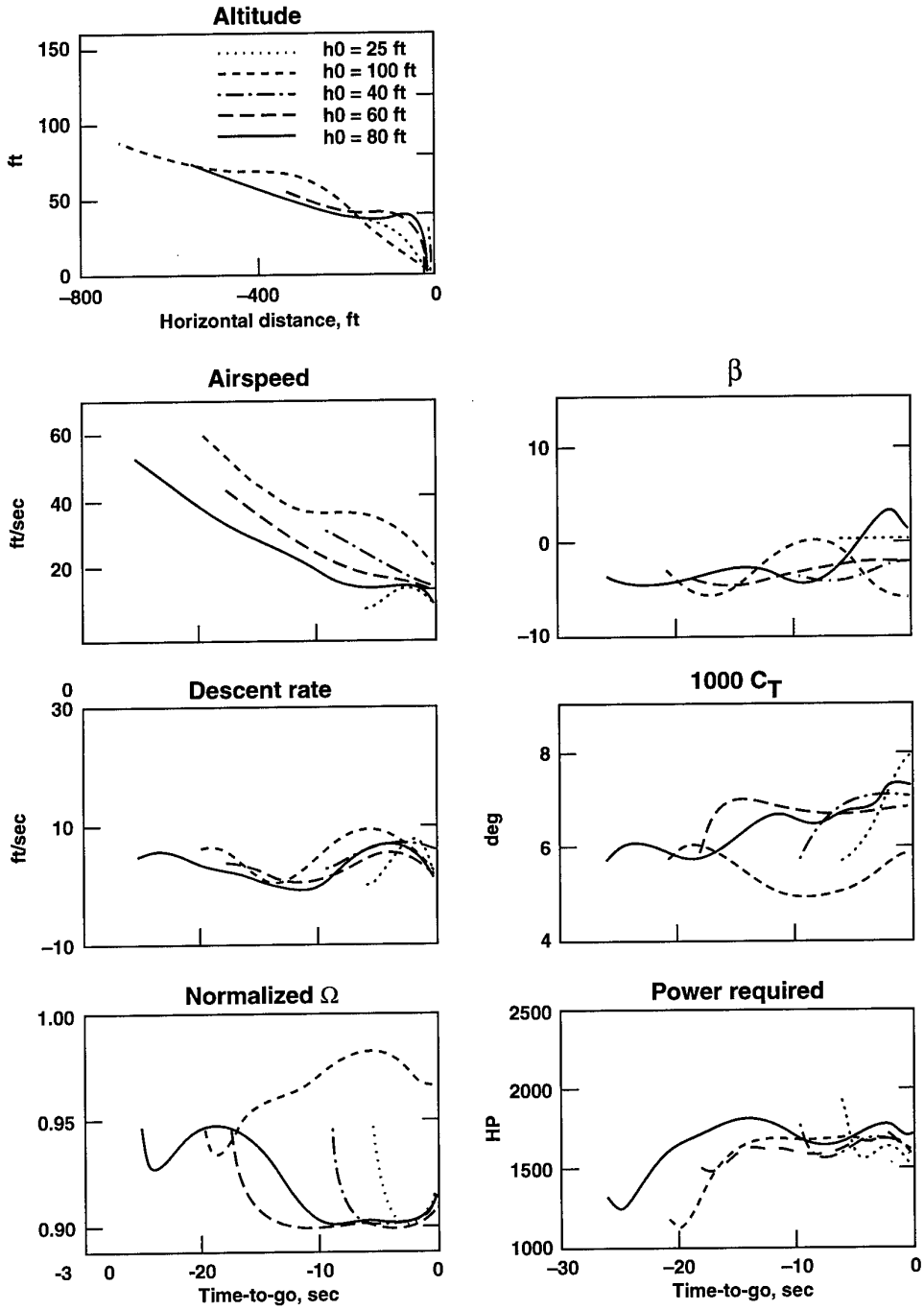

Fig. 14: Effect of initial altitude on optimal VTOL-CL trajectories: W = 16,000 lb, P_{OEI} = 1656 hp, $\gamma_0 = -6°$, and V_0 varied with h_0 on the AEO landing path.

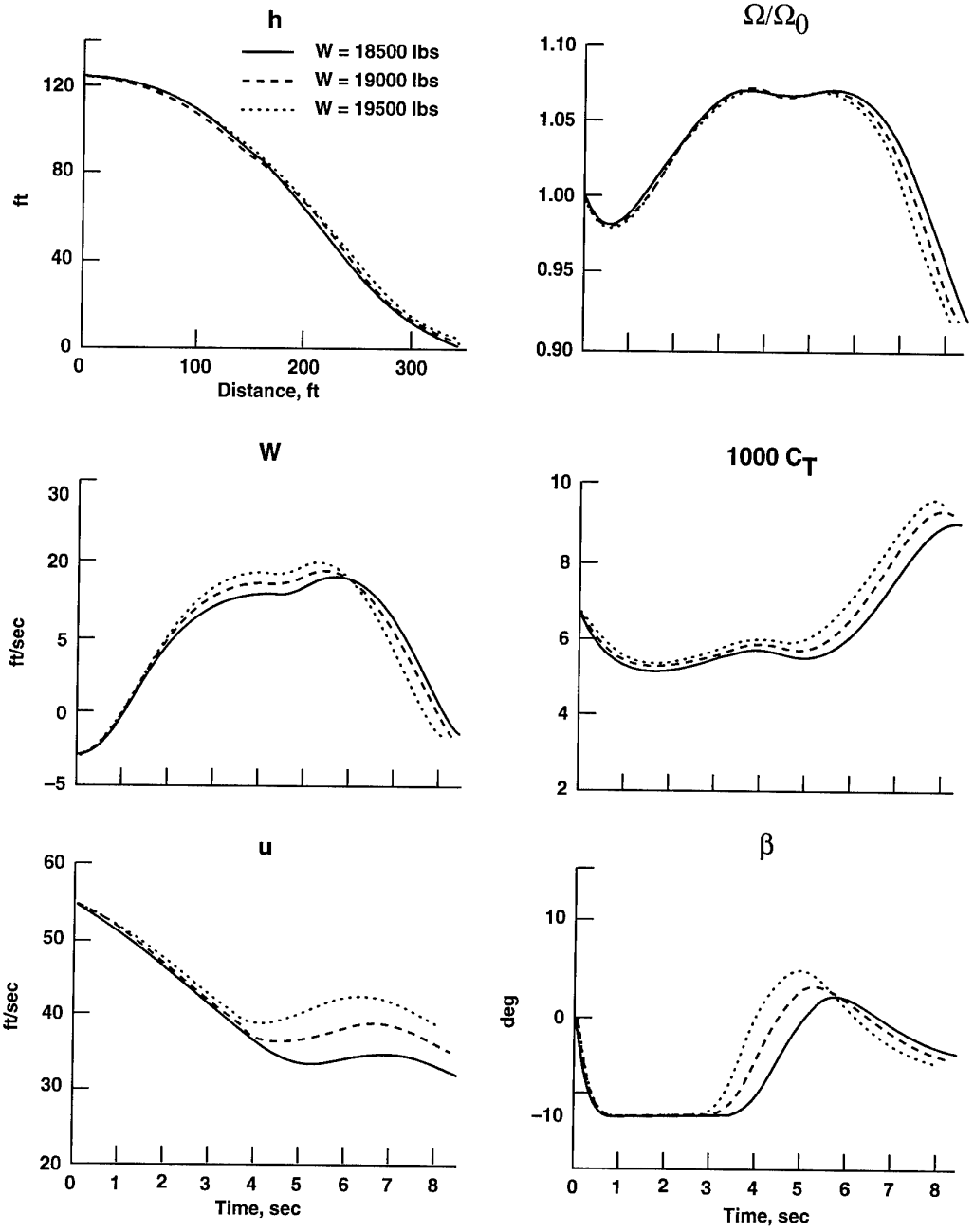

Fig. 15: Effect of gross weight on minimum runway CL trajectories: h_0 = 125 ft, γ_0 = –3°, and V_0 = 55 ft/sec.

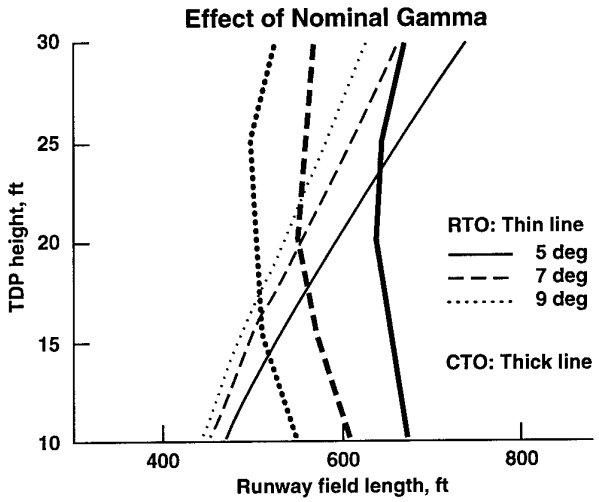

Fig. 16: STOL minimum runway length for $V_0 = 50$ ft/sec, $W = 18{,}610$ lb, and $U_2 = 65$ ft/sec (for CTO).

AN INVESTIGATION OF PRIMARY FLIGHT CONTROL FAILURE IN A PILOTED HELICOPTER

Scott R. Gibbard
Atlantis Aerospace Corporation
1 Kenview Blvd
Brampton, Ontario
Canada L6T 5E6

L.D. Reid
University of Toronto
Institute for Aerospace Studies
Toronto, Ontario
Canada M3H 5T6

SUMMARY

The application of fly-by-wire techniques to helicopters allows for a number of advanced control schemes that can be used to enhance performance and safety. An experiment has been carried out in a manned helicopter simulator to evaluate the possibility of making use of such a system to allow the pilot to retain control over the helicopter following catastrophic failure of the lateral cyclic primary control. It was demonstrated that a pilot can switch to pedals as the lateral control input provided that the tail rotor is controlled by an autopilot mode. The feasibility of this process has been evaluated for a range of system configurations and the corresponding handling qualities ratings are reported.

INTRODUCTION

The advent of digital flight control systems and fly-by-wire primary flight controls has led to considerable effort directed towards demonstrating their safety and reliability based on redundant hardware and software (Ref. 1). It is generally accepted that these systems can be as reliable as the traditional mechanical systems of the past. The simultaneous actuation of a number of aerodynamic control surfaces by a single channel of primary controls (such as implemented on the F-18 described in Ref.2) is now possible in applications intended to maximize the performance of the airframe. The present paper examines the possibility, in the context of a fly-by-wire helicopter (Ref. 3), of employing such a system to allow a helicopter pilot to recover from a catastrophic failure of the primary flight controls. The equivalent failure in a traditional mechanical control system would be the severing of all mechanical links between one channel of the primary flight controls and the associated swashplate, tail rotor, or aerodynamic control surfaces.

The ability of pilots to adapt to abrupt changes in vehicle dynamics has been documented in previous studies (Ref.4). In most instances the pilots were involved in part task simulation environments during the investigations. The present work looks at the feasibility of substituting one channel of primary flight control for another in a full task helicopter simulator. The investigation differs from previous ones in that the pilot must switch input channels rather than adapt to a change in vehicle dynamics. Specifically, this involved a failure of the lateral cyclic primary flight control and the substitution of the pedals as the lateral swashplate control input. Tail rotor control following this substitution was transferred to autopilot control.

SIMULATOR

The evaluation flights were flown in the UTIAS (University of Toronto Institute for Aerospace Studies) Flight Research Simulator (described fully in Ref. 5). The simulator incorporates a cab mounted on a 6 degrees-of-freedom hexapod motion system. The simulated helicopter is a Bell 205 as modelled by the ARMCOP computer algorithm developed by NASA and the U.S. Army Aviation Systems Command (Refs. 6,7). The algorithm employs a rotor disk model with tip-path dynamics. The complete model includes 6 rigid degrees-of-freedom (DOF), 3 rotor flapping DOF and rotor rotation. However, the Bell 205's teetering rotor system means that the rotor coning angle is preset, leaving 9 DOF in the operational model. The simulation runs on a Perkin-Elmer 3250 digital computer at a 33 Hz update rate.

The pilot's panel is an electronic flight instrument system (EFIS) generated on a 19 inch colour monitor by an IRIS 3130 workstation. Conventional flight parameters are supplemented by a 3-cue flight director (FD) which is coupled to the ILS during landing approaches. The FD system, described in Reference 5, provides cyclic and collective commands to the pilot. The forward visual scene is generated by a second IRIS 3130 workstation. A full colour display is collimated to optical infinity, resulting in a 40 degree horizontal by 29 degree vertical field-of-view. By the use of predictor algorithms the time delay associated with the visual display was reduced to less than 30 ms and for that of the motion system to between 30 and 50 ms.

FLYING TASKS

Two flying tasks were employed in this study. Task A was directed towards establishing reasonable control system gains. Task B involved an investigation of transition time constants.

Two tail rotor autopilot modes were used, both of which allowed feet-on-the-floor flying. These modes are Turn Coordination (TC) and Heading Hold (HH). The TC mode maintains sideslip near zero during maneuvering. The HH mode maintains the helicopter on the heading present at the time of mode engagement. Both of these control modes are fully described in References 5 and 8.

In both tasks each flight was begun in trimmed flight at 60 kts, 500 ft above ground level (AGL), and 1.1 nm from the threshold on the runway centreline.

An atmospheric disturbance signal composed of a weighted sum of 9 sine waves was employed (Ref. 9). These signals were input to the simulation as three components of body-axes wind effects, with a frequency content in the range 0.07 to 2.96 Hz. This disturbance was included to increase the pilot's workload during the trials. The core of the present study was the transition of lateral swashplate input from the lateral cyclic primary flight control to the pedals. When initiated, the transition takes place as depicted in Figure 1. Here δ_{lat} is the actual control signal sent to the lateral swashplate and K_{CS} is the control gain for the lateral cyclic before the time delay interval t_{delay} and for the pedals after t_{delay}. During the period of t_{delay} the swashplate is held at the trim value for level flight at the current airspeed.

Paper presented at the FVP Symposium on "Advances in Rotorcraft Technology", held in Ottawa, Canada, 27-30 May 1996, and published in CP-592.

The resulting system is shown in Figure 2. The logic and timing for mode transition is applied at the shaded areas.

To investigate the desired pedal gain to control the lateral swashplate, provision was made to adjust the gain as is shown in Figure 3. The command pedal signal, δ_{com}, is normalized to full swashplate deflection at ± 1.0. The control is computed such that at $\delta_{com} = \pm 1.0$ the lateral swashplate is deflected to the same degree as that normally achieved by full scale lateral cyclic inputs from the stick. This maximum deflection is represented by $\delta_{lc} = \pm 1.0$. In order to accommodate a range of pedal sensitivities around zero deflection, the pedal gain at $\delta_{com} = \pm 0.5$ (hereafter $\delta_{0.5}$) can be adjusted, giving the piecewise linear input/output characteristic shown in Figure 3.

Task A Description:
Task A was carried out for two wind disturbance levels, Level 1 having peak gusts of 3 kts for all three axes and Level 2 having peak gusts of 6 kts. The TC mode controlled the tail rotor both before and after the transition. The pedal gain parameter $\delta_{0.5}$ was tested at four levels (0.25, 0.45, 0.65 and 0.90). The transition timing of Figure 1 was selected to be fixed with $t_{fadeout} = t_{fadein} = 0.5$ s and $t_{delay} = 0.5$ s. It was emphasized to the pilots that the purpose of this experiment was to evaluate the handling qualities of the aircraft *after* the transition, *not* during the transition.

The Task A flying task was as follows:

- begin in trimmed horizontal flight, altitude 500 ft AGL, groundspeed 60 kts, heading $\Psi = 0°$, and 1.1 nm from the runway threshold on the centreline
- descend slowly to 450 ft AGL, holding groundspeed and heading constant; transition from lateral cyclic stick control to pedal control begins at 475 ft AGL and takes place over 1.25 s.
- regain control and level off at 450 ft AGL, 60 kts and hold for 10 s.
- perform a 15° banked turn to the right to heading $\Psi = 45°$.
- remain level at 450 ft AGL, $\Psi = 45°$ for 5 s.
- perform a 15° banked turn to the left to heading $\Psi = 0°$.
- remain level at 450 ft AGL, 60 kts, $\Psi = 0°$ for 5 s.
- decelerate to a groundspeed of 45 kts.
- remain level at 450 ft AGL, 45 kts for 5 s.
- descend to 350 ft AGL at 500 fpm, maintaining $\Psi = 0°$ and groundspeed 45 kts.
- hold 350 ft AGL, 45 kts and $\Psi = 0°$ for 10 s.

Task B Description:
Task B was carried out with a single wind disturbance of Level 1.5, having peak gusts of 4.5 kts. Four distinct flight control modes were employed:

Case 1: - TC engaged at all times.
Case 2: - HH engaged at all times.
Case 3: - Flight began with conventional pedal control. Pedal control of the tail rotor was faded out and TC faded in following the same scheme and timing as in Figure 2.
Case 4: - Same as Case 3 but HH was faded in to control tail rotor.

Based on preliminary flight trials, the pedal gain parameter was fixed at $\delta_{0.50} = 0.65$. For each of the 4 Cases, 7 treatments representing different time constant combinations in Figure 2 were studied. The t_{delay} parameter was fixed at 0.25 s and the values selected for t_{fadein} and $t_{fadeout}$ can be seen in Figure 9.

The Task B flying task was as follows:

- begin in trimmed horizontal flight, altitude 500 ft AGL, groundspeed 60 kts, heading $\Psi = 0°$, and 1.1 nm from the runway threshold on the centreline.
- follow the flight director in level flight; at 0.8 nm from the threshold you will intercept the 6° glideslope and the FD will direct you to begin your descent, while maintaining 60 kts groundspeed.
- at 375 ft AGL a warning tone will indicate the beginning of the fadeout period of lateral cyclic stick effectiveness. If rudder pedals were being used for yaw control, their effectiveness will also fade to zero and either TC or HH will take over tail rotor control.
- after a brief delay, control of the lateral swashplate by the pedals will be faded in.
- regain control of the helicopter, recapture the glideslope and localizer, and continue the approach down to 150 ft AGL.

Task B is shown graphically in Figure 4.

EXPERIMENTAL PLAN

A group of 5 evaluation pilots took part in this project on a voluntary basis. Their qualifications are summarized in Table 1. Because no single pilot had to perform all of the experimental cases, it was not necessary for each pilot to become proficient at all of the tasks. Training for Task B included several trials of Task A, as this familiarized the pilots with controlling lateral response with the pedals without the added complexity of tracking the flight director. The amount of training depended on several factors, including pilot experience, simulator experience, IFR proficiency and the type of trial being flown.

In general, a pilot was considered to be trained when the following criteria were met:

Task A Training Criteria:
(i) the pilot was comfortable flying the EFIS display.
(ii) the experimenter felt comfortable that the task was performed with reasonable proficiency.
(iii) the pilot was satisfied that he had complete control of the helicopter following transition of lateral control to the pedals.

Task B Training Criteria:
(i) both the pilot and the experimenter were satisfied that the pilot could fly a flight director approach using conventional controls.
(ii) the pilot was comfortable in controlling lateral response with the pedals.
(iii) the differences among TC, HH and normal yaw control were well understood.
(iv) the specifics of the approach procedure were well understood.

The 8 configurations of Task A (see Table 2) were evaluated by pilots 1 to 3. The 28 configurations of Task B (see Table 3) were evaluated by pilots 1 to 5. In the case of Task A each pilot evaluated every configuration. In Task B each pilot evaluated only a subset of all possible configurations. The order of the presentation of all these tasks was randomized to minimize sequence effects.

The primary evaluation metric was the Cooper-Harper Handling Qualities Rating (HQR) described in Reference 10. When a particular configuration was to be evaluated, the pilot flew the identical configuration through the flight sequence 4 times in succession. At the end of these trials he was asked to give a single HQR based on that portion of the flight following the onset of the transition process. In addition, any relevant pilot comments were encouraged and recorded.

Pilot Number	Age (years)	Background	Hours Fixed Wing	Hours Helicopter	Hours Simulator
1	47	Military	300	4000	300
2	38	Military	2200	1500	300
3	33	Military	200	1500	100
4	28	Civilian	110	1990	10
5	31	Civilian	48	2000	0

Table 1 - Pilot's Background

$\delta_{0.5}$ Gain	Disturbance Level	Pilot Number		
		1	2	3
0.25	1	3.0	7.0	2.0
	2	4.0	9.0	5.0
0.45	1	3.0	4.0	4.0
	2	3.0	4.0	3.0
0.65	1	5.5	4.0	5.0
	2	4.0	6.0	4.0
0.90	1	3.0	4.0	4.0
	2	5.0	7.0	7.0

Table 2 - Task A Handling Qualities Rating

Case	$t_{fadeout}$ (s)	t_{fadein} (s)	Pilot					Average
			1	2	3	4	5	
1. (TC)	0.25	0.25	2	4	-	2	3	2.75
	0.25	2.00	2.5	5	-	-	-	3.75
	0.25	6.00	-	-	-	6	4	5.00
	2.00	0.25	3	3	-	-	-	3.00
	2.00	2.00	4	3	-	-	-	3.50
	6.00	0.25	-	-	-	5	10	7.50
	6.00	6.00	-	-	-	8	8	8.00
2. (HH)	0.25	0.25	2.5	-	4	4	3	3.38
	0.25	2.00	3	-	4	-	-	3.50
	0.25	6.00	-	-	-	6	4	5.00
	2.00	0.25	4	-	4	-	-	4.00
	2.00	2.00	2	-	4	-	-	3.00
	6.00	0.25	-	-	-	5	6	5.50
	6.00	6.00	-	-	-	6	6	6.00
3. (Pedals→TC)	0.25	0.25	4	5	-	5	5	4.75
	0.25	2.00	5	6	-	-	-	5.50
	0.25	6.00	-	-	-	2	5	3.50
	2.00	0.25	6	3	-	-	-	4.50
	2.00	2.00	5	6	-	-	-	5.50
	6.00	0.25	-	-	-	3	7	5.00
	6.00	6.00	-	-	-	6	6	6.00
4. (Pedals→HH)	0.25	0.25	2	-	3	3	6	3.50
	0.25	2.00	2	-	3	-	-	2.50
	0.25	6.00	-	-	-	5	4	4.50
	2.00	0.25	4	-	3	-	-	3.50
	2.00	2.00	4	-	4	-	-	4.00
	6.00	0.25	-	-	-	6	6	6.00
	6.00	6.00	-	-	-	3	5	4.00

Table 3 - Task B Handling Qualities Rating

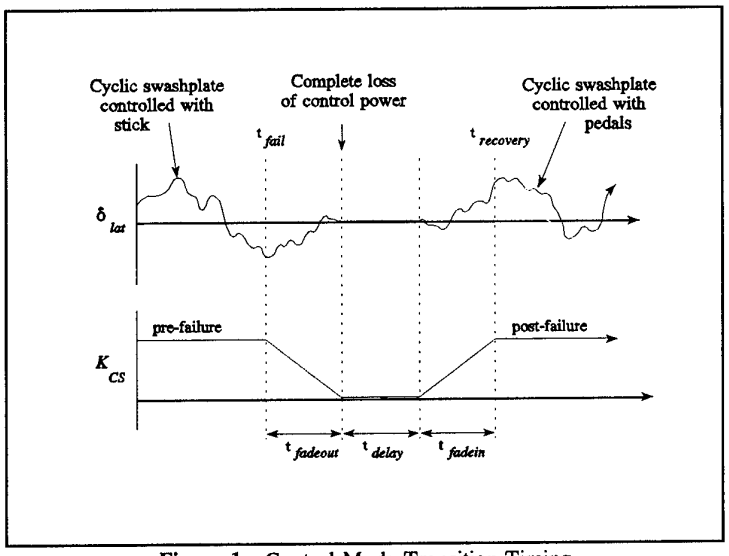

Figure 1 - Control Mode Transition Timing

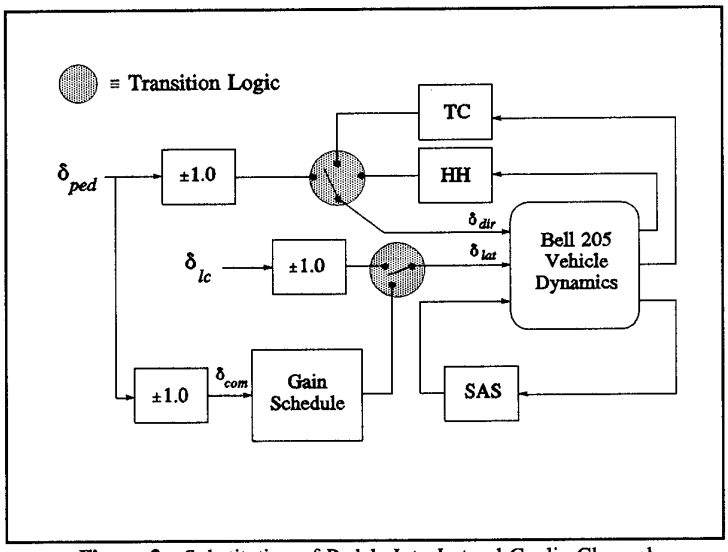

Figure 2 - Substitution of Pedals Into Lateral Cyclic Channel

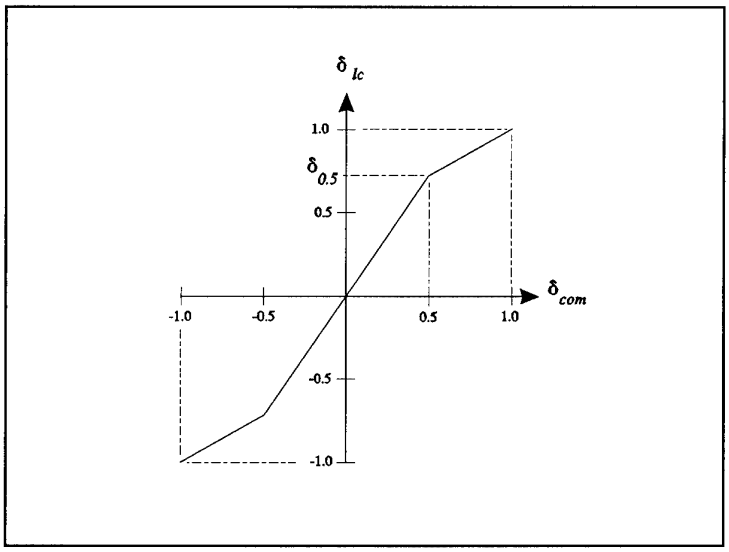

Figure 3 - Pedal Gain Schedule

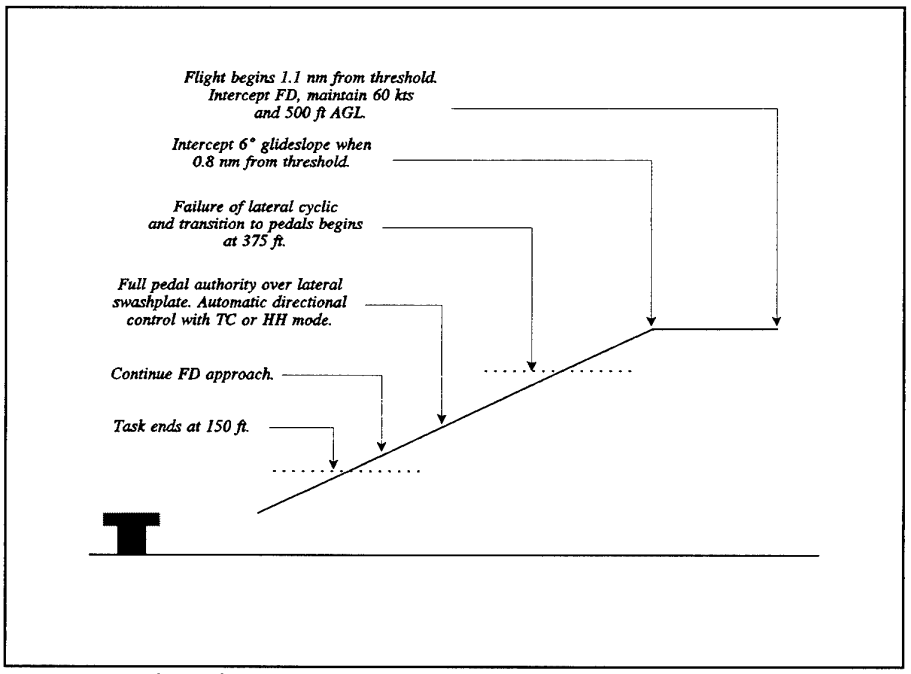

Figure 4 - Course Profile for Flight Director Landing Approaches

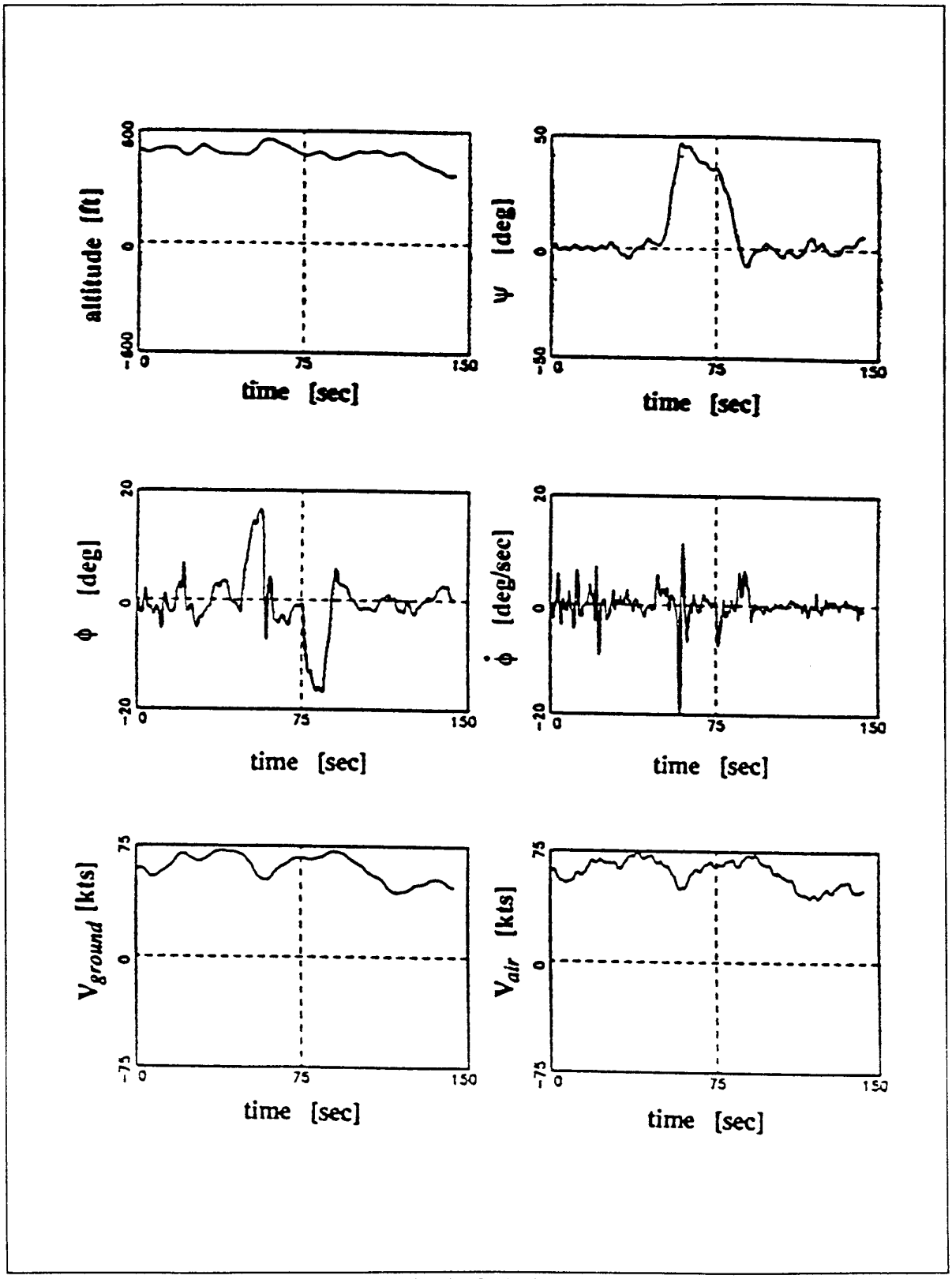

Figure 5 - Typical Time Histories for Task A, Case 1, Wind level 1.0

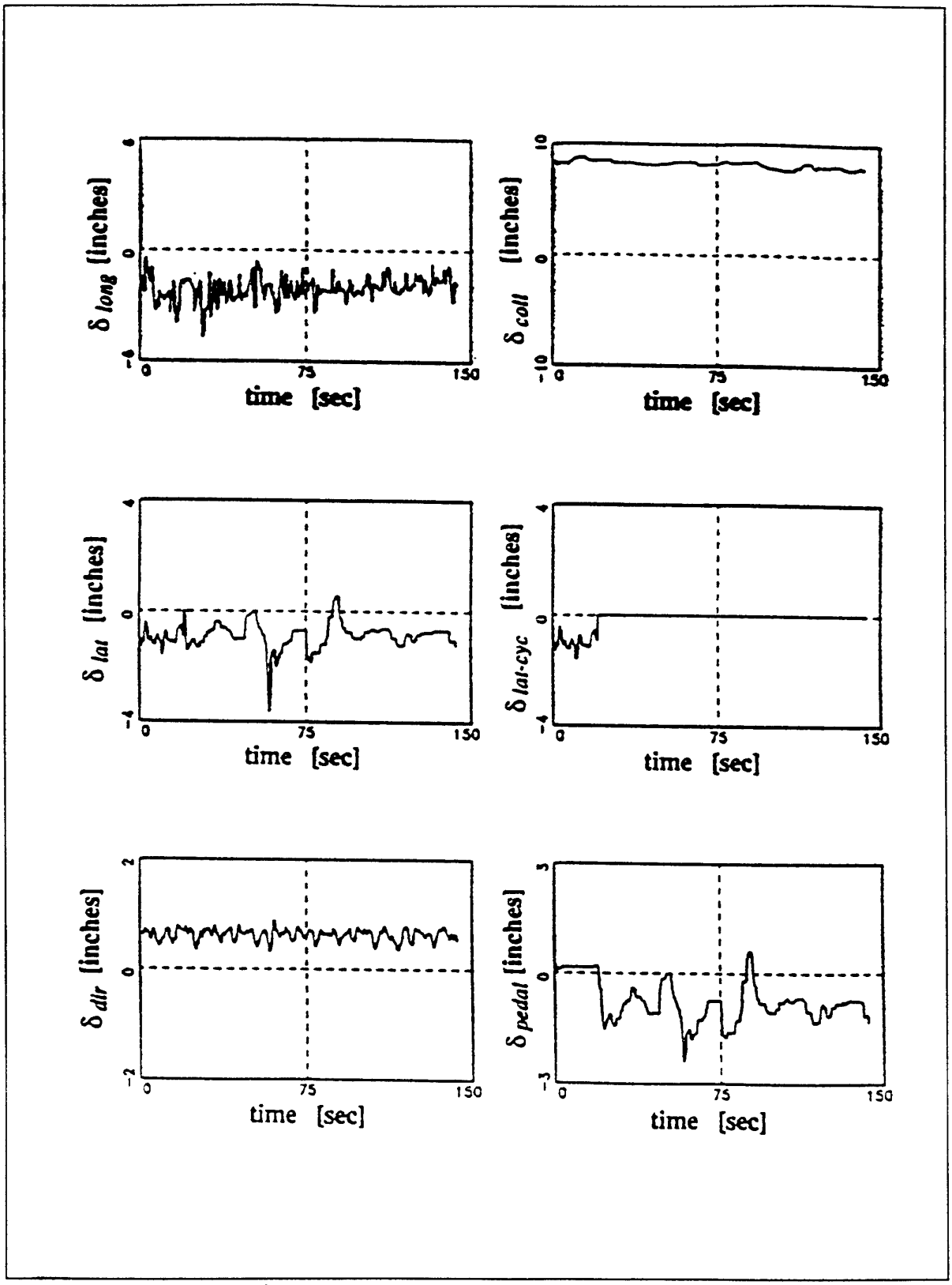

Figure 6 - Typical Time Histories for Task A, Case 1, Wind level 1.0

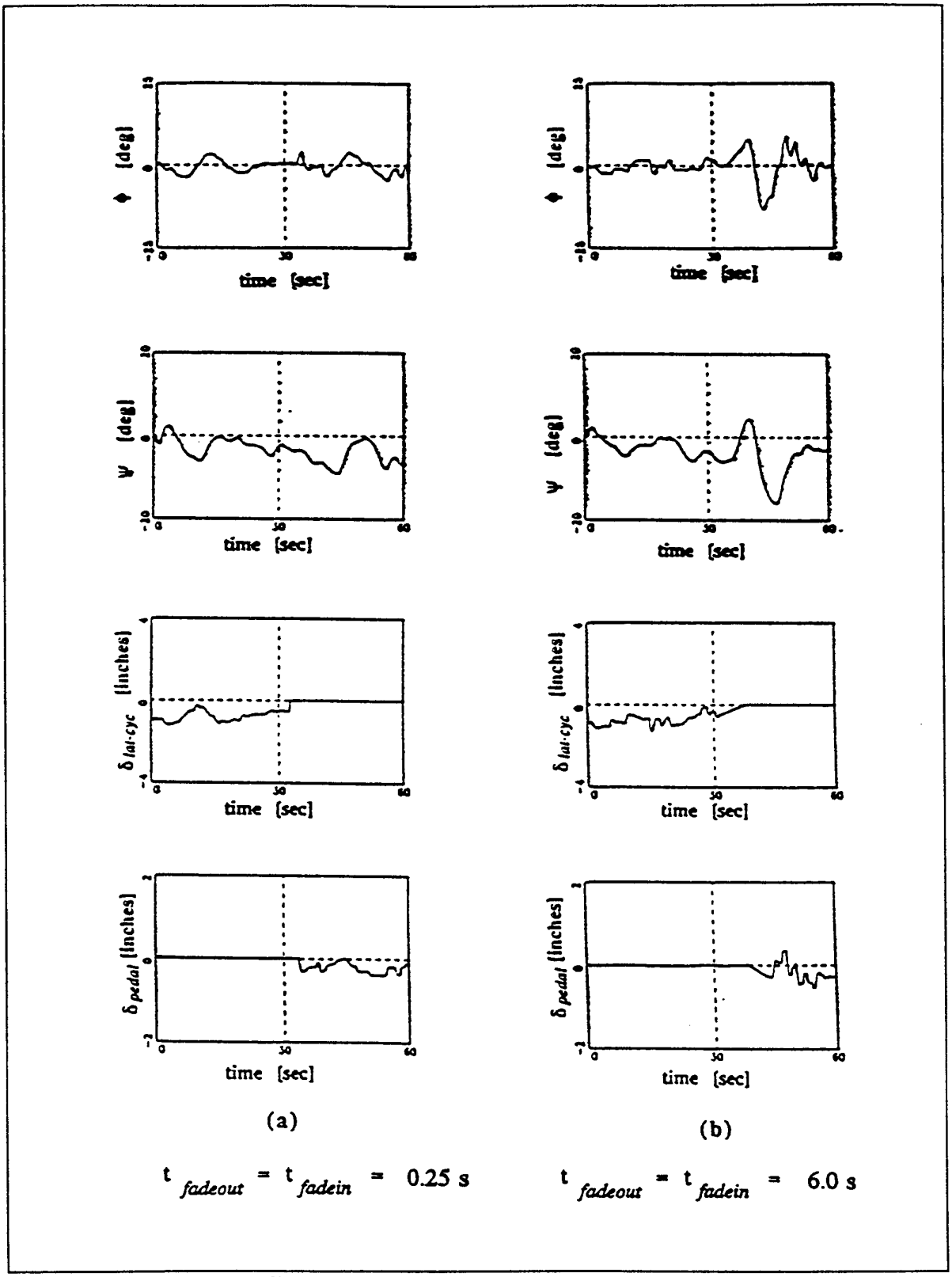

Figure 7 - Typical Time Histories for Task B, Case 1

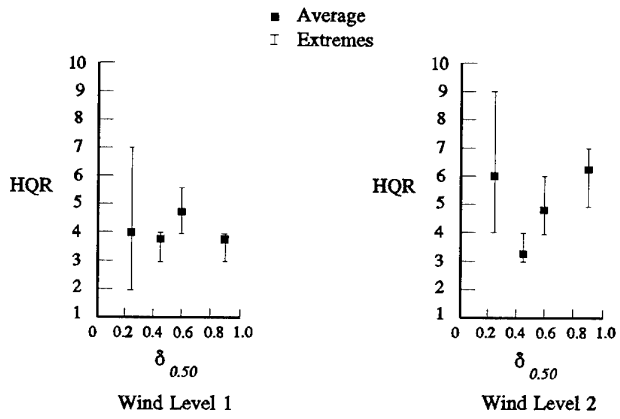

Figure 8 - Handling Qualities Ratings for Task A

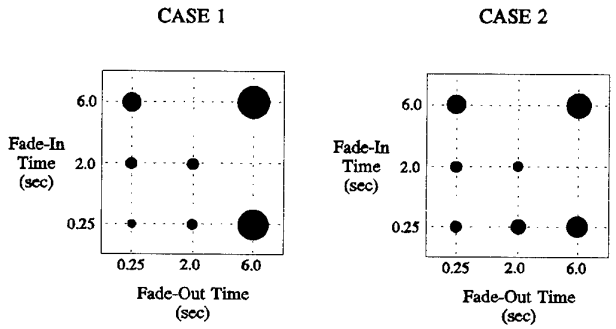

Figure 9 - Handling Qualities Ratings, Task 5, Cases 1 & 2

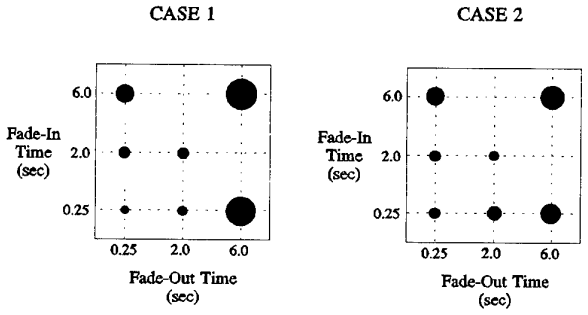

Figure 10 - Handling Qualities Ratings, Task 5, Cases 1 & 2

RESULTS AND DISCUSSION

Figures 5 and 6 show typical time histories for Task A, Case 1. The effect of the wind disturbance can be seen by comparing the groundspeed with the airspeed. As the TC mode is engaged throughout the flight, it can be seen that the tail rotor control term δ_{dir} is very steady throughout the flight. Also, because the pedal gains for Case 1 is very low (0.25), the pilot required an extreme amount of pedal activity after the transition to lateral swashplate control with the pedals (maximum pedal deflection is ± 3.25 inches).

Figures 7a and 7b show typical system time histories recorded during Task B, Case 1. Figure 7a is a rapid transition with $t_{fadeout} = t_{fadein} = 0.25$ s and Figure 7b is a slow transition with $t_{fadeout} = t_{fadein} = 6.0$ s. Here the helicopter is performing a TC approach and considerable heading (Ψ) variation results. In Figure 7a the time at which the transition occurs can be seen as a sudden change in the lateral swashplate input signal from the lateral cyclic $\delta_{lat\text{-}cyc}$ (which goes to zero) to the pedals δ_{pedals} (which grows from zero). In Figure 7b the same process takes place over a 6 s interval for each control signal source. It can be seen that the bank angle excursion (ϕ) and heading transient following transition is modest for the rapid transition of Figure 7a and excessive for the slow transition of Figure 7b. This is largely the fault of the longer interval with reduced control authority present in the latter instance.

The individual HQR data are recorded in Tables 2 and 3. Three pilots evaluated each configuration of Task A while at least two pilots evaluated each configuration of Task B. The data of Table 2 are plotted in Figure 8, showing the mean and extreme values. The data of Table 3 are plotted in Figures 9 and 10, where the diameter of each circle represents the mean of the corresponding HQR data.

Task A Results

The HQR results for Task A demonstrate several distinct effects. It was found that all of the pilots were able to retain control following the transition from cyclic stick to pedal control of lateral vehicle response. From Table 2 it can be seen that for the lowest pedal gain ($\delta_{0.50} = 0.25$) and the highest ($\delta_{0.50} = 0.90$), every pilot's HQR increased in going from Level 1 wind disturbance to the higher Level 2 disturbance. However, for the middle gains ($\delta_{0.50} = 0.45$ and 0.60) no obvious consistent effect of wind disturbance level is evident. The two extreme pedal gains drew complaints from the pilots of insufficient pedal authority and oversensitive pedals respectively. The two middle gains drew a mixture of comments on pedal sensitivities with no unanimous consensus.

The HQR summary of Figure 8 clearly shows the above mentioned trends. If a single pedal gain were to be selected for use with both wind disturbance levels it would appear that $\delta_{0.50} = 0.45$ would be the best choice. It also appears that a clearer distinction between gain levels can be made when the task workload is increased by employing a larger wind disturbance signal.

Task B Results

The HQR results for Task B were fairly consistent for the extreme values of transition values of ($t_{fadeout}$,t_{fadein}) equal to (0.25,0.25) and (0.60,0.60) and less so for the others (see Table 3). In Cases 1 and 2 where the pedals are not in use before the transition occurs, the pilots preferred fade times that were short and disliked those that were long (see Figure 9 and 10). In Cases 3 and 4 where the pedals are in use before the transition, it is seen that for each Case the mean HQR for equal values of $t_{fadeout}$ and t_{fadein} are the same, indicating less sensitivity to the overall transition time than found for Cases 1 and 2.
The pilot comments add much insight to these findings. One pilot (S1) indicated that he found the transition of lateral control to the pedals easier to contend with when he was already "on" the pedals as in Cases 3 and 4. A second pilot (S4) felt that cases involving HH were easier to handle because the autopilot held the heading during the transition when the pilot control authority was reduced. In Case 1 the pilot comments for ($t_{fadeout}$,t_{fadein}) near the origin in Figure 9 were generally of the type "abrupt but good transition," while for values far from the origin a typical comment was "no response for too long." In Case 2 the pilot comments for ($t_{fadeout}$,t_{fadein}) near the origin were "transition too short," while far away from the origin they commented "response too slow." Case 3 comments were similar to those for Case 2. Case 4 resulted in a different set of comments. The pilots felt that the short fade time produced "a comfortable transition" that was "not very noticeable." The long time delays were "not difficult."

CONCLUSIONS

An experiment was carried out in a helicopter flight simulator to investigate pilots' ability to adapt to an unusual transfer of lateral control from the cyclic stick to the pedals. It was found that for a modest range of system characteristics all 5 test pilots were able to make the transition to pedal control and continue the mission. As expected, the HQR assigned during the evaluation process were sensitive to pedal gain, with ratings degrading as gains were increased or decreased away from the optimal region.

The pilots were also sensitive to the fadeout and fadein times employed in the transition to pedal control. In cases where the pedals were not in use to control yaw before the transition (because the tail rotor was under autopilot control) it was found that the pilots preferred to have short fade times. In cases where the pedals were in use before transition the effect of fade times was less pronounced.

REFERENCES

1. Reid, L.D.,"Technical Evaluation Report on the Flight Mechanics Panel Symposium on Active Control Systems - Review, Evaluation and Projections," AGARD-AR-220, March 1985.

2. Moran, W.A.,"Operational and Developmental Experience with the F/A-18A Digital Flight Control System," presented at the AGARD Symposium on Active Control Systems, Toronto, AGARD CP-384, October 1984.

3. Richards, W.R.,"ACT Applied to Helicopter Flight Control," presented at the AGARD Symposium on Active Control Systems, Toronto, AGARD CP-384, October 1984. October 1984.

4. Weir, D.H., and Johnson, W.A.,"Pilot Dynamic Response to Sudden Flight Control System Failures and Implications for Design," NASA CR-1087, June 1968.

5. Reid, L.D., Advani, S., and de Leeuw, J.H.,"An Evaluation of Decelerating IFR Approaches Utilizing a Helicopter Flight Simulator," University of Toronto Institute for Aerospace Studies Report No. 336, May 1991.

6. Chen, R.T.N.,"A Simplified Rotor System Mathematical Model for Piloted Flight Dynamics Simulation," NASA TM 78575, May 1979.

7. Talbot, P.D., Tinling, B.E., Decker, W.A., and Chen, R.T.N.,"A Mathematical Model for a Single Main Rotor Helicopter for Piloted Simulation," NASA TM 84281, September 1982.

8. Baillie, S., Kereliuk, S., and Hoh, R.,"An Investigation of Lateral Tracking Techniques, Flight Directors and Automatic Control Coupling on Decelerating Approaches for Rotorcraft," Aeronautical Note NAE-AN-55, NRC No. 29604, October 1988.

9. Gibbard, S.R.,"The Investigation of Control Failures and Control Mode Transitions in a Piloted Helicopter Simulator," M.A.Sc. Thesis, University of Toronto Institute for Aerospace Studies, August 1992.

10. Cooper, G.E., and Harper, R.P.,"The Use of Pilot Rating in the Evaluation of Aircraft Handling Qualities," NASA TN D-5153, April 1969.

SIMULATION DE MISSION POUR LE TIGRE (VERSION APPUI PROTECTION)

J. F. RIGAL
G. COLAS
Simulation Test Engineers
Centre d'Essais en Vol - Section Etudes et Simulation
Base d'Essais d'Istres
13128 Istres Air
FRANCE

1. RESUME

Dans le cadre du développement de la version HAP de l'hélicoptère TIGRE, le processus d'évaluation des spécifications du système de mission a été effectué au centre de simulation du CEV à Istres. Les phases précédentes ont permis d'aborder les aspects relatifs à l'interface équipage-système dont les symbologies et procédures de pilotage, de navigation et de mise en oeuvre des armements, ainsi que les modes dégradés et l'intégration des équipements spécifiques à la version HAP dans le système de base TIGRE.

La présente phase du développement a permis d'effectuer des simulations de missions, assurant ainsi la validation globale de la charge de travail de l'équipage dans des conditions aussi proches que possible des missions réelles.

Dans ce cadre, le CEV a utilisé des moyens de simulation hautement représentatifs aussi bien pour les postes pilote et tireur, que pour la restitution de l'environnement extérieur. Ce dernier aspect est essentiel à la crédibilité des résultats et doit prendre en compte les éléments suivants:

- une base de données de terrain pour les visualisations (monde extérieur et capteurs) de taille suffisante (adaptée au profil des missions), certaines zones doivent présenter un niveau de détails élevé permettant le vol tactique,
- un environnement tactique significatif comprenant des dispositifs ECM, des zones irradiées (validation NRM), des menaces aériennes et au sol (du type interactives pré-programmées),
- une cabine pilotée pour un hostile ou un équipier, dans laquelle le pilote disposera d'un environnement suffisamment représentatif.

Les résultats ont porté sur différents aspects: amélioration des spécifications des systèmes embarqués, plus particulièrement la coopération et le travail en équipage, ce qui était l'objectif initial. En outre, cette phase de simulation a amené une contribution à la réflexion sur les procédures d'emploi opérationnel, ainsi qu'une expérience supplémentaire pour les moyens de formation et les futurs travaux en simulation d'études.

L'objet de cet exposé est de présenter les moyens et méthodes mis en oeuvre pour réussir les simulations de mission HAP, ainsi que les principaux résultats et enseignements.

2. INTRODUCTION

Dans le double but de garantir une interface équipage-système de qualité et d'assurer une bonne adéquation du TIGRE aux besoins des futurs utilisateurs, la logique suivante a été adoptée pour le développement de cet hélicoptère.

Chaque élément du cockpit, chaque fonction, après que leur définition papier a été approuvée par les services officiels français et allemands, sont implémentés sur simulateur afin d'être évalués et modifiés si cela est jugé utile. La définition implémentée sur les prototypes prend en compte les modifications effectuées à l'issue des campagnes de simulation. Chaque fonction est ensuite évaluée en vol par les services officiels, et de nouvelles demandes de modification peuvent en découler, avant les essais technico-opérationnels.

Ainsi, depuis 1991 de nombreuses campagnes d'essais en simulation se sont déroulées, à Ottobrunn chez ECD pour l'avionique de base et la version antichar, et depuis 1989 à Istres au CEV pour la version appui-protection. Pour clore ces campagnes, où toutes les fonctions ont été étudiées dans le détail, une simulation de mission est organisée pour fournir une vue d'ensemble du système dans un cadre aussi proche que possible de l'emploi opérationnel.

Le système de mission du TIGRE en fait un hélicoptère novateur dans de nombreux domaines, au moins en Europe. Il peut comprendre, selon la version, un FLIR de pilotage, un viseur de mât ou de toit avec une caméra thermique de nouvelle génération, des viseurs/visuels de casque, un collimateur tête haute, la gestion simultanée de 3 armements et 2 membres d'équipage en tandem. Pour l'ALAT, à qui est destinée la version HAP, le TIGRE représente un saut technologique considérable à bien des égards.

Le CEV a donc souhaité mettre en œuvre des moyens exceptionnels afin de conférer à la simulation de mission HAP un très grand réalisme qui permette, deux ans avant les évaluations technico-opérationnelles, d'évaluer la capacité opérationnelle - en termes d'interface Homme-Machine - dans un contexte de mission.

3. PRESENTATION DU CENTRE DE SIMULATION

Unique centre de simulation pilotée de la Direction des Constructions Aéronautiques (Délégation Générale pour l'Armement, dépendant du ministère de la défense), la section études et simulation du CEV a pour mission de développer,

Paper presented at the FVP Symposium on "Advances in Rotorcraft Technology", held in Ottawa, Canada, 27-30 May 1996, and published in CP-592.

mettre en oeuvre et exploiter des simulateurs pilotés d'études au profit de la définition et du développement des systèmes embarqués pour aéronefs civils et militaires. Pour évaluer l'adéquation aux besoins opérationnels, les essais en simulation nécessitent la représentation complète des systèmes embarqués et des interfaces "équipage-système" avec pour objectifs:

- de fournir des éléments d'appréciation technique concernant les évolutions des spécifications des systèmes embarqués,

- d'analyser les situations à risques ou à charge de travail élevée,

- d'assurer le support des essais en vols (rejouer des vols réels, préparer des vols complexes, rechercher des causes d'anomalies rencontrées en vol, former et entraîner les équipages d'essais).

Actuellement 7 simulateurs complets sont simultanément opérationnels; ils sont composés de leur cockpit, des calculateurs de simulation, de systèmes de génération graphiques, d'une salle de conduite des essais, et des moyens de restitution de l'environnement nécessaires aux essais (mouvement 6 axes, 3 sphères de projection, machines de génération synthétique d'images, simulation de cibles et d'équipiers, ...).

Pour un programme aéronautique tel que MIRAGE 2000, RAFALE ou TIGRE, on estime qu'un simulateur du CEV permet d'économiser l'équivalent d'un prototype.

4. LA SIMULATION DANS LE DEVELOPPEMENT DU TIGRE

La configuration des membres d'équipage dans l'hélicoptère TIGRE est la suivante: le pilote est en place avant et le tireur, commandant de bord, est en place arrière.

La version HAP qui fait l'objet de cet exposé se caractérise par: un viseur de casque pour chaque membre d'équipage, un collimateur tête haute (Head Up Display) pour le pilote, un viseur de toit (appelé également viseur principal ou viseur STRIX) avec voies directe optique, télévision noir et blanc et infrarouge pour le tireur, trois armements (canon de 30 mm en tourelle, roquettes 68 mm, missiles air-air Mistral). Chaque membre d'équipage possède deux moyens de visée, et est capable d'engager les trois armements.

L'avionique de base (commune aux différentes versions) a été simulée sur le simulateur ECD à Ottobrunn en 6 campagnes de 1991 à 1995. Le système d'armes HAP a été simulé à Istres sur le simulateur du CEV en 5 phases de 1989 à 1995. La dernière phase précédant la simulation de mission a consisté à vérifier la cohérence du système de base (évalué en Allemagne) avec le système d'arme HAP.

Chacune de ces phases était consacrée plus spécifiquement à un ensemble de fonctions ou d'équipements. A chaque nouvelle phase, une partie du système venait s'ajouter à ce qui avait été vu précédemment.

Outre les modes, les commandes et les symbologies qui sont typiquement l'objet des évaluations en simulation, on évalue la charge de travail du pilote et du commandant de bord, et la qualité du travail en équipage.

Il est clair qu'il ne suffit pas d'étudier séparément les pièces du puzzle pour que, mises ensemble, elles constituent un système cohérent et opérationnel. De gros problèmes peuvent passer inaperçus si l'on n'étudie pas simultanément et interactivement l'ensemble du système, et plus particulièrement les modes dégradés, avec une charge de travail de l'équipage réaliste (représentative de la mission). Il est notoire que les accidents sont toujours la conséquence de plusieurs causes simultanées; ils peuvent ne pas être mis en évidence en simulation si l'on concentre l'équipage en essais sur un seul aspect des choses.

Toutefois, certaines limites de la simulation sont incontournables: la sécurité du vol préoccupe nécessairement moins en simulation qu'en vol réel (l'équipage ne risque rien); les images de synthèse, même de qualité, ne permettent pas d'évaluer les hauteurs et les vitesses comme en vol, notamment près du sol (cas du vol tactique).

En revanche, d'autres éléments difficilement évaluables en vol sont étudiés de manière approfondie en simulation: gestion des pannes, cibles nombreuses, ECM, ...

5. OBJECTIFS DE LA SIMULATION DE MISSION

5.1. Différentes phases

Le planning de développement des prototypes, en particulier le planning de réalisation des logiciels embarqués, ont conduit à effectuer plusieurs phases de simulation de façon à prendre en compte les résultats dès que possible dans les versions et les implémentations successives de ces logiciels:

- une première phase en octobre/novembre 1995,
- une deuxième phase en février 1996,
- une troisième phase est en projet pour fin 1996 concernant un système de cartographie numérique et des liaisons de données venant en complément du système actuel.

Ce découpage en différentes phases résulte d'un compromis entre les contraintes du développement:

- les étapes planifiées du codage des logiciels embarqués, ce qui permet de réaliser les essais en vols des prototypes pour lesquels il est essentiel d'intégrer les résultats de simulation conformément au planning du développement,

- la volonté affirmée d'étudier globalement l'ensemble des systèmes dans un contexte représentatif de la mission opérationnelle pour obtenir une bonne crédibilité et un niveau de qualité sur les résultats obtenus.

5.2. Objet des évaluations

L'objet des évaluations de mission est la validation des procédures d'utilisation technique (c'est à dire telles que prévues dans les spécifications, les procédures d'emploi opérationnel sont de la responsabilité de l'ALAT) des systèmes de base TIGRE et de mission HAP dans un contexte proche de celui d'une mission, notamment en terme de charge de travail de l'équipage, ce qui correspond à:

- l'intégralité du système d'armes HAP dans un état de définition conforme aux "Modes et commandes spécification N°2" et donc au logiciel embarqué H3.2 lors de la première phase de simulation, et aux "Modes et commandes spécification N°3" et donc au logiciel embarqué H3.3 pour la seconde phase de simulation,
- une partie significative des fonctions du système de base (détection ECM, MFD, CDU, warning concept, navigation, AFCS).

Les résultats des évaluations, s'ils sont acceptés par les groupes nationaux et bilatéraux, pourront conduire à des évolutions des logiciels embarqués sur le prototype N° 4, soit le logiciel H3.3 pour le MEP-HAP, et le logiciel V3.1 pour le système de base TIGRE.

6. METHODES ET MOYENS D'ESSAIS

6.1. Architecture du simulateur

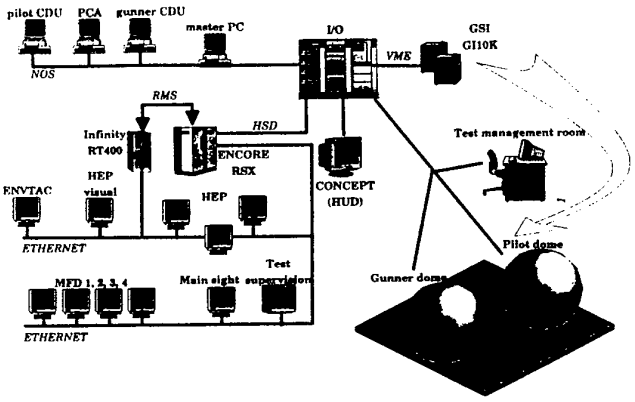

Le coeur du simulateur est composé de calculateurs temps réel couplés à une baie d'entrées/sorties. Des stations de travail et PC en réseaux permettent de simuler les éléments terminaux de la chaîne de simulation (visualisations graphiques sur MFD, symbologies du viseur clair et du viseur principal, CDU, génération sonore, etc.).

Les équipements de deux cockpits (l'un pour le pilote, l'autre pour le tireur), les équipements de la salle d'essais (d'où sont supervisées les évaluations) et les moyens de restitution de l'environnement sont couplés à la simulation par un dispositif informatique et électronique (baie d'entrées/sortie).

Un système de génération synthétique d'images permet la simulation des senseurs et la restitution du paysage extérieur.

Des moyens vidéo (incrustation, recopie) permettent la distribution et la commutation de ces images, ainsi que leur incrustation.

6.2. Moyens d'essais et d'environnement

Le centre de simulation du CEV met un certain nombre de moyens au service de la simulation TIGRE, que ce soit au niveau des moyens informatiques (machines et logiciels) ou au niveau des moyens de restitution de l'environnement.

6.2.1. Moyens informatiques

Le simulateur TIGRE HAP est architecturé autour de moyens informatiques récents et s'appuie sur des produits logiciels du commerce ou développés au CEV. Il intègre des modèles, soit fournis par les industriels (ECF, ECD, MTR, SFIM, etc.), soit développés au sein de la section simulation:

- la génération synthétique d'images, issue d'un produit du commerce (SOGITEC GI10K), permet de fournir cinq images: trois images pour le visuel extérieur, et deux pour la simulation des senseurs.

- la symbologie du viseur clair ou HUD (technologie de type cavalier) est générée par un calculateur spécialisé CONCEPT 60.

- les pages MFD (visualisations têtes basses) ainsi que la symbologie du viseur principal sont générées par des stations graphiques SILICON GRAPHICS connectées en réseau (ETHERNET).

- les deux CDU et le PCA sont émulés par des PC en réseau (NOS) et gérés par un "PC maître".

- la visualisation graphique de l'environnement tactique est réalisée sur station de travail SILICON GRAPHICS.

- les moyens de calcul (supportant les nombreux modèles) se composent de trois calculateurs TR de générations différentes couplés par un système de mémoire réfléchie: 2 calculateurs ENCORE RSX et un calculateur INFINITY RT400 (quadri-processeurs) cadencés à 40 ms et fonctionnant avec des contraintes TR fortes (déterminisme).

- les entrées/sorties du simulateur (provenant des cabines pilote et tireur et de la salle d'essais) sont gérées par une chaîne d'acquisition TR (développement spécifique réalisé par la société TITN). Cette baie d'entrées/sorties est connectée à l'un des calculateurs RSX via une ligne parallèle à haut débit (HSD).

- une station de travail SUN SPARC 20 permet un suivi en temps réel des données de simulation et de leurs évolutions (tracé de courbes).

Afin de développer, d'intégrer, de mettre au point, et puis mettre en oeuvre les différents modèles, des couches logicielles ont été développées par le CEV:

- sur les calculateurs RSX (système d'exploitation MPX), un moniteur temps réel offre un environnement souple et convivial pour l'ingénieur d'essais. Il permet de gérer facilement les aspects TR et le déterminisme des simulations (entrées/sorties, cadencement, priorité des tâches, etc.).

- sur les autres machines dotées d'un système d'exploitation UNIX (INFINITY RT400 et stations SILICON GRAPHICS), une structure d'accueil complète a été développée afin d'intégrer aisément des modèles et des applications graphiques, et de gérer les communications inter-tâches, inter-processeurs et inter-calculateurs; les modèles et applications peuvent être physiquement situés sur des processeurs ou des machines distants.

6.2.2. Cabine Pilote HAP

La cabine pilote est équipée des éléments suivants:

* un viseur clair THOMSON-CSF VH130 (collimaté à la même distance que la sphère),
* un bandeau d'armement BAP,
* deux écrans MFD,
* un CDU,
* un panneau de commande AFCS,
* des instruments secours sur la planche de bord,
* un panneau d'alarmes en banquette droite,
* des boutons "Master Alarm" et "DO-LIST",
* des poignées de pilotage cyclique et collectif,
* des commandes de réglages divers (écrans, éclairage cabine, ...).

6.2.3. Cabine Tireur HAP

La cabine Tireur est équipée des éléments suivants:

* un bras porte-occulaire avec micro-moniteur télévision pour visualiser les images des capteurs,
* un poste de commande armement PCA,
* deux écrans MFD,
* un CDU,

* un poste de servitudes du viseur STRIX,
* un panneau de commande AFCS,
* un panneau d'alarmes en banquette droite,
* des boutons "Master Alarm" et "DO-LIST",
* deux poignées de pilotage cyclique et collectif (non utilisables pour le pilotage mais utilisables uniquement pour les commandes "système"),
* deux poignées d'armement,
* des commandes de réglages divers (écrans, éclairage cabine, ...).

6.2.4. Modélisation du porteur et des systèmes

6.2.4.1. Mécanique du vol et pilote automatique

La modélisation de la mécanique du vol et du pilote automatique sont réalisés par des modèles fournis par ECF. Ces modèles ont été recalés suite aux essais en vol effectués sur le prototype N°2 en version HAP.

6.2.4.2. Moteurs

La modélisation des moteurs a été réalisée par MTR, le modèle permet le fonctionnement dans tous les modes normaux et dégradés, y compris les diverses pannes possibles des moteurs et le fonctionnement en "roue libre".

6.2.4.3. Indicateur de première limitation

Le modèle d'indicateur de première limitation permet le calcul de la première limitation atteinte par les moteurs, quelle que soit son origine. Il s'agit d'une information complexe à élaborer mais permettant une gestion facile des régimes moteurs pour l'équipage.

6.2.4.4. Viseur principal STRIX

Le modèle comportemental a été fourni par le fabricant (société SFIM). Il est associé avec une modélisation des calculateurs d'armement, des bus 1553B, de l'architecture vidéo et avec les images des senseurs produites par le système de GSI pour simuler et restituer l'ensemble du dispositif.

6.2.4.5. Conduites de tir

Les algorithmes réels des conduites de tir ont été mis au point au Centre Electronique de l'Armement (CELAR). Ce logiciel a ensuite été transféré au CEV pour animer de façon représentative les symbologies de tir.

6.2.4.6. Calculateurs embarqués du système de base

La simulation des calculateurs embarqués permet la gestion des écrans MFD, des CDU, de la navigation et du concept d'alarmes. Certaines liaisons par bus et liaisons filaires directes entre équipements sont également modélisés, permettant de simuler les modes dégradés correspondants.

6.2.4.7. Architecture du MEP-HAP et calculateurs d'armement

La modélisation du système d'armes a été développée de façon très poussée: elle comprend l'architecture des différents sous-systèmes et de leurs liaisons (différents bus et liaisons filaires), les modèles de chaque sous-système, les calculateurs d'armement (ainsi que les possibilités de reconfiguration, de pannes partielles et totales, les modes secours) et également l'architecture vidéo du TIGRE. Par exemple en cas de panne de l'un des calculateurs d'armement, toutes les conséquences fonctionnelles sont reproduites, y compris les effets sur la disponibilité des images vidéo et senseurs dans le cockpit.

6.2.4.8. Symbologies MFD

Les différentes pages des MFD sont simulées de façon complète ainsi que les modes dégradés des écrans et des générateurs de symboles. Seules quelques pages sont représentées de façon statique car les fonctions correspondantes ont été évaluées sur le simulateur SIMCO d'ECD.

Les pages et spécificités de la version HAP ont bien entendu été implémentées dans le simulateur, il s'agit des pages liées à la gestion de l'armement, des informations de pannes (alerte, labels des pannes, DO-LIST, conséquences fonctionnelles), de la page visionique (permettant la recopie des images des senseurs du viseur principal sur MFD).

La page tactique a été programmée de façon cohérente avec la situation tactique générale, elle indique à l'équipage les renseignements connus par le commandant d'unité.

6.2.4.9. Symbologies et logiques du CDU

Les pages les plus importantes de cet équipement ont été implémentées, notamment l'ensemble des pages de navigation et plus particulièrement les fonctions spécifiques de la version HAP telles que le recalage de navigation à l'aide du viseur principal. On notera toutefois que l'utilisation, à terme, d'un système de transmission de données diminuera l'impact de cet équipement sur la charge de travail de l'équipage.

6.2.4.10. Concept d'alarmes

Le concept d'alarmes a été programmé de façon complète, intégrant ses différentes composantes: sons (et les priorités des sons les uns par rapport aux autres), voyants et boutons sur les planches de bord, affichages sur MFD (label d'alerte, messages de DO-LIST, informations sur les conséquences fonctionnelles, ...). Les plus récentes évolutions et modifications de ce concept (correspondant à la version L013 de ces spécifications, et résultant des évaluations précédentes) ont été programmées.

6.2.4.11. Détection ECM

Le détecteur d'alertes et menaces TWE a également été modélisé de façon à restituer une information vraisemblable indiquant la direction et la gravité des menaces en fonction des moyens de détection utilisés. Par exemple, si la menace n'est détectée que par une seule antenne, le positionnement du symbole correspondant sur la page ECM des MFD pourra être imprécis.

6.2.4.12. Modes dégradés

La modélisation fine des modes dégradés est considérée par le CEV comme une nécessité pour obtenir des résultats de qualité et est une condition nécessaire à la représentativité des moyens de simulation.

Dans certains cas de pannes, une reconfiguration automatique du système permet de fonctionner dans un mode dégradé qui n'a pas de conséquence opérationnelle pour l'équipage Par exemple, dans le cas d'une perte de redondance, le système offre toujours à l'équipage les pleines capacités opérationnelles (donc c'est effectivement transparent, toutefois, la fiabilité du système est diminuée et le problème devra être traité dès le retour sur base en terme de .maintenance).

Dans d'autres cas, le fonctionnement en mode dégradé n'est pas transparent; il ne s'agit pas d'afficher seulement les informations de pannes, il est essentiel de modéliser les conséquences fonctionnelles des pannes, notamment en terme d'interactions entre les différents sous-systèmes.

Par exemple, une panne de liaison entre le calculateur d'armement et la tourelle canon impose un tir axial de cet armement à l'aide du HUD au lieu d'un tir asservi au viseur de casque; une dégradation des centrales de navigation va dégrader successivement différents sous-systèmes, en particulier les conduites de tir. Ces deux exemples montrent à l'évidence que l'interconnexion des systèmes se traduit par des modifications significatives des procédures de mise en oeuvre. L'impact sur la charge de travail de l'équipage est donc considérable. De plus la gestion des pannes et du warning concept doit intégrer ces éléments.

Comme expliqué précédemment la modélisation des modes dégradés a intégré l'architecture informatique et vidéo des principaux systèmes du TIGRE pour restituer fidèlement ces comportements en cas de dégradations.

6.2.5. Viseurs de casque

Chaque cabine est équipée d'un viseur de casque; il s'agit d'un casque de pilotage muni d'un réticule de visée pouvant afficher des informations discrètes sur l'armement et les alarmes (7 leds permettant d'éclairer une croix de visée et 6 informations) et d'un détecteur de position permettant de fournir aux différents modèles la position de la tête, et donc la ligne de visée, de chaque membre d'équipage.

Les positions brutes, perturbées par l'environnement électromagnétique des cabines, sont corrigées mathématiquement, un recalage initial est effectué à chaque début de mission afin d'obtenir une précision maximale.

Le viseur de casque est utilisé pour effectuer des tirs rapprochés au canon ou pour réaliser des désignations d'objectifs pour le missile air/air MISTRAL. Il sert également à désigner une cible à l'autre membre d'équipage; en effet, il est possible d'afficher sur MFD une image (thermique ou télévision) du viseur principal qui lui-même peut être asservi à la visée du casque pilote ou tireur.

6.2.6. Moyens de restitution de l'environnement

6.2.6.1. Génération sonore, téléphone de bord et radio

La génération sonore permet de restituer:

- le bruitage dynamique de l'hélicoptère,

- les bruits de départ des munitions,

- les sons d'alarmes entendus dans les écouteurs des casques (mixage avec le téléphone de bord) et dans le cockpit (cockpit horn),

- les sons "attendus", correspondants aux étapes successives de la mise en oeuvre d'équipements (par exemple les phases d'activation et d'accrochage des missiles).

Le téléphone de bord permet le dialogue entre les membres de l'équipage, les liaisons techniques avec la salle d'essais (conduite des essais), la simulation des dialogues avec le commandant d'unité.

6.2.6.2. Système de génération synthétique d'images

Chaque cabine (pilote et tireur) est installée dans une sphère de projection de 8 m de diamètre. Pour la visualisation du paysage extérieur, le système de projection permet un champ composé de 3 images jointives sur 192° x 60° en haute définition. Les images latérales sont décalées de 10° vers le bas pour s'adapter à la forme géométrique du cockpit et favoriser ainsi la vision latérale vers le bas (meilleure perception du sol).

Le système de GSI permet également la simulation des capteurs du viseur principal dans les voies optique directe, thermique et télévision noir et blanc: 2 images en basse résolution sont disponibles dont l'une pour le micro-moniteur du viseur principal (HID), et l'autre pour la recopie sur les MFD.

6.2.6.3. Base de données pour GSI

La base de données du terrain correspond à une zone géographique contenant Istres, les Alpilles, le sud-ouest du Luberon, Marignane, et le pourtour de l'étang de Berre, soit environ 60 km x 60 km.

Cette base de données réalisée spécialement pour la simulation de mission HAP est le fruit d'une collaboration entre le CEV et la société SOGITEC. A partir des fichiers DLMS décrivant l'altimétrie et la planimétrie du terrain, des phototextures génériques ont été réalisées et intégrées, des zones particulières ont été enrichies, des objectifs (convois, chars, radars, systèmes lance missiles, plots de ravitaillement, ...) ont été disposés selon le dispositif tactique retenu.

Cette base de données réalise un compromis remarquable entre le niveau de réalisme souhaité et les capacités du système de GSI disponible au CEV. Elle est une des meilleures réalisations actuellement utilisées en FRANCE dans le domaine des simulations pour hélicoptères.

De plus, une carte papier au format UTM (échelle 1/100 000) entièrement cohérente de cette BDD a également été réalisée et fournie aux équipages.

6.2.6.4. Visualisation des cibles

La visualisation des cibles aériennes peut être réalisée, soit par un système de projection indépendant, soit directement dans l'image du paysage.

Le halo de la cible projetée par un système indépendant est très visible, ce qui facile beaucoup trop la détection de la cible, et donc dénature la charge de travail correspondante.

Le choix s'est donc porté sur la visualisation des cibles intégrée au paysage, car son coût est moindre, mais cette solution présente également des avantages opérationnels: elle est cohérente avec le paysage et les effets de cache (relief, objets) sont pris en compte. Le seul inconvénient de cette solution réside dans la limitation de la visibilité de la cible aux champs projetés pour le paysage.

6.2.6.5. Installation en sphères des 2 cockpits

La restitution des champs des images projetées pour générer le paysage extérieur, ainsi que des positions angulaires (site, gisement) d'un objet (cible par exemple), doit être assurée correctement.

En fait, on doit considérer 3 points:

- l'oeil théorique de projection des images en sphère,

- la position de l'oeil du pilote dans le cockpit,

- le point de vue pour lequel les images sont calculées en temps réel.

L'oeil théorique est le point pour lequel on dimensionne un système de projection, en ce point les angles de visualisation seront respectés.

Il faut ensuite positionner l'oeil du pilote (dans son cockpit) à l'emplacement de l'oeil théorique du système de projection, et calculer les images synthétiques à partir de ce point. Pour un cockpit monoplace, les 3 points peuvent et doivent être confondus.

Dans le cas des cabines biplaces (en tandem ou côte-à-côte), un choix délicat doit être fait:

- soit respecter l'ergonomie du cockpit et admettre une erreur importante de restitution pour les champs projetés et pour les lignes de visée, par exemple le pilote et le copilote ne verront pas la piste au même endroit !

Une étude théorique (cf. § 10.1.) a permis de déterminer, pour la configuration tandem du TIGRE dans une sphère, que l'erreur est nulle pour un objet posé sur la surface de la sphère, et croit en fonction de la distance de l'objet (voir tableau ci-après). Cette solution est incompatible avec les objectifs de l'évaluation, notamment de l'utilisation opérationnelle qui est faite des viseurs de casque (par exemple transfert de cible d'un membre de l'équipage à l'autre).

- soit rompre l'ergonomie du cockpit en séparant les membres d'équipage (utilisation de 2 cockpits); cela semble difficile pour un équipage côte-à-côte, mais c'est une solution tout à fait réalisable pour un équipage en tandem. En effet, cette solution ne pose pas de problème de dialogue équipage puisque, dans le positionnement en tandem du TIGRE, les deux membres d'équipage ne peuvent pas communiquer visuellement. Il reste à évaluer les erreurs ainsi introduites.

La même approche théorique a permis de déterminer la configuration d'installation des cockpits pilote et tireur. Les solutions possibles étaient:

-1) installer chacune des 2 cabines dans une sphère différente avec une génération de paysage spécifique à chaque membre d'équipage; cette solution est théoriquement satisfaisante, mais son coût est prohibitif puisqu'elle nécessite deux systèmes indépendants de GSI (2 fois 3 canaux d'imagerie synthétique),

-2) installer chacune des 2 cabines dans une sphère différente avec une génération de paysage commune aux 2 membres d'équipage, chaque membre d'équipage étant à la même position d'oeil théorique; on peut ensuite choisir comme repère pour générer le paysage projeté:

* soit le point de vue du pilote,
* soit le point de vue du tireur,
* soit un point intermédiaire.

Avec une distance à la cible supérieure à 100 m, on peut garantir une erreur inférieure à 1 degré, cette erreur diminuant fortement en fonction de la distance; pour les distances de tir habituelles elle peut être considérée comme négligeable.

<u>Quelques résultats de l'étude théorique</u>

Pour une cible positionnée à 15 degrés en site et à 15 degrés en gisement par rapport au pilote, le tableau suivant présente les erreurs de visée pour le tireur en fonction de la distance de la cible dans chacune des 2 configurations:

- Configuration 1: cockpit en tandem intégré dans une sphère unique,

- Configuration 2: chaque cockpit dans une sphère spécifique avec un même paysage généré pour les 2 sphères.

	Configuration 1			Configuration 2		
D cible (m)	50	100	1000	50	100	1000
E gisement (deg)	3.56	3.78	3.97	0.43	0.22	0.02
E site (deg)	8.23	8.71	9.15	0.97	0.49	0.05

Finalement, la configuration retenue est la seconde, et le choix du repère pour le calcul de l'image (pilote ou tireur) peut être fait en fonction des objectifs de simulation pour privilégier l'un ou l'autre des membres d'équipage sans pénaliser le second. En l'occurrence, nous avons souhaité favoriser le pilotage avec HUD, qui nécessite une excellente harmonisation entre les 3 points de vue évoqués précédemment, ainsi qu'avec les symbologies présentées dans le HUD.

La solution adoptée consiste à installer chaque membre d'équipage dans une sphère de projection de 8 m de diamètre, le paysage projeté étant identique pour les deux membres d'équipage et couvrant 192° par 60° et étant calculé pour le point de vue du pilote.

6.2.6.6. Effets spéciaux

En liaison avec les conduites de tir, l'équipage peut détruire des cibles, visualiser l'impact ou la trajectoire de ses tirs afin de les rectifier. Une génération sonore du départ des munitions vient renforcer le réalisme.

Tous ces aspects, qui ne sont pas toujours simples à programmer et à mettre en œuvre, peuvent apparaître comme des gadgets visuels et sonores dans le cadre d'une simulation d'études.

Il n'en est rien et concrètement, ces effets spéciaux contribuent d'une manière très significative au réalisme de la simulation, et permettent une immersion rapide de l'équipage. Le tir, sans ces effets, semble particulièrement factice et irréel.

De plus, l'expérience a montré que la charge de travail n'est pas du tout représentative lorsque les membres d'équipage travaillent sans retour d'information. Notamment l'équipage perçoit immédiatement le départ de l'armement (il n'a donc pas besoin de contrôler ce départ sur ses symbologies). Bien que disposant de conduites de tir performantes (qui garantissent un excellent taux de succès si la procédure est correctement suivie), l'équipage va naturellement suivre des yeux la trajectoire des munitions et rechercher les points d'impact pour gérer la situation en fonction du résultat du tir (éventuellement corriger le tir, abandonner, dégager, se représenter sur l'objectif, ...). Cette gestion réaliste de la situation, en particulier des munitions, correspond aux objectifs de la simulation de mission car elle induit une charge de travail pour l'équipage.

6.2.6.7. Environnement tactique

Un logiciel de gestion et de visualisation de l'environnement tactique a été intégré dans la simulation. Depuis la salle de suivi d'essais, il permet de gérer des menaces au sol et aériennes: pré-programmation des comportements, conditions d'activation, etc. Ce logiciel permet de gérer en temps réel l'ensemble des données tactiques: amis, ennemis, modélisation de l'environnement électromagnétique (différents types de radars), menaces laser, zones irradiées, etc. Ce logiciel permet notamment de représenter d'une façon suffisamment réaliste l'interaction entre l'hélicoptère en essais (TIGRE HAP) et son environnement à partir d'une situation tactique prédéfinie.

Associée à ce logiciel, une visualisation de type cartographique permet le suivi du déroulement des missions. Cette cartographie est entièrement corrélée au terrain puisqu'elle a été générée à partir de la base données terrain du système de GSI (comme la carte papier fournie aux équipages).

Ces éléments sont complétés par un gestionnaire d'événements (tels que pannes, apparition de cibles ou de patrouilles amies ou dégradation des conditions météorologiques); ce logiciel permet le déclenchement automatique et de façon reproductible pour chaque équipage, des actions prévues dans les scénarios.

Les critères d'activation peuvent être liés au temps, à des lieux de passage, voire même des conditions complexes prenant en compte des actions de l'équipage.

6.2.6.8. Utilisation d'une cible pilotée

Cet hélicoptère cible est mis en œuvre par un autre pilote dans un simulateur simplifié et reconfigurable, fait d'une cabine générique, utilisant des écrans tactiles pour planche de bord, et d'un visuel du monde extérieur cohérent de la base de données où évolue le TIGRE. Ce moyen dispose des éléments suivants :

* une cabine spécifique (ancienne cabine Super-Frelon) équipée des organes de pilotage et des modèles de comportement (mécanique du vol, pilote automatique, navigation, radio-navigation),

* une planche de bord virtuelle constituée de 3 écrans tactiles de 19 pouces sur lesquels sont visualisés des symbologies de pilotage et navigation, des instruments classiques, une présentation cartographique,

* un visuel extérieur simplifié de caractéristiques:
  - altimétrie cohérente avec la BDD principale,
  - quelques objets dans le paysage,
  - la visualisation de l'hélicoptère HAP dans l'image (en tant que chasseur) et éventuellement d'autres mobiles, (bien entendu et réciproquement, le chasseur voit également sa cible dans son paysage synthétique !),
  - la planimétrie sera absente du visuel extérieur, mais cette absence sera compensée par une présentation cartographique en planche de bord.

La cible pilotée (ou équipier piloté), liée étroitement à cet environnement interactif, est un atout important. Les trajectoires prédéfinies de cibles programmées ne permettent évidemment pas de simuler un combat air-air de manière réaliste. Le CEV a développé une structure d'accueil permettant de faire communiquer en temps réel les modèles complets du TIGRE avec les modèles d'un autre hélicoptère en considérant en particulier les interactions entre systèmes d'armes.

6.3. Moyens de suivi d'essais et d'exploitation

6.3.1. Salle de conduite et de gestion des essais

Cette salle permet la mise en oeuvre des simulateurs et leur supervision. C'est un instrument indispensable pour la conduite des essais en simulation. Dotée de toutes les recopies des équipements des cockpits (écrans, instruments, boutons, voyants), elle permet de connaître exactement l'état du simulateur et de voir ce que voit l'équipage, cela permet une analyse en temps réel du déroulement des missions par le biais d'outils de contrôle et d'exploitation: espionnage de paramètres internes au simulateur, visualisations spécifiques pour le suivi d'essais (cartographie, situation tactique, etc.).

Cette salle est également dotée d'une station de suivi d'essais graphique qui permet de venir "espionner" les variables de simulation et de les représenter en temps réel sous forme de tracés défilants, bargraphes ou de manière générale, sous forme d'objets graphiques issus d'une bibliothèque de base ou développés au CEV. Cette station permet également l'enregistrement de données pour exploitation en temps différé grâce à des fonctions de rejeu de type magnétoscope.

6.3.2. Moyens audio et vidéo de debriefing

Des moyens audio et vidéo sont utilisés pour le debriefing et ont permis plusieurs enregistrements:

* micro-caméra en cabine pilote,
* copie vidéo directe du HID tireur,
* mixage des 4 MFD's sur une même image,
* viseur clair (HUD) superposé au paysage extérieur,
* visualisation tactique,
* sons (téléphone de bord, alarmes, bruits munitions).

6.4. Méthodes de travail

6.4.1. Documents officiels et Validation du simulateur

La traçabilité et la gestion de ces évaluations sont effectuées de la façon suivante:

- un programme d'essais présente aux participants, à l'industrie et aux services officiels les objectifs, identifie les fonctions et matériels objets de l'évaluation, et liste les moyens utilisés ainsi que le niveau de représentativité recherché pour chacun d'entre eux,

- une validation est effectuée par EUROCOPTER (éventuellement les autres sociétés impliquées) pour contrôler la conformité du simulateur aux spécifications industrielles et pour vérifier si le niveau de représentativité prévu est suffisant et s'il est atteint (principe du contrôle indépendant). Cette phase fait également l'objet d'un compte rendu contractuel appelé "Status Check du simulateur".

- les résultats de l'évaluation sont communiqués officiellement par un rapport d'essais. Celui-ci reprend et confirme les conditions d'expérimentations telles que la représentativité. Notamment, certains points peuvent s'avérer plus pénalisants que prévus ou au contraire les évaluateurs peuvent s'accorder pour en diminuer l'importance.

Dans tous les cas, les résultats de l'évaluation sont indissociables de la représentativité réelle, constatée et approuvée par les participants.

6.4.2. Différents scénarios

6.4.2.1. Préparation des scénarios et du contexte des missions

La définition et la mise au point des scénarios de mission, du contexte général et de la situation tactique est le résultat d'une préparation avec les pilotes d'essais du CEV, des équipages de la STAT, et des représentants de la société ECF.

Les scénarios ont été joués préalablement pour obtenir des éléments de référence et de comparaison (faisabilité, timing des missions par exemple).

Les pannes simulées ont été les suivantes:

- quelques pannes caractéristiques du système d'armement (modes dégradés HAP) telles que panne caméra IR, rupture des liaisons entre chaque sous-système d'armement et calculateur d'armement, panne totale nécessitant le passage en mode secours du système d'armement,
- pannes du système de base telles que panne AFCS, perte d'un moteur, panne d'un générateur de symboles de l'un des MFD (l'équipage devra, après la reconfiguration - il faut connecter deux MFD sur un même générateur de symboles - gérer et partager ces symbologies communes).

Les équipages ont été constitués pour toute la durée de l'évaluation et de la phase d'entraînement, les membres d'équipage restant au même poste (pilote ou tireur). Tous les équipages ont dû participer à l'entraînement et au briefing initial, avec une durée variable en fonction de leurs connaissances des systèmes de base et HAP.

Les scénarios comportent des éléments connus de l'équipage c'est à dire une partie seulement de la situation tactique générale, et des éléments inconnus, par exemple certaines menaces de type radars, convois ennemis, apparition des cibles et des pannes, changement des conditions météorologiques ...

6.4.2.2. Plans de vol

Une base de données de points de navigation, ainsi qu'une base de données de points de radionavigation ont été préparées et mémorisées comme cela aurait été effectué à l'aide du DID. Ces points servent de support à tous les scénarios. De plus, 5 routes sont mémorisées de la même manière.

6.4.2.3. Scénarios typiques

Ils sont proches des missions nominales décrites dans les documents de spécifications avec adaptation au contexte de simulation. Ces scénarios ont les caractéristiques suivantes :

- riches en événements,
- certains événements doivent être inconnus des équipages en évaluation,
- la densité des événements sera croissante au fur et à mesure des missions d'un même équipage,
- reproductivité et répétivité totale pour que tous les équipages voient les mêmes choses,
- durée d'un scénario ou d'une mission simulée: 45 mn environ, (les phases de vol de type transit ne sont pas jouées afin de gagner du temps car elles n'apportent pas de plus-value sur les résultats),
- 4 missions différentes de ce type ont été effectuées par chaque équipage lors de la première phase et 2 lors de le seconde phase.

6.4.2.4. Scénario "catastrophe"

Ce type de scénario doit permettre l'évaluation dans des conditions particulièrement dégradées ou difficiles, incluant une densité en événements très supérieure aux scénarios typiques, et/ou des événements à très faible probabilité d'occurrence (pannes multiples par exemple). Ce type de scénario doit induire une charge de travail, voire un niveau de "stress" très important pour l'équipage. Comme les scénarios typiques, il est également reproductible.

6.4.2.5. Scénarios d'entraînement

Vus la complexité et le volume des systèmes simulés, il est indispensable que les équipages soient briefés et entraînés préalablement. Les scénarios utilisés sont spécifiques à l'entraînement et sont différents des scénarios d'évaluation.

Ces scénarios doivent permettre aux équipages d'aborder et de mettre en œuvre tous les concepts, procédures, modes, commandes et symbologies. Ils permettent également une familiarisation et une bonne connaissance des moyens d'environnement (base de données de terrain par exemple).

6.4.2.6. Contexte général d'évaluation

6.4.2.6.1. Organisation générale

Des fiches de consignes et de description de la situation générale ont été remises à tous les équipages, ainsi qu'une fiche pour chaque mission. Ces fiches rappellent la situation tactique (Weapon Free Zones, Transit Corridors, menaces sol-air, ligne d'engagement, etc.) connue de l'équipage, l'objectif de la mission, la configuration de l'armement de l'appareil, les temps de passage, les consignes d'emploi de la radio, les conduites à tenir, etc.

Chaque session de simulation est précédée d'un briefing avec remise des fiches de mission et de la carte papier. Chaque mission est suivie d'un debriefing à chaud pour recueillir les impressions de l'équipage et les confronter avec les remarques des observateurs.

Pour chaque équipage, un debriefing global permet de reprendre tous les éléments évoqués, de voir les cassettes vidéo, et donc de reconsidérer ou d'étayer les différentes remarques.

Une réunion générale des participants permet ensuite d'harmoniser les différents points de vue pour présenter une synthèse de l'évaluation.

6.4.2.6.2. Equipages participants

Pour obtenir une richesse en terme de participation, le CEV a pleinement associé les représentants des futurs utilisateurs et a réuni pour cette évaluation:

- 2 équipages du CEV qui effectuent également les essais en vol des prototypes, et qui sont aussi des anciens personnels de l'ALAT,
- 2 équipages de la section technique de l'armée de terre (STAT) qui sont en charge du suivi du programme,
- 1 équipage venant directement des régiments de l'ALAT,
- 1 équipage d'instructeurs de l'école d'application de l'ALAT.

La provenance variée des équipages permet, grâce à la richesse et à la diversité de leurs expériences, de multiplier les points de vue et d'assurer une couverture optimale des besoins.

6.4.2.6.3. Suivi des essais

Depuis la salle de conduite des essais, plusieurs observateurs et l'ingénieur responsable de l'essai prennent des notes sur le déroulement des missions, notamment sur les circonstances particulières telles que les incompréhensions ou mauvaises interprétations de l'équipage, les bonnes séquences ou au contraire celles qui ont posé un problème. Ils analysent les points notables, s'interrogent sur les comportements, essaient de les expliquer tout en vérifiant le déroulement correct de la mission grâce aux moyens de suivi et d'exploitation.

Tous ces éléments sont ensuite confrontés avec les impressions de l'équipage d'une part et les enregistrements vidéo d'autre part. Bien entendu, il ne s'agit pas de juger ni des capacités, ni des compétences des équipages, mais de l'adéquation des spécifications aux besoins opérationnels.

7. RESULTATS

7.1. Remarques sur les spécifications des systèmes embarqués

Une approbation globale confirme les évaluations précédentes, et le système est bien perçu et correctement appréhendé par les équipages, son adéquation aux besoins est considérée comme bonne.

Quelques points spécifiques méritent une attention particulière:

- l'amélioration de la lisibilité des Do-list et prise en compte de règles pour leur rédaction,
- une meilleure lisibilité des modes d'orientation de la page tactique des MFD est souhaitée, car cela peut être source de confusions aux conséquences graves, ces points sont à noter pour l'intégration de la cartographie,
- la gestion des niveaux des menaces peut être améliorée,
- la configuration initiale des paramètres des armements doit être modifiée,

- la gestion des LSK sur les MFD doit respecter des règles générales, certaines ont été proposées par les évaluateurs,
- les symbologies en cas de panne moteur doivent être revues,
- une convergence avec les résultats des essais en vol du prototype N°4 est notée sur les points suivants: possibilité d'allégement des symbologies HUD, quelques problèmes d'ergonomie des poignées (problème pris en compte et traité par ECF).

7.2. Travail en équipage

Il a été possible, notamment, d'évaluer la charge de travail due au dialogue intra-équipage et de valider les moyens fournis par le système du TIGRE pour effectuer la communication entre pilote et tireur.

En effet, contrairement aux autres hélicoptères présents au sein de l'ALAT, le TIGRE présente la particularité d'une disposition de l'équipage en tandem, ce qui exclue toute communication visuelle. Ceci est une nouveauté pour nos pilotes et modifie quelques habitudes.

Ainsi, outre la communication orale par phonie, l'équipage dispose des moyens suivants:

- Possibilité de recopier un MFD de l'autre membre d'équipage sur son propre MFD. Ceci permet d'obtenir une référence visuelle commune ce qui n'est pas généralement le cas puisque les pages MFD sont largement configurables.
- Présence d'un "directeur d'ordre" sur le viseur clair. Cette symbologie supplémentaire informe le pilote sur la visée du tireur, lui fournit une consigne pour rallier, de manière optimale, le domaine de tir et lui indique si les meilleures conditions de tir sont réunies. Elle permet principalement au pilote de rentrer, et de rester, dans le domaine de tir, elle s'avère indispensable pour réaliser des tirs coopératifs, notamment des tirs proches de l'axe machine.
- La possibilité de visualiser sur MFD (image thermique ou télévision noir et blanc) la visée de l'autre membre d'équipage (utilisant le viseur de casque notamment) permet de lui désigner facilement un objectif.
- transfert de cible d'un membre de l'équipage à l'autre, notamment à l'aide des viseurs de casque,
- indication sur HUD du gisement de la visée du tireur permettant ainsi au pilote d'anticiper, et d'éviter le passage en butée du viseur principal,
- information sur l'état d'engagement des armements dans le cockpit tireur (voyants) et sous forme de symbologies dans le HID.

Le système du TIGRE met donc à disposition de l'équipage un nombre important de moyens de dialogue plus ou moins complexes.

Grâce aux évaluations de missions simulées, il a été possible de vérifier qu'ils étaient aisément mis en oeuvre et couvraient l'ensemble des besoins.

7.3. Réflexions sur le concept d'emploi et sur les procédures opérationnelles

Cette question reste évidemment de la responsabilité de l'ALAT. La nouveauté de l'hélicoptère TIGRE, de ses systèmes embarqués et de la configuration en tandem nécessite un profond changement des méthodes et habitudes des équipages.

Pour la première fois, il a été donné la possibilité à des équipages de jouer des missions significatives dans un environnement représentatif. Le simulateur a été le moyen d'amorcer cette réflexion sur des bases concrètes.

7.4. Simulation d'entraînement

Ces phases d'évaluation ont également conforté les travaux en cours sur la spécification des moyens de formation pour le TIGRE.

Quelques aspects méritent clairement des réflexions approfondies. On pense, par exemple, aux problèmes des systèmes de GSI et de leurs bases de données, pour lesquels la simulation hélicoptère constitue réellement une difficulté technique.

La simulation d'études, quand elle est aussi représentative, peut constituer un excellent banc de test pour certains moyens de formation, en particulier sur les aspects FMS (Full mission simulator) où les similitudes sont grandes.

7.5. Amélioration de la simulation pour les phases ultérieures

L'expérience de ces phases de simulation permet de réfléchir et d'envisager l'amélioration et l'enrichissement des moyens:

- l'ambiance sonore et radio peut être significativement améliorée en ajoutant un système de multiplexage des liaisons permettant ainsi de simuler différentes fréquences. Dans la réalité, d'autres appareils encombrent le réseau radio, et le commandant de bord doit rester attentif pour répondre seulement quand on s'adresse à lui et pour s'insérer dans le trafic radio opérationnel lorsque celui-ci est dense. On peut également simuler les difficultés à établir une liaison radio lorsqu'on est au milieu des obstacles.
- l'utilisation d'une cible ou d'un équipier piloté amène une réelle plus value dans la mesure où les scénarios utilisant cet outil sont minutieusement préparés, testés et mis au point; il ne s'agit pas de laisser la cible ou l'équipier évoluer à son gré: comme l'hélicoptère principal, il se voit confier une mission. De plus, les communications entre les différents hélicoptères et la salle d'essais doivent pouvoir se faire sur des canaux différents (voir point précédent).
- de nouvelles fonctionnalités concernant certains moyens de simulation tels que BDD, GSI, logiciel d'environnement tactique et effets spéciaux peuvent également être implémentées. Leur réalisme peut être amélioré.

8. CONCLUSION

En premier lieu, ces phases de simulation de mission ont nécessité une énergie et un travail considérable pour la préparation des moyens de simulation et des scénarios de mission, et ensuite pour la réalisation de cette évaluation. Nous tenons à remercier tout le personnel du centre de simulation et également les participants, personnels navigants et équipages du CEV, de la STAT et de l'ALAT ainsi que les représentants d'ECF.

La simulation de mission HAP a permis, et c'était son objectif principal, de valider la définition, et d'effectuer quelques modifications qui n'avaient pu être vues, ni lors des précédentes campagnes de simulation, ni lors des essais en vol. On notera que la proximité des essais en vols a permis de travailler avec les équipages qui effectuent les 2 types d'essais (complémentarité et convergence des remarques).

Le grand réalisme apporté à cette simulation est le garant de la crédibilité des résultats dans la mesure où un résultat de simulation ne peut pas être considéré indépendamment de la représentativité du moyen sur lequel il a été obtenu.

Cette évaluation a également permis, pour la première fois, de voir évoluer le TIGRE dans un contexte opérationnel réaliste, et les enseignements que l'on peut en retenir dépassent largement la définition du cockpit. Les bases d'une nouvelle étape dans la réflexion sur le concept d'emploi sont jetées. Les besoins pour la simulation d'entraînement pour les futurs équipages TIGRE sont plus précisément cernés.

Enfin, sur un plan plus technique, l'architecture de simulation mise en place constitue une base solide pour évaluer dans de bonnes conditions de représentativité les prochains développements envisagés pour le TIGRE: contre-mesures actives, détecteur d'alerte et de veille (radar de détection), transmissions de données, où un environnement riche et réactif est indispensable à la simulation. D'autres voies sont également étudiées pour participer à ce réalisme de l'environnement tactique, comme un dispositif d'animation automatique de cibles au comportement plus sophistiqué incluant des techniques d'intelligence artificielle.

9. GLOSSAIRE

AFCS: Automatic Flying Control System, pilote automatique

ALAT: Aviation Légère de l'Armée de Terre

BAP: Bandeau d'Armement Pilote

BDD: Base de données terrain pour GSI, (Data base for CGI)

CEV: Centre d'Essais en vol

CME: Contre Mesures Electroniques (voir ECM)

CDU: Control and Display Unit

DCAé: Direction des Constructions Aéronautiques

DGA: Délégation Générale pour l'Armement

DID: Data Insertion Device

DLMS: Data Land Mapping System

DO-LIST: liste d'actions à effectuer à l'équipage en cas de panne

EA ALAT: Ecole d'Application de l'ALAT située au LUC en Provence

ECD: EUROCOPTER DEUTSCHLAND

ECF: EUROCOPTER FRANCE

ECM: Electronic counter measure

FLIR: Forward Looking Infra Red

FMS: Full Mission Simulation

GSI: Génération Synthétique d'Images, (computer generation images CGI)

HAC: Hélicoptère Anti-Char (anti tank version)

HAP: Hélicoptère d'Appui-Protection (combat support version)

HID: Head In Display, écran situé dans le bras porte-occulaire du viseur principal

HSD: High Speed Data, interface d'entrée/sortie à haut débit

HUD: Head Up Display, viseur clair

IR: infra red ou infra-rouge

MEP-HAP: Mission Equipment Package for HAP

IPL: Indicateur de Première Limitation (voir PMI)

MFD: Multi Fonction Display (écran multifonctions)

MPX: système d'exploitation propriétaire de la société ENCORE COMPUTER, (ENCORE COMPUTER company's proprietary operating system)

MTR: consortium industriel en charge de la fourniture des moteurs du TIGRE

NRM: Nuclear Radiation Measurement

PC: Personal Computer

PCA: Poste de Commande Armement, (armament control panel)

PMI: Power Margin Indicator

SE/ES: sigle de la Section Etudes et Simulation, centre de simulation du CEV

SFIM: Société Française d'Instruments de Mesures

SIMCO: Simulateur HAC d'ECD

STAT: Section Technique de l'Armée de Terre

STRIX: Système de Télémétrie, de Reconnaissance et d'Identification tous temps, viseur principal de l'HAP monté sur le toit, (Roof mounted Sight)

TR: Temps Réel

TD: temps différé (par opposition à temps réel)

TWE: système de contre-mesures

UNIX: système d'exploitation couramment employé dans le monde informatique.

10. REFERENCES

1) "Etude théorique des sphères pour une utilisation avec cabines biplaces (tandem ou côte à côte)" Mr B. MALLET, Note interne CEV/SE/ES du 24.10.1995 (non diffusée).

Modular Roll-on / Roll-off Design Concept of a Rotorcraft Simulation Center

Klaus Niessen

CAE Electronics GmbH
Steinfurt 11, D-52222 Stolberg, Germany
Tel.: +49 2402 106200 * Fax: +49 2402 106270

Training Concept

It must be the objective of the army aviation corps' flight training to enable helicopter pilots to use their weapon system safely and efficienty by using the technical equipment and possibilities:

- at day and night
- in air mobile combat of combined arms
- under almost all possible weather conditions.

This is done in the so-called training equipment compound where the adequate training equipment is assigned to the respective training objective.

Partial skills are learned by means of simple procedure trainers and handling models before complex simulators and finally the original device, the helicopter, are used to merge the partial skills.

This training equipment compound allows to reduce costs and at the same time to reach those training objectives which will be demanded in the future.

Training equipment essentially consists of the following:

- **CBT** is an interactive **computer based training** equipment which is used for interactive learning of flight theoretical and technical aircraft knowledge, navigation training and radio communications.
- **Part Task Trainers** are used for hands-on training of partial capabilities. They are corresponding to the respective system in design, layout and operation.
- **Flight Simulators** and Combat Mission Simulators will be treated in detail during the further explanations.
- The **close-in combat simulator (AGDUS)** corresponds to the common equipment of the army.
- **SIRA**, the common equipment **for combat simulation**, must be extended to allow for the command and control of operations of air-mobile forces.
- The **basic training helicopter (SHS)** is an indispensable equipment for the basic and advanced training of aircrews. The helicopter is not replaceable - especially with regard to affective training objectives.

Flight Simulators

Flight simulators reproduce the complete (especially dynamic) behaviour of the helicopter so that all relevant targets of practical flight training to the level of mastery can be trained.

- 8 ea HGA simulators
- 2 ea UH-1D simulators and
- 2 ea CH-53 G simulators

will be delivered in the period from 1999 to 2000 for the simulation center.

A modularization would be an ideal solution for the realization of such a scope of delivery (12 flight simulators), especially with regard to future flight simulators or combat mission simulators which, as opposed to flight simulators, also reproduce the helicopter's mission equipment.

Planning of Simulator Hours

The number of simulators is based on a planned number of simulator hours per year as follows:

- 16894 for the basic training helicopter
  This means that with 2160 h per cockpit and year the training requirement will be satisfied with 8 SHS simulators.
- The simulator hours for the UH-1D are estimated at 5120 h per year; with 2480 h per cockpit and year 2 UH-1D simulators are required.
- For the CH-53G 4904 simulator hours per year are required. If - analogous to the UH-1D - also 2480 h per cockpit and year are estimated, 2 CH-53G simulators are required.

A Modular Simulator - Why ?

The modular architecture of one or several simulators located in one single center was the customer's idea considering that through definition of technical or functional communalities within the basic training devices, effects of rationalization can be achieved.

The possibility of reduction of the total amount is- for example - given because the simulator hours required for 2 type-specific helicopters A=1500h/year and B=3300h/year can be covered by 2 basic modules

Paper presented at the FVP Symposium on "Advances in Rotorcraft Technology", held in Ottawa, Canada, 27-30 May 1996, and published in CP-592.

and one type-specific module A and 2 type-specific modules B.

If we assume the conventional construction, 3 badly occupied individual simulators would be necessary. If all simulators have the same basic modules, this results in large numbers of identical modules.

With the procurement and production of larger quantities, a total cost reduction of a minimum of 10% can be realized. This cost reduction is achieved by a more efficient procurement, bulk discounts and more efficient production because of identical parts.

The considerably lower life cycle costs can be based on the facts that

- only one single modification development must be carried out for the modification of identical modules,
- fewer spare and replacement parts have to be stored and
- fewer maintenance personnel is necessary.

Moreover the later integration of new modules or elements is considerably simplified because of standardized interfaces.

Definition of Terms

First of all the essential terms have to be defined:

The **simulator** is the functional unit which consists of at least one basic module and one type-specific module.

The **simulation center** consists of 12 simulators.

A **module** is a combination of **elements** or functional units such as sound system, motion system, control loading system, etc.

Subquantities or parts of elements are **components** such as computer, disk storage, processors, pumps, panels,etc.

In general, the present concept of a modular simulator does not include any new additional elements in comparison with the conventional comprehension.

What is new is the uncompromising separation of separable elements and the definition of their interfaces as well as the resulting possible use of identical components on the module level.

A later objective is the highest possible flexibility in the operation of simulators through the exchange or use of different type-specific, sensor or tactics modules on one and the same basic module.

Basic Module

The basic module contains all those elements providing the functions equally necessary for all simulators.
A careful distinction must be made between hardware and software elements. Software, which is different for different simulators, does not belong to the basic module. The hardware however, that is the computer on which this software is running, can be designed as a standard for all simulators and belongs to the basic module.

As a consequence there must be only one basic module configuration for the simulation center.

A basic module consists of 3 groups of elements:

- **Group 1** are the primary elements which has each simulator, such as simulation computer, operating system, type-specific-independent and parameterizable type-specific, sensor and tactical software, interfaces, image generator, display system, motion system, control loading system, sound/audio system, data recording, etc.

- **Group 2** are the elements such as the database for out-of-cockpit view, but without special attributes for sensorics and tactics, as well as the instructor operator station.

- **Group 3** are the elements such as briefing/debriefing, database generation system, lessonplan station, energy supply, air-conditioning.

Type - Specific Module

Fundamentally the type-specific module contains all type-specific parts which are necessary for the representation of helicopter subsystems. Not included are the whole mission avionics system and the sensor parts which are necessary for accomplishing the mission such as night-vision-goggles, Forward Looking Infrared, etc.
For each helicopter type an individual type-specific module with corresponding interfaces to the other modules is required.

The type-specific module consists of elements like the cockpit including the complete equipment which means instrumentation, controls, a conventional cockpit interface with digital inputs and outputs and analogous inputs and outputs, seats with seatshaker as well as the Flight Controls such as Control Column, Collective Pitch and pedals.
Not included in the type-specific module is the cockpit instructor console if it can be realized separately from the cockpit.

Naturally, the functional separation of basic and type-specific module is not limited to the hardware, but also valid for the software.

Generic- / Specific Software

Generic or data-driven software is a parameterizable software which can be used universally for different modules of a module type. This software performs the tasks by initialization and configuration with type-specific data.

As the generic software is independent of specific requirements, it is a part of the basic module.
The appertaining specific data is part of the respective module whose functionality has to be reproduced.

Specific software is the one which performs a specific task of a certain module and cannot be used for tasks of another module of the same or a different module type.

Generic software is, for example, the motion model or weather model but also models for helicopter dynamics or the rotor blade.

Specific software is, for example, the Flight Director model of the different helicopter models.
Independent of the type, the generic as well as the specific software can run on the computer of the basic module.

Sensor Module

Each sensor type requires an individual sensor module. Such a module contains all elements necessary for recording, processing and displaying all mission dependent sensor signals from this sensor type.

The simulation of the out-of-cockpit view is one exception.

Typical sensor modules are:

- Night Vision Goggles
- FLIR
- Radar
- Sonar

A sensor module generally consists of the following components:

- Sensor image generation
- Post processors for specific image effects
- Sensor image presentation
- Sensor database
- Software for the simulation of certain operating modes
- Original device or controls and
- Interfaces within the module and to other modules

Tactics Module

The tactics module contains all elements of mission avionics, self-protection and weapon parts of the own helicopter as well as all parts for the generation and representation of the mission scenario.

As the helicopter simulators treated in this paper have no tactics module in the required realization phase, this will not be further considered.

Main Topics of Realization

In the development of 12 simulators by means of modern simulation technology the main emphasis is attached to:

- Implementation of the future-oriented modular concept to reduce procurement and life cycle costs by using the latest technology.

- Equipment of 11 channel high-performance image generators with 8 channels for dome projection, 2 channels for NVG simulation and one instructor eyepoint.
  With channel performances of 1,54 million pixels, a pixel filling rate of 300 million pixel / sec. and appr. 5000 polygons / channel, the image generator can simultaneously represent 64 moving objects with 6 degrees of freedom and manage 256 dynamic coordinate systems.

- For the display system a partial dome construction has been chosen. 8 lyquid crystal light valve projectors guarantee a field-of-view of 240° horizontally and 90° vertically with a resolution of 7.5 arcmin throughout the entire area.

- Realization of a realistic night-vision-goggles simulation.
  The original components are used and the image amplifier tubes are replaced by cathod ray tubes. The NVG are slaved to the head movements without delay by a 240 Hz headtracker and a precalculation of the line of vision.

- Design for a faster and uncomplicated change of cockpits in order to integrate type-specific modules of other helicopter types into the simulator without problems.

- The construction consists of three separable segments; the type-specific front cockpit, the middle, the on-board instructor console and the finally rear part, the so-called walk-away module. The parts can be driven to the back from the dome, are easily separable from each other and are - coupled in a new configuration - integrated again.

- Realistic simulation of helicopter dynamics by using a powerful and flexible rotor blade model.

- Use of a high performance hydraulic motion platform with 6 degrees of freedom and a control

structions.
A logical, graphical user interface improves the overview, optimizes interventions and reduces the attention levels.

- Each of the 12 simulators receives a debriefing station; their networking will avoid a fixed attachment of simulator and debriefing station and achieve a large organizational flexibility.
The central element of the debriefing station is an IOS identical graphics workstation with an independent image generator. Data filing and the presentation of all mission relevant information and actions, also with the out-of-cockpit view as

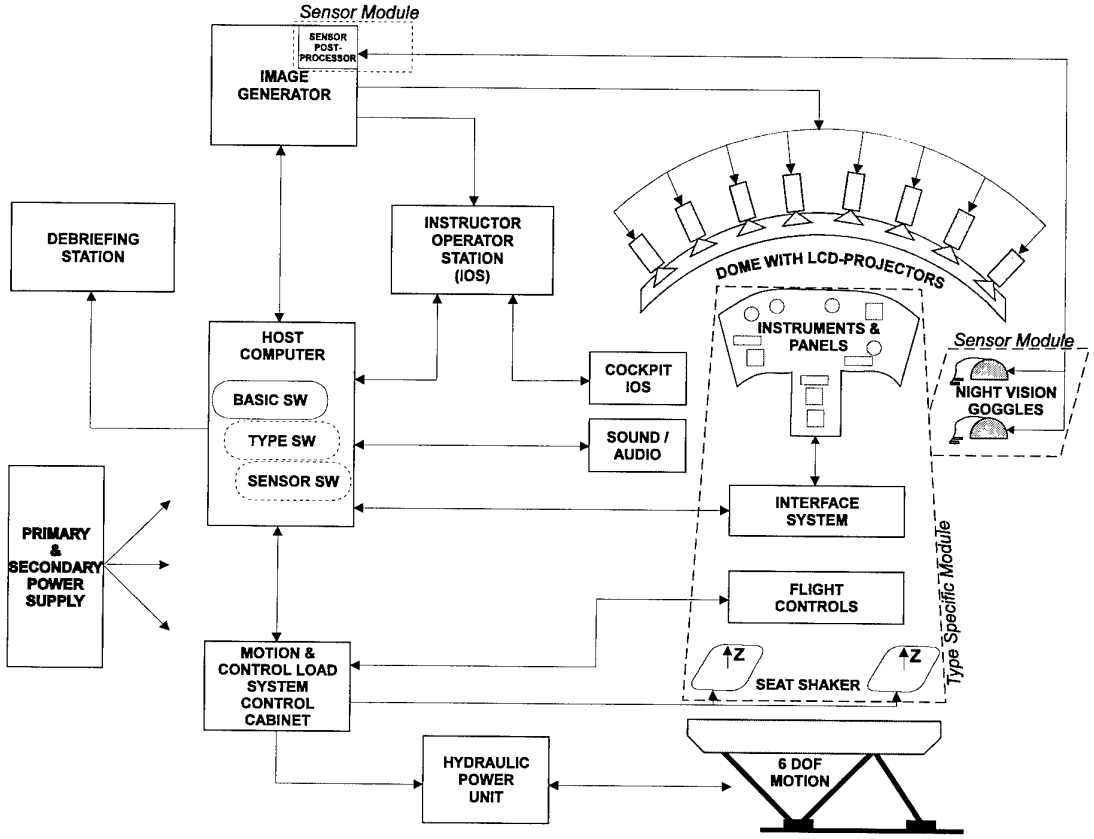

Figure 1: *Bockdiagram of 1 Simulator*

force simulation of latest technology by using electromechanical drives. The simulation of high-frequency vibrations of the cockpit cabin is also supported by a seatshaker each for the pilot and the co-pilot.

- Implementation of a standardized operating concept for all instructor and debriefing stations, for hardware layout as well as software functionality. The instructor has the possibility to control and monitor the training operations via an external IOS, an on-board IOS or a portable LCD panel. They all have an identical functionality and also enable the crew to use the simulator without in-

experienced by the crew and from other perspectives, communications, etc. are guaranteed. In addition, a lecture-room is equipped with a debriefing component of the same functionality so that a follow-up discussion can also be performed with a large audience.

- Software development will be in accordance with the Allgemeiner Umdruck 250, also called V-model, a standard of the German Armed Forces, comparable to DOD STD 2167 A. The software structure supports the modular architecture where all parameterizable type-

- specific-, sensor- and tactics-dependent parts asfar as possible extend to all modules and only the data records are assigned to the respective module.

- Realization of simulation software in the programming language ADA, expecting to be able to effect modifications and adaptations fast and at low costs and to port the basic module software for future helicopter simulators easily and without problems on any computer platforms.

- The 12 simulators of the center are networked via an FDDI-connection and can effect common exercises according to the DIS protocol.

  An open system will be integrated so that the networking can also be extended to other DIS capable simulators via a wide-area network.

- A prototype database with the size of 100.000 km^2 will be delivered together with the 12 simulators.
  This database contains one highly detailed training area of about 1.500 km^2 and 3 insets of about 2 - 6 km^2 each with very high detail.
  The database will also have the attributes for simulation of NVG view and for sensor modules, e.g. Infrared or FLIR, which may be required at a later time.

- Lessonplan and database generation will be taken into consideration especially in the light of provisions for preparing exercises in the sense of mission rehearsal.

- In order to obtain the IFR certification, the German Aviation Authority in Braunschweig will be involved as early as possible in the development process.
  The simulators should have this certification so that a certain percentage of IFR simulator hours will be accepted as actual flying hours.

- A high availability on the basis of the simulators' modular structure is to be obtained at reasonable maintenance expenditure.
  Common components relieve the logistics and a central system examination will facilitate maintenance and repair, supported by a mobile maintenance station.

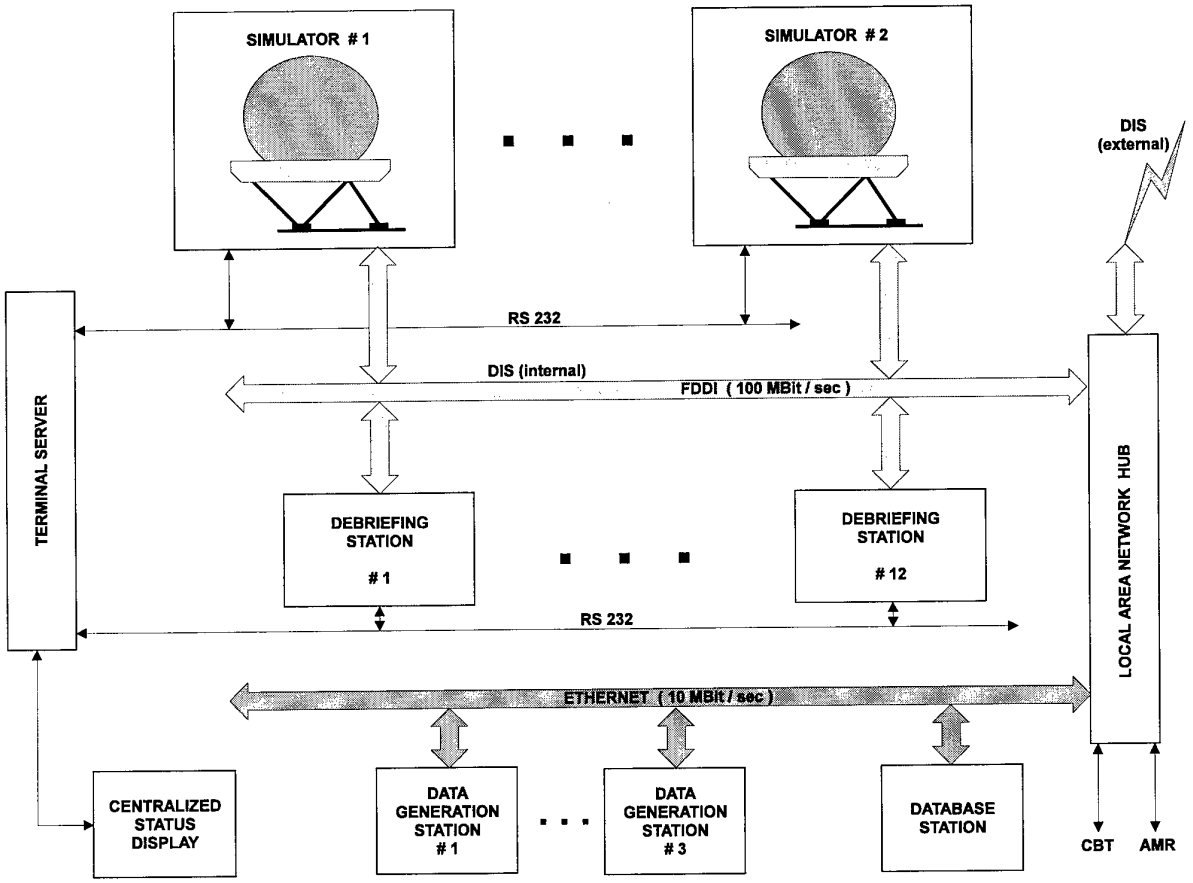

Figure 2: *Blockdiagram of Simulation Center*

Figures

Figure 1 outlines the layout of one of the 12 simulators. The individual modules are marked accordingly and linked to each other by clearly structured interfaces.
The hardware and software parts of the type-specific module can be seen very clearly here. It is this module which will finally turn a generic helicopter simulator into a UH-1D, CH-53G or SHS-type helicopter.

Figure 2 shows the combination of 12 simulators with supporting facilities such as debriefing stations, data generation stations, database station and the central status display.
Each simulator is linked via the network with the other elements so that there is no fixed assignment of a simulator to a data generation station or debriefing station. This allows very flexible training operations and an optimum use of free resources.

The combining of the simulators for exercising common missions among each other and with other DIS-capable simulators is effected via an FDDI connection.
The interfaces for linking the CBT component and the AMR (training equipment computer) are also allowed for.
For the simulation center 12 identical basic modules, 2 type-specific modules UH-1D, 2 type-specific modules CH-53G, 8 type-specific modules SHS and 8 identical sensor modules will be delivered in accordance with the modular concept.

Evaluation de la pilotabilité des hélicoptères de transport en utilisant les essais en vol de type ADS-33C
Formalisation de la méthodologie et de l'instrumentation d'essais

D. Fournier
Ingénieur Navigant d'Essais
Centre d'Essais en Vol
13128 Istres Air, France

D. Papillier
Ingénieur d'Essais
Centre d'Essais en Vol
13128 Istres Air, France

RESUME

Des essais en vol du type de ceux proposés par l'ADS-33 vont se généraliser lors des phases de développement et de qualification des futurs hélicoptères de transport. En s'appuyant sur les résultats d'une expérimentation menée sur un SA 332 Super Puma Mk II, ce document tente de formaliser la méthodologie et les moyens d'essais nécessaires.

1 INTRODUCTION

Au début des années 80 l'Aeroflightdynamics Directorate de l'US Army Aviation Troop Command commença à développer une norme de pilotabilité des hélicoptères militaires destinée à remplacer l'ancienne norme Mil-H-8501A considérée comme obsolète. Les études menées à l'origine dans le cadre du programme LHX de l'US Army (hélicoptère de combat) ont montré l'intérêt d'une telle norme pour les autres types d'hélicoptères militaires (observation, transport, naval). Ainsi est née l'Aeronautical Design Standard 33 (ADS-33) aujourd'hui à la révision D (réf 1 et 2).

Le NH 90, dont le premier vol a eu lieu le 18 Décembre 1995, est un hélicoptère de la classe 9 tonnes développé par quatre nations (France, Italie, Allemagne, Pays Bas) en deux versions, une version de transport tactique, une version de lutte anti-sous-marine et anti-surface. Cet appareil est équipé d'un système de commandes de vol numériques quadruplex à pleine autorité. Les spécifications du NH 90 demandent un niveau de pilotabilité 1 (handling quality level 1) dans toute l'enveloppe de vol opérationnelle. Pour répondre à cette exigence le contrat de développement prévoit que d'un commun accord les officiels et les industriels adaptent l'ADS-33 C au NH 90. En particulier un nombre limité de manoeuvres d'essais en vol (Flight Test Maneuvres) devront être démontrées en vol. Dans ce but, un groupe de travail (NH 90 ADS-33 Tailoring AD'Hoc Group) a été créé en 1993. Il regroupe des experts industriels et étatiques. En particulier, les Centres d'Essais en Vol Officiels (Official Test Centers) des quatre nations y sont représentés. En tant que membre de ce groupe de travail, le Centre d'Essais en Vol (CEV) a estimé qu'il lui était nécessaire d'approfondir son expérience dans le domaine en effectuant une expérimentation en vol sur un appareil de transport SA 332 Super Puma Mk II.

Dans ce document, seront présentés les objectifs de cette expérimentation ainsi que les principales conclusions qui en ont été tirées tant du point de vue de la méthodologie d'essais que des moyens d'essais à mettre en oeuvre.

2 OBJECTIFS DE L'EXPERIMENTATION

l'objectif de cette expérimentation était d'analyser la méthode d'essais et les moyens d'essais à mettre en oeuvre lors d'essais en vol de type ADS-33 dans les phases de développement et de qualification d'un hélicoptère militaire de transport. Il ne faut, en effet, pas confondre essais en vol de développement et de qualification et vols d'évaluation opérationnelle. Ces derniers sont réalisés sur un appareil de série ou de présérie ne possédant pas d'installation d'essais sophistiquée, leur but est essentiellement d'évaluer la capacité d'un appareil à remplir une mission opérationnelle particulière. La problématique des essais de développement et de qualification est fondamentalement différente, les vols sont effectués sur un prototype dont les coûts de mise en oeuvre (coût à l'heure de vol) sont très élevés. L'objectif de tels vols est de collationner pour les bureaux d'étude le maximum de données qui seront ensuite analysées pour en déduire des modifications éventuelles du prototype (développement) ou pour conclure au respect des spécifications (qualification). Il dispose à ces fins d'une installation de mesure et d'essais évoluée qui doit être utilisée. Il faut par contre qu'elle soit conçue à l'origine pour répondre aux exigences spécifiques des essais du type ADS-33.

Paper presented at the FVP Symposium on "Advances in Rotorcraft Technology", held in Ottawa, Canada, 27-30 May 1996, and published in CP-592.

3 METHODE ET MOYENS D'ESSAIS

3.1 Principes généraux

L'évaluation de la pilotabilité d'un hélicoptère selon la méthode ADS-33 repose fondamentalement sur le jugement du pilote. Il doit en effet évaluer sa capacité à effectuer la manoeuvre dans le respect des contraintes (précision de pilotage) qui lui ont été fixées ainsi que la charge de travail associée. Pour cela il s'appuie sur l'échelle de Cooper Harper et attribue une note (Cooper Harper Rating, CHR) de 1 à 10 (cf. figure 1). Deux niveaux de précision de pilotage étant requis (niveau désiré et niveau adéquat), une erreur sur l'appréciation de la précision effectivement atteinte fausse le résultat final de façon rédhibitoire. Il est donc impératif que le pilote dispose en temps réel d'un retour d'information sur la précision de pilotage effectivement atteinte.

L'autre élément fondamental qui soutient l'expérimentation présentée ici est qu'il s'agit d'étudier la pilotabilité d'un hélicoptère dans le cadre de son développement et de sa qualification. Il est donc indispensable qu'à l'issue des vols, en plus du jugement du pilote (CHR) des données objectives soient fournies aux ingénieurs des bureaux d'étude. Ces données donneront lieu à des analyses quantitatives permettant d'étudier les défaillances éventuelles détectées à travers un CHR élevé et d'envisager des solutions correctrices. Ces données viennent donc consolider le jugement du pilote.

Il va sans dire que l'ensemble de la méthode repose sur le postulat que les manoeuvres sont répétables. En effet l'ADS-33 exige qu'au moins trois pilotes réalisent les manoeuvres afin de comparer les résultats obtenus. Il est évident que comparer des résultats issus de manoeuvres par trop différentes serait inutile. Il faut donc définir les manoeuvres avec cette exigence en tête, il faut les simplifier au maximum (les « épurer » de ce qui pourrait être lié à une culture opérationnelle trop marquée) sans toutefois les dénaturer (les plus intéressantes sont les manoeuvres multiaxes). C'est une tâche difficile et longue. Une discussion sur ce sujet est hors des objectifs de ce document, les lecteurs pourront se reporter au document en référence 4 qui décrit, entre autre, les manoeuvres retenues pour le NH90. Les manoeuvres exécutées lors de cette expérimentation sont pour l'essentiel issues de celles présentées dans le document.

3.2 Retour d'information

Les manoeuvres à effectuer sont en général des manoeuvres à haut gain de pilotage. Les précisions de pilotage demandées au pilote sont donc élevées. Pour les paramètres du type vitesse, attitudes, les équipements traditionnels de pilotage sont suffisants pour que le pilote contrôle sa précision de pilotage. Pour la trajectoire horizontale et verticale les moyens traditionnels (environnement extérieur) se sont révélés insuffisants compte tenu des contraintes fixées. Il est par exemple très difficile à un pilote d'estimer de façon répétitive sa hauteur à +/- 2 ft et sa position à +/- 1m. Le problème se complique encore si l'on admet que la stratégie de pilotage doit rester du vol à vue. Les moyens de retour d'information ne doivent donc pas conduire à une stratégie du type vol aux instruments. Par exemple pour les manoeuvres près du sol (hover, hovering turn, pirouette,...) l'utilisation de l'indicateur de hauteur radiosonde sur la planche de bord pour le contrôle de précision en hauteur ne peut être retenue.

Concernant le retour d'information de position horizontale, pour chaque manoeuvre des tracés au sol ont été définis. Ils se composent :

- d'un tracé figurant la trajectoire nominale (de référence) que le pilote doit faire suivre à l'hélicoptère,
- de tracés figurant les écarts de trajectoire par rapport à la trajectoire nominale et visualisant ainsi la précision de pilotage requise.

Les deux niveaux d'écart (désiré et adéquat) requis par l'ADS-33 sont représentés.
Les figures 2 et 3 présentent les différents tracés qui ont été retenus.
Ces tracés se sont révélés particulièrement adaptés aux objectifs fixés. Ils permettent au pilote de visualiser des axes de déplacement, des points de passage et les précisons exigées pour la position horizontale.

Le problème de la restitution de la hauteur et des précisions associées est plus complexe. Il convenait d'abord de définir quel est le point de référence choisi, la trajectoire de ce point devant se situer à l'intérieur des contraintes de position horizontale et de hauteur. Aprés avis des différents pilotes participant à l'expérimentation, il a été décidé de prendre comme référence pour l'ensemble des manoeuvres la position du pilote (par opposition par exemple au centre de gravité de l'hélicoptère ou un point situé sur l'axe rotor). Au moyen de la mesure de la hauteur radiosonde, la hauteur du point de référence a été reconstituée. L'indicateur de hauteur radio sonde ne pouvant être utilisé, un moyen spécifique de visualisation a été développé par le CEV. Il s'agit du système ECLIPS. L'objectif primordial de ce système est de fournir au pilote une information de hauteur et de respect des précisions exigées, visible alors qu'il regarde à l'extérieur de l'hélicoptère. Ce moyen se présente comme un ensemble de trente diodes électroluminescentes disposées à la verticale. Ce moyen est fixé dans le cockpit au niveau du pare-

brise de façon a être vu par le pilote en vision périphérique (cf figure 4).
Son principe de fonctionnement est le suivant:

- au moyen d'un boîtier de commande on indique au système la manoeuvre qui va être exécutée, un boîtier programmé identifie ainsi la valeur en pieds d'une diode (par exemple 1 diode = 1 pied) ainsi que les fourchettes de hauteur correspondant aux précisions désirées et adéquates;
- le pilote stabilise l'hélicoptère aux environs de la hauteur de référence requise par la manoeuvre. On initialise alors le système. Un boîtier électronique acquiert cette hauteur et illumine la diode centrale;
- au cours d'une modification de la hauteur lors de la réalisation de la manoeuvre les diodes s'éclairent successivement (vers le haut si l'hélicoptère monte et vers le bas s'il descend);
- chaque diode peut prendre trois couleurs (vert, ambre, rouge), la couleur des diodes est modifiée en fonction des fourchettes de variation de hauteur autorisées pour la manoeuvre. Tant que la hauteur reste à l'intérieur de la précision désirée les diodes sont vertes, elles deviennent ambres lorsque l'on atteint la performance adéquate et passent au rouge ensuite.

Ce système a montré qu'il permettait au pilote d'avoir conscience de la performance atteinte sans modifier fondamentalement sa stratégie de pilotage.

3.3 Mesure de trajectoire

La restitution de trajectoire dans le plan horizontal a été réalisée au moyen d'une caméra vidéo de verticale avec incrustation dans l'image de la verticale du point de référence (position pilote) (cf figure 5). Cette caméra possède un champ de 53° qui, compte tenu des hauteurs de vol, a permis une visualisation correcte de la position de l'appareil par rapport aux tracés au sol (cf § 3.2 ci-dessus). Il est ainsi possible de reconstituer la trajectoire horizontale et surtout de vérifier en temps réel le respect ou non par le pilote des précisions demandées et le respect du profil de trajectoire demandé. Les manoeuvres mal exécutées ont ainsi pu être exécutées à nouveau. L'observation du réticule de verticale par rapport aux exigences de précision permet également de consolider le jugement du pilote (cf figure 6). Il est en effet aisé tant en temps réel qu'à la lecture des enregistrements vidéo de vérifier l'écart par rapport aux précisions exigées. Les enregistrements vidéo ont constitué un très bon support lors du débriefing des vols. Précisons que l'image de la caméra n'était pas présentée au pilote en temps réel mais à l'ingénieur d'essais; il ne s'agit donc pas d'une aide au pilotage.

3.4 Mesure des paramètres de comportement de hélicoptère

3.4.1 exploitation en temps réel

Les paramètres importants pour la conduite de l'essai (vitesses, assiettes longitudinale et latérale, cap, hauteur, positions de commandes...) étaient disponibles en temps réel sur les écrans de l'ingénieur d'essais disposés en cabine. Ils permettent en corrélation avec la mesure de trajectoire de pouvoir juger en temps réel la qualité de la manoeuvre, permettant ainsi d'éventuellement la faire exécuter à nouveau. Il permettent également de consolider le jugement du pilote (par exemple vérification du respect des critères de tenue de cap ou de vitesse).

3.4.2 exploitation en temps différé

Les mêmes paramètres que ci-dessus auxquels furent ajoutées les vitesses angulaires ont permis en temps différé une analyse plus précise et complète des manoeuvres. En particulier l'analyse combinée des assiettes, vitesses angulaires et accélérations angulaires ont permis d'étudier les corrélations entrée/sortie et les corrélation entre les différents axes. De même l'analyse de l'activité sur les commandes au moyens de l'enregistrement des positions de commandes a permis l'étude des fréquences de coupure sur les différents axes pour différentes manoeuvres ainsi que les diverses corrélations (cf figure 7). Ce travail a été réalisé par Eurocopter France.

3.5 Méthode d'essais - influence des paramètres d'environnement

Les principaux paramètres d'environnement à considérer sont: le vent, la masse, le centrage, les moments d'inertie, l'environnement visuel.

Pour chaque manoeuvre les conditions de vent (force, direction) sont spécifiées. L'expérimentation a cependant montré que le vent pouvait masquer d'éventuelles anomalies de pilotabilité. D'une part, lors de certaines phases de vol il est difficile de faire la distinction entre l'effet des turbulences et une défaillance éventuelle de l'appareil. D'autre part, pour d'autres phases de vol, le vent peut avoir des effets stabilisateurs. Il convient donc dans un premier temps d'effectuer les manoeuvres sans vent afin d'obtenir des réponses de l'appareil les plus pures possible puis dans un deuxième temps d'effectuer les manoeuvres avec le vent spécifié.

La masse de l'appareil n'est pas apparue comme un facteur sensible, les modifications de centrage et de moment d'inertie le sont bien plus. Il est toutefois assez facile pour un bureau d'étude de déterminer les cas critiques de façon à les évaluer en vol.

L'évaluation de la pilotabilité en environnement visuel dégradé correspond à des exigences opérationnelles de vol en conditions diurnes et nocturnes avec de mauvaises conditions météorologiques. Lors de cette expérimentation trop peu de vols ont été effectués en environnement dégradé pour permettre de savoir si les valeurs de performances attachées aux manoeuvres étaient correctes ou non. Il est toutefois clair que le pilotage en environnement visuel dégradé est très différent du pilotage en environnement visuel normal. Le pilote ne se comporte pas de la même façon même s'il possède des aides au pilotage, il est en effet plus sujet au pompage piloté même si les actions aux commandes sont plus douces. Ce facteur d'environnement mériterait une expérimentation spécifique.

3.6 Méthode d'essais - Utilisation de l'échelle de Cooper Harper

La notation de Cooper Harper lie dans une échelle unique les deux notions principales de l'évaluation de la pilotabilité d'un appareil qui sont: la charge de travail du pilote et la performance obtenue.

De multiples niveaux d'appréciation par le pilote de sa charge de travail sont définis (les termes sont volontairement laissés en anglais pour éviter toute interprétation des rédacteurs):

- intense pilot compensation
- considerable " "
- maximum tolerable " "
- extensive " "
- moderate " "
- minimal " "

L'appréciation de la charge de travail est laissée au pilote, toutefois l'utilisation stricte de l'arbre de décision de l'échelle de Cooper Harper n'autorise guère de confusion dans l'évaluation. Tout au plus le pilote peut avoir le choix entre deux notes consécutives à l'intérieur d'un même niveau.

La graduation dans les niveaux de performance obtenue est double:
- performance désirée (desired performance),
- performance adéquate (adequate performance).

Les deux niveaux sont déterminés a priori en fixant des tolérances sur l'exécution de la tâche à réaliser, ces tolérances sont fixées par des considérations opérationnelles (stationnaire près des arbres, station sonar,...). L'échelle de Cooper Harper fixe le niveau de transition entre la performance désirée et la performance adéquate entre les notes 4 et 5 et la transition entre la performance adéquate et une performance non acceptable entre les notes 6 et 7.

L'expérimentation a montré que l'utilisation, ainsi décrite, de l'échelle de Cooper Harper posait problème quant à la perception des transitions entre deux niveaux et quant à la prise en compte de la pondération relative de la charge de travail et de la performance atteinte.

Transition entre niveaux: la question « Is it satisfactory without improvement ?» n'est pas suffisamment explicite pour guider le pilote dans son choix vers les niveaux 1 ou 2. Dans ces conditions, le choix s'effectue à partir de l'estimation de sa charge de travail pour réaliser la performance désirée : « minimal compensation » ou « moderate compensation ». Toutefois il est difficile pour un pilote de savoir si sa charge de travail de pilotage l'occupe à 20%, 50% ou plus. De plus, d'un pilote à l'autre cette estimation est très variable. La transition entre les niveaux 2 et 3 est plus facilement appréciable puisqu'elle se juge sur le fait que la performance adéquate a été ou non atteinte.

Pondération relative charge de travail/performance atteinte: la réalisation par le pilote de la performance désirée assure une note au moins égale à 4. Or il peut très bien arriver que celui-ci estime que sa charge de travail pour atteindre la performance désirée dépasse le niveau «moderate». Cette combinaison n'apparaît pas explicitement dans l'échelle. La note de 4 lui apparaît ainsi sous estimée vis à vis de la charge de travail qu'il estime «considerable» ou «extensive». De la même façon, il est possible que la performance adéquate ne nécessite de la part du pilote qu'une compensation « moderate » ou « minimal ». La note de 5 apparaissant alors surestimée vis à vis de la charge de travail.

Ces problèmes sont révélateurs de l'impossibilité de mesurer la charge de travail de pilotage. La solution passe par une approche du problème par différents axes. Il convient de garder comme base le jugement subjectif que chaque pilote porte à la fois sur la réalisation ou non de l'objectif fixé (performance) et sur la charge de travail requise. Ce jugement doit toutefois être corrélé par des mesures objectives visant à vérifier la réalisation de la manoeuvre et de la performance mais aussi à approcher la charge de travail par des mesures quantitatives (activité sur les commandes, couplages, corrélations entrées/sorties,...) même si elles ne représentent qu'une partie de celle-ci. Il faut également établir un questionnaire de débriefing qui permette au pilote de revenir plus en détail sur sa notation en étudiant chacune des caractéristiques qui participent à la pilotabilité d'un hélicoptère. Un exemple d'un tel questionnaire issu des études du programme Euro-ACT est fourni en figure 1. Enfin, si dans l'ensemble des pilotes évaluateurs, l'un d'entre eux a un jugement atypique, il ne faut pas le rejeter en utilisant de façon par trop systématique des méthodes statistiques. Il convient par contre de

pousser l'investigation au moyen du questionnaire pour déterminer si ce jugement n'est pas dû à une défaillance sur une caractéristique précise qui aurait pu échapper à la majorité des pilotes mais qui pourrait dans des cas marginaux être problématique vis à vis de la sécurité du vol. Enfin un axe d'étude pourrait être d'introduire dans la réalisation de la manoeuvre une tâche secondaire et de tenter de mesurer le rapport tâche principale/tâche secondaire (par exemple en utilisant un critère de réussite de la tâche secondaire).

4 CONCLUSIONS

Cette expérimentation a montré que des essais en vol du type ADS-33 pouvaient être utilisés pour le développement et la qualification de la pilotabilité d'un hélicoptère de transport en prenant un certain nombre de précautions.

La méthode repose par essence sur le jugement des pilotes quant à la facilité avec laquelle il peuvent réaliser des manoeuvres-type tout en respectant une précision de pilotage prédéfinie. Il convient donc de définir des manoeuvres (tâche et précision) qui soient répétables, il faut fournir aux pilotes des moyens qui leur permettent de situer ce qu'ils sont en train de réaliser par rapport au niveau de précision qui leur est demandé. Il faut pouvoir au moyen de mesures consolider le jugement des pilotes en analysant la tâche réalisée, la précision effectivement atteinte, la réponse de l'hélicoptère et l'activité des pilotes sur les commandes. Les mesures doivent être complétées par un questionnaire de débriefing qui permet d'analyser dans le détail l'ensemble des caractéristiques de l'hélicoptère qui participent à la pilotabilité.

Cette expérimentation devrait être complétée par des études visant à mieux cerner l'influence de l'environnement visuel dégradé ou visant à la définition de tâches secondaires et de critères associés afin de mieux cerner la quantification de la charge de travail de pilotage.

REFERENCES

(1) ADS 33C, August 1989
(2) ADS-33D, July 1994
(3) Strachan, Shubert, Wilson : « Development and Evaluation of ADS-33C handling Qualities Flight Test Maneuvers for Cargo Helicopters » 50th AHS Forum, Washington DC, May 1994
(4) Benquet, Rollet, Pausder, Gollnick: « Tailoring of ADS-33 for NH90 Program » 52nd AHS Forum, Washington DC June 1996.

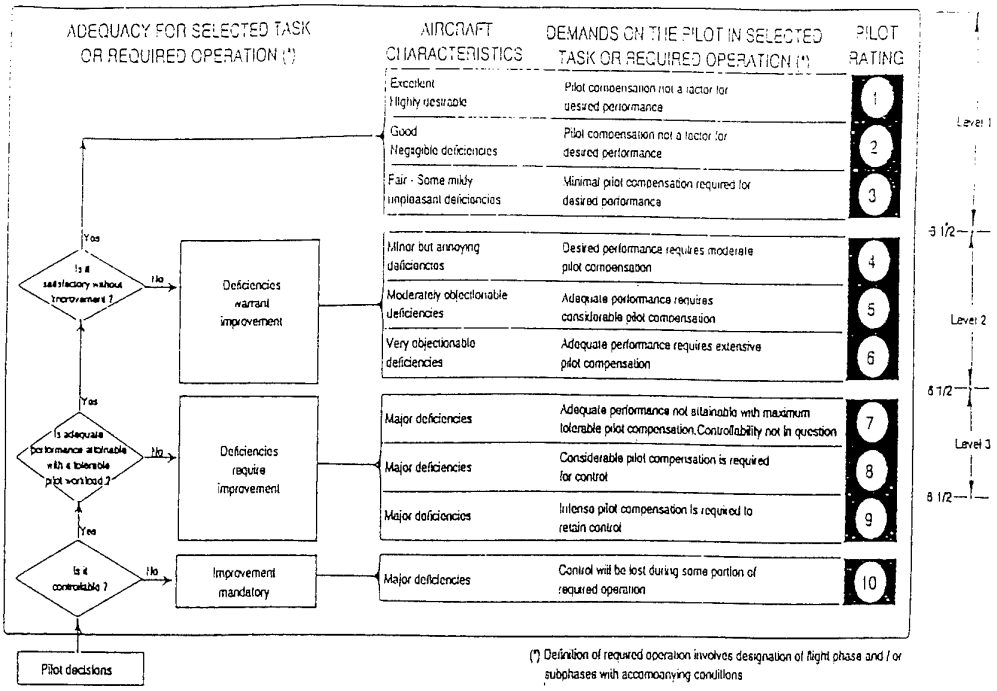

Cooper Harper : arbre de décision

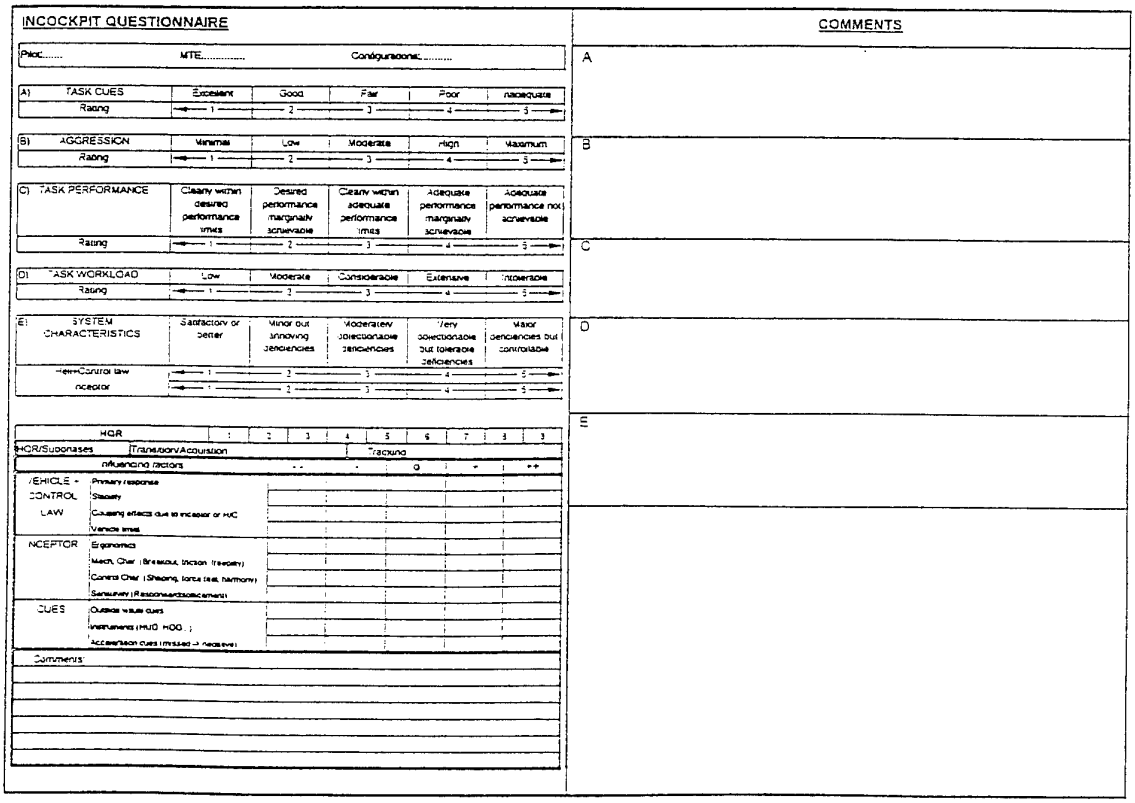

questionnaire Euro-ACT
figure 1

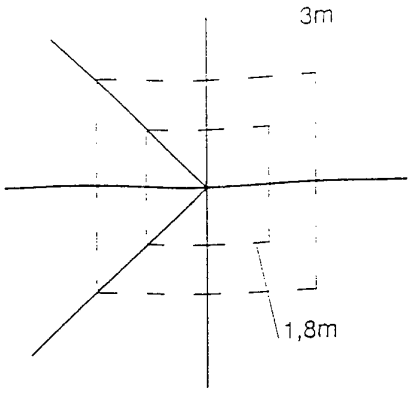

HOVER

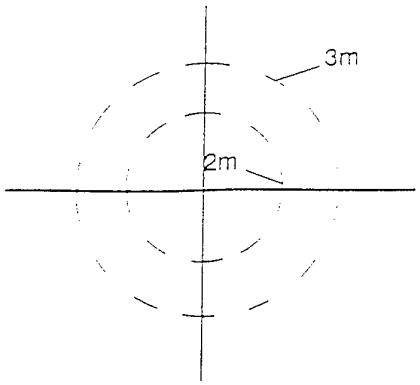

HOVER TURN

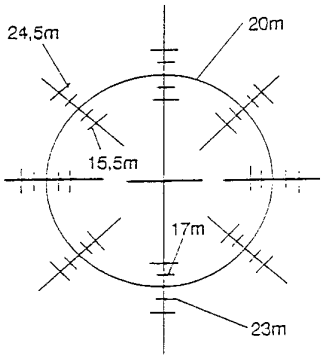

PIROUETTE

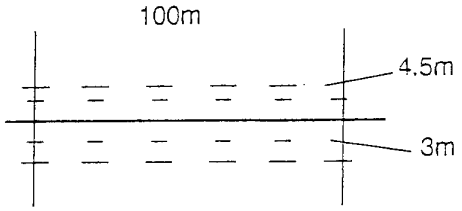

SIDESTEP

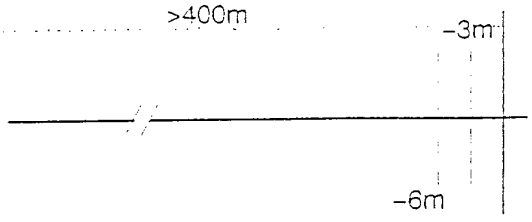

ACCELERATION/DECELERATION

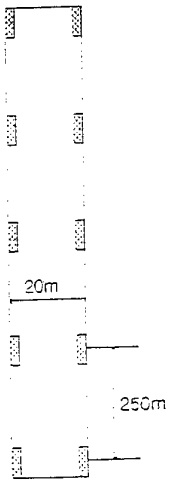

SLALOM

Exemples de tracés au sol

figure 2

Hover: en blanc trajectoire, en jaune tolérance sur la précision

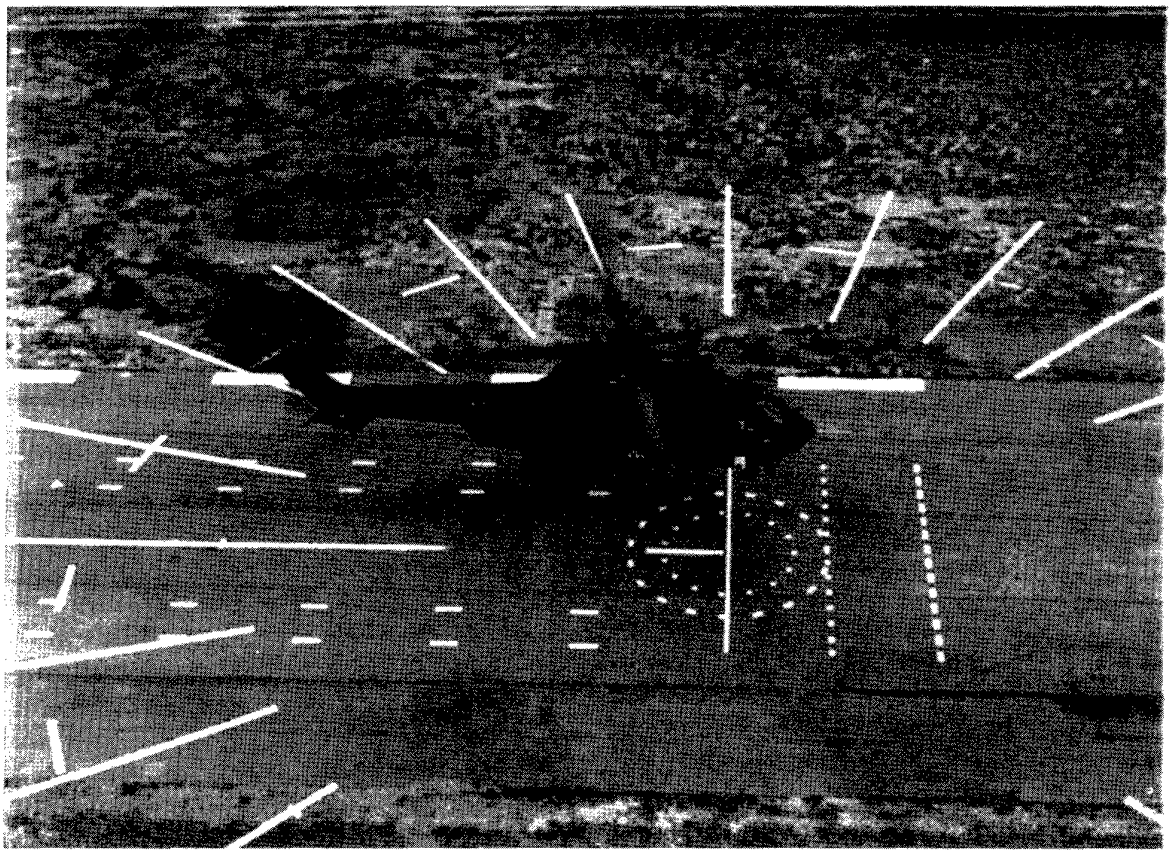

Pirouette et Hovering Turn

figure 3

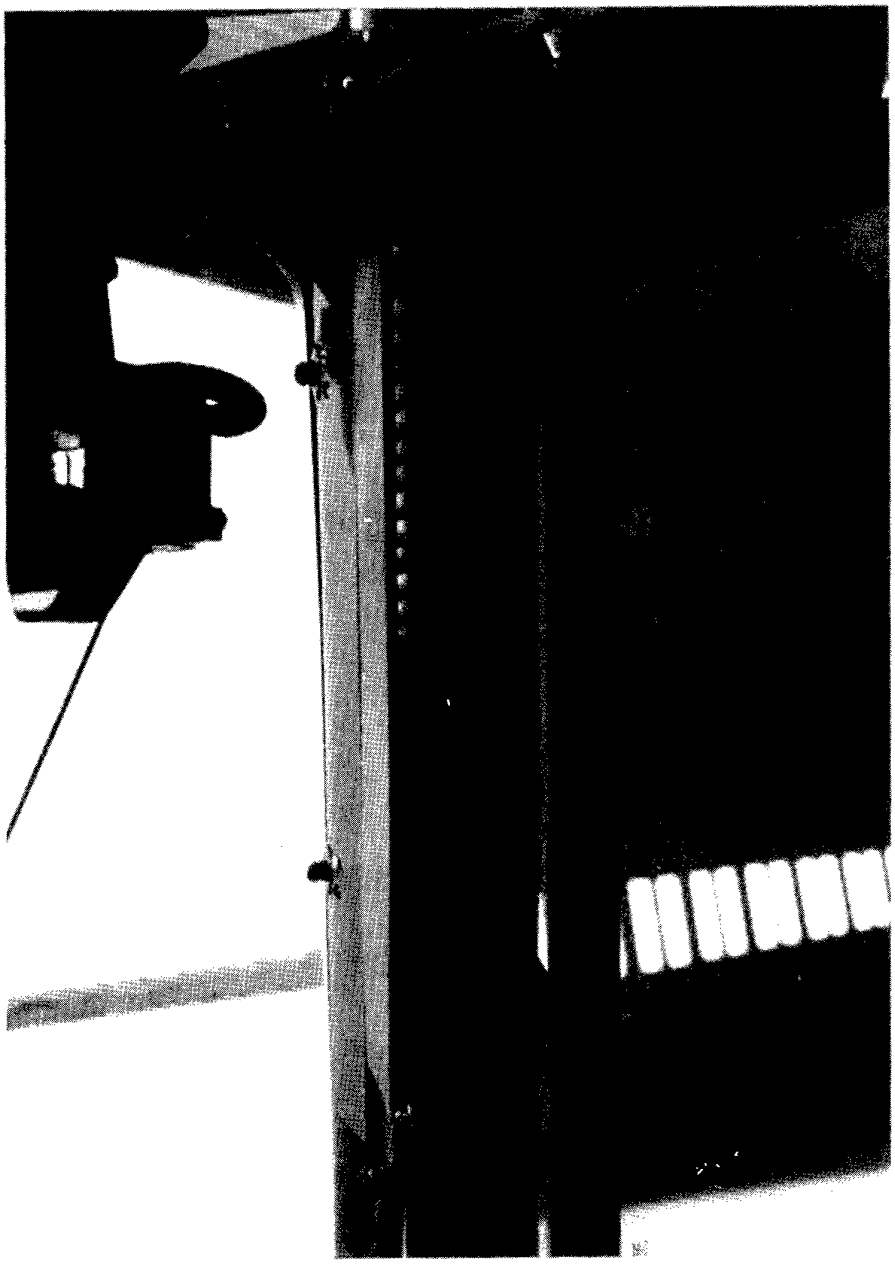

Système ECLIPS

figure 4

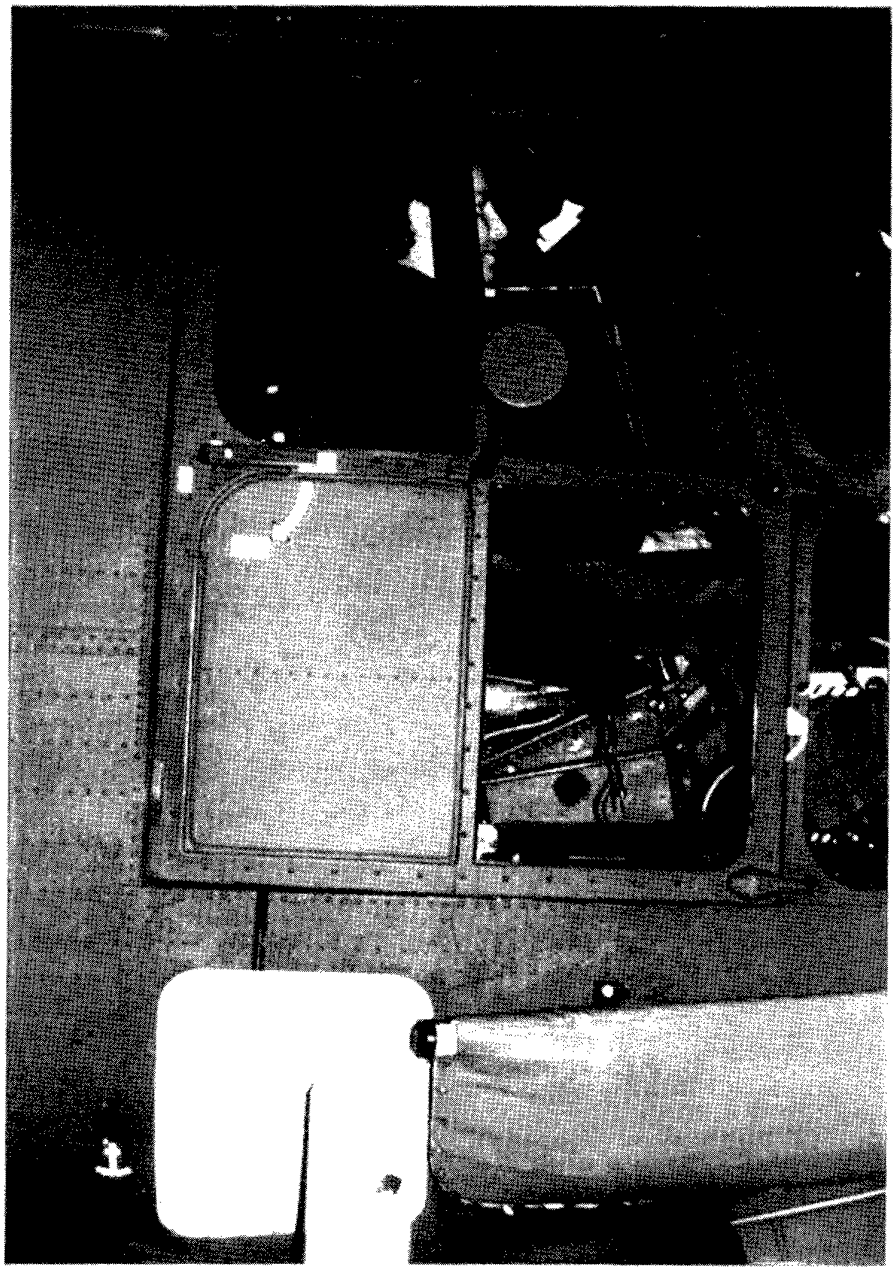

Montage de la caméra vidéo de verticale (boîtier orange)

figure 5

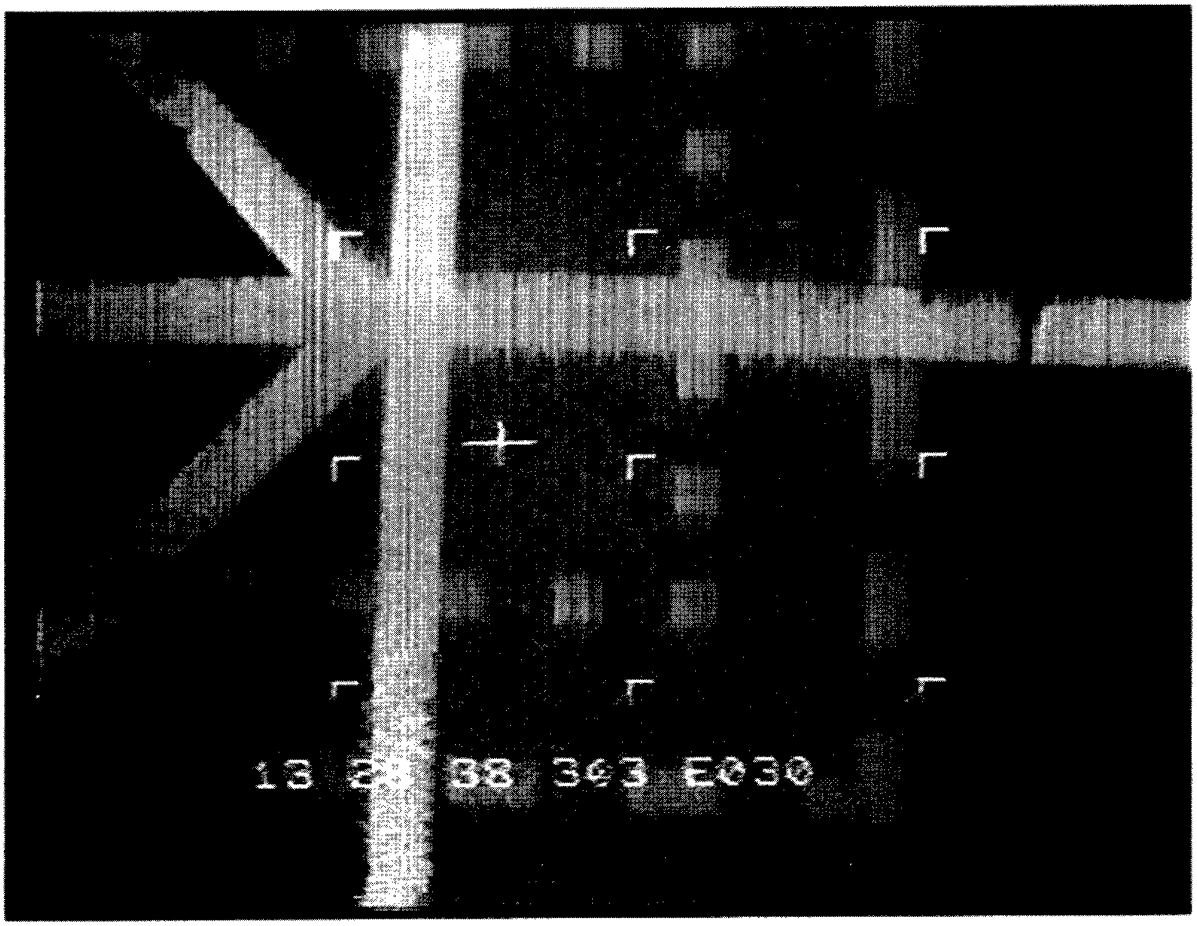

Photo de l'image vidéo de la camera de verticale

figure 6

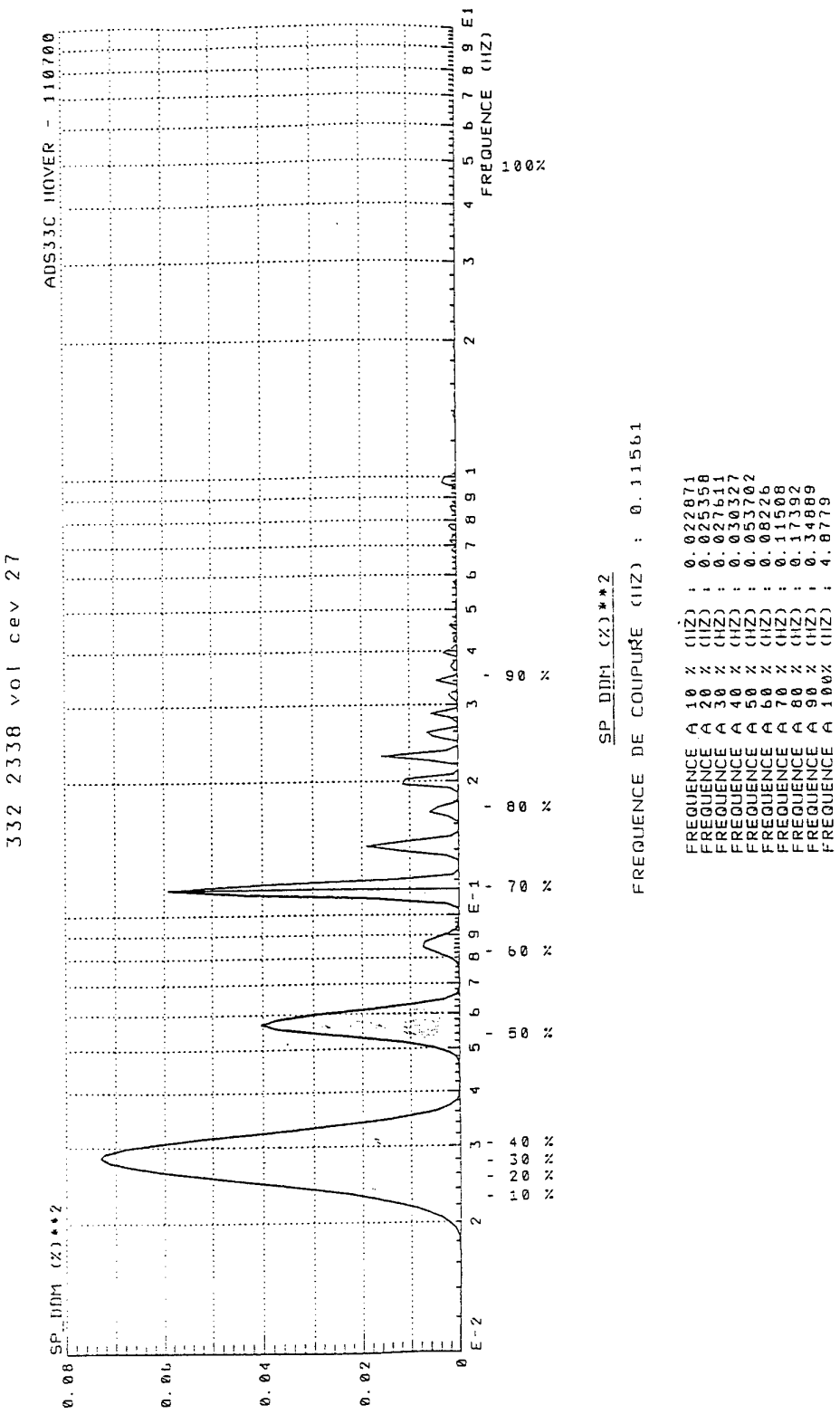

exemple de calcul de fréquence de coupure (manoeuvre Hover- tangage)

figure 7

ADS-33 Flight Testing - Lessons Learned

Carl J. Ockier
DLR - Institute of Flight Mechanics
Lilienthalplatz 7
38108 Braunschweig
Germany

Volker Gollnick
German Armed Forces Flight
Test Center (WTD-61)
85077 Manching
Germany

SUMMARY

A comprehensive evaluation of the ADS-33D handling qualities specification for military rotorcraft was completed with the BO 105 helicopter. The evaluation addressed both the quantitative and qualitative ADS-33 criteria. The evaluation of the quantitative or open-loop criteria in hover and in forward flight directly addressed applicability and repeatability of the criteria. The evaluation of the qualitative criteria or ADS-33 flight test maneuvers in the good visual environment addressed applicability and validity issues. This paper presents some of the major results of the quantitative and qualitative evaluations and extracts some lessons from the comparison of the results of both evaluations.

INTRODUCTION

ADS-33, the new specification for handling qualities of military rotorcraft [1], was developed under the leadership of the US Army as a replacement for the obsolete MIL-H-8501A. To the testing of helicopter handling qualities, ADS-33 meant nothing less than a revolution. Almost overnight, the classic determination of static and dynamic stability was replaced with new, often unknown techniques. Although a lot of knowledge was gained from the early flight tests conducted by the US Army and Navy [2], there is still a lot to be learned about ADS-33.

This paper presents the major results of a complete evaluation of the current D version of the ADS-33 specification. The evaluation was conducted with a standard BO 105 helicopter and concentrated on the quantitative (open-loop) and qualitative (demonstration maneuver) criteria in the good visual environment. The objectives of this study were: (1) to gain experience with the use of ADS-33 and to develop safe flight testing techniques; (2) to verify the applicability and repeatability of the ADS-33 criteria; (3) to identify possible inconsistencies between the quantitative and qualitative criteria; and (4) to complete the handling qualities data base for the BO 105 helicopter.

Conduct of the Flight Tests

The ADS-33 flight tests were conducted by the German Aerospace Research Establishment (DLR) in cooperation with the German Armed Forces Flight Test Center (WTD-61). The tests took place between 1992 and 1995 at Braunschweig Airport, Celle Army Base, and at the German Forces Test Center in Manching. Six test pilots – three German and three American – participated in the tests. Helicopter mass for the tests was between 75 and 85 percent of the BO 105s 2300 kg maximum gross weight.

The flight tests for the quantitative handling qualities evaluations were conducted in calm winds out of ground effect. For practical reasons, all necessary control inputs were made by hand. Before making the inputs, the aircraft was carefully trimmed to an unaccelerated, level flight condition. The quantitative evaluations were carried out for two flight conditions: hover (<5 kt) and forward flight at 80 kt.

The qualitative handling qualities flight tests were carried out in calm to moderate winds under good visual conditions (UCE=1). During pre-tests, the safety margins and power limitations were verified, and where necessary modifications to the original ADS-33D maneuver descriptions were made (usually, this meant reducing the maximum airspeed to 100 or 110 kt). The evaluations consisted of a training phase, during which the evaluation pilot was given ample time to practice the maneuver, and an evaluation phase, usually two or three runs during which the handling qualities were evaluated. After each flight, during which no more than two maneuvers were flown, the evaluation pilot completed, for each maneuver flown, a 3 page de-briefing questionnaire – answering questions regarding the achieved performance, the workload, and other aspects influencing the handling qualities. At the end of the questionnaire, a handling qualities rating (HQR) was reached using the Cooper-Harper [3] decision process.

The BO 105 Helicopter

All experiments were carried out with the DLRs standard BO 105C helicopter (Fig. 1). In its civilian version, the light twin-engined BO 105 helicopter is popular for police, EMS, and light transport operations. The German military derivative of the BO 105, fitted with a stronger tail rotor and a yaw SCAS, is primarily used for anti-tank and liaison missions. Although the BO 105 was designed in the 1960s and first flew in 1971, its innovative design is still relevant for today's – and tomorrow's – helicopters. The hingeless rotor system allows the generation of large rotor moments, necessary to attain the agility required in modern helicopters. This makes the BO 105 a particularly interesting helicopter for handling qualities testing. Of course, the low maximum speed (V_{max} = 120 kt) and the absence of stability augmentation or automatic flight control systems are not features of the next generation military helicopters. Nevertheless, the handling qualities of the BO 105 should in many respects be representative of future light helicopters – especially when operating in a 'degraded' mode.

Paper presented at the FVP Symposium on "Advances in Rotorcraft Technology", held in Ottawa, Canada, 27-30 May 1996, and published in CP-592.

Fig. 1: The DLR's BO 105 helicopter.

Instrumentation and Ground Courses

During the evaluations, the BO 105 was fitted with a standard instrumentation package. Recorded data included: attitude, heading, angular rates, accelerations, velocity components from the HADS sensor, indicated rotor speed and torque, height, and control positions. All data recording was done digitally, with sampling rates between 100 and 400 Hz. With these elevated sampling rates, the anti-aliasing filters could cause no measurable phase shift over the frequency range of interest. Additional filtering was done off-line using zero phase shift filters.

The test courses for the qualitative handling qualities evaluations were mostly made according to the guidelines in ADS-33, except for the landing area which was marked on the ground and not on an elevated platform. During the forward flight maneuvers, the helicopter position was laser tracked and the target aircraft for the yo-yo maneuver was tracked using kinetheodolites. Most flight test maneuvers were recorded on airborne and ground video.

EVALUATION OF THE QUANTITATIVE ADS-33D CRITERIA

The quantitative ADS-33 criteria measure the open-loop response of the helicopter. They are useful as a design guide for the flight controls engineer and as an analysis tool for the handling qualities engineer. Since the emphasis of the BO 105 tests was on evaluating the repeatability of the criteria, most pilot inputs were repeated several times, so that the typical spread of the data could be assessed. Fig. 2 gives an overview the evaluated criteria. In this and all subsequent figures the Level boundaries corresponding to the most demanding mission task elements (MTEs) are used, regardless of whether the concerned MTEs are relevant for the BO 105. Following is a discussion of the pitch-roll-yaw on-axis criteria, the vertical axis criteria and the interaxis coupling criteria. A more detailed discussion of the quantitative evaluations in forward flight can be found in [4].

Pitch, roll and yaw on-axis criteria

The four on-axis criteria for pitch, roll and yaw cover the mission task spectrum between high and low pilot gain tasks and between precision and aggressive flight. High gain precision tasks are covered by the bandwidth/phase delay criteria. Aggressive high gain maneuvering is defined by attitude quickness criteria. Criteria that pertain primarily to low gain or open loop tasks are the mid-to-long term stability criterion for precision tasks, and the large amplitude criterion for aggressive tasks.

Bandwidth/Phase Delay Criteria

The bandwidth and phase delay parameters are used to determine the helicopter's handling qualities in small amplitude, high gain tracking tasks. The effects of bandwidth and phase delay on handling qualities were studied extensively in recent years [5], as were the methods to compute these parameters [6,7].

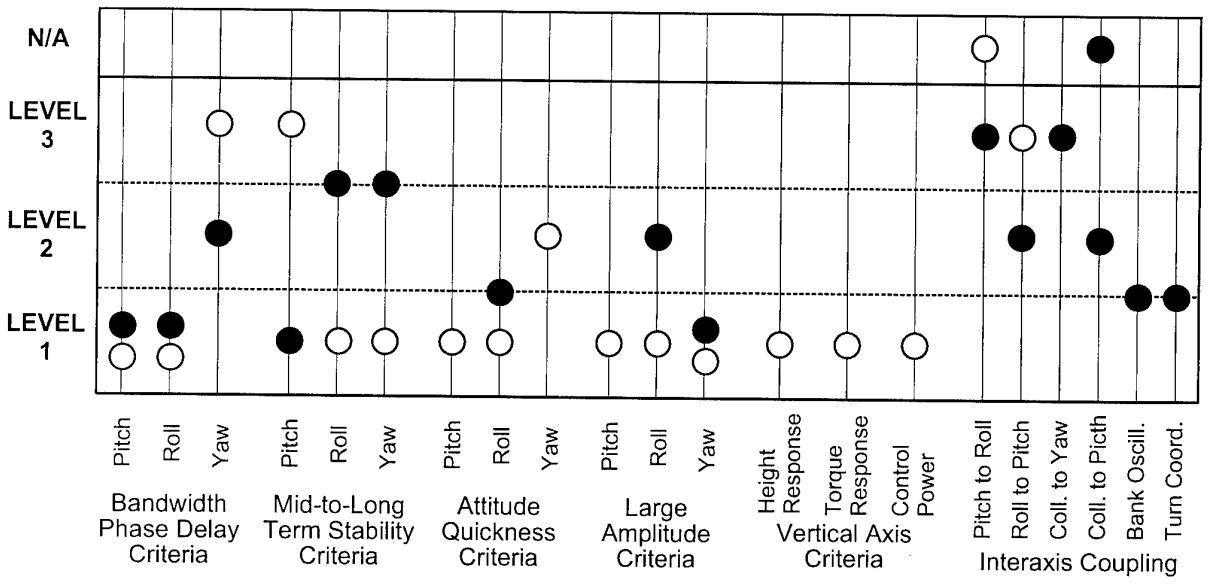

Fig. 2: The handling qualities of the BO 105 determined from the quantitative criteria. The open sympols are for hover (<5 kt) and the closed symbols are for forward flight (80 kt).

With the BO 105, multiple frequency sweeps were used to determine the angular frequency response of the pitch, roll and yaw axes. The combination of sound flight test techniques, unfiltered data recording, and proven computational techniques produced frequency responses with a high coherence over the frequency range of interest and with good consistency over different data runs [4]. For the pitch axis, the BO 105's bandwidth and phase delay were computed as 2.7 rad/sec and 84 msec in forward flight and as 2.9 rad/sec and 71 msec in hover (although the phase margin in hover was only a few degrees more than the required minimum of 45 degrees, so that small phase differences could easily degrade the BO 105 to Level 3). For the roll axis, bandwidth and phase delay were 5.8 rad/sec and 48 msec at 80 kt and 5.1 rad/sec and 42 msec in hover, with sufficient phase margins.

The computation of bandwidth and phase delay for the yaw axis turned out to be more difficult. In hover, the available phase margin was less than 45 deg/sec, at least over the frequency range where coherence was acceptable (Fig. 3). This automatically reduces the BO 105s yaw bandwidth to Level 3 – a very severe conclusion that warrants further research. In forward flight, the phase delay was hard to determine because of the poor coherence around $2\omega_{180}$, where non-linear effects dominated the response [4].

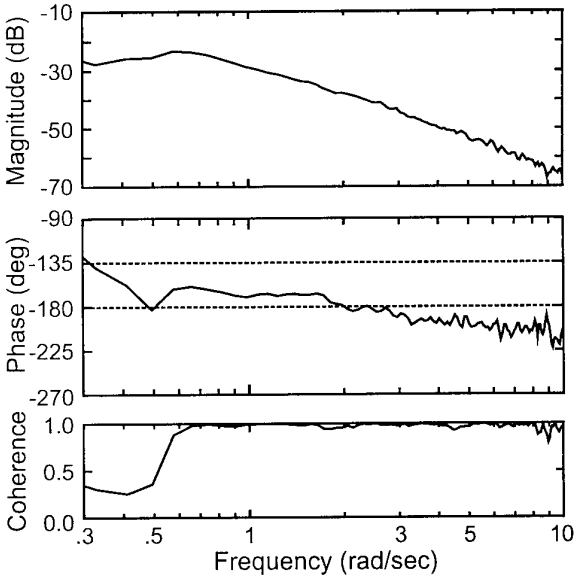

Fig. 3: Frequency response of heading to pedal for the BO 105 helicopter in hover.

Mid-to-Long Term Stability Criteria

The mid to long term criteria are the classical dynamic stability criteria, so important for low pilot gain operations. For unstabilized helicopters, such as the BO 105, they evaluate the frequency and damping of the Dutch roll and Phugoid modes. For augmented helicopters, they analyze oscillatory remnants of the control system. The mid-to-long term criteria pertain to frequencies below the highest bandwidth frequency and hence rotor-body oscillations are not typically considered.

The evaluation of the stability criteria is based on the premise that frequency and damping of any oscillatory modes can be determined from the time history of the free response to a pulse input. For the BO 105, this was true only for forward flight, where the Phugoid and Dutch roll modes could be determined with relative ease [4]. In hover, the BO 105 was too unstable and too coupled to be able to extract any oscillatory characteristics from the time histories. As a result, data had to be obtained with parameter identification [8]. The BO 105s unstable Phugoid mode was identified with a frequency of .33 rad/sec and a damping of -.15 in forward flight (Level 1) and with a higher frequency of .5 rad/sec and a lower damping of -0.61 in hover (Level 3). The opposite result was obtained for the Dutch roll mode, where the forward flight mode is Level 2/3 with a frequency of 2.5 rad/sec and a damping of .14 and the hover mode is Level 1 with a frequency of 1.5 rad/sec and a damping of .51.

Attitude Quickness Criteria

The attitude quickness or moderate amplitude criteria measure the helicopter's agility, or the ability to maneuver aggressively with an elevated pilot gain. The criteria, defined for all three axes in hover and only for the roll axis in forward flight, evaluate moderate amplitude attitude changes between 10 and 60 degrees for the roll and yaw axes and between 5 and 30 degrees for the pitch axis. The attitude quickness criteria are based on two parameters extracted from the response to a pulse controller input: the ratio of the maximum angular rate to maximum angle change and the minimum angle during the transition (see Fig. 4).

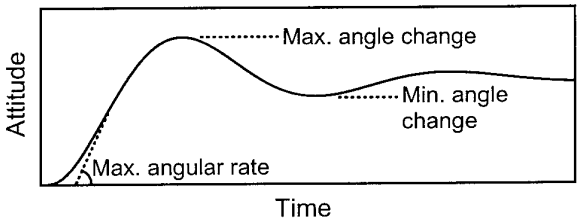

Fig. 4: Definition of the attitude quickness parameters.

To determine the criteria, large and even maximum amplitude pulse inputs were used to excite the helicopter. The response to the inputs generally was a complicated dynamic response, unlike the smooth 2nd order response of Fig. 4. This made measuring the minimum angle change difficult. The response to a lateral pulse input in hover (Fig. 5) shows that although a minimum bank angle can be determined, there are obviously additional dynamics that make the determination of this parameter onerous.

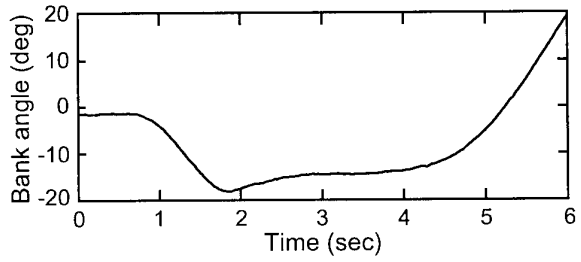

Fig. 5: Typical bank angle response to a lateral pulse inputt in hover.

The attitude quickness of the BO 105 was computed for the roll axis in hover and at 80 kt [4], and for the pitch axis in hover (Fig. 6). In the three cases, Level 1 or borderline Level 1-2 handling qualities were obtained for the most demanding mission tasks. No data were obtained for very large attitude changes, because of the dangers associated with sustaining large bank and pitch angles in a free response.

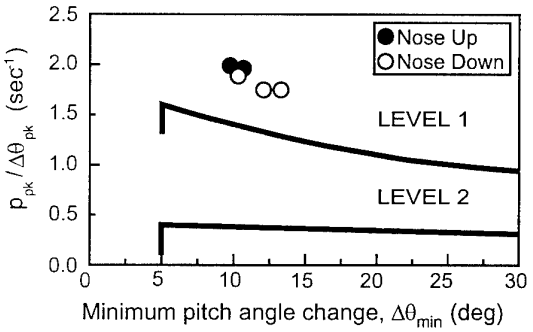

Fig. 6: Pitch attitude quickness of the BO 105 helicopter in hover.

Attitude quickness could not be determined for the heading response in hover because of a divergent periodic response following a pulse pedal input. As an alternative, heading quickness was evaluated with maximum angle change rather than minimum angle change plotted on the horizontal criterion axis (Fig. 7). Using this altered format, the BO 105 was found to have Level 2 handling qualities.

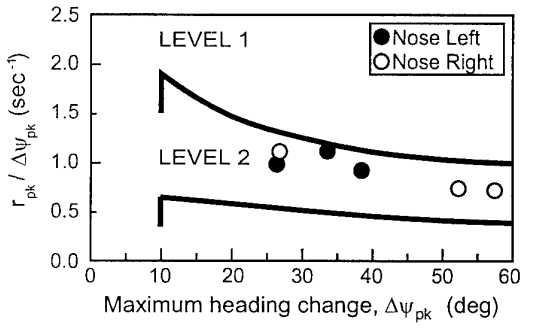

Fig. 7: Heading quickness (modified) for the BO 105 in hover.

Large Amplitude Criteria

The large amplitude criteria are a measure of the control power in the pitch, roll and yaw axes. The hover pitch and hover and forward flight roll axis criteria are defined as the minimum achievable angular rates, at least for rate command systems. These maximum rates were obtained during short, very large amplitude pitch and roll inputs. In hover, the BO 105 has Level 1 pitch and roll control power. In forward flight, the BO 105 has Level 2 handling qualities for the air combat mission.

The large amplitude yaw axis criteria are defined as the minimum yaw rate in hover, and as the minimum achievable heading change in forward flight. In hover, the BO 105's maximum design yaw rate of 90 deg/sec was easily achieved (Level 1). In forward flight, the maximum sideslip angle (or heading change) that were recorded, using other controls to maintain a constant attitude, were in excess of 30 degrees, which is clearly Level 1 [4].

The control power criteria for Level 1 pitch axis handling qualities in forward flight are defined in terms of the steady load factors that are attainable. Load factors in excess of the Operational Flight Envelope (OFE) limits were reached at 100 kt during the pull-up push-over maneuver (Level 1). Flight tests at lower forward velocities, where attaining these load factors would be a lot more difficult, were not made.

Vertical Axis Criteria

The vertical axis criteria assess the response to a collective controller input. A change in the collective blade pitch of the helicopter's main rotor has two immediate effects: a desired effect – it causes the helicopter to accelerate vertically – and an undesired effect – it causes the rotor speed to change. In most modern helicopters, rotor speed is automatically controlled by the engine governor, so that, in theory, the pilot needs not worry about it. In practice, the governor is unable to follow instant large changes in torque demand, so that the pilot has to use collective to avoid dangerous under and over-speed conditions. Because rotor speed is nothing but a parasitic degree of freedom and because the governor is usually part of the engine and not of the flight control system, the rotor speed degree of freedom is often ignored in handling qualities discussions. Nevertheless, this degree of freedom can be a major contributor to workload and is often a source of serious handling qualities problems [9]. ADS-33D has three quantitative vertical axis criteria, which all pertain to hover and low speed flight: height response, torque response, and vertical axis control power criteria. A fourth criteria, addressing the rotor speed, is of a more qualitative nature and will not be addressed here.

Height Response Criteria

The height response criteria measure the dynamics of the rate of climb to a collective step input. The height response criteria require the response to be approximately first order, with limits to the equivalent time delay and time constant. The criteria parameters are determined from the response to a step collective input, using parameter identification. Results show the primitive least squares method proposed in ADS-33D was too sensitive to the selection of the starting point of the step input (all step inputs having a finite duration), so that a slightly more sophisticated least squares method, which used the actual input and response, had to be used. Figure 8 shows the results of the analysis. All data points in this diagram have a 'goodness of fit' within the limits. As can be seen, two different control input strategies were used: (1) collective steps with the other controls fixed and (2) collective steps with the other controls used to maintain attitude and heading. Apart from the more pleasant flight testing with the second type of input, there were no major differences in time delay between the two input signals. The time constant for the collective steps with constant attitude and heading was generally a bit higher, probably due to the power needed for antitorque.

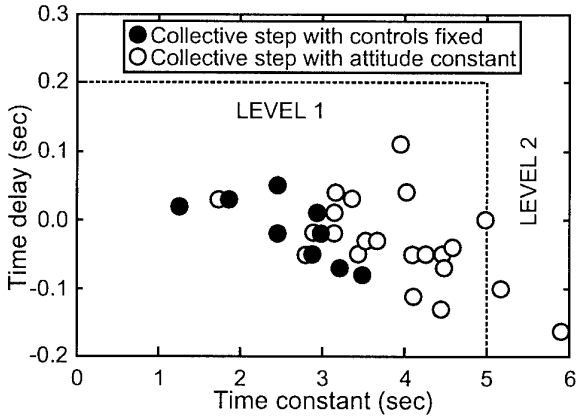

Fig. 8: Identified time constants and time delays of the BO 105's vertical axis response in hover.

The parameter identification above was repeated in the frequency domain, where a first order response was fit to the height rate to collective response obtained from a collective frequency sweep. The time constant and time delay thus computed were very close to the results of Fig. 8.

Torque Response Criteria

The torque response criteria directly address the parasitic degree of freedom of the helicopter – the engine. The ADS-33D criterion places requirements on the dynamics of the displayed torque response. In the BO 105, displayed torque was measured from the input of the torque indicator. Criteria parameters are overshoot ratio and time to first peak.

As with the height response criteria, two types of inputs were used: collective steps with all other controls fixed and collective steps with constant attitude and heading. Since it was difficult to sustain the inputs with all controls fixed for as long as 10 seconds, only a few of these inputs are shown in Figure 9. Fig. 9 shows a large spread in the time to first peak. The BO 105 has Level 1 handling qualities, despite its slow torque response.

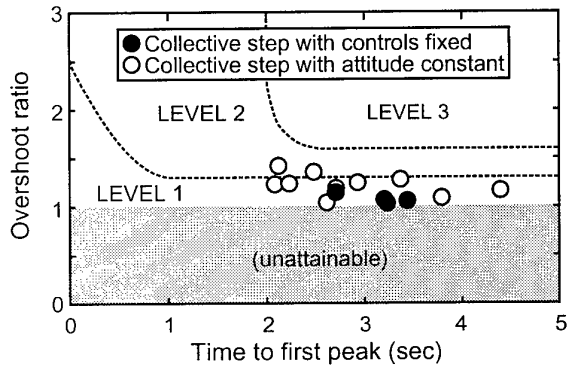

Fig. 9: Parameters of the torque response criterion for the BO 105 in hover.

Vertical Axis Control Power Criteria

The vertical axis control power criteria measure the ability to build up a rate of climb following a collective pitch input. This ability will depend on the height response characteristics as well as on the weight conditions of the vehicle. Experiments with the BO 105 showed that maximum rate of climb in 1.5 seconds after a collective step input was 2.9 m/sec, which is more than 3 times the Level 1 requirement.

Interaxis coupling criteria

The complex dynamics of main rotor, tail rotor, fuselage, engine, and wake cause the single rotor helicopter to be coupled in almost all axes. The handling qualities implications of interaxis coupling are not yet fully understood, just as there are many deficiencies in the physical understanding of the exact coupling causes. In ADS-33D several criteria address interaxis coupling with quantitative requirements – although at least as many coupling criteria present only qualitative requirements (e.g. height-due-to-yaw coupling).

Pitch-Roll Coupling

The ADS-33D criteria for helicopter pitch-roll coupling are expressed in the time domain. The off to on-axis coupling ratio, which defines the criteria, is measured from the response to a step input. The peak off-axis response is measured within four seconds following the input, the on-axis response is measured at the end of a four second observation period. Measurements of the pitch-due-to-roll coupling criteria showed significant differences depending on the direction and amplitude of the input. In forward flight, left rolls generally produced around 15% coupling, where right rolls produced about 35% coupling. In hover, the situation was reversed, with left roll producing more than 100% coupling and right rolls producing about 30% coupling. The same erratic behavior was noted for roll-due-to-pitch coupling, although it was more difficult to gather good data because of problems associated with maintaining a pitch input for the required length of time.

These deficiencies with the ADS-33 time domain criteria were the subject of an in-depth study of pitch-roll coupling in helicopters by the US Army and DLR [10]. In this study, an alternative pitch-due-to-roll coupling criterion that uses the frequency domain was suggested. Using the available frequency sweep data, the roll-due-to-pitch coupling handling qualities were determined for both hover and forward flight (Fig. 10). With this definition, which addresses pitch-due-to-roll coupling only, the BO 105 is predicted to have clear Level 2 handling qualities.

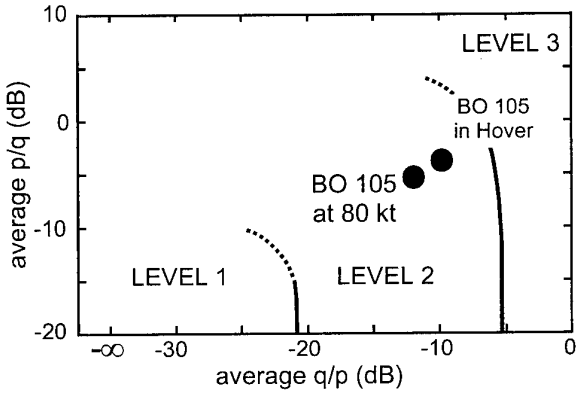

Fig. 10: The pitch-due-to-roll coupling criteria of [10] applied to the BO 105 in hover and forward flight.

Yaw-due-to-Collective Coupling

The hover and low speed yaw-due-to-collective coupling criteria measure the yaw rate build-up in the first three seconds that follow a collective step input. The criteria parameters are the normalized peak yaw rate measured within the three second observation window, $|r_1 / \dot{h}_3|$, and the normalized yaw buildup in the last two seconds of the observation window, $|r_3 / \dot{h}_3|$. These coefficients are normalized with the rate of climb that exists at the end of the three seconds. The yaw rate buildup in the yaw to collective coupling criterion is the inevitable result of the torque/anti-torque imbalance that follows a change in the collective pitch of the main rotor. In the BO 105, the torque change is not compensated for by a collective-to-pedal mixing unit, hence the yaw rate buildup is relatively severe.

Two different types of collective step inputs were used to determine the criterion: collective steps with the other controls fixed and collective steps with the attitude (but not the heading) constant. The latter produced more consistent results, as collective steps with the other controls fixed produced off-axis velocity components. Figure 11 shows the yaw-due-to-collective coupling criteria for the BO 105. As can be seen, the BO 105 has Level 3 handling qualities.

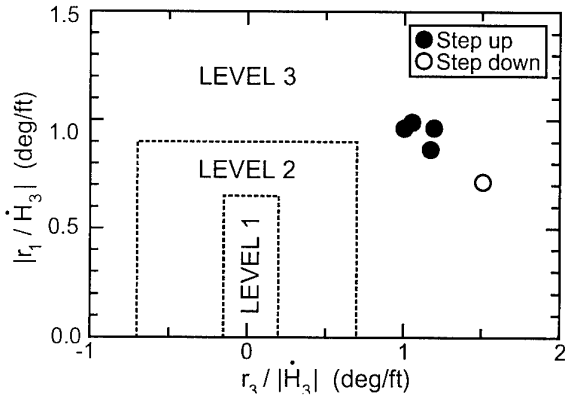

Fig. 11: The yaw-due-to-collective coupling criteria for the BO 105 in hover.

Pitch-due-to-Collective Coupling

The pitch-due-to-collective coupling criteria measure the pitch response during the first three seconds following a collective step input in forward flight. Collective steps with the other controls fixed showed Level 2 handling qualities for small collective steps with the BO 105 [4]. For large collective steps, the cri- terion could not be determined because of rotor speed con- siderations and the large pitch amplitudes that developed.

Roll-Sideslip Coupling

The complex yaw-sideslip coupling criteria mainly measure the helicopter's ability to perform coordinated turns. The roll-sideslip criteria, derived from old fixed-wing requirements, address turn coordination as well as bank angle oscillations following a lateral pulse input. Measurements with the BO 105 revealed difficulties in determining this criteria [4]. The roll-sideslip handling qualities for the BO 105 are estimated between Level 1 and Level 2.

EVALUATION OF ADS-33D HANDLING QUALITIES FLIGHT TEST MANEUVERS

The qualitative ADS-33 criteria, also known as the demonstration maneuvers, are a comprehensive assessment of the rotorcraft's handling qualities during stylized maneuvers representative of typical mission task elements (MTEs). The qualitative criteria in ADS-33 are included as an independent assessment of the rotorcraft's handling qualities. For the BO 105 tests, the qualitative assessment was completed for all maneuvers in the good visual environment. All of the ADS-33D flight test maneuvers were evaluated, except for the *roll reversal at reduced and elevated load factors* maneuver. Most maneuvers were evaluated by three experienced test pilots: one pilot with almost 4000 hours on the BO 105 and two test pilots with little or no time on this type of helicopter. This paper presents some of the main results of the flight tests (with additional details to be found in [11,12]).

Precision maneuvers

ADS-33 lists five precision maneuvers in the good visual environment: *hover*, *hovering turn*, *landing*, *slope landing*, and *pirouette*. All of these maneuvers were performed with the BO 105 according to the descriptions in ADS-33D. The test courses for these maneuvers consisted of a hover board, a pirouette circle, and a landing and slope landing area.

Figure 12 shows the handling qualities ratings (HQRs) for the precision maneuvers. All maneuvers received HQRs between 4 and 5, on the border between desired and adequate performance in the Cooper-Harper scale. The excellent consistency of the HQRs, despite the enormous differences in background of the different pilots, should at least be partially attributed to the excellent descriptions of the maneuvers.

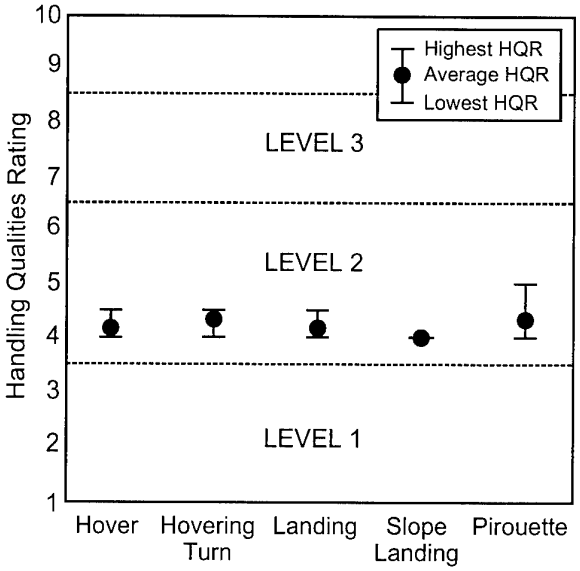

Fig. 12: Handling qualities ratings for the BO 105 in the precision maneuvers.

In this paper, two precision maneuvers will be described to demonstrate some of the typical problem areas that can be uncovered with these maneuvers.

Hover

The objective of the hover maneuver is to establish and maintain a precision hover within a 6 ft wide and long and 4 ft high box, the position of which is marked by a hover board and lines on the ground. Fig. 13 shows the pilot's control activity during the maneuver. The control inputs are

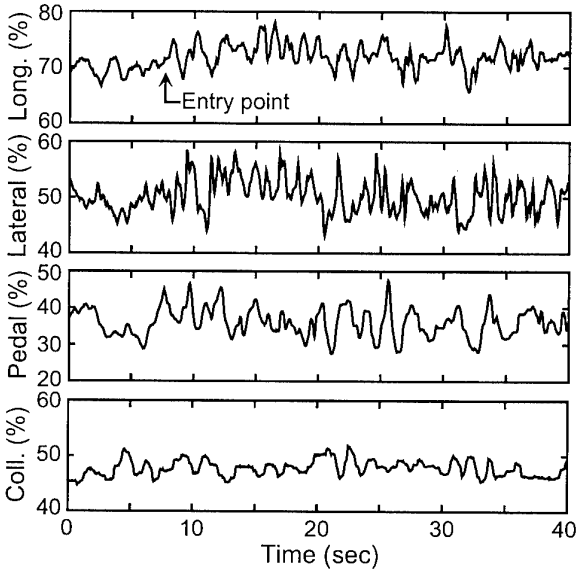

Fig. 13: Pilot control inputs during the hover maneuver.

typical of a high gain task; there is a lot of low amplitude control activity in all axes. A frequency analysis showed pitch and roll inputs up to frequencies of about 15 rad/sec, well above the bandwidth frequency of the BO 105. The handling qualities ratings for the hover maneuver ranged between 4 and 4½. The driving factor for this rating was the BO 105s poor yaw damping, which presented the only difficulty in meeting desired performance. Interaxis coupling was hard to notice and did not seem to have a significant influence on the handling qualities.

After completing the maneuver, the pilots complained about difficulties in assessing the longitudinal position of the helicopter. Future experiments may require adding lines on the ground to provide extra longitudinal cues.

Landing

The ADS-33 landing maneuver requires the pilot to touch down on a relatively small platform within 10 seconds after passing an altitude of 10 ft. For practical reasons, a ground marked landing area (Fig. 14) was substituted for the elevated landing platform suggested in ADS-33D. The hover maneuver was performed with an 8 kt quartering headwind, although this did not seem to affect performance significantly.

Fig. 14: The BO 105 during the landing maneuver.

The landing maneuver was started at an altitude of about 50 ft at a distance that allowed an approach with the landing area in the field of view. The control strategy was to build up a steady descent that would bring the helicopter to a hover just above the ground with only a minimum of collective pitch adjustments (i.e., let the ground effect do the work). Without the disturbances from the collective inputs, the pilot could then concentrate on getting over the desired position before touching down. When properly executed, this maneuver would give the pilot about 5 seconds to position the helicopter over the landing area and touch down. This was generally considered too short and sometimes slightly harder landings were made in order to meet the 10 second deadline. All pilots agreed that the 10 seconds available for the landing task was unrealistic and not operationally relevant. Also, the differences between desired and adequate performance, where a larger landing area is to be gained with no time limits, were considered too large. Further concerns were raised about missing cues for heading control, even though lines that extended out from the landing area were available.

Like the hover maneuver, the landing received HQRs between 4 and 4½. All pilots were able to meet desired performance, while being moderately aggressive on the controls. Yaw control and maintaining a descent rate throughout the maneuver required more than minimal compensation. Some yaw-due-to-collective coupling was noted, even though collective inputs were generally kept small. Power management did not seem to affect handling qualities at all.

Aggressive maneuvers

ADS-33 lists twelve aggressive maneuvers typical of NOE-flight and air and ground combat. These maneuvers cover the entire velocity range from sideward flight to hover to high speed forward flight. The BO 105 performed all aggressive maneuvers, except for the *roll reversal at reduced and elevated load factors* maneuver, which was dropped for safety reasons. Trials with the *roll reversal* maneuver showed the BO 105 dangerously approaching its structural limits. For some maneuvers, the starting velocities had to be reduced to conform to the BO 105s performance limits. All maneuvers were flown in calm to moderate winds.

Figure 15 shows the handling qualities ratings for the aggressive ADS-33 maneuvers with the BO 105. Eight out of

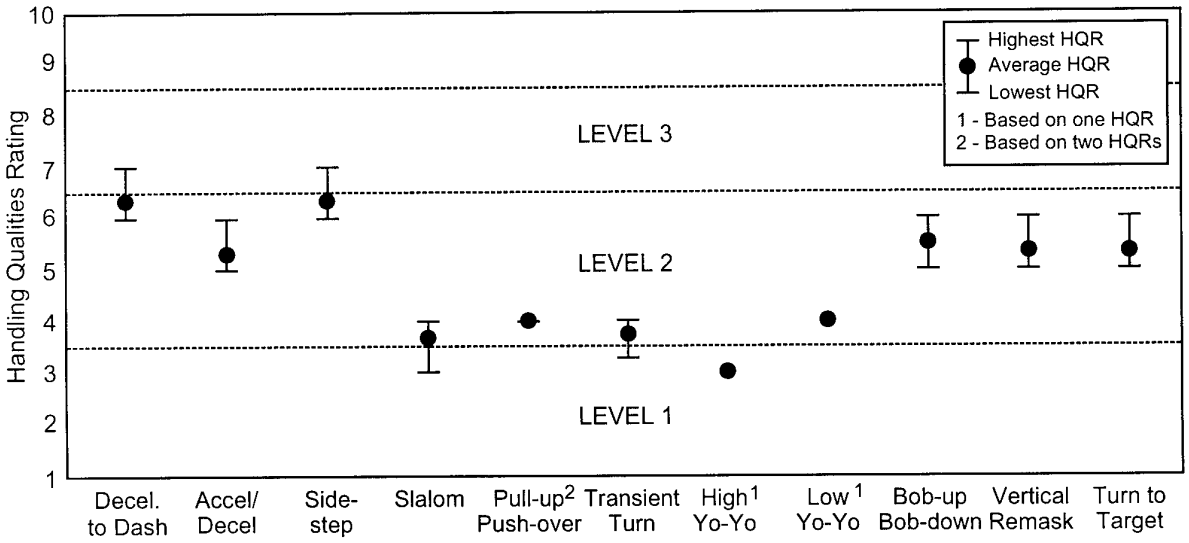

Fig. 15: Handling qualities ratings for the BO 105 in the aggressive maneuvers.

the eleven maneuvers were evaluated by three pilots. In each case, the HQRs differed by no more than one point. This excellent agreement between the pilots, who differed largely in background, should provide the necessary confidence in the maneuvers that were not rated by three pilots.

An analysis of the handling qualities ratings in Fig. 15 shows that HQRs on the Level 1-2 boundary were obtained for the *slalom*, *pull-up push-over*, *transient turn*, and *yo-yo* maneuvers, for which pitch and roll control dominates the task. Tasks that required large collective inputs, like *acceleration/deceleration*, *deceleration-to-dash*, *bob-up bob-down* and *vertical remask* received handling qualities ratings in the Level 2 to borderline Level 2-3 range. The *turn-to-target* and *sidestep* maneuvers who were mostly affected by interaxis coupling, and to a lesser degree by engine governor problems, also received Level 2 to borderline Level 2-3 handling qualities ratings. In this paper, three maneuvers, one from each of the above problem areas, will be discussed.

Transient Turn

The objective of the transient turn maneuver is to perform a 180 degree turn in less than 10 seconds, starting from 120 kt. The pilot is allowed to use all controls, including collective and pedals, to increase the rate of turn. With the BO 105, the entry speed was lowered to 100 kt, in order to maintain a safe margin to the envelope limits.

The freedom to use collective and pedals to increase the rate of turn makes it possible to perform the maneuver using different control strategies. Two slightly different control strategies are shown in Figures 16 and 17. Pilot A, using virtually no collective or pedal inputs, makes an almost coordinated turn with a load factor of about 2.4 g and with a velocity reduction of no more than 30 kt. Pilot B, who uses collective and some pedal, is able to complete the turn slightly faster with a maximum load factor of only about 2 g (which is at the very edge of desired performance). As a result, both pilots perceive somewhat different handling qualities. Pilot A, who assigned an HQR of 4 for this task, noted some 'mushing' at higher load factors, a significant amount of pitch-due-to-roll coupling, and had no problems with rotor speed and power management. Pilot B, who assigned an HQR of 3, did not note any effects of the elevated load factor, but had some (minor) problems with rotor speed management and also found some pitch-due-to-collective coupling in addition to the unavoidable pitch-due-to-roll coupling. A third pilot, who took the middle road, used moderate amounts of collective with a high load factor to perform the maneuver. He noted roll-due-to-pitch and pitch/ roll-due-to-collective as minor but annoying deficiencies which warranted an HQR of 4.

The apparent freedom to perform the transient turn maneuver, with or without the use of collective and pedals, but always within the set performance standards, does not seem to cause troubling differences in the perception of handling qualities. As with all ADS-33 maneuvers, it is important to try to meet all aspects of the achievable performance (whether it be desired or adequate performance), without trying to do more than necessary.

The handling qualities for the transient turn maneuver, on the borderline between Level 1 and 2, are typical of the BO 105s handling qualities for maneuvers that require primarily roll and pitch inputs. The excellent on-axis handling qualities are degraded by the substantial amounts of interaxis coupling.

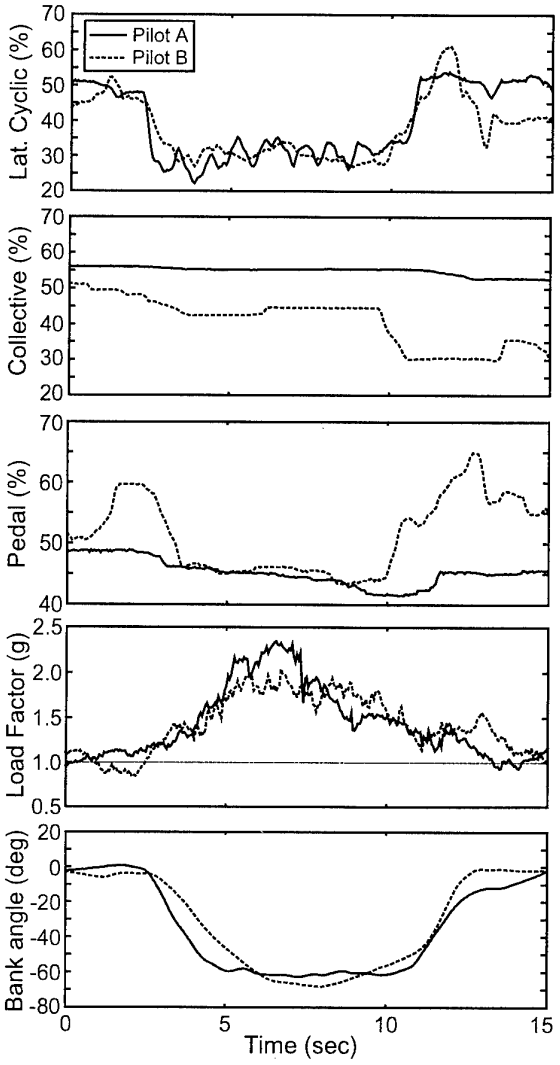

Fig. 16: Control inputs and helicopter response for two pilots performing the transient turn maneuver.

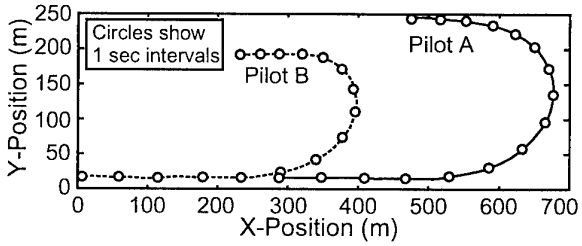

Fig. 17: Helicopter ground tracks during the transient turn maneuver.

Acceleration/deceleration

The acceleration/deceleration maneuver is a typical NOE task, characterized by strong collective inputs and aggressive maneuvering in the longitudinal axis. The averaged handling qualities rating for the accel/decel maneuver was 5.3, with all pilots failing to meet the desired performance requirements. Although interaxis coupling was noted,

power and rotor speed management were the driving factor for the handling qualities rating. The requirements to achieve 95 percent torque within 1.5 seconds at the start of the acceleration and to lower collective within three seconds to initiate the deceleration exposed the deficiencies of the engine governor. Workload was further increased by having to simultaneously observe heading and attitude with outside cues and rotor speed and torque with cues inside the cockpit.

Figure 18 shows some typical differences in control strategy between the pilots. Pilot A, who is very familiar with the BO 105, uses a very aggressive control strategy. He makes rapid power changes to achieve desired performance, but cannot prevent rotor speed from exceeding the Operational Flight Envelope (OFE). Pilot A assigned an HQR of 6 for this maneuver. Pilot B, who is unfamiliar with the BO 105, is not so aggressive. He accepts not being able to meet desired performance and so is able to keep rotor speed more or less within the OFE. Pilot B reached an HQR 5 for this maneuver.

All pilots remarked on the problems of having to decelerate with 30° pitch up and at the same time having to achieve hover over a designated spot. Although this requirement could be met, it required a fair amount of training and a good sense of timing. It is suggested that the end position requirement be relaxed. The pilots also complained about the requirement to achieve 95% torque within 1.5 seconds and to lower collective within 3 seconds. These requirements are very demanding and may not be realistic for helicopters like the BO 105.

The requirements of the deceleration-to-dash maneuver are very similar to the demands of the accel/decel task. Both maneuvers mostly evaluate rotor speed and torque control characteristics, together with collective to pitch and yaw coupling. The evaluations showed the deceleration-to-dash maneuver to be even more demanding on the BO 105 than the accel/decel.

Sidestep

The sidestep maneuver is a very aggressive maneuver at the edge of the BO 105s capabilities. The maneuver consists of an aggressive lateral acceleration with 25 degrees of bank to the maximum sideward velocity, followed by an aggressive deceleration with at least 30 degrees of bank back to hover. The BO 105 reached its maximum sideward velocity almost immediately, so that most of the time was spent regaining hover (Fig. 19). Lateral displacement during the maneuver was in the order of about 100 to 150 ft.

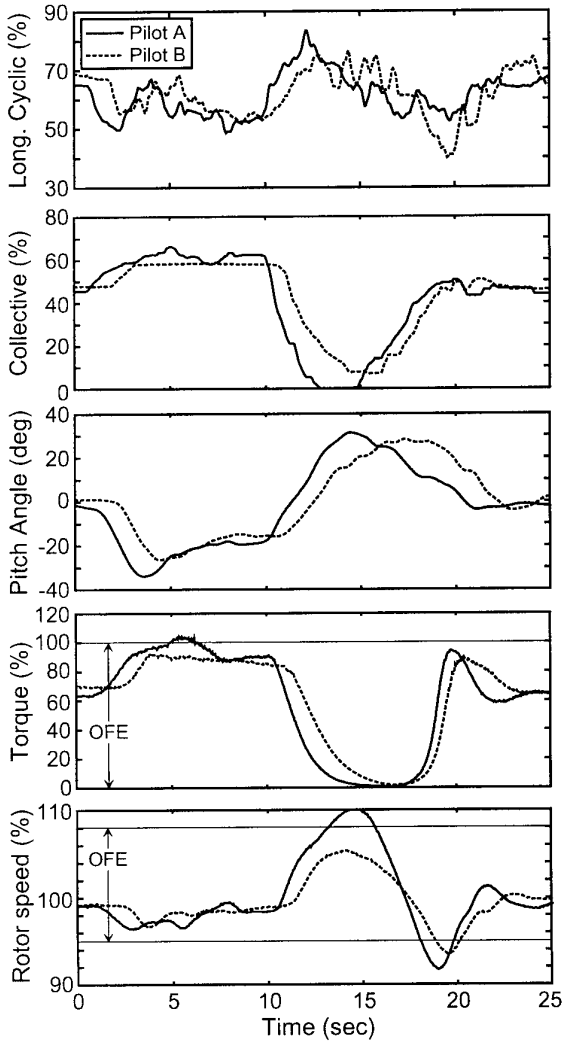

Fig. 18: Control inputs and BO 105 response for two pilots flying the acceleration/deceleration maneuver.

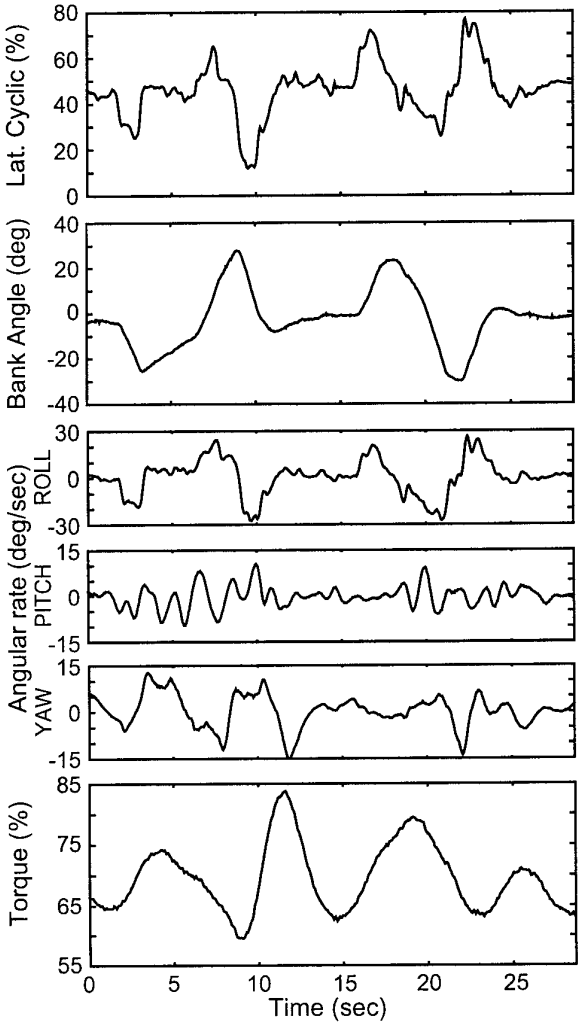

Fig. 19: Lateral cyclic input and the helicopter response during the sidestep maneuver.

The mean handling qualities rating for this maneuver was 6.3, which reflects the numerous difficulties encountered. Despite its high control power, the BO 105 was unable to meet desired performance, even adequate performance was hard to attain. Controlling the helicopter through the high roll rates and bank angles required a lot of lead compensation. Fig. 19 shows a time history of the lateral cyclic inputs, bank angle, angular rates, and indicated torque response of the BO 105 during the sidestep. The bank angle response shows the difficulty in regaining hover after the initial input has been made. The almost oscillatory torque response is indicative of the power control problems during the maneuver. Since the sidestep maneuver takes the BO 105 almost beyond its performance limits, a lot of the pilot's efforts went into controlling the rotor speed and torque.

Heading control necessary to compensate for the severe yaw coupling, aggravated by the poor yaw damping characteristics, was another major source of handling qualities problems. The third problem encountered was pitch-due-to-roll coupling, as evidenced by the nearly oscillatory pitch rate response. Or, as one pilot commented: "Added to the yaw oscillations and rotor/power train oscillations it [pitch-roll coupling] pushed the pilot workload over the top". Coupling seemed more severe on roll out, "due to collective inputs required to maintain altitude during the 30° bank angle".

These results underline that the sidestep is capable of exposing both engine and multi-axis coupling problems in lateral axis maneuvering. Nevertheless, the evaluation pilots considered the maneuver irrelevant for helicopters like the BO 105. The rapid succession of lateral acceleration and deceleration was found unrealistic, as were the imposed bank angle requirements. It is suggested that bank angle requirements be reduced, at least for non-attack helicopters like the BO 105, or that bank angles be made part of the performance requirements. It is also suggested, that the lateral acceleration and deceleration phases of the sidestep are separated by a phase where the helicopter laterally translates with constant velocity.

COMPARISON OF THE QUANTITATIVE AND QUALITATIVE EVALUATIONS

During the design of ADS-33, the limitations of the quantitative criteria were correctly recognized [13]. No matter how large the handling qualities data base, it will always be impossible to define a set of quantitative criteria that is so comprehensive that desirable handling qualities can be guaranteed over the entire maneuver spectrum – unless undue restrictions are imposed. For that reason, the quantitative criteria are supplemented by the demonstration maneuvers. This allows the discovery of handling qualities deficiencies not covered by the quantitative criteria. At the same time, it is recognized that failing to meet the quantitative criteria should result in less than desirable handling qualities – which may or may then not be exposed by the ADS-33 demonstration maneuvers. In general, a comparison of the results of a qualitative and a quantitative evaluation is likely to raise a number of questions, schematically summarized in Fig. 20.

Limitations of the Quantitative Evaluations

The evaluation of the quantitative criteria of the BO 105 provides not more than a snapshot of the BO 105's handling qualities in hover and at 80 kt. Because of the limited flying time available, no evaluations were made at other velocities, at different weight and cg conditions, or at different altitudes. Some criteria were not evaluated at all, either because they were irrelevant to the BO 105, because they were too difficult to measure (e.g. gust response characteristics), or because they required a qualitative rather than a quantitative statement.

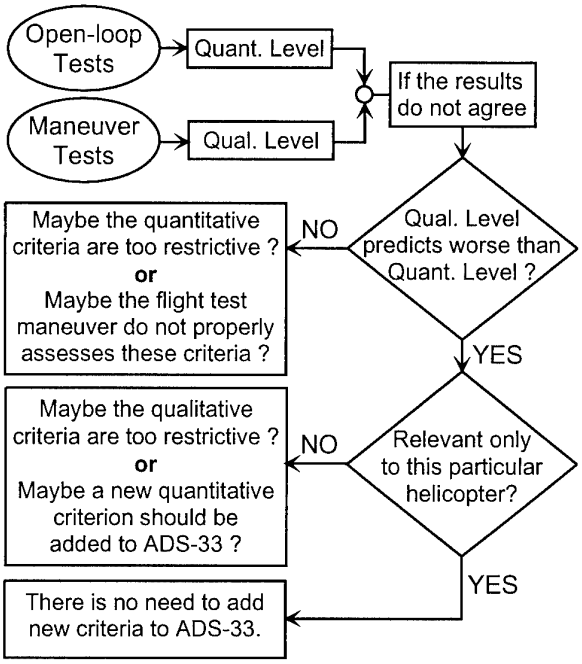

Fig. 20: Obligatory questions resulting out of discrepancies between the results of the quantitative and qualitative evaluations.

Limitations of the Qualitative Evaluations

The qualitative evaluation of the BO 105s handling qualities covered all maneuvers in good visual conditions (but of course at only one configuration of weight and cg). Most maneuvers were performed by three experienced test pilots who agreed on the handling qualities rating – even when there existed differences in piloting technique.

Figure 21 shows the dominant controller frequencies that were observed during the different maneuvers. This figure is based on a relatively simple analysis of the time histories of the pilot's control activity. Control inputs for the hover, *vertical remask* and *yo-yo* maneuvers extended up to 15 rad/sec, which is well beyond the neutral stability frequency of all primary axes. Other maneuvers, like *deceleration-to-dash* and *pull-up push-over*, demand relatively little of the short term response, although the inputs still exceed the bandwidth frequency. Very few maneuvers seemed to assess the long term response of the helicopter, which may be a reason for the differences between the Level 3 assessment of the unstable Phugoid and the borderline Level 1-2 handling qualities during maneuvers like *hover, landing* and *slope landing*.

Comparison of the Results

Short term and large amplitude response

Both the quantitative and qualitative evaluations showed the BO 105 with an excellent short term pitch and roll response. Some shortcomings to the roll quickness were noted during the *sidestep* maneuver, and pitch control power was a problem during the *pull-up push-over* maneuver. Nevertheless, Level 1 handling qualities seems quite reasonable.

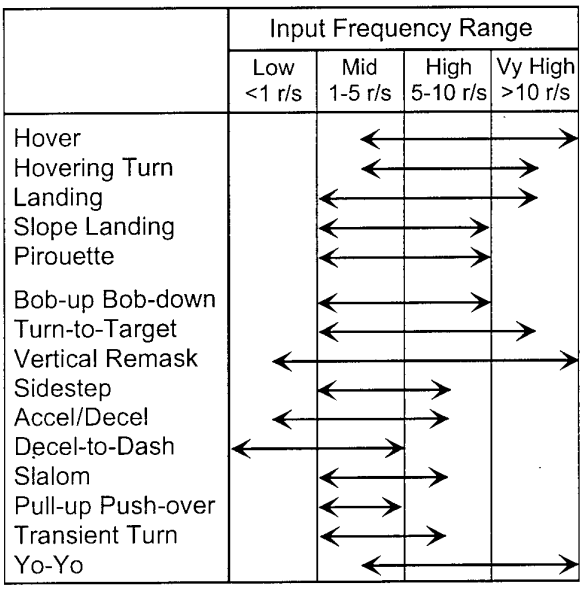

Fig. 21: Dominant pilot input frequencies for the ADS-33 maneuvers.

The poor yaw axis bandwidth was a major source of problems during the flight evaluations. Almost all hover/low speed maneuvers suffered from the poor yaw axis bandwidth in some way or another. Poor yaw damping was most noticeable during the hovering turn maneuver, which received a Level 2 (HQR 4.3) rating.

Mid-to-long term response

As could be expected of an unaugmented helicopter, the quantitative criteria revealed the poor stability of the BO 105. In forward flight, the instability of the Phugoid is acceptable (Level 1) but Dutch roll is too lightly damped (Level 2/3 for aggressive maneuvers). In hover, this picture is reversed: the Phugoid is highly unstable (Level 3) with a well damped (Level 1) Dutch roll.

These results were not fully confirmed during flight tests. Although roll-yaw oscillations were noted during some forward flight maneuvers, they were not considered a serious factor in the handling qualities. In hover, poor pitch and yaw axis stability were occasionally mentioned, but never really factored in any of the hover/low speed maneuvers (most of which had handling qualities ratings around 4). This raises a few questions which are beyond the scope of this paper. The analysis of the pilot input frequencies, however, seems to suggest that phugoid stability is not an issue in most of the good visual environment maneuvers tested (suitable divided attention maneuvers may be required to assess this criterion).

Vertical axis response

The quantitative evaluation of the vertical axis response suggested Level 1 vertical axis handling qualities for the BO 105. Yet, flight tests showed that maneuvers that relied heavily on the use of collective inputs (*decel-to-dash, accel/decel, bob-up bob-down, vertical remask* and *sidestep*) returned HQRs in the upper Level 2 range. Pilot comments for these maneuvers mentioned the demands on rotor speed and power management as the main contributor to the workload. For the *bob-up bob-down* and *vertical remask* maneuvers, the power margin was considered too narrow to achieve desired performance – despite the predicted Level 1 control power. Vertical damping seemed sufficient, although the poor rotor speed characteristics made stopping large descent and climb rates difficult.

The discrepancy between the BO 105s Level 1 quantitative and Level 2/3 qualitative results brings us to the obligatory questions in Figure 20. Although there are particularities of the BO 105s engine governor that play a role, the general problem of rotor speed management is not unique to the BO 105. Therefore, efforts to establish quantitative criteria for rotor speed control, though difficult to define, may be a necessary area of research in the coming years.

Interaxis coupling

The weak point of the BO 105 was clearly identified from the quantitative evaluations as the severe interaxis coupling. The BO 105 was identified as having Level 2 and 3 handling qualities on all interaxis coupling criteria except those involving turn coordination. The flight test evaluations with the ADS-33D maneuvers did not contradict this, although there are a few qualifications that need to be made. Pitch-roll coupling was noted during several maneuvers, both in forward flight and in hover, and was the major driver of the handling qualities rating in the transient turn maneuver. Yet, all these maneuvers returned average HQRs in the lower Level 2 range (HQR 4.5) so that the frequency domain criteria from [10] would seem to be more appropriate than the ADS-33D time domain criteria. Yaw-due-to-collective coupling, aggravated by the poor on-axis yaw handling qualities, was noted during most hover maneuvers, although the resulting handling qualities ratings never degraded into Level 3, as predicted by the collective-to-yaw coupling criterion.

During the flight test maneuvers, other couplings with an impact on handling qualities were noted, the most important of which was probably the pitch/roll-due-to-yaw coupling that was one of the main drivers for the Level 2 rating on the Turn to Target maneuver.

In summary, the coupling criteria seem to contain a number of deficiencies. These may have to do with the general time domain format of the criteria. As was learned in [10], coupling is primarily a high frequency phenomenon that the time domain criteria of ADS-33D may ineffectively capture. More research is needed to fully establish the effects of interaxis coupling on helicopter handling qualities.

CONCLUDING REMARKS

The most important conclusion to be drawn from this evaluation is that ADS-33D has superbly passed a difficult test with an unaugmented, highly maneuverable helicopter. The overall handling qualities picture obtained from ADS-33D confirmed in about 80 hours of evaluations more than we had learned about the helicopter through many years of flight testing.

Apart from this all important conclusion, there are many individual recommendations to be made, most of which are beyond the scope of an overview paper (please refer to [4,6,11,12]):

- Despite recent – partially unfounded – criticism from the flight test community, the introduction of frequency domain criteria to the evaluation of helicopter handling qualities testing is an example that deserves repetition. It appears like the coupling criteria would make excellent candidates.

- The use of parameter identification for the estimation of the height response to a collective step provides an interesting tool for the analysis of the vertical axis response. An extension to the estimation of rotor speed response might provide a useful analysis tool for engine and helicopter control systems designers alike. Beyond this, the use of parameter identification might be useful for the determination of the classic stability parameters (at least for unaugmented helicopters).
- The flight test maneuvers in the qualitative evaluation provide the necessary counterpart to the quantitative evaluations. The description of the maneuvers has improved significantly from ADS-33C, and provided an excellent basis for testing the BO 105.
- The aggressive maneuvers in ADS-33D may lie very close to the limits of performance of attack helicopters and are certainly difficult to achieve with other helicopters. A reformulation of the maneuvers to incorporate helicopters with different roles and missions seems necessary.

REFERENCES

1) "Handling Qualities Requirements for Military Rotorcraft," Aeronautical Design Standard 33D (ADS-33D), US Army Aviation and Troop Command, St. Louis (Mo), July 1994.

2) Key, D.L., Blanken, C.L. and Hoh R.H., "Some Lessons Learned in Three Years with ADS-33C," Piloting Vertical Flight Aircraft: A Conference on Flying Qualities and Human Factors, San Francisco (Ca), Jan 1993.

3) Cooper, G.E. and Harper, R.P., "The Use of Pilot Rating in the Evaluation of Aircraft Handling Qualities," Nasa TN D-5153, April 1969.

4) Ockier, C.J., "Flight Evaluation of the New Handling Qualities Criteria Using the BO 105," *Journal of the American Helicopter Society*, Vol. 41 (1), Jan. 1996.

5) Pausder, H.-J. and Blanken, C.L., "Generation of Helicopter Roll Axis Bandwidth Data through Ground-Based and In-Flight Simulation," AGARD CP-519, Oct. 1992.

6) Ockier, C.J. and Pausder, H.-J., "Experiences with ADS-33 Helicopter Specification Testing and Contributions to Refinement Research," AGARD CP-560, Jan. 1995.

7) Ham, J.A., Gardner, C.K. and Tischler, M.B., "Flight-Testing and Frequency-Domain Analysis for Rotorcraft Handling Qualities," *Journal of the American Helicopter Society*, Vol. 40 (2), April 1995.

8) Kaletka, J. and Gimonet, B., "Identification of Extended Models from BO 105 Flight Test Data for Hover Flight Condition," 21st European Rotorcraft Forum, St. Petersburg, Russia, Aug. 1995.

9) Corliss, L.D., "A Helicopter Handling Qualities Study of the Effects of Engine Response Characteristics, Height-Control Dynamics, and Excess Power on Nap-of-the-Earth Operations," *Journal of the American Helicopter Society*, Vol. 28 (3), July 1983.

10) Ockier, C.J., Pausder, H.-J. and Blanken, C.L., "An Investigation of the Effects of Pitch-Roll (De)-Coupling on Helicopter Handling Qualities," DLR FB 95-08, Feb. 1995. (Also: NASA TM 110349.)

11) Ockier, C.J. and Gollnick, V., "Evaluation of Selected Demonstration Maneuvers Using the BO 105 S-123 – 1994 Flight Test Results," DLR Institute of Flight Mechanics, IB 111-95/21, May 1995.

12) Soijer, M.W., "Evaluation of Selected Quantitative and Qualitative ADS-33D Maneuvers Using the BO 105 – Preliminary Results of the 1995 Flight Tests," DLR Institute of Flight Mechanics, IB 111-95/27, Aug. 1995.

13) Key, D.L. and Hoh, R.H., "New Handling Qualities Requirements and How They Can Be Met," 43rd Annual Forum of the American Helicopter Society, St. Louis (Mo), May 1987.

ONERA & DLR Cooperation on the "Smart Helicopter Concept"

- Handling Qualities Data Base for Hover and Low Speed Flight -

by

G. Bouwer [1]
A. Taghizad [2]
H. Mödden [1]

[1] Deutsche Forschungsanstalt für
Luft- und Raumfahrt e.V. (DLR)
Institut für Flugmechanik
D - 38108 Braunschweig, FRG

[2] Office National d'Études et de Recherches Aérospatiales (ONERA)
Direction des Études de Synthèse
BP-72, 92322 Châtillon - Cedex, France

SUMMARY

The handling qualities of a helicopter in the hover / low speed range were investigated with a lateral tracking task. The desired behaviour of decoupled rate command / attitude hold and attitude command systems were programmed in conceptual models with numerous sets of bandwidth / phase delay configurations. In a first step, the task was flown in a fixed base simulator. Then selected configurations were investigated in flight on a helicopter in-flight simulator. In the ground simulator, the pilots clearly preferred attitude command systems. In the flight tests, none of the attitude command systems was rated Level 1. For rate command / attitude hold systems, the configurations were rated with Level 1 and Level 2 with a clear boundary at a bandwidth of 2.5 rad/sec.

NOMENCLATURE

δ_y	Evaluation pilot lateral stick position
L_p	Model roll damping
L_δ	Model roll control sensitivity
ω_ϕ	Model roll eigenfrequency
τ_p	Model roll axis filter constant
b_M	Model roll acceleration
p_M	Model roll rate
Φ_M	Model roll attitude

INTRODUCTION

Increasing levels of mission performance are required for civil and military use of the next generation of helicopters. This aspect is pervading the application of new technologies to facilitate the pilot's task.

Flying a helicopter in adverse weather with high precision close to the ground means a drastic change of the piloting task. New cockpit technologies and high authority digital control systems will be implemented with the potential to tailor the flying qualities of the integrated helicopter system [1].

In 1992 the "Smart Helicopter Concept" cooperation between Office National d'Etudes et de Recherches Aérospatiales (ONERA) and Deutsche Forschungsanstalt für Luft- und Raumfahrt (DLR) was started. Task II of this cooperation is the investigation of handling qualities in hover and low speed.

The first step in the ONERA/DLR cooperation was a synthesis of existing specifications on helicopter Handling Qualities (HQ) [2]. A review of FAR Part 27/29, MIL-F-83300 and ADS-33 [3] specifications was performed, and some gaps were identified in each of these specifications.

The main conclusion of this study is that the new military handling qualities specification ADS-33 is a good guideline for the specific investigations within the Smart Helicopter Concept. Indead, FAR and MIL requirements cover only conventional helicopters HQ aspects. FAR uses mainly qualitative requirements. It does not take into account any technical solution as design specifications. Its overlaying certification topic is operational safety; mission effectiveness is not considered, therefore a mission orientation is missing. MIL-F-83300 is a much more detailed requirement, which addresses most of the HQ topics directly and quantitatively. As a military specification it tries to specify both aspects, operational safety and mission effectiveness; and it is highly related to technical solutions. Nevertheless, MIL specification does not take into account future helicopter capabilities through active control technology and additional cockpit equipment (Inceptors, HUD).

The ADS-33 represents a novel type of specifications which is necessary for helicopters, augmented by means of active controls and avionics. However, the deficiencies of ADS-33 for the Smart Helicopter Concept are mainly the limited database for the requirements and the military point of view. The main topics, used for our application on the lateral axis are the short term criteria of ADS, the response-type classification and rank ordering of ADS. Short term criteria are especially important because civil missions often require tracking control strategies.

Paper presented at the FVP Symposium on "Advances in Rotorcraft Technology", held in Ottawa, Canada, 27-30 May 1996, and published in CP-592.

The next step in ONERA/DLR cooperation was a mission analysis of civil helicopters in hover and low speeds [4]. This work enabled the definition of a task scenario for the HQ database generation. The essential results out of the mission analysis are listed below:

1.) In general, civil hover and low speed helicopter operation is careful maneuvering (small attitudes with corresponding small control inputs; mid term and short term response characteristics, predictability of the response rather than control power, stabilisation).

2.) This kind of operation often contains high gain precision strategies (small control amplitudes but high control frequencies; importance of short-term response; time delay).

3.) Multi axis operations due to inherent couplings : wind effect due to the helicopter's high gust sensitivity in the hover flight regime, short term and mid term couplings.

4.) Distinct control strategies exist:

a) Lateral and longitudinal are the most important controls with equal importance. Especially for position control that seems to be a keypoint for civil hover and low speed operations.

b) The collective control is also important, but only for height control close to the ground where it has first priority; in general though this is a secondary control.

c) The yaw axis with the corresponding pedal controls is the least important one. This is totally different from military operations where the most demanding requirements are related to the yaw axis, regarding targeting. Pedals are only used for stabilisations after gust disturbances and for careful heading changes in hover and low speed. The requirements for the corresponding response character- istics are comparatively low; only a good damping of yaw oscillations is required.

APPROACH

The handling qualities data base was is expected to provide the relation between pilot opinions and the parameters bandwidth (ω_{BW}) / phase delay (τ_p). So, varying ω_{BW} and τ_p was necessary. In addition, the response type effect on the task performance had to be an outcome of this database. For our investigations the selected behaviours were Attitude Command Attitude Hold (ACAH), and Rate Command Attitude Hold (RCAH).

This activity was done, in a first step, on a ground based simulator. The simulator used for this work was the CEV (French Flight Test Center) ground based facility at Istres. As a preliminary work, the characteristics of this simulator were evaluated and its capability to be used for the Smart Helicopter concept was succesfully proven [5,6]. As an outcome of the previous investigations (review of specifications, mission analysis), a Conceptual Simulation Model (CSM) and a task scenario for a lateral axis maneuver were defined and implemented on the simulator. The CSM is a collection of flight mechanics equations combined with some mathematical equations in order to reproduce easily the desired behaviour of a fly-by-wire helicopter (Response-Type), with adjustable characteristics. It is to be emphasized that simulation trials were mainly organized in order to validate our approach and the best procedure. The background provided from these trials enabled us to optimize the flight test conditions.

Two pilots during 1 week evaluated the handling qualities of 28 configurations of ACAH response types and 17 configurations of RCAH response types. Figures 1 and 2 illustrate these configurations in a bandwidth / phase delay diagram.

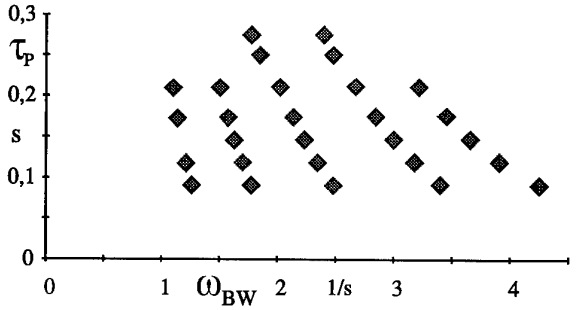

Figure 1 : Bandwidth / Phase Delay Diagram of Simulated Attitude Command Attitude Hold Systems

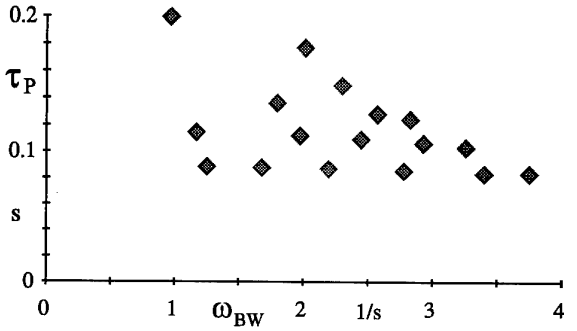

Figure 2 : Bandwidth / Phase Delay Diagram of Simulated Rate Command Attitude Hold Systems

The second step of these investigations was to test the selected configurations in flight. The helicopter used was the DLR in-flight simulator ATTHeS. The previously defined task scenario was adapted to flight testing, and the ACAH and RCAH control laws were implemented on ATTHeS. About 20 hours of flight tests were allocated to this investigation. Three pilots during 2 weeks evaluated the handling qualities of 10 configurations of RCAH and 10 configurations of ACAH. Figures 3 and 4 illustrate these points in a bandwidth / phase delay diagram.

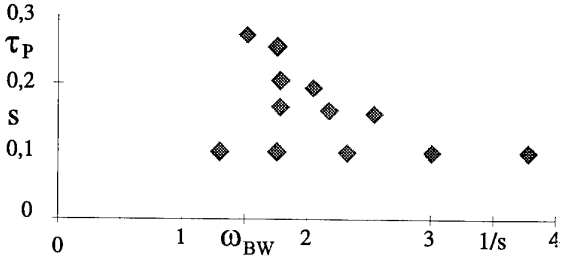

Figure 3 : Bandwidth / Phase Delay Diagram of Flown Rate Command Attitude Hold Systems

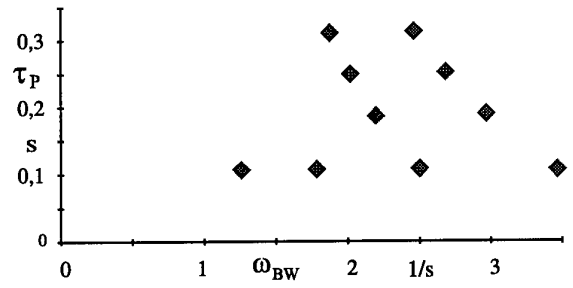

Figure 4 : Bandwidth / Phase Delay Diagram of Flown Attitude Command Attitude Hold Systems

GROUND SIMULATION

The Simulator System

The CEV simulator in Istres is a ground based simulator placed in a 10 m diameter dome. It is equiped with a CGI visual system, for which the scenario is adapted to helicopter flight conditions (buildings, trees, wires). The fixed based cockpit is basically a french/german Tiger configuration with conventional sticks. A Head-Up-Display is also available. The field of view of the visual system is ± 20° in vertical and ± 90° in the lateral axis. The overall time delay is estimated to 120 ms. A detailed description of the simulation system is given in [7].

The Conceptual Model

The generation of a handling quality database needs to have the possibility of sweeping main HQ parameters (τ_p, ω_{Bw}) and to select different response types. That is the role of the Conceptual Simulation Model (CSM). CSM is a selection of flight mechanics equations combined with some mathematical equations (appendix 1) in order to reproduce easily the desired behaviour of a fly-by-wire helicopter with adjustable characteristics. Two response types have been implemented on this model: the Rate Command Attitude Hold (RCAH) and the Attitude Command Attitude Hold (ACAH).

Flight Task Development and Adaptation

These first handling qualities investigation mainly focussed on the lateral axis behaviour. The mission analysis provided several important characteristics of helicopter missions in hover and low speed. The main parameters taken into account in these first tests are:

1.) carefree maneuvering

a) small amplitudes,

b) corresponding small control inputs,

c) mid-term and short-term response characteristics,

d) stabilisation.

2.) high gain precision control strategy

a) small control amplitudes but high control frequencies

b) main HQ parameters: bandwidth and phase delay.

The provided Mission Task Element (MTE) is called Precise Dynamic Position Control (figure 5). The objective of this MTE is to follow a target or "rabbit" in the lateral axis with high precision. At the starting point, the helicopter hovers in front of the target. Then the target starts moving, accelerating from 0 to 15 kts, keeping a constant speed during 75 meters and decelerating from 15 kts to stop at the finish point. The pilot has to follow the target "face to face", keeping the helicopter within a 3 meter radius horizontal circle moving with the rabbit, and has to control the height with a maximum error of ± 1,5 meters. The lateral overshoot at the end point should not exceed 3 meters. The task should be run in both directions (left and right).

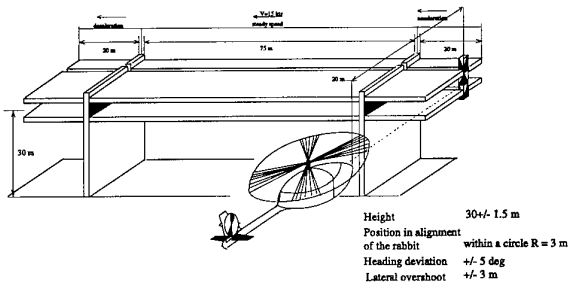

Figure 5 : The Task for the Piloted Simulation

For the first version of this MTE, some of the requirements were selected in comparison with the ADS sidestep. Two pilots from CEV and one pilot from DLR participated in the optimization of these limits. The objective for this work was to get a "realisable but difficult" task. The presented result is the convergence of pilot opinions with respect to the realisation limits of the MTE.

Head-Up-Display

During the development of this task, it was clearly shown, that using only the external view was not completely sufficient for the pilots to realise the performance. Therefore, the Head-Up-Display was used in order to provide additional informations to the pilots. A specific cueing was developed for the Precise Dynamic Position Control (figure 6).

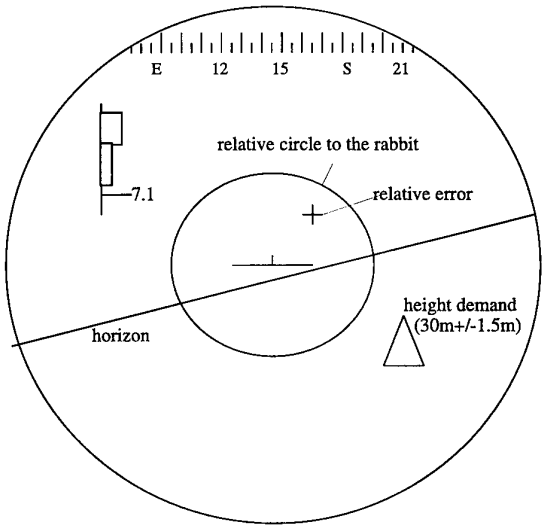

Figure 6 : View of the Head-Up-Display

The main information provided from the HUD is the relative position of the helicopter to the rabbit. A cross, moving within a circle, represents the helicopter. The circle is the limit of the adequate performance in the horizontal plane. Its center is the rabbit. The objective is to superimpose the cross with the circle center, or at worst, to avoid leaving the circle.

The HUD also provides additional height cues. When the height requirements are not respected, a danger triangle appears on the bottom-right side of the screen, accompanied with a bell.

Pilot comments tend to confirm that this task is perfectly defined on the simulator. According to them, all the required information for performance evaluation is available in a simple manner.

Simulation Results

According to the pilots, this task is very well adapted to test civil helicopter lateral axis handling qualities at low speeds. In addition, this MTE is very different from ADS-33 specifications for a lateral MTE (sidestep), because it requires a precise dynamic control of the helicopter's position. Pilots appreciated the definition of desired performance limits. But adequate performance limits had to be clearly defined. This work was done for the flight tests.

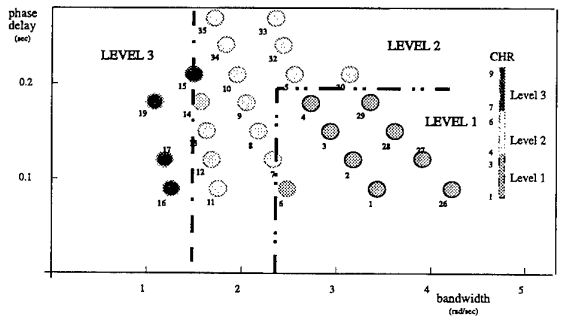

Figure 7 : Results of the ACAH Configuration in the Bandwidth-Phase Delay Plane

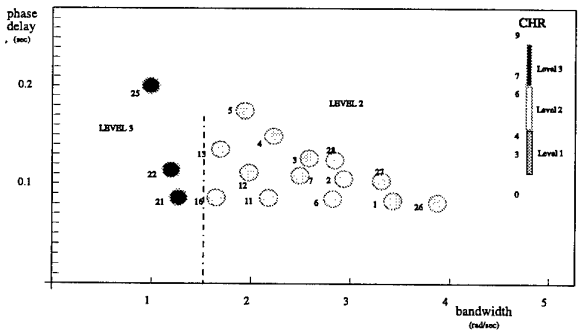

Figure 8 : Results of the RCAH Configuration in the Bandwidth-Phase Delay Plane

Figures 7 and 8 show the results of the pilots' Cooper-Harper ratings, presented on a bandwidth / phase delay diagram. They illustrate the two tested response-types ACAH (figure 7) and RCAH (figure 8). The pilot ratings harmonize very well. The low number of RCAH configurations is due to the fact that during the trials, pilots preferred the ACAH control law. For ACAH, a limitation on handling qualities levels appeared for the bandwidth of about 2.5 rad/sec for Level 1 and 1.5 rad/sec for Level 2. A maximum limit on phase delay is also shown for Level 1 handling qualities at about 0.19 second. The interpretation of pilots preferance for ACAH response-type rather than for RCAH is difficult. One reason may be the underestimation of the lateral aerodynamic drag coefficient in the Conceptual Simulation Model.

FLIGHT TEST

The Helicopter In-flight Simulator ATTHeS

The DLR Institute of Flight Mechanics was operating the helicopter in-flight simulator ATTHeS (Advanced Technologies Testing Helicopter System) for a decade [8]. Shortly after the flight tests for this project, ATTHeS crashed during a routine ferry flight. In the crash, the helicopter was destroyed and the crew, test pilot Klaus Sanders and mechanic Jürgen Zimmer, lost their lifes.

ATTHeS, shown in figure 9, was based on a BO 105 helicopter. The testbed was equipped with a full authority non redundant fly-by-wire (FbW) control system for the main rotor and fly-by-light (FbL) system for the tail rotor. The testbed required a two-men crew, consisting of a simulation pilot and a safety pilot. The safety pilot was equipped with the standard mechanical link to the rotor controls whereas the simulation pilot's controllers were linked electrically/optically to the rotor controls. The FbW/L actuator inputs which were commanded by the simulation pilot and/or the control system were mechanically fed back to the safety pilot's controllers. With this function, the safety pilot was able to monitor the rotor control inputs. The testbed could be flown in three modes:

Figure 9 : In-Flight Simulator ATTHeS

1. the FbW/L disengaged mode, where the safety pilot had the exclusive control,

2. the 1:1 mode, where the simulation pilot had the full authority to fly the baseline helicopter, and

3. the simulation mode, where the simulation pilot was flying a simulated helicopter command model with full authority.

In the 1:1 and simulation modes the flight envelope of the testbed was restricted to 50 ft above ground in hover and 100 ft in forward flight.

For in-flight simulation purposes, the most promising method for a control system design is to force the host helicopter to respond on the pilot inputs as an explicit calculated command model. This gives the ability to decouple the helicopter axis and to tailor each axis individually for the desired application. The explicit Model Following Control System (MFCS) design of ATTHeS provided the airborne simulator with the demanded level of simulation fidelity. A detailed description of the ATTHeS in-flight simulator system is given in [9].

The Flight Task

The principle flight task arrangement is shown in figure 10. On top of a car a special designed arrangement of lamps was mounted [10]. At a distance of 80 m to the car, the helicopter was hovering with an height of 50 feet. Helicopter states and controls were recorded on board. In addition, a video camera on the car pointed to the helicopter and recorded the flights. Upon a sign via radio, the car driver accelerated to 30 km/h and delcelerated again as shown in the lower part of figure 10.

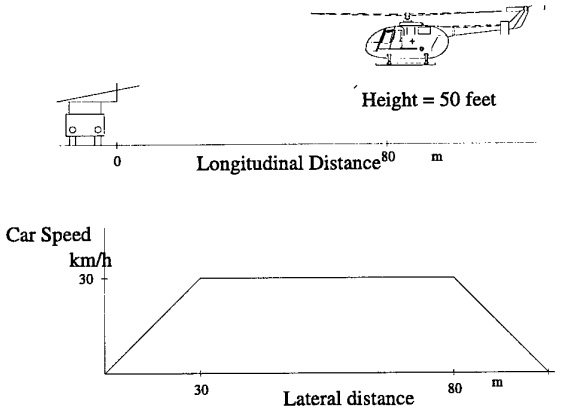

Figure 10 : Lateral Position Tracking Task

The rate command parameters are related to the model equation for the desired roll rate

$$\dot{b}_M = (-\dot{p}_M + L_\partial \cdot \partial_y - L_p \cdot p_M)\tau_p$$

the attitude command parameters are related to the model equation

$$\dot{b}_M = (-\dot{p}_M + L_\partial \cdot \partial_y - 1.4\omega_\Phi^2 \cdot \Phi_M)\tau_p$$

$$\dot{p}_M = b_M$$

In all cases the filter parameter τ_p was 20.0 rad/s. Pitch and roll axis had the same principal behaviour, the parameters were harmonized. The resulting parameters for the bandwidth-phase delay diagrams after [3] were calculated offline including 90 ms delay of the basic helicopter and the sampling delay.

The time histories of typical states during the lateral tracking task with a Level 1 rate command configuration in figure 11 are discussed from top to bottom. The lateral pilot control and the lateral actuator have the highest activity, both are similar in this rate command configuration because the basic BO 105 has nearly a rate command behaviour. Commanded and real roll attitude coincide well. The longitudinal pilot control has very little activity in contrary to the longitudinal actuator, which indicates a high pitch coupling of the BO 105, which is very well suppressed by the MFCS. Desired pitch attitude and real pitch attitude again have very little activity, the control error is less than two degrees. Collective pilot control and actuator coincide, because they are connected 1:1, the pilot has to control the radio altitude himself with collective inputs. The pilot doesn't make any pedal inputs because of the heading hold in the yaw axis, whereas the tail rotor actuator shows high activity to hold the Heading with an error less than five degrees during maneuvering.

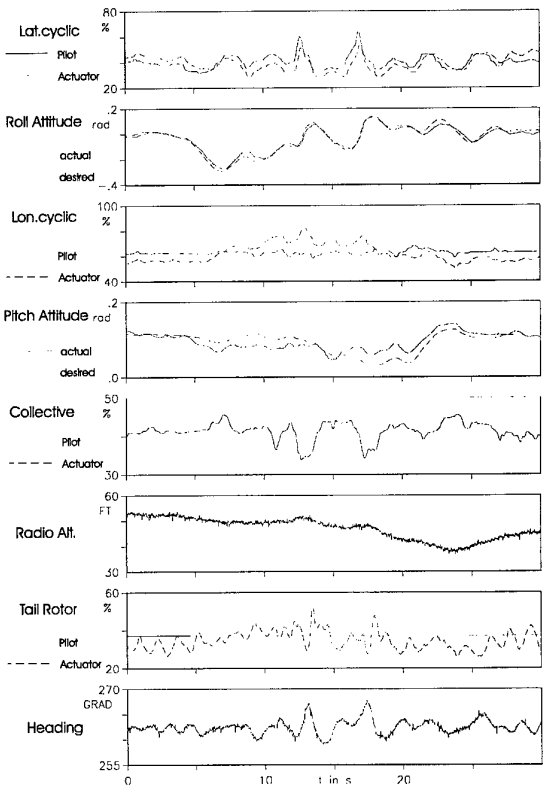

Figure 11 : Time Histories of typical States during Lateral Tracking

Commanded Model Verification

To prove the command models validity, selected models were verified in flight with frequency sweep inputs of the pilot. Frequency analysis of these time histories lead to the Bode Plot in figure 12.

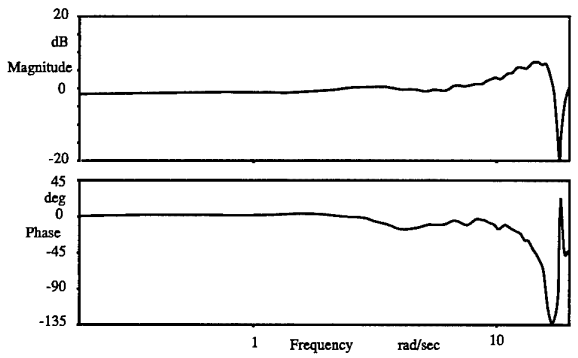

Figure 12 : Bode Plot of Real Roll Rate to Desired Roll Rate

The input signal was the desired roll rate, the output signal the actual roll rate of ATTHeS.At low frequencies up to 2.5 rad/sec the magnitude is constant 0 dB and the phase shift is zero, which indicates perfect matching. At 3 rad/sec the influence of the not fully suppressed dutch roll can be observed. At about 15 rad/sec the low damped mode of the rotor-body coupling can be seen. Nevertheless, the phase is not larger than 135 degrees. At frequencies larger than 17 rad/sec the result is not interpretable because of a strong drop in the coherence function. In general it can be stated, that ATTHeS matched very well the desired dynamics.

Task Performance Analysis

After each test the pilots had to fullfil a questionnaire, collecting information about the task performance, the workload, the vehicle's control dynamic characteristics and the corresponding Cooper-Harper rating. As mentionned above, during the flight tests a video camera on the car recorded the flights. Figure 13 shows an image through this camera, on which the desired and adequate performance limits were determined with calibration flights. Thus, with this video, it is possible to visualize during the flight tests the helicopter's position within the performance limits. A comparison with pilot comments and their Cooper-Harper ratings provides the level of harmony between the ratings and the real task performance in flight. Table 1 illustrates these conclusions for two selected test points. From this analysis, it was concluded, that pilot ratings harmonized very well with the measured task performance for all pilots.

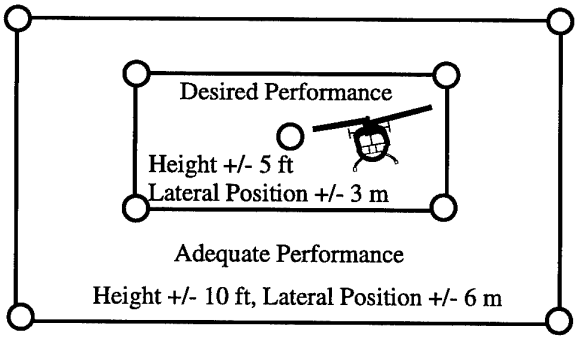

Figure 13 : View of the Camera on the Tracking Target

Overall Handling Qualities Ratings

During the flight tests, pilots clearly preferred the RCAH control law to ACAH.

The Cooper-Harper ratings for the ACAH test points in flight are not interpretable, because several problems emerged in flight with this response-type. Most of the investigated configurations were in the Level 2 handling qualities, some of them in Level 3. Contrary to the simulator investigations, none of the attitude command test points was rated to be Level 1. During the flight tests with ACAH, pilots complained about the difficulty they had to maintain the stick outside the trim position. Investigations during the trials showed that the problems encountered with this control law were due to the implementation of this specific command in real flight conditions. Two reasons were mainly identified. The first one was the relatively high stick forces on the controls of ATTHeS, which made this task difficult to fly. Further analysis showed that pilots were also disturbed by the fact that the helicopter body motion prevented them from maintaining the stick in a fixed position. At last, the effect of fuselage's inertial motion reaction on the stick during bank angle changes, was also identified as a reason for the discomfort encountered with this control law.

Figure 14 shows the average handling qualities rating for the flown Rate Command / Attitude Hold configurations in the bandwidth-phase delay diagram. The ratings harmonize very well and show a clear limit between Level 1 and Level 2 handling qualities around the bandwidth 2.5 rad/sec. Pilots comments collected for test points number 5 and 7 suggest a tendency to a Level 1 limitation on phase delay at 0.2 sec. Pilots appreciated the task realisation in flight, they confirmed that this MTE was very well adapted to test the lateral axis handling qualities of helicopters in hover and low speed.

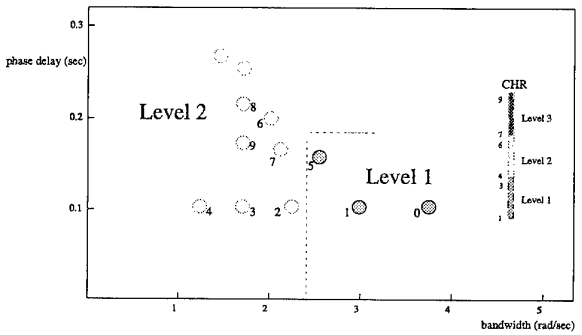

Figure 14 : Bandwidth / Phase Delay Diagram of Rate Command / Attitude Hold Systems

CONCLUSIONS

A handling qualities data base was generated from simulation trials and from in-flight tests on the DLR's ATTHeS. The main objective for this data base was to identify Level 1 configurations of HQ and its boundary with Level 2. The simulation trials were mainly used to provide a background on these handling qualities investigations and to validate the adopted approach, in order to prepare the flight tests. They also provided first results for the HQ data base.

According to the pilots, the implementation of the "Precise Dynamic Position Control" task on the simulator was appreciated. Indeed, the good definition of the Head-Up-Display cues compensated the lack of a sufficiant external view, which could appear as being indispensable. All the information useful to estimate the task performance were available to pilots in a simple manner.

From the flight tests, a clear area of Level 1 handling qualities was identified with the RCAH response type. The ACAH encountered some technical problems in flight, requiring some more investigations to get it operational. These topics are:

1- The influence of the stick forces and control sensitivity. Pilots emphasized the importance of the phase when they had to maintain the stick to a position outside trim (zero force). More investigations are required to analyse the effect of this parameters on handling qualities.

2- Helicopter's body motion and it's inertia coupling to the stick is a disturbing effect to maintain the stick in a fix position.

Further investigations are necessary to analyse in detail all the parameters which influence the ACAH control law performance in flight. In the framework of these investigations the effect of active inceptors on this specific response-type could also be taken into account.

The RCAH controller provided very good results in flight. One of the reasons of its success was the very good decoupling of yaw axis. The directional hold was appreciated by all the pilots.

Finally, pilots commented that this task was very well adapted to check helicopter's lateral axis handling qualities in hover and low speeds. From both tests (simulations and in-flight) a very good harmony between pilots Cooper-Harper ratings was noted.

Acknowledgement

Thanks are due to many people at DLR and ONERA who helped making possible the simulation experiments at ONERA and the flight tests at the military airport at Celle, the test pilots from CEV (Centre d'Essais en Vol) and DLR and especially Klaus Sanders and Jürgen Zimmer.

References

[1] Gmelin, B., Pausder, H.J., and Hamel, P. "Mission Oriented Flying Qualities Criteria for Helicopter Design via In-Flight Simulation", AGARD-CP-423, Paper No. 4, 1986.

[2] Mödden, H. "Review of Specifications for the Smart Helicopter Concept of ONERA/DLR", DLR Institute Report IB 111-93/29, Braunschweig, 1993

[3] NN, "Aeronautical Design Standard ADS-33D" United States Army Aviation and Troop Command, St. Louis, Mo, July 1994

[4] Mödden, H., "Mission Analysis for the Smart Helicopter Concept of DLR/ONERA", DLR Institute Report IB 111-93/57, Braunschweig 1993

[5] Taghizad, A. "Evaluation Of The CEV Ground Simulation Facility For The Smart Helicopter Concept Of ONERA/DLR", ONERA, Direction des Etudes de Synthèse, Report RT 13/5161, Salon de Provence, 1993

[6] Taghizad, A., "Handling Qualities Simulation Tests At CEV. ONERA/DLR Cooperation on the Smart Helicopter", ONERA, Direction des Etudes et de Synthèse, Report RT 23/5161, Salon de Provence, 1995

[7] NN, "Présentation des Moyens de Simulation TIGRE/GERFAUT", Centre d'Essais en Vol, Section Etudes et Simulations, Décembre 1993

[8] von Grünhagen, W., et. al. "A High Bandwidth Control System for a Helicopter In-Flight Simulator", International Journal of Control, Vol. 59, No.1, 1994

[9] Bouwer, G. "A Robust Digital Model Following Controller for Helicopters", European Space Agency, ESA-TT-1041, April 1989

[10] Mödden, H. "Improved Flight Test Equipment for ATTHeS: Multicolor Signalling Systems with Modular Components for the Smart Helicopter Concept of DLR & ONERA -Precise Dynamical Position Control Tasks in Hover and Low Speed - (Part I: For Flight Tests in 1995)", DLR Institute Report IB 111-95/05, Braunschweig, 1995

Test Point	time in Desired Perform.	time in Adequate Perform.	CHR	Pilot Remark on Perform.	Pilot Workload Remark
RCAH-0	22 sec	0..1 sec	2	desired	all points are good
RCAH-4	23 sec	0..1 sec	4	desired	importants efforts mainly to control roll spare capacity moderate anticipation is necessary in roll

Table 1 : Measured Task Performance and Pilot Ratings

Appendix : Conceptual Model Equations of Motion

1. RCAH Conceptual Model :

$$\dot{u} = rv - qw - g\sin(\Theta) + k_{dragx} V_A^2$$

$$\dot{v} = pw - ru + g\cos(\Theta)\sin(\Phi) + k_{dragy} V_A^2$$

$$\dot{w} = qu - pv + g\cos(\Theta)\cos(\Phi) + \left(k_{col}(t-\tau) + Z_w w\right)$$

$$w = u\frac{\tan(\Theta)}{\cos(\Phi)} - v\tan(\Phi) \qquad (height\ hold)$$

$$\dot{p} - L_p p = k_{lat}\partial_{lat}(t-\tau)$$

$$\dot{q} - M_q q = k_{lon}\partial_{lon}(t-\tau)$$

$$\dot{r} - N_r r = k_{ped}\partial_{ped}(t-\tau)$$

$$\dot{r} = 0 \quad (turn\ coordination)$$

$$\dot{\Phi} = p + \tan(\Theta)\left(q\sin(\Phi) + r\cos(\Phi)\right)$$

$$\dot{\Theta} = q\cos(\Phi) - r\sin(\Phi)$$

$$\dot{\Psi} = coef_1 r + coef_2 \frac{g}{u}\tan(\Phi)$$

2. ACAH Conceptual Model :

$$\dot{u} = rv - qw - g\sin(\Theta) + k_{dragx} V_A^2$$

$$\dot{v} = pw - ru + g\cos(\Theta)\sin(\Phi) + k_{dragy} V_A^2$$

$$\dot{w} = qu - pv + g\cos(\Theta)\cos(\Phi) + \left(k_{col}(t-\tau) + Z_w w\right)$$

$$w = u\frac{\tan(\Theta)}{\cos(\Phi)} - v\tan(\Phi) \qquad (height\ hold)$$

$$\dot{p} = \dot{\Phi} - \tan(\Theta)\left(q\sin(\Phi) + r\cos(\Phi)\right)$$

$$\dot{q} - \dot{\Theta} + r\frac{\sin(\Theta)}{\cos(\Theta)}$$

$$\dot{r} - N_r r = k_{ped}\partial_{ped}(t-\tau)$$

$$\dot{r} = 0 \quad (turn\ coordination)$$

$$\ddot{\Phi} + 2D\omega_0\dot{\Phi} + \omega_0^2\Phi = k_{lat}\delta_{lat}(t-\tau)$$

$$\ddot{\Phi} + 2D\omega_0\dot{\Theta} + \omega_0^2\Theta = k_{lon}\delta_{lon}(t-\tau)$$

$$\dot{\Psi} = coef_1 r + coef_2 \frac{g}{u}\tan(\Phi)$$

Notation

V_A	Resultant speed
u	Forward velocity
v	Sideward velocity
w	Vertical velocity
p	Roll rate
q	Pitch rate
r	Yaw rate
g	Gravitation (= 9.81 m/s^2)
k	Constant
t	Time
Φ	Euler angle roll
Θ	Euler angle pitch
Ψ	Euler angle yaw = heading
L_p	Roll damping
M_q	Pitch damping
N_r	Yaw damping
D	Damping
$\omega 0$	Natural frequency
τ	Time delay

Indices

dragx	Longitudinal drag
dragy	Lateral drag
lon	Longitudinal
lat	Lateral
col	Collective
ped	Pedal

DEVELOPMENT OF A TACTICAL HELICOPTER INFRARED SIGNATURE SUPPRESSION (IRSS) SYSTEM

P.R. Sully
Air Vehicles Research Sector, Research and Development Branch
National Defence Headquarters
Ottawa, Ontario, Canada K1A 0K2

D. VanDam
W.R. Davis Engineering Limited

J. Bird
Institute for Aerospace Research
National Research Council

D. Luisi
DAEPM(C), Department of National Defence

SUMMARY

The world-wide availability of increasingly sophisticated but light weight infra-red missile systems is presenting a serious threat to tactical helicopters in regional and peace-keeping operations. Part of the response to this threat lies in reducing as much as possible the infra-red signature of these helicopters. This paper briefly describes the nature of the threat presented by such missiles. The design and development of countermeasures in the form of IR suppression systems to reduce the engine exhaust produced signature is detailed. The results of experimental investigations and trials completed to date are described, along with the estimated potential for improving survivability. Future programmes and plans are summarized.

INTRODUCTION

The increasing use of Canadian Forces helicopters in regional and peace-keeping operations, coupled with the world-wide proliferation of shoulder-launched infra-red (IR) guided missiles has made countermeasures and signature reduction a high priority item in the Canadian Department of National Defence (DND) research and development programme. The major threat is from IR (heat-seeking) missiles which are cheap and easy to use. The development of infra-red signature suppression (IRSS) systems has necessitated studies of these threats and the corresponding requirements for signature reduction, modelling of the helicopter IR signatures and missile lock-on ranges. Following these, detailed specifications were required for the suppressor system in terms of aerothermal performance, power loss, weight etc. Extensive experimental evaluations of the helicopter air management system were carried out before final designs were completed. Prototype IRSS systems were fabricated and preliminary structural and engine cell tests have been carried out. Fitment in the CH-146 Griffon helicopter has been confirmed. Initial flight evaluations are planned on the NRC Bell 412, and a complete evaluation of the effectiveness of the IRSS system will be carried out on the CH-146.

THE IR THREAT

All aircraft emit energy in the infrared (IR) portion of the electro-magnetic spectrum which makes them potential targets. For this reason, IR seekers have exploited techniques to acquire and intercept airborne targets by passively detecting IR energy from the engine exhaust emissions and aircraft aerodynamic heating. Other advantages of IR seekers are that they require no special fire control system aboard the launch platform, no special radio-frequency (RF) radiation from the target, and the technology of infrared detectors makes it possible to acquire a target at sufficient ranges to provide useful engagement boundaries (May and Van Zee, 1983). This results in a missile which is cheap to manufacture, easy to use and has a "fire-and-forget" capability. Between 1979 and 1993, IR guided missiles have destroyed 89% of all downed aircraft (gunfire, and RF missiles included).

Since the atmosphere limits practical use of the IR spectrum to certain bands, it is important to discuss the bands of interest for IR weapons. First generation IR seekers operate in the 1.9 - 2.9 μm waveband - which spectrally match emissions from hot metal parts such as engine exhaust components. However, these IR seekers are mostly effective in tail aspect engagements only, and can be easily seduced by active IR countermeasures (IRCM) such as flares. Second generation IR seekers use the 3 - 5 μm band, which has the advantage of an all aspect engagement capability (all aspect target lock-on) resulting from strong plume emissions (4.3 to 4.55 μm band) and from aircraft skin emissions. Since plume emissions extend well beyond the aircraft body, they can be viewed with little obscuration over all but near nose-on viewing angles. Aircraft body or skin emissions can also provide all aspect lock-on capability. Some of these seekers employ sophisticated techniques for

Paper presented at the FVP Symposium on "Advances in Rotorcraft Technology", held in Ottawa, Canada, 27-30 May 1996, and published in CP-592.

countering flares also known as IR counter-countermeasures (IRCCM). A flare which comes into the field of view of the seeker may be rejected while the seeker continues to track the targeted aircraft. There has been a vast improvement in IRCCM over the past several years and thus flares which are capable of decoying one advanced missile type may be totally ineffective against another more advanced IR missile type (Deyerle, 1994). The next is the third generation IR missile threat which employ imaging type seekers using focal plane arrays operating in the 0.4 - 1.1 μm and 1 - 5 μm bands (Pollock, 1993). Imaging seekers use an array of detectors that detect energy from the scene and build a spatial map of that scene. By design, imaging seekers are inherently immune to IR countermeasures. They are not readily decoyed by flares because the flare appears as a point-source (i.e. it does not look like an extended aircraft with an exhaust plume).

IR MISSILE PROLIFERATION

IR missile threats to aircraft consist mainly of shoulder launched surface to air missiles (SAM) and air-to-air missiles (AAM). These missiles originate mainly from the former Soviet bloc and Western bloc countries and are being proliferated worldwide to countries that could become hostile in the future. A representative list of IR missiles is shown in Table 1.

Missile Type	Foreign Missiles	Western Missiles
Surface-to-Air (SAM)	SA-7, SA-9, SA-13, SA-14, SA-16, SA-18	CHAPARRAL, REDEYE, STINGER B/RMP
Air-to-Air Missiles (AAM)	AA-2, AA-3, AA-5, AA-6, AA-11	AIM 4D, AIM 9L/M, MISTRAL MICAL, IRIS

Table 1: Representative List of IR Missiles

Note: The total number of missiles is estimated to be in the thousands.

REQUIREMENT FOR IR SUPPRESSION

All missile systems which employ the IR portion of the spectrum for guidance are susceptible to IR countermeasures (IRCM). These CM can be active or passive. Active IRCM make use of high-energy narrow band flares which are intended to seduce IR tracking systems from their intended source, or high-energy IR jamming sources (IR lamps or IR lasers) which are intended to defeat the tracking algorithms of the IR missiles by introducing false signals. Passive IRCM are those actions which are intended to reduce the IR signature of aircraft. This is intended to minimize the threat's capability to acquire and track its intended target by reducing the acquisition range of the aircraft or to cause the aircraft to blend into the IR background, (similar to when an aircraft is camouflaged against detection in the visible portion of the EM spectrum).

The current configuration of the Defensive Electronic Warfare Suite (DEWS) aboard CF aircraft include the following systems: radar warning receiver, missile approach warning system, and expendable countermeasures dispenser (flare/chaff). However, the performance characteristics of the defensive IR system (expendable flares) is limited. Studies have shown that the expendable flare system, even with an IR jammer combination, provides only limited protection against the current generation of IR threats. A more appropriate form of protection is to reduce or eliminate the IR signature of the aircraft itself. This would reduce acquisition ranges against most, if not all IR threats. Thus, DND has identified the requirement for an IR suppressor for the Canadian Forces CH-146 helicopter. For the purpose of this study, the SA-7 seeker model was chosen as the reference IR threat (typical of SAM threat proliferated in third world countries).

IR SIGNATURE MODELLING

The first step in the IR suppressor development program was to establish the benefits, in terms of reduction in susceptibility, resulting from the installation of an IR suppression system. A thermal model of the candidate helicopter was developed to evaluate the various types or levels of IR suppression currently available. The resulting signature levels were compared to the baseline or unsuppressed helicopter.

The modelling process is described in Birk and VanDam, 1991. A comprehensive IR signature model of a helicopter must include the following effects:

i) self emitted radiation from the helicopter solid surfaces and exhaust gases;
ii) reflected and absorbed IR radiation originating from other sources such as the ground, sky, sun and moon;
iii) background radiance; and
iv) atmospheric attenuation between the helicopter and observer.

For the purposes of this development program a simplified version of the above model was used. This was considered appropriate since the model would be used for comparison purposes only. The following assumptions were made in the development of the thermal model:

i) The helicopter was modelled as simple grey body surfaces with dimensions representative of the helicopter;
ii) all reflected and absorbed radiation was neglected.

iii) the background was treated as a uniform black body radiating at a fixed temperature; and
iv) atmospheric effects were accounted for using a simple atmospheric transmissivity model based on the following expression;

$$\tau = e^{-\alpha R}$$

Where

τ = spectral transmissivity
α = atmospheric extinction coefficient (for a specific spectral range and atmospheric condition)
R = range

As identified above, the main objective of the thermal model was to have a generally simple model of the helicopter with enough detail to show the effect of varying levels of IRSS. IRSS as discussed in this paper refers only to the gas turbine exhaust system and does not include surface finishes, internal ventilation etc.

The IR video footage of the Twin Huey (DREV, 1991) clearly shows the gas turbine exhaust system to be the dominant source of radiation from the aircraft followed by the heated section of the tailboom.

For this reason that area of the helicopter was modelled in the most detail. For modelling purposes, the helicopter was subdivided into a number of isothermal zones consisting of the main body, heated section of the tailboom, engine nacelle, engine exhaust ejectors (tailpipes), engine exhaust ducts (nozzles), engine exhaust plumes and the oil cooler. The temperature and emissivity of each surface zone were either measured or estimated based on experience.

The operational condition which was selected as the worst case or design point was based on the following:

i) helicopter operating in hover condition;
ii) engines operating at gearbox limit (ie. approximately 1100 HP); and
iii) the helicopter is in the horizontal plane.

Figure 1 shows a polar plot of the IR signature in the 3-5 micron waveband of the baseline helicopter the above assumed conditions. The relative contributions of the major components have been shown separately. These results of the thermal model have been validated based on measured data (DREV, 1990). The actual results are classified and therefore only general comparisons will be presented in this paper.

The figure shows that the IR signature of the aircraft varies significantly from front to rear views as is expected. The

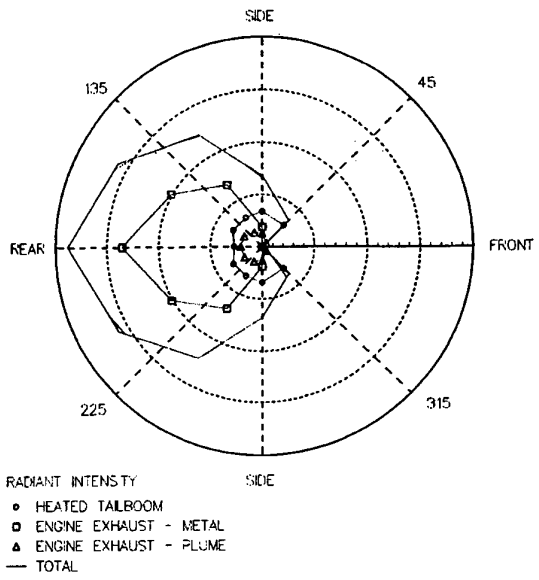

Figure 1: IR Signature - Unsuppressed Helicopter

signature is the lowest for the front views and peaks at the rear view at which angles the engine exhaust system and specifically the nozzles are visible. The heated section of tailboom accounts for a significant amount of the IR signature from side-on to rear view angles. The plume signature is approximately 10% of the signature of the exhaust metal from rear view angles which is typical for gas turbine exhaust systems.

Varying levels of IR suppression were applied to the thermal model to estimate the change in IR signature. The varying levels of IRSS were representative of existing suppressor designs ranging from simple upward bent ducts (Winn et al, 1975) to more sophisticated technology which employs both hot metal and plume suppression (Bartholomew et al, 1981).

The first generation IR suppressors which basically blocked the view of hot metal using insulated upward bends were effective against the simple uncooled reticle seekers but not against the more sophisticated threats. For this reason they are not considered further.

The topic of this paper is limited to the discussion of two of the concepts which are representative of today's technology. These are suppressors which provide both metal and plume cooling. Suppressor #1 has been designated the Film Cooled Tailpipe (FCT) and suppressor #2 has been designated the Optical Block Suppressor (OBS). The major difference between the two is the fact that the OBS provides full optical blockage while the FCT allows a view of the engine exhaust nozzles for the rear view angle. The performance of the two devices in terms of visible metal and plume temperatures are comparable. The

device which provides full optical blockage does however cause higher losses to the engine performance.

Figure 2 shows the resulting aircraft IR signature with the two IRSS concepts included. The figure shows a significant reduction in the signature of the helicopter for both concepts with the biggest difference between the FCT and OBS being the view of the engine exhaust components at the rear view angle.

The side-on signature is reduced to approximately 30% of the baseline and the signature from the rear views has been reduced to approximately 40% of the baseline for the FCT and 8% of the baseline for the OBS. The side-on signature for both the FCT and OBS are mainly due to the heated section of the tailboom.

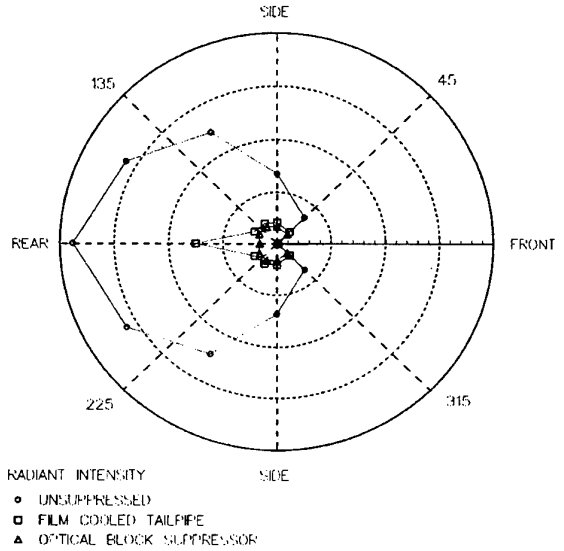

Figure 2: IR Signature - Suppressed Versus Unsuppressed.

The conclusions which were made as a result of the signature modelling were:

i) the signature of the aircraft could be significantly reduced with IRSS; and
ii) there were various options or suppressor types available for reducing the signature.

THREAT MODELLING

The ultimate goal in reducing the IR signature of the aircraft was to decrease the susceptibility of the aircraft to IR guided seekers. A model of the threat was therefore required to try and quantify the benefits of IR signature reduction in terms of seeker lock-on ranges.

As discussed earlier, the threat which DND considered to be the most appropriate for this development program was the SA-7 shoulder launched surface to air (SAM) IR missile. This threat is representative of the type of technology which is cheap and readily available worldwide.

Figure 3 shows the predicted seeker lock-on ranges versus contrast radiant intensity for a number of IR SAM's for comparison purposes (DAVIS, 1991). The results are based on a surface with an area of 900 cm^2 with a temperature varying from 50 to 450°C under clear day conditions. The figure clearly shows the relative performance of the SA-7 (low temperature operation (LTO)) in comparison to the Stinger and imaging IR (IIR) type seeker.

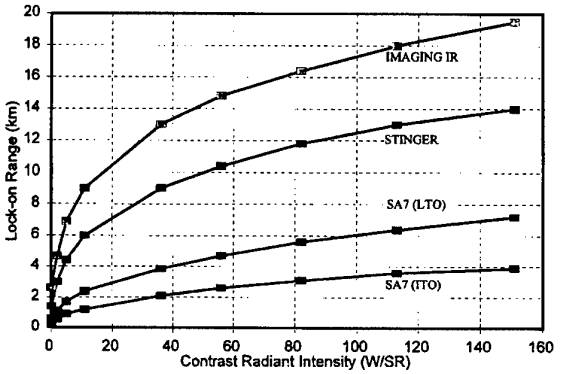

Figure 3: IR Seeker Lock-on Range Versus Contrast Intensity

Figure 4 shows the predicted lock-on ranges for the baseline helicopter as well as for the helicopter fitted with the two suppressor concepts. The results are similar to the IR signature plots in that the lock-on ranges are the lowest for front view angles and highest for the rearward view angles. The predicted lock-on ranges for the baseline helicopter compare well with known values obtained from DND. For the helicopter fitted with the FCT IR suppressor the seeker locks on the heated section of the tailboom for all views except the rear view in which the engine exhaust nozzles are visible. All lock-on ranges for the OBS fitted helicopter are on the heated section of the tailboom.

The results clearly show the benefits in terms of reduction in lock-on range resulting from the installation of engine exhaust IR suppressors. The results of the IR signature and threat modelling supported the decision to develop an IR suppressor for the helicopter.

Specifications for the further development of the IR suppressor were established based on the results of the modelling and the known performance (ie. power loss, weight etc.) of the various suppressors designs.

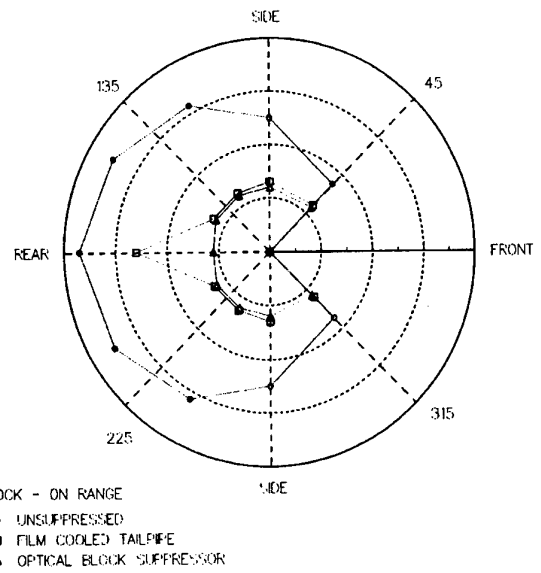

Figure 4: Lock-on Range - Unsuppressed Versus Suppressed

FCT DESIGN AND DEVELOPMENT

This section of the paper will focus on the design and development of the FCT IR suppressor. This suppressor concept was developed first since it would likely involve less modifications to the aircraft and result in lower power loss etc.

It is worthwhile noting that no currently available IR suppressors could be easily fitted on this aircraft.

SPECIFICATIONS

The general specifications which were developed for the FCT are as outlined below:

i) consider the SA-7 SAM as the main threat;
ii) provide both metal and plume cooling to obtain the desired signature levels;
iii) require no modifications to the helicopter for installation;
iv) the suppressor must work in all flight conditions; and
v) the performance of the air management system must be maintained.

The detailed performance specifications which were identified for the device were as follows:

i) the maximum allowable capacity reduction was 400 N;
ii) the maximum allowable back pressure on the engine was 4 kPa;
iii) maximum allowable engine power loss was 4% (this was ultimately reduced to 1.5% for the FCT); and
iv) the maximum average lock-on range was 2.5 km.

These specifications are based on hover conditions at full power (gearbox limit) under clear day conditions. The target value for engine power loss of 1.5% was suggested by Bell as a more reasonable level for the FCT type of device.

AIR MANAGEMENT SYSTEM

Figure 5 shows the exhaust system arrangement for the helicopter. As shown in the figure, each engine is fitted with a completely separate inlet and exhaust system referred to as the air management system (AMS). The engine exhaust is ejected from the rear of the helicopter through exhaust ducts or tailpipes which are angled slightly upward and towards each other.

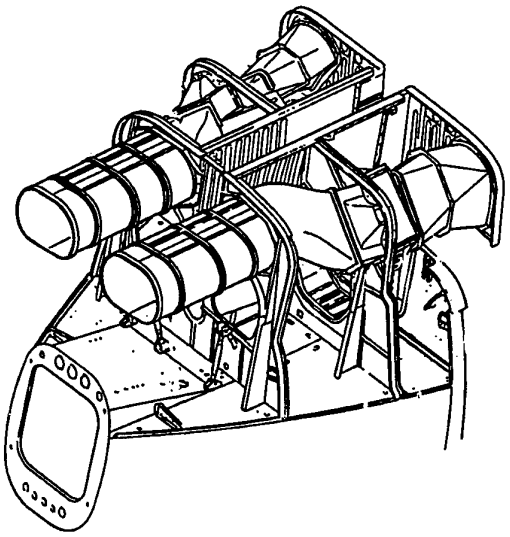

Figure 5: Exhaust System Arrangement

Figure 6 shows an airflow schematic for the AMS. This system is responsible for delivering combustion air to the engine and exhaust products to the environment. The bypass air acts as a carrier for air laden particles. The high velocity exhaust flow is used as an ejector to drive the particle separator bypass air flow.

A door is also installed in the bypass duct which can be used to eliminate the bypass flow in conditions when full engine power is required (ie. single engine operation etc).

The AMS of the helicopter was identified as a critical component in the design of the IR suppressor. The requirement to maintain the bypass or particle separator bypass flow rate warranted a detailed study of this flow. The complete AMS of the helicopter was installed on a hot gas generating wind tunnel at the DAVIS test facility to conduct full scale testing.

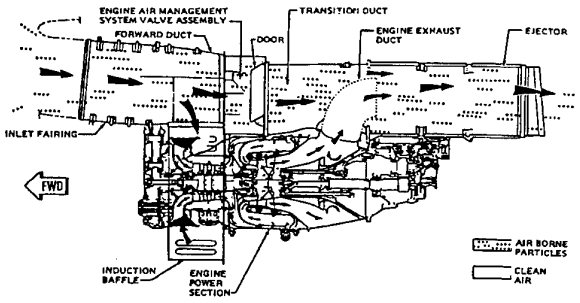

Figure 6: AMS Airflow Schematic

Actual helicopter components were used for the test program. The test rig was capable of simulating the engine exhaust flow conditions in full scale. Figure 7 shows a test prototype installed on the AMS.

Figure 8 shows the results of the testing of the baseline AMS (Birk and VanDam, 1994). The results presented here are the ratio of secondary or bypass flow rate to engine exhaust or primary flow rate versus a back pressure applied at the exit plane of the tailpipe. Screens of varying porosity were used to apply the varying back pressures. It should be noted that all IR suppressors will impart a back pressure on the exhaust system to some varying degree.

The figure shows that the AMS is very sensitive to back pressure: with a back pressure of approximately 750 Pa (3" water) the bypass flow, Q_s, as a fraction of primary flow Q_p, is reduced to zero.

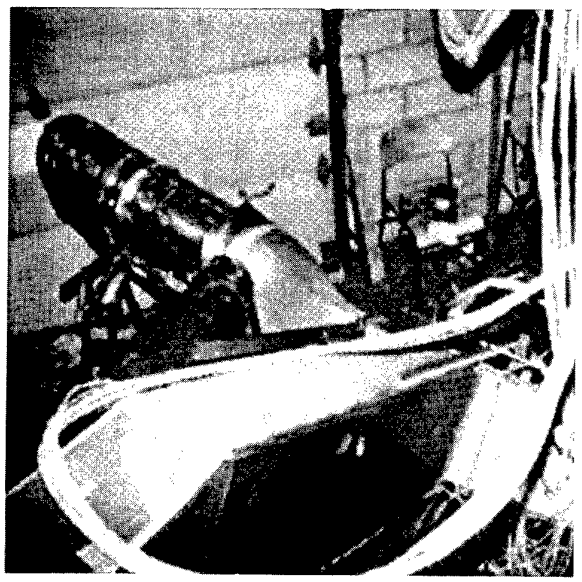

Figure 7: Photo of DAVIS Hot Gas Test Facility

The upper curve shown in the figure is the predicted perfect mixer limit for the AMS. The perfect mixer analysis approach can be used to estimate the theoretical limits of an ejector performance under ideal flow conditions. The model was based on the following assumptions:

i) one dimensional, steady, incompressible flow of an ideal gas
ii) all streams mix perfectly to a uniform velocity and temperature distribution; and
iii) all gases modelled as air.

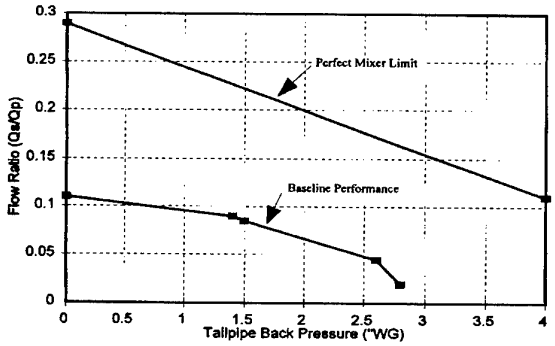

Figure 8: AMS Performance

It is recognized that a number of factors including wall friction, flow separation, non-perfect mixing and inlet losses will reduce the performance from the maximum predicted. The results show that there is still significant room for improvement in the performance of the AMS.

Further hot flow testing of the AMS identified the following:

i) the existing nozzle was efficiently turning the exhaust flow;
ii) the engine nozzle was a major flow blockage and resulted in a large drag loss;
iii) the flow in the tailpipe was severely distorted due to flow separation and the positioning of the exhaust nozzle; and
iv) the exit flow was severely distorted which indicates poor mixing in the tailpipe.

The above observations were used to design flow modifying devices to improve the AMS pumping performance. The modifications included the following:

i) a flow wedge downstream of the nozzle to reduce drag loss;
ii) enhanced perimeter nozzles to improve mixing between primary and secondary streams;
iii) a flow turning vane to improve flow distribution in the tailpipe;
iv) a flow partition to increase the effective L/D ratio of the tailpipe.

The results of the test program are shown in Figure 9. The results have been non-dimensionalized with respect to the perfect mixer performance to account for varying test conditions and component geometries. As the results indicate, the performance of the AMS has been doubled from that of the baseline. This means that for no applied back pressure on the exhaust, the secondary flow rate has

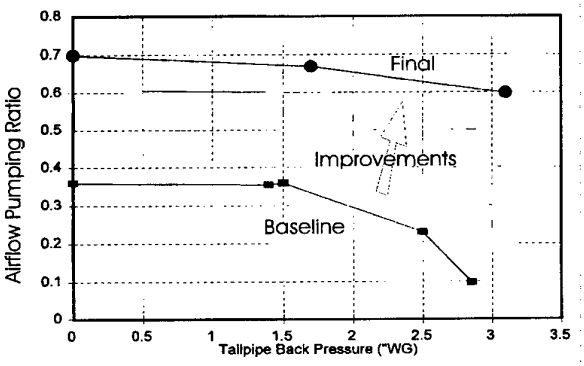

Figure 9: Results of AMS Improvements

doubled, or with the addition of approximately 1000 Pa (4" water) of back pressure the secondary flow remains the same as the baseline.

FCT AEROTHERMAL DESIGN FEATURES

The main aerothermal features which were incorporated into the design of the FCT were an improved nozzle design, a flow wedge downstream of the nozzle to improve the flow channel geometry and the use of film cooling for both visible metal and plume cooling. These features are shown in Figure 10.

The other flow modifying devices were maintained as options in the event that additional capability was required from the FCT. The OBS may also utilize some of the other features.

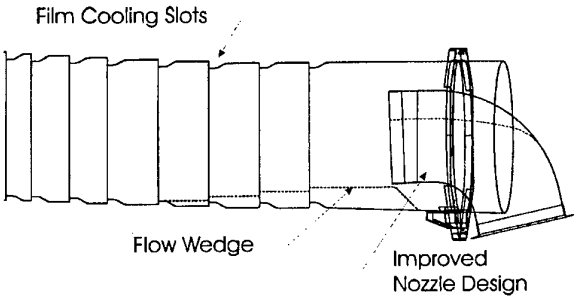

Figure 10: FCT Aerothermal Design

FCT INSTALLATION DESIGN

At this point in the design process it was assumed that the existing engine nozzle and tailpipe would be completely replaced with similar sections of the FCT as opposed to modifying existing components.

The requirement to have no modifications to the aircraft meant that the FCT would have to fit within the same space envelope as the current exhaust system components. The device was also required to utilize the same mounting points and mounting hardware as the current exhaust components. These requirements would ultimately allow the FCT to be installed in kit form which would be mission dependant.

A detailed fabrication drawing package was generated for the FCT based on the aerothermal design, the installation design and the structural analysis of the device.

FCT STRUCTURAL DESIGN

A detailed mechanical design was conducted on the FCT to ensure its structural integrity for the flight test program (VanDam and Hiscoke, 1996).

A review of the material selection for the existing exhaust components showed that the tailpipe was fabricated from type 321 stainless steel and the nozzle was fabricated from type N155 high nickel steel. The complete FCT was fabricated out of type 321 SS for ease of manufacturing. Components of the tailpipe including mounting flanges and seals were purchased from the original equipment manufacturer.

Finite element modelling was utilized for vibration, shock and thermal fatigue analysis. Fatigue resulting from helicopter induced vibrations, specifically the rotor and engine, were considered the critical design parameter for this analysis. Figure 11 shows a view of the finite element model of the tailpipe section of the FCT.
test.

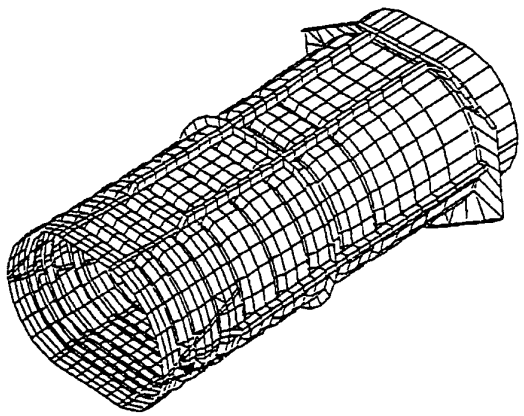

Figure 11: FCT Finite Element Model

Vibration results (ie. natural frequencies, mode shapes and transfer functions) from the FE model were verified by test. The FCT was installed in a test fixture and excited in all three orthogonal axis. Figure 12 shows the FCT installed in the test fixture during the shaker tests.

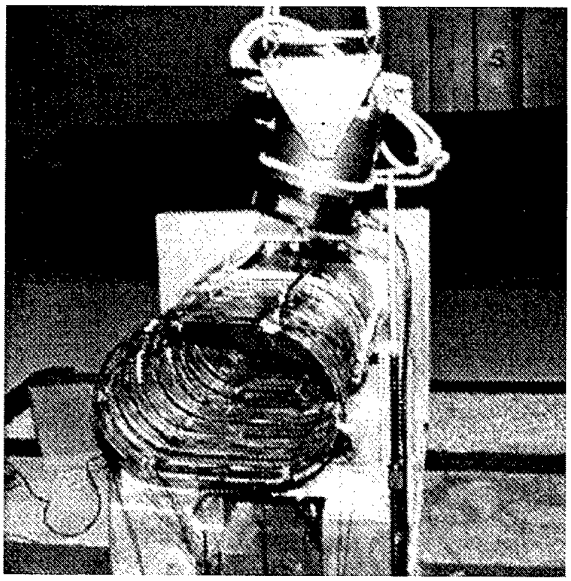

Figure 12: FCT Vibration Test

Table 2 shows the results for the first five modes of vibration which occur below the fundamental forcing frequency of the engine (ie. 110 Hz).

FCT PROTOTYPE FABRICATION

Both a left and right hand version of the FCT IR suppressor were fabricated for performance verification testing.

Mode	Frequency (Hz)	
	FE Model	Test Results
1	44	48
2	62	61
3	72	70
4	77	75

Table 2: Comparison of FE Model Results to Test Results

Figure 13 shows the FCT being assembled in a fixture for welding. As shown the FCT consist of nine independent ring section held together by axial stiffeners. All the various sections of the FCT were hand formed and are of a welded construction. Items such as the mounting flanges and seals are rivetted in the same manner as the factory components. Figure 14 shows the nozzle section being assembled for welding. The sections of the nozzle were also hand formed.

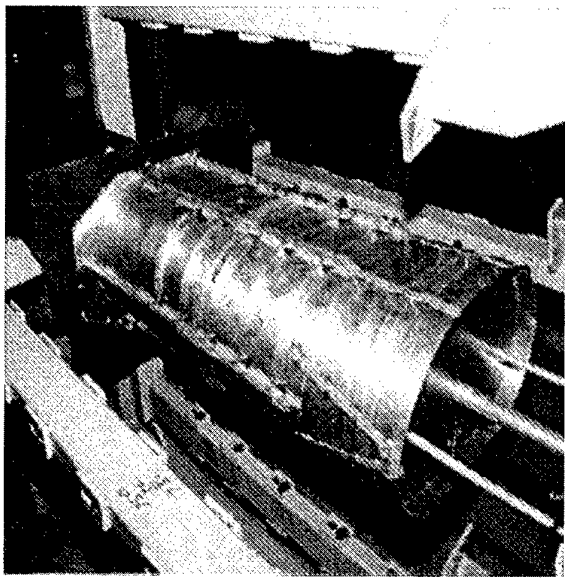

Figure 13: Photo of FCT Fabrication

INSTALLATION VERIFICATION

The first step in the verification testing of the suppressor was to ensure that it would fit within the space envelope of the helicopter. It should be noted that drawings of the helicopter were not provided during the design and development of the FCT.

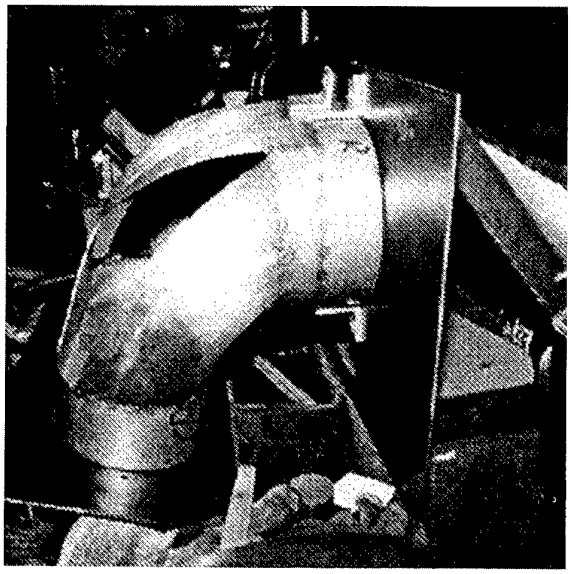

Figure 14: FCT Nozzle Fabrication

All dimensions were measured from the Bell 412 helicopter at NRC. Figure 15 shows the installation verification of the FCT using the NRC Bell 412 helicopter. As shown the device was successfully installed in the aircraft.

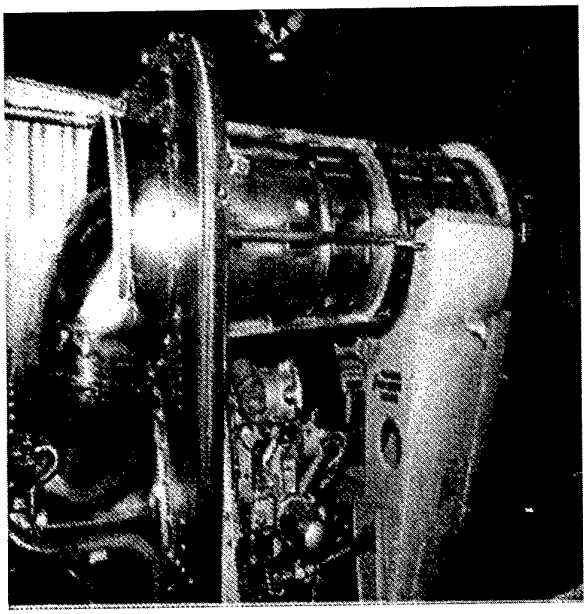

Figure 15: FCT Fitment Check

FCT PRELIMINARY PERFORMANCE

The completed prototype was installed on the hot gas wind tunnel for preliminary verification testing prior to being installed on an actual engine (VanDam and Hiscoke, 1996).

Table 3 presents the key results of the testing.

The results show that the back pressure and resulting engine power loss are considerably lower than the original design targets.

The signature of the helicopter with the FCT installed has been estimated based on the results of the wind tunnel testing. Figure 16 shows the predictions.

Parameter	Result	Spec
Back Pressure (Pa)	665	4000
Power Loss (%)	0.7	1.5
Weight Increase (kg)	4.5	40
Particle Separation Flow (%)	100	100

Table 3: Preliminary Test Results

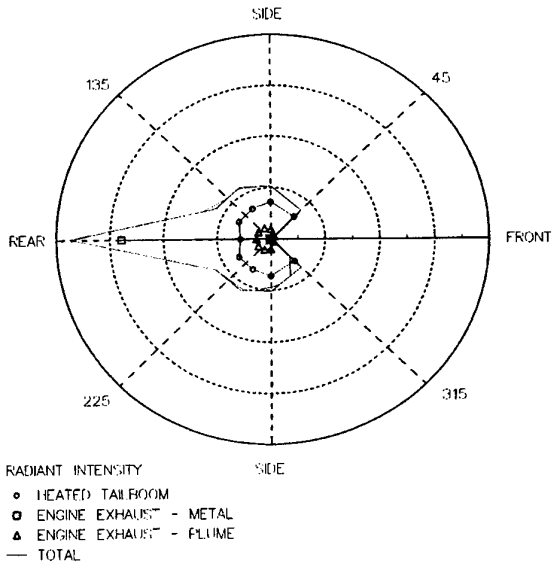

Figure 16: IR Signature - FCT Installed

As shown in the figure the signature is quite small except for the rear views in which the engine nozzle is in view. The signature levels are slightly lower than those shown in Figure 2 which provides a relative comparison of the suppressed and unsuppressed helicopter. The heated zone of the tailboom is the dominant signature source for all of the other views of the aircraft. The signature of the engine exhaust including both metal and plume have been reduced well below what is required for the threat.

The next phase in the development program was to install the FCT on an actual T400 engine in a test cell to measure the performance with actual engine inlet and flow conditions.

TEST CELL EVALUATION

The aim of this activity was to evaluate the interaction of a prototype infrared suppressor with a T400 helicopter engine installation in a test cell. Specifically the test objectives were:

i) measure the effect of replacing the existing exhaust ejector with each of the prototype suppressor on the performance of the engine, and air management system; and
ii) measure the performance of the suppressor with actual engine inlet and exhaust flows.

To meet these requirements, test facilities and procedures were developed to simulate the helicopter installation and evaluate system performance (Bird and Barry, 1996). Specifically, the helicopter AMS and tailpipe ejector were integrated into the T400 engine test facility in #2 Cell at the National Research Council Canada (NRC) (Figure 17). Baseline performance of the engine and AMS

could then be measured using the existing helicopter configuration. Engine performance was then re-measured following replacement of the existing exhaust nozzle and tailpipe with the prototype suppressor.

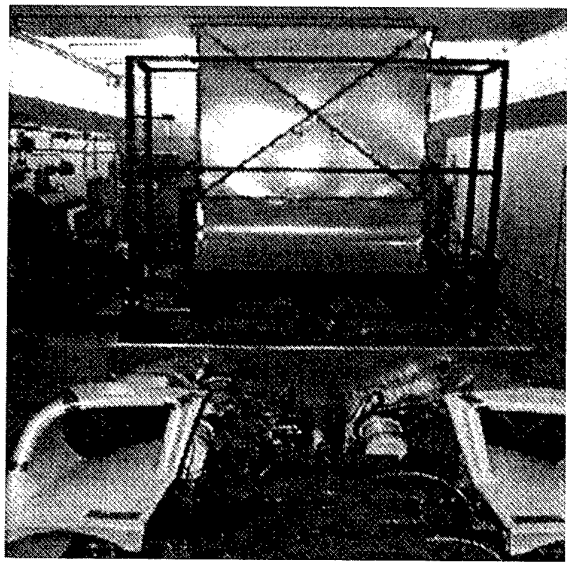

Figure 17: IR Suppressor Installed on T400 Engine at NRC

The performance parameters to be measured had been specified in the DND Statement of Work (DASP, 1994). The key parameters were: engine power, gas generator speed, fuel flow, inter-turbine temperature, AMS airflows (total and engine inlet), and exit flow pressure and temperature. Each parameter was measured at several engine power settings relevant to CF operations. Test runs were to be conducted over a range of ambient temperatures for each configuration to determine ambient temperature effects and to verify the repeatability of the results. Suppressor testing included measurement of the suppressor skin temperatures and plume temperatures. Suppressor mounted instrumentation was provided by Davis Engineering (Davis, 1995). IR images of metal and gas radiation patterns were also gathered. Reference thermocouples were the basis for the IR image interpretation.

The verification of AMS performance required the measurement of engine and AMS airflow. Typically only engine airflow would be measured in a test cell installation and therefore, the following approach was developed for the test program:

i) measure the individual engine (power section) airflow with a high accuracy airmeter and bellmouth;
ii) correlate these airflows to the aerodynamic speeds of the individual engine gas generators;
iii) calibrate an airmeter section inserted into the AMS inlet section to the power section airflow with AMS bypass airflow shut-off; and
iv) determine the AMS bypass flow as the difference between the AMS total airflow and the power section airflow.

The correlation to aerodynamic or corrected speed allowed the calculation of airflow during any subsequent testing after the removal of the airmeter and bellmouth. It would have been preferable to correlate this calibrated airflow to pressure measurements in the inlet scroll of the power section. However, this was not possible without extensive disassembly of the engine. The gas generator speed-airflow correlation was assumed constant over the short test period required. This correlation was to be checked at the end of the tests.

Test data were acquired with micro-processor-based data acquisition systems which incorporated on-line pressure calibration. Flow traverses of the tailpipe flows were conducted with eight-element, total pressure and temperature probes. Engine power was absorbed and measured for each power section with a water brake dynamometer. Test data were taken at a gearbox output speed of 6000 rpm, for each power section for power levels up to 680 kW (910 HP), the one engine inoperative limit for the helicopter installation. Particular data were taken at 420 kW (560 HP) which would be the normal operational maximum set by the helicopter transmission limit. Double data points were recorded following a stabilization period of 10 minutes.

The test data were corrected for the pressure losses in the test cell inlet and exhaust and for the specified reference conditions: ambient conditions (Temperature = 288.15 K, pressure = 101.325 kPa, and Humidity: 60% RH) and fuel properties (Lower heating value = 42 MJ/kg, temperature = 288K). Acquired data sets were validated through a series of consistency checks ,eg. engine schedules, calibration checks, redundant measurements, and component performance tracking before proceeding with the data comparisons.

The performance comparisons for the evaluation were selected based on the requirements of DASP, 1994 and Davis, 1995. For each power section, the following comparisons were made:

i) corrected power as a function of inter-turbine corrected temperature;
ii) ratio of total AMS airflow to power section corrected airflow as a function of corrected speed;
iii) suppressor exit total pressure and total temperature, average and profiles, as a function of corrected power;
iv) AMS secondary airflow as a function of ram pressure ratio, ie. ratio of

tailpipe exit static pressure to AMS inlet pressure;

v) corrected fuel mass flow as a function of corrected speed;

vi) engine tailpipe corrected pressure and temperature as a function of corrected power; and

vii) compressor pressure ratio as a function of corrected compressor speed.

The assessment of power section compressor delivery pressure was provided to ensure consistency of compressor performance from which the airflow-speed correlation was derived.

At the time that this paper was prepared, testing test had only been completed on the baseline configuration. The IR suppressor is currently installed and testing is in progress. Some limited data are available. Figure 18 provides a comparison of the engine power change for the suppressor installation. As shown the performance loss is small.

Figure 19 shows the typical bypass flow rate for the baseline AMS, resulting from the airflow calibration process. The suppressor results will be compared to this baseline when available.

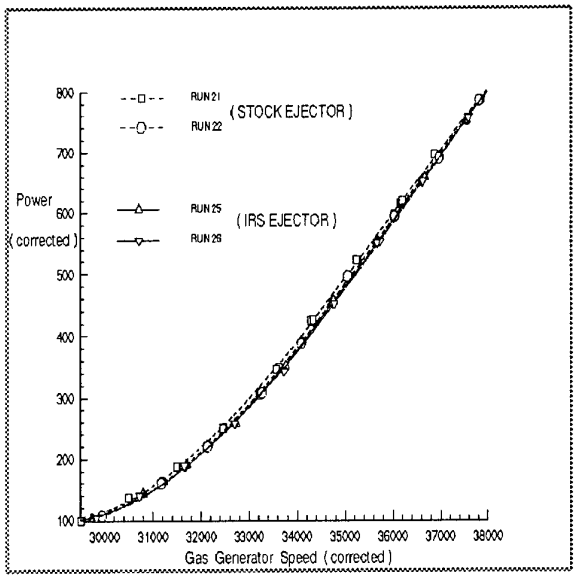

Figure 18: Engine Power Change for Suppressor Installation

FLIGHT EVALUATION

The Film Cooled Tailpipe will be evaluated in flight onboard both the Bell 412 (FRL/NRC) and CH-146 helicopters. Testing will be conducted in three phases:

i) Tailboom Heating and Vibration Testing

The Bell 412 baseline helicopter exhaust system will be characterized for its

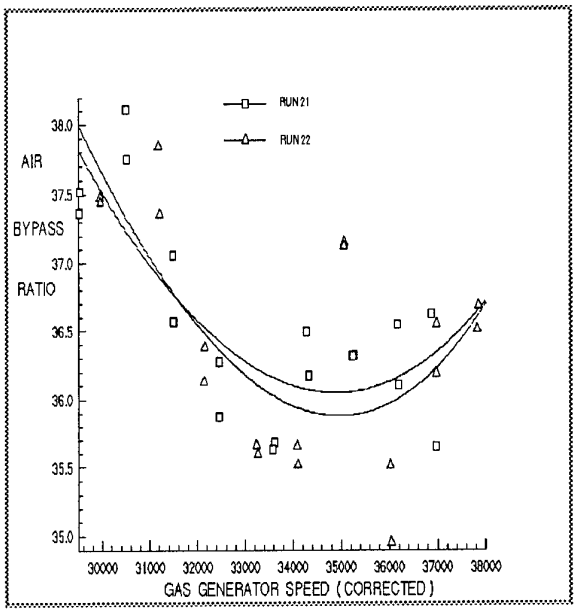

Figure 19: AMS Pumping Ratio Change for Baseline Installation

effects on tailboom heating, and vibration characteristics of its exhaust components (tailpipe). These tests are currently being conducted by the Flight Research Lab/NRC.

ii) Performance Verification & Flightworthiness Testing

The IRSS will be certified for flight onboard a CH-146 helicopter at the Aeronautical Engineering Test Establishment (AETE), CFB Cold Lake. The focus will be to determine if the IRSS has any adverse effects on aircraft performance, engine performance, and overall flying qualities. AETE will be checking aircraft performance at various aircraft flight regimes (i.e. hover, low airspeed flight, single engine flight, and trimmed flight control positions throughout the forward flight envelope).

iii) IR Signature Measurements & IR Seeker Engagement

The final phase of flight testing will be conducted during NATO Trial EMBOW VII (3 - 27 Sept 96). This will be to evaluate the operational effectiveness of the IRSS. The Defence Research Establishment Valcartier (DREV) (Spectral Exploitation Group) will conduct IR signature measurements of the baseline CH-146 in forward flight, hover and at various aspect angles with respect to the measurement site. These measurements will be repeated with the IRSS equipped CH-146 to provide a relative assessment of IR signature reduction. In-flight countermeasures effectiveness testing will determine how well a CH-146 equipped with IRSS & decoy flares can defend itself against medium to high threat IR seeker

heads (SA-7, SA-13, SA-18, SA-16, Stinger B, and AA-11).

CONCLUSIONS

IR Guided seekers have been identified as a major threat to aircraft both in combat and in peacekeeping roles. The types of countermeasures currently employed against these weapons are IR jammers, flares in conjunction with missile approach warning systems and engine exhaust IRSS. The focus of this paper was on engine exhaust IRSS which will significantly reduce the IR signature of the helicopter and therefore ultimately increase the effectiveness of the other countermeasures.

An extensive modelling capability in terms of IR signature and seeker lock-on ranges has been developed and validated. The modelling has been used to quantify the benefits resulting from the addition of an engine exhaust IR suppressor to the helicopter. The results of the analysis have warranted the design and development of an IR suppressor for this specific helicopter.

The development program has been successful in designing the FCT IR suppressor for the CH-146 helicopter. The device satisfies all of the specified design requirements. The resulting design provides improved protection for the helicopter with minimal performance penalties. The suppressor has been designed as a retrofit to existing aircraft and requires no modifications for installation.

A full performance verification test program is currently in progress to prove the performance of the device both in an engine test cell and on an actual aircraft for flight testing.

FUTURE WORK

Development work is underway to further improve the performance of the FCT suppressor. The main goal of this work will be to provide optical blockage of the engine exhaust nozzles to remove the signature spike from rear view angles. The heated section of the tailboom has been identified as the dominant IR signature source for all other view angles and therefore warrants further investigation. The hot exhaust gases currently impinge on the tailboom resulting in a large heated zone. This will be eliminated or reduced by directing the flow of exhaust gasses away from the tailboom in combination with further reductions in exhaust plume temperatures.

REFERENCES

W.R. Davis Engineering Limited Report, Helicopter Infrared Signature Suppression System Phase II: Technology Review (CDRL 005), August 1991.

DREV Twin Huey IR Video, ASE Trials, June 1991 - Valcartier.

DREV Report 4561/90, Characterization and Reduction of the Infrared Signatures of Helicopters (U), March 1990 - Valcartier.

Winn, A., et al, Performance and Handling Qualities - AH-1G Helicopter Equipped with Three Hot Metal/Plume Infrared Suppressors, USAAEFA 75-01, April 1975.

Bartholomew, D., et al, Preliminary Airworthiness Evaluation of the UH-1H with Hot Metal Plus Plume Infrared Suppressor and Jammer, USAAEFA 80-6, June 1981.

W.R. Davis Engineering Limited Report, Research and Development of an Infrared Signature Suppression System for the Bell 212/412 Helicopters, Phase I Report, Air Management System Improvements (CDRL 002), January 1994.

W.R. Davis Engineering Limited Report, Helicopter Infrared Signature Suppression System, Phase II: Set Design Requirements (CDRL 006), February 1992.

W.R. Davis Engineering Limited Report, Hot Flow Testing of the Film Cooled Tailpipe IRSS Device for the Bell 212/412 Helicopter (CDRL 005), February 1996.

W.R. Davis Engineering Limited Report, Infrared Signature Suppression System for the Bell 212/412 Helicopter, Film Cooled Tailpipe - Final Design Report (CDRL 002), January 1996.

May Jr., J. And Van Zee, M.E., Electro-Optic and Infrared Sensors, General Dynamics, Pomona, California, Microwave Journal, September 1993.

Deyerle, C., Advanced Infrared Missile Counter-Countermeasures, USAF, journal of Electronic Defence, January 1994.

Pollock, D.H., The Infrared and Electro-Optical Systems Handbook: Countermeasure Systems, Vol. 7, ERIM, SPIE Optical Engineering Press, 1993.

Bird, J.W. and Barry B.C., Infrared Suppressor System - Engine Test and Evaluation: Test Plan Letter Report, 1250 (DND), Structures, Materials and Propulsion Laboratory, Institute for Aerospace Research, National Research Council, 1996.

National Defence - DASP, Statement of Work: IRSS Project 2715-40-90A1 (DASP-3-4-2), 1 November 1994

W.R. Davis Engineering Limited, Performance Verification Testing of the Infrared Signature Suppression System for the Bell 212/412 Helicopter (CDRL 003). December 1995.

MODEL 412 COMPOSITE TAILBOOM

G. Mussett
R.Fews
Bell Helicopter Textron Canada
12800, rue de l'Avenir
Mirabel, Quebec, J7J 1R4, Canada.

SUMMARY

Bell Helicopter Textron is developing a technology demonstrator in the form of a Composite Tailboom for the Model 412 and 212 helicopters, to potentially replace the existing metallic design.

The composite tailboom has been designed for producibility and low cost whilst maintaining the capability to withstand the operating environment of the Model 412 and 212 helicopters.

During the development of the tailboom, concurrent engineering philosophies were used so that manufacturing and tooling considerations were recognised in the design concept stage resulting in a very economical and producible design. Additionally the composite tailboom has been designed for fatigue with a high degree of redundancy in critical areas making it very tolerant to in service damage. This has been proven by an extensive material qualification and structural test program at Bell Helicopter.

The composite tailboom is scheduled for flight test and FAA certification in 1996.

1 BACKGROUND

The Bell Helicopter Model 412 and Model 212 are twin engine commercial medium lift helicopters (6000 lb -12000 lb gross weight) derived from the HUEY-UH1 helicopter used by the US Military. The two bladed Model 212 entered service in 1971 followed by the four bladed Model 412 in 1981 and now there are 920 Model 212's and 450 Model 412's operating world wide. Both the Model 412 and 212 are now manufactured at Bell Helicopters facility in Mirabel Canada. Typical missions for Model 212 and 412 include offshore support, search and rescue, emergency medical services and external loads such as logging. Operating in these roles the tailboom is subjected to a high temperature, corrosion and fatigue environment. Figure 1 shows a schematic view of a Model 412 Helicopter.

The tailboom on the Model 212 and 412 comprises a monocoque boom section with an integral vertical fin and attaches to the main fuselage via four bolts. The tailboom supports the tailrotor, its drive system and the synchronized elevator. A baggage

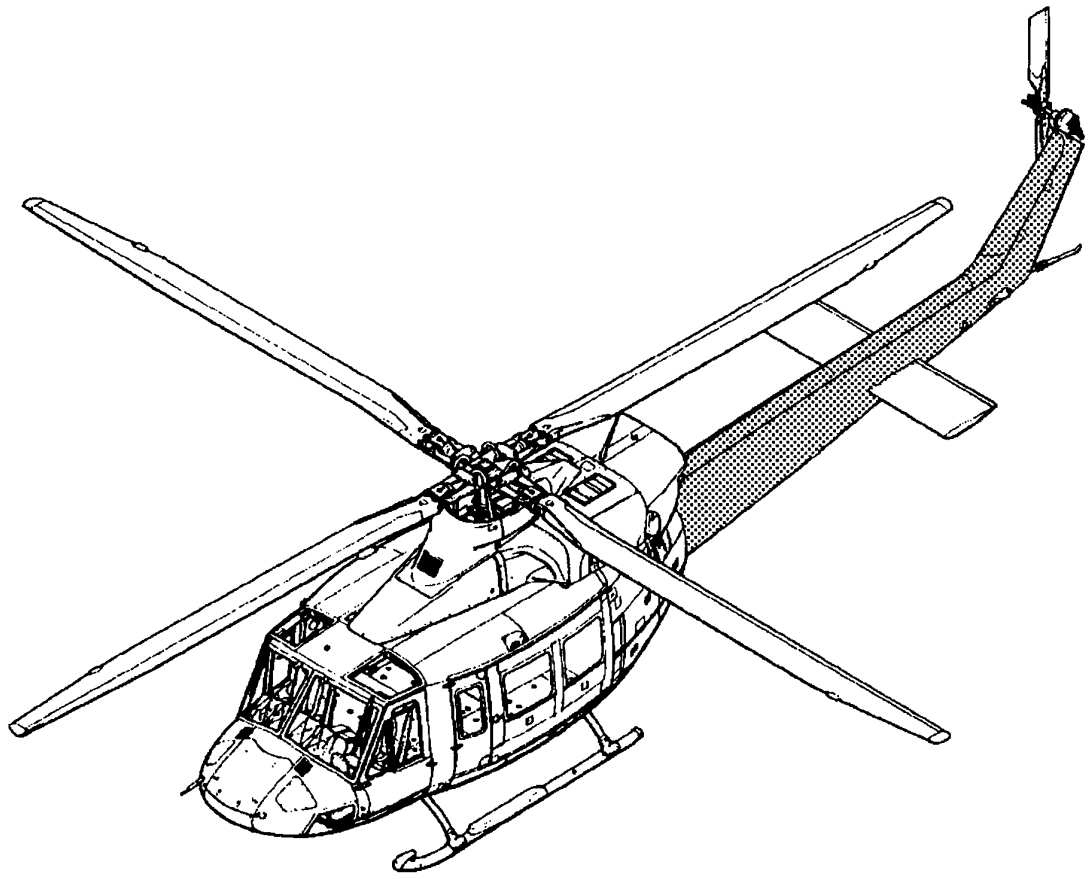

Figure 1
Bell Model 412

Paper presented at the FVP Symposium on "Advances in Rotorcraft Technology", held in Ottawa, Canada, 27-30 May 1996, and published in CP-592.

compartment that carries up to 400lb of cargo makes up the forward section of the tailboom.

Technical advancements in the producibility of composite structure at Bell has provided the opportunity to upgrade the Model 412. In 1992 Bell Helicopter started a project to enhance the Model 412 in the form of a new composite tailboom design.

2 DESIGN

2.1 Design Approach

The primary project goal is to develop an FAA certified composite tailboom for the Model 412 that meets the customer needs. These included reducing operating costs by improving reliability, increased baggage volume, weight reduction and cost competitiveness with the existing metal tailboom in production. Additional design objective included the ability to withstand the high engine exhaust temperatures, improved dynamic and vibration characteristics, a flaw tolerant safe life design and provision for increased tailrotor thrust.

Developing a composite design that is cost competitive meant that designing for producibility was of major importance. Therefore, manufacturing and tooling considerations needed to be recognised at the design concept stage. To accommodate all the design goals as well as designing for producibility a concurrent engineering team was set up, comprising engineers from design, stress, dynamics, weights, cost, manufacturing, tooling, materials and product support. Following a revision of tailboom design criteria and extensive trade studies on manufacturing methods, tooling, materials, and cost the engineering team developed a design concept that is very economical and producible.

2.2 General Description

The composite tailboom comprises a carbon-bismaleimide bonded assembly with the existing dynamic components attached via mechanical fasteners.

The bonded assembly is a honeycomb stiffened monocoque structure assembled from a minimum number of components. The basic construction comprises minimum gauge carbon bismaleimide facesheets sandwiched around a phenolic fibreglass honeycomb core. Figure 2 shows an exploded view of the bonded assembly comprising a four piece skin construction with internal substructure. Note that there are no mechanical fasteners used in the bonded assembly. The four main skins extend the full length of the tailboom and includie the vertical fin as an integral part of the side skins. These main skins include integral angles and tee caps that are cured to the inner facing skins to accommodate the internal substructure. For load introduction areas doubler packs are incorporated into the main skins to give the extra strength and stiffness required. This replaces conventional longerons and stiffeners.

The internal substructure includes a baggage compartment floor and roof, bulkheads and frames in the boom section, forward and aft fin spars and two fin ribs. In total there are only seventeen components making up the bonded assembly. These components are bonded together using two different joint configurations shown in figure 3. The four main skins are joined to each other along their length using a bonded splice joint. The internal structure is bonded to the main skins via integral angles and tee caps in a lap joint configuration. Where fittings are mechanically fastened to the bonded assembly the core is cut away and doublers added so that fasteners attach to solid laminate only.

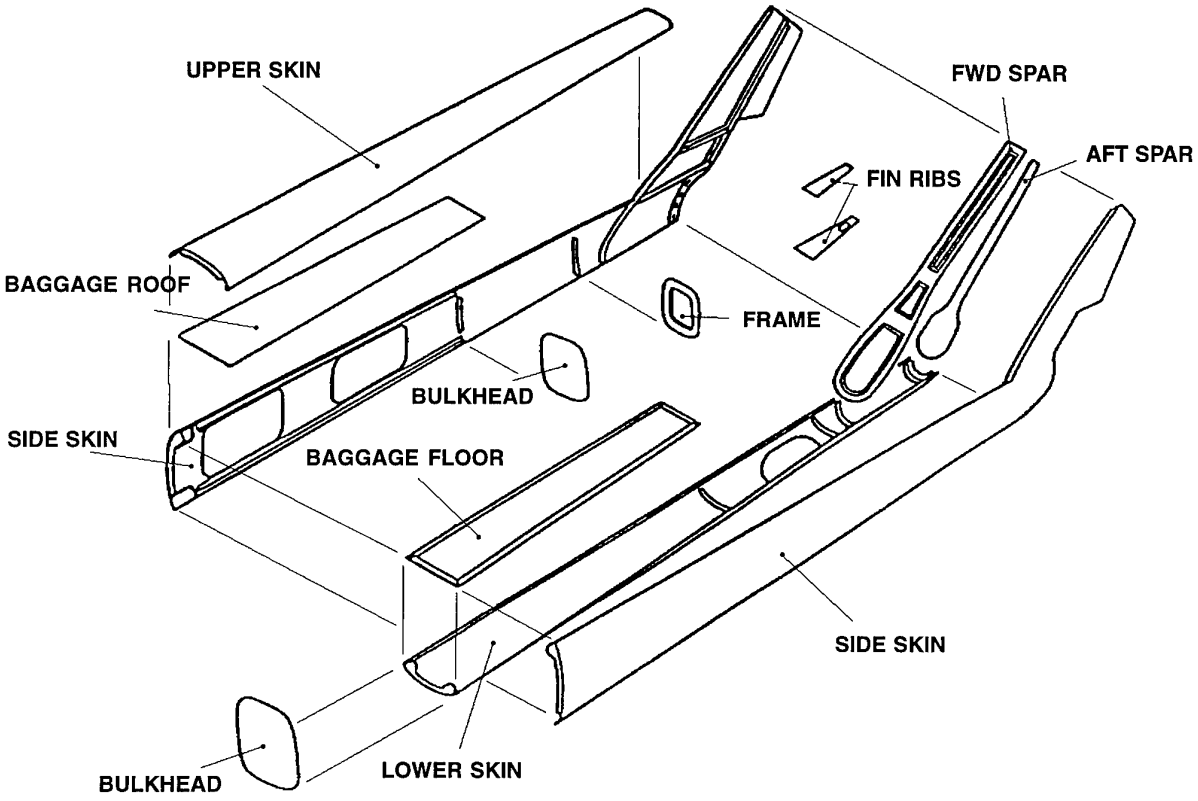

Figure 2
Exploded View of Composite Tailboom Construction

Wherever possible on the new design the existing dynamic components have been used. These include the tailrotor and its drive system, the synchronized elevator, the anti-torque control system and the tailskid. Modifications have been required on the elevator control system and the tailrotor driveshaft. The tailrotor driveshaft modification was required to account for the difference in thermal expansion between the carbon tailboom and the aluminium driveshaft caused by heating from the engine exhaust. All of the fittings on the tailboom including the main fuselage attachment fittings have been redesigned to interface with the new composite construction.

The new tailboom design includes an increased size baggage compartment with two doors compared to the single door on the existing tailboom. The driveshaft covers, all access doors and fairings have all been redesigned using carbon-bismaleimide. To protect against lightning strike the outer surface of the tailboom is covered in a copper mesh which is grounded to the fuselage.

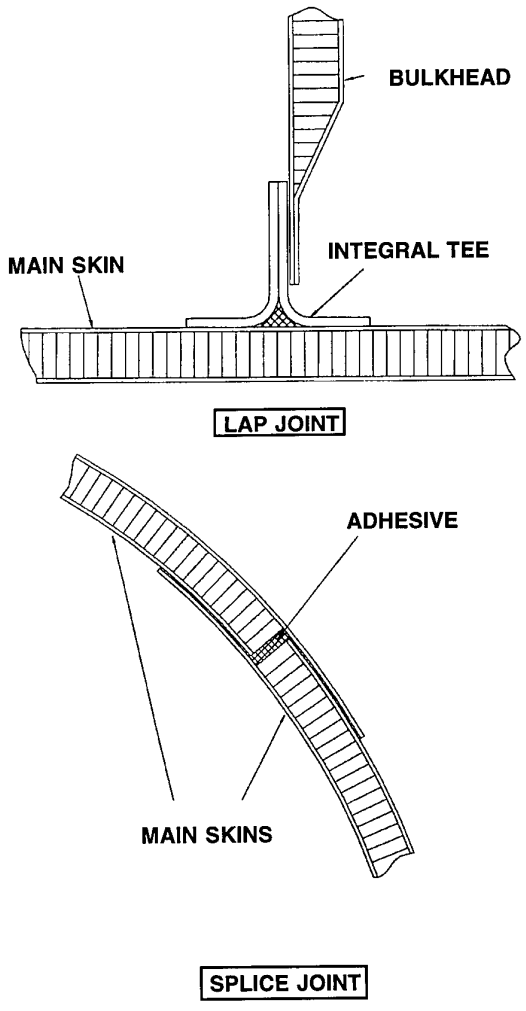

Figure 3
Composite Tailboom Joint Configurations

2.3 Materials

The main criteria for material selection is to minimise in-service problems. This includes a material that will not corrode, has good fatigue characteristics and is able to operate at high temperatures. The material must also have good strength to weight ratio. For these reasons bismaleimide carbon reinforced resin was chosen as the main material for the tailboom.

The composite tailboom is constructed using plain weave fabric and unidirectional tape. The bismaleimide resin system has the ability to operate in a 350F wet environment as compared to traditional epoxy resin systems which are limited to 280F wet operating environments. The sandwich core is a woven fibreglass reinforced phenolic honeycomb chosen for its good shear properties and high operating temperature. Bismaleimide film adhesive is used to bond the facing skins to the core. The outer surfaces of the main skins have a thin film adhesive layer that contains the copper shielding used for lightning protection.

Due to the poor galvanic compatibility between carbon and aluminium, steel and cadmium plate the preferred material on the composite tailboom for fittings and fasteners is titanium. Aluminum has been used for some of the fittings where it is impractical to use titanium. In these cases a glass bismaleimide barrier is placed between the carbon and the fitting.

2.4 Design for Producibility

The primary objective in designing for producibility is to achieve low recurring costs during manufacture. This has been achieved on the composite tailboom by minimising the number of parts, reducing the layup cycle time and simplifying the assembly process. Having manufacturing development and tooling engineers involved in the design from the fist day of the program has allowed the design concept to evolve around these basic principles.

The use of composites allows very large continuous components to be designed, the size being restricted only by the limits of the manufacturing facility available such as autoclave size and layup area. In the case of the composite tailboom it has been possible to design components such as the side skins the full length of the tailboom (21ft) within the size limits of the existing manufacturing facilities at Bell. Designing skin panels the full length of the tailboom has allowed the main structure to be designed with minimum components. A four piece skin construction was chosen to maintain a simple component shape for the main skin details and to ease the assembly process. The simple geometric shape of the main skins has led to simplified cure tool design and an easier layup process. The four piece skin construction allows a two stage final assembly operation giving greater access during assembly and subsequent inspection.

Another major factor in reducing the parts count and simplifying the joining and assembly operation is cobonding or cocuring tees and angles to the main skins. Cocuring is the process of simultaneously curing a composite detail and bonding it to another component during the same cure cycle. In this case the prepreg resin acts as the adhesive between the two components. Cobonding is when a detail is precured and then bonded using a film adhesive to another component during its cure cycle. Figure 4 shows a cocured tee section located on the inner facing sheet of a main skin panel held in place by mandrels during the cure cycle.

The composite tailboom design has been generated in 3D CATIA. Lines Engineers generated an Outer Mold Line (OML) model which has been used as the single source database for all subsequent activities. This includes tool design who used the

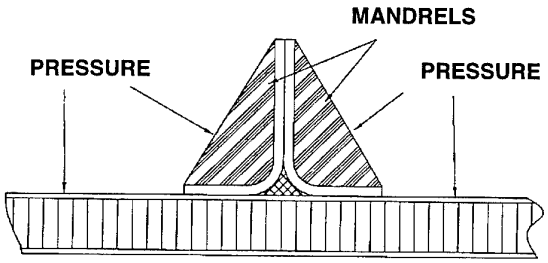

Figure 4
Cocured Tee Section

O.M.L surfaces to develop NC programs for the machining of the skin tooling and details. Having an electronic model of the tailboom from which tooling is generated has led to an exceptional fit of components during the final assembly operation. A major design philosophy is to maintain a true O.M.L surface for all points on the outer skin surfaces. All design features are then built up from the O.M.L surface inwards. This allows for easy modification of the layup tool and its details as a result of any future design changes.

The face sheets of all the O.M.L skin panels are either flat or wrappable, having only single contour in any one place, ie a single piece of paper can be placed over the entire tool surface without cutting or wrinkling the paper. Additionally the face sheets were deemed as 'sacred' meaning that no internal plies or buildups are allowed within the facesheet layup. This meant that for each component all of the facesheet plies shared common EOP's. These features allow all of the facesheets to be preplied, compacted and trimmed on the flat and placed into the tool as one detail. All stiffening, load introduction, and close out plies are preplied into packs and compacted as details prior to assembly layup. This allows a modular assembly process in the tool as opposed to a ply by ply layup reducing cycle time and tooling requirements in production.

The bond assembly stage is done using simple 'through the part' bonding with an oven cure. For example on the main skin splice joints, pressure is applied to the joint using rubber faced cleco bars. This process alleviates complicated and expensive bonding operations and curing in an oven ensures uniform bondline temperatures throughout the tailboom.

2.5 Design for Strength and Stiffness

The main design drivers for the dynamics and stress engineers is to optimize the boom stiffness for dynamic characteristics and to have a flaw tolerant safe life design under repeated loading. Figure 5 shows a Nastran Finite Element model of the composite tailboom, created so that dynamic characteristics, strength and weight could be optimised. Extra plys of 0 degree tape were added to the side skins to optimize the tailboom resonant frequency lateral mode so that it lies above the tailrotor one per rev frequency thus reducing vibration levels.

One of the composite tailboom certification requirements is to meet FAR 29.571(b)(1) flaw tolerant-safe life, ie with flaws present the structure must withstand repeated loading with no flaw growth for the life of the aircraft. The primary method of compliance of this requirement for the composite structure is to be done by structural test. This is discussed further in section 4. To meet this requirement many of the fatigue critical areas were designed out of the tailboom. Having a continuous side skin that includes the fin eliminates the need for a fin boom joint and has given the designers the opportunity to create a very smooth transition in this area with the ply layup tailored efficiently for maximum strength. These features have totally eliminated what was previously a fatigue critical area on the metal boom. Having a bonded assembly with a minimum number of large details as the primary load path between the tailrotor and the fuselage has eliminated all the fatigue critical fastened joints and reduced the number of bonded joints to a minimum. A bonded joint can be fatigue critical if it is subjected to repeated peel loads, such loads can be created if adjacent panels buckle under normal flight loads. Care has been taken on the tailboom to avoid any peel loading on the joints and to design the structure as non buckling. Fatigue

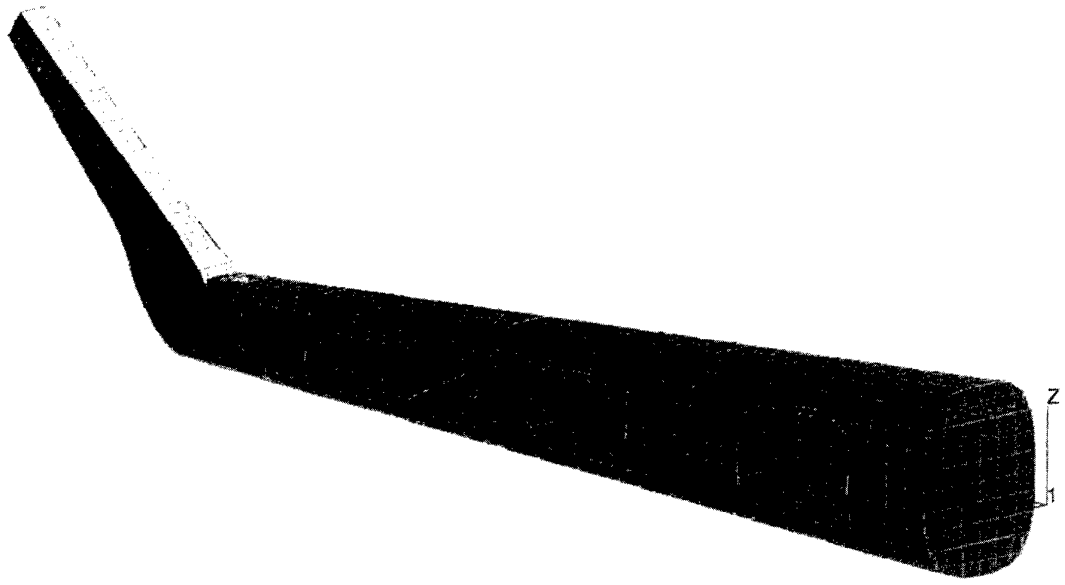

Figure 5
Nastran Finite Element Model

critical areas that still exist on the composite tailboom include the attachment of fittings to the bonded assembly via mechanical fasteners. In particular this includes the fuselage attachment fittings, the elevator attachment fittings and the tailrotor attachment casting on the fin tip. For these joints the fastener hole bearing stresses have been designed below the endurance limit for both the carbon and the metal fitting. Additionally the metal fittings have been analysed to show that they meet the flaw tolerant safe life requirements of FAR 29.571 (b)(1).

For static strength requirement existing Model 412 and 212 external loads were used and the tailboom was designed with a provision for 20% future growth in tailrotor thrust. Generally, from a strength view point, the composite tailboom is a very efficient design utilising the benefits of sandwich panels and making effective use of fibre orientation and ply build up where they are required. Doubler packs that include mainly 0 degree tape plies have been used to efficiently transfer load into the main skins in load introduction areas eliminating the need for longerons and stiffeners. This is further emphasised by the use of honeycomb sandwich construction that provides lightweight nonbuckling panels requiring no stiffeners. Generally the overall construction of the composite tailboom provides a very redundant structure that should prove very tolerant to in-service damage.

2.6 Design for Reliability

Designing for reliability was the major factor in the decision to use composite materials for the tailboom. The Model 412 tailboom is required to operate in a diverse range of harsh environments. This includes temperatures up to 350F due to engine exhaust gases, cold conditions down to -70F, wet, humid and sea salt spray conditions and fatigue loading from the tailrotor and elevator. Metal structure subjected to these conditions can suffer from corrosion and fatigue cracking of joints pushing up operating costs. The careful material selection and the configuration of the new composite tailboom design will considerably reduce these problems. Section 4.0 describes much of the testing that has been done under critical environmental and loading conditions to prove the reliability of the composite tailboom design.

3.0 TAILBOOM MANUFACTURE

3.1 Manufacturing Development

From the initial stage of the composite tailboom program the manufacturing development engineers started working in parallel with design to develop manufacturing processes and techniques. This work included material process development, material and design risk reduction tests, and development of manufacturing techniques for specific design features.

3.1.1 *Material Process Development*

One of the greatest challenges for manufacturing development was to develop the processing of the carbon bismaleimide (BMI) so that it could be repeatable for large scale primary structure. Prior to the composite tailboom program BMI had only been used at Bell in a limited way for secondary structure and the use of BMI throughout the aircraft industry was and still is very limited. This meant that manufacturing development had to start with a "blank sheet of paper". A large amount of effort went into the development of the cure cycle for the BMI tailoring it to Bell's bagging technique and the type of construction being used on the composite tailboom. Many material characteristics needed to be optimised such as material tack, resin content, void content, glass transition temperature and percentage of cross linking. A modified edge bleed system at low cure pressure was developed. To achieve the required material characteristics from the cure cycle, parameters such as ramp rates, dwell temperatures and durations, pressure and vacuum were all experimented with. BMI degrades nylon at high temperatures and so several bagging materials needed to be tested for compatibility before a suitable high temperature BMI resistant bagging film was found.

3.1.2 *Material and Design Risk Reduction*

Once the manufacturing process for the BMI had been developed, exhaustive testing and studies of the basic panel construction were performed as a risk reduction activity to prove the panel design concepts and the material suitability for the tailboom construction. This development work consisted of environmental testing, material compatibility and formability, adhesive quality, and panel concept evaluation.

Environmental testing included hot water soaks, moisture pickup under hot humid conditions, salt spray, galvanic corrosion, high temperature exposure and aging. Material compatibility studies and tests were performed to look at surfacing, paste adhesives, core splice adhesives, and lightning strike screens.

Test were done to look at the formability of the fabric and tape, the placing of thick preplied doubler packs into curved tools without wrinkling, curved panel spring back after cure, and the suitability of tool release agents.

The adhesive quality tests examined the viability, strength and process repeatability of the core to facesheet cocure bond. Several sandwich panels with BMI adhesives at different weights were manufactured and the adhesive filet inspected for cure quality, material composition (resin/adhesive), and adhesive displacement. Flatwise tension tests were then performed so that the optimum adhesive weight and strength could be determined.

A series of panels were manufactured so that an evaluation of some basic panel design properties could be performed. This included visual quality, panel weight, surface quality, leak checks, and pressure and temperature resistance. The surface quality evaluation comprised assessing the minimum amount of surface preparation required for painting and the quality of the surface after painting. Leak tests included immersing panels in hot and cold water for long periods and checking for panel leaks visually and by weight gain. Simulated post cures were performed subjecting panels to high temperatures to assess the effect of any internal panel air pressure.

These risk reduction tests were performed prior to the material qualification tests for certification that are described in section 4.1.

3.1.4 *Fabrication and Tooling Techniques*

The development of fabrication and tooling techniques for specific design features was a major driver of the design, tailoring many features for producibility.

The manufacture of the cocured tees and angles onto the main skins using mandrels in the main skin layup tool required several development activities. The offset of the mandrels on all of the curved skin panels needs to be known precisely so that the manderals can be machined to the correct shape. A perfect fit of the mandrels will ensure that an even pressure is obtained on the top surface of the laminate. Two factors effect this offset, firstly the cured laminate thickness and secondly the compression of the sandwich construction during cure. Many laminates and sandwich panels were cured and measured to establish satisfactory statistical data to estimate the offset.

The level of fixation required for the installation of the mandrels for the cocured tees needed to be determined to allow for

movement during the cure. Forming curved tees and angles without having to resort to darting of the plies was a manufacturing and structures objective. This was simply achieved by using only 45 degree fabric that can be formed around the skin curvature for the tees and angles without excessive stretching.

Another manufacturing feature that required significant development work was the secondary bonding process for the tailboom bonded assembly. The objective was to obtain a bondline thickness of .005" to .008" by use of mechanical pressure with uniform heating of the joints throughout the complete tailboom assembly. Bars are clamped to the bondlines using cleco's that apply minimal clamping pressure. The assembly is then heated in an oven, curing the bondline. Many tests were performed to optimize the bondline thickness and quality. Variables included the amount and type of adhesive, the pitch of the cleco's, the thickness of the cleco bars and the amount of adhesive squeeze-out obtained.

3.2 Tooling

The principal tools used on the composite tailboom program are the four main skin layup tools. Figure 6 shows the Right Hand Skin Tool. A tool material was required that has the same thermal expansion as carbon bismaleimide. Available options included the high nickel alloy invar, or composite tools. Invar tools were chosen as they have an infinite life and the invar can be machined directly from NC programs eliminating the need for a master making them cheaper than composite tools. The skin tools are fairly large tools over 20ft in length and so a major concern in using invar is the large mass of the tool affecting the heatup rate of the skins during the autoclave cure cycle. For this reason finite element models of the skin tools were generated to perform a thermal and a stiffness analysis. A minimum weight substructure was required to lessen the overall mass of the tool and so the results from the stiffness analysis were used to optimize the configuration of the substructure. A thermal evaluation of the autoclave was performed and this information fed into the finite element model so that the thermal analysis could accurately evaluate the effect of the tool mass on the autoclave cure cycle. These results were then used to further modify the substructure to achieve the desired results. The final outcome is an invar tool design that allows equivalent cure times to composite tooling.

The internal substructure of the composite tailboom is made up from flat or very small details. For these simple detail tools thermal expansion is of little concern and so aluminum NC machined or flat plate tools are used. The design of the bond structure allows some float of these internal details to accommodate any minor discrepancies.

For future production of the composite tailboom Ultrasonic Ply Cutters and Laser Ply Projection Locators will be used in conjunction with the layup tools to speed production of the detail parts.

Once all of the composite details have been made, only minimum tooling is required to perform the assembly operation. An assembly jig is used for the location of all the composite details for the bonded assembly. This tool simply locates the composite details for a prefit operation in which the cleco holes are drilled for the pressure bars. After bonding this tool is also used for locating the fittings that make up the mechanical assembly.

3.3 Tailboom Fabrication

The first composite tailboom bond assembly to be produced is shown in figure 7. The manufacture of this first boom was very successful with very few problems encountered throughout each stage of the fabrication process. The extensive manufacturing development and design approach used had paid off. Detail parts produced were of very high quality with virtually no defects present on the first articles made. The final assembly operation proved to be very simple with the parts fitting together so well that no gaps requiring shimming were present in any of the joints over the entire bonded assembly.

The manufacture of this first bonded tailboom assembly has shown the potential for future low cost production.

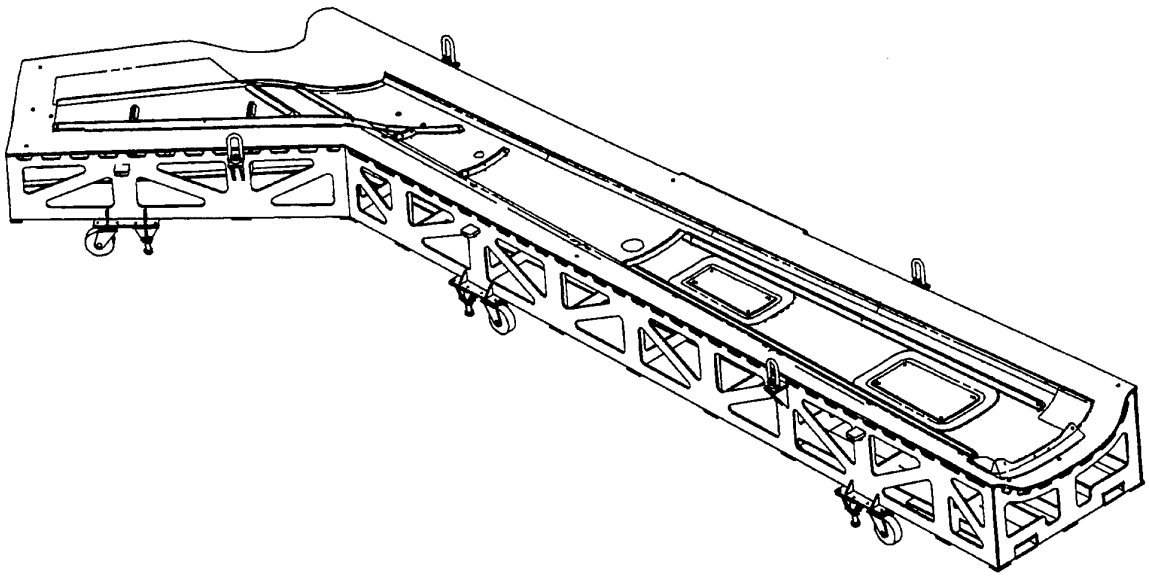

Figure 6
Right Hand Skin Layup Tool

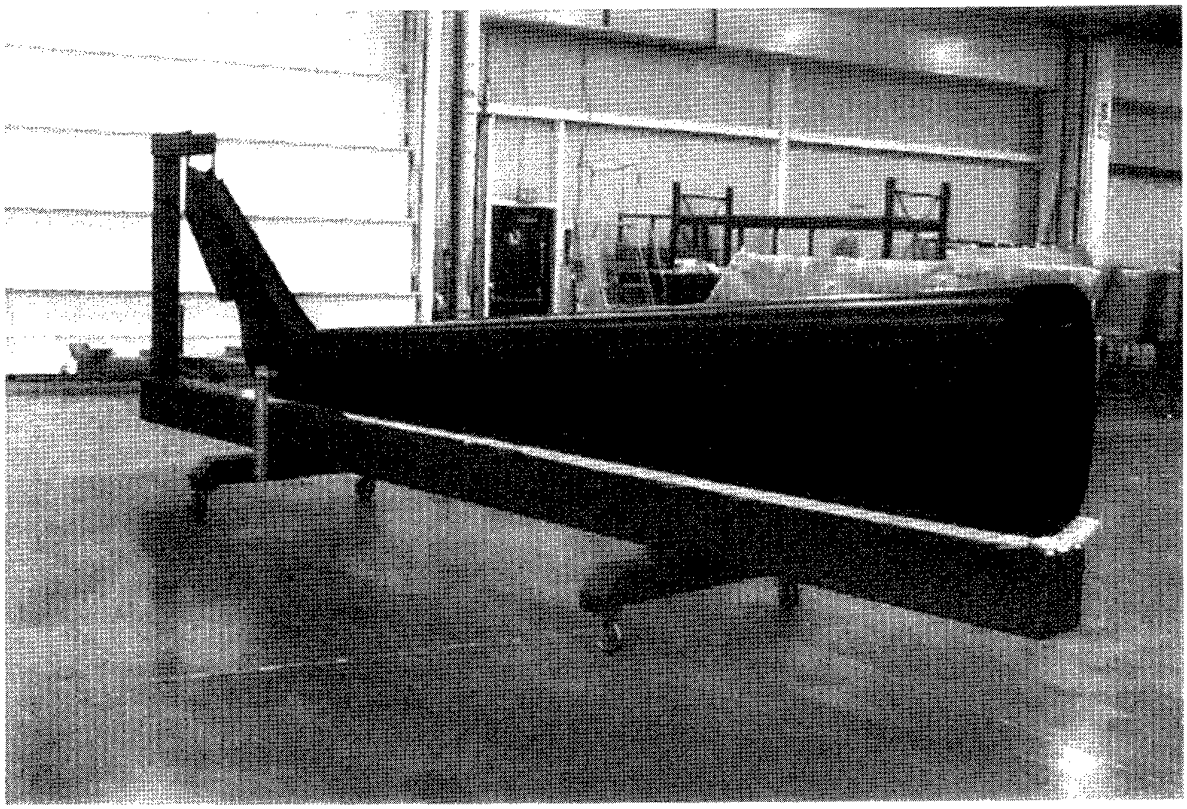

Figure 7
Composite Tailboom Bonded Assembly

3.4 Inspection

The use of BMI carbon and the unique design features of the composite tailboom meant that non-destructive inspection (NDI) standards and techniques needed to be established. A series of panels were manufactured incorporating many of the design features on the composite tailboom. The panels contained imbedded pieces of teflon tape representative of manufacturing flaws of different sizes. The panels were used to develop NDI standards by establishing ultrasonic signals for acceptable quality material and identification of flaws. Ultrasonic NDI techniques used for the composite tailboom include squirter system for sandwich construction, pulse echo for solid laminates, contact through transmission for local verification and harmonic bondtesting for bondlines.

4.0 CERTIFICATION TESTING

The M412 Composite Tailboom structure will be certified by the Federal Aviation Administration (FAA) under Federal Aviation Regulation (FAR) Part 29. To achieve this, a certification plan was produced based on guidelines from FAA Advisory Circular AC-107A 'Composite Aircraft Structure'. The plan uses a 'Building Block Approach' that combines laboratory tests, full scale article tests, flight test and analysis to evaluate the structural integrity of the materials and design of the composite tailboom.

4.1 Material Qualification

A program of tests have been performed to qualify the materials which have been used in the composite tailboom design. These materials include carbon BMI prepreg tape and fabric, BMI adhesive films, pastes and syntactic film core.

The tests for the BMI prepreg materials comprised laminae tests for material qualification and laminate tests to determine material design allowables. The material qualification tests of the tape and fabric included traditional physical property tests, laminate chemical resistance tests, and laminae mechanical property tests.

The design allowables were determined by testing laminates of differing fibre orientations that represent actual design laminates. Design allowables generated include open hole tension, filled hole tension, open hole compression and joint bearing. Allowables were derived in consideration of material and process variability, and critical service environment using computational methods per MIL-HDBK-17.

4.2 Structural Testing

Structural laboratory testing on the composite tailboom has been done a three levels, design verification elements, subcomponents, and a full scale static test.

4.2.1 *Design Verification Element Tests*

The design verification element tests generated design values for critical design elements with consideration for critical environment, repeated loading, and manufacturing defects. The element tests included baggage floor joints, skin splice joints, sandwich cocure effects and endurance tests for bolted joints, adhesive joints, and laminates.

The baggage floor joint tests consisted of elements representative of a section through the baggage floor to side skin cocured tee joint. Loading included static and repeated loads representative of peel and bending from baggage mass and tensile pulloff loads from tailboom bending. Tests were conducted at room temperature and elevated temperature wet conditions with manufacturing defects and cleco holes included in the test specimens.

The skin splice joint tests consisted of elements representing two configurations of the main skin splice joint. Loading included static and repeated loads representing tensile lap shear on the adhesive. Again tests were conducted at room temperature and elevated temperature wet conditions with manufacturing defects and cleco holes included in the test specimens.

The sandwich cocure effect tests were performed to generate knockdown factors to apply to the laminate design allowables discussed in section 4.1. The knockdown factors account for the sandwich panel facesheet discontinuities caused when the laminates are cocured to the honeycomb core. Knockdown factors were generated for tension and compression static loading conditions under room temperature and elevated temperature wet conditions.

The endurance tests for laminate bearing in a bolted joint, adhesive lap shear joints and laminates were performed to generate S-N diagrams and endurance limits for these elements. During the flight test high cycle loads will be measured and compared with the endurance limits generated to show that these high frequency loads are non damaging to the composite tailboom structure. The tests were performed under critical environmental conditions.

4.2.2 *Subcomponent Tests*

The subcomponent tests represent three critical design areas of the composite tailboom, the vertical fin, the fuselage attach fittings and the tailboom skin panels. The purpose of the tests is to verify the static and repeated loads capability of these design

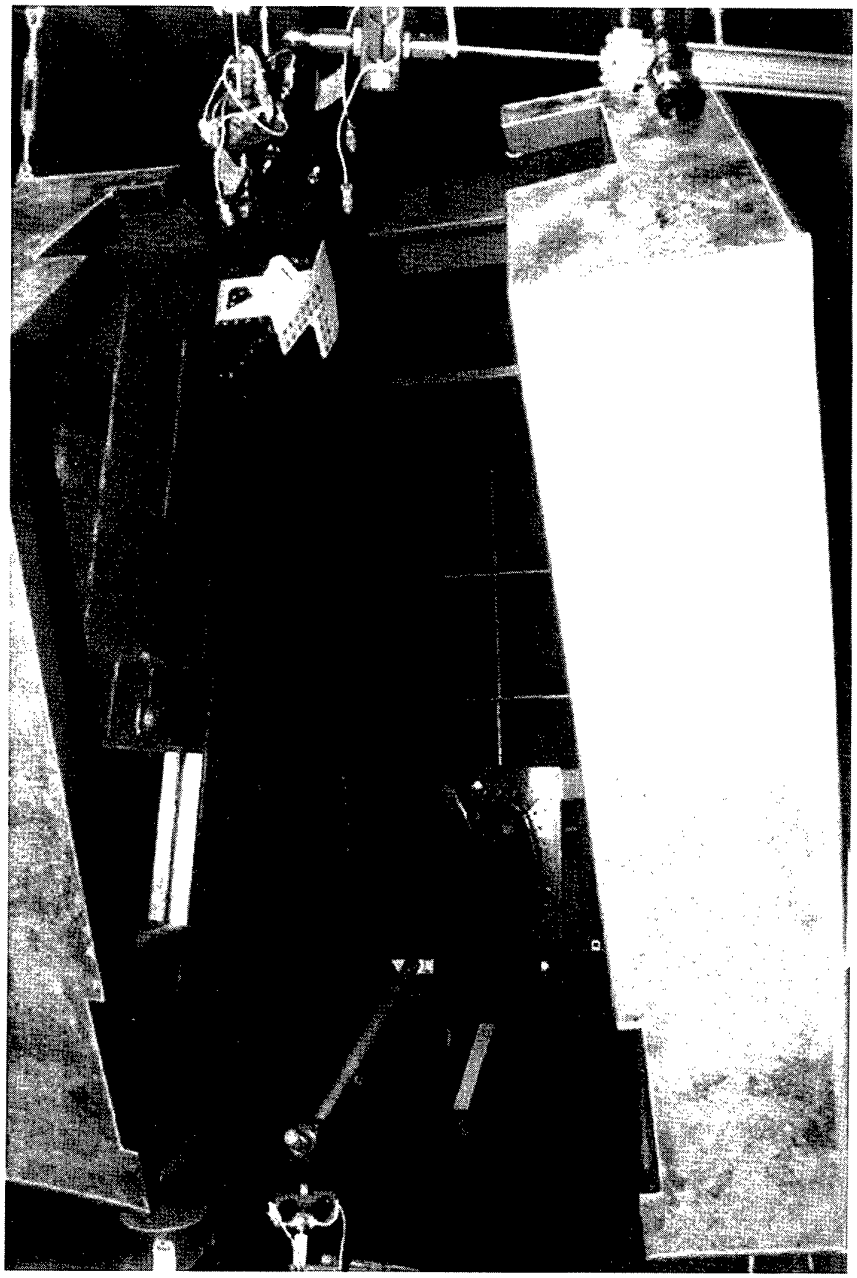

Figure 8
Vertical Fin Test

areas under critical environmental conditions. Test specimens include manufacturing defects, impact damage and field repairs at critical locations.

Before any subcomponent tests were started a series of impact resistance and tool drop tests were performed to determine the energy levels required to create barely visible impact damage (BVID) on different areas of the tailboom. This information was used to apply representative in-service damage to the subcomponent tests. FAA AC-107A describes BVID as damage that can be realistically expected in service below the established threshold of detectability and the airforce standard MIL-A-8722 describes BVID as a 0.1" depth dent using a hemispherical impactor. Impact energy levels were determined for damage up to 0.1" depth damage on the tailboom panels and from the results energy levels were chosen that would give an appropriate level of damage for the composite tailboom per FAA AC-107A.

The Vertical Fin Test is the largest of the subcomponent tests and was used to evaluate the structural integrity of the most critical region of the tailboom which included the tailrotor gearbox attachment, the vertical fin structure, the tailskid attachment and the fin/tailboom load transition section. The test specimen, built on development composite tooling was the first major piece of structure built for the composite tailboom program and was used by manufacturing development to prove many of the fabrication techniques and processes. The specimen contains 21 planned manufacturing flaws and 6 inservice BVID sites. The manufacturing defects are all placed at critical locations in the form of laminate voids, disbond of cocured and precured members, core to skin disbonds and main skin splice joint disbonds. The size and position of the defects and damage is such that they represent the maximum limit of the acceptance criteria for inspection. Repairs included a riveted titanium patch field repair to a large skin puncture and autoclave cure repairs to adhesive disbonds that could occur during manufacture. Overall the test specimen was considered to be discrepant, damaged and repaired far beyond any production standard tailboom that would be put into service. This meant any test results from this specimen could be considered conservative and valid for a worst scenario situation in production and in-service.

Figure 8 shows the vertical fin test specimen mounted in the test fixture. The specimen attaches to the fixture via a bolted joint at its most forward boom section. Loads are applied via hydraulic actuators to the specimen at 4 locations representing tailrotor thrust, tailrotor and driveshaft torque, fin aerodynamic forces and tailskid loads. These loads are combined to represent the repeated loading spectrum and the 3 most critical flight and landing load conditions. The specimen was surrounded by an environmental chamber so that temperature and humidity could be controlled. The specimen and test fixture were fully instrumented to measure applied loads, strains, displacements, temperature and humidity. Computerised control and data acquisition units were used to monitor and control the test parameters.

The first phase of the vertical fin test was to prove the repeated loads capability per FAR 29.571(b)(1) flaw tolerant safe-life evaluation. The repeated loading represents a Ground Air Ground (GAG) spectrum for 2 aircraft lifetimes. The GAG spectrum comprised tailrotor thrust and torque derived from existing M412 flight test data representing a severe heavy lift operation with periodic autorotation. The repeated loads test was conducted at 250F dry representing the conditions that can repeatedly occur on the vertical fin from the engine exhaust gases. During the test regular data recovery and periodic NDI and visual inspection was performed to monitor the specimen for no flaw growth. Before and after the repeated loads test the fin structure was subjected to the maximum operating (limit) loads to prove that the structural integrity has been maintained. The repeated loads test was successful with no flaw growth detected and no failures or permanent deformation in the limit load tests.

The second phase of the vertical fin test was to prove the ultimate load (1.5xlimit) capability of the structure. The environmental condition chosen for the test was hot wet (160F, 95%Relative Humidity) with a specimen preconditioned wet (1.3% moisture content). The hot wet compressive properties of carbon composite are considerably reduced and so hot wet conditions were considered the most critical for the ultimate test. These conditions are not likely to occur very often in service due to drying of the structure from the exhaust gases, however an aircraft left standing for a long period in hot humid conditions and then flown could see hot wet conditions for a short time before the exhaust gases dry the tailboom. To achieve 1.3% moisture content, the test specimen was left in the environmental chamber at 160F and 95% relative humidity. To monitor the moisture content a number of test panels with the same characteristics as the vertical fin were placed in the chamber with the test specimen and then periodically weighed to establish the amount of moisture gain.

The ultimate test was successful with no failures of the fin specimen occurring for the three critical load conditions tested. After the ultimate test the specimen was loaded to failure under the most critical loading condition. The fin structure failed at a BVID site on the side skin under compression at 170% limit load. This result was considered very satisfactory considering the degraded condition of the test specimen and the severity of the loading and environmental conditions.

Two subcomponent tests representative of the tailboom side skin panels were performed to verify panel stability in shear and compression. The compression panel is representative of the righthand side skin aft of the elevator where maximum panel compression occurs. The test procedure for the compression panel is similar to the vertical fin test and is summarised as follows. The test specimen is a flat rectangular sandwich panel (51" x 15") and contains planned manufacturing defects, BVID, and a field repair. The panel is simply supported on all sides and loaded in pure compression on its shorter sides. The panel was subjected to the repeated load cycles under 350F dry conditions followed by an ultimate test at 160F wet conditions. The test was successful with the panel facing skins failing at 250% of the design load in compression.

The shear panel is representative of the right hand skin panel between the two baggage bay door openings where maximum panel shear occurs. The test specimen is a flat square sandwich panel (24" x 24") and contains planned manufacturing defects, BVID, and a field repair. The panel has shear load introduced along each of its 4 sides via a test fixture. The panel was subjected to an ultimate test only under 160F wet conditions. The test was successful with the facing skin failing at 400% of the design load in shear. For both the compression and the shear panel tests the structural design objective was achieved with full fibre strength being reached with no premature failures due to panel or skin instability or core to skin disbonding.

The final subcomponent test is the fuselage attach fitting which will verify the structural integrity of the composite to titanium fastened joint. The M412 composite tailboom attaches to the fuselage via four titanium attach fittings and load is transferred from the fuselage to each attach fitting via a single bolt which clamps the two mating faces together. Each attach fittings is fastened to solid laminate doubler packs on the composite tailboom structure using approximately 25 titanium Hi-Lok pins.

Figure 9 shows the test specimen which represents a quarter section of the forward tailboom structure and the upper left fitting. The composite section of the test specimen contains planned manufacturing flaws, BVID, and a field repair. The upper left fitting experiences tensile loading only and has the highest loading of the four fittings during flight manoeuvres. The specimen will be subjected to repeated loads and an ultimate test under critical environment in a similar manner to that discussed earlier for the vertical fin test. Particular attention will be paid to any hole wear or fretting in the titanium composite joint interface during the repeated loads test.

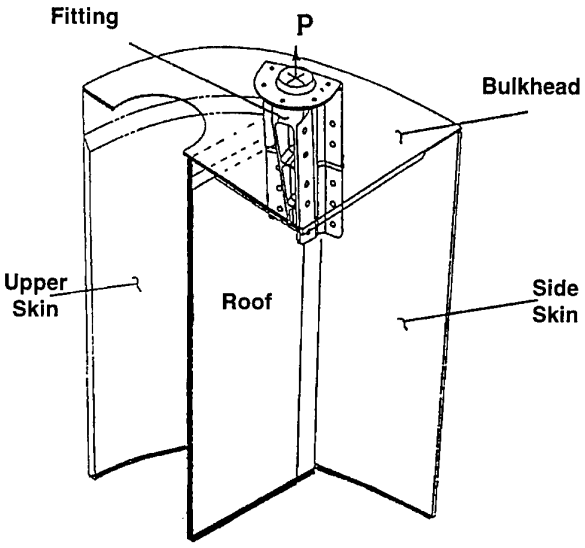

Figure 9
Attach Fitting Test Specimen

4.2.3 *Full Scale Static Test*
A full scale composite tailboom will be statically tested at ambient conditions to qualify the structure at the critical design loads. Environmental effects will be accounted for by comparison of recorded strains at ultimate loads to design allowables derived in the Material Qualification test program. Three critical loading conditions will be tested and the test loads applied so that the shear forces, torsion and bending moments closely match the theoretical values. The tailboom will be mounted in a test fixture and loads applied through hydraulic actuators and reacted at the four attach fitting points. Measurements of loads, strains and tailboom displacements will be recorded during the test.

4.2 Ground and Flight Tests

Ground and flight tests will be conducted to verify the performance of the Model 412 helicopter with a composite tailboom installation. Ground testing will include static tests of the modified elevator and tailrotor control systems, a ground vibration test to evaluate the dynamic response of the tailboom and aircraft installation, a drive system ground run to evaluate the modified tailrotor drive system installation and an electrical systems evaluation. Flight testing will verify handling qualities, flight strains, tailboom temperatures, dynamic and vibration characteristics and the electrical systems.

5.0 CONCLUSIONS

Fabrication of the first tailboom bonded assembly showed that the design concept worked well. Designing for producibility and extensive manufacturing development work had paid off resulting in a simple structure that is easy and cheap to assemble. Extensive structural and environmental testing has shown that the materials and structural configuration used should prove to be extremely reliable in service. The Model 412 Composite Tailboom Program is now into its final phase of flight testing and certification concluding what is proving to be a very successful program.

CRASH RESISTANT COMPOSITE SUBFLOOR STRUCTURES FOR HELICOPTERS

A.F. Johnson and C.M. Kindervater
German Aerospace Establishment DLR
Institute of Structures and Design
PO Box 800320
D-70503, Stuttgart, Germany

H.G.S.J. Thuis and J.F.M. Wiggenraad
National Aerospace Laboratory NLR
PO Box 90502
NL-1006 BM Amsterdam
The Netherlands

ABSTRACT

The paper describes the application of composite materials to the design of crash resistant beam and frame elements for helicopter subfloor structures, and discusses alternative fabrication technologies for these structural elements. These elements require a dual function structural concept with load carrying capability under flight loads and energy absorption under crash loads. The realisation of this dual function by innovative design with fibre reinforced composite materials is described. In order to utilise these lightweight structural concepts in helicopters, cost effective technologies for series production of composite components are required. The paper discusses three fabrication methods based on autoclave technology, resin transfer moulding (RTM) and thermoforming, taking a sine-wave floor beam as a demonstrator component for the technologies.

1. INTRODUCTION

Future helicopter structures for both military and civil use will consist extensively of fibre reinforced composite materials to permit lighter structures. However, the design of such structures must satisfy stringent crashworthiness specifications, see for example MIL-STD 1290A [1]. To achieve crash-worthiness the design of the helicopter must contain mechanisms which absorb sufficient energy to limit accelerations on the occupants, and which maintain a protective shell large enough to allow a safe evacuation of the occupants. A helicopter design concept which meets the structural and crashworthiness requirements is described in [2] and illustrated in Fig. 1, with energy absorbing elements incorporated in the landing gear, the subfloor and the seats. The subfloor is an assembly of composite beams joined together by intersection elements into floor boxes. Energy absorption is mainly achieved by crushing the vertical webs of the beams and the intersection elements. The paper concentrates on the design and fabrication of a basic composite floor beam element, and its integration into a floor box. Design concepts for the key elements of sine wave beams, cruciform intersection elements and a composite sandwich 'tensor' skin, which is designed to improve energy absorption in a subfloor under water impact, are described in §2.

Now that composite structural concepts have been established for EA subfloor structures, attention is turning to cost-effective fabrication methods for composite components, which are suitable for future series production. In a modular helicopter subfloor structure the basic element is the sine-wave beam, and three fabrication methods for this component are described: in §3 autoclave technology and resin transfer moulding (RTM) for thermoset composite beams, and in §4 the thermoforming of thermoplastic composite beams. Both RTM and thermoforming are suitable for automated production methods. An evaluation of the three fabrication technologies in relation to tooling, equipment, materials and production time is made. Finally in §5 some static and dynamic compression test results on sine-wave beams, cruciforms and tensor skins are presented.

2. SUBFLOOR DESIGN CONCEPTS

In crash accidents with a high vertical component of the impact velocity the crash loads have to be absorbed mainly by controlled structural deformation. A systems approach should be applied whenever possible which comprises the landing gear, the subfloor and the high mass retention structure and seat/restraint systems with tuned energy absorbing characteristics. However, helicopters and light fixed-wing aircraft have little crushable airframe structure. Such designs typically consist of a framework of longitudinal beams and lateral bulkheads covered by the outer skin and cabin floor. The total structural height is often only about 200 mm. The design of intersections of beams and bulkheads

Paper presented at the FVP Symposium on "Advances in Rotorcraft Technology", held in Ottawa, Canada, 27-30 May 1996, and published in CP-592.

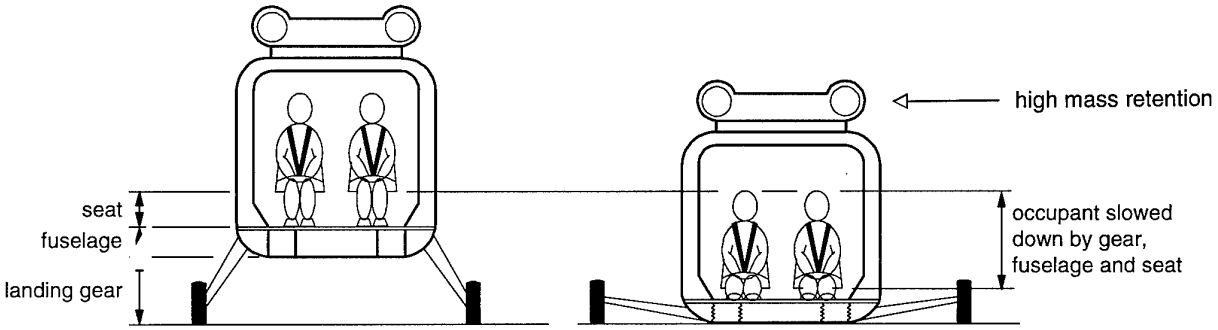

Fig. 1 Helicopter crashworthiness concept, see [2]

(cruciforms), the beam webs and floor sections (boxes) contribute essentially to the overall crash response of an airframe subfloor assemblage. Under vertical crash loads cruciforms are 'hard point' stiff columns which create high deceleration peak loads at the cabin floor level, and cause dangerous inputs to the seat/occupant system. Subfloor crush characteristics should have a moderate initial stiffness and then a slightly increasing or constant crush force level. To minimise cost and weight penalties a dual function structural concept should be realised in the floor structure: load carrying capability for normal operation; and energy absorption for crash loads in the subfloor, which should maintain cabin floor structural integrity. Compared to metals, totally different design concepts are being developed and verified for composite structures. High energy absorption with composites is obtained for compressive loading where brittle fracturing of the composite into sublaminates occurs. Under tensile or bending loads structural integrity may be lost at initial fracture and energy absorption can be low. To guarantee post crash structural integrity, i.e. a protective shell around the occupants, load bearing carbon fibre composite structures have to be hybridised with tougher fibres such as aramid fibres (Kevlar or Twaron) or high performance polyethylene (Dyneema SK 60). Thus structural crashworthiness comprises both energy absorption and structural integrity.

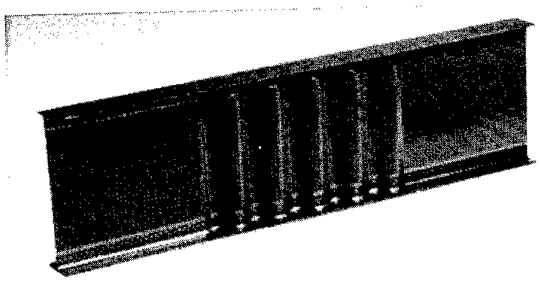

Fig.2 Composite sine-wave beam

2.1 Sine-wave beams

Composite beams with sinusoidal or trapezoidal corrugated webs (Fig. 2) are the most efficient subfloor design concepts yet evaluated for helicopters. They are efficient at carrying shear and compression loads in normal flight, have high energy absorption under crushing loads and, with hybrid lamination techniques, have good structural post-crash integrity. Drawbacks of the sine-wave beam concept, however, are the high fabrication costs, the interface with other structural elements (i.e. adjacent fuel tank bladders) and the difficulty in incorporating suitable trigger mechanisms, which reduce peak loads when the beam is crushed during impact, without lowering the shear load performance. The determination of the static load capacity, which in thin shell structures is limited by buckling, the influence of materials hybridisation and geometry on crush characteristics, and the selection of trigger mechanisms are the main design aspects of sine-wave beams.

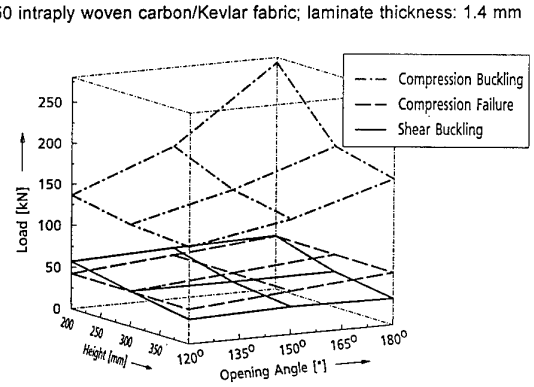

Fig. 3 Buckling and failure loads of sine-wave webs

Shear and Compression Buckling Behaviour

This has been studied by Finite Element (FE) analysis of various corrugated web configurations in order to optimise the sine-wave geometry [3]. Investigated were the effects of geometrical parameters such as free buckling length (spar height 150, 200, 300 and 400 mm), laminate thickness (1.4, 1.75 mm), the opening angle of the wave elements (120°, 150° and 180°), and the effect of hybridisation. The basic web laminate

consisted of a 50/50 intraply woven carbon/aramid fabric with epoxy resin. The radius of the wave element was held constant at R=20 mm. Buckling critical combinations of geometrical parameters are small laminate thickness, large spar height and opening angle of the tangent circular ring section (wave element) between 90° and 120°. The results are summarised in Fig. 3. An optimum for all the analysed laminate thicknesses and spar heights is an opening angle of 150°. An increase of the angle up to 180° does not result in most cases to higher buckling load but leads to higher weight due to increasing cross section. Compression buckling loads are higher than strength failure loads, which is a crucial fact for crash resistance, because compression strength dominated failures result in more efficient crush energy absorption.

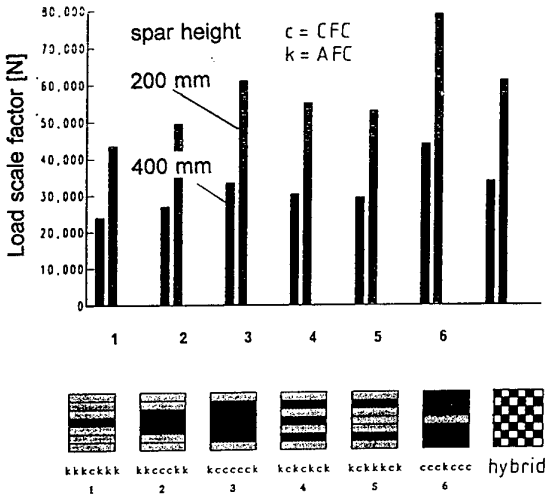

Fig. 4 Effect of hybridisation on shear buckling of sine-wave webs

Influence of Hybridisation

Fig. 4 shows further theoretical results on hybridisation of carbon fibre and aramid fibre plies in a sinusoidal corrugated web with opening angle of 150° and constant laminate thickness 1.4 mm based on 7 prepreg plies. Two spar heights (h = 200 and h = 400 mm) are considered. The sine-wave web with the lowest aramid share (laminate 6) shows the highest shear buckling loads. However, the post-crash integrity of this laminate is not satisfactory. Acceptable shear buckling resistance can be achieved when the proportion of aramid plies is between 30-50% (laminate 3 and intraply woven hybrid). These webs provide under crash loading a good post crash structural integrity. Higher proportions of aramid fibres improve the integrity further but lead to severe reduction in shear stiffness.

Specific energy absorption

The larger the included angle of the circular segments in the sine-wave beam web the more energy will be absorbed. However large included angles increase beam weight. An NLR study [4] demonstrated that a sine-wave web with an included angle of 110° provides the highest specific energy absorption level (absorbed energy divided by the crushed mass).

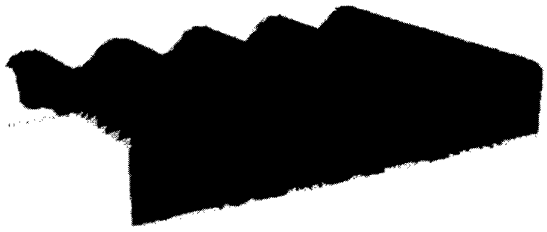

Fig. 5 DRAPE simulation

Drapability of fabric

The larger the included angle the more difficult it is to laminate the fabric layers on the mould without fibre bridging in the concave areas and without wrinkling of the fabric in the double curved flange web interface. Simulations with the Delft University computer code DRAPE [5] indicated that an included angle of 110° in combination with a radius of 20.0 mm is the maximum angle one can allow without excessive wrinkling of the fabric in the corners (see Fig. 5). This is one aspect of composite prepreg formability which is discussed further in §4.3.

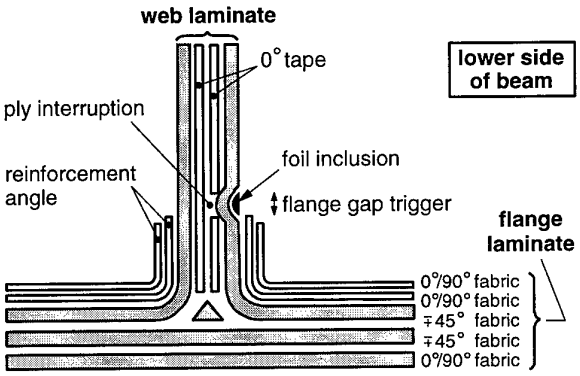

Fig. 6 'Flange gap' trigger with ply drop-off

Influence of Trigger Mechanisms

Triggers are stress concentrators in the structure which initiate failure locally, causing reductions in the peak load and initiating progressive crushing. The two main types of trigger in use are notch triggers, which consist of small cut-outs in the sine-wave webs, and ply drop-off triggers in which there is a narrow region along the web containing an interruption to one or more of the load bearing plies, as shown in Fig. 6. In a test programme [3] on trapezoidal and sine-wave webs it was found that notch type triggers caused about 50% peak load reduction compared to untriggered webs under static crushing, Fig. 7. Whereas an embedded ply drop-off under static load caused only 20% peak load reduction. However, under dynamic crushing (v_o = 8 m/s) a peak load reduction of about 40-60% compared to the untriggered version was observed in ply drop-off triggers. In conclusion it is found that the notch trigger has a more significant influence on the static response

but gives higher crush force efficiency. In a well designed trigger it is important that the beam shear strength and stiffness should not be significantly reduced. Sine-wave beams with ply drop-off triggers have been tested and found to have a shear load reduction of less than 5% which is a very acceptable compromise for crash resistance structures, see [3], so these are currently preferred for sine-wave floor beams.

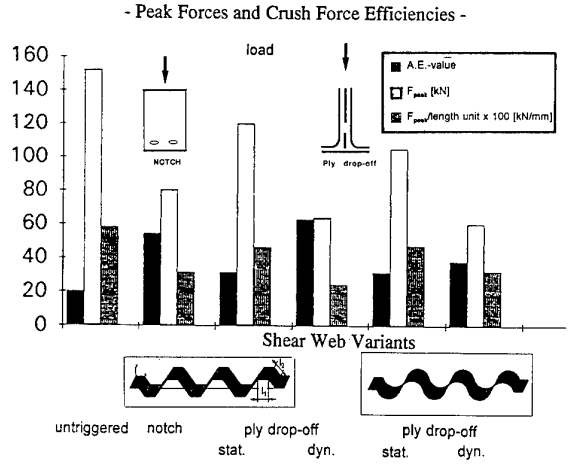

Fig. 7 Effect of trigger type on crush behaviour

When these various influences on sine-wave beam properties are taken into account, it is obvious that any final design will be a compromise. Thus lower opening angles are easier to fabricate and give higher specific crush energies, whereas larger opening angles increase stability and shear failure loads. Further compromises have to be made on the level of hybridisation with carbon and aramid fibres or fabrics, and in the type of triggering.

2.2 Cruciform elements

Cruciforms are formed by intersections of beams and bulkheads and represent typical floor structure subelements. These are the 'hard' points in the subfloor structure, with the stiffness of the cruciform elements controlling peak loads, which may be intolerable for crew and passengers in the case of a crash. Various cruciform designs were investigated [3] within the basic subfloor crashworthy design concept. A stiffness reduction is possible with correctly designed triggers provided the operational loads are not affected. Starting from an aluminium baseline cruciform taken out from a commuter type aircraft, composite cruciforms having single and multiple notched edge joints, corrugated edge joints, tapered sections were studied, Fig. 8. A moderate initial stiffness and then a constant or slightly increasing crush force level in combination with post crash structural integrity are the major cruciform design goals for vertical energy absorption.

Further design improvements led to a hybrid cruciform variant - the HTP-element, Fig. 8. The element has a column-like mid-section formed by a Y-shaped split of the shear web laminate, an integrated bevel trigger at the bottom of the shear webs, and tapered edge joints at

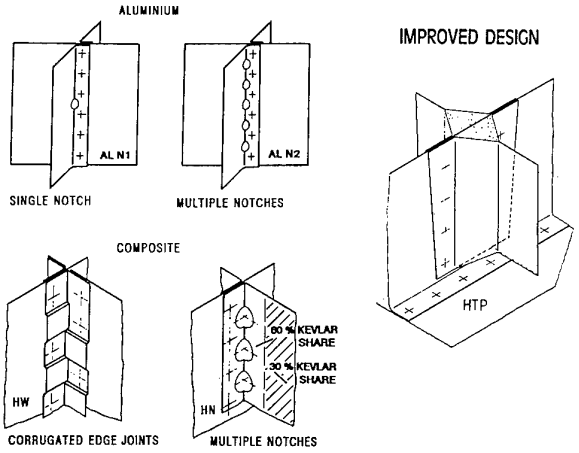

Fig. 8 Trigger variants for cruciform elements

the keel beam attachment. The keel beam and shear web laminates have a J-shaped connection to the outer skin. In several static and dynamic crush tests 3-4 times higher absolute energy absorption compared to the other elements could be achieved. The specific absorbed energy of an aluminium cruciform with a single notch reaches only 28% of the value of the HTP-element. From the cruciform test series the following conclusions for cruciform crash resistant designs can be drawn:

a. Multiple notching for peak failure load reduction results in low energy absorption.
b. Post-crush structural integrity can be achieved by hybridisation of carbon and aramid laminates.
c. Carbon composite cruciforms have high energy absorption and high weight savings(30%) compared to aluminium, but disintegrate during crushing.
d. Hybrid carbon/aramid elements have weight savings between 15-20% compared to aluminium, with the same or much higher absolute energy absorption.

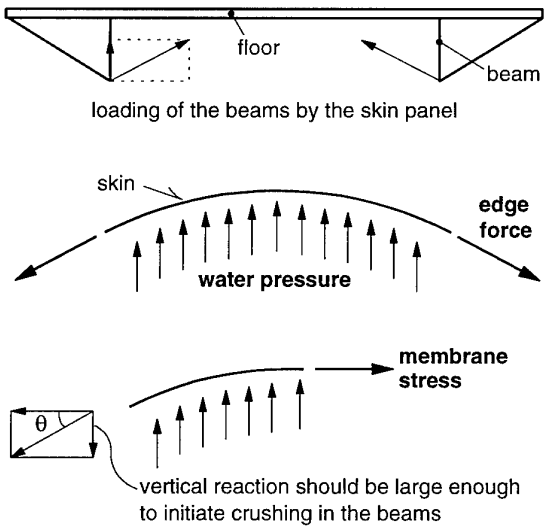

Fig. 9 Force equilibrium in bottom skin panel under water impact

2.3 Tensor-skin concept

As discussed above crash energy can be absorbed by a number of structural elements such as the landing gear, the subfloor and the seats. In the case of an impact on water a number of these structural elements may be less successful in absorbing energy. For instance the landing gear will meet little resistance when impacting a water surface. When the subfloor impacts a water surface the skin panels will be loaded by a transverse load induced by the water pressure. Due to the brittleness of composite skin panels the transverse loading will generally lead to a skin failure. When the skin panels fail the beams of the subfloor structure may not be loaded to the same extent as in land impact accidents, hence they are not as effective in absorbing energy. The subfloor can only absorb crash energy during an impact on water when the skin panels transfer the water pressure loads to the energy absorbing beam elements. This load transfer can only take place when the skin deflects substantially without failing, since large deflections of the skin will result in a vertical load component which will load the beams in the subfloor as shown in Fig. 9.

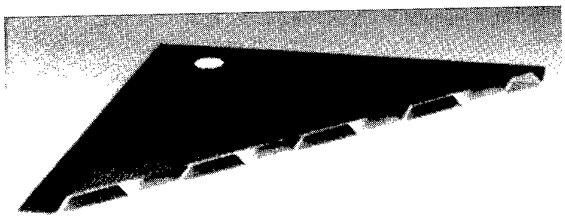

Fig. 10 Tensor skin sandwich panel

At NLR a composite sandwich skin concept ("tensor"-skin) has been developed (see Fig. 10). The tensor skin provides a mechanism which allows a composite skin to unfold and deflect before membrane stresses build up [6]. Hence, reaction forces to the membrane stress have a large vertical component from the start, limiting the membrane stresses in the skin needed to react to the water pressure and loading the beams with the compression forces needed to crush them. The tensor-skin concept makes use of high performance poly-ethylene (PE) fibres which can survive the large deformation during the unfolding process while maintaining their strength in tension [7]. The faces of the tensor-skin can be carbon/epoxy, aramid/epoxy or hybrid carbon/aramid epoxy materials. The PE/epoxy core is configured as a corrugated plate, thereby containing the necessary folds. The design loads for the sandwich tensor skin panels are mainly in-plane shear with respect to the operational loads, and membrane tension of the stretched core with respect to crash loads.

3. THERMOSET COMPOSITE SINE-WAVE BEAM

3.1 Design

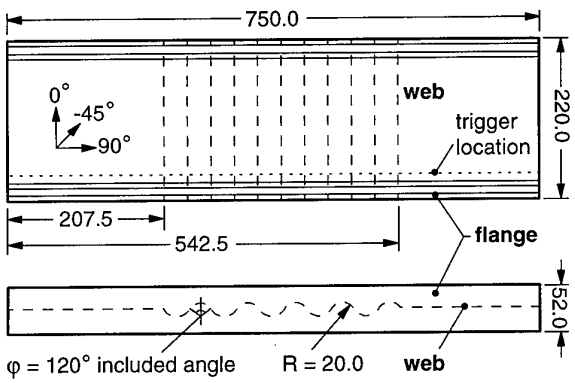

Fig. 11 Thermoset sine wave beam design

The sine-wave beam (see Fig. 11) used in this study was designed for "generic" loading conditions, i.e., for shear loading of 220 N/mm, with a web thickness of approximately 1.2 mm for stability. The beam consists of a web with ten circular segments with a radius of 20.0 mm and an included angle of 120° combined with two double flanges (I-beam concept). To provide optimal crash energy absorbing characteristics and structural integrity [8], the web laminate was composed of outer faces of hybrid carbon/aramid fabric with unidirectional (UD) carbon fibre plies in the centre, as seen in the laminate construction in Fig. 6. The high strength and stiffness of the carbon fibres is used to absorb most of the crash energy by crushing whereas the resilient aramid fibres provide post crush integrity and contain the carbon fibres so they fracture into many small segments. The flange laminates allow easy attachment to the neighbouring structure, and were designed to provide the necessary bending stiffness of the sine-wave beam and the required bearing strength of the flanges.

To initiate the right failure mode and to reduce peak loads during a crash the thermoset sine-wave beam was configured with a "flange-gap" trigger in the lower side of the beam as indicated in Fig. 11. The "flange gap" trigger is a variant of the ply drop-off trigger, with an eccentricity induced by a foil inclusion (see Fig. 6). The trigger has a gap in one of the main load carrying 0° plies just above the beam flange. This trigger concept provides a sufficient reduction of the peak load before crushing, a predictable failure mode, a crushing mechanism with sufficient energy absorption and satisfactory post-crush integrity [9].

3.2 Fabrication techniques

Tooling concepts

Because of its complex shape, fabrication of the composite sine-wave beam is cumbersome and in the traditional autoclave process with thermoset prepreg a number of problems arise, which have an influence on design of the tooling.

Laminating (tacky) prepreg plies in the concave areas of the tool (especially in the double curved flange-web interface) is difficult and *fibre bridging* in these areas is likely to occur, whereby the fibres bridge across the concavity and are no longer in full contact with the tool. As mostly one-sided tooling concepts in combination with a vacuum bag are used in autoclave processing, the autoclave pressure applied to the vacuum bag creates tensile stresses within the bridged laminate which may lead to distortion of the fabricated part. The bridged laminate is usually resin starved, because resin flows into the cavity behind the laminate, and has a very high void content resulting in poor laminate quality.

In order to create a uniform heating profile in the tool and to reduce heating time, the thickness of the tool should preferably be uniform and minimised resulting in a tool with the same contour as the sine-wave beam. Applying the *vacuum bag* to this complex shaped tool is very time consuming and difficult because of the large number of folds which have to be applied. In the mean time these folds make the vacuum bag vulnerable to cracking. If the vacuum bag cracks in an early stage of the prepreg consolidation process , the quality of the cured laminate will be poor due to lack of pressure.

To overcome these difficulties two different tooling concepts for thermoset sine-wave beams were developed: a tool for Autoclave Processing and a tool for Resin Transfer Moulding (RTM), see [9]. The two tooling concepts had to satisfy the following conditions:

a. No fibre bridging during the consolidation process of the resin.
b. The height of the cured beam had to be controllable to limit the amount of shimming when assembling the sine-wave beams into a subfloor box.
c. No additional laminating blocks were allowed.
d. The sine-wave beams had to be net shaped to eliminate trimming of the cured sine-wave webs.
e. No vacuum bag was to be used in autoclave fabrication.

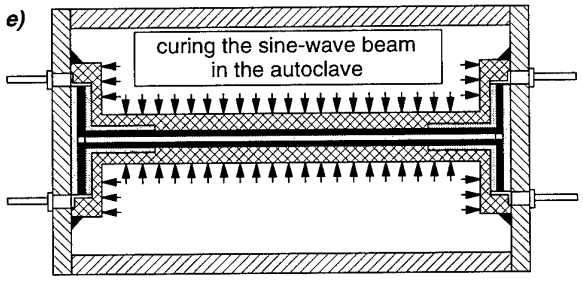

Fig. 12 Autoclave fabrication concept

The autoclave fabrication concept

The global lay-out of the tool used for the autoclave process consists of a metal frame with two airtight flexible carbon fibre reinforced elastomer panels (see Fig. 12), which constitute the tool surfaces. The autoclave fabrication concept can be described in the following five basic steps:

a. Laminating prepreg layers on the elastomeric panels.
b. Laminating the fillers, the flange laminates and joining the elastomer panels.
c. Assembling the elastomer panels into the metal frame.
d. Sealing all edges with tacky tape and connecting the vacuum hoses.
e. Curing the sine-wave beam in the autoclave

The elastomer panels are used as male laminating blocks. This eases the laminating process, reduces the amount of fibre wrinkling and fibre bridging in the area of the flange-web interface and reduces the laminating time in comparison to laminating (tacky) prepreg layers into a female mould. Because the elastomer panels are airtight no vacuum bag has to be used during the autoclave process. The thin elastomer panels also guarantee a uniform heating of the laminate during the consolidation process in the autoclave. Because of their "soft" surface, small cavities between the elastomer panels and the sine-wave beam laminate are closed when pressure is applied to the panels in the autoclave which eliminates fibre bridging. The metal frame assures that the height of the cured beam can be controlled as accurately as needed.

The RTM fabrication concept

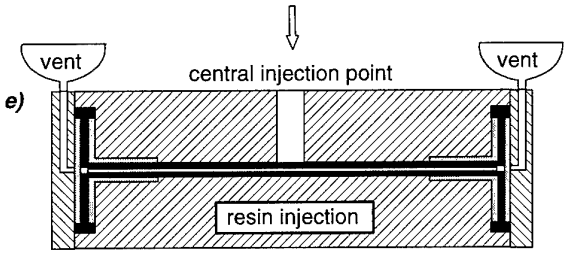

Fig. 13 RTM fabrication concept

The autoclave process uses prepregs, that is sheets of UD fibres or fibre fabrics which are preimpregnated with uncured resin. The prepregs are 'tacky' and convenient for hand laminating into the tool geometry. The RTM fabrication concept is quite different, being based on the injection of a low viscosity liquid resin into a closed tool containing fibre or fabric preforms (Fig. 13). The resin is injected under pressure so that a closed metal tool is required. Fig. 14 shows the elements of the aluminium RTM sine-wave tool. Resin is injected through a central injection point located at the centre of the sine-wave web. Four vents located at the corners of the tool allow air to be replaced by resin during injection. The RTM sine-wave fabrication concept can be described by the following phases:

a. Assembling the fibre fabric preform.
b. Positioning the preform, the fillers and flange laminates in the RTM tool.
c. Sealing and closing the tool.
d. Heating the tool to a temperature of 55°.
e. Assembling the vents and injecting the resin.
f. Curing the resin at room temperature.
g. Releasing the cured component.

Epoxy resin LY 5052 in combination with hardener HY 5052 was used. An injection pressure of 15 bar without vacuum assistance in the mould was used during the injection process. The sine-wave beams produced with this technique had a fibre volume fraction of approximately 52%, no voids and an impregnation of the complete preform. Because of the full metal tool, outer dimensional tolerances can be controlled as accurately as needed. However, the main advantage of the RTM process over the traditional autoclave technology, is the possibility to automate the process thus reducing fabrication costs in series production, and permitting higher part quality through control of the machines.

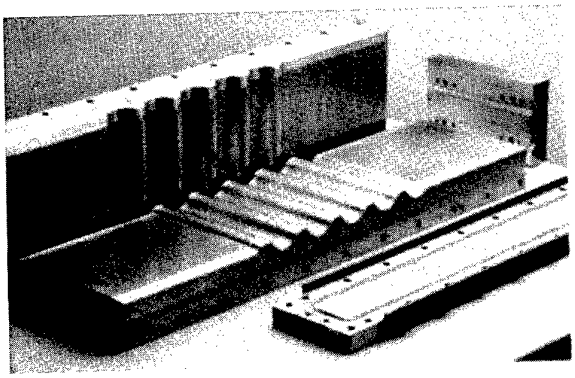

Fig. 14 Elements of the RTM tooling

Evaluation of the thermoset fabrication techniques
The RTM fabrication concept turned out to be very easy in practice with the exception of the positioning and preparing the dry preform. Because the dry fibres lacked any tack, the fibres showed a lot of fibre spring back when positioned in the mould. This problem could be solved by preparing the preform in a preforming press, in which the fibres have a small quantity of thermoplastic binder so that after preheating and pressing the preform retains the required geometry. However this will increase the investment cost one has to make. Because of the high injection pressure of 15 bar used to inject the resin (caused by the high viscosity of the resin) the mould has to be very stiff (and heavy) to guarantee the dimensional tolerances, thus requiring matched metal tooling. This problem may be solved by using a different lower viscosity resin.

The autoclave fabrication concept developed here turned out to be the preferred fabrication concept of the two. The tools (the airtight elastomer panels and the metal frame) had a low weight and were easy to handle. Because the elastomer panels were used as male laminating blocks, positioning the tacky prepreg plies was no problem. Since no vacuum bag was used, preparing the mould for autoclave processing was very simple and fast. However, this approach is labour intensive and not very suitable for automisation. Thus for larger production runs with better quality control the additional investment in the RTM process is required.

4. THERMOPLASTIC COMPOSITE SINE-WAVE BEAM

4.1 Design

Thermoplastic and thermoset composites
In §3 two fabrication techniques for composite subfloor beam structures based on fibre reinforced epoxy resins were described in detail. These are the traditional composites used in aircraft construction. Epoxies are thermosetting resins which are polymerised by a chemical catalyst in a process which usually requires controlled temperature and pressure, as provided in the autoclave. For high quality components the fabrication process, consisting of lamination or resin injection, cure under pressure and temperature, postcure at high temperature, and cooling may take several hours. In order to speed up the fabrication process and to improve component quality, there is in the last few years considerable interest in thermoplastic composite systems. Thermoplastics are polymers which are already polymerised, above their melt temperature they flow easily and on cooling they set hard again. New high performance thermoplastics such as polyetherimide (PEI) or polyetheretherketone (PEEK) have been developed and combined with carbon or aramid fibres in prepreg sheets or tapes for aircraft applications. Components can be fabricated by preheating the prepreg sheets above their melt temperature and thermoforming in a press in matched metal tools. This 'stamping' process can be carried out rapidly, and theoretical cycle times for preheating, forming and demoulding a composite component could be as low as 10 minutes. This technology was investigated at the DLR in a demonstrator project to fabricate a sine-wave beam equivalent to a standard epoxy composite beam traditionally produced by hand lamination in the autoclave.

Thermoplastic design concept
A design and manufacturing concept for a thermoplastic composite sine-wave beam was developed using the same basic component geometry as an existing epoxy composite beam, with the same carbon- and aramid-fibre fabrics, hybrid laminate layup and stacking sequence. A PEI matrix system was chosen which requires a forming temperature of 340°C. The required carbon and aramid fabric/PEI prepregs are commercially available from Ten Cate under the tradename Cetex. The carbon fabric prepreg chosen was CETEX CD 0282 with 5H satin and the aramid prepreg was CETEX VD 0175 with 1/3 crowfoot fabric. Fig. 15 shows the I-beam geometry

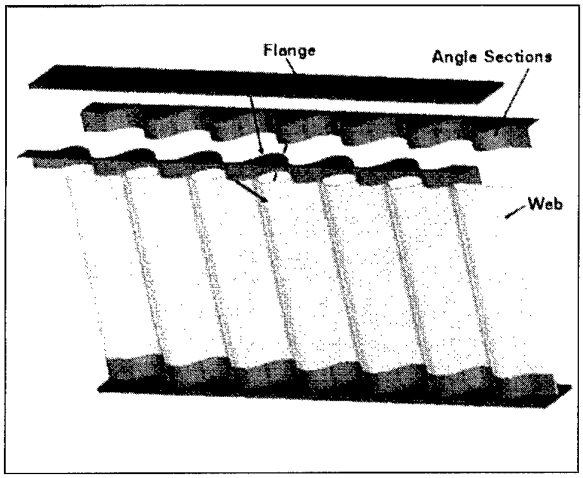

Fig. 15 Design concept for thermoplastic sine-wave beam

and design concept for the thermoplastic variant. The sine wave web is to be thermoformed, and connected to the plane flanges by four thermoformed angle sections. The sine-wave web is an 8-ply laminate containing both carbon and aramid fibre fabric reinforced PEI plies, whilst the angle sections consist of 3 plies of carbon fabric/PEI.

The corrugated web geometry consists of an assemblage of 12 circular tangent ring segments ('sine waves') with flat plates at both ends, similar to the beam shown in Fig. 2. The opening angle of the single segments is 132,5°. The I-beam section considered has 45 mm wide symmetric flanges on top and bottom, an overall length of 500 mm and a height of 200 mm. In order to meet both requirements for shear stiffness and crashworthiness a mixed lay-up of the form $[A_{45}, A_{45}, C_{45}, C_0]_S$ containing 4 carbon (C) and 4 aramid (A) fabric reinforced plies was used for the sine wave web. The subscripts denote the orientations of the warp fibres relative to the longitudinal axis of the part. The placement of the aramid fabric layers at the outside of the laminate is chosen due to the better post crash structural integrity of this stacking sequence compared to others, see §2.1. The angle sections consisted of three carbon fabric reinforced plies in a $[C_{45}, C_{45}, C_{45}]$ lay-up. Triggering is by a ply drop-off trigger of the central carbon fabric plies along the sine wave web just above the intersection with the angle section.

4.2 The thermoforming process

The design of the thermoplastic beam shown in Fig. 15 is suited for automated manufacturing by thermoforming: the two flanges, the web and four connecting angles are manufactured separately and the single parts are bonded or welded together in a second manufacturing step. For the prototype beams a thermoforming process with matched male and female aluminium tools is used for the corrugated web and the connecting angles. Female tooling with rubber pads are an alternative to matched metal tools, as shown schematically in Fig. 16. CAD files for fabrication of the tooling of the sine wave web and the two angle sections (right and left corners) were produced. These files were then used to provide the cutting parameters for the computer driven milling machine, with which the matched aluminium tooling was manufactured.

The main steps in the fabrication process consist of:
a. Stacking up the prepreg plies and consolidating into flat plates.
b. Preheating of preconsolidated laminates in IR array.
c. Transfer to colder press.
d. Thermoforming of sine web and corner sections in the press
e. Cooling under pressure in the press, then in air at RT.
f. Water jet trimming of subcomponents
g. Assembly of beam by adhesive bonding or welding.

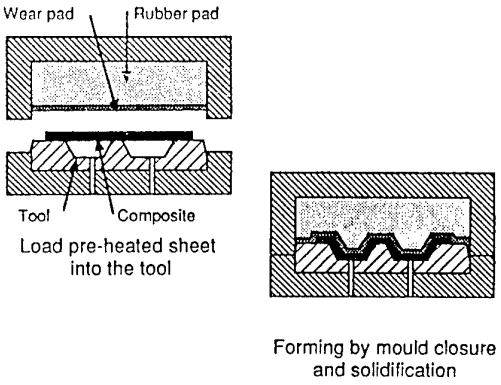

Fig. 16 The thermoforming process

The preconsolidation of the laminated sheets consists of a pressureless contact heating of the plies to melt temperature of 340°C, a 15 min consolidation at 2 bar followed by another 15 min at 20 bar, and subsequent cooling under pressure. This provides a set of laminated thermoplastic flat plates with the correct stacking sequence. These plates have an indefinite shelf life, so that this preconsolidation step may be separated completely from the thermoforming process if required. The laminated sheets are then cut by water jet into plates of a size appropriate for the thermoforming of the parts. These plates are then preheated to 340°C in an IR heater array and transferred immediately to the DLR 400 tonne press, which contains the tools preheated to 190°C. Press closure speed is 20 mm/s which gives a forming time of about 3 s, with a maximum forming pressure of about 60 bar. The first cooling stage takes place in the press under this constant pressure, before part removal and final cooling in air at RT. After water jet trimming assembly by adhesive bonding or resistance welding is carried out in a second stage. Preheating in an IR array takes typically 1-2 mins, transfer and pressing can be completed in less than 30 s, and cooling with the press closed and then open requires about 5 mins before the part can be removed. For series production of the flanges a pultrusion process, and for the webs a roll-

forming process, could also be considered and may be more economic compared to thermoforming.

Evaluation of the thermoforming process
Potentially thermoforming is a very fast production process for composite component elements, in comparison with fabrication methods for thermosetting composites. However, final assembly is an additional step which was not required in the case of the epoxy fabrication methods discussed in §3, where the sine-wave beam with flanges was fabricated as a single integral component. Thermoforming is also a more costly high temperature process requiring more expensive metal tooling, a preheating facility and a large industrial press. Generally this additional investment would be justified by larger production runs of the component, or higher quality control requirements which are possible in a machine controlled process.

Considerable experience is also required in order to produce high quality components, particularly in tool design. Several factors influence the quality of the thermoformed parts. The first is the maximum thickness tolerance of the laminate which can be accommodated by the tool. Small deviations from the nominal thickness lead to an inhomogeneous pressure distribution on the material, which can result in a poor surface quality and inadequate consolidation. This effect may also influenced by the small thickness changes which take place in a ply when it undergoes large in-plane deformations during forming. The second factor is the presence of frozen-in stresses which cause post-moulding distortions in the component. These are due to the high processing temperature and the mismatch in thermal expansion coefficients between fibre and matrix. These first two effects can be reduced with hotter tooling, higher pressures and longer cooling times, which of course increases the cycle time of the process. The third factor is drapability as discussed in §2.1, or more accurately here the formability of UD and fabric prepreg over complex geometries. For double curvature geometries low formability can lead to folding or wrinkling of fabrics, fibre waviness and even fibre fracture in a thermoformed component.

Simulation of the thermoforming process
In order to better understand the problems with the thermoforming process and to give a framework for selection and optimisation of process parameters, a simulation software has been developed for thermoplastic composites. The software generalises an explicit FE code PAM-STAMP [11] developed for metal stamping and computes temperature and pressure distribution, part thickness variation, fibre reorientation during forming and identifies potential regions of materials defects such as poor consolidation and fabric wrinkling. The main deformation and flow mechanisms during forming of thermoplastic composites are interply shear where prepreg plies slide over each other, which is important in forming single

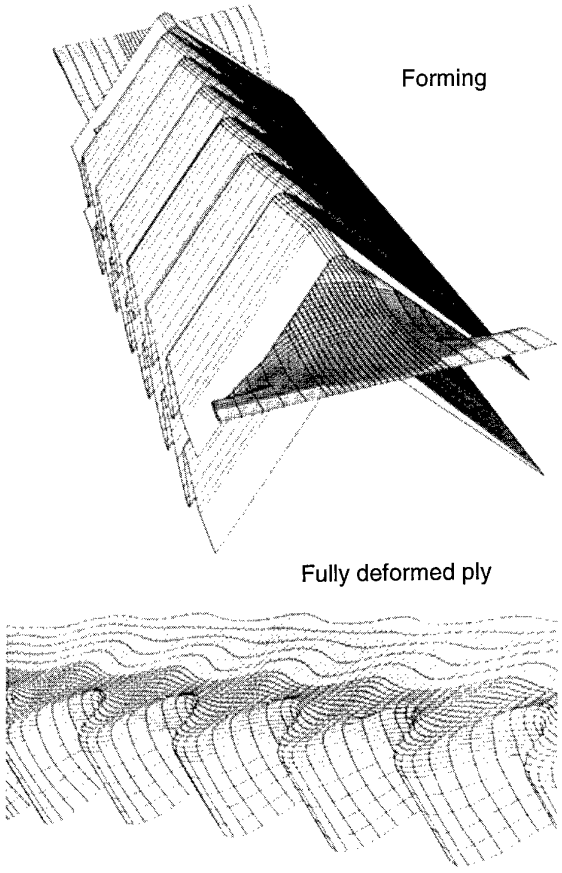

Fig. 17 Thermoforming simulation with PAM-STAMP

curvature shapes, and intraply shear which is required to form double curvature geometries. This causes UD plies to rotate and in fabric plies intraply shear deformations lead to significant changes in fabric angle, and hence to fibre directions in the component. When intraply strains are too high, this can lead to locking and hence local folding or wrinkling in fabrics. In the simulation software new rheological models have been developed to model these deformation processes and prepreg rheological properties determined, as discussed further [12].

Software simulations were carried out to support the process development. In particular they show whether a particular geometry is formable with a selected laminate construction. For the sine-wave beam here, they show that the sine-wave plate which has only a single curvature should be easy to form with the laminate construction defined in §4.1. However this is not the case with the angle section., because of the complexity of the geometry it is only possible to form this double curvature shape without extensive wrinkling if the fabric plies are at 45° to the section longitudinal axis. This is because a required stretch ratio of about 1.25 is required in the fabric in order to form the sine-wave shape, and this is only possible in a fabric stretched at 45° to the fibre directions. Thus in this subcomponent the fabrication aspects determine the possible fibre reinforcement directions. Fig. 17

Table 1: Test results of crush tests on sine-wave beams and cruciforms.

Compo-nent	Fabrication concept	Test	Peak Load (kN)	Average crush load (kN)	Crush length (mm)	Absorbed energy (kJ)	Spec. Absorbed energy (kJ/kg)
Sine 1[1]	Autoclave	Static	92.1	35.0	180	5.64	36.2
Sine 2[1]	Autoclave	Static	83.0	34.3	180	5.58	35.9
Sine 3	Autoclave	Dyn. 9.8 m/s	68.0	17.0	195	3.32	19.7
Sine 4[2]	Autoclave	Dyn. 9.8 m/s	28.0	15.0	190	2.85	17.4
Sine 5[3]	Autoclave	Static	54.0	17.2	142	2.45	21.9
Sine 6[3]	Autoclave	Static	56.5	16.9	114	1.94	21.5
Cruc. 1[4]	Autoclave	Static	53.7	36.2	125	4.53	30.0
Cruc. 2	Autoclave	Dyn. 9.8 m/s	44.0	26.6	132	3.50	21.8
Cruc. 3[5]	Autoclave	Static	83.3	46.1	130	5.99	34.7

[1] Sine-wave beams with three plies UD carbon in the web
[2] Dynamic test at 10° offset
[3] Sine-wave beams with two plies UD carbon in the web
[4] Hybrid with CF plies outside
[5] HTP-element, hybrid with AF plies outside

shows the simulation of the angle section forming as the tool is closing on the laminate, and the final deformed geometry of one of the prepreg plies. Note that the tool geometry in the FE simulation used the same CAD geometry file as that used for machining the aluminium tools, also that the deformed fabric ply wrinkles on the inside of the concavities. The simulation also showed that on the curved surfaces where the shear strains are highest that the fabric angle was reduced from 90° to about 50°. It was found that the thermoformed angle sections had the local wrinkles and the large variation in fabric angle as predicted by the software. As this is only a connecting element without a significant load bearing function, it was decided that these process induced defects would not be significant in practice. However, this example indicates that the final fibre orientations in the thermoformed component cannot freely be defined by the designer, but are dependant on the forming process and tool geometry.

5. COMPRESSION TESTS ON SUBFLOOR ELEMENTS

5.1 Sine-wave beams

A number of static and dynamic compression tests have been carried out on sine-wave beams and the results are summarised in Table 1. The table shows the influence of the web laminate construction on the static crush properties, with the 3 UD ply carbon beam having higher crush loads and energy absorption than the 2 UD ply web beam. Fig. 18 shows a representative crush curve measured during a test on a thermoset sine-wave beam fabricated in the autoclave. Failure initiates at the location of the trigger, followed by a stage where the upper part of the web shears at a relatively low load into the lower part of the web with the angle reinforcements (web locking mechanism), until the web bottoms and picks up load. The dynamic drop tests were carried out on a 3 UD ply beam and

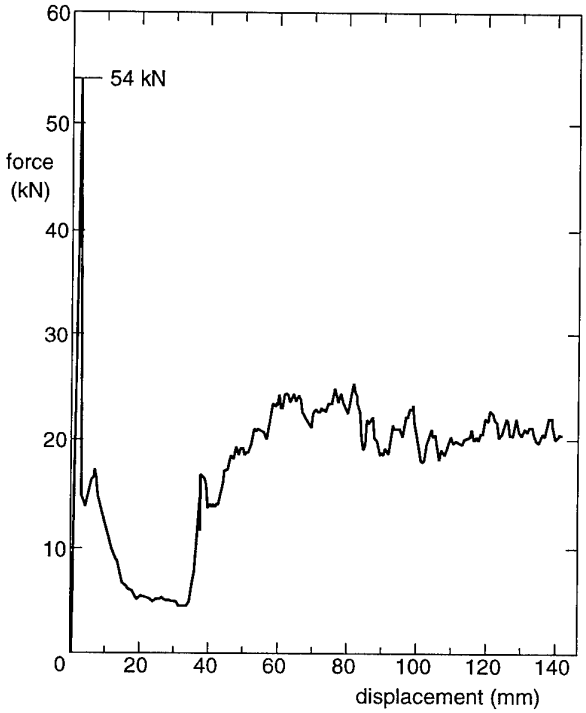

Fig. 18 Load-deflection response in a beam crush test

demonstrated that the failure sequence was identical to that observed in the static tests. However, the tests showed that the sine-wave beams in a dynamic test absorb only about 50% of the energy absorbed in a static test, with much lower average crush loads. The web locking mechanism was found to provide good post-crush integrity both under static and dynamic loading conditions. The reasons for the lower energy absorption in the dynamic tests is not yet fully understood. Contributory effects are changed materials properties at higher loading rates, the influence of dynamic effects on the trigger leading to different, more brittle, failure modes being initiated, and the reduced influence of friction on the energy absorbed at higher impact velocities.

5.2 Cruciform elements

Table 1 also contains some static and dynamic crush test data on hybrid CF/AF cruciform elements. The main difference between Cruciforms 1/2 and Cruciform 3 is that Cruciform 3, which is referred to as the HTP-element in §2.2, has the 45° aramid plies on the outside in the keel and transverse beams, whereas in the first two cruciforms these aramid plies are interior, with carbon plies on the outside. All have J-triggers on the transverse and keel beams. The table shows that load levels, absorbed energy and specific absorbed energy (defined here per mass of damaged material) are similar to those found in the sine-wave beams. Once again it is seen that the dynamic loads and energy absorption are lower than the static crush values.

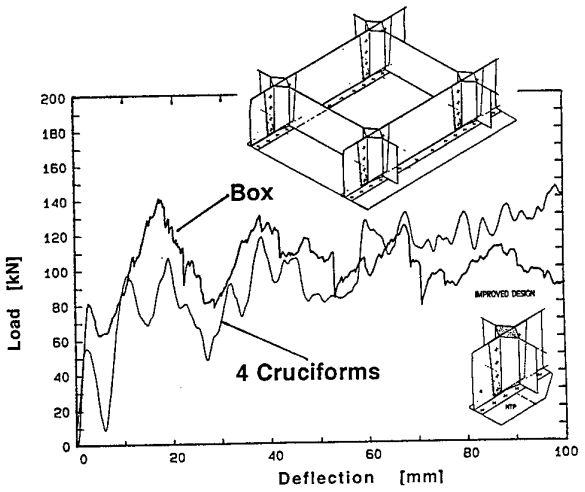

Fig. 19 Crush characteristics of subfloor box and four superimposed cruciforms

Subfloor box structures

Based on the HTP-cruciform test results a crash resistant CF/AF-hybrid subfloor box was designed to the specification of an existing aluminium structure for a commuter airframe. The two keel beams together with the lateral bulkheads form 4 HTP-cruciform type elements. The keel beams and the bulkheads had the form of ribbed plate construction and were connected to the outer skin with J-triggers at the base. All parts were bonded and riveted together. The static test result for the floor box compared with the fourfold test values of a single HTP-element are shown in Figure 19. The box fails first at 80 kN, a second peak occurs at 140 kN, and then a fairly constant average crushing force of about 100 kN develops up to a stroke of 135 mm. The superposition of the crush characteristics of four single HTP-cruciforms up to 80 mm stroke shows that 80 percent of the energy in the box structure is absorbed by folding and fracturing of the cruciforms, and about 20 percent by the beams and bulkheads. The overall structural integrity of the box was poor, since the floor beams were not specially designed for energy absorption. The importance of the test results, shown very clearly in Fig. 19, is that the cruciforms can be the dominant elements in the behaviour of a subfloor structure. Thus particular attention must be given to cruciform design and trigger concepts.

5.3 Tensor skins

A sine-wave beam configuration with two layers of unidirectional carbon tape in the web (Sine 5 and Sine 6 in Table 1) was used for the design of the tensor skin panels. A design case was considered where the tensor skin panel is able to initiate crushing in two sine-wave beams in a box of the subfloor section. This means that the tensor skin panels should survive transverse loads of at least 2 × 57 kN = 114 kN. The inner face of the tensor skin panel consisted of carbon/aramid crowfoot fabric, the outer face consisted of aramid crowfoot fabric embedded in epoxy. Both faces had a three ply [45,0,45] lay-up. The core of the tensor panel had a three ply $[45]_3$ PE-epoxy lay-up.

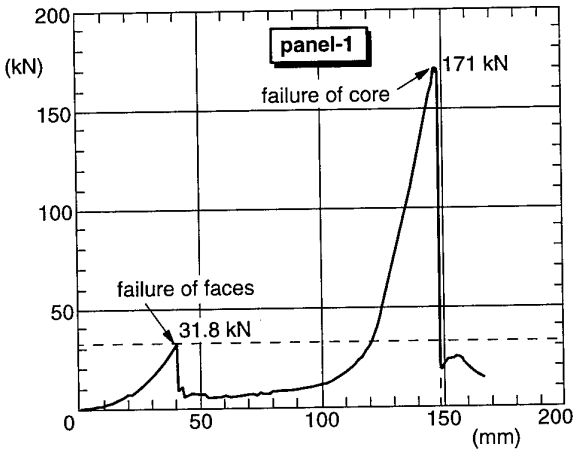

Fig. 20 Load-deflection behaviour of tensor-skin panel

The panel was clamped around all four sides, and indented by a blunt indenter simulating the water pressure in a quasi-static test. As expected the two faces failed early, the corrugated core unfolded and stretched as required to fail at a high load level. Figure 20 shows the load-deflection curve measured during the test of the tensor panel. First the outer face failed at 32 kN, simultaneously with a more gradual tearing of the inner face, after which the load dropped, and the core unfolded. At the end of the unfolding process, the core stretched and the load increased again until final failure occurred at 171 kN with a deflection of 150 mm. Based on this test it was concluded that the sandwich tensor skin meets the design requirement of 114 kN. A shear test has not been carried out yet. However, the core can easily be adapted by changing its geometry if shear loads would lead to premature buckling or failure.

6. CONCLUSIONS

The paper discusses design concepts for helicopter subfloor structural elements out of carbon and aramid fibre reinforced plastics, which have a dual structural and energy absorption function. The basic subfloor element, which is discussed in most detail, is the sine-wave beam. Sine-wave beams have been designed and fabricated with the capability to absorb crash energy, show post crush integrity and with a trigger mechanism that has the potential to sufficiently reduce the crash peak loads. This capability was demonstrated on single beams tested statically and dynamically.

Three different fabrication techniques for fabricating composite sine-wave beams were developed, based on hand lamination with autoclave technology and resin transfer moulding for a thermosetting epoxy composite beam, and thermoforming in a heated press for a thermoplastic PEI composite beam. All three techniques proved to be well suited to the fabrication of net shaped composite sine-wave beams with controllable outer dimensional tolerances. Both the RTM process and thermoforming are suitable for machine controlled series production.

The design of related subfloor structural elements was also discussed. These included a cruciform element at the intersection of two or more floor beams, which requires careful design since if it is too stiff it can dominate the floor crush response and cause peak loads which are too high. Finally a composite skin concept ("tensor skin") has been developed which can provide crashworthiness to a helicopter in case of an impact on water. A test on a tensor skin panel demonstrated the capability of the panel to survive a transverse pressure load, that simulates the water pressure, and to transfer this load to the substructure, i.e. the sine-wave beams.

REFERENCES

1. MIL-STD-1290 A (AV), Military standard light fixed wing and rotary-wing aircraft crash resistance, US Dept. of Defense, September, 1988.
2. J.D. Cronkhite, Design of airframe structures for crash impact, AHS Specialist's Meeting on Crashworthy Design of Rotorcraft, Atlanta, April, 1986.
3. C.M. Kindervater, Crash resistant composite helicopter structural concepts - thermoset and thermoplastic corrugated web designs, AHS National Technical Specialist Meeting, Williamsburg, October 1995.
4. H.G.S.J. Thuis, The influence of included angle variations on the specific energy absorption of composite sine-wave webs, NLR TR 93066 L, 1993.
5. O.K. Bergsma, Computer simulation of 3D forming Processes of Fabric Reinforced Plastics. Ninth International Conference on Composite Materials ICCM-IX, Madrid, Spain, 1993.
6. H.G.S.J. Thuis and J.F.M. Wiggenraad, A tensor skin concept for crashworthiness of helicopters in case of water impact. NLR TP94045 L, presented at the AHS 50th Annual Forum Washington, DC, May 11-13, 1994
7. H.G.S.J. Thuis and J.F.M. Wiggenraad, Development of a fuselage skin concept to enhance the crashworthiness of helicopters in water impact accidents, NLR TR 93491 L, 2-11-1993
8. H.G.S.J. Thuis and V.H. Metz, The Influence of trigger Configurations and Laminate Lay-up on the Failure mode of Composite Crush Cylinders. Composite Structures, Vol. 25, 1993.
9. W. Lestari, H.G.S.J. Thuis and J.F.M. Wiggenraad, The development of a trigger mechanism to reduce peak forces in crash loaded composite sine-wave spars, 20th European Rotorcraft Forum, Amsterdam, 4-7 October 1994.
10. H.G.S.J. Thuis, H.P.J. de Vries, The development of two tooling concepts for the production of composite sine-wave beams. NLR TP 95017 L, presented at the 8th International Conference on Composite Structures Paisley September 1995.
11. PAM-STAMP, Engineering Systems Int. SA, 20 Rue Saarinen, Silic 270, F-94578 Rungis-Cedex, France.
12. A.F. Johnson and A.K. Pickett, Numerical simulation of the forming process in long fibre reinforced thermoplastics, CADCOMP 96, Udine, July, 1996.

INTRODUCTION OF BERYLLIUM ALUMINUM CASTINGS IN THE RAH-66 COMANCHE EOSS PROGRAM

J.P. Seinberg
D.P. Tetz
Lockheed Martin Electronics & Missiles
5600 Sand Lake Road, MP-183
Orlando, FL. 32819-8907
and
K.R. Raftery
Nuclear Metals, Inc.
2229 Main Street
Concord, MA. 01742

SUMMARY

Beryllium aluminum alloys, containing greater than 60 weight percent beryllium, are very attractive materials for lightweight and high-stiffness applications. However, due to the inherent problems associated with casting these alloys, processing of beryllium aluminum has generally been restricted to rolling and extrusion of pre-alloyed powder metal compacts. Nuclear Metals, Inc. (NMI), with technical and financial support from the Lockheed Martin Electronics and Missiles (LMEM) RAH-66 Comanche Electro-Optical Sensor System (EOSS) program, has recently developed a family of castable beryllium aluminum alloys suited for production using state-of-the-technology investment casting processes. These new alloys, identified as Beralcast®, yield a fine grain homogenous microstructure with attractive mechanical, physical and thermal properties.

The problems associated with producing beryllium aluminum castings, including molten metal reactivity and a wide solidification range, have been resolved by NMI and LMEM. As a result of the efforts to date, over fifty different Comanche EOSS components of various sizes and complexities will be produced using Beralcast® alloys. In certain cases, where designs are being modified to take full advantage of the Beralcast® properties, component weight savings of up to 50% over conventional materials can be achieved.

Current focus is on the optimization of both casting and associated secondary support processes, material characterization, non-destructive testing, and cost reduction. Developmental program goals, over the next eighteen months, being addressed in a series of programs funded by NMI, LMEM and the Army Aviation Research and Development Center, will provide the technology for the fabrication of large, complex precision investment castings. As a result of these efforts, Beralcast® investment castings will be available in time to support the RAH-66 Comanche EOSS demonstration/validation (Dem/Val) flight hardware program.

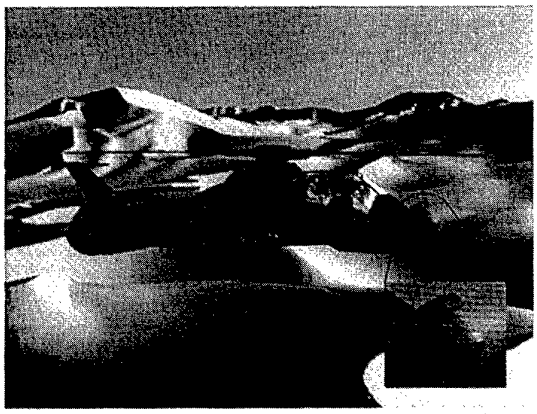

Figure 1: RAH-66 Comanche Highlighting the Electro-Optical Sensor System

1. INTRODUCTION

Today's sophisticated electro-optical, electronic and flight systems demand continued advances in the areas of materials and processing technology. Increasingly stringent military application requirements in such programs as, RAH-66 Comanche, F-22 and PAC-3 Patriot missile upgrade, have resulted in the need for lighter weight, higher stiffness, and more stable,

Paper presented at the FVP Symposium on "Advances in Rotorcraft Technology", held in Ottawa, Canada, 27-30 May 1996, and published in CP-592.

structural housings, electronic packaging and flight hardware with demonstrated producibility and affordability.

Traditional materials possessing the desired properties are often limited in producibility while the materials that are producible to complex configurations frequently require a trade-off in properties sought. Common, lightweight investment cast flight materials, such as, aluminum, titanium and magnesium alloys, as well as metal-matrix composites of these metals, can often achieve complex configurations but have significant weight, stiffness, producibility and/or application problems. Continuous oriented or short fiber resin-matrix composites are very lightweight and stiff but are expensive to produce and not suited to complex configurations that require isotropic properties. Ceramics and ceramic-matrix composites are mostly restricted to specialized applications due to low ductility. Powder metallurgy (PM) produced beryllium meets the criteria of being lightweight and stiff but is inherently, a brittle, anisotropic material that is expensive and limited to configurations that can be machined or formed from hot pressed or hot isostatically pressed (HIP'd) billet product.

In 1991, the RAH-66 Comanche EOSS design presented a challenge to finding a suitable lightweight, high-stiffness, material. Based upon an extensive material trade study, LMEM downselected beryllium aluminum alloys as the most promising material to meet these requirements.

Utilizing the best attributes of each component material and eliminating many individual shortcomings, beryllium aluminum alloys containing greater than 60 weight percent beryllium are very attractive for lightweight, high-stiffness applications. Beryllium aluminum alloys combine the high modulus of elasticity and low density characteristics of beryllium with the excellent processing characteristics and the mechanical property behavior of aluminum. Until recently, however, this material has been commercially available only in a pre-alloyed powder metal wrought form which is, like beryllium, limited to configurations that can be fabricated by machining or forming. This limitation has typically resulted in "buy to fly" ratios of up to 20:1, where the majority of the material used for the part ends up as machined turnings.

The complexity and design to cost (DTC) goals of current and future hardware require a more applicable and cost effective fabrication process, i.e. casting rather than machined "hogouts". For over thirty years, however, attempts to produce investment cast beryllium aluminum hardware were unsuccessful. Beryllium aluminum alloys are difficult to cast primarily due to the exceptionally large differentials in solidification temperatures and lack of solubility between beryllium and aluminum, and the high reactivity of molten beryllium with most other materials.

During the past five years, NMI, with technical and financial support from the LMEM RAH-66 Comanche EOSS program, has developed a family of castable beryllium aluminum alloys termed Beralcast®. These alloys consist of Beralcast® 363 for structural applications, Beralcast® 191 for electronic packaging and, Beralcast® 310 for wrought products made from cast ingots. Table 1 shows the general advantages of Beralcast® material when compared to aluminum and beryllium.

Table 1. General Beralcast® Advantages

Advantages over Cast Aluminum	Advantages over PM Beryllium
• 22% lower density with near equivalent strength to A356 aluminum	• 3 times greater ductility than hot pressed beryllium
• 3 times stiffer (modulus of elasticity in tension)	• Castable for complex & precise net shape configurations
• 4 times better in damping coefficient for stability and jitter reduction	• Weldable for defect repair
• 40% lower in coefficient of thermal expansion (CTE) for matching of mating parts	• Reduced scrap generation and lower cost

2. HISTORY/EVOLUTION OF BERYLLIUM ALUMINUM DEVELOPMENT

The commercial possibilities of beryllium aluminum have been recognized for over seventy-five years. However, the first beryllium aluminum material commercially produced (called "Lockalloy") was not developed until the 1960's by Lockheed and NASA (with NMI participating in some of the early development as a subcontractor to Lockheed) as a high efficiency replacement for magnesium alloys in compression critical structures. Lockalloy was a powder metallurgy (PM) product consisting of 62

weight percent beryllium and 38 weight percent aluminum[1]. This composition was selected, primarily for its elastic modulus (matching the stiffness of steel). Since beryllium and aluminum are mutually insoluble, Lockalloy was looked on as a composite rather than the usual solid solution composition. As a composite structure, it reflected the most desirable properties of each constituent. Lockalloy development efforts culminated in successful applications in missiles as extruded skin stiffeners and on the YF-12 aircraft in rolled sheet form. Kawicki-Beryllico, Inc. (KBI) adapted the process and scaled-up their facilities for production quantities. However, difficulties with producing the alloy economically limited its use to specialized applications, and by the late 1970's, KBI went out of business and Lockalloy was no longer commercially available.

In the 1980's, interest in beryllium aluminum reappeared as a less expensive alternative to pure beryllium . The beryllium aluminum family of materials developed during this time period (primarily based on the original Lockalloy composition) had potential uses in specific applications. However, like beryllium and the original Lockalloy composite material, applications were limited to "smaller" wrought parts that could be made by common powder metallurgy techniques or machined from hot pressed blocks or shapes.

In 1991, LMEM was in the process of evaluating several materials in order to meet the stringent weight and stiffness requirements of the Comanche EOSS program. A concept to fabricate beryllium aluminum investment castings, presented by NMI, appeared to be promising, but required considerable development. LMEM and NMI began a series of development programs to further assess technical feasibility and, based on promising early results have continued this initial development and currently have programs planned through 1997. Summaries of early and current programs are presented in Tables 2 and 3, respectively.

Table 2: Early Stage Beralcast® Development

Development Program	Time Frame	Primary Focus
Pre Phase I:	Oct.-91 - Nov.-91	• Initial Proof of Principle
Comanche Program		
Phase I	Dec.-91 - Jan.-92	• Initial Proof-of-Principle
Phase II	Feb.-92 - Oct.-92	• Initial Alloy Development • Initial Casting Process Development
Phase IIA	Nov.-92	• As-Cast Material Properties • Initial Post Cast Conditioning
Phase IIB	Dec.-92 - Jan.-93	• Material Property Repeatability • Post Cast Conditioning Evaluation
IR&D Programs		
NMI	1991 - 1993	• Additional Alloy Development • Crucible & Mold Contamination & Reactivity Elimination • Pilot Plant Manufacturing • Production Facility Scale-up
LMEM	Mar.-93 - Dec.-93	• Casting Process Controls • Material Property Controls • Preliminary NDI Processes
NMI Capital Improvements	1993	• Installation of "Large-Scale" Furnace Facility

Table 3: Current Stage Beralcast® Development

Development Program	Time Frame	Primary Focus
Comanche EOSS Beryllium Aluminum Specification:	1994 - 1995	• Investment Casting Process Control • Material Qualification and Control
Comanche Streamline Program:		
Phase I:	May-94 - Aug.-94	• Concurrent Engineering Guidelines • Design to Cost Plan • Optical Platform Tooling Trade Study
Phase II:	July-94 - Aug.-95	• Initial Material Characterization (Beralcast® 363) • Material Stability Evaluation • NDI Test and Evaluation • Design to Cost and Concurrent Engineering
Comanche MANTECH:	Mar.-95 - Aug.-96	• Expanded Materials Characterization(Beralcast® 363) • Secondary Support Process Development (Welding, Finishing, Thermal Treatments, Mech. Fastening, etc.) • Updated NDI Process Development
Phase III:	May-95 - May-96	• Initial Material Characterization (Beralcast® 310) • Additional Secondary Support Process Development (Adhesive/Pin Joining, Finishes, etc.)
Manufacturing Technology (MANTECH) Program:		
Phase I:	Aug.-94 - Mar.-95	• Large, Complex Casting Process Development
Phase II:	Apr.-95 - May-96	• Large, Complex Casting Process Development (Continued)
Phase III:	May-96 - Sept.-97	• Recycle Process Development • Computer Modeling & Simulation Development
NMI IR&D and Capital Improvement	1994 - 1997	• Parallel Beralcast® Research and Development • Installed Beralcast® Investment Casting Facility • Production Facility Scale-up

2.1 EARLY DEVELOPMENT PROGRAM

Early program phases focused on development of a castable beryllium aluminum composition, initial manufacturing control processes, preliminary material characterization, and preliminary nondestructive inspection procedures. Between 1991 and 1992, initial material development and casting process development demonstrated some limited success. Castable alloys with moderately good material properties were developed and demonstration castings were produced. However, problems existed with material property repeatability, material contamination, and mold reactivity. These problems led to a decision on the Comanche program not to incorporate beryllium aluminum castings in the EOSS design for the Dem/Val Phase. However, LMEM was still convinced that beryllium aluminum castings had great potential and made the decision to continue to support the development effort, along with NMI, as an internal research and development (IR&D) activity.

In 1993, after NMI developed and evaluated over 400 beryllium aluminum alloy compositions, a family of Beralcast® alloys that met or exceeded the Comanche EOSS requirements was identified. Beralcast® 363 was selected for structural applications based on its combination of strength, ductility, and producibility. In addition, Beralcast® 191 was selected for thermal applications based on its high thermal conductivity, and Beralcast® 310 was selected for extrusions. During this period, a crucible composition that eliminated contamination of the cast material during the melting process and a mold composition that eliminated reactivity with molten Beralcast® material were developed. Casting processes and procedures were also

developed which resulted in the ability to repeatedly fabricate high quality, precision castings of moderate size and complexity. In addition, initial post cast processes such as welding, straightening, stress relieving, and preliminary nondestructive inspection (NDI) techniques for radiography and dye penetrant, were developed for Beralcast® castings. Finally, NMI designed and installed a new, environmentally controlled Beralcast® investment casting facility. This facility included a "large scale" tilt pour furnace that increased NMI's melt capacity over tenfold to approximately 100 lbs.

Using Beralcast® 363 alloy along with the new crucible and mold compositions, the new casting processes and procedures, and the new tilt-pour furnace, two medium sized, moderately complex castings were successfully poured. Using radiographic and dye penetrant procedures, and cutting up one casting, it was determined that there was a vast improvement in casting finish, microstructure, and material properties from results a year earlier. As a result of the successful IR&D programs, the Comanche program reinstated Beralcast® investment castings into the Dem/Val Phase of the EOSS program. The designs of fifty four (54) primary and secondary structural parts of various sizes and complexities were changed to take advantage of the improved weight and stiffness properties of beryllium aluminum. These parts included cast support structure, cast housings for sensors, lenses, and mirrors, and extruded structural tubing.

2. 2 CURRENT DEVELOPMENT PROGRAM

The goal of the current program is to transition from development to production readiness by advancing the Beralcast® technology to a state where large, high complexity, and precision Comanche EOSS hardware can be economically and reliably fabricated in a production operation. This program is composed of a series of sequential development phases funded by LMEM, NMI and the Army Aviation Research and Development Center.

Efforts conducted to date have resulted in several major advances in the technology of cast Beralcast® materials, processes and capabilities. These advances include: generation of Beralcast® material properties, process development for investment casting large, complex configurations, secondary support process development, and NDI process development. Other significant accomplishments include: generation of a Comanche EOSS process control specification for Beralcast® castings, publication of preliminary Beralcast® design guidelines and development of a DTC plan for reducing casting costs prior to full-scale production.

Beralcast® material characterization has been conducted over the past two years to generate material properties for Beralcast® 363, 310, and 191. Currently, this testing is continuing for Beralcast® 363 in order to generate S-basis allowables in accordance with MIL-HDBK-5 requirements. In addition, thermal and dimensional stability studies have been conducted which have demonstrated that the stability of Beralcast® 363 cast material is equal to or greater than that of A356 aluminum cast material.

Process development for large, complex castings used the Comanche EOSS Optical Platform (reference Figure 2) and included an extensive hard tooling and rapid prototype trade study and the demonstration of tooling and mold fabrication capabilities. The process was demonstrated by successfully investment casting two monolithic aluminum EOSS Optical Platforms (reference Figure 2), and fabricating six sets of Beralcast® 363 Optical Platform segments from wood patterns (reference Figure 3). The initial segment sets consisted of four segments each which, with resolution of control process parameter issues such as feed and gating control, resulted in the final segment set being reduced to two large, consolidated segments. In 1996, NMI completed a facility upgrade which increased the Beralcast® casting capacity by an additional 60% in order to handle the largest and most complex Comanche EOSS parts. This upgrade, along with continued casting process development, has permitted the fabrication of the first monolithic Beralcast® 363 Optical Platform in April 1996.

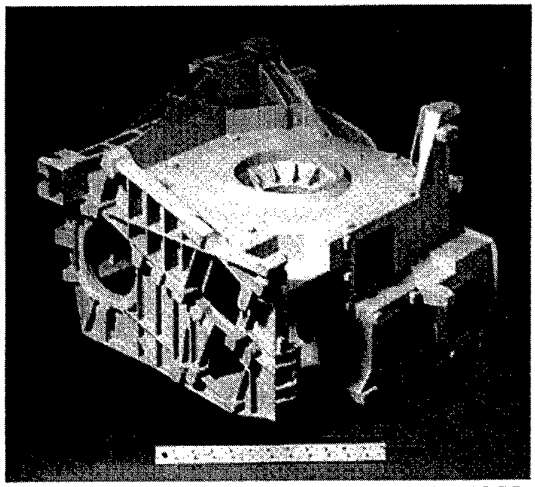

Figure 2: Monolithic Aluminum Comanche EOSS Optical Platform Casting

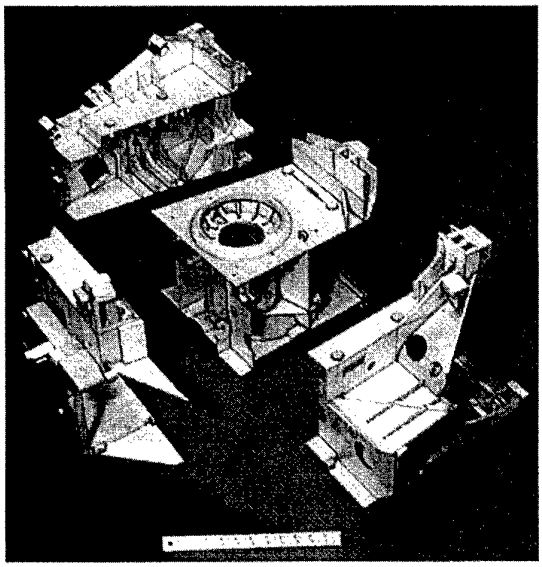

Figure 3: Comanche EOSS
Optical Platform Wood Pattern Segments

In addition to the focus on material characterization and primary casting process development, secondary support processes required for hardware production have been developed. These processes include: casting weld repair, structural joining, thermal stress relief, mechanical finishing, and environmental finishes. Casting weld repair techniques being investigated include gas tungsten arc welding (GTAW) and gas metal arc welding (GMAW). Structural joining techniques being addressed include adhesive bonding, pin and threaded fastener (helicoil) installation, welding (including electron beam), and brazing. Post cast conditioning (HIP) and thermal stress relief processes have been optimized to minimize fabrication generated stresses without inducing detrimental microstructural changes. Mechanical finishing procedures and guidelines, including turning, milling, boring, drilling, reaming, tapping, lapping, and electrical discharge machining (EDM), have been developed to economically meet Comanche EOSS fabrication and dimensional design requirements. Environmental finishing processes for chemical film, anodize, and nickel plating have been developed for Beralcast® and are similar to those of other cast materials and meet Comanche requirements. Salt fog testing to verify the effectiveness of these processes is currently in progress.

NDI process development in the current program has included the maturation and validation of both radiographic and dye penetrant techniques for the evaluation of Beralcast® investment castings. Significant accomplishments include: the development of a nondestructive inspection Beralcast® database, substantiation of radiographic standards and casting grades, and the development of acceptance/rejection criteria based on empirical and analytical data. NDI methods have matured sufficiently to allow them to be used for confirmation of input material and test specimen quality, as well as the assessment of the effects of process or parameter changes.

The final development phase planned for the current program is the MANTECH Phase III recycled material and computer modeling study. During the recycled material task, an optimized process for the multiple use of recycled material will be developed and recycled material characterization testing will be conducted to provide sufficient data to substantiate its use in place of virgin material. The computer modeling and simulation task will focus on mold, feed and gating design modeling, as well as solidification modeling and simulation. These techniques will aid in reducing the number of casting iterations needed to successfully produce deliverable castings and reducing the amount of Beralcast® material required. This will eventually establish a basis for continuous process improvement and cost reduction.

3. INVESTMENT CAST BERYLLIUM ALUMINUM (BERALCAST®) ALLOYS

Beryllium aluminum metal matrix materials exhibit the best characteristics of both beryllium and aluminum. By uniformly distributing beryllium within a continuous matrix of very ductile, non-reactive material, i.e. a face centered cubic (FCC) metal, marked improvement in formability and reduction in sensitivity to fracture can be obtained. Aluminum (a FCC metal) does not react with beryllium, is ductile, and is relatively lightweight, making it a suitable candidate as a matrix material[2].

However, binary beryllium aluminum alloys, such as Lockalloy are inherently difficult to cast due to the mutual insolubility of beryllium and aluminum and the wide solidification temperature range of this alloy system. The solid solubility of beryllium in aluminum is approximately 0.9 weight percent at the eutectic temperature while the solubility of aluminum in beryllium is negligible. A binary alloy of 60 weight percent beryllium and 40 weight percent aluminum has a liquidus temperature (temperature at which solidification begins) of approximately 1160 °C (2120 °F) and a solidus temperature (temperature of complete solidification) of approximately 643 °C (1189 °F), resulting in an approximately 517 °C (963 °F)

solidification range. During the initial solidification, primary beryllium dendrites form in the liquid to make a two phase solid-liquid mixture. The beryllium dendrites produce a tortuous channel for the liquid to flow through and fill during the last stages of solidification. As a result, shrinkage cavities develop, and these alloys typically exhibit a large amount of microporosity in the as-cast condition. This feature greatly affects the properties and integrity of the casting. Porosity leads to low strength and premature failure at relatively low ductility. In addition, binary alloy castings have a relative coarse microstructure of beryllium distributed in an aluminum matrix, and such coarse microstructures generally result in low strength and low ductility. Accordingly, previous attempts to produce binary beryllium aluminum alloys by casting were unsuccessful.

During the past five years, a much more ductile beryllium aluminum (Beralcast®) family of alloys has been developed. Beralcast® alloys represent an in-situ two phase matrix composite consisting of selected alloy combinations of beryllium, germanium, silver, cobalt, silicon, and aluminum as described in Table 4.

Beralcast® 363 is the primary alloy in the Beralcast® family of materials. Beralcast® 363 alloy elements were selected to improve castability, microstructure and enhance mechanical properties without post cast thermal treatments[3]. It has been found that including silver, germanium and cobalt creates an as-cast alloy having very desirable properties with greatly improved strength and ductility over cast binary beryllium aluminum alloys. In the aluminum matrix phase, silver increases the strength and ductility of the alloy while germanium also increases ductility and aids in castability as a fluidity enhancer. These advantages are believed to be related to interactions between silver and germanium in the Beralcast® alloys, and not due to the silver or germanium acting alone. The beryllium phase is strengthened through the addition of cobalt which increases yield strength of the alloy by up to 25 percent without a decreasing ductility. Although Beralcast® 363 alloys do not require post cast thermal treatment to obtain strength and ductility suitable for structural usage, HIPing has been found to further increase both strength (approximately 5 percent for yield strength and approximately 15 percent for ultimate tensile strength) and ductility (up to 100%) without causing dimensional distortion in precision cast parts.

Beralcast® 191 represents an alloy variant formulated for better thermal properties. With a moderate decrease in strength properties and a modulus of elasticity the same as Beralcast® 363, thermal conductivity of the 191 alloy can be increased by approximately 75%. The strength of Beralcast® 191 is provided by the primary beryllium phase while ductility results from the aluminum, silicon, silver alloy matrix phase. Silicon provides fluidity, required for casting, while the silver provides for strengthening of the aluminum phase. Beralcast® 191 alloy typically receives a solution, quench and aging (SQA) post cast thermal treatment to optimize precipitation of a secondary silicon-silver phase within the aluminum matrix.

Beralcast® 310 represents an alloy similar to the 191 alloy. The alloy may be wrought (e.g. extruded) after casting to increase ductility and strength. The enhanced properties observed in the Beralcast® 310 alloy are provided by the warm work imparted during fabrication. Wrought Beralcast® 310 properties are highly directional and textured along the axis of deformation.

Material characterization for Beralcast® 363, 310 and 191 has included the testing of more than one thousand specimens. This testing has resulted in the generation of statistically significant data on seventeen different chemical, mechanical, physical, thermal and electrical properties. Several of the typical ("average") properties for Beralcast® alloys are provide in Table 5 below. (17)

Table 4: Nominal Beralcast® Family Compositions

Element	Beralcast® 363 (Weight Percent)	Beralcast® 191 (Weight Percent)	Beralcast® 310 (Weight Percent)
Beryllium (Be)	Balance	Balance	Balance
Aluminum (Al)	27.5 - 34.5	28.5 - 34.5	28.5 - 34.5
Silver (Ag)	2.65 - 3.35	1.80 - 3.20	1.80 - 3.20
Cobalt (Co)	0.65 - 1.35	N/A	N/A
Germanium (Ge)	0.55 - 0.95	N/A	N/A
Silicon (Si)	N/A	0.65 - 2.35	0.05 - 0.15

Beralcast® material can be cast with a relatively fine microstructure into highly complex shapes without microporosity or segregation that is detrimental to mechanical properties. Typical microstructures of alloys 363, 191 and 310 are shown in the photomicrographs below (Figures 4, 5, and 6). In each photomicrograph, the dark phase represents the beryllium and the light phase the aluminum alloy matrix. Alloy 363 and 191 as-cast microstructures are, typically, equiaxed while the microstructure of alloy 310 yields a distinctly textured and aligned morphology due to post cast fabrication processing.

Table 5: Typical ("Average") Beralcast® Properties

Property Description	Beralcast® 363	Beralcast® 191	Beralcast® 310
Density, Maximum: g/cm^3 @ 25°C (lbs/in^3 @ 77°F)	2.19 (0.079)	2.19 (0.079)	2.19 (0.079)
Modulus of Elasticity in Tension: GPa @ 25°C (mpsi @ 77°F)	217.2 (29.9)	217.2 (29.9)	217.2 (29.9)
Yield Strength: MPa @ 25°C (ksi @ 77°F)	212.3 (31.0)	137.9 (20.0)	325.4 (47.2)
Ultimate Tensile Strength: MPa @ 25°C (ksi @ 77°F)	289.6 (42.0)	196.5 (28.5)	422.6 (61.8)
Elongation: (2.54 cm (1 in) Gage): All Orientations: % @ 25°C (77°F):	(All Orientations) 4.0	(All Orientations) 1.7	(Longitudinal) 13.2
Reduction in Area: (2.54 cm (1 in) Gage): All Orientations: % @ 25°C (77°F):	(All Orientations) 4.2	(All Orientations) 2.0	(Longitudinal) 17.4
Poisson's Ratio:	0.2	0.2	TBD
Axial Fatigue (R=1.0, 10^7 cycles): MPa @ 25°C (ksi @ 77°F)	117.2 (17)	TBD (TBD)	(Longitudinal) 220.6 (32)
Compressive Strength: MPa @ 25°C (ksi @ 77°F)	226.1 (32.8)	TBD (TBD)	318.5 (46.2)
Double Shear Strength: MPa @ 25°C (ksi @ 77°F)	247.5 (35.9)	TBD (TBD)	299.9 (43.5)
Bending Modulus: GPa @ 25°C (mpsi @ 77°F)	174.4 (25.3)	TBD (TBD)	179.3 (26.0)
Pin-Type Bearing (e/D-1.5): Yield Strength: MPa @ 25°C (mpsi @ 77°F)	406.8 (59.0)	TBD (TBD)	492.3 (68.0)
Pin-Type Bearing (e/D-1.5): Ultimate Strength: MPa @ 25°C (mpsi @ 77°F)	465.4 (67.5)	TBD (TBD)	566.1 (71.4)
Pin-Type Bearing (e/D-2.0): Yield Strength: MPa @ 25°C (mpsi @ 77°F)	476.4 (69.1)	TBD (TBD)	566.1 (82.1)
Pin-Type Bearing (e/D-2.0): Ultimate Strength: MPa @ 25°C (mpsi @ 77°F)	618.5 (89.7)	TBD (TBD)	606.1 (87.9)
Coefficient of Thermal Expansion (CTE, α_{mt}): µm/m (ppm) °C @ 25°C (°F @ 77°F):	12.7 (7.0)	12.0 (6.6)	(Longitudinal) 13.2 (7.3)
Specific Heat: J/kg-°C @ 20°C (Btu/lb-°F @ 68°F):	1359.8 (0.58)	TBD (TBD)	TBD (TBD)
Thermal Conductivity: W/m-°K @ 25°C (Btu/h-ft-°F @ 77°F):	108 (62.4)	190 (109.8)	TBD (TBD)

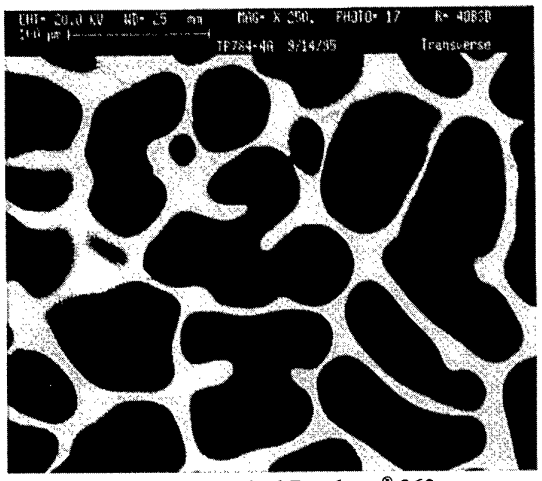

Figure 4: Typical Beralcast® 363
As-Cast Microstructure (Transverse)

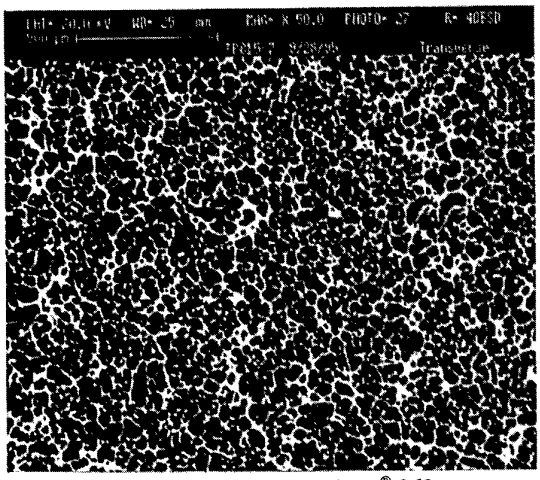

Figure 5: Typical Beralcast® 363
As-Cast Microstructure (Transverse)

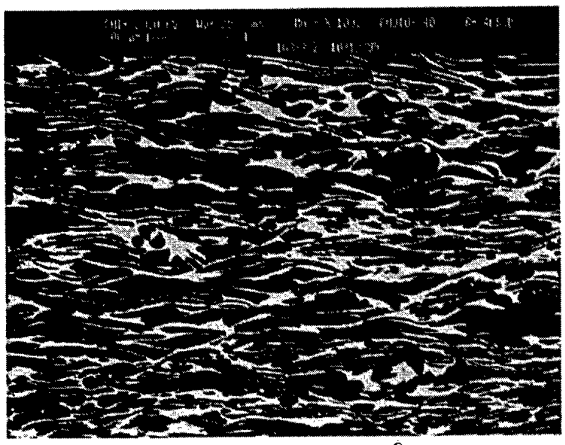

Figure 6: Typical Beralcast® 310
Cast and Extruded Microstructure (Transverse)

4. BERALCAST® MANUFACTURING:

In addition to material and process development, NMI and LMEM have conducted extensive validation of the entire manufacturing process. This included verification of part to part consistency using both destructive and non-destructive inspection techniques. During manufacturing process development, emphasis was placed on utilizing known, mature manufacturing processes. This permitted benchmarking of this casting process against aluminum casting processes. With the exception of alloy melting and casting equipment, the only discernible differences between these processes are the extensive ventilation equipment required for Beralcast® to limit the amount of airborne particles generated during manufacturing.

Beralcast® investment castings are currently produced at NMI's Concord, Massachusetts facility. For this facility, NMI installed a vacuum induction melting tilt-pour furnace specifically for melting and casting Beralcast® material[4]. Although vacuum melting was not required, it was preferred to assure melt degassing and prevent melt oxidation. The casting furnace, shown in Figure 7, has been configured with various size melting coils and crucibles to allow production of melts from 7 kgs (15.4 lbs) to 75 kgs (165 lbs). The crucibles and coils are positioned in the vacuum melt chamber which is situated above the vacuum mold chamber. These two chambers are separated by a vacuum isolation valve which isolates each chamber. This allows alloy melting under vacuum in the upper chamber while molds are loaded into or removed from the lower chamber.

Figure 7: Vacuum Induction Investment Casting Furnace

The mold chamber can handle individual molds as large as 0.9 meters (2.95 feet) in any dimension and is equipped with internal heating elements to preheat and maintain mold temperatures up to 1000 °C. (1832 °F). The mold chamber contains a lift platform that positions molds small enough to pass though the vacuum isolation valve, less than 0.6 meter (1.97 foot) in diameter, directly under the melt crucible for filling. This limits the fall height of the melt stream and aids in minimizing melt turbulence and metal splashing. For larger molds that cannot fit though the vacuum isolation valve, a process which uses a pouring tube to direct the molten metal from the upper chamber to the mold in the lower chamber, has been developed.

A typical melt cycle begins with preparation of the beryllium aluminum charge materials and alloy additions. Castings can be produced from either virgin elemental materials or recycled input materials. Elemental materials consist of low grade vacuum cast beryllium (99.5% purity) and high purity aluminum, grade 1188 or equivalent. The alloying elements consist of commercial grades of germanium, cobalt and silver for Beralcast® 363, and silver and silicon for Beralcast® 191 and 310. Recycle input materials consist of high-quality remelted beryllium aluminum cast material. The use of master melting of qualified ingot materials has also been validated but is not economically feasible using the current maximum melt capacity. Master melts will be introduced into the production process once the melt capacity has been increased beyond 400 kgs (880 lbs) and will result in reduced costs and increased productivity.

The charge is loaded into the melt crucible and the furnace chamber is then evacuated. Once the desired vacuum is achieved, the melt is uniformly heated to sufficiently melt and adequately stir the charge. Once molten, the charge is held at sufficient temperature to insure adequate degassing. Melt temperature is closely monitored using thermocouples and pyrometry techniques.

Investment molds, produced from a unique formulation developed specifically for this alloy, are baked out to remove moisture prior to casting preheat. These molds are fabricated using either conventional wax patterns or rapid prototype patterns. NMI has demonstrated all of the current rapid prototype casting pattern fabrication techniques but predominantly utilizes Stereo Lithography Apparatus (SLA) or wood prototype patterns. Molds are fabricated for NMI at Nu-Cast Inc. (NCI), Londonderry, New Hampshire, a leading producer of thin-walled, lightweight aluminum castings, where a dedicated mold fabrication line has been installed to support the manufacture of Beralcast® investment molds. Once molds are assembled and the patterns are removed they are delivered to NMI for casting. Prior to casting at NMI, the molds are preheated to aid in mold filling either outside of the casting furnace in air or inside the furnace vacuum mold chamber. Externally heated molds are used when castings are produced using multiple pouring techniques where one furnace charge is used to fill more than one mold. Mold preheat temperature is selected based on the size, wall thickness and complexity of the casting. Larger parts with thin walls generally require higher mold preheat temperatures.

Once both the melt and mold have reached the desired temperatures, the vacuum isolation valve between the furnace and mold chamber is opened and the mold is positioned under the crucible. The casting is poured by tilting the crucible containing the molten charge after which the mold is retracted back into the mold chamber. The isolation valve is then closed to allow for either reheating of the remaining charge or charging of another melt while the casting solidifies under vacuum in order to control the cast microstructure. When the casting has completely solidified, the mold chamber is backfilled with inert gas to accelerate cooling and facilitate handling.

After the casting has cooled to room temperature, the mold is removed using a high pressure water jet, the gates and risers are manually trimmed, and the cast surface is cleaned by abrasive grit blasting. The casting is then straightened, weld repaired, if required, and then released for initial inspection, prior to post cast processing, such as HIPing or SQA, if required. Final inspection typically consists of dye penetrant, radiography, visual, and dimension inspection. In addition, depending on customer requirements, integral or excised test specimens are mechanically tested to verify material properties.

Inspected castings are released for final machining by NMI or one of several qualified machining facilities which possess the necessary ventilation equipment to safely machine beryllium containing alloys. Cutting, grinding, etching, and machining are all controlled to limit the generation of airborne beryllium alloy dust or fumes. All of these operations are performed under strict environmental and health safety controls consistent with OSHA regulations for beryllium containing materials.

5. COST REDUCTION:

An important factor, monitored throughout the entire process development program, was the economic viability of the technology. The RAH-66 Comanche EOSS program has a stringent weight requirement, which led to the use of beryllium aluminum, but also has equally stringent cost goals. These goals require that the cost of this technology be substantially reduced in order to be viable. In order to meet the cost goals of the program, two approaches were utilized: concurrent engineering to lower hardware costs during the design phase of the program, and DTC to reduce the projected cost for the production phase of the program. Concurrent engineering was applied to the designs of both the castings and finished machined hardware. The intricacies of the beryllium aluminum casting process require slight design modifications to account for shrinkage differentials and increased fillet and corner radii requirements[5]. The concurrent engineering procedures consisted of a hardware design review which encompassed the entire manufacturing process. It included assessments of the design for: wax injection tooling, mold manufacture, casting manufacture, post cast processes, inspectability, machinability, and finishing processes. The cost savings from this approach include reduced tool cost and lead time, reduced casting design cycle, reduced material cost, and reduced machining cost.

In order to reduce production costs, a DTC plan was generated for the Comanche EOSS program. This defined program cost goals, current cost projections, and concepts to achieve the cost goals. As a result of efforts to date, the projected shipset cost of the Beralcast® hardware in the production Comanche EOSS system has been reduced five fold since 1993 (reference Figure 8).

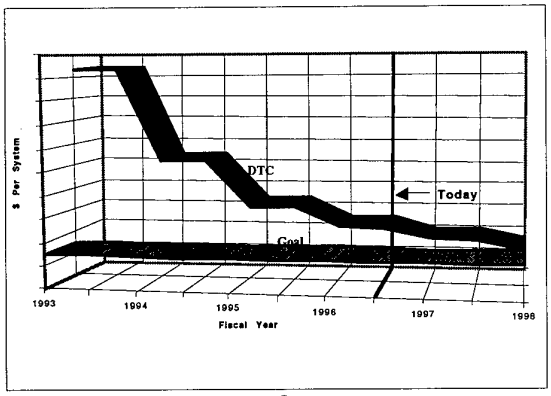

Figure 8: Beralcast® DTC Progression

Major cost reduction concepts include utilization of lower cost casting material, such as recycled beryllium aluminum, process improvements for the production of beryllium input material, and the replacement of the current casting fabrication facility with a new production casting fabrication facility.

NMI is planning to expand their current casting facility to a production level that will meet the growing demand for Beralcast® castings. This facility will lower costs, increase the melt capacity eightfold, and increase casting throughput capacity tenfold over the current facility. The facility will also include the support and ancillary equipment necessary to process these castings through final inspection and will include expanded machining capabilities to support short lead time, rapid prototype applications. NMI anticipates that this facility expansion will be completed during the 1997 calendar year.

5. CURRENT AND FUTURE BERALCAST® APPLICATIONS:

Beralcast® investment castings are being used and considered in many applications where weight and stiffness are critical to the design. Uses also include applications where there are volume constraints combined with complex thermal load management, such as, in electronic packaging applications. Table 6 shows some of the potential applications for Beralcast® technology.

Table 6: Applications for Beralcast® Technology

• A higher performance and/or lower cost replacement material for cast aluminum, magnesium, titanium, metal and nonmetallic composites, beryllium and powder metallurgy beryllium aluminum.
• Electro-optical housings, infrared systems, optical material: Night vision lightweight FLIR systems.
• Aircraft/missile/satellite structure: Missile guidance components (PAC-3) Engine gearbox (F-22) Miniature inertial measurement units (MIMU)
• Thermal control components: Heat sinks, liquid flow through (LFT) & pin fin heat exchangers, brazed chassis, etc.
• Electrical and electronic packaging: Chassis, enclosures, assemblies/boxes, air plenums, heat sinks, etc. (F- 22 and V-22)
• Computers and audio components, as well as medical and recreational equipment.

6. CONCLUDING REMARKS:

NMI and LMEM have developed the capability to produce complex Beralcast® investment castings in order to meet the stringent weight, stiffness and economic requirements of the RAH-66 Comanche EOSS program. This technology is currently being utilized or considered by several other military and aerospace programs.

Some of the results of this effort include: the generation of Beralcast® casting design guidelines, the development of a material properties database, the development of a validated casting process, the installation of a prototype and low rate production casting facility, production of castings in sizes ranging from 5 to 82 cm (~2 to ~32 in.) in maximum dimension and from a few grams (ounces) to over 20 kgs (44 lbs.), the demonstration of casting fabrication for low to high complexity parts on a consistent and repeatable basis, the development of secondary support processes (e.g., weld repair, stress relief, and environmental finishes), the development of machining and joining procedures, the development of nondestructive inspection processes (e.g., radiography and dye penetrant), and the development of cost reduction programs such as concurrent engineering and design to cost.

7. REFERENCES:

1. London, Gilbert J. "Alloys and Composites", Beryllium Science and Technology, Volume 2, pgs. 297-308.

2. Nachtrab, William T., Levoy, Nancy F. and Raftery, Kevin, R. "Lightweight, High Strength Beryllium-Aluminum Alloy". U.S. Patent No. 5,421,916; 6/6/95, Pgs. 1-8.

3. Nachtrab, William T., Levoy, Nancy F and White, Raymond L. "Ductile, Lightweight, High Strength Beryllium-Aluminum Cast Composite Alloy". U.S. Patent No. 5,417,778.

4. Nachtrab, William T., Raftery, Kevin R. and Sanborn, Thomas D. "Beryllium Aluminum - A New Alloy for Investment Casting". 3rd Near Net Shape Manufacturing Conference, 10/27/93.

5. King, William C. and Raftery, Kevin R. "Concurrent Engineering Procedures for Beralcast®, Beryllium-Aluminum Investment Casting". NMI Internal Control Document, 8/9/95, pgs. 1-26.

REDUCTION OF THE NOISE SIGNATURE OF THE EUROCOPTER EC 135

G. Niesl
EUROCOPTER DEUTSCHLAND
Dep. D/EE41
D-81663 München, Germany

G. Arnaud
EUROCOPTER FRANCE
Dep. DF/DTAE
F-13725 Marignane, France

SUMMARY

The paper presents an overview of the acoustic design of the EUROCOPTER EC 135 helicopter. The layout of the different noise relevant components were supported by measurements on the test bench and in the wind tunnel. The experimental and theoretical investigations were accompanied by acoustic measurements on the BO 105 and the BO 108. The results are discussed with respect to neighbourhood noise emission and acoustic detectability aspects. The low noise design of the fan-in-fin tail rotor (FENESTRON®) and the positive effect on the improved noise signature of the EC 135 is presented and compared to BO 105 and BO 108 with a conventional tail rotor. The main rotor of the EC 135 shows a reduced noise signature especially at higher Mach numbers due to the reduced blade thickness at the tip region, the introduction of a new airfoil generation, and an advanced blade shape. The low noise concept of the EC 135 is proved by noise measurements with ground based microphones.

NOMENCLATURE

SPL	Sound Pressure Level
SEL	Sound Exposure Level (time integrated A-weighted noise level)
PNL	Perceived Noise Level
EPNL	Effective Perceived Noise Level
MCP	maximum continuous power
v_H	maximum cruise speed at MCP
ktas	knots true airspeed
M_{TO}	Take-off weight
BVI	Blade Vortex Interaction
FAR	Federal Aviation Regulation
ICAO	International Civil Aviation Organisation
DNW	German-Dutch Wind tunnel

FENESTRON® is a registered trademark of EUROCOPTER FRANCE

1. INTRODUCTION

Because of their considerable high noise levels and their characteristic noise signature, helicopters suffer from the disadvantage that they can be heard from great distances. A low noise level is important for military operations, on the one hand to allow the helicopter a large field of unthreaded operations, on the other hand to minimise the warning time between detection and approaching at the enemy position. In peace time, also military helicopter operations have a low acceptability near populated areas mainly due to their noise emission. Here, the maximum flyover noise level and the duration of the flyover are the main parameters affecting the neighbourhood noise.

From the civil side, the helicopter noise must comply with the maximum permitted noise levels given by the civil certification rules (Ref. 1, 2). Even if the current limitations are regarded as non-stringent, a certain risk not to comply with the limits exists due to the lack of accurate prediction technology in the early design stage especially for interaction noise and the noise emission at high flight speeds. In addition to the noise certification constraints, in highly populated areas local authorities introduced restrictions to helicopter operations which are applied in some cases also to military helicopter bases.

During military operation, the implications from the noise emission are different. The dominating requirement is a low detectability of the helicopter by the human ear and even more demanding by acoustic sensing devices. For long distances, the lower main rotor harmonics dominate the noise emission of the helicopter especially of the approaching helicopter. Due to the low sound attenuation of the air and the low ground absorption at these very low frequencies, the helicopter harmonic noise propagates readily over distances of several kilometers which makes it not only possible to detect the helicopter quite early but also enables a friend/enemy recognition due to the main and tail rotor RPM ratio.

Figure 1: EC 135

Within the common development of the EC 135 helicopter, EUROCOPTER DEUTSCHLAND and

Paper presented at the FVP Symposium on "Advances in Rotorcraft Technology", held in Ottawa, Canada, 27-30 May 1996, and published in CP-592.

EUROCOPTER FRANCE made intensive efforts to reduce the noise emission. Some of the measures were already successfully applied to several EC helicopter like the BO 105 CBS-5 and the Tiger. Even if the measures are aiming on environmental noise reduction, most of them were also effective with regard to acoustic detection requirements.

The paper describes the noise reducing technologies which were developed during the design process of the EC 135 helicopter (Figure 1). It can be shown, that the acoustic signature of the EC 135 will comply well with both, military and civil applications of the helicopter.

2. DETECTABILITY ASPECTS

There are four main aspects which influence the acoustic detection probability: The characteristics of the noise source, the sound radiation conditions concerning damping and absorbing effects, the masking of the sound by other sources at the receiver, and the characteristics of the human ear or the noise detecting sensor. Considering the unweighted radiated acoustic energy, helicopters in horizontal flight condition have their main noise emission in the low frequency range up to about 500 Hz. At these low frequencies, the damping effects during the sound propagation are very small and do nearly not influence the sound radiation. But, the audible threshold of the human ear rises very rapidly at low frequencies, thus the critical frequency range for acoustic detection of helicopters is given from about 100 Hz to 500 Hz, dependant on the influence of masking noise sources. Figure 2 illustrates the contrary frequency dependencies of the different parameters influencing the military acoustic detection.

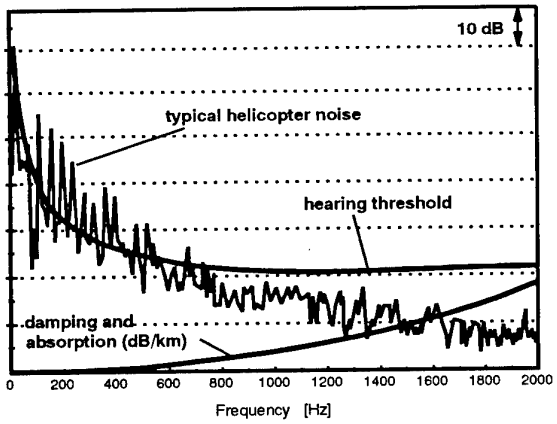

Figure 2: Interdependence of helicopter noise, hearing sensitivity and atmospheric sound attenuation

For the estimation of the aural detection distances, theoretical and/or experimental helicopter noise data were used in far field sound radiation models (ref. 3, 4). These calculations are based on 1/3-octave band data because this is considered as a minimum requirement due to the pulsating nature of the rotor noise. Besides the spherical spreading of the noise, the propagation models cover the sound attenuation in air, the attenuation caused by atmospheric turbulence, and the ground absorption. After the propagation of the sound to the observer, the resulting noise is compared with the threshold for aural detection. The definition of the threshold is based on

- the hearing characteristics of the human ear,
- the masking of the helicopter noise by background noise or other noise sources (e.g. engine noise, combat field noise, ship noise environment), and
- the sensitivity of the human ear to detect tonal components (human response to pure tones).

Both, the characteristic of the helicopter noise and the propagation conditions, may lead to very large detection distances up to 10 km under worst circumstances.

3. MAIN ROTOR NOISE REDUCTION

Starting from the BO 105 rotor design, different measures were theoretically investigated and tested first in the wind tunnel and then on the BO 105 or the BO 108 which can be considered as a prototype version of the EC 135 with an conventional type 2-bladed tail rotor.

3.1 Blade Shape and Profile

The first approach in main rotor noise reduction concerns the blade shape and the influence of the blade profile. The blade tip design was supported by the calculation of the critical Mach number distribution on and around the blade tip. As an example, in Figure 3, the calculated Mach number contours are shown for the upper blade surface for various blade tip designs at the 90 deg rotor azimuth position. The comparison shows the reduced supersonic regions on the blade surface by intensifying the complexity of the blade tip from the rectangular shape (Fig. 3a) to the tapered (Fig. 3b, 3c) and finally to the parabolic blade tip configuration (Fig. 3d). The investigation included also the effect of the new airfoil family DM-H which was developed by DLR Braunschweig and EUROCOPTER DEUTSCHLAND. These profiles provide a general improvement of the transonic characteristics and a significant drag reduction in comparison to the NACA 23012 airfoil used on the BO 105 helicopter.

By sweeping the quarterline at the blade tip (parabolic tip), the incident Mach number can be reduced, the supersonic region is limited, and the spreading of these regions beyond the blade tip is cut down. At higher flight speeds, the supersonic region is extended to the „sonic cylinder" around the rotation axis. Here, the freestream velocities appear to exceed the sonic speed in the rotating reference frame which is responsible for the excitation of a highly efficient noise source.

In order to explore the connected noise emission of main and tail rotor, tests were performed in the German Dutch wind tunnel (DNW) to separate the noise radiation of main and tail rotor and the related main/tail rotor interactions. Within this research programme conducted by the DLR Braunschweig (Ref. 5),

two 40% geometrically and dynamically scaled model rotors were used: a conventional BO 105 main and tail rotor system and an advanced main and tail rotor based on the design of the BO 108 helicopter. The latter one involves the use of tapered blades and the DM-H airfoil family on the main rotor (Fig. 3c) and an aerodynamically improved tail rotor with S102E profiles, a linear twist and a trapezoidal blade shape. The acoustic data were gathered in the open test section of the DNW aeroacoustic test facility. The rotor trim conditions for the simulated flight procedures were recalculated by flight mechanic codes and supported by flight test data of the BO 105.

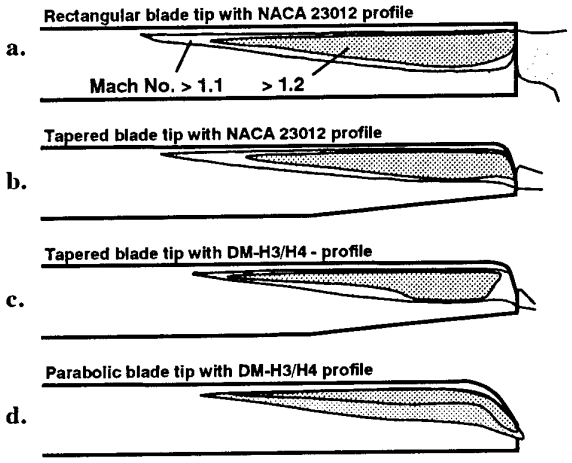

Figure 3: Mach number distribution for different blade planforms and airfoils (270 km/h flight speed, M=0,86 and 90 deg azimuth position)

In Figure 4, noise contour plots measured in a plane 2.4 m below the model rotor hub are shown for both model rotor systems. An average noise reduction throughout the contour plot was obtained for the new BO 108 rotor system by about 1.3 PNdB, whereas the maximum noise was reduced by 2 PNdB. The noise reduction was confirmed by a flight test of the advanced rotor on a BO 105 helicopter. For a flight speed of 55 m/s, the EPNL value (3 microphones) was reduced by 1.3 EPNdB, which corresponds well with the average reduction measured in the wind tunnel.

The maximum noise in Figure 4 is radiated for both rotor systems by the tail rotor on the retreating main rotor blade side. The dominance of the noise emission of conventional tail rotor configurations in horizontal flyover condition can be seen from Figure 5, where the mid frequency noise radiation for the isolated main rotor, the isolated tail rotor and the main/tail rotor configuration is shown at 60 m/s flight speed. Since the mid frequency noise from wind tunnel test results correlates well with the A-weighting of full scale helicopter testing, the neighbourhood noise level during flyover and take-off is influenced mainly by the two-bladed tail rotor.

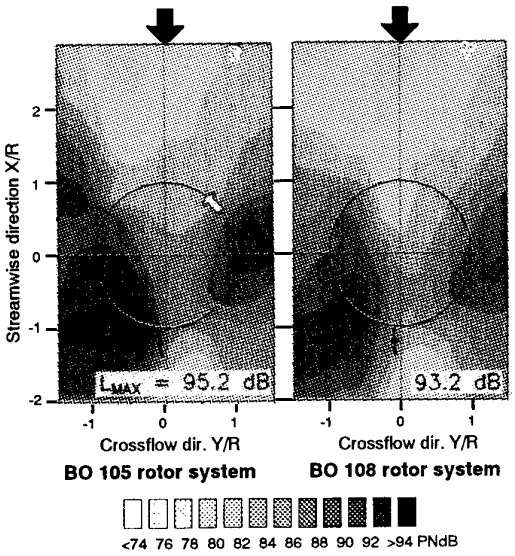

Figure 4: Noise contours (PNL- levels) during flyover condition (60 m/s) for a BO 105 and a BO 108 main/tail rotor system measured in the DNW wind tunnel (DLR, Ref. 5)

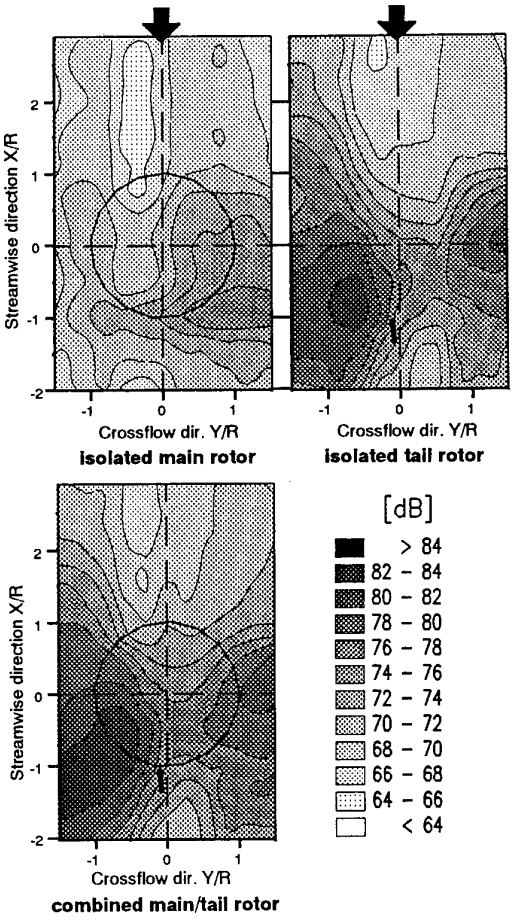

Figure 5: Mid frequency noise contours during flyover condition (60 m/s flight speed) for a BO 105 main/tail rotor system (DLR, Ref. 5)

With respect to the low frequency noise emission important for the military detectability aspect, the main rotor noise dominates the noise contour. Figure 6 shows that the low frequency noise ahead of the helicopter is up to 8 dB higher for the isolated main rotor compared to the tail rotor noise.

For the most upstream microphone position (mic. no. 9) of the measurement array on the advancing blade side, Figure 7 shows the sound pressure time histories for the BO 105 and the BO 108 model rotors. Major reductions of the main rotor thickness noise are achieved by reduction of the sharp negative peaks in case of the BO 108 rotor blades. Taking into account the wind tunnel measurement configuration, this microphone position corresponds to a position at about 150 m ahead of a helicopter at a flight altitude of 50 m. At this flight speed the noise ahead of the helicopter is determined by the main rotor thickness noise.

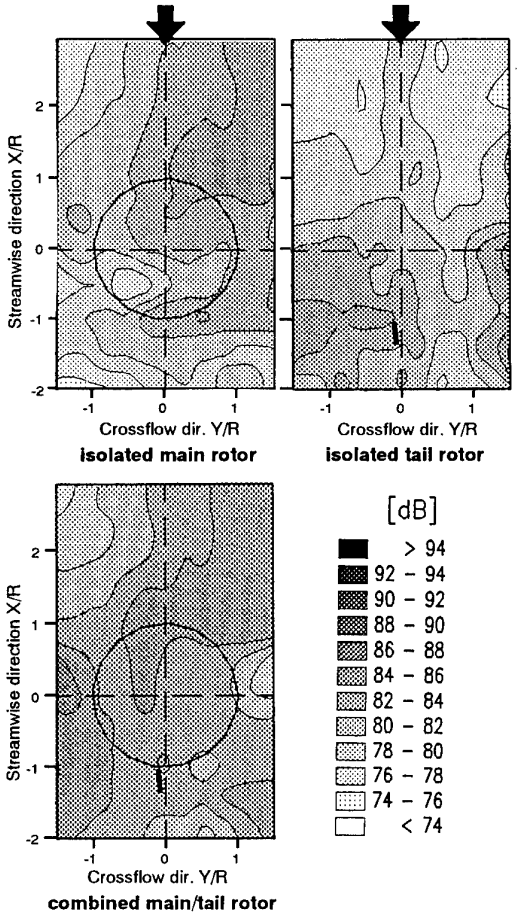

Figure 6: Low frequency noise contours during flyover condition (60 m/s flight speed) for a BO 105 main/tail rotor system (DLR, Ref. 5)

The thickness of the advanced BO 108 rotor was reduced at the blade tip by 25% compared to the thickness of a conventional BO 105 rotor blade (NACA 23012). As the thickness noise component of the Ffowcs-Williams and Hawkings (FWH) equation is directly proportional to the absolute thickness of the blade, the thickness noise was significantly reduced.

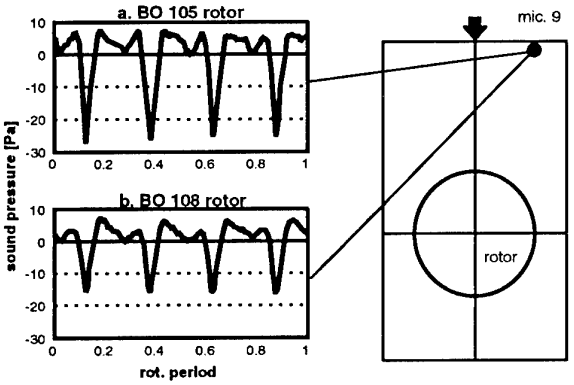

Figure 7: Sound pressure time histories for the most upstream microphone position on the advancing blade side

In several flight test campaigns, the noise emission of the different rotor planforms was measured and compared to the BO 105 with the conventional rectangular tip shape (Figure 8). Starting from the BO 105 rotor, the ICAO flyover noise level was reduced by 1.3 EPNdB by introducing the tapered planform and the DM-H profile family. By applying the parabolic tip design, a further reduction of 1.1 EPNdB was measured on the BO 108. Especially at higher flight speeds, the parabolic blades show advantages in the noise emission and in performance.

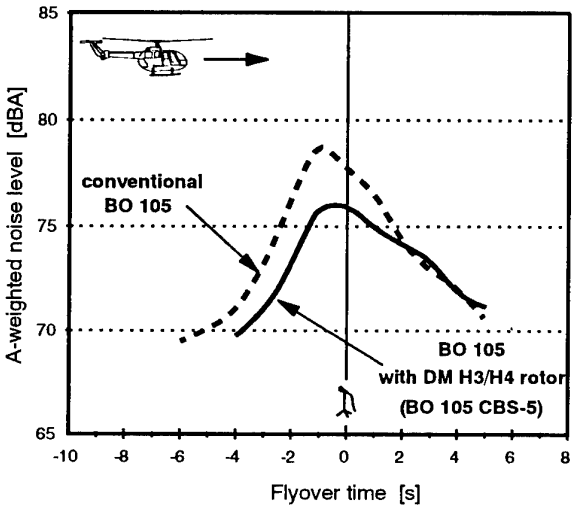

Figure 8: Sound pressure level during flyover condition (150 m altitude) on centerline microphone for various main rotor configurations (120 kts flight speed)

3.2 Main Rotor Tip Speed

The tip speed is the most dominating parameter for the noise emission of the overall rotor layout. In most flight conditions, the acoustic dipole term is dominant, which follows a 6th to 7th power of the sound pressure. At high flight speeds with advancing tip Mach numbers higher than 0.8, the monopol and quadrupol terms become important with a dependency of the radiated sound by up to the 14th power.

An important aspect of the development of the EC 135 helicopter was the reduction of the nominal tip speed and introduction of a variable tip speed concept. A careful layout of the main rotor acoustics was therefore conducted, supported by ECD and DLR noise prediction codes and measurements in the DNW wind tunnel and on the BO 108 helicopter in flyover and approach condition.

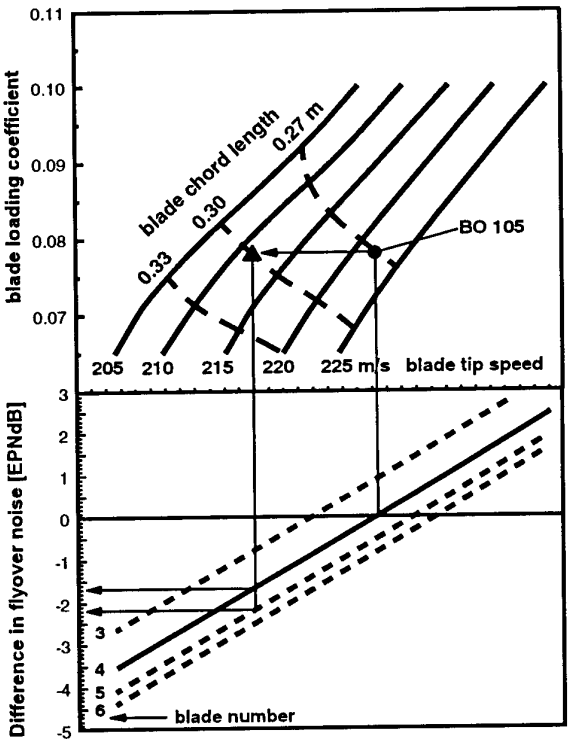

Figure 9: Influence of the rotor design parameters blade area, blade number, and tip speed on the design of a 2.5 tons size helicopter (NACA 23012, ICAO flyover condition)

A change of the rotor rotational speed always implies a change of other rotor layout parameters. An efficient noise reduction of a rotor must cover all initial design parameters such as tip speed, disc loading and solidity. For a specific helicopter design like the EC 135, the disc loading is given by the envisaged take-off weight and rotor diameter within a small frame. The noise effect of the two remaining parameters is illustrated in Figure 9, based on noise prediction codes for a moderate flight speed of 120 kts. Starting from the BO 105 rotor dimensions as a reference, it can be seen that the noise reduction by decreasing the tip speed is limited if the solidity (here: chord length) is not adequately increased. By a blade loading parameter comparable to the BO 105 reference rotor, a 5% reduction of the tip speed (from 222 m/s to 211 m/s) will result in a noise reduction of about 1.6 dB.

First tests of the noise sensitivity with rotor speed were conducted during the noise certification of the BO 105 helicopter (Ref. 6) in a range from 95% to 102% RPM for flyover condition. Due to the low drag divergence Mach number of the NACA 23012, a significant difference of the flyover noise by 2.9 EPNdB was measured.

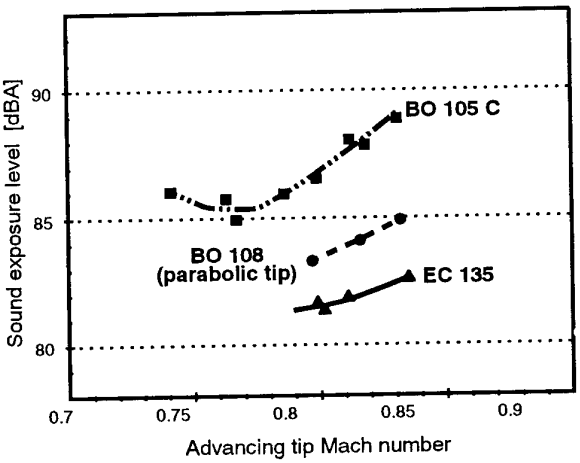

Figure 10: Flyover noise measurement (centerline microphone) in dependency of the advancing blade tip Mach number.

The investigation was continued on a BO 108 with parabolic blades and, finally on a EC 135. Figure 10 shows the Sound Exposure Level (SEL) versus the advancing blade tip Mach number for the BO 105, the BO 108 and the EC 135. The considerable higher drag divergence Mach number of the DM-H3/H4 profiles leads to a smoother noise dependency of the BO 108 and EC 135 compared to the BO 105. As the main rotors of the BO 108 and the EC 135 are similar, the difference is caused by the choice of the anti-torque concept.

The flight testing was supported by wind tunnel tests in the DNW. Figure 11 shows the noise contour and the sound pressure time history of the BO 108 rotor with only 90% rotor speed. If compared to the contour of the BO 108 at 100% rotor speed (Figure 4), an average noise reduction of 1.8 dB is obtained. The thickness noise peaks in the sound pressure time history for the most upstream microphone position are reduced significantly compared to the peaks indicated in Figure 7 for the 100% rotor speed measurement.

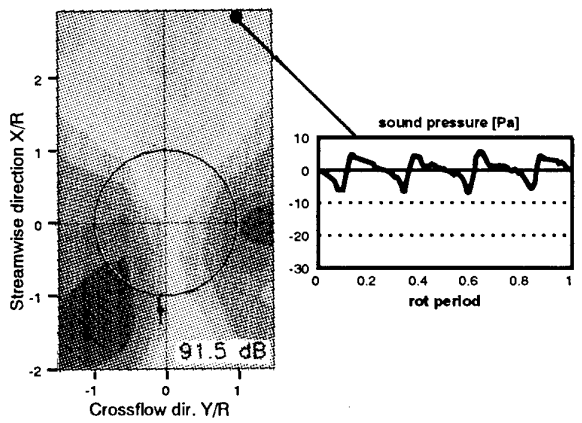

Figure 11: Noise contour and sound pressure time history for the BO 108 rotor system with reduced rotational speed (90% RPM)

3.3 Main Rotor Blade Number

A remaining parameter for the main rotor layout is the number of blades on which the rotor solidity is distributed. As seen in the lower part of Figure 9, the choice of a 5-bladed rotor reduces the main rotor noise by about 0.5 EPNdB. However, regarding the overall noise emission of the helicopter, the advantage of a 5-bladed rotor compared to 4 blades is only dominant for the approach flight condition, whereas during horizontal flyover and take-off, the other noise sources (tail rotor, engines) reduce the influence of the main rotor blade number. Considering the three flight procedures relevant for noise certification, the 5-bladed rotor will only have an advantage of about 0.2-0.5 EPNdB, depending on the influence of BVI noise emission in approach condition.

4. REDUCTION OF FENESTRON NOISE

In the late eighties, studies aiming at understanding the very mechanism of noise creation on a fan-in-fin tail rotor were performed at EUROCOPTER FRANCE in conjunction with the research laboratory of Ecole Centrale de Lyon. They were oriented not only to decrease the overall noise level of the Fenestron, an important source of noise at old generation Fenestrons for medium size helicopters during take-off and flyover, but also and particular to suppress the typical shrill noise emission in the medium range frequencies (around 700 to 1000 Hz).

Indeed, pure tones emerging in the 1000 Hz range must be avoided. As far as civil regulations are concerned, the existence of such pure tones highly penalise the overall noise level of the helicopter in certification conditions due to the tone corrections (PNLT) which can add a 3 to 6 dB penalty for take-off and /or flyover procedures. Therefore, a 1 to 2 dB gain can be expected when suppressing pure tones on the overall aircraft.

Moreover, populations are particular sensitive to pure tones, specially in the 1000 Hz range, and react aggressively to such disturbances. Hence, to increase the acceptance of helicopters near populated areas, a particular attention must be paid to eliminate such pure tones.

With respect to military missions, it is advantageous to shift the noise radiation to higher frequencies due to the high atmospheric absorption for such frequencies. However, pure tones coming from the tail rotors help in recognition of helicopter: the tail rotor RPM can be clearly identified and the ratio of main rotor to tail rotor RPM is immediately obtained. The aircraft is clearly identified as friend or enemy due to its dominant rotational noise sources. This is true for conventional tail rotors as well. Suppression of pure tones by modulation technique, easy and efficient on a Fenestron as we will see changes the Fenestron in a broadband noise-like source, hiding it in the surrounding broadband noise of a battlefield, and preventing from quickly detecting the type of the aircraft. Moreover, on a Fenestron, the shroud surrounding it filters part of the thickness noise radiated in front of the aircraft towards helicopter main detection directions, thus leading to a dramatic reduction of Fenestron noise level in the overall spectrum, contrarily to conventional tail rotors.

Along with the modulation technique, a reduction of the overall noise of the Fenestron by conventional acoustic means such as RPM reduction, helps reaching both, civil and military targets. To develop efficient and robust industrial means for noise reduction, one must understand the physics of the phenomena involved on a Fenestron. Studies indicated, and measurements confirmed that three mechanisms are responsible for the Fenestron noise emission (illustrated in Figure 12):

- atmospheric turbulences ingestion: they provoke loads fluctuations on the rotor blades. If these turbulence are extended, the resulting spectrum will look like a rotational spectrum. The turbulence is so long that it is ingested all blades cut it: a pseudo-period of this phenomenon can be determined and narrow peaks appear in the spectrum. Small disturbances will produce additional broadband noise.

- steady and periodic loads on the rotor blades, among them those due to the presence of obstacles downstream of the rotor which block or deviate the oncoming airstream and can be evaluated by the potential calculation or using conformal transformation techniques. They are called, by analogy, "potential noise". The obstacles can be the strut supporting the tail rotor gear box (or a stator), the transmission shaft, the pitch setting command, etc.. . They generate a typical rotational noise in the lower multiples of the reference frequency of the Fenestron. This reference frequency is defined as $f_0 = B \times \Omega$ where B is the number of rotor blades and Ω the tail rotor RPM.

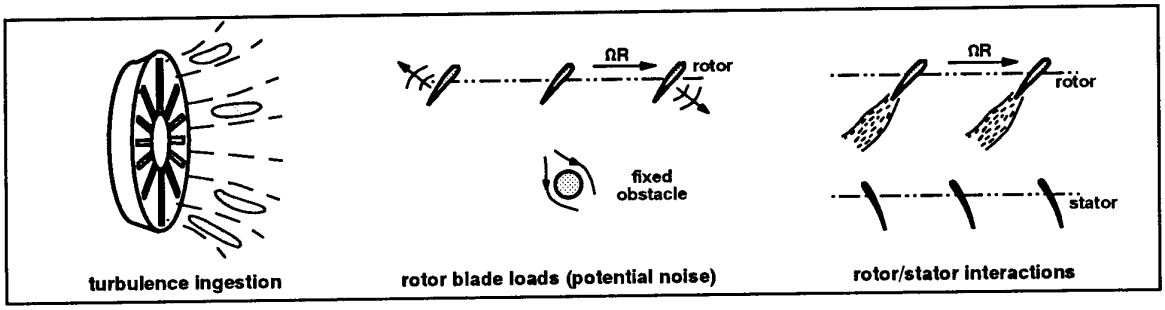

Figure 12: Generation mechanism of Fenestron noise

- Interactions between the rotor and the stator on the stator blades: The wake of the rotor blades, very sharp and turbulent, periodically hit the stator vanes. Thus, these air foiled vanes, although fixed, bear fluctuating loads, and noise of dipole type is emitted at the blade passing frequency and its multiples in a wide range of the spectrum.

To help designing a new Fenestron, a fully numerical code was developed based on the results of these studies, called RAF (ref. 7). From the specification of the geometrical characteristics of the Fenestron, characteristics of the atmospheric turbulence, axial and tangential velocity distribution through the plane of rotation obtained from a previous calculation, and pitch attitude, RAF calculates the load distribution on the rotor and on the stator, then the spatial pressure distribution using the Ffowcs-Williams and Hawkings analogy in the frequency domain.

Today, only hover calculations are made which already considerably helps in general design. These were validated by comparison with recent experiments performed in the anechoic wind tunnel of CEPRA 19 at Saclay (France) on a 850 mm diameter, 8 bladed rotor Fenestron rotor equipped with a stator (ref. 8).

During the experiments, effects of the blade spacing (modulation effects), tip speed variation, thrust variation, stator positioning, obstacles geometry, forward speed variation (for forward flight application), and yawing attitude were investigated both, in hover and forward flight. Figure 13 illustrates the effect of modulation, while Figure 14 shows the effect of RPM and thrust variation.

As illustrated, the code is currently able to predict modulation effects: the radiated acoustic energy, initially concentrated on the 8Ω frequency and its multiples is spread over many frequencies. Although the relative importance of 2Ω is not reproduced, the relative importance of 8Ω, 10Ω, 12Ω (emerging), and 14Ω (not appearing), 16Ω (almost eliminated while it dominated in the non modulated Fenestron) is correctly predicted. This range of frequencies plays the major role in the general noise level when the Fenestron is mounted on the helicopter, and directly determines the amount of pure tone correction, if any.

Of course, the code is not able to reproduce the broadband and the surrounding noise of the isolated Fenestron in the wind tunnel (scattered peaks in the simulation, fulfilled spectrum in the experiment) but this latter will vanish in the overall spectrum of the helicopter and is at least 10 dB below the rotational noise of the isolated Fenestron.

Experimental comparisons between hover and forward flight spectra of the modulated Fenestron proved that the modulation effect, after averaging to get rid of directivity effects, was similar. Thus, designing a good modulation law with RAF for hover case guarantees a good behaviour of the Fenestron in the whole range of flight, as far as this parameter is concerned.

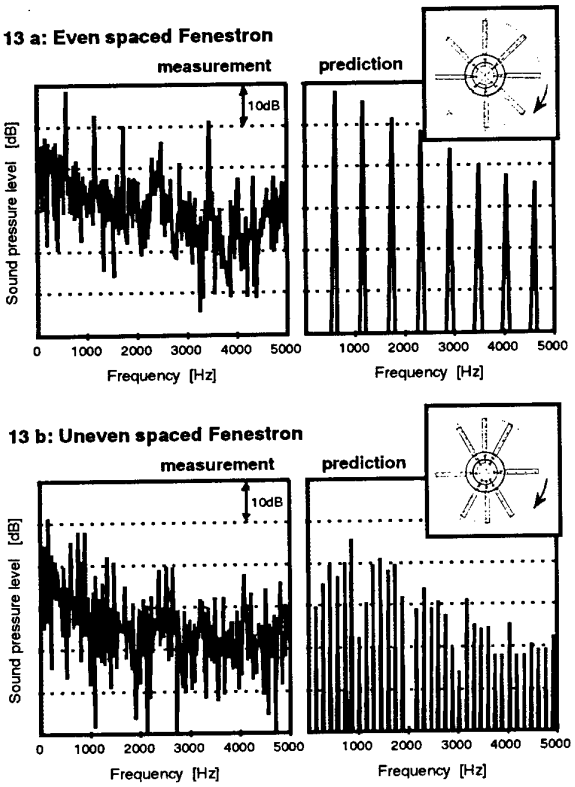

Figure 13: Comparison between theory and measurements for the effect of phase modulation on a Fenestron

Correlations between calculations and experiments on RPM and thrust effects (Figure 14) in hover show that RAF correctly predicts the amount of noise reduction due to tip speed reduction: an average of 3 dB reduction

is observed for a 10% tip speed reduction, similar to the measurement results.

However, RAF fails in the prediction of the gradient of noise versus thrust for a highly loaded Fenestron (the reduced thrust coefficient for hover typically ranges between 0,4 and 0,6). A possible explanation for such a failure may rely in the use of the Amiet modelisation of atmospheric turbulence ingestion which is almost independent of rotor thrust variation. Recent experiments (ref. 9) on the atmospheric turbulence effect on rotor noise revealed a stronger dependence of this type of noise to rotor thrust.

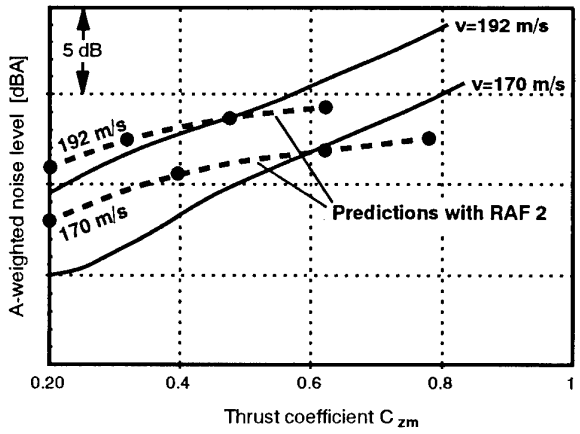

Figure 14: Effect of tip speed and thrust on the Fenestron noise emission

Figure 15 shows the effect of the stator position as measured during the experimental campaign when the stator was moved one rotor blade chord downstream from its initial position, corresponding to a 1 chord gap between the rotor plane and the stator leading edge. Around 2 dB can be saved in the range of load coefficient representative of the helicopter flight spectrum thanks to the decrease of turbulence in the rotor wake downstream.

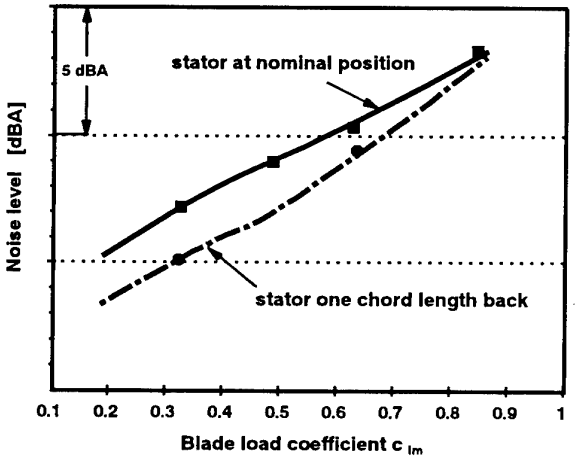

Figure 15: Effect of stator position on Fenestron noise

5. EC 135 NOISE EMISSION

5.1 Aircraft Description

The EC 135 is a light weight, twin engine multipurpose helicopter with a take-off weight of 5800 lb. The helicopter is offering a seat capacity for the pilot and up to 6 passengers. The EC 135 has a bearingless, all composite four-bladed main rotor system (Ref. 10, 11) with newly designed rotor blades and optimised blade geometry. Table 1 gives all data relevant for the exterior noise. The EC 135 has an aerodynamically optimised airframe structure with a high percentage of fibre composite components and increased interior width, cargo compartment, and fuel tank capacity. Figure 16 shows the design of the EC 135 with the overall dimensions.

Dimensions	
design gross weight	5800 lb.
maximum speed v_H (MCP, 0m ISA+10 deg)	140 ktas
rate of climb	1570 ft/min
Main rotor	
diameter	10.2 m
chord length	0.3 m
airfoil section	DM H3/H4
number of blades	4
rotor rpm (100%)	395.2
tip speed at 100% RPM	211.1 m/s
blade planform	parabolic tip
Tail rotor	Fenestron
diameter	1.0 m
chord length	0.05 m
airfoil section	OAF139-095
number of blades	10
rotor rpm (100%)	3584
tip speed at 100% RPM	187.7 m/s
blade planform	rectangular

Table 1: Aircraft general data EC 135

For yaw control, a new 10-bladed Fenestron tail rotor was developed by EUROCOPTER FRANCE (ref. 12). This Fenestron is the result of most recent research activities conducted in the fields of aerodynamics (for performance purposes), acoustics (for environmental aspects) and construction design (for Direct Operation Costs decrease).

The concept of a Fenestron fitted aircraft such as the EC 135 has proven its advantage in terms of operational safety compared to an aircraft with a conventional tail rotor. After the loss of the anti-torque function, the helicopter can still land safely, thanks to the large anti-torque aerodynamic surface provided by the shroud and the fin. The completely shrouded rotor prevents any personnel's injury on ground and has considerable decreased the rate of accidents involving contacts with ground, trees, electrical power lines or other obstacles (ref. 13). The accident probability can

be considerably reduced by placing the tail rotor high on the fin. However, this means for light helicopters as in the class of EC 135, a weight penalty and more complexity.

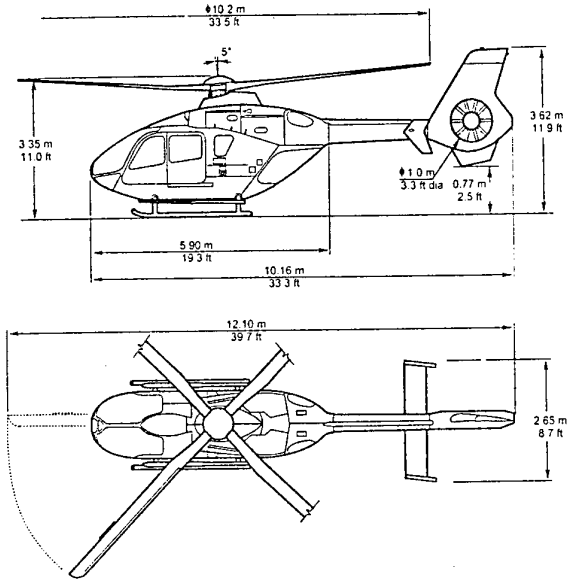

Figure 16: Dimensions of the EC 135

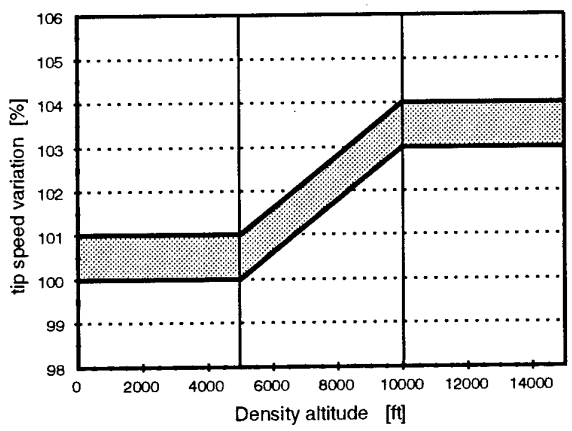

Figure 17: Rotor rotational speed dependency of the EC 135

Two turbine engine configurations are available: The EC 135 T with two TURBOMECA ARRIUS 2B engines and the EC 135 P with two Pratt&Whitney PW 206 B engines. Both engines provide a variable rotational speed by the Full Authority Digital Engine Control (FADEC) system. The resulting rotor rotational speed law versus density altitude can be seen from Figure 17: up to a density altitude of 5000 ft which is high enough to cover most of the heliports in the world, the rotor rotational speed is hold at 100% with a slight increase up to 1% at high flight speeds. The 100% RPM corresponds to a main rotor tip speed of 211.8 m/s and 187 m/s for the Fenestron. The low tip speed for the tail rotor system is of special importance for the light helicopter class, as this helicopters suffer mainly from the tail rotor noise during take-off and flyover. The selected tip speeds for the EC 135 will provide a balance between main rotor and Fenestron noise emission.

Above 5000 ft density altitude, the rotor speed increases linearly to a value of a maximum rotor rotational speed of 104% at 10.000 ft. The increase of the rotor speed is necessary not to penalise the helicopter performance at high altitudes.

5.2 Design of the EC 135 Fenestron

For the performance requirements mainly, the EC 135 has been equipped with a 1000 mm diameter Fenestron. The shrouded duct houses a gearbox, the rotor with 10 blades, 50 mm in chord, in light alloy with special leading edge protection against erosion by sand laden atmosphere, a stator in the diffuser part, and a thin transmission shaft (Figure 18). The shroud, duct, and fin, which supports the Fenestron in forward flight to assure the aircraft anti-torque, are manufactured in compound sandwich (Nomex honeycomb, glass/ carbon hybrid, high temperature and non toxic resin).

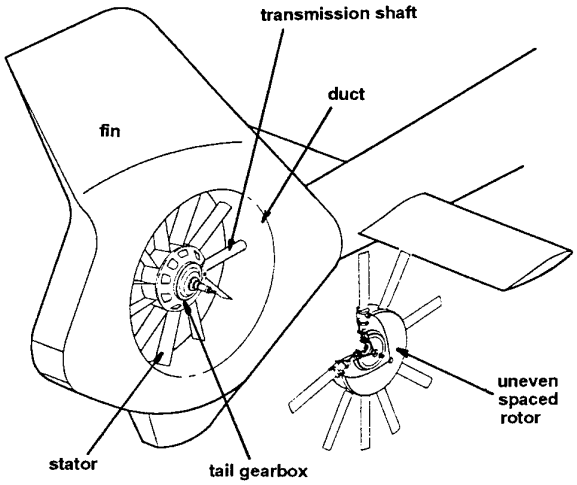

Figure 18: Fan-in-fin tail rotor for the EC 135

An optimised modulation was designed to fit both, acoustic and technological requirements: maximum spacing between blades to allow pitch full authority, selection of number of blades, etc.. An optimised phase modulation was designed to fit both acoustic and technological requirements: maximum spacing between blades to allow pitch full authority, selection of number of blades etc.

Figure 19 represents the rotational part of noise emission radiated in the rotating plane and corresponding to the optimised selected modulation architecture as calculated by RAF for a hover case. The blade passing frequency (10/rev) is no more dominant: adjacent frequencies have been created mainly 8/rev, 10/rev, 12/rev and 14/rev.

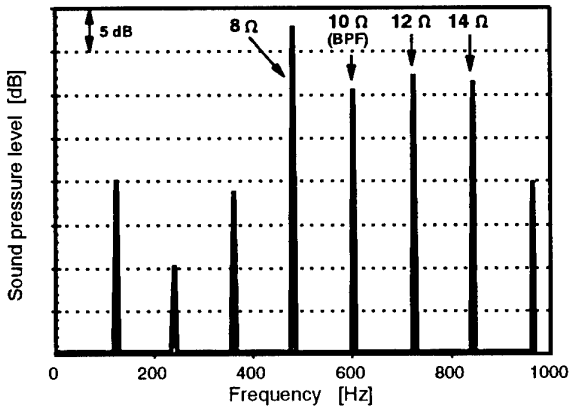

Figure 19: Prediction of the frequency spectrum for the EC 135 Fenestron

Compatibility of such a modulation law with the stator architecture was also numerically checked. It led to the following final design: 10 unevenly spaced rotor blades, 11 evenly spaced stator vanes and the transmission shaft.

A characteristic noise spectrum in the range of the EC 135 Fenestron frequencies can be seen on Figure 20 for a trim condition representative for hover flight and measured on an isolated bench. The blade passing frequency (10Ω) energy level was reduced and part of the energy was equally transferred on adjacent frequencies (8Ω and 12Ω mainly) as was calculated in the design phase with the RAF code. No peaks emerge more than 5 dB above the other ones. With the Fenestron mounted on the helicopter and in presence of the main rotor, Fenestron peaks will not significantly emerge from broadband noise and will be mixed with main rotor peaks in this range of frequencies. The EC 135 Fenestron signature is weak and hidden in the whole helicopter and surrounding spectrum.

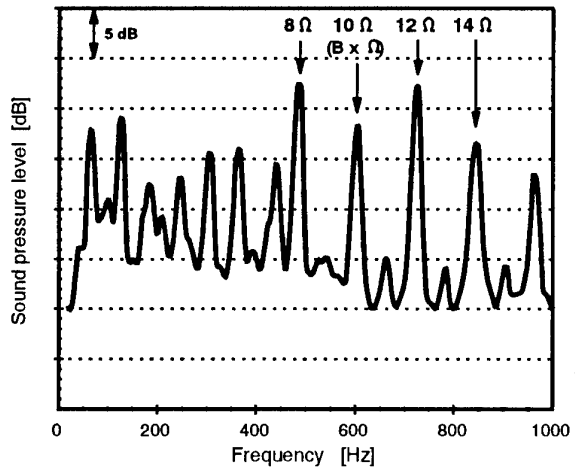

Figure 20: Frequency spectrum of the EC 135 Fenestron on the test bench with phase modulation

5.3 Noise Emission in Hover Condition

The acoustic testing started by measurement in hover condition. Figure 21 shows the A-weighted noise level and the unweighted low frequency noise (0-200 Hz) of the EC 135 in 200 ft distance and a take-off weight of 2600 kg. There are some modulations with azimuth angle on the A-weighed noise levels which are mainly caused by the Fenestron and the engine noise emission.

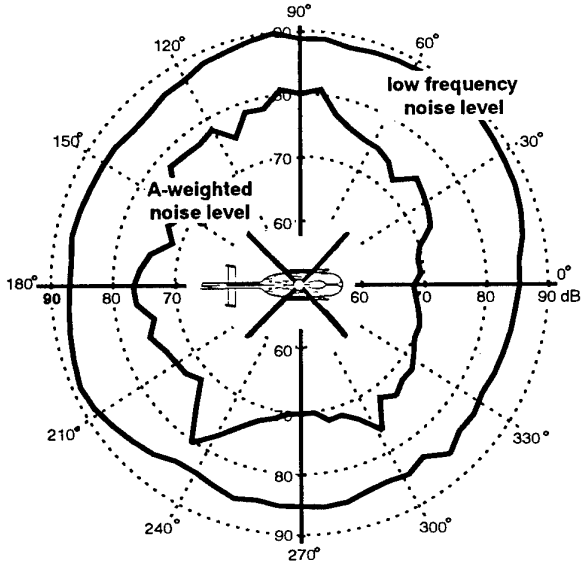

Figure 21: A-weighted noise emission during hover for the EC 135 (M_{TO}=2600 kg) for a distance of 200 ft and an altitude 15 ft.

Due to the absence of a conventional tail rotor, the low frequency noise emission is much more homogeneous with azimuth angle as this frequency range is influenced at the EC 135 only by the main rotor noise.

The noise reduction obtained in hover for the EC 135 is quite impressive if compared to the conventional BO 105 C. Here, it must be kept in mind that the tip speed of the BO 105 with 220 m/s is quite high. Related to the same take-off weight, the overall noise level of the EC 135 is reduced by 6 dBA in average in hover condition. There are two directions at about 235 deg and 300 deg. on the suction side of the Fenestron with slightly increased noise emission. These are the only noise emission directions where Fenestron harmonic noise is not fully covered by the overall helicopter broadband noise.

5.4 Acoustic Detectability

In Figure 22, the summarised effect of an aural detection range calculation for the EC 135 at 126 kts flight speed and the BO 105 at 120 kts speed is shown. Both calculations are based on measured flyover noise signatures and a long distance noise radiation code. Within the assumed low noise environment (no significant masking noise), a decrease of the detection

range of about 30% is provided by the acoustic design of the EC 135.

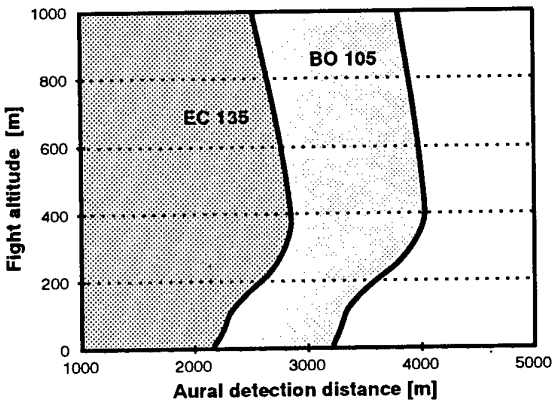

Figure 22: Calculated aural detection ranges for the EC 135 and the BO 105 in dependency of the flight altitude

Figure 23 shows the analysis of the first four main rotor harmonics for the EC 135 during flyover in 150 m altitude with 209 and 220 m/s tip speed. As expected, the first harmonic (4/rev) show no significant influence by the rotor rotational speed variation. At this moderate flight speed, the thickness component dominates the main rotor spectrum. For a given performance, the low frequency noise emission is smaller effected by the tip speed than the higher harmonic noise (Ref. 15). The other harmonics are reduced in the range ahead of the helicopter by 5 to 10 dB which means a reduction of their acoustic detection range by more than 50%.

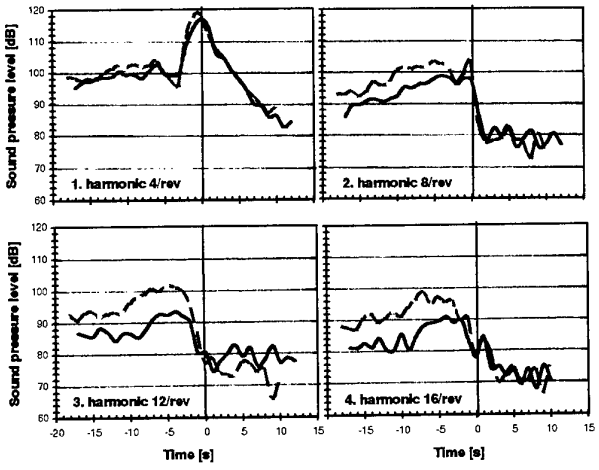

Figure 23: Sound pressure level time history for the first four main rotor harmonics during flyover with 250 km/h for 209 m/s tip speed (solid line) and 220 m/s (dashed line)

The effect of the rotor tip speed reduction can be seen in more detail from Figure 24. The frequency spectrums in the upper part of the Figure show the noise measured 800 m ahead of the approaching EC 135 helicopter on the advancing blade side at 150 m sideline from the flight path. A very significant effect is obtained for the first 10 harmonics if the tip speed is reduced. The intensity of the harmonics is reduced by 5 to 10 dB whereas the higher harmonics above 300 Hz nearly vanish in the background noise. At the flyover position (lower Figures), no influence of the main rotor noise can be noticed. The radiated noise is dominated by broadband noise which is nearly not affected by the tip speed variation. This is mainly due to the influence of engine noise during the helicopter flyover: It dominates for this flight phase, and it is independent of the defined RPM variations.

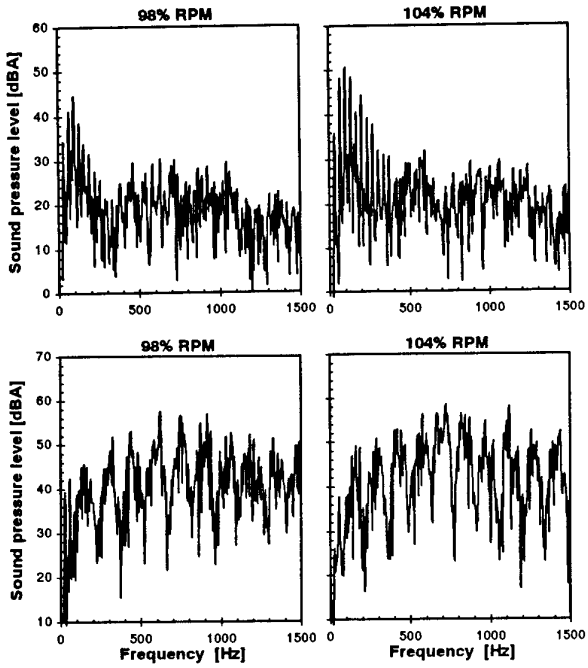

Figure 24: Frequency spectrums (sideline microphone) of the EC 135 (134 kts flight speed) at 800 m ahead of the helicopter (upper figures) and during flyover (lower figures)

5.5 Noise Certification Measurements

Noise certification measurements for the EC 135 were conducted in accordance with the new simplified method described in the standards ICAO Annex 16, Chapter 11 (Ref. 1), and FAR Part 36, Appendix J (Ref. 2). The new noise certification standards were adopted for helicopters not exceeding 6000 lb maximum certification take-off mass. An applicant must show compliance with maximum noise limits for the flyover procedure conducted at a level flight altitude of 150 m (492 ft). The reference flight speed is 126 ktas for the EC 135 which corresponds to 0,9 v_H. The acoustic data acquisition requires to record noise level time histories on a microphone position directly below the flight path. From the time histories, the time integrated Sound Exposure Levels (SEL) are derived including corrections for the reference flight (flyover duration time) and altitude deviations. The data

analysis performed to determine the certification levels ended with a margin of 5.8 dB to the LBA (ICAO) limits for the EC 135 P. The corresponding margin for the EC 135 T version is 7 dB. The measured data indicate the highest margin to the Chapter 11 noise limits for the EC 135 of all measured helicopters which verifies the success of the applied noise reduction measures. It should be noted that this result was achieved at a considerable higher flight speed (126 ktas) compared to most of the other helicopters.

CONCLUSION

During the design of the EC 135, a variety of noise reducing measures for both main and tail rotor were introduced in order to reduce the environmental noise emission. The spectrum was significantly modified from a rotational noise spectrum to a broadband noise like spectrum. Most of the measures applied to the main rotor and the use of the Fenestron concept also provided a positive effect on the aural detection for military applications.

Compared to the similar existing helicopters with a conventional two bladed tail rotor unit like the BO 105, the EC 135 noise is reduced by 3 to 4 dB depending on flight condition. The noise certification (LBA-ICAO Annex 16, Chapter 11) was obtained with a margin of 7 dB (EC 135T). The estimated aural detection range for the EC 135 was reduced by about 30% compared to the BO 105.

ACKNOWLEDGEMENT

The authors will express their appreciation for the contributions of Dr. W. R. Splettstößer, DLR Braunschweig, M. H. J. Marze, acoustic specialist of EUROCOPTER France, and M.M. Roger, professor and researcher for acoustics at Ecole Centrale de Lyon (France).

References

/1/ ICAO Environmental Protection, Annex 16, Volume 1, Aircraft Noise, 11. Nov. 1993

/2/ Federal Aviation Regulation 14 CFR Part 21 and 36, "Alternative Noise Certification Procedure for Primary, Normal, Transport, and Restricted Categories of Helicopters not Exceeding 6000 Pounds Maximum Take-off Weight", Federal Register, Vol 57, Sept. 1992

/3/ R. G. Loewy, "Aural Detection of Helicopter in Tactical Situation", Dep. of Mechanical Engineering, University of Rochester, New York

/4/ J. B. Ollerhead, "Helicopter Aural Detect-ability", USAAMRDL-TR 71-33, Wyle Labor-atory, Hampton, Virginia, 1955

/5/ K.-J. Schultz, W.R. Splettstößer, "Helicopter Main Rotor/Tail Rotor Noise Radiation Characteristics From Scaled Model Rotor Experimentation in the DNW", pres. at the 14th DGLR/AIAA Aeroacoustic Conference, Aachen, Germany, May 1992

/6/ W.R. Splettstößer, K.-P. Anders, K.-H. Spiegel, "Noise Certification and Sensitivity Studies on the Helicopter BO 105", DFVLR-Mitt. 86-13, 1986

/7/ F. Fournier, "Mise au point d'une méthode de calcul adaptée au bruit de Fenestrons d'hélicoptères", Thèse de doctorat de l'Ecole Centrale Lyon, 1988

/8/ F. Toulmay, D. Falchero, G. Arnaud, "Prediction of Helicopter Exterior Noise: Numerical Methods as Conceived by an Industrialist", AGARD CP552, Berlin, Oct. 1994

/9/ D. B. Signor, G.K. Yamauchi et al.,"Effect of Ingested Atmospheric Turbulences on Measured Tail Rotor Acoustic", Journal of the American Helicopter Society, Vol 1, pp 77-90, 1990

/10/ C. Zwicker, "Configuration and Program Status of EUROCOPTER's New Light Twin Helicopter EC 135", pres. at the 19th European Rotorcraft Forum, Cernobbio, Italy, 1993

/11/ G. Polz, D. Schimke, "New Aerodynamic Rotor Blade Design at MBB", Pres. at the 13th European Rotorcraft Forum, Arles, France, Sept. 1987

/12/ M. Vialle, G. Arnaud, "A New Generation of Fenestron Fan-in-Fin Tail Rotor on the EC 135", pres. at the 19th European Rotorcraft Forum, Cernobbio, Italy, 1993

/13/ A. Vuillet, F. Morelli, "New Aerodynamic Design of the Fenestron for Improved Performance", AGARD CP No. 423

/14/ D.Ewald et al.,"Noise Reduction by applying modulation principles", Journal of the Acoustical Society of America, Vo. 49, No. 5, pp1381-1385, 1971

/15/ F.J. Perry, A.C. Pike, "Helicopter Aeroacoustics and the Impact of Noise Regulations on Design", Symposium The Quiet Helicopter, Royal Aeronautical Society, 17. March 1992

DUCTED TAIL ROTOR DESIGNS FOR ROTORCRAFT AND THEIR LOW NOISE FEATURES

Bryan Edwards
Jim Andrews
Chris Rahnke
Bell Helicopter Textron, Inc., P.O. Box 482, Dept. 81
Fort Worth, Texas 76101, USA

ABSTRACT

During the development of an advanced ducted tail rotor (DTR) design, a concentrated and successful effort was made to research and incorporate the low noise features of a DTR suitable for intermediate size rotorcraft. The design, whirl stand testing, and flight evaluations of this DTR configuration are described.

Results of noise testing are presented for multiple design configurations to study the parametric effects of blade spacing, tip shape, rotational speed, and inflow turbulence. The acoustic effects of each parameter are presented, and measured noise reductions are identified. Isolated model ducted-rotor configurations are described, leading to additive noise level reductions of more than ten decibels for the DTR design. Installed on a Bell Model 222U helicopter, the DTR reduces total noise during hover and forward flight by an average of 2 to 6 dBA compared to the Model 222U configured with a standard tail rotor. A dramatic improvement in sound quality was found in subjective comparison tests.

The performance and handling qualities of the test helicopter with the DTR prove to be similar to those characterizing a standard tail rotor. Component loads are well within design limits. These design qualities are discussed and substantiating test data are presented.

INTRODUCTION AND HISTORY

A protected antitorque system can reduce the risk of component damage as well as enhance the safety of operators, passengers, and ground personnel. However, development of a practical system must overcome formidable design constraints. The antitorque system design should not adversely affect important operational and flight characteristics such as performance, acoustic signature, and reliability and maintainability, and must meet stringent cost and weight criteria. Bell has examined a number of protected anti-torque systems over the years. Each incorporated a duct-like feature, starting with a thin ring concept and leading to the most recent full duct concept, which has been called the "ducted tail rotor," or DTR.

Early Thin Ring Concept

During the period between 1978 and 1985, Bell conducted extensive wind tunnel and flight tests of a thin structural ring placed around a Model 206 helicopter standard tail rotor. The ring was less than 5 centimeters (2 inches) thick, serving as a vertical stabilizer in lieu of the standard vertical fin. Directional stability was enhanced by the integration of a vertical fin on the forward portion of the ring, visible in the sketch of Fig. 1. This design concept was termed the "ring fin." The major advantage of the ring fin concept was its ability to protect the tail rotor with minimal impact on weight and cost. Low-speed handling was also improved because of the reduction in fin blockage; but only minor improvements were evident in the acoustic signature, and no thrust augmentation was achieved. Due to a declining market, the targeted production opportunity did not materialize.

Development of the Current Full Ducted Concept

Following the ring fin work, additional studies were conducted to enhance the design analysis of ducted tail rotors (DTR). The analysis was calibrated with data from several whirl stand and low-speed wind tunnel tests. Basic design data was obtained for variations in duct thickness, duct geometry, and tip clearance effects. The success of the early tests, along with the good analytical model, provided the confidence to proceed to the next step, a flight demonstrator.

The demonstrator program was started in 1993, using a Bell Model 222U as the test-bed aircraft. In determining the size of the demonstrator DTR, a tradeoff between performance requirements and weight, inertia, and drag penalties was examined. In order to keep the weight, inertia, and drag penalties low, the DTR diameter was set so that there would be only a modest

Fig. 1. Bell's early "ring fin" tail rotor design.

Paper presented at the FVP Symposium on "Advances in Rotorcraft Technology", held in Ottawa, Canada, 27-30 May 1996, and published in CP-592.

performance degradation compared to the standard tail rotor. The maximum thrust capability was maintained by increasing the tip speed from 207 m/s (678 ft/s) to 220 m/s (720 ft/s). This initial design had four equally spaced blades with square tips, as shown in the photo in Fig. 2. A key feature of this design is the relatively thin duct. The duct thickness is 20% of the rotor diameter. A comparison with the standard Model 222U tail rotor is given in Table 1:

Table 1. Comparison of M222U and M222 DTR.

Aircraft:	M222U	M222 DTR
Gross weight	3,742 kg (8,250 lb)	3,742 kg (8,250 lb)
Tail rotor diameter	2.1 m (6.88 ft)	1.3 m (4.29 ft)
Number of blades	2	4
Solidity	0.154	0.371
Tail rotor blade aspect ratio	4.13	3.43
Duct thickness / diameter	–	0.2
Tail rotor tip speed	206 m/s (678 ft/s)	220 m/s (720 ft/s)
Tail rotor gearbox rating	138 kW (185 hp)	138 kW (185 hp)

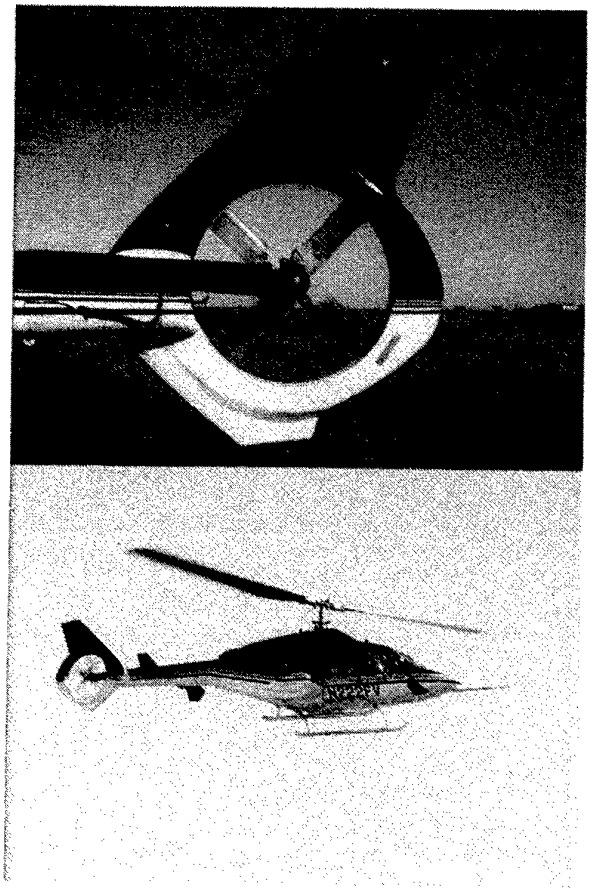

Fig. 2. Four-bladed DTR on Bell Model 222U helicopter.

This initial design was tested at Bell's Flight Research Center in Arlington, Texas, and then was flown to Leadville, Colorado for high-altitude tests (field elevation 9,920 ft). The purpose of high-altitude testing was to establish the DTR aircraft's capability for hovering in winds at altitude. At Leadville, the DTR demonstrated sufficient thrust capability in winds up to 35 kn for an increase in referred gross weight of 363 kg (800 lb) compared to the standard tail rotor. The DTR demonstrated right sideward flight capability of 45 kn at altitude. This performance was achieved without exceeding the standard M222U tail rotor drive train power rating.

While the performance and loads of the early DTR demonstrator were very promising, the original design was considered unacceptable because of the annoying tones. The acoustic problem with the initial DTR design was due to two reasons:

- The DTR had an increase in the blade passage frequency due to a combination of smaller diameter, higher tip speed, and more blades compared to the standard tail rotor. This resulted in a noise of higher frequency, which was more annoying. It also meant that tail rotor noise was less masked by the main rotor noise.
- The noise was very directional and unsteady.

Several attempts were made to improve the DTR's noise through the use of spinners and fairings on the gearbox support tubes and controls. While the design modifications provided some success, the tail rotor noise was still far from acceptable. At this point it was decided to examine more extensive configuration changes by using a whirl stand model, and then evaluate the most promising changes on the DTR demonstrator.

The initial whirl stand test examined the effects of spinners, fairings, and gearbox support strut size and location on the noise of a 0.82-scale, four-bladed model DTR. Variations in the spinner, fairings, and support structure did not provide the large reduction in noise that was needed. Two configuration changes that did provide notable noise reductions were thinner airfoils at the tip and an uneven blade spacing. The most favorable uneven blade spacing (or "scissored" blade spacing) is shown in Fig. 3. The minimum angle between the blades is 70 degrees, patterned after an early Bell scissored main rotor concept (Ref. 1). The first large amplitude harmonic for the equal blade spacing corresponds to a 4/rev tone, while the first large amplitude harmonic for the scissor rotor corresponds to a 2/rev tone. Essentially the acoustic energy has been shifted to a lower frequency. The lower frequency noise was less annoying, and it was expected that it would be partially masked by the main

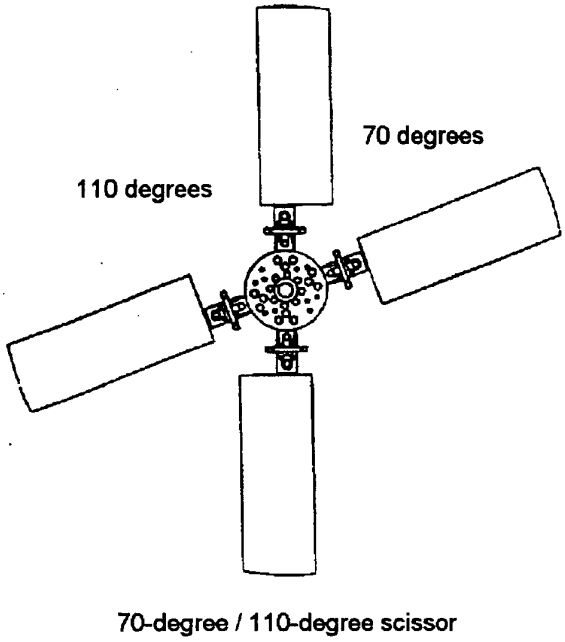

Fig. 3. Most favorable blade spacing for four-bladed DTR model found in initial whirl stand tests.

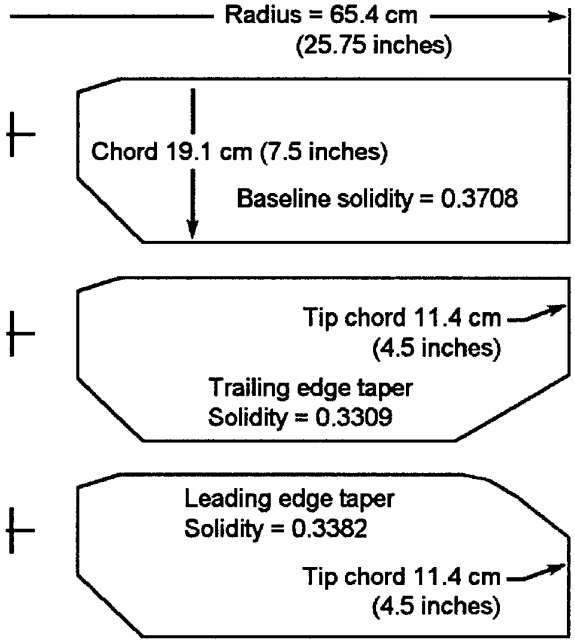

Fig. 4. Blade geometries and tip shapes evaluated on scissored four-bladed DTR.

rotor when installed on the demonstrator aircraft. Both the thin tip and scissored blades were incorporated into new flight test hardware.

The incorporation of the thin tip concept in the flight test hardware was not by means of thinner airfoils but through the use of a tapered planform tip shape. The use of a planform taper had the double benefit of a dimensionally thinner tip and of moving the blade loading inboard. The three tip shapes shown in Fig. 4 were flown on the DTR demonstrator incorporating a scissored four-bladed rotor. The tapered tips had a slight performance degradation compared to the square tip rotor. As can be seen in Fig. 5, the inboard end of the blade is fairly thick. By reducing the amount of efficient tip airfoil, the average blade profile drag coefficient increased. In addition, by reducing the blade loading at the tip, the suction on the duct decreased, resulting in a 6% reduction in thrust produced by the duct. Overall, the three configurations flew well. The trailing edge taper tip (termed the aft taper tip) proved to be the quietest of the three tips. While the scissored rotor was quieter than the equally spaced DTR, it still suffered from a high frequency "buzz" that was directional and unsteady. This led to another whirl stand test, which occurred in mid-1995, and which produced the dramatic noise reduction that changed the DTR design from unacceptable to acceptable.

WHIRL STAND TESTS

Based on the initial whirl stand tests results and the followup flight evaluation, a number of design modifications for improving the sound quality of the DTR had been suggested. An extensive static model test was then planned as the most efficient means to assess the potential of each modification. The goal of the model testing was to evaluate as wide a range of rotor and duct configurations as possible, quickly and efficiently. After a downselection process based on the whirl stand test results, the most promising candidate designs would be taken to flight test and evaluated by measurement and a sound jury.

Model Test Setup

A model rotor and duct test rig was installed in Bell's whirl stand facility. The walls of this test facility form a cylindrical chamber that can be vented near the floor and ceiling to minimize recirculation of air when the

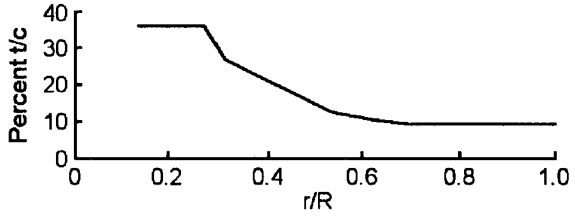

Fig. 5. Thickness distribution of baseline scissored four-bladed DTR.

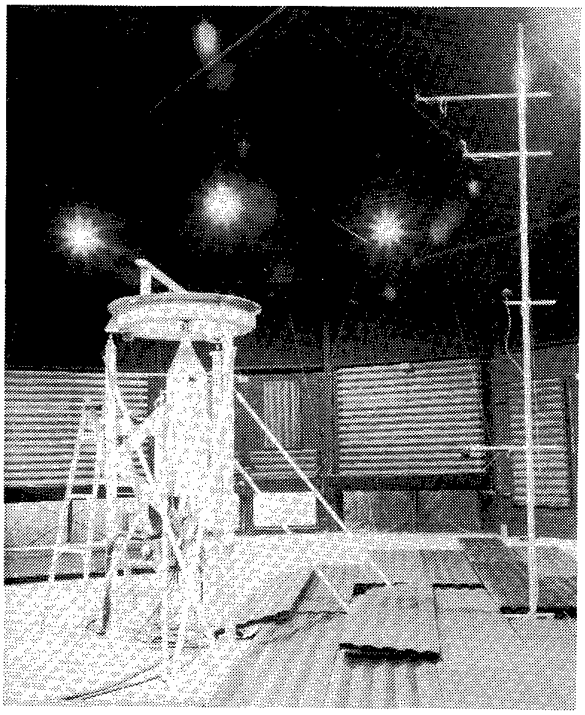

Fig. 6. Whirl stand test setup.

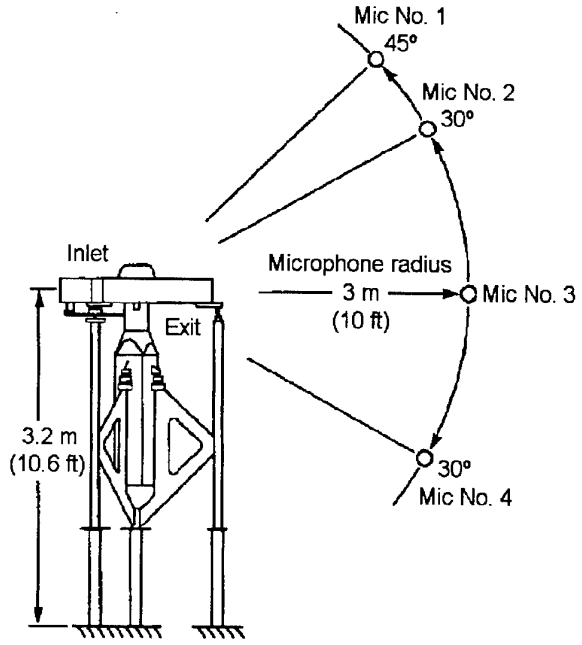

Fig. 7. Microphone locations for DTR model during whirl stand tests.

model is being tested. The model was mounted with its rotor plane horizontal. Absorptive panels, visible in the photograph of Fig. 6, were installed on the walls, ceiling, and floor to reduce acoustic reflections in the test cell. Three load cells in the rotor support structure measured thrust. The rotor mast was instrumented for torque.

The rotor was installed inside a circular solid wooden duct which was scaled from the flight test duct geometry, positioned 3.23 m (10.6 ft) above the test facility floor. The rotor diameter was 107.6 cm (42.34 inches), or 82% of the full scale rotor diameter, with a tip-to-duct clearance of 0.8 cm (0.3 inches). A total of 135 conditions were tested, including variations in number of blades, blade spacing, tip speed, thrust, airfoils, duct tip clearance, duct configuration, drive shaft support structure size and proximity to the rotor, spinner size, and centerbody configuration.

Four microphones, also visible in the photograph of Fig. 6, were set up near the model. The specific locations with respect to the model rotor are indicated in the sketch of Fig. 7. Each was positioned about 3 m (10 ft) from the rotor hub. Based on earlier testing, Microphone No. 2, which was located at 30 deg above the rotor plane on the inlet side, was expected to pick up the most dominant noise. The other positions were monitored to ensure that, as the model rotor configuration was changed, any noise variation seen was a true noise change, and not simply a directivity shift.

Model Rotor Configurations Tested

The rotor blades were constructed of steel spars with laminations of wood and fiberglass, with mono-ball bearings installed at the root end of the spars to provide blade pitch movement. Three steel hubs were used that had multiple sets of hole patterns to accommodate the variations in number of blades and blade spacing tested. Blade pitch angle was provided by securing the pitch horns to the hub at the required pitch settings. To simplify manufacturing, the model blades were untwisted and used a 10% thickness/chord airfoil along the entire span.

Since the four-bladed scissors rotor was the best evaluated in initial DTR testing, it was considered the starting point, or baseline rotor, for this series of whirl stand tests. The physical characteristics of the principal rotor configurations tested are listed in Table 2, and a sketch of each one is shown in Fig. 8. These represent the configurations which were of fundamental interest or represented a marked improvement during the evaluation process.

"Even spacing" indicates the blades had conventional equal spacing between each blade, i.e., 90-deg typical spacing for a four-bladed rotor, and 72-deg typical spacing for a five-bladed rotor. The "uneven spacing" for the four-bladed scissor rotor consisted of the paired 70-/110-/70-/110-deg spacing, which had previously

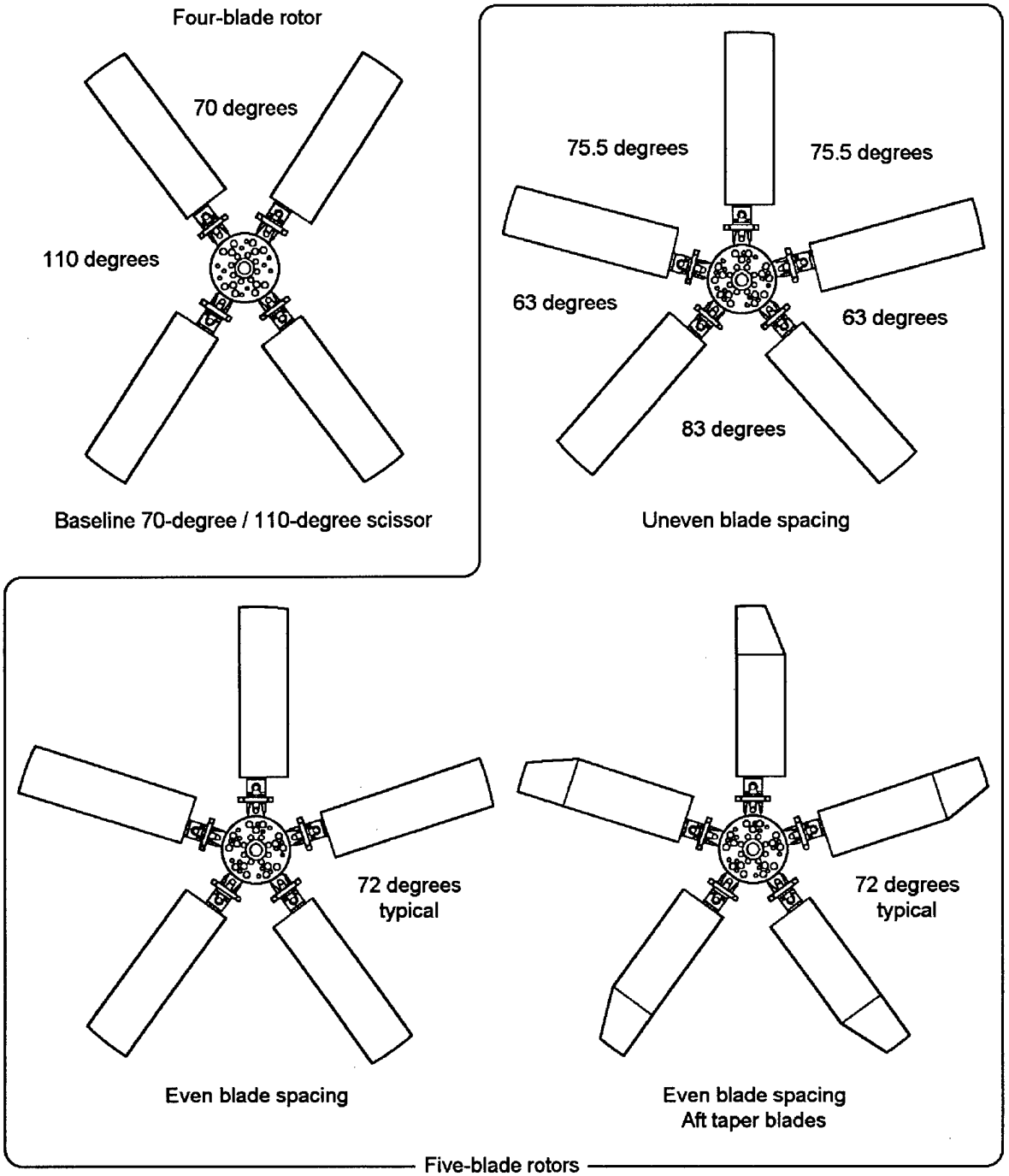

Fig. 8. DTR model configuration tested on whirl stand.

demonstrated acoustical improvements. For the five-bladed rotor, the blades had an irregular 83-/63-/75.5-/75.5-/63-deg spacing, as illustrated in Fig. 8. The aft taper tip refers to the trailing edge taper illustrated in Fig. 4. Other uneven spacings were evaluated for both the four- and five-bladed configurations, but did not offer as much potential for noise reduction. A full discussion of the design process employed in selecting candidate spacings for reduced noise and good rotor balance is given in Ref. 2.

The first two configurations in Table 2 are the four- and five-bladed rotors with equal solidity. At the same tip speed they will provide the same thrust capability with roughly the same performance. Configuration 3 introduced the effects of tip shape, and Configurations

Table 2. Principal rotor configurations tested.

Configuration	No. of blades	Spacing	Chord (cm)	Chord (in)	Tip shape	Solidity
1	4	Uneven	13.4	5.27	Square	0.317
2	5	Even	10.7	4.23	Square	0.318
3	5	Even	10.7	4.23	Taper	0.284
4	5	Uneven	10.7	4.23	Square	0.318
5	5	Uneven	10.7	4.23	Taper	0.284
6	5	Uneven	13.4	5.27	Square	0.396

4 and 5 introduced the effect of blade spacing. Configuration 6 used wide-chord blades to maintain thrust capability at the reduced tip speed. Each configuration was evaluated at the same thrust level.

Test Procedure

After an initial acoustic modeling validation effort, each rotor configuration to be evaluated was stabilized at the desired operating condition, and the sound at all microphone locations was recorded and examined. Based on the test results, the planned test matrix was then reviewed and amended as necessary. In this manner the testing was continuously directed toward the rotor configuration most likely to return the highest noise benefits while monitoring any performance changes.

As discussed previously, the initial DTR design had been characterized by an annoying sound during flight in which the tail rotor harmonics increased and their levels fluctuated. It was speculated that this sound fluctuation was caused by a combination of inflow turbulence induced by the main rotor downwash, ingestion of the engine exhaust, and unsteady flow over the gearbox support tubes.

The early whirl stand testing was directed toward making the baseline model configuration emulate this annoying sound. Experimentation with tabs on the duct inlet to "trip" the flow, and other means of introducing small-scale turbulence at the blade tips, showed little effect. The full-scale noise characteristics were finally approximated by introducing large-scale turbulence into the inflow. This was done by mounting a board nonradially across the duct inlet, about 0.3 m (1 ft) upstream of the rotor disk. The board, visible in the photograph of Fig. 9, caused a turbulent inflow that changed the model's noise characteristics from a steady drone to a fluctuating sound with a rich harmonic content, just as had been observed during flight tests of the four-bladed rotor. Subjective assessments of the model rotor sounds by people who had witnessed the earlier flights confirmed that the sounds were very similar. This increased the confidence that the physics of the sound-generating mechanisms were being duplicated by the whirl stand test setup. This test setup was then maintained as the most realistic approximation to full scale. Actual evaluations of rotor design changes then began.

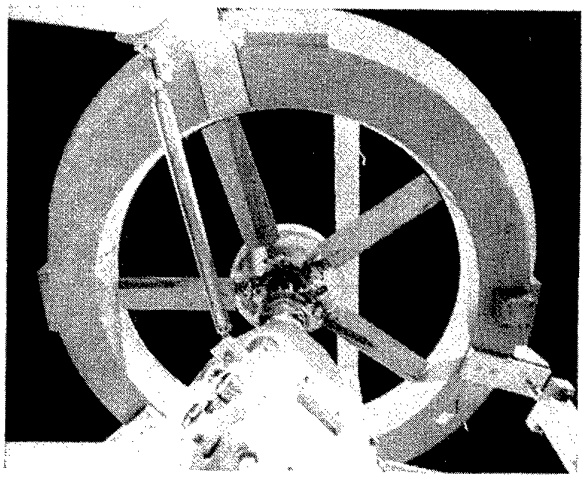

Fig. 9. DTR model and turbulence generator installed on whirl stand.

Each rotor configuration was tested at three thrust values and four rotor tip speeds. The low thrust value was set with the blade at flat pitch. The high thrust value was set by the maximum power capability of the test stand motor. The third thrust value was an intermediate point. Considerable effort was made to keep these thrust values constant with changes in rotor configuration. This would enable the acoustics data to be compared on an equal thrust basis. The tip speeds chosen were 220, 207, 195, and 183 m/s (720, 680, 640, and 600 ft/s).

The acoustic metric which seemed to track most closely with sound quality considered the dominant harmonic tones (1st through 12th harmonic), weighted them according to the A-weighting curve, and logarithmically summed the results. This gave a single number that was used in ranking the model rotor configurations.

Recognizing that even the best metric available would not fully reflect sound quality, the recorded sounds were digitized and stored on a computer, and a "point-and-click" playback capability was employed to play the recorded sounds back to a panel of listeners. This offered a convenient way to compare the changes in the character of the sound of each rotor configuration. As the test progressed, the subjective ranking which came from this panel of listeners carried at least as much weight as the chosen acoustic metric in downselecting to the best rotor configurations.

Model Rotor Test Results

The progressive acoustic improvements achieved during the whirl stand test and downselect process are summarized in the bar chart of Fig. 10. These are

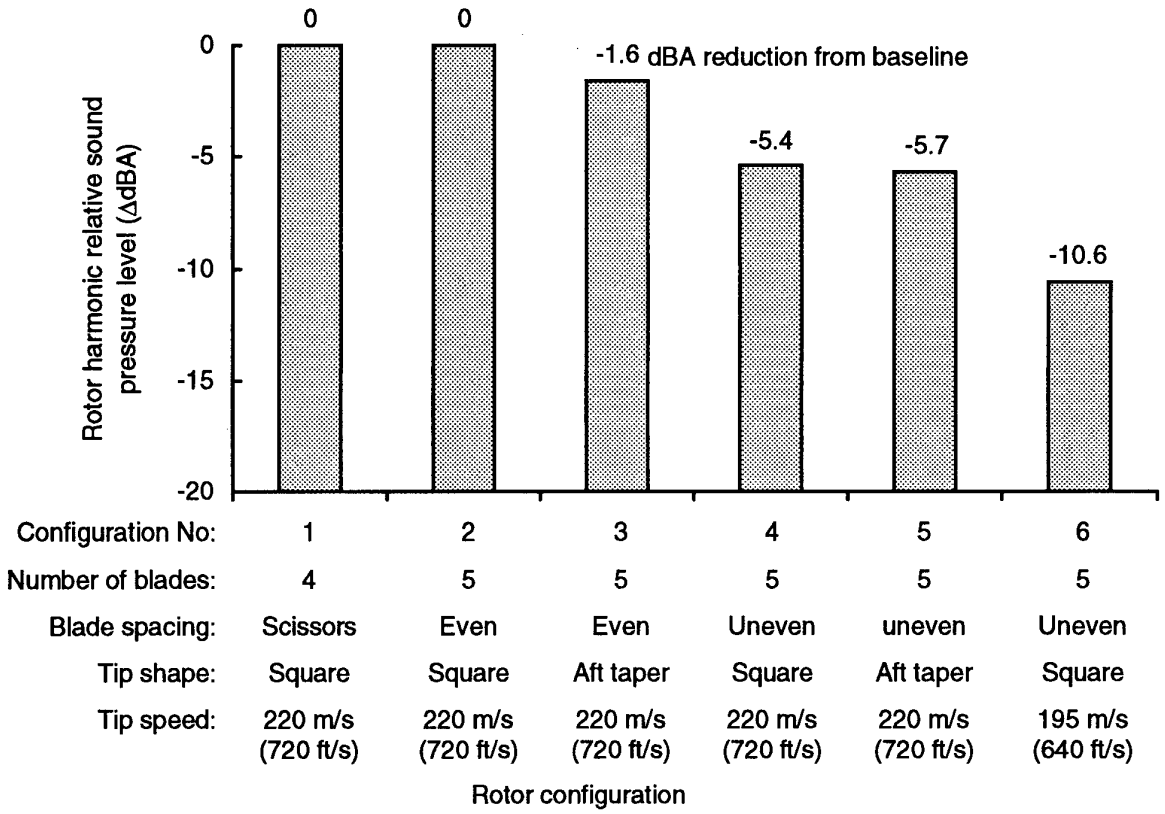

Fig. 10. DTR model whirl stand test showed the potential for 10.6 dBA harmonic noise reduction.

compared on a constant thrust basis and discussed below.

Configuration No. 1
The baseline four-bladed scissors rotor (Configuration No. 1 as described in Table 2), which was the best DTR configuration to date as the whirl stand test began, was the starting point for this series of tests. Any acoustic improvements were measured against this baseline. Configuration No. 1 is shown as the zero point on the noise scale, and the noise reductions achieved by the other candidate rotor configurations are shown relative to this point.

Configuration No. 2
Configuration No. 2 generated the same noise as the baseline, indicating that a five-bladed rotor with even spacing was no louder than the four-bladed rotor with uneven spacing. Tip shape (square tips) and tip speed (720 ft/s) were the same in both tests.

Configuration No. 3
Configuration No. 3 changed only tip shape, and achieved a harmonic noise reduction of 1.6 dBA. This aft taper tip had a trailing edge planform taper starting at 80% radius, as previously illustrated in Fig. 4. At 100% radius, the chord length is only 60% that of the square tip, introducing less blade area into the acoustically critical tip–duct region.

Configuration No. 4
Configuration No. 4 introduced the substantial benefits of blade spacing, demonstrating a harmonic noise reduction of 5.4 dBA. This rotor was identical to Configuration No. 2 except that, instead of the five blades being spaced a constant 72 deg apart, they were spaced unevenly in an irregular 83-/63-/75.5-/75.5-/63-deg spacing, illustrated earlier in Fig. 8. As the rotor was being tested, an immediate difference in sound quality was noticed. Compared with the single blade passage frequency (and related harmonics) of the evenly spaced rotor, this rotor had multiple low-amplitude subharmonics in addition to reduced-amplitude blade passage frequency and harmonics. The acoustic effect of unevenly spaced blades has been documented in Refs. 3 through 7, among others.

The spectral content of this rotor is compared with the evenly spaced one in the inset of Fig. 11. Note the spectral differences in character. The evenly spaced rotor has very well-defined rotor harmonics, with the 5/rev (324 Hz) frequency, and its multiples very apparent. The unevenly spaced rotor, however, has a large number of less defined tones of lower amplitude, some showing up at the 5/rev frequency and its multiples, and many others showing up at sidebands of 5 per rev and multiples of the sidebands. In other words, the effect of the uneven spacing is to redistribute the acoustic energy, reducing the energy present in the

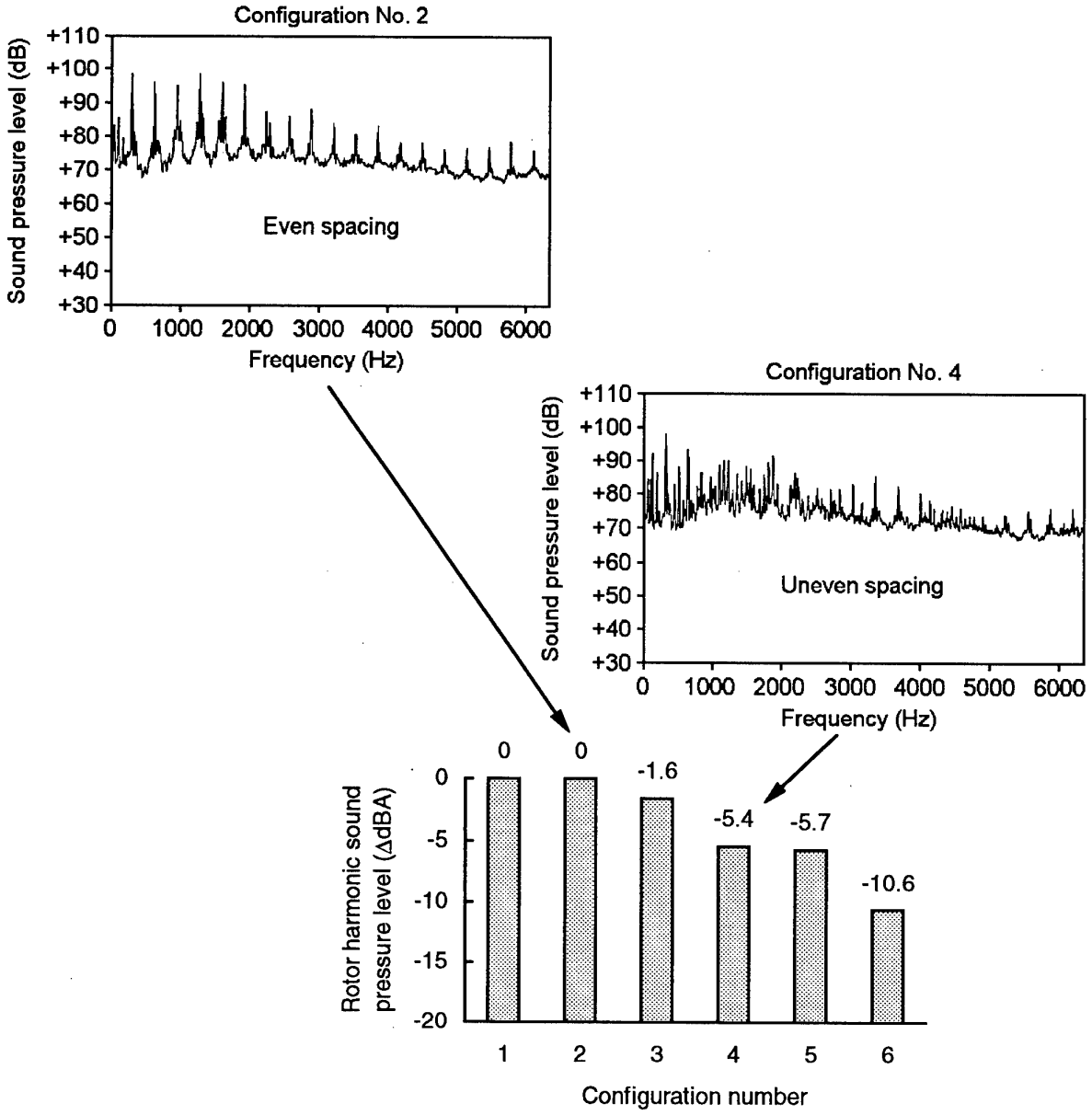

Fig. 11. Uneven blade spacing broadened spectral content and lessened the annoyance of the sound.

dominant 5/rev tone and its harmonics, and distributing it more uniformly throughout the audible spectrum. This redistribution has the effect of making the tonal content less objectionable, and tending to make the character of the rotor sound more like a broadband "hum" rather than a tonal "buzz." Ref. 7 offers a discussion of the selection and design process which led to the specific blade spacing tested.

Configuration No. 5

Configuration No. 5 represented a check of the additive effects of the tip shape as applied to the already reduced noise levels of Configuration No. 4. Combined with the reduced harmonic levels of the unevenly spaced rotor, this tip shape demonstrated an additional noise reduction of 0.3 dBA.

Configuration No. 6

Configuration No. 6, the final step in the process of testing toward an acceptable rotor design, was an unevenly spaced 5-blade rotor identical to that of Configuration No. 4, but with tip speed reduced from the original 220 m/s (720 ft/s) to 195 m/s (640 ft/s). This tip speed reduction alone reduced noise by 5.2 dBA.

Summary of Whirl Stand Test Results

The whirl stand test results showed directly that the baseline model rotor harmonic noise could be reduced

by 10.6 dBA by selecting a rotor with five unevenly spaced blades and reducing tip speed to 195 m/s (640 ft/s). If the aft taper tips were also utilized, an additional 0.3 to 1.6 dBA reduction could be expected.

Subjective evaluations of the sound of each rotor agreed with the measured data. The computer playback capability was used to great advantage in evaluating the sound quality differences among the rotor configurations. As the sounds were played back to a panel of listeners, there was unanimous agreement that the model rotor's sound quality had been dramatically improved.

The test results of model rotors to this point were very encouraging, indicating that a substantial noise reduction was possible. These tests had quickly evaluated a large matrix of potential design improvements. Because these improvements were based on the assumption that the inflow conditions that could be expected in the demonstrator helicopter were adequately simulated during the whirl stand tests, some reservations remained about the "real-world" effects of main rotor downwash and inflow turbulence upon the noise generating mechanisms. The noise reduction potential and sound quality improvements indicated by the model rotor testing outweighed these reservations, and full-scale hardware was fabricated incorporating the best five-bladed configuration in preparation for flight test evaluation.

FIVE-BLADE DTR FLIGHT TESTS

The new DTR flight test configuration incorporated the aft taper tips, five unequally spaced blades, and reduced tip speed. With the tip speed reduction comes a thrust capability reduction unless the rotor solidity is increased. In this case the solidity was increased to 0.422 by retaining the same chord (13.4cm) as the four-bladed rotor and adding a fifth blade. The fifth blade allowed the thrust capability to be maintained with the tip speed reduced to 195 m/s (640 ft/s) from the original 220 m/s (720 ft/s). The lower tip speed required a new tail rotor gearbox to be designed, built, and qualified for flight. The tooling used to make the aft taper tip for the four-bladed scissored rotor was used to make the fifth blade for the final flight test configuration. A five-bladed hub was designed, and this proved to be 1.6 cm (5/8 inch) larger than the scissored rotor's hub. The outer 1.6 cm (5/8 inch) of the blade was cut off to maintain the same blade tip clearance. The photo of Fig. 12 shows this configuration installed on the aircraft. A limited flight test program was conducted in early 1996 and produced basic low-speed performance and handling qualities, high-speed drag evaluation, and most important, the acoustic results.

The acoustic flight demonstration program compared the Model 222U DTR demonstrator helicopter with an acoustically similar Model 230 equipped with a standard two-bladed tail rotor. Flight conditions tested included in-ground-effect (IGE) hover with left and right pedal turns, 120-kn flyovers at 150 m altitude, 6-deg approach at 60 kn, and a maximum power climb at 60 kn. Both aircraft flew each condition one after the other in the presence of a listening jury comprised of marketing and engineering personnel. Three tripod-mounted microphones were deployed in a straight line, one directly under the helicopter's flight path and the others at 150 m to either side of the flight track. These measurements are considered preliminary, since the wind conditions during the demonstration were less than ideal. However, they provide a valid comparison between the two types of antitorque systems and illustrate the qualitative acoustic benefits of the present configuration DTR.

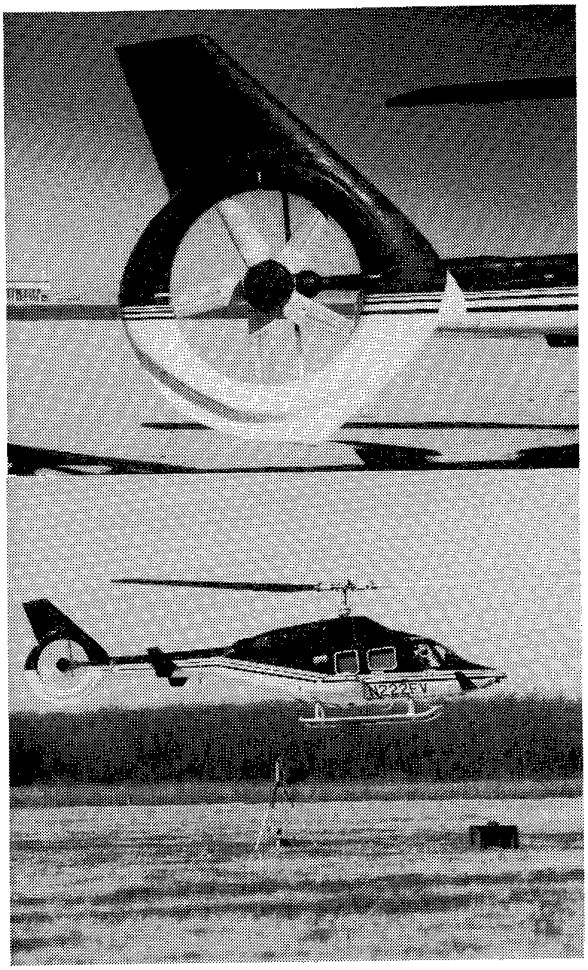

Fig. 12. Five-bladed DTR on Bell Model 222U helicopter.

ACOUSTIC RESULTS

Hover

The DTR showed a dramatic acoustic improvement during hover, which included slow left and right 360-

deg pedal turns. The DTR noise levels were lower than those of the standard tail rotor, and its tonal content changed from the traditional discrete frequency "buzz" to a more broadly distributed "hum." This beneficial characteristic was readily evident during the hover test as it had been during the whirl tests.

Fig. 13 shows the average A-weighted sound pressure level (SPL) measured during the hover test. The DTR reduced total helicopter noise 2 to 6 dBA during hover. The DTR's noise benefit is most noticeable at viewing angles aft of the helicopter, where tail rotor noise typically dominates during hover.

Forward Flight

During forward flight, as in the hover condition, the DTR showed the same dramatic acoustic improvement. A representative noise time history comparing DTR with the standard tail rotor is shown in Fig. 14 for the takeoff condition. The beneficial effects of the DTR are most pronounced when the helicopter is uprange, approaching the observer. Tail rotor sound is most dominant during this uprange portion of a flyover. The spectral content of the noise measured at about 300 m (1,000 ft) uprange, shown as an inset in the figure, indicates most tail rotor harmonics reduced by 5 to 20 dB, and total helicopter noise reduced by 6 dBA. Overhead, the DTR is 5 dBA quieter than the standard tail rotor. The acoustic benefits of the DTR are also more pronounced directly under the flight track than at the 150-m sideline microphones, presumably because of the shielding effects of the duct structure itself. After the helicopter passes overhead, tail rotor noise becomes less dominant, and the difference between the DTR and the standard tail rotor becomes less pronounced.

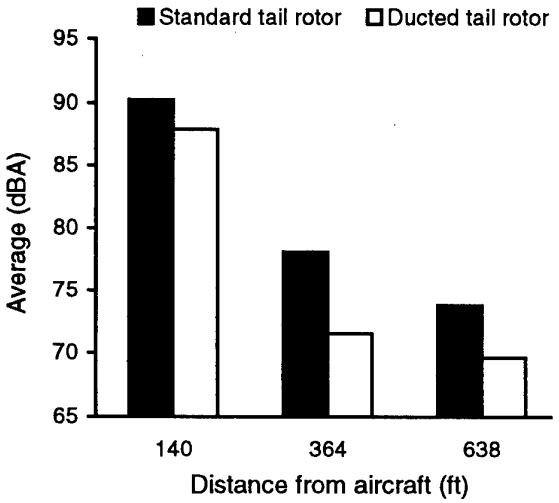

Fig. 13. IGE hover with 360° left and right pedal turns.

In terms of effective perceived noise decibels (EPNdB), a noise metric used in helicopter noise standards, the DTR reduces total helicopter noise by a three-microphone average of 3 EPNdB for the flyover, takeoff, and approach conditions combined.

In all the flight demonstrations, the sound quality of the DTR was markedly improved over that of a standard tail rotor. This improvement is due not only to the introduction of the duct itself, but also to the uneven blade spacing, lower rotational tip speed, and blade tip shape. Written comments, solicited from the 35-person sound jury present at the demonstration flight, were very positive and indicated that application of the DTR design to the product line should be considered. Typical comments from the jury included "[tail rotor noise] hardly noticeable," "very acceptable," and "excellent."

DTR FLIGHT CHARACTERISTICS

In addition to the noise characteristics, the DTR flight test program was to determine the effect that configuration changes had on performance, handling qualities, and component loads. Results from the different phases of testing provided insight into the use of analytical tools for future refined DTR designs. Performance, low-speed handling, and component loads were within expectations, and the results obtained greatly broadened the DTR technology data base.

Ground Run

Performance data taken during ground runs of the DTR demonstrator are compared to analysis predictions in Fig. 15. During ground runs, the DTR thrust was derived from tailboom lateral bending. This was found to be reasonably accurate when the main rotor collective was reduced to flat pitch to minimize downwash on the tailboom. The analysis indicated the low tip speed five-bladed rotor would have a very slight performance advantage over the high tip speed four-bladed rotor. The ground run data in Fig. 16 shows no measurable difference between the four- and five-bladed designs. The expected performance advantage is smaller than the measurement resolution. The only other difference between the four- and five-bladed designs is that the five-bladed design requires an additional 1 to 2 deg of blade pitch to maintain thrust capability, as indicated in Fig. 17.

Hover

Due to the emphasis on acoustic testing, only four hover performance points were taken of the five-bladed rotor in low wind conditions. Since this is a statistically small sample, the DTR hover performance is best determined by using the four-bladed rotor data and noting that the five-bladed rotor is as good, or better. The four-bladed DTR hover performance is shown compared to the standard tail rotor in Fig. 18.

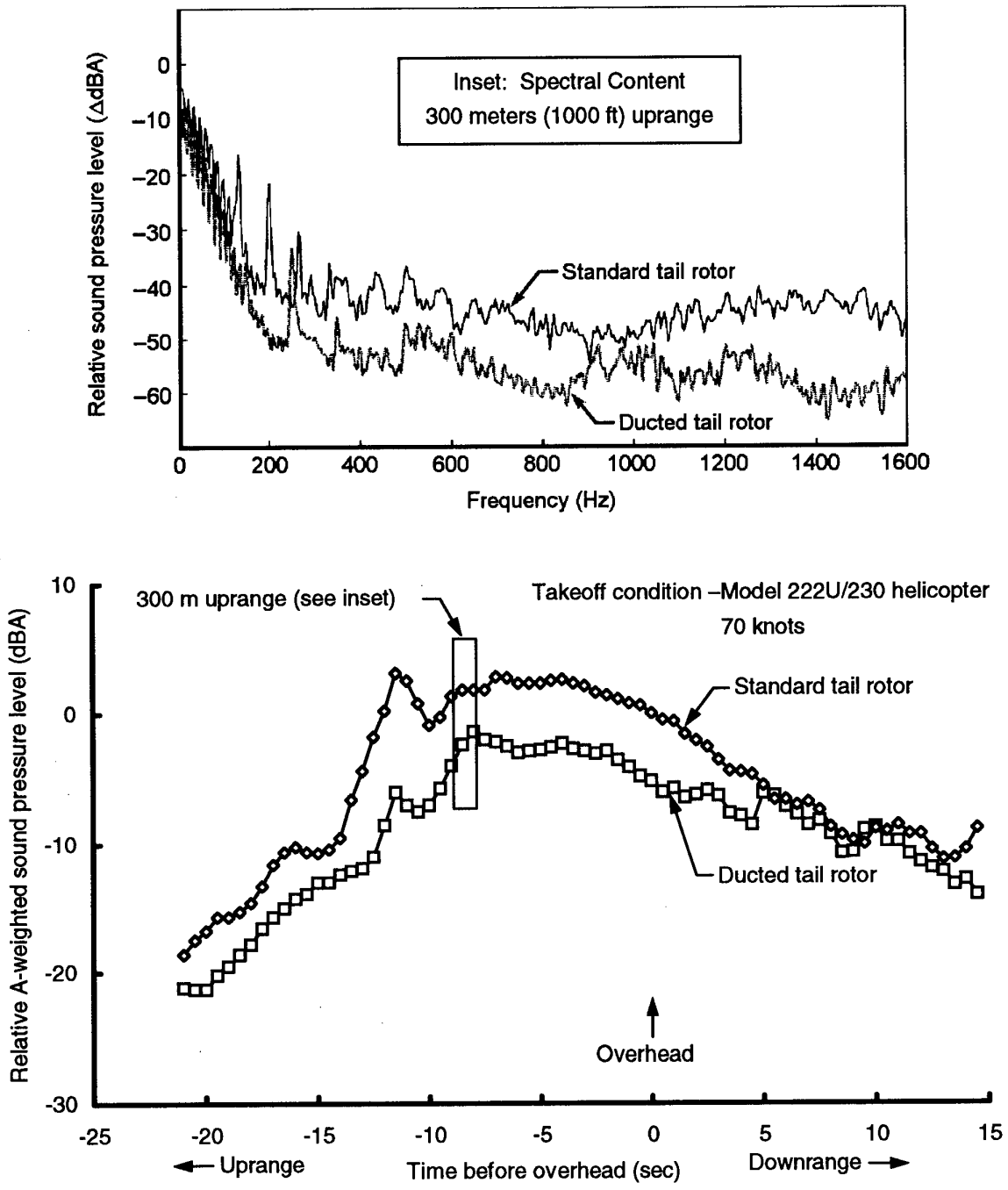

Fig. 14. Improved noise characteristics with ducted tail rotor.

For both curves, the thrust is derived from main rotor torque. This thrust value includes all the downwash forces on the tailboom and horizontal elevator endplates. However, since this is the same for both aircraft, the performance difference is valid. For a typical hover thrust value of 222 daN (500 lbf), the standard tail rotor requires 64 kW (86 hp), and the four-bladed DTR 77 kW (103 hp), a 13-kW (17-hp) penalty. Analysis indicates that the five-bladed DTR should require 2.2 kW (3 hp) less to produce 222 daN (500 lbf) of thrust than the four-bladed DTR, thus reducing the penalty to 10.4 kW (14 hp). This equates to a 1.5% increase in engine shaft power required to hover. This modest performance penalty could be reduced to zero by increasing the diameter of the ducted rotor. However, this larger rotor and the surrounding duct would weigh more and produce more drag in forward flight.

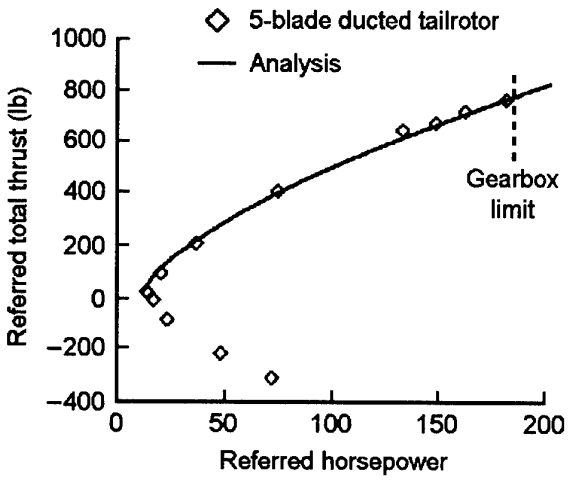

Fig. 15. Ground run performance.

Sideward Flight

Right sideward flight performance is shown in Fig. 19. At 35 kn, the power required is 97 kW (130 hp). With the gearbox rated at 138 kW (185 hp) maximum continuous power, this leaves plenty of margin for maneuvers or gusts. The low-speed flight pilot workload was less than for the standard tail rotor, due in part to the DTR's higher rotor disk loading.

Forward Flight

The only significant handling quality deficiency with the Model 222U demonstrator aircraft was the occurrence of lateral directional oscillations with left sideslip. These oscillations may have been due in part to low tail volume, high fin incidence, and poor fin sectional properties. Flight tests with the fin tufted indicated that the flow on the lower half of the vertical fin is separated during left sideslip, but attached with zero or right sideslip. A final solution will require additional flight testing.

The drag increase over the baseline Model 222U was 0.13 m^2 (1.4 ft^2). Because of the high fin incidence and shrouding of the tail rotor, the DTR tail rotor required less power than the standard tail rotor in forward flight (Fig. 20). The higher drag and lower power required combine to produce a 2-kn penalty compared to the standard tail rotor.

Loads

As seen in Figs. 21 and 22, measured rotor hub and blade steady and oscillatory (dynamic) loads are within or slightly greater than predicted design load values. These data were obtained during five-bladed DTR flight test for in-ground effect hover and level flight conditions. Also shown in Fig. 22, the effect of rotor configuration on oscillatory loads is not significant

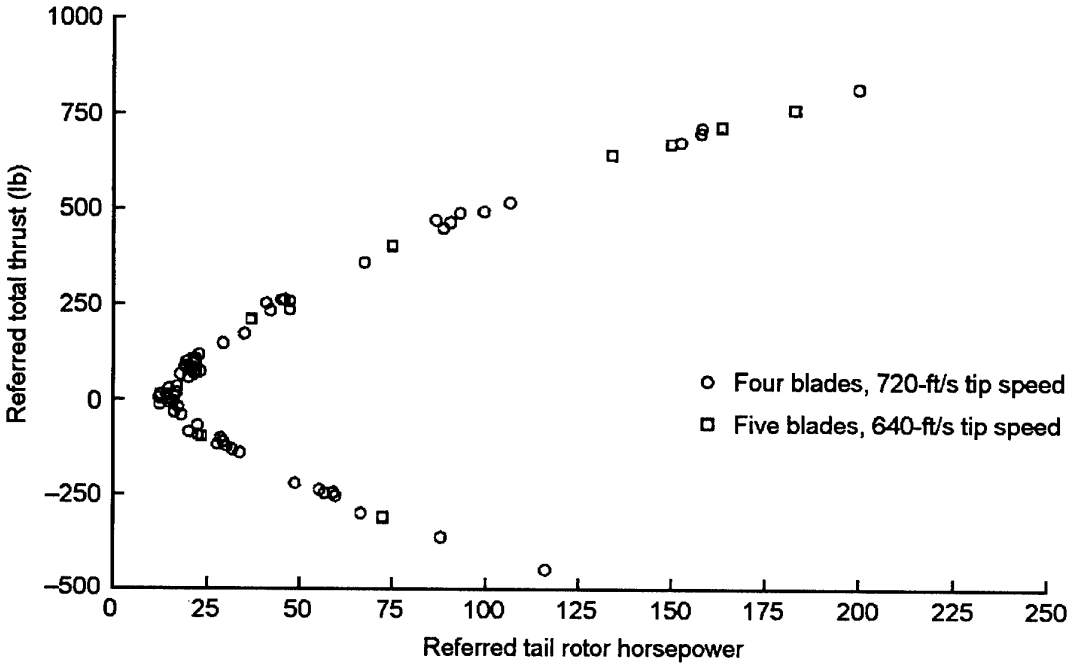

Fig. 16. Ground run performance comparison.

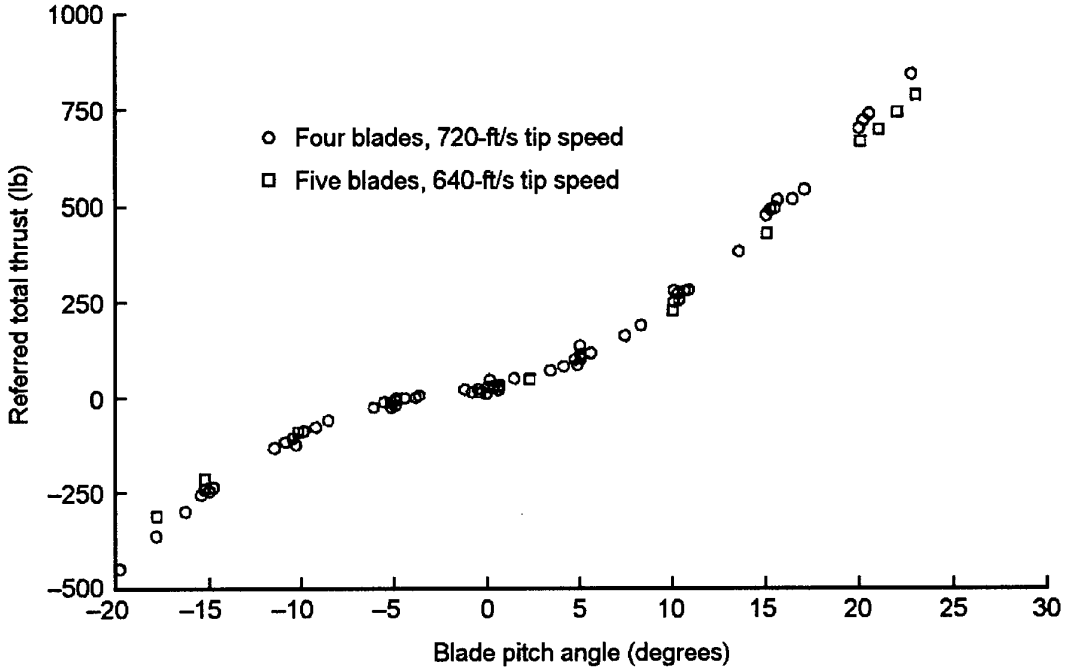

Fig. 17. Ground run performance comparison.

when accounted for in the design. Additional conditions were flown for the five-bladed and the four-bladed DTR configurations, and the measured steady and oscillatory loads data showed similar results.

CONCLUDING REMARKS

The whirl stand and flight tests have demonstrated that a DTR can meet operational needs, including low noise, performance, loads, and handling qualities. Installed on a Model 222U demonstrator helicopter, Bell's DTR, with five unevenly spaced blades and an aft taper tip, operating at a reduced tip speed, substantially decreases tail rotor noise and dramatically improves the sound quality of the helicopter. Total helicopter noise reductions of up to 6 dBA are realized during hover and forward flight, along with reductions in individual tail rotor harmonics of 5 to 20 dB. Effective perceived noise levels are reduced 3 EPNdB (three-microphone average) for takeoff, level flight, and approach conditions. A marked improvement in total helicopter noise is especially noticeable as the helicopter is uprange of a sound jury, while similar improvements are evident during hover operations. The annoying tail rotor "buzz" is changed to a more pleasing "hum." The DTR configuration tested required 1.5% more engine power to hover than the standard tail rotor, but demonstrated superior sideward flight capability and also reduced pilot workload. The increased drag of the duct costs about 2 kn in forward flight.

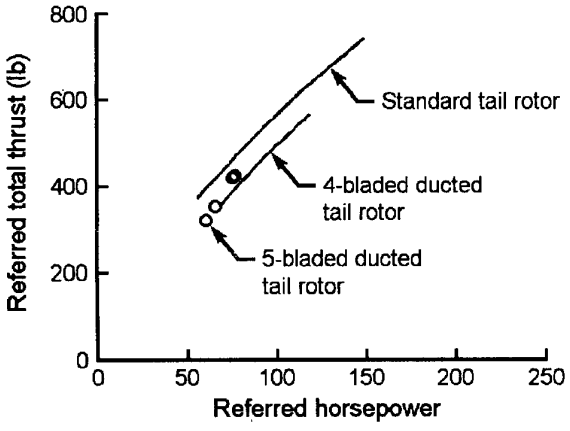

Fig. 18. Hover performance comparison.

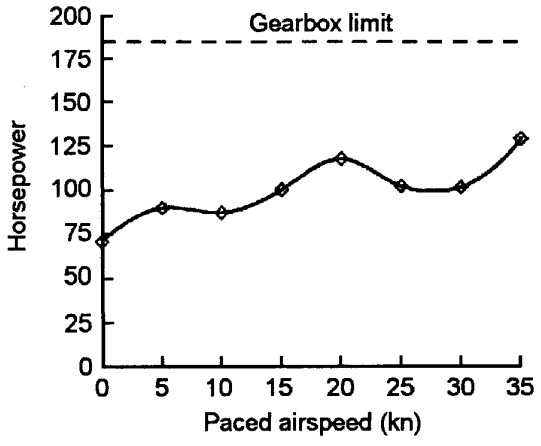

Fig. 19. Right sideward flight performance.

Since retrofits to existing helicopters would involve extensive redesign, these must be examined on a case-by-case basis. Cost, weight, and performance studies are now underway to determine the DTR's applicability to new designs.

REFERENCES

1. Prouty, R. W., "The Angle On the Scissors Rotor," *Rotor and Wing*, January 1996, p. 46.

2. Riley, R. G., "Effect of Uneven Blade Spacing on Ducted Tail Rotor Acoustics," American Helicopter Society 52nd Annual Forum, June 4–6, 1996.

3. Mellin, R. C., and Sovran, G., "Controlling the Tonal Characteristics of the Aerodynamic Noise Generated by Fan Rotors," *Journal of Basic Elements*, March 1970. pp.143-154.

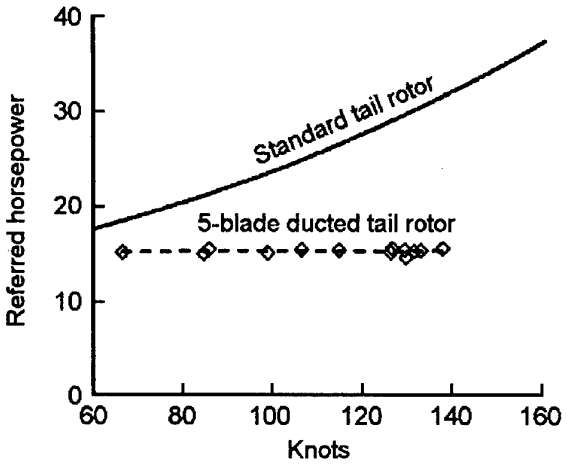

Fig. 20. Tail rotor power required in forward flight.

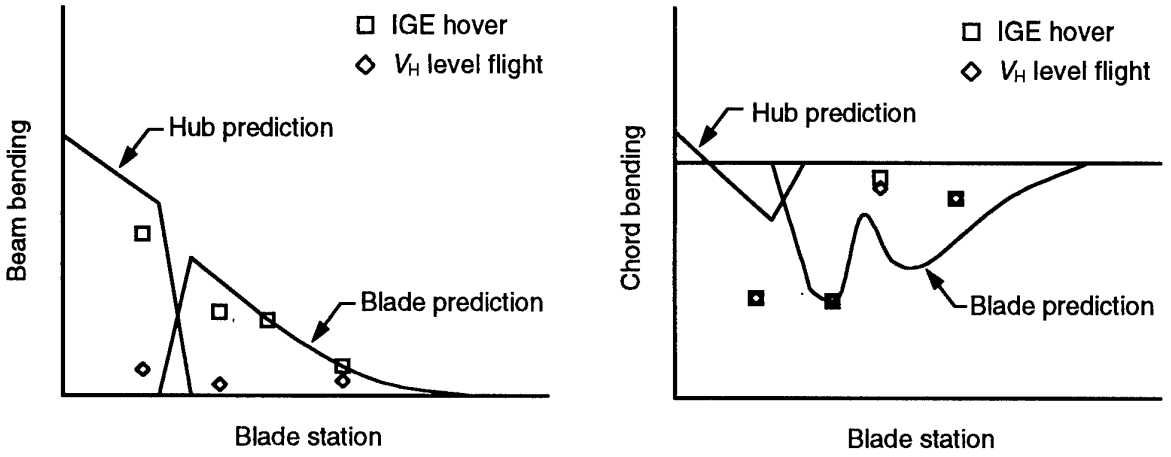

Fig. 21. Measured vs. predicted rotor hub and blade IGE hover and V_H level flight steady loads for five-bladed unevenly spaced rotors.

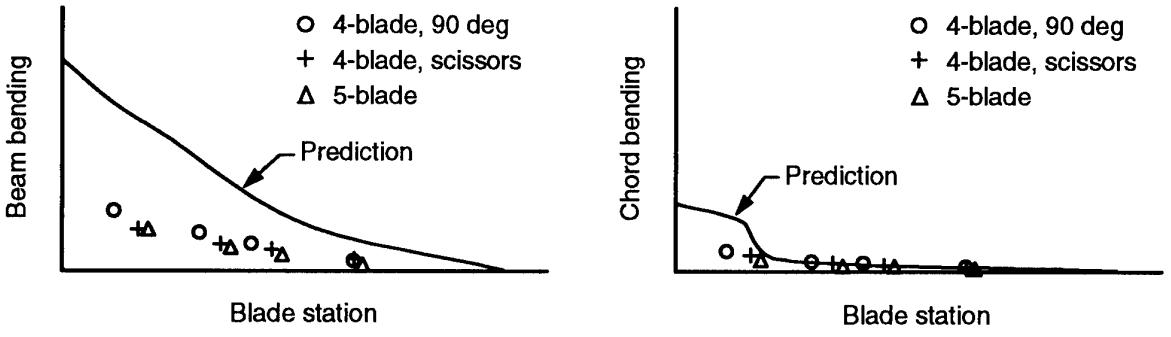

Fig. 22. Measured vs predicted rotor hub and blade V_H level flight oscillatory loads for four-bladed 90 degree spaced, four-bladed scissors, and 5-bladed unevenly spaced rotors.

4. Vialle, Michel, and Arnaud, Gilles, "A New Generation of Fenestron Fan-In-Fin Tail Rotor on EC 135," Nineteenth European Rotorcraft Forum, Sept 14–16, 1993.

5. K.D. Kryter and K.S. Pearsons, "Judged Noisiness of a Band of Random Noise Containing an Audible Pure Tone," *JASA* Vol 38, (1965), pp. 106-112.

6. D. Ewald, A. Pavlovic, and J. Bollinger, "Noise Reduction by Applying Modulation Principles," *JASA*, Vol 49, No. 5 (Part 1), 1971.

7.. P. Shahady, C. Lyon, J. Schauer, M. Chopin, and M. Ewing, "The Effects of Modulated Blade Spacing on Static Rotor Acoustics and Performance," 1973.

Mesures en vol et prévision du bruit interne d'un hélicoptère ECUREUIL

A. Morvan et J-M. David
OFFICE NATIONAL D'ÉTUDES ET
DE RECHERCHES AEROSPATIALES
Direction des Structures
29, avenue de la Division Leclerc
BP 72, 92322 CHÂTILLON CEDEX, France

RÉSUMÉ

Afin de caractériser les sources responsables du bruit interne dans la cabine d'un hélicoptère et de valider la modélisation de l'appareil basée sur la méthode SEA (Statistical Energy Analysis) qui permet la prévision de ce bruit interne, une campagne de mesures en vol sur un hélicoptère Ecureuil monomoteur a été effectuée par la Direction des Structures de l'ONERA sur le site d'EUROCOPTER FRANCE à Marignane, pendant que parallèllement était réalisée la modélisation.

On décrit l'instrumentation mise en place sur l'hélicoptère, la procédure d'enregistrement et d'exploitation des mesures et on analyse les résultats pour différentes vitesses de vol.

On présente ensuite le développement du modèle SEA de l'Ecureuil et la manière de prendre en compte les diverses sources d'excitation avec, en particulier, une modélisation de l'excitation aérodynamique due à la couche limite turbulente, basée sur un modèle numérique simplifié.

Enfin on présente une comparaison calculs-mesures portant sur des niveaux vibratoires et sur la pression acoustique moyenne dans la cabine.

ABSTRACT

In order to characterize the potential sources of noise in a helicopter cabin and to validate a model of the cabin based on the SEA (Statistical Energy Analysis) method used as a predictive method, measurements were made by the ONERA Structures Department vibroacoustical team at EUROCOPTER FRANCE in Marignane while the SEA modeling was being carried out.

Experimental equipment used in the single-engine helicopter ECUREUIL, data recording and analysis procedures are described and results are analyzed for different flight speeds. The SEA model of helicopter cabin is then presented and the way to take into account the different sources of excitation in this model. A model of aerodynamic excitation (due to turbulent boundary layer) is based on a simplified numerical approach.

Finally, a comparison between measurements and computation for vibration response of structural parts and acoustical pressure in the cabin is presented.

1. INTRODUCTION

Des méthodes de prévision du bruit interne dans les hélicoptères et plus généralement dans les structures aéronautiques peuvent être bâties sur l'Analyse Statistique Energétique (SEA) dans les domaines moyenne (MF) et haute fréquence (HF) compte tenu des progrès réalisés ces dernières années dans ce domaine.

Dans le cadre des développements de méthodes de prévision du comportement dynamique haute fréquence des structures mécaniques complexes, la Direction des Structures de l'ONERA a effectué depuis 1986 un ensemble de recherches centrées sur la SEA [9,10,11,12,13,14,15,16]. Ces travaux ont abouti à la création d'un code de SEA à vocation industrielle ("PEGASE") [17,18,19]. Parallèllement des méthodes numériques ont été développées en basse fréquence (BF) et moyenne fréquence pour la prévision du comportement vibratoire des structures [2]. Ces méthodes et les codes numériques correspondant ont été développés et validés dans le cadre des études de discrétion acoustique. La méthode (MF) a été également validée dans le cadre de la prévision du bruit interne sur un hélicoptère de type DAUPHIN [4].

Dans le cas des hélicoptères, la méthode SEA est bien adaptée à la prévision du bruit interne dans la cabine dans les domaines MF et HF compte tenu que la structure est constituée d'éléments structuraux à forte densité modale qui entourent différentes cavités acoustiques internes et compte tenu aussi que les spectres d'excitation sont des spectres large bande qui s'étendent dans les domaines MF et HF.

A la demande d'EUROCOPTER-France (ECF) et dans le but de valider la méthode SEA et l'application du code PEGASE à la prévision haute fréquence du bruit interne dans une cabine d'hélicoptère, une campagne de mesures du bruit interne d'un hélicoptère en vol a été réalisée en 1992 par la Direction des Structures de l'ONERA sur l'Ecureuil SA 350Z monomoteur [5].

Le but de cette campagne de mesures était de générer une base de données expérimentales destinée à être utilisée de deux façons.

- La première a consisté à caractériser les différentes sources de bruit dans la cabine et à mesurer les réponses vibratoires et acoustiques de l'appareil dans les domaines

Paper presented at the FVP Symposium on "Advances in Rotorcraft Technology", held in Ottawa, Canada, 27-30 May 1996, and published in CP-592.

moyenne et haute fréquence.

- La seconde a permis la mise en oeuvre et la validation de modèles SEA qui seront utilisés ultérieurement dans la prévision du bruit interne des futurs hélicoptères.

Ces mesures ont permis de valider un premier modèle SEA de l'Ecureuil réalisé par ECF [6] en utilisant le logiciel LASCAR développé par l'Aérospatiale-Missiles.

Un modèle SEA de l'ONERA a ensuite été mis en oeuvre à l'aide du logiciel PEGASE [7].

2. DESCRIPTIF DE LA CAMPAGNE DE MESURES

La finalité des mesures à effectuer en vol était de constituer une base de données expérimentales permettant :

- d'identifier et de caractériser les sources potentielles du bruit cabine, qu'elles soient d'origine :

  . vibration mécanique transmise par voie solidienne,

  . excitation acoustique transmise par voie aérienne (interne ou externe),

  . excitations d'origine aérodynamique induites par des écoulements (couche limite turbulente),

- de mesurer la réponse vibratoire et acoustique interne de l'hélicoptère.

Les sources ainsi mesurées peuvent alors être appliquées comme des entrées au modèle SEA de l'hélicoptère; les sorties calculées, énergies des sous-systèmes mécaniques et des cavités acoustiques dont en particulier la cavité cabine, sont alors comparées aux réponses correspondantes mesurées sur l'appareil.

2.1 Instrumentation de l'hélicoptère

2.1.1 Mesure des sources

Les excitations mécaniques étaient mesurées par :

- 6 accéléromètres (4 en Z, 1 en X, 1 en Y) sur le plancher mécanique aux pieds des barres BTP,

- 1 accéléromètre en Z près d'un plot d'attache du moteur,

- 1 accéléromètre en Z sur le palier de sortie vers la BTA.

Pour estimer les excitations acoustiques étaient disposés :

- 2 microphones dans la cavité BTP,

- 2 microphones extérieurs sur le toit de la cabine, sous le rotor,

- 1 microphone près d' une entrée d'air moteur,

- 1 microphone à proximité du jet de la tuyère.

Enfin 3 capteurs de pression pariétale étaient montés affleurants sur la verrière et le vitrage d'une porte avant, afin d'appréhender les excitations d'origine aérodynamique.

2.1.2 Mesure des réponses

Les 7 sous-systèmes mécaniques retenus pour la comparaison calcul-mesure, pour leur rôle important dans la transmission de l'énergie vibratoire et acoustique vers la cavité interne cabine, étaient :

- le plancher mécanique de la BTP,

- la partie haute de la cloison arrière cabine,

- la partie basse de la cloison arrière cabine,

- le plafond de la cabine,

- le portillon arrière gauche,

- la portière avant gauche,

- la verrière.

L'énergie vibratoire de chacun de ces sous-systèmes était établie à partir des réponses de 5 accéléromètres répartis aléatoirement, normaux aux parois.

L'énergie acoustique dans la cavité cabine était mesurée par 5 microphones au niveau habituel des têtes pilotes et passagers. Enfin 1 microphone mesurait la pression acoustique dans la soute arrière de l'appareil.

2.2 Enregistrement et exploitation des mesures

La procédure retenue était la suivante : enregistrement analogique en continu des signaux issus des capteurs pendant les vols de mesure, puis, à terre, relecture et transfert pour numérisation des voies enregistrées à un laboratoire mobile pour validation en temps très peu différé.

Le nombre total de capteurs étant d'environ 60, le matériel embarqué, hormis les capteurs eux-mêmes, se composait de boîtiers conditionneurs, d'un commutateur 4x32 voies et d'un enregistreur magnétique analogique 28 pistes FM, dont une voie phonie. L'enregistrement de l'ensemble des capteurs s'effectuait en trois séquences de 27 voies, certains signaux de référence correspondant à des sources étant répétés sur les trois séquences, afin de rechercher les cohérences entre les réponses et chacune des sources potentielles. La numérisation, le traitement du signal et l'analyse, effectués en léger différé juste après le vol, utilisaient les ressources d'un laboratoire mobile équipé d'un système d'acquisition DIFA, géré par stations de travail Hewlett-Packard, sous logiciel LMS.

2.3 Configurations de vol traitées

Les mesures ont été effectuées dans 4 configurations de vol de l'hélicoptère Ecureuil :

- vol stationnaire hors effet de sol (65 % du couple nominal),

- vol avançant à 82 noeuds (50 % du couple nominal),

- vol avançant à 105 noeuds (65 % du couple nominal),

- vol avançant à 130 noeuds (95 % du couple nominal) ;

le choix de ces configurations permettant d'apprécier les influences respectives de la valeur du couple délivré et de la vitesse aérodynamique.

2.4 Analyse des résultats et commentaires

Sans présenter de manière exhaustive tout le contenu de la base de données élaborée après cette campagne de mesure, nous pouvons illustrer le contenu de celle-ci et mettre en évidence les différences de morphologie entre les princi-

pales excitations, causes du bruit interne, et montrer leur résultante, le spectre fréquentiel du bruit cabine.

2.4.1 Excitations mécaniques

La Figure 1 présente l'accélération en Z au pied d'une des barres BTP, ceci dans les 4 configurations de vol. Nous avons ici un spectre de raies dans lequel on retrouve, bien naturellement, toutes les fréquences d'engrènement présentes dans la chaîne cinématique constituant la BTP, ainsi que des harmoniques ou combinaisons de ces fréquences. Le régime moteur étant bien régulé et donc quasi constant malgré les variations du couple délivré, les fréquences des raies ne bougent pas en fonction de la configuration de vol; seules les amplitudes varient un peu en fonction de la vitesse de vol, donc du couple transmis. Nous avons présenté ici une excitation par voie solidienne, mais la même remarque vaut pour les excitations acoustiques (voie aérienne) dues au bruit dans la cavité BTP et donc de même origine.

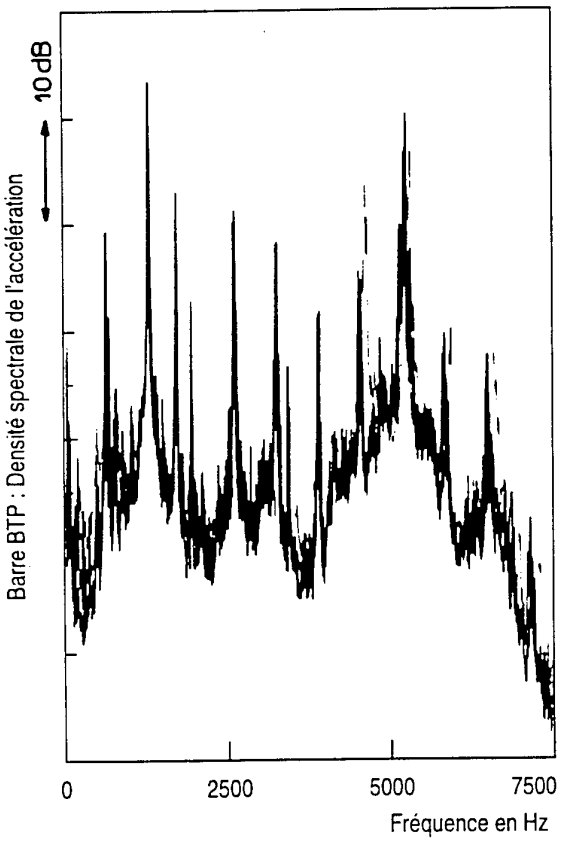

Fig. 1

2.4.2 Excitation aérodynamique

La Figure 2 présente le spectre de pression pariétale en un point de la verrière pour les 4 vitesses de vol. On retrouve la morphologie typique d'un spectre d'excitation par couche limite turbulente, de nature bruit large bande, avec une bosse à une fréquence dépendant des caractéristiques de la couche limite et donc du point de mesure choisi. Cette fois nous constatons une augmentation du niveau sur tout le spectre directement corrélé à la vitesse de vol ; la fréquence de la bosse ne variant pratiquement pas.

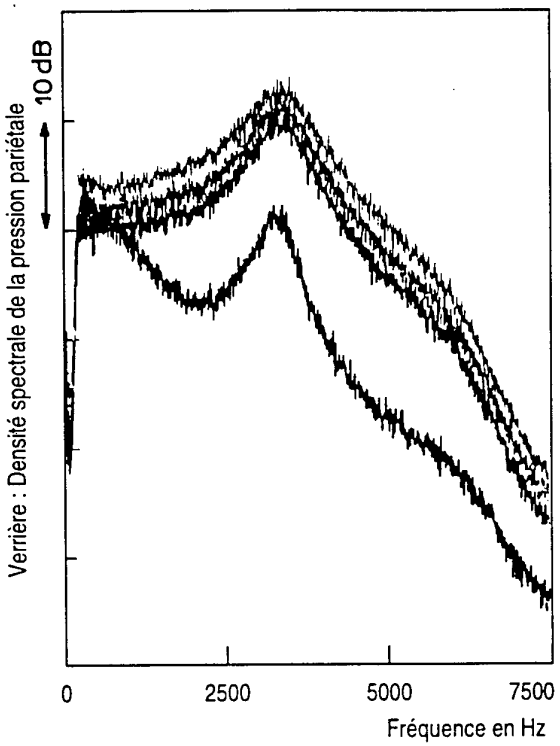

Fig. 2

2.4.3 Bruit interne cabine

La contribution des différentes sources à la génération du bruit cabine fait que celui-ci (Figure 3) présente une combinaison des caractères spécifiques rencontrés sur les spectres des sources: spectre de raies à fréquences fixes et bruit large bande augmentant régulièrement en niveau avec la vitesse de vol de l'hélicoptère.

3. MISE EN OEUVRE D'UN MODÈLE SEA À L'ONERA

Un modèle SEA **simplifié** de la cabine prenant en compte uniquement les éléments principaux (voir Figure 4) où transite l'énergie a été développé à la Direction des Structures de l'ONERA. Cette modélisation a conduit à environ **40** sous-systèmes SEA. Ces sous-systèmes sont de type plaque mince, poutre, coque mince en flexion constitués soit de matériaux métalliques ou en composite sandwich-NIDA et de type cavité acoustique interne.

L'application du code "PEGASE" sur ce modèle a été effectuée dans la bande de fréquence [300 – 10000] Hz pour des bandes 1/3 d'octave et pour trois des quatre configurations de vol de l'appareil décrites au paragraphe précédent. Les comparaisons calcul-mesures ont porté sur les niveaux d'énergie vibratoire des 7 éléments principaux de type structure (**vitesses quadratiques moyennes au carré**)

et sur le champ de pression dans la cavité cabine passagers (**pressions quadratiques moyennes au carré**) pour lesquels les mesures ont été réalisées.

La difficulté majeure dans la réalisation de ce modèle a été l'estimation et la reconstitution des puissances introduites dues aux différentes sources d'excitation qui participent au bruit interne et qui ont été identifiées expérimentalement.

Pour la bande de fréquences traitée, elles se résument à trois types:

1) une excitation **mécanique** induite sur le plancher "mécanique" par les barres BTP et provenant des différentes raies d'engrenement de la boîte de vitesse dont le spectre est un spectre de raies,

2) une excitation **acoustique** provenant du rayonnement de la boîte de vitesse et du carter et se propageant au plancher et,

3) une excitation **aérodynamique** provoquée par la couche limite turbulente qui se développe sur la partie avant du fuselage pour les vols avançants et dont le spectre est un spectre large bande dans la gamme MF et HF.

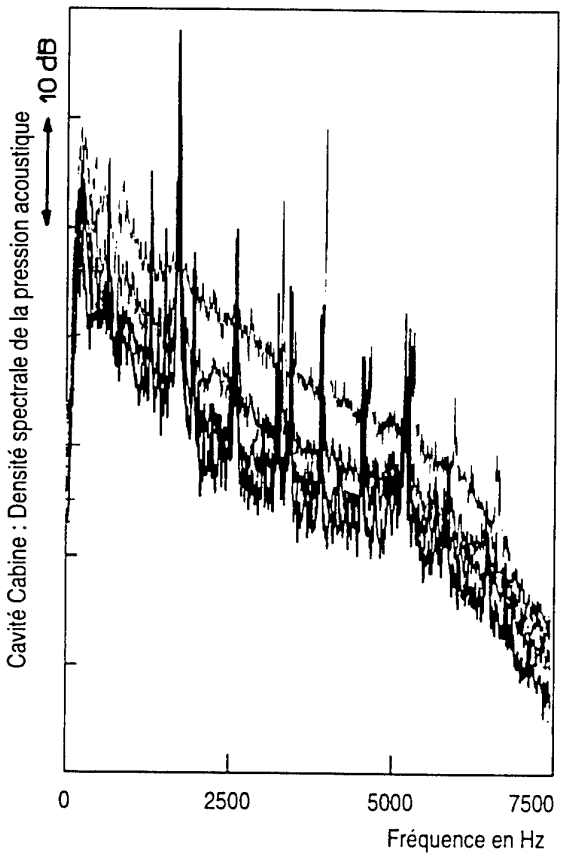

Fig. 3

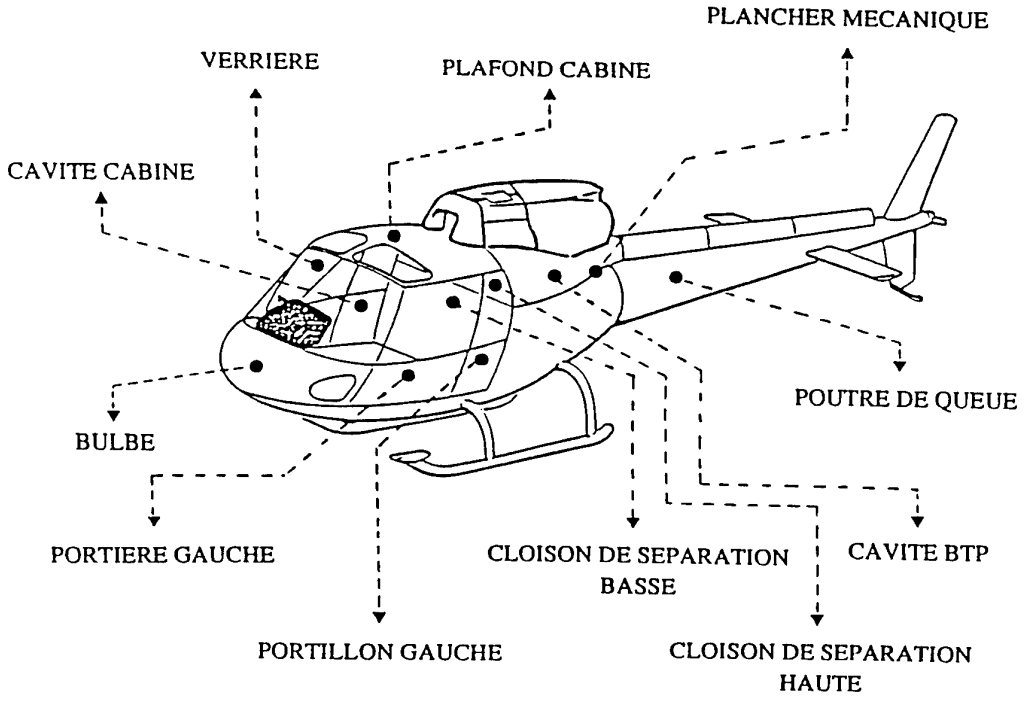

Fig. 4

3.1 Modélisation de l'excitation sur le plancher

En ce qui concerne l'excitation induite sur le plancher "mécanique", qui englobe l'excitation mécanique par les barres et la partie rayonnement acoustique du carter, la puissance introduite dans le modèle SEA a été déterminée "de façon globale" en effectuant un **recalage** des niveaux d'accélération mesurés sur le plancher. On ne disposait pas en effet de mesures suffisantes permettant de remonter directement aux forces introduites dans les barres et l'on ne sait pas estimer la part relative de l'excitation acoustique due au rayonnement de la boîte.

3.2 Modélisation de l'excitation aérodynamique

Quant à l'excitation de couche limite induite sur les éléments structuraux du fuselage avant, une **évaluation numérique** de cette excitation a été réalisée à l'aide d'un modèle simplifié de couche limite [8].

Le modèle de puissance introduite développé à cet effet est le suivant :

$$< \Pi_{in}(\omega_0) >= \frac{\pi}{2} \frac{S}{M_T} \frac{0.65U_0}{0.115\omega_0} \frac{0.65U_0}{0.7\omega_0} n_T(\omega_0) \bar{P_a}^2(\omega_0)$$

où $\bar{P_a}^2(\omega_0)$ est la pression moyenne pariétale appliquée sur les différents éléments soumis à l'excitation de la couche limite, U_0 est la vitesse de l'écoulement autour de la cabine (soit la vitesse de l'hélicoptère pour les configurations en **vol avançant**), ω_0 la fréquence centrale de calcul, S la surface de l'élément, M_T sa masse totale et $n_T(\omega_0)$ sa densité modale totale.

Ce modèle nécessite par conséquent l'évaluation de la pression moyenne pariétale $\bar{P_a}^2(\omega_0)$ (moyenne fréquentielle et moyenne spatiale).

Dans un premier temps, on a utilisé pour $\bar{P_a}^2(\omega_0)$ les résultats de mesure de pression pariétale dont nous disposions.

Dans un deuxième temps, afin d'améliorer le caractère prévisionnel de la méthode pour les futurs hélicoptères en vol, un modèle numérique d'évaluation de la pression moyenne pariétale a été développé. Puisque $\bar{P_a}^2(\omega_0)$ est la moyenne fréquentielle et spatiale de l'auto-spectre de pression pariétale, on utilise, pour alimenter ce modèle, le modèle **analytique** de CORCOS qui semble donner les meilleures prévisions (comparé à l'utilisation d'autres modèles tels que ceux de CHASE, BENARROUS, etc...) et qui fait intervenir les paramètres de la couche limite. On évalue alors ces paramètres numériquement à l'aide d'un modèle simplifié de couche limite de la façon suivante :

1) on introduit un profil moyen axisymétrique de l'hélicoptère qui permet de calculer en fluide incompressible le champ des vitesses extérieures,

2) puis un calcul de couche limite est effectué, permettant de déterminer le long du profil les différentes zones de la couche limite (laminaire, transition, turbulente) et les principaux paramètres de celle-ci. Ce calcul est réalisé à l'aide du logiciel "3C3D" qui a été développé et validé par le CERT-ONERA [1].

- La Figure 5 montre l'évolution de l'épaisseur de déplacement de la couche limite δ^* obtenue sur le Plafond-Cabine (**trait continu fort**) et les Portières (**trait pointillé fort**) pour la vitesse de vol de l'hélicoptère de 194 km/h (105 noeuds).

- La Figure 6 montre ensuite la comparaison entre mesure (**trait continu fort**) et calcul (**trait pointillé fort**) de la pression moyenne pariétale $\bar{P_a}^2(\omega_0)$ appliquée sur le Plafond-Cabine pour la vitesse d'avance de 194 km/h.

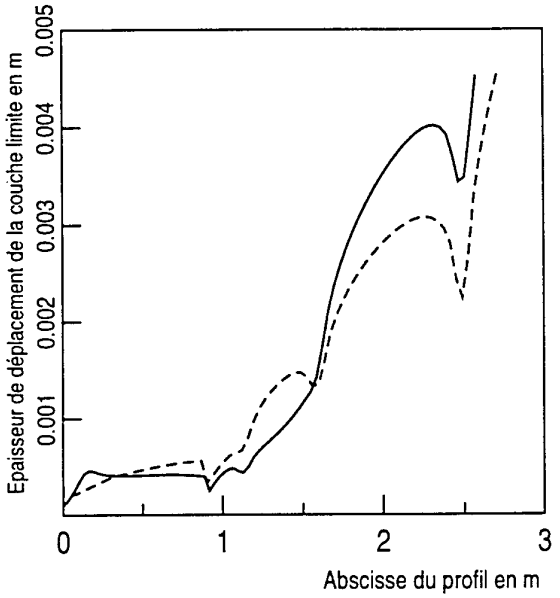

Fig. 5

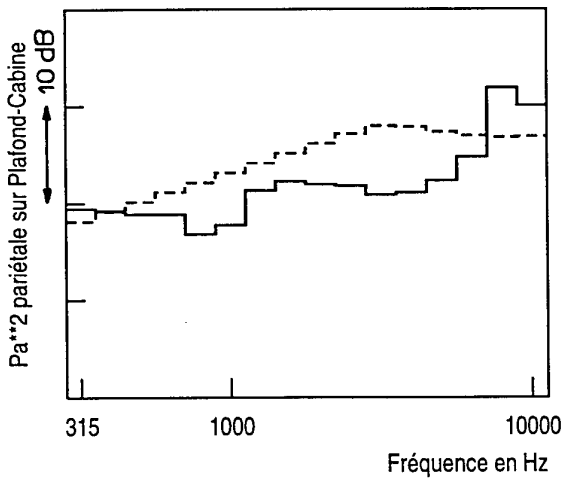

Fig. 6

On peut ainsi noter sur ce dernier résultat une bonne corrélation entre mesure et calcul.

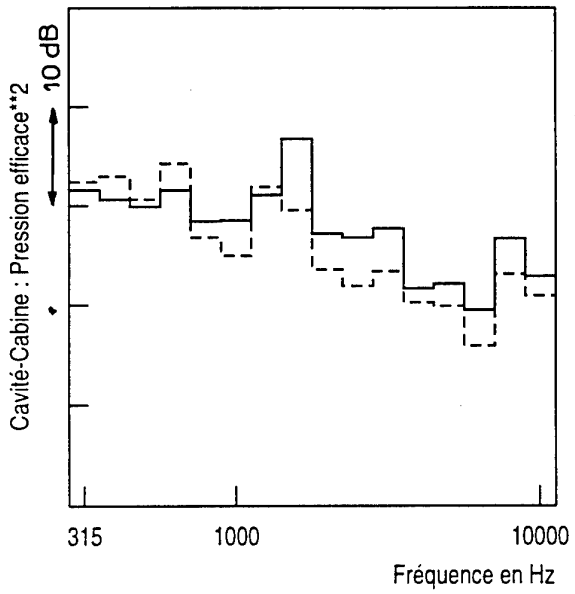

Fig. 7

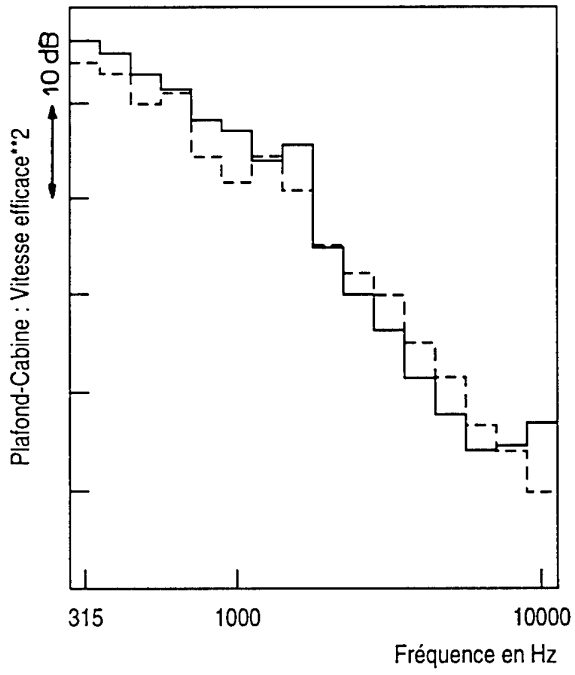

Fig. 8

4. COMPARAISON CALCULS-MESURES

Le code PEGASE fournit dans un premier temps la **valeur moyenne** de la réponse de chaque sous-système.

- La Figure 7 montre la comparaison entre mesure (**trait continu fort**) et la prévision par le calcul (**trait pointillé fort**) de la **pression moyenne efficace** obtenue dans la Cavité-Cabine pour le vol avançant à 194 km/h.

- La Figure 8 montre la comparaison entre mesure (**trait continu fort**) et la prévision par le calcul (**trait pointillé fort**) de la **vitesse moyenne efficace** du Plafond-Cabine obtenue pour le vol avançant à 194 km/h.

Dans un deuxième temps, on a la possibilité avec ce code d'effectuer une analyse de sensibilité du modèle autour des valeurs moyennes. Cette analyse permet de prendre en compte la dispersion des paramètres SEA autour de leur valeur moyenne, de tester la robustesse du modèle vis-à-vis de paramètres importants et de déterminer les paramètres principaux qui pilotent la réponse dans la cabine (ici les excitations). L'analyse se fait via l'introduction d'un taux de dispersion moyen des paramètres autour de leur valeur moyenne ; le code calculant alors l'**enveloppe de la réponse** autour de la valeur moyenne.

Ceci est illustré par les Figures 9 et 10 qui montrent la comparaison entre la mesure (**trait continu fort**) et l'enveloppe de la réponse prévue par le calcul (trait pointillé fin) de la **pression moyenne efficace** dans la Cavité-Cabine et de la **vitesse moyenne efficace** du Plafond-Cabine obtenus pour le vol avançant à 194 km/h.

On peut constater sur ces résultats que globalement l'enveloppe de la réponse estimée par le calcul contient les résultats de la mesure.

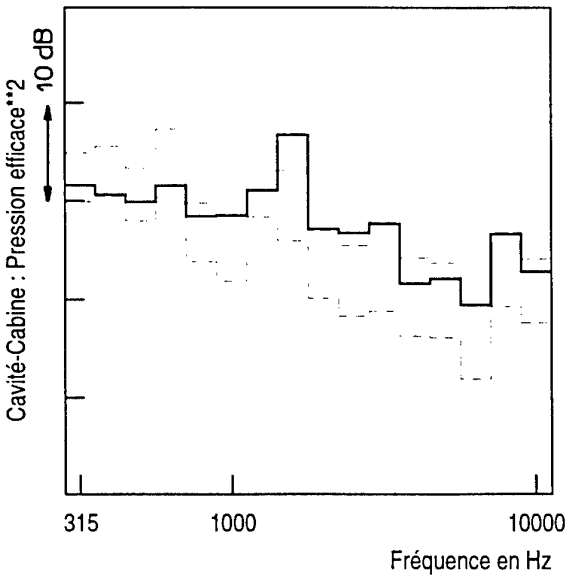

Fig. 9

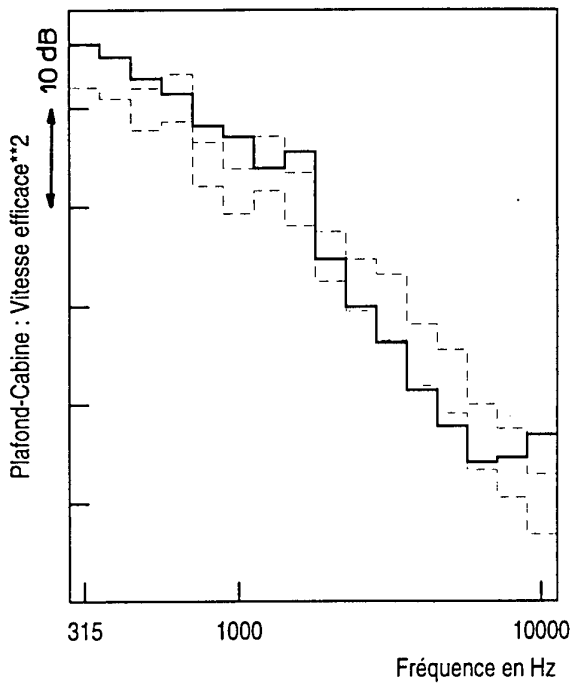

Fig. 10

5. CONCLUSIONS ET PERSPECTIVES

Les études qui ont été menées par la méthode SEA sur la prévision du bruit interne dans une cabine d'hélicoptère ont montré que :

- la SEA est une bonne méthode prévisionnelle du bruit interne dans les structures aéronautiques complexes pour les domaines Moyenne Fréquence et Haute Fréquence,

- l'évaluation numérique de l'excitation de couche limite en utilisant un modèle simplifié de couche limite est très satisfaisante,

- la part de l'excitation aérodynamique due à la couche limite sur le fuselage avant étant plus faible que la contribution de l'excitation mécanique sur le plancher par les barres BTP et de l'excitation acoustique due au rayonnement de la boîte de vitesse, il est nécessaire dans l'avenir de faire porter nos efforts sur l'évaluation de ces excitations afin d'améliorer le caractère prévisionnel de l'approche SEA pour la prévision du bruit interne pour les futurs hélicoptères en vol.

Afin d'étendre la base de données expérimentales à un hélicoptère moyen porteur et de préciser la mesure des sources de bruit interne cabine d'origine mécanique, une campagne de mesures en vol similaires va avoir lieu en Mai 1996 au CEV d'Istres sur un appareil Dauphin dédié à la recherche. On mesurera à cette occasion les forces instationnaires injectées dans le plancher mécanique au pied de chacune des barres BTP; des ponts de jauges de contraintes, collés sur les barres et étalonnés en dynamique, fourniront une mesure des forces transmises, tant en traction-compression qu'en flexion dans deux plans orthogonaux, permettant ainsi, associées aux mesures d'accélération en X, Y et Z au pied des barres BTP, de calculer les puissances mécaniques d'entrée sur ce sous-système plancher.

Parallèllement à ces études de prévision du bruit interne, une campagne de validation des logiciels de calcul vibroacoustique dans les domaines BF, MF et HF est actuellement effectuée par la commission SFM-SFA (Société Française des Mécaniciens et Société Française des Acousticiens) qui regroupe différents laboratoires et centres de recherche. Plusieurs cas test ont été définis par la commission et ont été réalisés à ce jour [20,21,22,23,24] ou sont en cours de réalisation.

6. RÉFÉRENCES BIBLIOGRAPHIQUES

1. Arnal D., Habiballah M. et Coustols E., "Théorie de l'instabilité laminaire et critères de transition en écoulement bi et tridimensionnel", La Recherche Aérospatiale, ONERA, **2**, 1984.
2. Soize C., Desanti A. et David J.M., "Numerical Methods in Elastoacoustics for Low and Medium Frequency Ranges", La Recherche Aérospatiale, **5**, 1992, pp 25–44.
3. Soize C., David J.M., Desanti A. et Félix D., "Réponse forcée des milieux élastiques à un champ de pression aléatoire. Cas de corrélations spatiales courtes", RT ONERA $n°$ 67/3454 RY 065R, 1987.
4. Dussac M., Martin P., Marze H.J., Chabas F., David J.M., Desanti A., Meidinger N. et Soize C., "A Finite Element Method to Predict Internal Noise Levels at Discrete Frequencies for a Partially Composite Helicopter Fuselage", Boston (Ma), AHS Annual Forum, 1989, May 22-24.
5. Guillaumie L., Menelle M. et Morvan A., "Mesures en vol sur un hélicoptère ECUREUIL appliquées à la validation d'un modèle SEA", RT ONERA $n°$ 14/3654 RY 020R, Décembre 1992.
6. Dussac M. et Morvan A., "Evaluation of Helicopter Inter-
nal Noise by Enhanced Statistical Energy Analysis", 19th European Rotorcraft Forum, Cernobbio (Como), Italie, September 14-16, 1993.
7. David J.M., "Prévision du bruit interne dans une structure d'hélicoptère par la méthode SEA", RT ONERA $n°$ 15/3654 RY 030R, Juin 1994.
8. David J.M., "Évaluation numérique de l'excitation de couche limite pour la prévision du bruit interne dans une cabine d'hélicoptère par la SEA", RT ONERA $n°$ 16/3654 RY 042R, Avril 1995.
9. Soize C., "Analyse Energétique Statistique (SEA). Etude bibliographique 1975-1986 (Tomes I et II)", RT ONERA $n°$ 72/3454 RY 166R, Juillet 1987.
10. David J.M. et Soize C., "Prediction of the High-Frequency Behavior of Coupled Fluid-Structure Systems by the SEA Method and Applications", in "Computational methods for fluide-structure interaction", Editeurs J.M. Crolet et R. Ohayon, Longman Scientific and Technical, Harlow, 1994, pp. 55 –77.
11. David J.M. et Soize C., "Statistical Energy Analysis : Formulation and Software Developments", Congrès EURO NOISE'95, Lyon, 21-23 Mars 1995, Tiré à part $n°$ 1995-17.
12. Chabas F. et Soize C., "Approche SEA des couplages HF structure-fluide dense externe infini", RT ONERA $n°$ 76/3454 RY 176-178R, Janvier 1988.
13. Chabas F., "Approche SEA des couplages hydro-élastiques HF. Détermination des facteurs de perte par couplage", RT ONERA $n°$ 88/3454 RY 088R, Février 1989.
14. David J.M. et Soize C., "Approche SEA des vibrations HF des structures couplées avec un fluide dense non borné", RT ONERA $n°$ 97/3454 RY 098R, Mai 1990.
15. Menelle M., Guillaumie L. et Morvan A., "Étude du comportement hydro-élasto-acoustique d'une coque cylindrique en haute fréquence. 2ème campagne expérimentale", RT ONERA $n°$ 122/3454 RY 018R, Septembre 1992.
16. David J.M., "Analyse des vibrations HF par la SEA d'une coque en eau avec comparaisons expérimentales", RT ONERA $n°$ 120/3454 RY 121R, Août 1992.
17. Soize C. et David J.M., "Développement et implantation dans le logiciel PEGASE d'Analyse Statistique Energétique d'un modèle d'incertitudes sur les paramètres SEA moyens", RT ONERA $n°$ 107/3454 RY 093R, Décembre 1990.
18. Chabas F., "Analyse dynamique HF des systèmes mécaniques par l'Analyse Statistique Energétique. Logiciel PEGASE", RT ONERA $n°$ 89/3454 RY 186R, Août 1989.
19. David J.M., "Manuel d'utilisation du logiciel d'Analyse Statistique Energétique PEGASE", RT ONERA $n°$ 108/3454 RY 093R, Janvier 1991.
20. David J.M., "Validation des progiciels de calcul vibroacoustique SFM-SFA. Cas test de calcul $n°$ 1.3", RT ONERA $n°$ 10/2894 RN 032R, Octobre 1995.
21. David J.M., "Validation des progiciels de calcul vibroacoustique SFM-SFA. Cas test de calcul $n°$ 1.10", RT ONERA $n°$ 11/2894 RN 032R, Octobre 1995.
22. David J.M., "Validation des progiciels de calcul vibroacoustique SFM-SFA. Cas test de calcul $n°$ 1.1", RT ONERA $n°$ 12/2894 RN 032R, Octobre 1995.
23. David J.M., "Validation des progiciels de calcul vibroacoustique SFM-SFA. Cas test de calcul $n°$ 1.7", RT ONERA $n°$ 13/2894 RN 032R, Octobre 1995.
24. Morvan A., Guillaumie L. et Menelle M., "Validation des progiciels de calcul vibroacoustique SFM-SFA. Cas test expérimental $n°$ 1.1e", RT ONERA $n°$ 14/2894 RN 032R, Février 1995.

UPGRADING OF CLASSICAL LIFTING-LINE THEORY TO OBTAIN ACCURATE FLIGHT MECHANICAL HELICOPTER MODELS: IMPROVED CORRECTION FOR SWEEP EFFECTS.

Th. van Holten
Faculty of Aerospace Engineering
Delft University of Technology
Kluyverweg 1
2629 HS Delft
The Netherlands

SUMMARY

In the usual analysis of the helicopter rotor, models and concepts are used which originate from classical lifting line theory. A theory, strictly valid for the analysis of straight high aspect ratio wings in steady flow.
In the case of a helicopter rotor blade, the validity of these models is questionable since its sections encounter unsteady and yawed flow. Asymptotic theory shows how in this case more correct models may be synthesized.

The present paper deals with an improved correction for the effect of sweep on the tilt of the rotor's tip path plane. Its application to a simple test case shows that the prediction of its lateral tilt is considerably affected. The new model for sweep effects might thus explain the often observed peak of the lateral tilt at small flight velocities.

NOTATIONS

Symbols

a_0	rotor coning angle	rad (deg)
a_1	longitudinal tilt angle of tip path plane	rad (deg)
A	blade aspect ratio, $A= b^2/ S= b/ c$	
b_1	lateral tilt angle of tip path plane	rad (deg)
b	blade span	m
c	blade chord	m
$C_{l\alpha}$	lift curve slope	rad^{-1}
C_T	rotor thrust coefficient	
I_p	blade polar moment of inertia with respect to its center of rotation	$kg{\cdot}m^2$
l	section lift	N/m
N	number of blades	
r	radial coordinate of a blade section	m
R	rotor radius	m
t	time	s
U	velocity	m/s
V	flying speed	m/s
v_i	rotor induced velocity	m/s
x	nondimensional radial coordinate of a blade section	
x, y, z	Cartesian coordinates	m
α	angle of attack	rad
β	blade flapping angle	rad
γ	blade Lock number, $\gamma= \rho C_{l\alpha} cR^4/ I_b$	
δ	as defined	
ϵ	as defined	
θ	pitch angle	rad
λ_i	inflow ratio component, $\lambda_i= v_i/\Omega R$	
λ_c	inflow ratio component, $\lambda_c= V\sin\alpha_c/\Omega R$	
Λ	local sweep angle	rad
μ	advance ratio, $\mu= V\cos\alpha_c/\Omega R$	
σ	rotor solidity, $\sigma= Nbc/\pi R^2$	
ρ	air density	kg/m^3
ψ	blade azimuthal coordinate	rad
Ω	rotor rotational velocity	rad/s

Subscripts

c	control plane
e	effective
P	perpendicular to control plane
T	tangential to control plane

INTRODUCTION: GENERAL BACKGROUND

The basic concepts of classical-lifting line theory are still in widespread use in the helicopter industry. Especially for the purpose of flight-dynamics analyses, and certainly in the case of real-time simulations, the classical concepts derived from this theory play a major role, and will do so for a long time to come.

The notion that blade sections may be treated as two-dimensional aerofoils placed at an effective angle of attack, is typically a lifting-line concept. This classical view on section-behaviour makes it possible to absorb experimental two-dimensional data (including compressibility and unsteady effects) into a three-dimensional analysis. Combined with a relatively favourable computing time this explains the continued use of lifting-line theory for the purposes mentioned above.

Although fully three-dimensional analyses of helicopter blades have become feasible, such methods are best used for zooming in upon certain details of the flow, for instance tipflows and blade/vortex interactions. Note that "section characteristics" and the "induced angle of attack" concept have no meaning in a fully three-dimensional lifting surface theory.

Although the aplication of classical lifting-line concepts to rotor blades is generally accepted, this leads to some fundamental problems and inconsistencies. These arise from the fact that rotor blades experience a combination of unsteady and yawed flow, and are often subjected to appreciable compressibility effects at the same time.
In the case of fixed wing analysis it was realized at an early stage, that the usual lifting-line concepts, when used under such circumstances, would cause fundamental singularities to occur in the calculation of the induced angles of attack along the wing.

For convenience this problem is often ignored in helicopter analysis, or bypassed by using other inflow models than trailing vortex sheets. However, this involves the risk of ending up with an inconsistent analysis, and systematic errors.

As a result of the research described in ref.1 a lifting-line theory was developed from basic principles, in order to avoid such problems. This more consistent and more accurate analysis was however not very convenient to use. For instance, it could not be

Paper presented at the FVP Symposium on "Advances in Rotorcraft Technology", held in Ottawa, Canada, 27-30 May 1996, and published in CP-592.

integrated with popular inflow models like the dynamic inflow model by Pitt and Peters (ref.3), or similar analyses.

Recently, research based on the rigorously derived lifting-line theory has been resumed again, prompted by the requirements of rotor analysis for real-time simulation. It is now attempted to derive simple "engineering" corrections which may be applied to conventional rotor analyses. These corrections are implemented by using the characteristics of "effective" two-dimensional aerofoils which replace the aerofoils defined by the exact blade shape. "Effective" camber or other corrections are derived from the exact form of lifting-line theory mentioned above.

In the present paper, the first result of this new approach, an improved correction for sweep effects, will be derived. This because the simple sweep correction as usually applied to the section characteristics, introduces a significant error.

1. THE SIMPLE SWEEP CORRECTION

The usual analysis of rotor behaviour is based on a blade-element consideration like the one shown in fig.1.

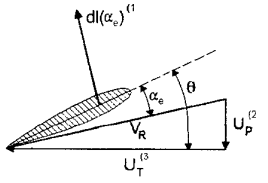

(1) Concept of blade-section ≡ 2D aerofoil

(2) Based on concept of Prandtl-like induced velocity

(3) Based on "Simple sweep correction"

Figure 1: Velocities relative to a blade element

In order to arrive at the elementary contributions to the total rotor thrust and torque, a large number of simplifying models are used:

- It is assumed that the lift of a blade-element corresponds to the lift of a two-dimensional aerofoil placed at an effective angle of attack.
  This is a typical lifting-line concept, which by asymptotic analysis may be shown to be correct to the order $O(A^{-1})$, where A denotes the aspect ratio.

  The effective angle of attack is in usual rotor analysis taken as (see fig.1):

$$\alpha_e = \theta - \arctan\left(\frac{U_P}{U_T}\right) \qquad (1)$$

- In the case of a centrally hinged blade (see fig.4):

$$U_P = v_i + V\sin\alpha_c + \frac{d\beta}{dt}r + V\beta\cos\alpha_c\cos\psi - \Omega R\left(\lambda_i + \lambda_c + \frac{d\beta}{d\psi}x + \mu\beta\cos\psi\right) \qquad (2)$$

- The tangential velocity U_T is taken as:

$$U_T = \Omega r + U\cos\alpha_c\sin\psi = \Omega R(x + \mu\sin\psi) \qquad (3)$$

  The second term on the r.h.s. is based on the "simple sweep correction", i.e. it is assumed that as far as the lift is concerned only the velocity components perpendicular to the span are relevant.

In relation to flight mechanical models much attention has been given to inflow-models to determine the value of v_i, see for instance the review by Chen (ref.4).
Another topic on which research has concentrated, is the relation $C_l(\alpha_e)$. The latter may be linear or non-linear, steady or unsteady, compressible or incompressible, and based on any combination of these.

As far as boundary layer effects are concerned, e.g., profile drag, the simple sweep correction has always been recognized to be invalid. Three-dimensional effects are taken into account, sometimes even including centrifugal and Coriolis forces, to replace the assumption of two-dimensional section characteristics.

Little attention has been paid to the validity of the simple sweep correction in relation to the lift. By Van Holten (ref.2) it was pointed out that considerable errors are likely to be introduced by this assumption. However, the special formulation of lifting-line theory which takes sweep effects correctly into account (ref.2) is relatively complicated.
As stated before, a simple approximate correction for sweep effects, to be incorporated into the usual flight mechanical rotor models, will be derived in this paper.

2. PHYSICAL INTERPRETATION OF SWEEP EFFECTS

Let us first look at the usual derivation of the simple sweep correction. A windtunnel is imagined (see fig.2) whose walls have openings through which a wing slides.

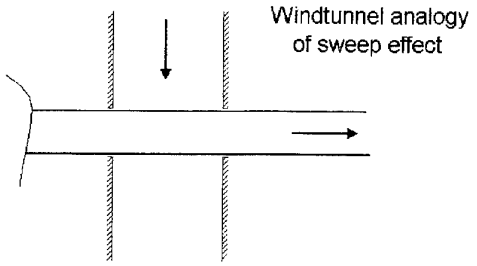

Figure 2: Windtunnel analogy of sweep effect

There is no twist in the wing, and what the flow in the windtunnel "feels" would not be different from a two-dimensional wing section, at least in inviscid flow.

From this thought experiment it is concluded that the lift force is not influenced by the relative velocity components parallel to the wingspan, at least in the linear part of the lift-curve where viscosity does not play a major role. This leads to the simple sweep correction which is usually applied in rotoranalysis.

It is clear that the simple sweep correction is not valid for the forces that depend strongly on viscous effects, such as the profile drag. This consideration has led to the well-known correction by Bennett (ref.5) for the profile-power of a rotor in forward flight.

Even in inviscid flow, the simple sweep correction would break down if one imagines a windtunnel through which a twisted wing is sliding. In such a case, what the flow inside the tunnel would "see" is a wingsection whose lift varies in time. The conclusion is, that for a wing with lift varying along the span the sweep effect is analogous to an unsteady flow effect.

By Van Holten (ref.2), a formulation of lifting line theory was derived which takes the effects of unsteady and swept flow rigorously into account. This theory leads to the same conclusion, viz. that the effect of sweep may be equated to unsteady effects of an aerofoil. It is furthermore shown in ref.2 that the equivalent unsteadiness is of a special type: apparent mass effects do not play a role in this case.

3. RESULTS FOR THE SWEPT WING

In the appendix of this paper a quantification of the sweep effect is given in the case of a swept, uncambered wing in parallel flow (see fig.3).

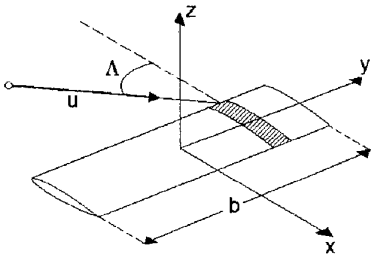

Figure 3: Swept, uncambered wing in paralel flow

The aspect ratio A is assumed to be large, and effects of the order $O(A^{-2})$ are neglected. This accuracy corresponds to the usual lifting line assumptions.
The sweep angle Λ is assumed to be relatively small, therefore also effects of the order $O(\epsilon)$ may be neglected, with $\epsilon = \tan\Lambda/A$.

It then appears that the lift of a section of such a wing is determined by the differential equation

$$l - l'\epsilon \ln|\epsilon| = 2\pi\alpha \tfrac{1}{2}\rho(U\cos\Lambda)^2 c \qquad (4)$$

where:

l	sectional lift;
$l' = dl/dy'$	with $y' = y/(b/2)$ the spanwise coordinate of the section non-dimensionalized by the semi-span;
$\epsilon = \tan\Lambda / A$	with Λ the sweep-angle and A the aspect ratio of the wing.

In case of constant lift along the span, this expression yields the simple sweep correction.

4. APPROXIMATE SWEEP CORRECTION FOR THE HELICOPTER ROTOR BLADE

An approximate correction for sweep effects in the case of a helicopter rotor blade is obtained by using an equation for the lift which is analogous to the one derived above for the swept wing in parallel flow.

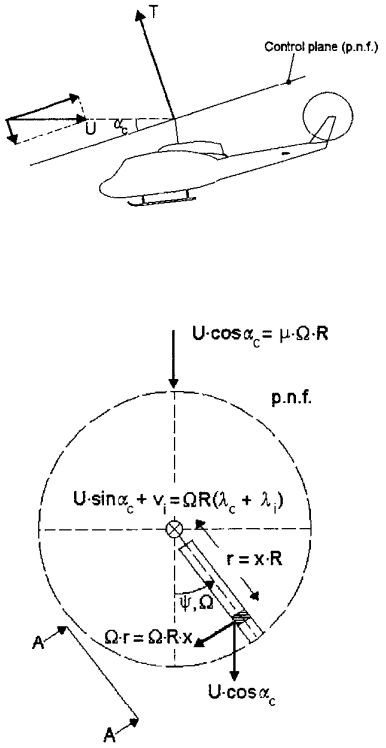

Figure 4: Signs and notations

We will now consider the case of a centrally hinged helicopter blade without twist, so that by analogy with eq.(4), see fig.4 for notations:

$$\frac{l(x) - \frac{1}{2}\epsilon\ln|\epsilon|\frac{dl}{dx}}{C_{l_\alpha}\frac{1}{2}\rho(\Omega R)^2(x + \mu\sin\psi)^2 c} = \theta - \frac{U_P}{U_T} - \theta - \frac{\lambda_i + \lambda_c + \frac{d\beta}{d\psi}x + \mu\beta\cos\psi}{x + \mu\sin\psi} \qquad (5)$$

This expression is cleaned up a bit by defining the special lift coefficient l_c:

$$l_c = \frac{l}{\frac{1}{2}\rho(\Omega R)^2 c} \tag{6}$$

so that eq. (5) is transformed into:

$$l_c = C_{l_\alpha}\theta(x + \mu\sin\psi)^2 + \\ - C_{l_\alpha}\left(\lambda_i + \lambda_c + \frac{d\beta}{d\psi}x + \mu\beta\cos\psi\right)(x + \mu\sin\psi) + \\ + \frac{dl_c}{dx}\frac{1}{2}\epsilon\ln|\epsilon| \tag{7}$$

where σ denotes the rotor solidity, N the number of rotor blades and the perturbation parameter ϵ is given by

$$\epsilon = \frac{\tan\Lambda}{A} = \frac{\mu\cos\psi}{x + \mu\sin\psi}\frac{\pi\sigma}{N} \tag{8}$$

5. APPROXIMATE SOLUTION

An approximate solution is based on the following consideration. If one would omit the last term in (7) containing the correction of $O(\epsilon \ln|\epsilon|)$, the classical results would be obtained. The lift distribution $l_c(x)$ thus obtained will contain an error of order $O(\epsilon \ln|\epsilon|)$, which is inconsistent with lifting-line theory. The same is true when the function dl_c/dx is derived from the classical lift distribution. The error would again be of order $O(\epsilon \ln|\epsilon|)$. However, after substitution of this classical function dl_c/dx into the last term of (7), the finally resulting error becomes of a higher and irrelevant order. This because of the multiplication by the factor $\frac{1}{2}\epsilon \ln|\epsilon|$.

We may therefore use the classical solution $l_c(x)$ to derive dl_c/dx in eq. (7):

$$\frac{dl_c}{dx} = C_{l_\alpha}\left(2\theta - \frac{d\beta}{d\psi}\right)(x + \mu\sin\psi) + \\ - C_{L_\alpha}\left(\lambda_i + \lambda_c + \frac{d\beta}{d\psi}x + \mu\beta\cos\psi\right) \tag{9}$$

A second, cruder approximation has been introduced for the term $\frac{1}{2}\epsilon \ln|\epsilon|$. This term is approximated by

$$\frac{1}{2}\epsilon\ln|\epsilon| = -\delta\cos\psi \tag{10}$$

with δ the value of $\text{abs}(\frac{1}{2}\epsilon \ln|\epsilon|)$ in the point x=.75, ψ=0:

$$\delta = \frac{4}{6}\frac{\mu\pi\sigma}{N}\ln\left(\frac{4}{3}\frac{\mu\pi\sigma}{N}\right) \tag{11}$$

Substituting eqs. (9) and (10) into (7) we can work out the following integrals, on assuming a truncated Fourier-series for the flapping angle; $\beta = a_0 - a_1\cos\psi - b_1\sin\psi$:

$$C_T = \frac{\sigma}{2}\frac{1}{2\pi}\int_0^{2\pi}d\psi\int_0^1 l_c dx = \\ = \frac{C_{l_\alpha}\sigma}{4}\left(\frac{2}{3}\theta\left(1 + \frac{3}{2}\mu^2\right) - (\lambda_i + \lambda_c) + \delta(\mu a_0 - b_1)\right) \tag{12}$$

and

$$a_0 = \frac{\gamma}{2C_{l_\alpha}}\frac{1}{2\pi}\int_0^{2\pi}d\psi\int_0^1 l_c dx = \\ = \frac{\gamma}{8}\left(\theta(1 + \mu^2) - \frac{4}{3}(\lambda_i + \lambda_c) + \delta\left(\mu a_0 - \frac{4}{3}b_1\right)\right) \tag{13}$$

Furthermore, because we consider a centrally hinged rotor blade without spring stiffness in the hub, the 1-P components of the flapping moment must vanish:

$$\frac{1}{2\pi}\int_0^{2\pi}\cos\psi\,d\psi\int_0^1 l_c x dx = \\ = -\frac{4}{3}\mu a_0 - b_1\left(1 + \frac{1}{2}\mu^2\right) + \delta\left(\frac{8}{3}\theta - 2(\lambda_i + \lambda_c) + \mu a_1\right) = 0 \tag{14}$$

and

$$\frac{1}{2\pi}\int_0^{2\pi}\sin\psi\,d\psi\int_0^1 l_c x dx = \\ = -\frac{8}{3}\mu\theta - a_1\left(1 - \frac{1}{2}\mu^2\right) - 2\mu(\lambda_i + \lambda_c) - \delta\mu b_1 = 0 \tag{15}$$

Together with the relation $\lambda_d = \lambda_c + \mu a_1$, where λ_d denotes the nondimensional component of the flight velocity perpendicular to the tip path plane (in contrast to λ_c which denotes the same w.r.t. the control plane), the equations (12) through (15) form a set from which θ, a_0, a_1 and b_1 may be solved for given values of C_T, μ, λ_d and λ_i. The latter quantities are easily obtained from the helicopter trim condition.

6. RESULTS

Fig.5 shows some results for a typical trim condition. For comparison, fig.6 shows, for the same trim condition, the results obtained from the classical analysis where just the simple sweep correction is used.

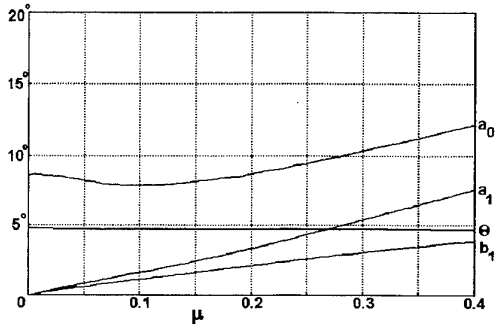

Figure 5: Results from present analysis

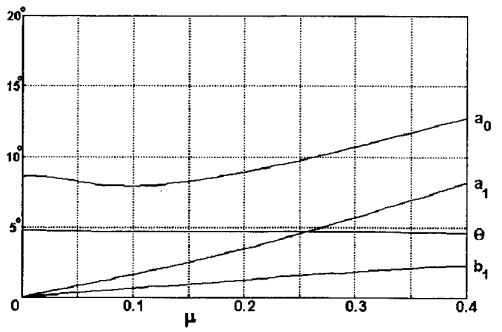

Figure 6: Results with, classical, simple sweep correction

The comparison shows that the only quantity significantly influenced by the correction for sweep effects, is the lateral tilt angle of the rotor disc b_1. This angle is roughly doubled by the sweep correction.

By comparing eqs.(14) and (15) and neglecting some higher-order terms, it is thus found:

$$b_1 = \frac{\frac{4}{3}\mu a_0}{1 + \frac{1}{2}\mu^2} + \delta\frac{a_1}{\mu} \qquad (16)$$

where the first term on the r.h.s. represents the classical result, and the second term represents the effect of the sweep correction.

7. LATERAL TILT AT SMALL ADVANCE RATIOS

It is well known that the lateral tilt of the rotor disc is severely underpredicted by the classical result. See, e.g., the comparison with experimental data in fig.7, taken from ref.6.

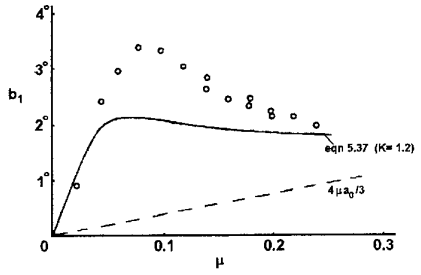

Figure 7: Classical theory vs. experiment, (Bramwell, ref.6)

A large part of this discrepancy can be contributed to the crude assumption; that the induced velocity is uniformly distributed over the rotor disc. A more realistic distribution goes some way to explain the difference between the classical theory and the experiments, see again fig.7. However, it has never been possible to account fully for the experimentally observed peak of the lateral tilt in the flight region around $\mu = 0.1$.

The sweep correction as derived above might give the answer to this question. One should realize that in the region of medium flight speeds one may expect in-plane induced velocities to occur. Such an in-plane component of the induced velocity has never been considered in the usual analyses, since it would hardly influence the flapping angles. However, it would affect the additional sweep effects as considered in the present analysis.

From qualitative considerations one can see that the induced velocity has no in-plane component in the case of hover. Neither are in-plane induction effects present in high-speed flight, where the rotor may be considered as a circular wing. However, in the intermediate region in-plane induction velocities do occur, as may be inferred from fig.8.

These in-plane induction velocities will further increase the lateral rotor tilt angle, at these intermediate flight velocities. A further quantification of this effect will thus be needed, by deriving an extension of existing inflow models, so that in-plane induction velocities are included.

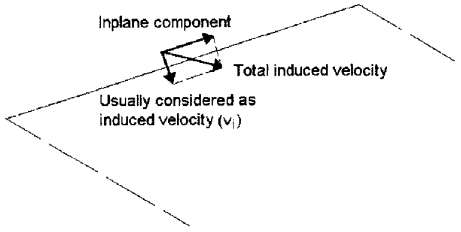

Figure 8: The in-plane induced velocity component

CONCLUSIONS

- The conventional methods of rotoranalysis contain a large number of simplifying assumptions. One of these assumptions is, that the generation of lift by a blade section depends on the velocity component perpendicular to the bladespan only. Closer consideration reveals that this assumption is too crude and inconsistent with other approximations implicit in usual rotor analyses.
- In the paper an improved correction for such "sweep effects" is derived. Application to the simple case of a centrally hinged rotor blade shows that the lateral tilt of the rotor is profoundly influenced.
- Furthermore, it is argued on the basis of qualitative arguments that the improved sweep correction might explain the peak of the lateral rotor disc tilt, often observed at low flight velocities.
- A further quantification awaits an improved model for induced velocities, where also in-plane induction effects are taken into account.

REFERENCES

1. Holten, Th. van, "Some notes on unsteady lifting-line theory," J. Fluid Mech., vol. 77, part 3, pp. 561-579, 1976.
2. Holten, Th. van, "On the validity of lifting line concepts in rotor analysis," Vertica, vol. 1, pp. 239-254, 1977.
3. Pitt, D.M., and Peters, D.A., "Theoretical prediction of dynamic inflow derivatives," Vertica, vol. 5, no.1, pp. 21-34, 1983.
4. Chen, R.T.N., "A survey of nonuniform inflow models for rotorcraft flight dynamics and control applications," paper no. 64, 15th European Rotorcraft Forum, Amsterdam, 1989.
5. Bennett, J.A.J., "Rotary wing aircraft," Aircraft Engineering, 1940.
6. Bramwell, A.R.S., "Helicopter Dynamics," Edward Arnold Ltd, Baltimore, Maryland, U.S.A., 1986.
7. Moon, P., and Spencer, D.E., "Field theory for engineers," D. van Nostrand Company, 1961.

APPENDIX A: DERIVATION OF EQUATION (4)

In this appendix one finds the derivation of equation (4) given in paragraph 3. One should note that the coordinate system and notations used in this appendix differ somewhat from the rest of the article.

Notations

Symbols

$\underline{a}_\eta$, $\underline{a}_\varphi$	unit vectors, as defined	
A	wing aspect ratio	
b	wing span	m
c	chord length	m
C	constant, as defined	
C_l	lift coefficient	
$\underline{i}$, $\underline{k}$	unit vectors, as defined	
K_0	modified Bessel function of the second kind	
l	section lift	N/m
p	pressure perturbation	N/m^2
t	time	s
U	free stream velocity	m/s
$\underline{V}$= (u,v)	velocity perturbation vector	m/s
x, y, z	Cartesian coordinates	m
x', y', z'	nondimensional Cartesian coordinates	
α	angle of attack	rad
γ	Euler's number	
ϵ	perturbation parameter, as defined	
Λ	sweep angle	rad
ρ	air density	kg/m^3
η, φ	eliptical coordinates	rad

Subscripts

0	wing section

Preliminary: Theory of the two-dimensional aerofoil using the method of the acceleration potential

As a preliminary we derive the equations for a flat-plate aerofoil in steady flow, using a description in terms of the pressure perturbations (fig.A-1).

Two-dimensional incompressible flow and small perturbations are assumed, so that the following equations apply:

$$\frac{D\underline{V}}{Dt} = \frac{\partial \underline{V}}{\partial t} + (\underline{U}\cdot\underline{\nabla})\underline{V} = -\rho^{-1}\,\mathrm{grad}\,p \quad \text{(Euler's eq.)} \qquad \text{(A-1)}$$

$$\mathrm{div}\,\underline{V} = 0 \quad \text{(continuity equation)} \qquad \text{(A-2)}$$

where $\underline{U} = \underline{i}\,U$ is the free-stream velocity, $\underline{V}$ is the velocity perturbation with components ($\underline{i}u$, $\underline{k}v$), and p denotes the pressure perturbation (see fig.A-1). Taking the divergence of (A-1) and substituting (A-2) yields de Laplace equation for p:

$$\nabla^2 p = 0 \qquad \text{(A-3)}$$

in terms of Cartesian coordinates (x,y,z) the following boundary-value problem results for the flat-plate aerofoil. The pressure perturbation should satisfy Laplace's equation:

$$\frac{\partial^2 p}{\partial x^2} + \frac{\partial^2 p}{\partial z^2} = 0 \qquad \text{(A-4)}$$

The pressure perturbation should vanish at large distances from the wing:

$$p \to 0 \quad \text{for} \quad x^2 + z^2 \to \infty \qquad \text{(A-5)}$$

According to (A-1) the normal component of the pressure gradient on the aerofoil surface should vanish:

$$\frac{\partial p}{\partial z} = 0 \quad \text{on the aerofoil surface} \qquad \text{(A-6)}$$

In linearized theory this boundary condition is applied to the part of the x-axis between $-c/2 < x < c/2$, with c denoting the chord length. At the leading edge however, there will in general exist a streamline kink, which implies a pressure singularity:

$$p \to -\infty \quad \text{at the leading edge} \qquad \text{(A-7)}$$

The strength of this singularity should be such that the flow becomes tangential to the aerofoil surface. Because it has already been required by (A-6) that the curvature of the flow on the surface is zero, it is sufficient to require the flow to be tangential at just one point of the surface. A convenient choice is the point just past the leading edge singularity which will be denoted as the point $(-c/2+0^+, 0)$, so that:

$$v(-c/2+0^+,\,0)/U = -\alpha \qquad \text{(A-8)}$$

where α is the geometrical angle of attack.

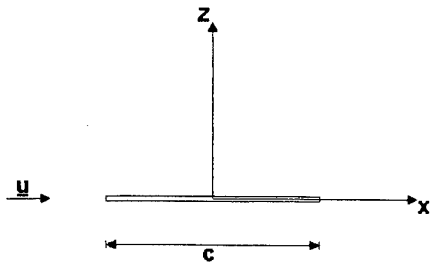

Figure A-1: Flat-plate coordinate system and definitions

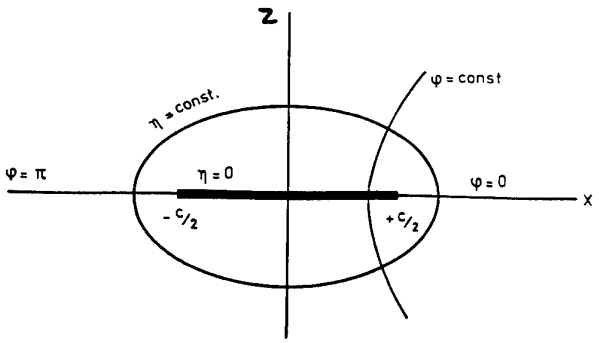

Figure A-2: Flat-plate eliptic coordinate system

For the solution it is convenient to introduce elliptic coordinates. sketched in fig.A-2 and conforming to the transformation formulae

$$x = \frac{c}{2}\cosh\eta\cos\varphi \qquad \text{(A-9)}$$

and

$$z = \frac{c}{2}\sinh\eta \sin\varphi \qquad \text{(A-10)}$$

The value of η ranges between 0 and ∞, with lines η = constant representing ellipses degenerating for $\eta = 0$ into the aerofoil chord. The coordinate ϕ ranges between $-\pi$ and $+\pi$, the lines ϕ = constant representing hyperbolae orthogonal to the ellipses. In terms of the elliptic coordinates, Laplace's equation (A-3) reads (see, for example, Moon & Spencer 1961, ref.7):

$$\frac{\partial^2 p}{\partial \eta^2} + \frac{\partial^2 p}{\partial \varphi^2} = 0 \qquad \text{(A-11)}$$

and the pressure gradient is:

$$\text{grad } p = \frac{1}{\frac{c}{2}\sqrt{\cosh^2\eta - \cos^2\varphi}}\left(\underline{a}_\eta \frac{\partial p}{\partial \eta} + \underline{a}_\varphi \frac{\partial p}{\partial \varphi}\right) \qquad \text{(A-12)}$$

where $\underline{a}_\eta$ and $\underline{a}_\varphi$ denote unit vectors perpendicular to the surfaces η = constant and ϕ = constant respectively.

The boundary conditions (A-5), (A-6) and (A-7) transform into

$$p \to 0 \text{ for } \eta \to \infty \qquad \text{(A-13)}$$

$$\frac{\partial p}{\partial \eta} = 0 \quad \text{for} \quad \eta = 0 \qquad \text{(A-14)}$$

except at the leading edge, where

$$p \to -\infty \quad \text{for} \quad \eta = 0,\ \varphi = \pm\pi \qquad \text{(A-15)}$$

The antisymmetric solution of (A-11) satisfying the conditions (A-13), (A-14) and (A-15) is given by

$$\frac{p}{\frac{1}{2}\rho U^2} = -\frac{C_l}{\pi}\frac{\sin\varphi}{\cosh\eta + \cos\varphi} \qquad \text{(A-16)}$$

The constant C_l in the right-hand-side has the physical meaning of the lift coefficient, as may be checked by integrating the pressure on the surface of the flat plate.
In order to relate the lift coefficient C_l to the angle of attack, the kinematic condition (A-8) is applied.

According to Euler's equation (A-1) the evaluation of the velocity at time t_0 in a given point is equivalent to the computation of the velocity acquired by a particle of air coming from infinity upstream, travelling through the pressure field and passing the point considered at the required time t_0.
In the case considered this translates the condition (A-8) for a particle arriving at time 0^+ in the point $(-c/2+0^+, 0)$ into:

$$v(-c/2+0^+, 0) = \int_{-\infty}^{0^+}\frac{Dv}{Dt}dt =$$

$$= -\frac{1}{\rho}\int_{-\infty}^{0^+}\frac{\partial p}{\partial z}[x(t), 0]dt = \qquad \text{(A-17)}$$

$$= -\frac{1}{\rho U}\int_{-\infty}^{-\frac{c}{2}+0^+}\frac{\partial p}{\partial z}(x, 0)dx$$

According to (A-16) and (A-12) the vertical component of the pressure gradient on the x-axis for $x \le -c/2$ is given by:

$$\left(\frac{\partial p}{\partial z}\right)_{z=0,\ x\le -\frac{c}{2}} = -\frac{1}{2}\rho U^2 \frac{C_L}{\pi}\frac{1}{\frac{c}{2}\sinh\eta}\frac{1}{\cosh\eta - 1} \qquad \text{(A-18)}$$

so that eq.(A-17) may be transformed into

$$v(-c/2 + 0^+, 0)/U = -\frac{C_l}{2\pi}\int_{0!}^{\infty}\frac{d\eta}{\cosh\eta - 1} \qquad \text{(A-19)}$$

It should be remembered that a special physical meaning is attached to this integral: the vertical velocity component v is sought in the point just <u>past</u> the leading edge singularity. This is expressed by the exclamation mark in the lower boundary of the integral.

Without this special meaning the integral of eq.(A-19) would be singular. The actually sought value of the integral (A-19) may be found easily however by going back to eq.(A-17). According to the divergence theorem the integral in eq.(A-17) may be replaced by :

$$v(-c/2 + 0^+, 0) = -\frac{1}{\rho U}\int_0^{\infty}\left(\frac{\partial p}{\partial x}\right)_{x=0} dz \qquad \text{(A-20)}$$

on account of the fact that on the surface of the aerofoil $\partial p/\partial z = 0$.

Once again this integral may be transformed in terms of elliptical coordinates:

$$v(-c/2 + 0^+, 0)/U = -\frac{C_l}{2\pi}\int_0^{\infty}\frac{d\eta}{\cosh^2\eta} = -\frac{C_l}{2\pi} \qquad \text{(A-21)}$$

We see that this result is in agreement with the classical result of thin-aerofoil theory

$$C_l = 2\pi\alpha \qquad \text{(A-22)}$$

The important result, needed in the following development of the theory, is the conclusion

$$\int_{0!}^{\infty}\frac{d\eta}{\cosh\eta - 1} = -1 \qquad \text{(A-23)}$$

when the special physical meaning as explained above is attached to this singular integral.

Analysis of the section of a swept wing

According to the rigorous lifting-line theory of ref.2 the vertical perturbation velocity on the surface of a section of a swept wing must be determined as follows. One considers again a particle of air, coming from infinity upstream (see fig.A-3), and integrates its vertical acceleration up to a point just past the leading edge of the section considered. However, in this case the pressure gradient experienced by the particle is different from above. It corresponds, at any particular time, to the wingsection whose spanwise-coordinate equals the instantaneous spanwise position of the particle. For a further explanation, see fig.A-3.

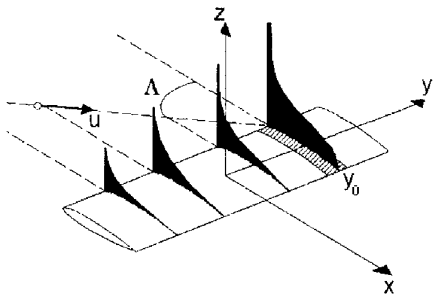

Figure A-3: Particle influenced by different sections

If the spanwise position of the section where the particle arrives at time t=0 is denoted by y_0, then the x- and y-coordinates of the particle are given by

$$x = -\frac{c}{2} + U\cos\Lambda \cdot t \qquad \text{(A-24)}$$

$$y = y_0 + U\sin\Lambda \cdot t \qquad \text{(A-25)}$$

and the relation between these coordinates is:

$$y(x) = y_0 + \tan\Lambda \cdot \left(x + \frac{c}{2}\right) \qquad \text{(A-26)}$$

In terms of elliptical-cylinder coordinates, and introducing the nondimensional spanwise coordinate y'= y/(b/2) with b the span of the wing:

$$y'(\eta) = y_0' - \epsilon(\cosh\eta - 1) \qquad \text{(A-27)}$$

where

$$\epsilon = \frac{\tan\Lambda}{A} \qquad \text{(A-28)}$$

The perturbation parameter ϵ is of order $O(A^{-2})$, if we consider small sweep angles.

The integral which determines the vertical velocity perturbation just behind the leading edge has the same form as eq.(A-17), except for the fact that now C_l is no longer a constant. Rather, C_l is a function of the spanwise coordinate of the particle, which in turn is a function of t:

$$v(-c/2 + 0^+, 0) = \int_{-\infty}^{0^+} \frac{Dv}{Dt} dt =$$

$$= -\frac{1}{\rho}\int_{-\infty}^{0^+} \frac{\partial p}{\partial z}(x(t), 0, y(t))dt \qquad \text{(A-29)}$$

The pressure field of all the sections whose influence is "felt" by the particle has the form of a flat-plate pressure field:

$$p = -\frac{l[y(\eta)]}{\pi c}\frac{\sin\varphi}{\cosh\eta + \cos\varphi} \qquad \text{(A-30)}$$

so that

$$\frac{\partial p}{\partial z} = -\frac{l[y(\eta)]}{\pi c}\frac{1}{\frac{c}{2}\sinh\eta}\frac{1}{\cosh\eta - 1} \qquad \text{(A-31)}$$

Substituting this and the relation $y(\eta)$ according to (A-27) into (A-29) yields:

$$v\left(-\frac{c}{2} + 0^+, y_0, 0\right) = \frac{1}{\rho U\cos\Lambda\pi c}\int_{0!}^{\infty}\frac{l[y(\eta)]d\eta}{\cosh\eta - 1} \qquad \text{(A-32)}$$

According to the rigorous-lifting line theory of ref. 2 the result of this integration up to order $O(A^{-1})$ depends on the sectional lift $l_0 = l(y_0')$ as well as on the local value of the spanwise gradient of the lift $l_0' = (dl/dy')_0$. All the higher derivatives of the lift in spanwise direction appear to have an influence of order $O(A^{-2})$ and smaller.
For this reason we may, with sufficient accuracy, approximate the lift distribution along the span of the wing by:

$$l(y) = l_0 + \left(\frac{dl}{dy'}\right)_0 (y' - y_0')e^{-C|y' - y_0'|} \qquad \text{(A-33)}$$

with C a positive quantity, and the spanwise coordinate y' defined by y' = y/(b/2). For a further explanation see fig.A-4.

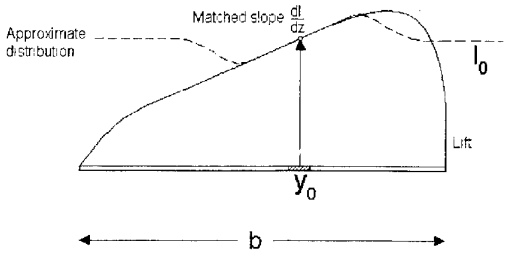

Figure A-4: Actual and approximated lift distribution

The integral in (A-32) becomes, after substituting this approximated lift distribution:

$$I = \int_{0!}^{\infty}\frac{l[y(\eta)]\,d\eta}{\cosh\eta - 1} =$$

$$= l_0\int_{0!}^{\infty}\frac{d\eta}{\cosh\eta - 1} + \qquad \text{(A-34)}$$

$$+ \epsilon l_0' e^{C|\epsilon|}\int_0^{\infty} e^{-C|\epsilon|\cosh\eta}d\eta$$

Recalling the special meaning attached to the singular integral on the r.h.s., the integrations may be performed, and yield the following result:

$$I = -l_0 - \epsilon l_0' e^{C|\epsilon|}K_0(C|\epsilon|) \qquad \text{(A-35)}$$

where K_0 is the modified Bessel-function of the second kind, and of zero order. This expression may be expanded using

$$e^{C|\epsilon|} = 1 + C|\epsilon| + \ldots$$

$$K_0(C|\epsilon|) = -\gamma - \ln\left(\frac{1}{2}C|\epsilon|\right) + \ldots$$

where γ is Euler's number.

Remembering that ϵ is of order $O(A^{-2})$, whereas it is consistent with lifting line theory to neglect terms of this order, it appears that the only relevant terms in the expansion of (A-35) are:

$$I = -l_0 + l_0'\epsilon \ln|\epsilon| \qquad \textbf{(A-36)}$$

The kinematic condition for the swept-wing

$$\frac{v\left(-c/2 + 0^+, y_0, 0\right)}{U\cos\Lambda} = -\alpha \qquad \textbf{(A-37)}$$

thus leads to the differential equation

$$\frac{1}{\rho(U\cos\Lambda)^2\pi c}\left(-l_0 + l_0'\epsilon \ln|\epsilon|\right) = -\alpha \qquad \textbf{(A-38)}$$

In the case of constant lift along the span of the wing, this expression indeed yields the simple sweep correction. In case there is a variation of lift along the span, a differential equation must be solved in order to find the correct value of the lift.

ROTORCRAFT - PILOT COUPLING

A Critical Issue for Highly Augmented Helicopters?

by

Peter G. Hamel

Deutsche Forschungsanstalt für
Luft- und Raumfahrt e.V. (DLR)
Institut für Flugmechanik
D - 38108 Braunschweig, FRG

SUMMARY

Rotorcraft-pilot coupling (RPC) has became a critical issue for flight safety. Based on experience in the field of aircraft-pilot coupling (APC), definitions and limited prediction opportunities of three RPC categories are discussed. Time delay, rate-limiting elements and pilot manipulators of full-authority FbW/L flight control systems provide new potentials of unfavorable rotorcraft-pilot coupling phenomena.

Some limited RPC flight test experience at AFDD and DLR is presented. Research requirements for soliciting RPV prevention methodologies and technologies are laid down. New flight test techniques prediction tools and advanced technologies are proposed to improve RPC immunity.

1. HISTORY AND BACKGROUND

1.1 General

Civil and military flight vehicles have been associated with instabilities due to airframe/pilot interactions since the early days of human flight. these so-called Aircraft-Pilot Coupling (APC) problems have a multitude of technical reasons combined with various kinds of human behaviors.

Brilliant historical accounts on APC phenomena, originally called Pilot-Induced Oscillations (PIO) have been recently published by D.T. McRuer [1, 2].

The rapid advances in the field of digital flight control technologies provided new flexibility to the airframe designer. Computerized flight controls will enable the pilots to concentrate more on the mission. This is especially challenging for rotorcraft systems which have to be flown in the mechanically mode with *all hands and feet.*

On the other side, increased automation in the cockpit and flight control environment have not necessarily mitigated but increased the sensitivity of Aircraft-Pilot Coupling phenomena: the power and responsiveness of high gain full authority digital flight control systems makes them more susceptible to various *nonlinear* effects such as time delays, actuator rate limits and amplitude saturation. The increased potential of dangerous APC has been underlined by several historical and recent spectacular incidents and accidents [1 - 5].

1.2 Definitions and Objectives

Pilot Induced Oscillations (PIO), or, adverse Aircraft-Pilot Coupling (APC), describe high gain feedback interactions between the human pilot and flight vehicle dynamics. The designation APC removes also some of the stigma associated with these incidents and which might be attached to the pilot.

APC is associated generally with abnormal trigger events which may be related to changes of vehicle characteristics or pilot behaviour. Whereas changes of vehicle characteristics are related to configuration changes such as flap deployment, variations of flight control laws or system failures, the pilot may change his task aggressiveness by gain changes, e.g. amplitude/rate or frequency contents of his control inputs. Also, emotional elements may have a certain influence in high stress situations when the pilot feels *disconnected from the stick* (..."the airplane had never done anything like that before. It surprised me, it really shocked me ...I thought something had broken and I didn't see any warning lights", [4]).

Further, atmospheric disturbances such as turbulence upsets, wind shear conditions or wake vortex encounters may also provide triggering events for adverse APC situations.

Adverse APC is safety critical in that it is loss of control and that when it is encountered it is dangerous as a structural failure of the airframe. Therefore, APC in general is concerned with flight safety issues. The cost of these problems in development programme delays and financial terms are often not envisaged but they may become significant.

The objectives of this paper can be defined as following:

(1) Assess the status of current studies and related research on adverse Aircraft-Pilot Coupling (APC),

(2) Review historic and recent incidents/accidence regarding adverse Rotorcraft-Pilot Coupling (RPC) issues,

(3) Identify new potentials of RPC as a future threat to flight safety of highly augmented rotorcraft and

(4) Recommend international research efforts devoted to RPC anatomy and prevention possibilities.

Paper presented at the FVP Symposium on "Advances in Rotorcraft Technology", held in Ottawa, Canada, 27-30 May 1996, and published in CP-592.

1.3 Aircraft-Pilot Coupling (APC) Research

As a result of growing numbers of APC-related incidents and accidents of civil and military aircraft with active control systems and/or advanced cockpit technologies various review teams and research groups have been formed in recent years.

They include the Study Committee on *Effects of Aircraft-Pilot Coupling on Flight Safety* of the United States Research Council (Aeronautics and Space Engineering Board) under the leadership of D.T. McRuer (1995 - 1996) and various recent initiatives and activities of the Flight Vehicle Integration Panel (FVP) of the Advisory Group of Aerospace Research and Development (AGARD) [6 - 7]. Further research is directed by NASA [8], US Air Force [9] and DLR/FFA [10]. Surveys on recent and ongoing APC research concerned mainly with fixed wing aircraft are given in [1 and 11]. Evaluations of available material and flight data bases resulted in revisiting theoretical approaches and originating unified steps and standards to assess and characterize adverse aircraft-pilot coupling phenomena more generally [12, 13, 14]. The world of potentially severe PIOs or APCs respectively is divided into three categories described below.

1.4 Three Categories of APC

The classification scheme suggested by McRuer [1, 2] takes into account various pilot behavior models and closed loop analysis procedures from past experience. Data bases utilized rely more or less totally on fixed-wing in-flight simulation, flight test and flight incident/accident data bases. Rotorcraft related data bases are extremely limited and practically only concerned with sling load/helicopter-pilot interactions (see section 2.1).

- Category I

  Linear Pilot-Vehicle System Oscillations.

  The effective controlled vehicle dynamic characteristics are essentially linear as well as the pilot's behavioral dynamics. The oscillations are associated with high gain open-loop system dynamics. These are critically formed by increasing time delay effects.

Generally, Cat. I APC tendencies are sufficiently predicted by simply providing "good" flying qualities as defined in USAF MIL-STD-1797 (fixed-wing) or US Army ADS-33D (rotary wing) under "Level 1" requirements with emphasis placed on those criteria of most importance in high-gain closed loop piloting tasks.

Aeroelastic related linear phenomena are not as yet generally predictable. They require extended mathematical models including flexible mode dynamics.

- Category II

  Quasi-Linear Pilot-Vehicle System Oscillations with Control Actuator/Surface Rate or Position Limiting.

  The rate limiting elements (RLE, [15]) modify the Cat. I situation by introducing amplitude-sensitive effective time delays which determine the magnitude of limit-cycle type oscillations. Additionally, nonlinearities such as stick command shaping or aerodynamic characteristics may also be included [1].

Specific Cat. II APC conditions tend to be equivalent to those of Cat. I except for the dominance of control system and/or aerodynamic nonlinearities. Oscillatory APC condition may be analytically described by linear parts of the open-loop pilot-vehicle dynamics and a composite describing function representing the nonlinearity as a function of input amplitude and frequency. This approach was successfully applied as early as 1964 [16].

A straight forward Cat. II prediction criterion is proposed in [17]. This new flying qualities parameter (OLOP: **O**pen **L**oop **O**nset **P**oint) predicts potential adverse APC conditions due to rate limiting in the flight control system of highly augmented flight vehicles. No describing functions techniques are required. The method determines the closed-loop frequency where the RLE is actived first time for maximum input amplitude.

Then, OLOP is defined as the open-loop frequency response at the closed loop onset frequency [17]. OLOP can be readily used in the flight control systems design process dealing with feedforward and feedback gains and RLE parameters.

- Category III

  Essentially-Nonlinear Pilot Vehicle System Oscillations with Transition.

  These APC conditions depend on nonlinear transitions in either the effective controlled flight vehicle dynamics, or in the pilot's behavioral dynamics [1]. Transitions or shifts in controlled element dynamics may be associated with the control input amplitude, or due to variations or failures in the flight vehicle external configuration (e.g. aerodynamics, structural components, propulsion system) or internal architectures (e.g. flight control laws, software configuration). Pilot transitions may be related to changes in the flight mission implying different aggressiveness in the manual control task and/or switched motion cueing (e.g. from attitude to load factor).

Cat. III APC are highly critical and less predictable for modern digital FbW/L flight control systems designed for more or less unstable flight vehicle configurations. The control laws of these highly augmented flight vehicles are optimized for optimum and carefree handling qualities (Level 1) with embedded flight envelope protections. For these purposes, various nonlinear *soft* and *hard* system elements are implemented to counter anticipated control problems.

The Cat. III problem arises if the pilot is faced with unanticipated or unimagined hard - and/or software interferences of the control - configured flight vehicle. A more elaborate discussion on Cat. III APCs, e.g. the alteration potential of effective flight vehicle or pilot dynamics is given by D.T. Mc Ruer [1, 2].

2. INTEGRATED PILOT-ROTORCRAFT SYSTEM

2.1 Potential Sources of Rotorcraft-Pilot Coupling (RPC)

The next generation of military rotorcraft will have to be capable of precise and aggressive maneuvering close to the ground at night and in poor weather. By using Active Control Technologies (ACT), the rotorcraft's handling qualities can be tailored to specific demands of individual mission phases. Hence, different flight control laws will be programmed for different flight phases, e.g. rate command for Nap-of-the-Earth (NOE) flight and attitude command for precision hovering. Handling qualities requirements such as ADS-33D will provide guidelines for the design of integrated flight control systems. They also provide the bottom line for acceptance flight testing. Figure 1 shows the generics of an integrated flight control system of a future rotorcraft. Different components like *inceptors* (manipulators), *effectors* (actuators and rotor blade controllers),

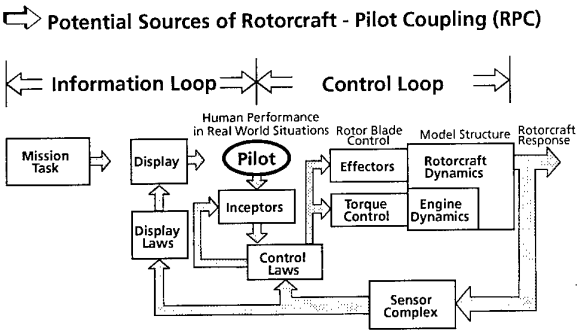

Fig. 1 Integrated Rotorcraft-Pilot System

sensors, display and software interfaces (control and display laws) form the integrated rotorcraft system, which has to be ultimately handled and evaluated by the pilot. Besides the bare rotorcraft dynamics, each component in Figure 1 introduces additional higher order dynamics which will enter into the final evaluation of the integrated rotorcraft-pilot system. These higher-order dynamics of actively controlled rotorcraft will result in reduced system bandwidth and increased system phase delay which is directly related to the total effective time delay of the rotorcraft-pilot system. System bandwidth and effective time delay are two of the most important flight control design and specification parameters of ADS-33D. Effective time delays of more than 200 msec, resulting from 50 - 70 msec inherent rotor response delays, some 30 msec actuator delay and additional delays due to digital computing, sensor signal shaping and filtering, may reveal poor handling qualities due to high-gain tasks. They exhibit potential sources of adverse Rotorcraft-Pilot Coupling.

Potential dynamic interactions of rotorcraft have been discussed by D.T. Mc Ruer [1]. Based on a CH-53E roll rate to lateral cyclic transfer function Figure 2 provides a concrete illustration of the huge amount of dynamic models involved in helicopter dynamic interactional features. As

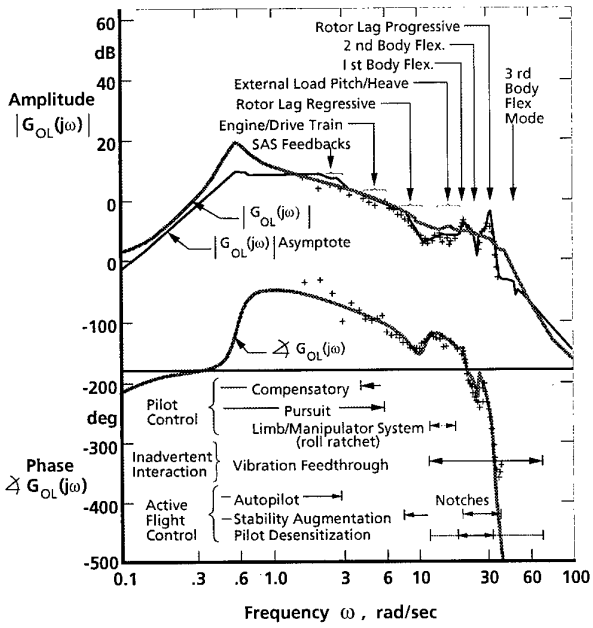

Fig. 2 Large Rotorcraft Dynamic Interactional Features

Mc Ruer states: "... extensive interactions between a large number of phenomena that have diverse origins and that untangling their big mess demands further interactions among many cooperative disciplines".

From a historical viewpoint a collection of adverse Rotorcraft-Pilot Coupling occurrences has been assembled in Figure 3 [18 - 26]. The most dramatic RPCs involving large operational rotorcraft with relatively conventional flight controls were associated with the coupling of lower flexible mode frequencies in combination with external (sling) loads [1, 2, 19, 21, 22].

Type	Year	Associated with	Ref.
▷ BO 46	1964	Rotor Control/Gyro System Coupling	[18]
▷ CH-47	1968	Rotor/Sling Load Bounce	[19]
▷ AH-56	1970	Flexible Control Actuation System	[20]
▷ CH-53 E (USN)	1978	Flexible Mode-Sling Load Interaction	[21]
▷ CH-53 G (GAF)	1980	Flexible Mode-Sling Load Interaction	[22]
▷ UH-60 ADOCS	1988	Excessive Time Delays	[23]
▷ V-22	1989	Flight Control/Flexible Mode Interaction	[24]
▷ BO 105 ATTHeS	1993	Time Delay/Attitude Command	[25]
	1995	Biomechanical/Airframe Coupling	[26]

Fig. 3 Rotorcraft-Pilot Coupling Occurrences

Other adverse RPC incidents / accidents involved man-machine control behavior in biodynamic environments [20, 27] plus excessive time lag [18] or delays [23, 25, 26].

2.2 Rotorcraft Indicators of Concern

From Figures 1 and 2 of section 2.1 it can be concluded that the potential of RPCs related to future combat and transport rotorcraft will be challenged by the following four features:

- Rotorcraft Dynamic Features
  - Limited inherent Stability
  - Rigid Body/Flexible Modes Coupling
  - Control/Response Coupling
  - Vibration Environment
  - Very large Airframes
  - Underslung Loads
- The Fly-by-Wire/Light Factor
  - Full-Authority Control Effectors
  - Control Laws and Degraded Modes
  - Envelope Protection and Load Limiting
  - Manipulator Dynamics and Stick Filtering
  - Bandwidth & Time Delay Effects
- Pilot Dynamics Features
  - Behavior Patterns
  - Flight Training and Experience
  - Increasing Task Demands
- Pilot-Rotorcraft Interface
  - Biodynamic Interferences
  - Usable Cue Environment
  - Mode Switching
  - Envelope Protection
  - General Effects of Automation.

3. THREE RPC CASES

3.1 UH-60 ADOCS (Cat. I Example)

The Advanced Digital Optical Control System (ADOCS) demonstrator program was conducted in the 1980's with the overall objective of providing the technology base for the engineering development of an advanced battlefield-compatible flight control system (Fig. 4). Performed by Boeing Helicopter under contract from the US Army Applied Technology Directorate (AATD), Ft. Eustis, Virginia, it provided an extensive base of experience on the design, testing,

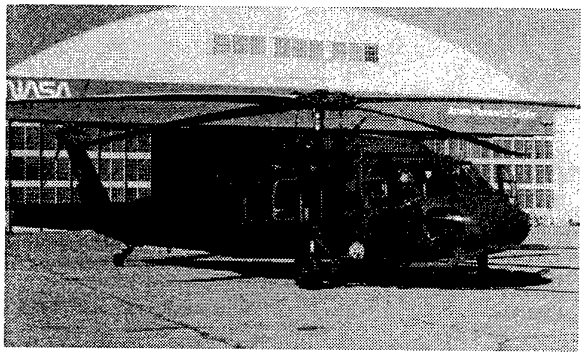

Fig. 4 UH-60 ADOCS Demonstrator

and analysis of a full flight-envelope advanced combat rotorcraft [23]. Shown in Fig. 5 is a simplified depiction of the flight-test configuration for the pitch channel. Command inputs from the pilot's manipulator, a multi-axis side-stick controller, are sampled and then filtered before being passed to the digital flight computer. An explicit model-following concept was implemented to take advantage of the capability to independently set the command and stabilization response characteristics, thus providing multi-mode responses. The equivalent time delay of each the elements is indicated along with their percentage of the total delay. The total equivalent time delay was 223 msec. There were similar delays in the roll and yaw axes (260 and 224 msec respectively).

UH-60 ADOCS
Advanced Digital Optical Control System Demonstrator
Elements of Time Delay

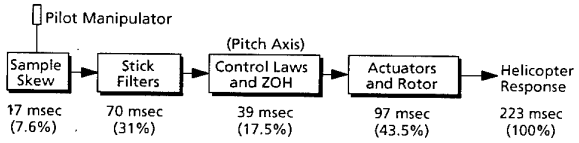

Fig. 5 Rotorcraft-Pilot Coupling (Cat. I, Example 1)

The evaluation of aircraft's handling qualities is very dependent upon the task and environment in which the task is performed. That is, as task requires a higher and higher pilot gain, generally there is degradation in the handling qualities. This may be accentuated with a side-stick controller. For the final ADOCS evaluation by the Aeroflightdynamics Directorate (AFDD), the pilots evaluations were categorized into low gain, medium gain, high gain, and ultra-high gain tasks (Fig. 6). For the low and medium gain tasks, the ADOCS demonstrated essentially all Level 1 ratings. For the high gain tasks, the handling qualities ratings degraded into Level 2. For the ultra-high gain tasks, the handling qualities generally degraded even more. A repeatable 1 Hz lateral oscillation was observed for several of the high to ultra-high gain tasks. For example, during the performance of the vertical landing from a hover a persistent adverse 1 Hz lateral RPC was observed on the telemetry. This was not always observed by the evaluation pilot however and though the workload during the descent was very low, exhibiting excellent Level 1 characteristics, the overall rating for this maneuver varied between 4 and 5. Comprehensive frequency-domain testing is needed to uncover these potentially degrading time-delay effects, as quantitative time-domain testing techniques (steps and pulses) are not sufficiently sensitive to time delays.

UH-60 ADOCS
Advanced Digital Optical Control Flight Demonstrator

Exhibited RPC in several high to ultra-high Gain Tasks
- Vertical Landing - 1 Hz lateral
- Dash / Quickstop - 1 Hz lateral during Flare
- Slope Landing - sometimes divergent 1 Hz lateral

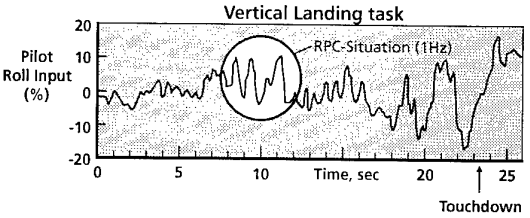

Fig. 6 Rotorcraft-Pilot Coupling (Cat. I, Example 1)

3.2 BO-105 ATTHeS (Cat. I Example)

The effects on handling qualities due to time delays in conjunction with a high bandwidth response was investigated in a collaborative study by the Institute for Flight Mechanics of the German Aerospace Research Establishment (DLR) and the Aeroflightdynamics Directorate of the US Army Aviation and Troop Command under a US/German MOU [25, 28]. Using DLR's variable-stability helicopter, BO-105 ATTHeS (Figure 7), both rate and attitude command response types with added time delays up to 160 msec

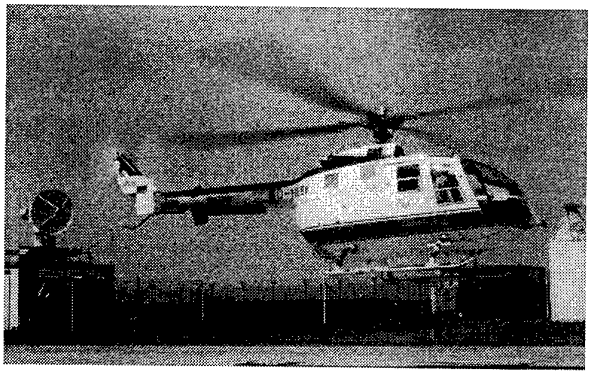

Fig. 7 BO-105 ATTHeS In-Flight Simulator

were investigated (Fig. 8). The evaluation task consisted of a modified slalom task with precise tracking phases through a set of groundmarked gates. These gates were 3 m in width and varied in length from 90 to 150 m. The overall course was 1550 m in length. The transition phases between gates were intended to be a lower frequency disturbance with the main emphasis being the higher frequency acquisition and tracking phases just prior to and through the gates.

BO 105 ATTHeS
Variable Bandwidth/Time Delay In-Flight Simulation

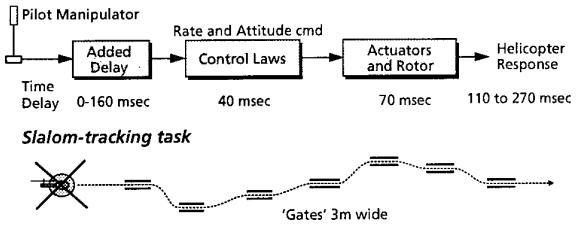

Fig. 8 Rotorcraft-Pilot Coupling (Cat. I, Example 2)

Figure 9 shows the time history for an attitude command response ω_{BW} = 1.7 rad/sec) and with an added time delay of 160 msec (τ_p = 270 msec). One can still recognize the gate transition phase in the control and bank angle time histories, although during the gate acquisition and tracking phases the pilot is using a lot of almost periodic inputs to try and maintain track within the gates. The result is an oscillatory RPC-response which is clearly visible in the bank angle response. After the flight evaluation the pilot commented the tendency for a "roll pilot induced oscillation" and said this was a "very poor configuration." The handling qualities rating for this case was an HQR = 6 which implies very objectionable but tolerable deficiencies with only adequate performance attainable with extensive pilot compensation.

BO 105 ATTHeS
Variable Bandwidth/Time Delay In-Flight Simulation

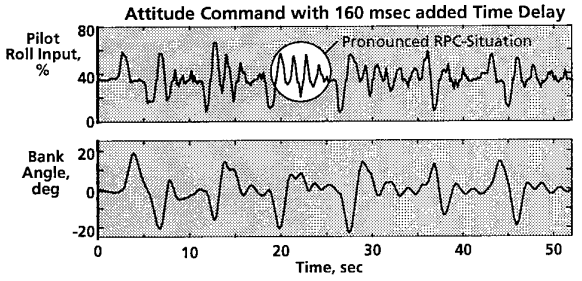

Fig. 9 Rotorcraft-Pilot Coupling (Cat. I, Example 2)

Category I Rotorcraft-Pilot Coupling may be predicted using the bandwidth and phase delay requirements from Aeronautical Design Standard ADS-33D. Figure 10 shows the bandwidth and phase delay of the two RPC configurations discussed above. Both RPC cases, which had a phase delay of about 200 msec were predicted with marginally adequate to inadequate (borderline Level 2-3) handling qualities. Figure 10 also shows the bandwidth and phase delay of the DLR in-flight simulator with no added time delay. As can be seen, the helicopter possesses desired (Level 1) handling qualities in this case.

3.3 BO-105 ATTHeS (Cat. I/III Example)

Figure 11 shows an example of a Category I/III Rotorcraft-Pilot Coupling that was experienced with the DLR in-flight simulator ATTHeS [26, 28]. The command model implemented on ATTHeS was an attitude command system with

⇨ Cat. I Cases may be prediced by ADS-33 D Bandwidth Requirements

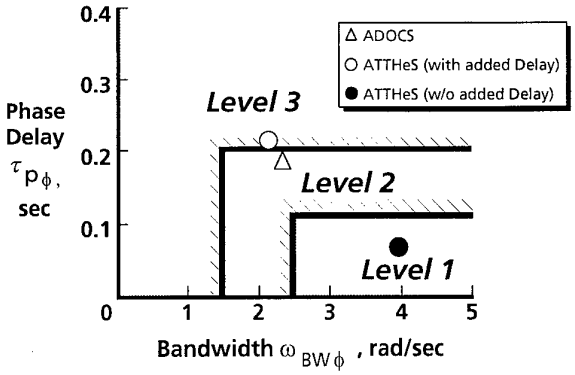

Fig. 10 Rotorcraft-Pilot Coupling (Cat. I, Prediction by ADS-33D)

a basic time delay of 90 msec and an added time delay of 100 msec. The task was a lateral position tracking task, during which the pilot tried to maintain a hover relative to a hover board mounted on a vehicle that was moving. Figure 11 shows the experiment set-up and the velocity profile of the vehicle.

BO 105 ATTHeS Sidestep Tracking Task
Flight Control Law:
Attitude Command with 100 msec added Delay

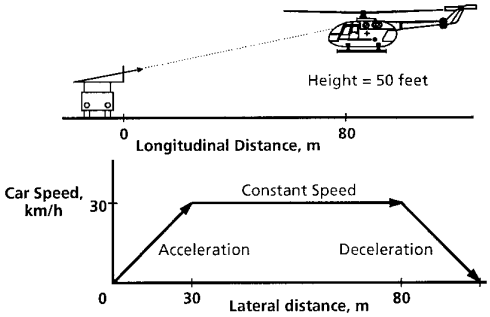

Fig. 11 Rotorcraft-Pilot Coupling (Cat. I/III, Example)

Fig. 12 shows the lateral stick input and the bank angle response for the lateral position tracking task. A pronounced RPC can be recognized at the start of the lateral transition. During the debriefing, it was found out, that although time delay was a contributing factor, the most important reason for this RPC was biodynamic coupling between the aircraft, the lateral cyclic controller, and the pilot. This can best be explained by examining the sequence of events. When the vehicle starts its lateral translation, the pilot needs to bank to the right in order to follow the vehicle, so he makes a lateral stick input to the right and tries to maintain that stick position (necessary because of the attitude command system). The helicopter control system responds to the input by generating a roll rate to the right. The inertia acting on the stick and the pilot's arm now makes the stick lag this right rolling motion. Since stick position is measured relative to the helicopter, a left stick input is sensed, so the control system responds with a left roll rate. Now, the pilot gets into the loop and a classic RPC develops, which continues until the pilot can backs-out of the control loop or ultimately releases the stick.

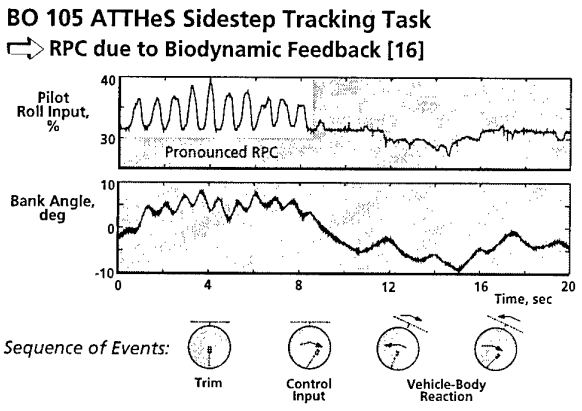

Fig. 12 Rotorcraft-Pilot Coupling (Cat. I/III, Example)

Comparison of the vehicle handling qualities with the bandwidth and phase delay criteria of ADS-33D did not reveal the very severe RPC tendency of this vehicle-stick response. Although the phase delay was evaluated as a result of the added time delay, handling qualities were predicted as adequate (Level 2), which is not consistent with the severe RPC shown in Figure 12.

Similar biodynamic feedback phenomena associated with control stick dynamics have been observed during flight experiments at NRC, Canada, and others [29].

4. RPC ASSESSMENT

4.1 Cat. I RPC

From the afore discussed three RPC flight cases it can be concluded that the *bandwidth* and *phase delay* criteria of the current D-version of the Aeronautical Design Standard 33 (ADS-33) *Handling Qualities Requirements for Military Rotorcraft* have some potential to predict adverse Cat. I-type RPC cases at the Level 2/3 boundary (Figure 10).

A potential difficulty with the analysis of flight test data associated with *bandwidth / phase delay* criteria is the frequency for gain and phase margins, and twice the cross-over frequency may be outside the range of good coherence. Especially *phase delay* (phase slope) estimates may become sensitive because of poor data coherence due to rotor dynamics and other nonlinear effects at higher than bandwidth frequencies. These effects have to be quantified and need more research [30].

Reproducable *phase delay* (phase slope) estimates at bandwidth frequencies are indispensable for reliable Cat. I-RPC predictions, as small changes in pilot gain may result in large changes in phase lag, "a perfect setup for a PIO" [31].

Some of the ADS-33 standardized flight test maneuvers such as roll-slalom tracking provide the level of aggressiveness required for unmasking critical RPC tendencies. Nevertheless as yet only limited RPC oriented flight test data bases have been gathered by fly-by-wire / light technology demonstrators (e.g. UH-60 ADOCS) or airborne simulators (e.g. BO 105 ATTHeS) [25, 28, 30].

4.2 Cat. II RPC

No specific rotorcraft prediction methods are available. At least, the ADS-33 *attitude quickness* criterion developed as a measure for rotorcraft agility, or the ability to maneuver aggressively may have some application potential for exposing control actuator rate limiting [31].

Fixed-wing related APC prediction criteria utilizing describing function methods offer some good potential for rotorcraft applications [12, 13, 15].

Still more attractive becomes Duda's OLOP-criterion which does not require describing functions but the following steps [14]:

- Define simple high-gain pilot model
- Calculate *linear* closed-loop frequency response from pilot model input to input of rate-limiting element (RLE)
- Determine closed-loop onset frequency where rate limiter is actuated first time for maximum pilot input amplitude and
- Identify open-loop frequency response at the closed-loop onset frequency.

Fixed-wing aircraft simulation and flight data analysis look promising but rotorcraft simulation and flight data gathering and evaluation is still missing. Also, OLOP boundaries for rotorcraft with rate limiting elements in the feedforward or feedback path have still to be investigated and validated.

4.3 Cat. III RPC

No specific rotorcraft related prediction methods readily available. Cat. III RPC assessment methods are the most challenging issue for highly-augmented and full authority fly-by-wire / light rotorcraft.

What measures (research and flight test techniques) have to be taken in order to unmask unforeseen (hidden) events which are contradictory to software solutions or dedicated system nonlinearities originally designed and implanted to provide optimum (level 1) flying qualities or to counter anticipated problems (e.g. load limiting and / or flight envelope protection)?

5. RPC PREVENTION

5.1 Prevention Methodologies

There is no unique methodology or clear set of recommendations which can be applied to prevent adverse rotorcraft-pilot coupling problems. Two specific aspects of RPC prevention methodologies have to be highlighted:

(1) **Successive system assessment** during the design process including

Analytical modeling of

- Rotorcraft dynamics and aeromechanics,
- Pilot dynamic behavior (control-theoretic or fuzzy control equivalents),

Ground-based pilot-in-the-loop simulation,

In-flight (airborne) simulation and

Prototype testing

yielding cumulative data bases for potential / rotorcraft-pilot coupling evaluations.

The second aspect is concerned with stringent requirements for the design and implementation of

(2) **Flight test techniques** for

- System identification purposes and
- High-gain maneuvering.

System identification flight testing is essential for all handling qualities investigations of highly augmented rotorcraft as it can provide validated mathematical models extracted right in time during the flight envelope expansion phase [32].

German (DLR [33] and US (NASA / AFDD / Boeing [34]) fly-by-wire / light rotorcraft flight experience have clearly demonstrated the advantages of explicit model following flight control laws for tailoring of the rotorcraft response to achieve favourable handling qualities. The philosophy of model following control based on feedforward regulation provides safer and more accurate mode control. The performance, however, depends strongly on the validated mathematical model of the bare rotorcraft dynamics which have to include for high-gain and bandwidth requirements (aggressive maneuvering) not only rigid-body but also higher-order rotor and control system dynamic effects [35 - 37].

Pilot-in-the-loop investigations utilizing these validated high-fidelity mathematical models are one of the best prerequisites to identify and alleviate potential RPC conflicts.

More details about rotorcraft system identification flight test techniques such as control input design are published in [35].

High-gain demonstration maneuvers for RPC immunity testing should include

- Slalom tracking (AFDD/DLR) which provide appropriate acquisition and precision tracking phases [25] and
- Sidestep tracking (DLR/ONERA) which includes rapid successions of lateral acceleration and deceleration phases and a dynamic precision hovering task [26].

Another high gain/high bandwidth flight test technique involves random multi-axis tracking originally developed by DLR (GRATE, [38]) and complemented by NASA (ATLAS, [39]) for unmasking adverse APC phenomena. Fore more details read section 8.3.5 of Reference [32]. This method has still to be explored for RPC applications.

5.2 Prevention Technologies

There are mainly two technology options to prevent adverse RPCs:

(1) **FbW/L manipulator technologies**

- Adaptive filtering,
- Active manipulators (active sidesticks)

and

(2) **FbW/L control law schemes**

- Alternative control schemes,
- Explicit model following.

Rotor-induced vibrations and other inertial forces during aggressive maneuvering can exert forces on the body and limbs of the pilot, exciting nonvoluntary control commands of the manipulator (pilot inceptor) which may deteriorate rotorcraft control precision, increase control activity and may cause rotorcraft-pilot coupling effects due to parasitic positive feedback paths. These phenomena have already been researched [40].

Adaptive filtering may restore tracking performance and suppress or prevent adverse RPCs due to biodynamic feedback [41]. Still more research is needed for establishing guidelines for designing RPC-free fly-by-wire/light (FbW / L) manipulator / flight control laws.

One disadvantage of passive stick feel systems is the inability to change stick dynamics and to sense control system or rotor load limits which will vary with trim conditions. On the other hand active force feedback or cueing manipulators are still subject of basic research.

Active sidesticks definitely can improve critical RPC situations by giving the pilot immediate kinesthetic feedback on the consequences of controller inputs, and can be used to indicate trim status. Also, active sidearm controllers could transfer control of the rotorcraft from one pilot to another in an emergency.

Recent advances in active inceptor technology utilizing electromagnetic instead of electromechanic force loading indicate promising options of active and adaptive manipulators for future highly augmented and RPC resistant FbW/L rotorcraft (Figure 13, [42]).

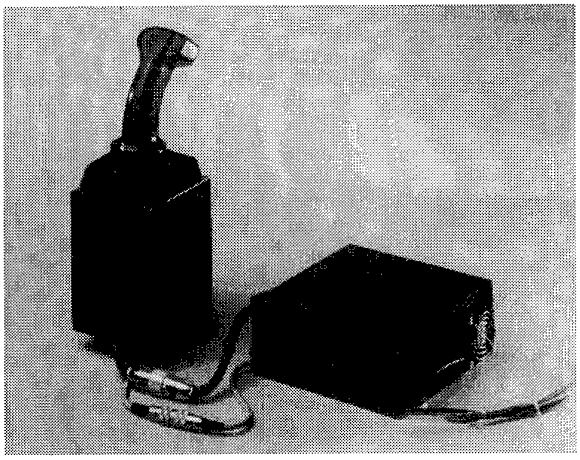

Fig. 13 Active Electromagnetic Sidestick (DLR / TU BS)

Alternative control schemes have been proposed and flight tested by A'Harrah and others in order to alleviate potential APC-Problems during actuator rate limiting [43]. Results of a DLR experiment implemented on the in-flight simulator ATTAS demonstrated both the negative effect of rate saturation and the effectiveness of alternate control schemes (ACS) to reduce the equivalent time delay and to improve the tracking performance [44]. There is a great potential to transfer this fixed-wing APC alleviation technology to RPC applications.

Finally, *explicit model following* control schemes, as discussed in chapter 5.1, show strong promises and challenges for future highly augmented FbW / L rotorcraft. The basic helicopter is forced to respond to the pilot's inputs as an explicitly calculated command model [33]. This kind of

feedforward control yields the required flexibility for variations of the command model response behavior. Low gain-feedbacks are solely required to compensate for modeling inaccuracies and disturbance rejection and, hence, offer a reduced potential for critical RPC conditions.

6. CONCLUSIONS AND RECOMMENDATIONS

In this paper, a survey was given of rotorcraft-pilot coupling (RPC) phenomena which may adversely affect mission performance and flight safety:

1. Potential unfavorable RPCs are mainly associated with interdisciplinary interactions between the pilot and effective dynamics of the rotorcraft, including rigid-body dynamics, flexible rotor aeromechanics, propul-sion system and flight control system components. In connection with lower frequency flexible rotor modes and large underslung loads severe rotorcraft-pilot cou- plings may occur during precision flight tasks such as on-the-spot-hovering.

2. With the introduction of full-authority fly-by-wire/light flight control systems in combination with new manipulators such as sidesticks a multitude of favorable options offering task-oriented optimum and carefree handling qualities becomes available. With these promising but sophisticated *hard* and *soft* technologies a total system integrity qualification process regarding unfavorable RPC potentials becomes mandatory.

3. Within project development and acceptance flight testing adequate time for executing standardized aggressive maneuvering should be provided to unmask any sources for adverse rotorcraft-pilot handling deficien-cies. These deficiencies may have been undeliberately introduced by nonlinear elements such as rate limiters for alleviating loading problems on the rotor system.

4. Only very limited flight test data bases for Cat. I RPC research are available. Diligent pilot-in-the-loop handling qualities research is required for data gathering in all three RPC categories (Cat. I-III) using ground-based and airborne flight simulators.

5. Elements of the US Army ADS-33D criteria provide certain guidance for predicting unfavorable Cat. I RPC conditions. ADS-33D also define selected high gain tracking tasks which have sufficient levels of aggressive-ness for indicating RPC tendencies. Random multi-axis tracking tasks designed for fixed-wing pilot-in-the-loop handling qualities testing and training show promises for RPC applications.

6. Explicit model following control laws, active force feel systems (active sidesticks) and electro-optic cockpit information systems can greatly enhance mission flexibility of future FbW/L rotorcraft without compromising human factors and related RPC flight safety issues. But integrated technology readiness still has to be flight demonstrated.

7. Prediction methods as well as certification or acceptance standards for RPC immunity need NATO-wide coordinated research. An interdisciplinary AGARD Expert Group may organize a FVP-led Specialists' Meeting or Working Group entitled *Rotorcraft-Pilot Coupling and related Phenomena.*

7. ACKNOWLEDGEMENTS

The author would like to express his appreciation to Chris L. Blanken, Guest Scientist form the US Army Aeroflightdynamics Directorate (AFDD) under the auspices of the US-German Memorandum of Understanding on Helicopter Aeromechanics, and Carl J. Ockier, Scientist, both Institute for Flight Mechanics, DLR, for their valuable contributions to chapter 3 (three RPC cases) of this paper. Special thanks are due to Bärbel Fischer for preparing the final manuscript.

8. REFERENCES

[1] Mc Ruer, D.T., "Active Control Technology and Interdisciplinary Interactions", AGARD-CP-560, Paper K , January 1995.

[2] Mc Ruer, D.T., "Pilot-Induced Oscillations and Human Dynamic Behavior", NASA CR 4683, July 1995.

[3] Kullberg, E., et al., "SAAB Experience with PIO", AGARD-AR-335, Paper 9, February 1995.

[4] Dornheim, M.A., "Report Pinpoints Factors Leading to YF-22 Crash", AW & ST, 9 Nov. 1992, pp. 53 to 54.

[5] Dornheim, M.A., et al., "Boeing Corrects Several 777 PIOs", AW & ST, 8 May 1995, p. 32.

[6] N.N., "Active Control Technology: Applications and Lessons Learned", AGARD-CP-560, January 1995.

[7] Mc Kay, K. (Editor), "Flight Vehicle Integration Panel Workshop on Pilot Induced Oscillations", AGARD-AR-335, February 1995.

[8] A'Harrah, R.C., "Communique with DLR and Others", NASA Headquarters, Washington D.C., 14 July 1992.

[9] Flynn, W.A., "An Investigation of Pilot Induced Oscillation Phenomena in Digital Flight Control Systems", AGARD-CP-560, Paper 23, January 1995.

[10] Duda, H., "Analysis of Adverse Aircraft-Pilot Coupling in the Roll-Axis Using Frequency Domain Criteria", DLR-IB 111-15/24 (1995).

[11] Mc Kay, K., "Pilot Induced Oscillation - A Report on the AGARD Workshop on PIO, 13th May 1994", AGARD-CP-560, Paper PIO, January 1995.

[12] Klyde, D.H., et al,, "Unified Pilot-Induced Oscillation Theory", STI TR-1313-1, September 1995.

[13] Duda, H., "Effect of Rate Limiting Elements in Flight Control Systems - A new PIO Criterion", AIAA-Paper 95-3304 (1995).

[14] Duda, H., "Prediction of Adverse Aircraft-Pilot Coupling in the Roll Axis due to Rate Limiting in Flight Control Systems", DLR IB 111-96/13 (1996).

[15] Hanke, D., "Handling Qualities Analysis on Rate Limiting Elements in Flight Control Systems", AGARD-AR 335, Paper 11, February 1995.

[16] Ashkenas, I.L., et al., "Pilot Induced Oscillations: Their Cause and Analysis", STI TR-239-2, June 1964.

[17] Duda, H., "The Open Loop Onset Point. A New Flying Qualities Parameter to Predict APC Problems due to Rate Saturation in FCS", DLR-IB 111-96/1 (1996).

[18] Reichert, G., "Stabilitätsprobleme mit dem Versuchshubschrauber Boelkow BO 46", Private Communication, Braunschweig, 23 August 1996.

[19] Gabel, R., et al., "Test Approaches to External Sling Load Instabilities", 24th Annual Forum, AHS, 1968, Paper 230, 12 p.

[20] N.N., "Lockheed Flight Testing AH-56 with Modified Controls, Blades", AW & ST, 30 March 1970, pp. 66 - 67.

[21] Kaplita, T.T., "Helicopter Simulation Development by Correlation with Frequency Sweep Flight Test Data", 45th Annual Forum, AHS, 1989, pp. 681 - 692.

[22] Buchacker, E., " Experience with SIFT Flight-Test-Techniques at the German Air Force Flight Test Center", AGARD-CP-333, Paper 24, June 1982.

[23] Tischler, M.B., et al., " Flying Quality Analysis and Flight Evaluation of Highly Augmented Combat Rotorcraft", AIAA J. Guidance, Vol. 14, No. 5, pp. 954 -963, Sept. - Oct. 1991.

[24] Parham, T., et al., "V-22 Pilot-in-the-Loop Aeroelastic Stability Analysis", 47th Annual Forum, AHS, Phoenix, May 6 - 8, 1991, pp. 1307 - 1319.

[25] Pausder, H.-J., and Blanken, C.L., "Investigation of the Effects of Bandwidth and Time Delay on Helicopter Roll-Axis Handling Qualities", NASA CP-3220, January 1993.

[26] Bouwer, G., et al., "Smart Helicopter Concept – Handling Qualities Data Base for Hover and Low Speed Flight", AGARD-CP-592, Paper 11, December 1996.

[27] Jex, H.R., "Problems in Modeling Man-Machine Control Behavior in Biodynamic Environments, NASA SP-281, pp. 3 - 13, 1971.

[28] Ockier, C.J., "Pilot Induced Oscillations in Helicopters - Three Case Studies", DLR-IB 111-96/12 (1996).

[29] Morgan, J.M., "An Initial Study into the Influence of Control Stick Characteristics on the Handling Qualities of a Fly-by-Wire Helicopter", AGARD-CP-508, Paper 18, February 1991.

[30] Key, D.L., "Rotorcraft Potential APC", Aircraft-Pilot Coupling Workshop, US National Research Council, Aeronautics and Space Engineering Board, Irvine, 27 - 30 November 1995.

[31] Hoh, R.H., and Mitchell, D.G., "The Role of Handling Qualities Specifications in Flight Control Sys-tem Design", AGARD-CP-560, Paper 1, January 1995.

[32] Wünnenberg, H. (Editor), "Handling Qualities of Unstable Highly Augmented Aircraft", AGARD-AR-279, May 1991.

[33] von Grünhagen, W., et al., "A high Bandwidth Control System for a Helicopter In-Flight Simulator", International Journal of Control, Vol. 59, No. 1, pp. 239 -261, January 1994.

[34] Landis, K.H., et al., "Advanced Flight Control Technology Achievements at Boeing Helicopters", Inter-national Journal of Control, Vol. 59, pp. 263 - 290, January 1994.

[35] Hamel, P.G. (Editor), "Rotorcraft System Identification", AGARD-AR-280, September 1991.

[36] Hamel, P.G., and Kaletka, J., "Rotorcraft System Identification - An Overview of AGARD FVP Working Group 18", AGARD-CP-552, Paper 18, August 1995.

[37] Tischler, M.B., "System Identification Methods for Aircraft Flight Control Development and Validation", NASA TM-110369, October 1995.

[38] Koehler, R., et al., "GRATE - A new Flight Test Tool for Flying Qualities Evaluations", AGARD-CP-452, Paper 6, July 1989.

[39] Shafer, M.F., et al., "Initial Flight Test of a Ground-deployed System for Flying Qualities Assessment", AIAA-Paper 89-3359, August 1989.

[40] Idan, M., and Merhav, S.J., "Effects of Biodynamic Coupling on the Human Operator Model", AIAA Journal of Guidance, Vol. 13, No. 4, pp. 630 - 636, July -August 1990.

[41] Velger, M., et al., "Adaptive Filtering of Biodynamic Stick Feedthrough in Manipulation Tasks on Board Moving Platforms", AIAA Journal of Guidance, Vol. 11, No. 2, pp. 153 - 158, March - April 1988.

[42] Meins, J., et al., "Advanced Sidestick Controller with Electromagnetic Loading System", CEAS Symposium on Simulation Technology, 30 October - 1 November 1995, Delft, The Netherlands.

[43] A'Harrah, R.C., "An Alternative Control Scheme for Alleviating Aircraft-Pilot Coupling", AIAA-Paper 94-3673 (1994).

[44] Martin, J.R., and Buchholz, J.J., "SCARLET: DLR Rate Saturation Flight Experiment", AGARD-AR-335, Paper 8, February 1995.

An Empirical Correction Method for Improving Off-Axes Response Prediction in Component Type Flight Mechanics Helicopter Models

M. Hossein Mansur and Mark B. Tischler
Aeroflightdynamics Directorate
Aviation Research, Development, and Engineering Center
US Army Aviation and Troop Command
MS 211-2, Ames Research Center
Moffett Field, CA 94035-1000
USA

SUMMARY

Historically, component-type flight mechanics simulation models of helicopters have been unable to satisfactorily predict the roll response to pitch stick input and the pitch response to roll stick input off-axes responses. In the study presented here, simple first-order low-pass filtering of the elemental lift and drag forces was considered as a means of improving the correlation. The method was applied to a blade-element model of the AH-64 Apache, and responses of the modified model were compared with flight data in hover and forward flight. Results indicate that significant improvement in the off-axes responses can be achieved in hover. In forward flight, however, the best correlation in the longitudinal and lateral off-axes responses required different values of the filter time constant for each axis. A compromise value was selected and was shown to result in good overall improvement in the off-axes responses. The paper describes both the method and the model used for its implementation, and presents results obtained at hover and in forward flight.

NOMENCLATURE

$c_{d_{filter}}$	filtered elemental drag coefficient
$c_{d_{table}}$	elemental drag coefficient from table
$c_{\ell_{filter}}$	filtered elemental lift coefficient
$c_{\ell_{table}}$	elemental lift coefficient from table
f_1	lift coefficient table
f_2	drag coefficient table
M	local Mach number of blade element
p	helicopter roll rate, deg/sec
q	helicopter pitch rate, deg/sec
R	rotor radius, ft
V_o	longitudinal component of airspeed, ft/sec
α	angle of attack of blade-element, deg
δ_{lat}	lateral stick input, in
δ_{lon}	longitudinal stick input, in
τ_a	first-order filter time constant, 1/sec
Ω	rotor rotational speed, rad/sec
μ	advance ratio, nd
ψ_a	static aerodynamic phase lag, deg

BACKGROUND

Component-type flight mechanics simulation models of most existing helicopters are unable to correctly predict the off-axes roll response to a longitudinal input and pitch response to a lateral input of the actual vehicle. Linear models, identified from flight data at a specific flight condition, correctly capture the off-axes behavior. Such identified models, however, are only applicable to flight near their reference condition and cannot be applied over the entire flight envelope. Further, they obviously cannot be used during the aircraft development phase, before flight data become available.

Simulation model fidelity is especially important for modern development programs where accurate on- and off-axes response prediction is required for high-bandwidth flight control design purposes (ref. 1). Some researchers speculate that the off-axes discrepancies of flight mechanics simulation models are due to inadequate modeling of the main rotor wake and dynamic inflow (refs. 2 and 3). Others suggest that the discrepancies are the result of insufficient modeling of rotor/fuselage interaction. Yet others propose that only by including blade flexibility can the off-axes discrepancies be corrected. The answer is not clear and has led to the conclusion, as voiced by Professor Curtiss of Princeton, that "off axis response characteristics of single rotor helicopters are not understood" (ref. 4).

In recent years, considerable research effort has been devoted to improving the modeling of the rotor wake. In 1994, Rosen and Isser developed a complex model of rotor wake distortion during pitch and roll motion of a hovering helicopter (ref. 5). This rigorous approach takes into account the influences of shed and trailing vortices together with geometric unsteady effects. It has shown promise in correctly predicting the off-axes responses of the AH-64 and the UH-60. However, to date, it has only been applied to the case of an isolated rotor in hover. Furthermore, the model is too complex to apply to flight mechanics models in its present form, especially if the model is intended for real time simulation.

Presented at the AGARD Flight Vehicle Integration Panel Symposium on "Advances in Rotorcraft Technology", May 27-30, 1996, Ottawa, Canada.

Paper presented at the FVP Symposium on "Advances in Rotorcraft Technology", held in Ottawa, Canada, 27-30 May 1996, and published in CP-592.

To avoid this complexity, researchers at the Aeroflightdynamics Directorate have taken an empirical approach to improving the predictive capability of helicopter models. The goal is not to rigorously model the physics of the problem, but to develop simple modifications that would improve the off-axes correlation of existing and future component-type models. The work originated with the analysis of full scale wind-tunnel test data from the Sikorsky Bearingless Main Rotor (SBMR). That study showed that by increasing the swashplate phase angle used in the analysis model beyond its actual geometric value, it was possible to achieve much better correlation with the off-axes test data (ref. 6). Applying the same technique to a component type model of the UH-60, however, did not improve the off-axes correlation in free flight. The phasing of the swashplate only affects the rotor response to control inputs and not to shaft motion. It was, therefore, thought that for free flight it would be more appropriate to include this correction through an azimuthal rotation in the fixed-frame aerodynamic components, termed the "aerodynamic phase lag", ψ_a. The two correction approaches yield an identical improvement in the fixed-shaft, wind-tunnel case. The aerodynamic phase lag approach proved successful in subsequent identification studies of the UH-60 in hover and forward flight (Fletcher, ref. 7). Physical sources of this identified effective aerodynamic lag include: a) wake geometric distortion due to pitch and roll motion (ref. 5, 8), b) increased 2D unsteady indicial response lag (Theodorsen type) under compressible flow conditions (ref. 9), and c) perhaps in-plane inflow swirl (ref. 2).

In a similar effort, Arnold, et. al. (ref. 3) have recently explored the effects of three possible methods of improving the off-axes response. These are, a) an extended version of momentum theory including wake distortion terms, b) a first-order aerodynamic lag model, and c) an aerodynamic phase correction. The latter two methods follow the empirical approach of AFDD (refs. 1, 7). Arnold et. al. have shown that all three approaches result in similar improvements in the off-axes responses when applied to a simplified model of the coupled pitch and roll dynamics in hover. Also, they have shown that considerable improvement in correlation with flight data is achieved when the extended momentum theory approach is applied to an existing non-linear simulation model. The extended momentum theory work of Arnold parallels the work by Keller (ref. 8) who has shown that the inclusion of induced velocity variations due to shaft rate improves correlation in the pitch response to lateral cyclic inputs. Finally, Von Grunhagen (ref. 2) of the DLR has included apparent angular momentum, arising from the in-plane swirl of the wake, in the dynamic inflow equations and shown improvements in the off-axes prediction.

In the effort presented here, the aerodynamic phase lag technique was applied to a blade-element model of the AH-64 known as BEMAP (ref. 10). Following the implementation of Arnold (method b above), first-order low-pass filtering of the lift and drag coefficients per blade-element was used to implement the desired phasing. The time constant could then be varied until good off-axes correlation was achieved. Herein, the delay was applied to the lift and drag coefficients at the elemental level in an attempt to mimic the actual generation of the forces on the elements (similar to Theodorsen effect but of much higher delay). Also, in the current study the modification is applied to a full-flight-envelope flight-mechanics model, rather than the simplified representation of the pitch and roll responses used in reference 3.

This paper describes the details of the model and the aerodynamic phase lag correction technique. It also provides frequency-domain comparisons of the responses of the modified model with flight data in hover and forward flight. Summary results from SBMR and UH-60 work at AFDD are provided to show the general applicability of the technique, and trends in the empirical phase lag for a range of rotor geometries and flight conditions.

BLADE ELEMENT MODEL FOR APACHE (BEMAP)

The Blade-Element Model for APache (BEMAP) is a version of McDonnell Douglas Helicopter Systems' (MDHS) FLY Real Time (FLYRT) (ref. 11) in which the map-type main-rotor has been replaced with a blade-element type module (ref. 10). The new rotor module was developed following the general structure of the main-rotor module of Sikorsky's Gen Hel model of the UH-60 Black Hawk helicopter (ref. 12). The kinematic and inertial equations for modeling the AH-64 rotor were derived with the aid of the symbolic manipulation program MACSYMA (ref. 13) based on a flap-lag-pitch hinge arrangement and following the work of Chen (ref. 14). Though the Apache uses a flap-pitch-lag hinge arrangement, the simpler f-l-p sequence was used to avoid the added complexity of treating blade pitch as a degree of freedom.

Simple 2D strip theory, augmented with yawed flow corrections and Pitt-Peters dynamic inflow, is used to calculate the aerodynamic forces generated by each blade element. The yawed flow corrections are applied as described in reference 12. The Pitt-Peters inflow model is based on the version outlined by Peters and Ha Quang (ref. 15). It was implemented as a modification of the implementation used by Ballin (ref. 16) in which the normal induced inflow is calculated based on the aerodynamic thrust coefficient using an iterative scheme. Lift and drag coefficients are extracted from bi-variate maps as functions of local angle of attack and Mach number. These coefficients are used to calculate the elemental lift and drag forces. The elemental forces are then summed over all the blade elements to calculate the aerodynamic forces and moments per blade. The aerodynamic forces and moments on each blade are then used, along with the inertial, gravitational, and flapping and lead-lag restraint forces and moments to calculate the flapping and lead-lag dynamics. Finally, the forces and moments are summed over all the blades to calculate the total forces and moments at the aircraft C.G.

The new rotor was integrated into FLYRT to create BEMAP. This also required the modification of the trim and equations-of-motion modules. The modules representing other components of the Apache helicopter, i.e. fuselage/empennage/wings, vertical tail/tail rotor, horizontal stabilator, and landing gears, however, were used directly from FLYRT (ref. 11). BEMAP was extensively validated against flight data as described in reference 10. Some of the same data will be used later in this paper as a basis of comparison to highlight off-axes improvements.

IMPLEMENTATION OF THE AERODYNAMIC PHASE LAG

The delay, or effective phasing, of the elemental forces is accomplished by processing the lift and drag coefficients for

each element through a first-order filter. As mentioned before, the lift and drag coefficients at each time step are found from lookup tables as functions of local angle of attack and Mach number at that element.

$$c_{\ell_{table}} = f_1(\alpha, M) \quad (1)$$

$$c_{d_{table}} = f_2(\alpha, M) \quad (2)$$

The angle of attack and Mach number are based on the local flow resulting from aircraft motion, blade rotation, blade flap and lead-lag, rotor inflow, and wind. The filtering is done for every blade-element using:

$$\tau_a \dot{c}_{\ell_{filter}}(i,j) + c_{\ell_{filter}}(i,j) = c_{\ell_{table}}(i,j) \quad (3)$$

$$\tau_a \dot{c}_{d_{filter}}(i,j) + c_{d_{filter}}(i,j) = c_{d_{table}}(i,j) \quad (4)$$

where i is the blade index and j is the element index (1-4 and 1-5 respectively for this model). This filtering is depicted graphically in figure 1.

The time constant of the first-order filter, τ_a, is selected in terms of an equivalent static aerodynamic phase lag, ψ_a:

$$\tau_a = \frac{1}{\Omega} \tan \psi_a \quad (5)$$

so that this implementation (τ_a in rotating frame) and previous implementations (ψ_a in fixed frame) result in the same steady-state response (ref. 3).

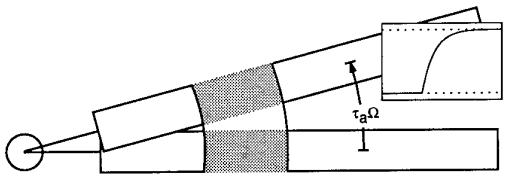

Figure 1: Implementation of first-order filter on lift and drag coefficients

For each airspeed (hover and 60 kts), the time constant was varied until the most improvement in the off-axes response was achieved. The aerodynamic lag was assumed independent of rotor azimuth for all airspeeds. This was considered to be a reasonable approach even though using 1st harmonic variation in τ_a for the lateral and longitudinal inputs might have resulted in better correlation in forward flight, as will be discussed later.

GENERATING MODEL RESPONSES

A frequency-domain approach was taken in the evaluation of the model responses (with and without the aerodynamic phase lag correction) and for their comparison with flight data. Non-parametric frequency responses for the actual aircraft were already available from reference 10. Simulation model responses without the aerodynamic phase correction could also have been used from the same reference. The latter responses, however, were based on 6 DOF linear models generated using a simple numerical perturbation technique. It was decided to employ a more rigorous approach for this effort.

The new approach basically mimics the process of frequency sweep testing of an actual aircraft. Instead of pilot-generated sweeps, however, computer generated sweeps were used. These were generated using a modified version of a FORTRAN code described in reference 6. Briefly, the code allows the user to 1) specify the total duration and sample rate, 2) the duration of initial and ending zero signal, 3) the duration of signal fade-in to maximum amplitude at a constant minimum frequency, and 4) the duration of signal fade-out at a constant maximum frequency. White noise of specified standard deviation can also be added to the fundamental signal to improve spectral content. In addition, white noise can be specified as the input to the 3 remaining controls and its standard deviation adjusted relative to the white noise used for the main control. Figure 2 shows a typical frequency sweep input used for this work.

The sweeps were used as inputs to the model, one axis at a time, and model responses recorded. The main difficulty with running frequency sweeps through an unpiloted simulation model is maintaining attitude and airspeed close to initial trim. Given the long duration of a typical sweep (90 seconds), some additional control has to be provided. This was added in the form of low-gain rate and attitude feedback loops on roll, pitch, and yaw (figure 3), similar to the work by Ballin et. al. (ref. 16). These loops have no effect on the extracted dynamic response obtained from multi-input/multi-output spectral analysis, since the frequency responses are based on the total input to the mixer (Sum4, Sum5, and Sum6 in figure 3).

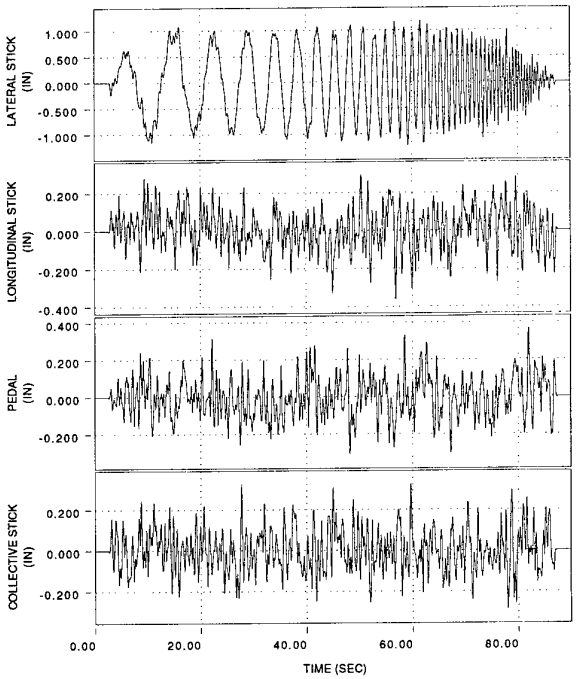

Figure 2: Typical computer generated frequency sweep input including white noise

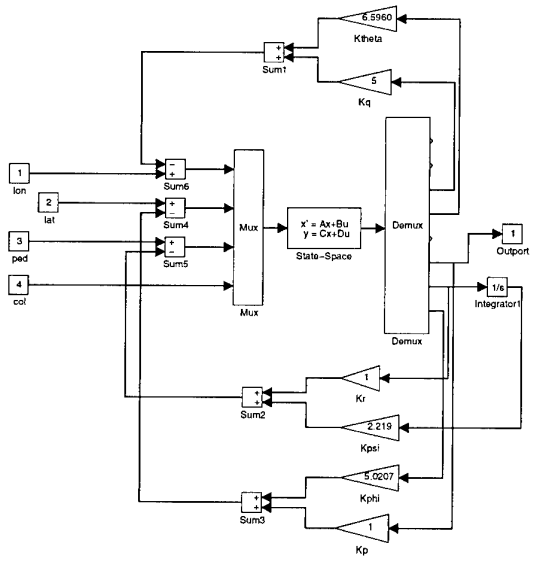

Figure 3: Feedback loops to maintain attitude during frequency sweep

First, 6 DOF linear models of the simulation were generated, using standard linear perturbation techniques, at the airspeeds of interest. These where then used, in MATLAB®, to find suitable rate and attitude feedback gains (figure 3). The simulation was then modified with the new feedback loops and exercised with typical frequency sweeps to insure that attitude and airspeed excursions were limited to acceptable levels. Finally, test data were taken at hover and 60 kts with and without the aerodynamic phase lag correction.

Model time histories generated above where then processed through the Comprehensive Identification from FrEquency Responses (CIFER®, ref. 17) tool to generate Bode plots for comparison with flight data. For each case, two 90 second runs were concatenated to give a total run length of 180 seconds. Five windows, varying from 5 to 40 seconds in length, were used to process the data. The larger windows were used to provide good low frequency coverage while the smaller windows provided good averaging and high frequency identification accuracy. The data was further processed to eliminate the effects of off-axes inputs and to combine the results from all the windows. In some cases the entire process (starting from the generation of inputs) was repeated because the model results did not have sufficient coherence in the frequency region of interest (1 to 10 rad/sec). Nevertheless, in a few of the cases good coherence could not be achieved across the entire frequency region of interest even after several attempts.

Figure 4 shows a comparison of the frequency response curves obtained using the identification approach with curves obtained using the 6 DOF linear-perturbation-model approach. As expected, the two approaches show similar results in the mid-frequencies while the new approach is clearly superior at higher frequencies, capturing the regressing rotor dynamics.

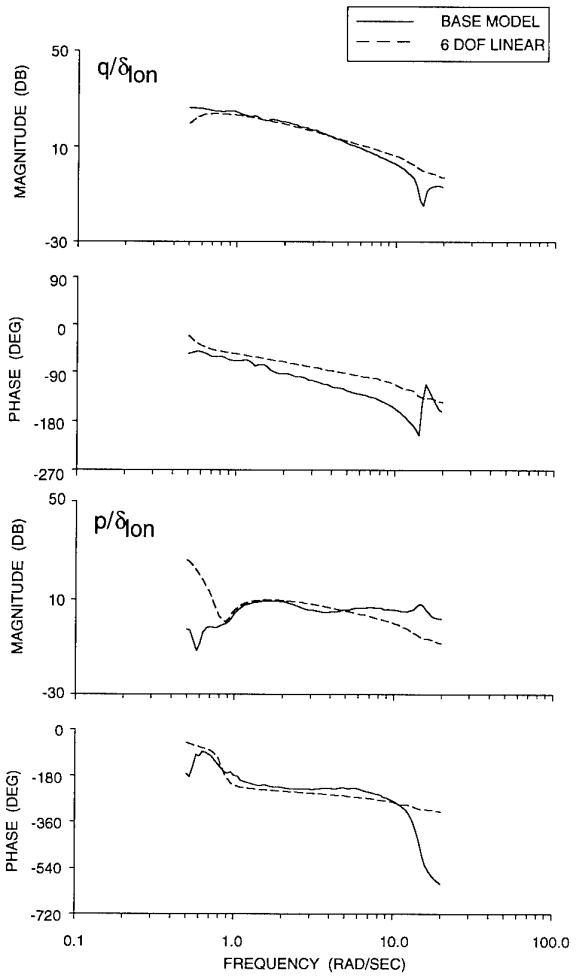

Figure 4: Results of new frequency response generation approach vs. the old 6 DOF approach

COMPARISON OF MODEL RESPONSES WITH FLIGHT DATA

Hover

The responses of the modified AH-64 model were compared with available flight data in the frequency domain. Results in hover indicate that using a time constant equivalent to an aerodynamic phase lag of $\psi_a = 36$ deg., the modified AH-64 model correlates significantly better with the flight data. Figure 5a depicts the on-axes roll-rate to lateral input response of the model in hover, with and without the aerodynamic phase lag correction. As may be seen, the on-axes response of the baseline simulation model is quite good. Within the frequency range of interest (between 1 and 10 rad/sec for flight mechanics models), the baseline model shows very good correlation in both phase and magnitude. It is also seen that the addition of the aerodynamic phase lag does not degrade the on-axes correlation.

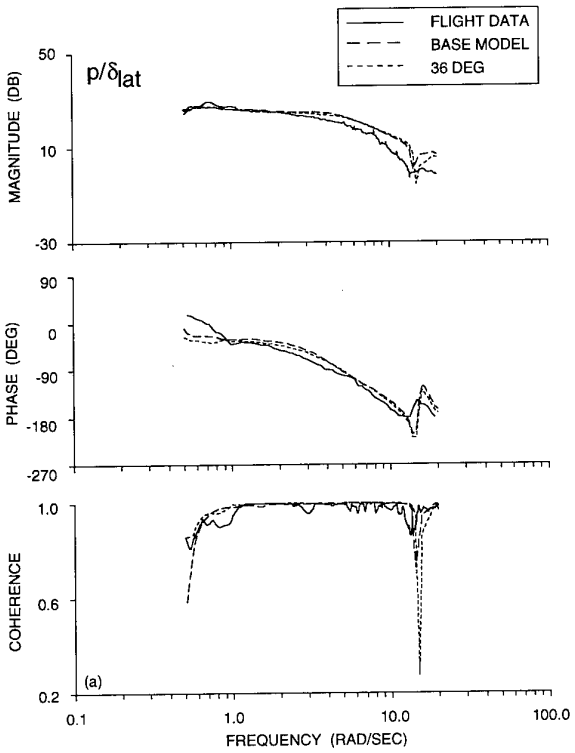

Figure 5a: Roll-rate response to lateral input at hover

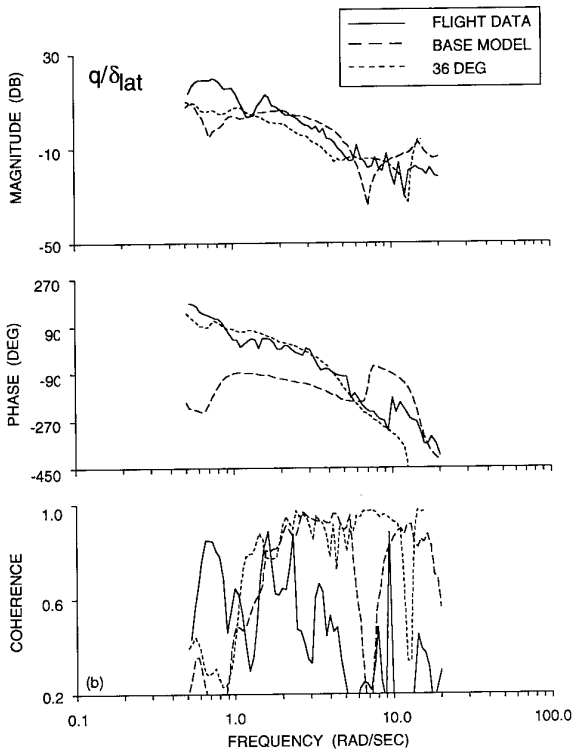

Figure 5b: Pitch-rate response to lateral input at hover

Figure 5b depicts the off-axes pitch-rate responses to the same lateral input. It may be seen that the baseline simulation model exhibits the familiar inability to match the off-axes response as indicated by the up to 180 deg. mismatch in the phase correlation. Figure 5b also shows that the addition of the 36 deg. of aerodynamic lag almost completely corrects the phase correlation error in the 1-5 rad/sec frequency range where flight data has acceptable coherence, without degrading the magnitude correlation. Note that the coherence of the off-axes flight data is significantly lower than the on-axes data and falls below the acceptable values for a portion of the 1 to 10 rad/sec interest region. This is caused by low output signal magnitude and may be due to the large moment of inertia of the aircraft in pitch. Nevertheless, the general trend of improvement in correlation should be valid.

Moving on to pitch inputs, figure 6a depicts the on-axes pitch-rate to longitudinal input response of the model in hover, with and without the aerodynamic lag correction. The on-axes response of the baseline simulation model is again good. Within the frequency range of 1 and 10 rad/sec, the baseline model shows very good correlation in both phase and magnitude. Also, the addition of the filter does not degrade the on-axes correlation.

Figure 6b depicts the off-axes roll-rate responses to the same longitudinal input. Here, unlike in the lateral input case, the coherence of the off-axes flight data is adequate, probably because the roll moment of inertia of the aircraft is small (compared to pitch). Again, the baseline simulation model exhibits the familiar inability to correctly model the off-axes response. The figure shows that as 10 rad/sec is approached, the phase correlation error is 180 degrees. This means that at

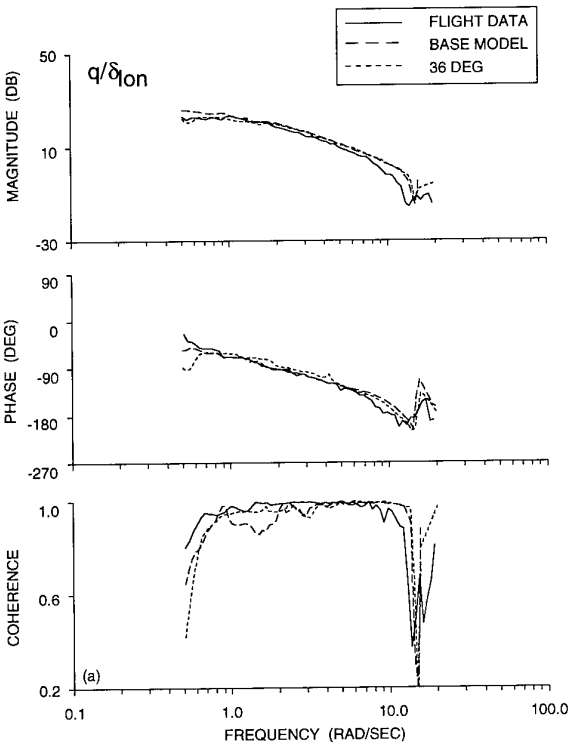

Figure 6a: Pitch-rate response to longitudinal input at hover

those frequencies, the baseline model essentially goes the wrong way. The figure also shows that the addition of the 36 degrees of lag again results in a significant improvement in the phase correlation. Furthermore, this is achieved without any degradation of the magnitude response. As a matter of fact, the magnitude response is slightly improved.

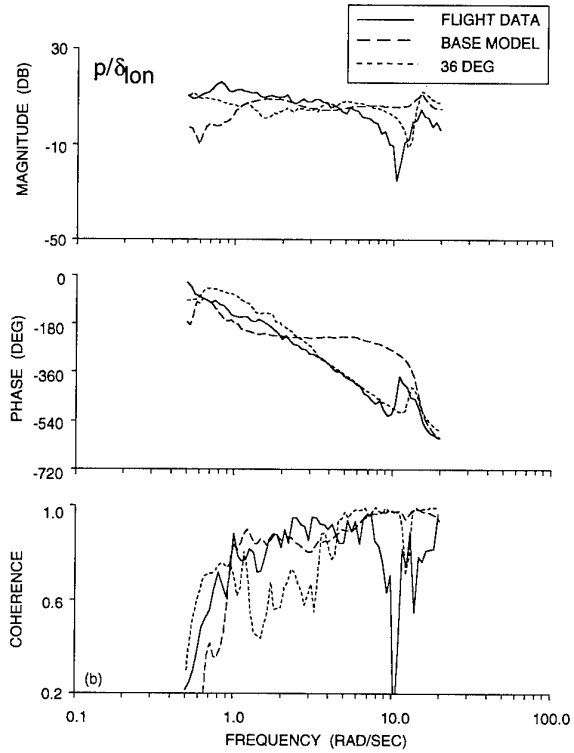

Figure 6b: Roll-rate response to longitudinal input at hover

Forward Flight at 60 Kts

The results of using the aerodynamic phase lag correction to improve the correlation at 60 kts were mixed. It was obvious from the start that the filter time constant used in hover would not be applicable to 60 kts and that a smaller value would be needed. A range of values, from 15 to 30 degrees, were therefore investigated. Results indicated that different amounts of aerodynamic phase lag would be needed in each axis to obtain the best correlation. An aerodynamic phase lag of 24 degrees was shown to result in the best correlation of the pitch-rate response to lateral input, as shown in figure 7. On the other hand, the baseline simulation model (without any aerodynamic phase lag correction) showed the best correlation of the roll-rate response to longitudinal input. This suggests that a 1st harmonic variation of the value of the aerodynamic lag may be the optimum solution. For this study, however, the implementation required that the same delay value be used in both axes. Therefore, a compromise value of the aerodynamic phase lag had to be found. The goal was to provide improvement in the pitch-rate to lateral input response without degrading the roll-rate to longitudinal input response of the baseline model. Sample runs showed 19 degrees to be this compromise value. The forward flight results that follow are therefore for 19 degrees of aerodynamic phase lag correction.

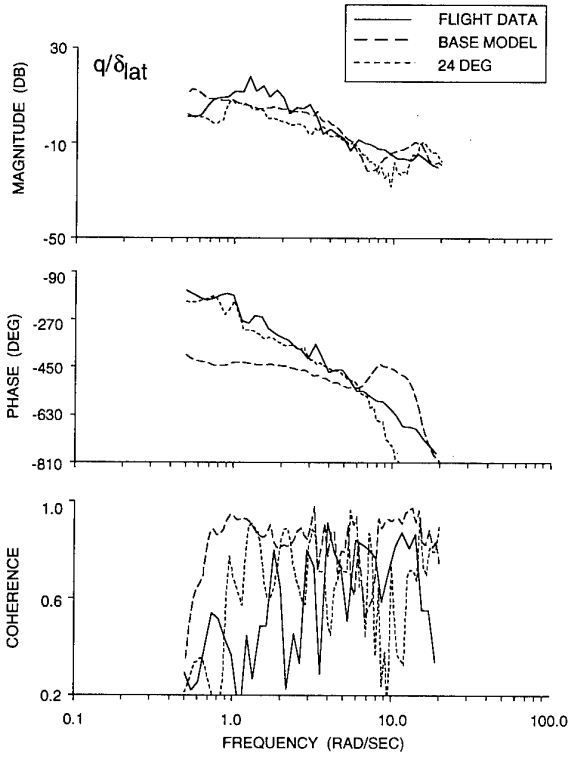

Figure 7: Pitch-rate response to lateral input at 60 kts

Figure 8a depicts the on-axes roll-rate to lateral input response of the model at 60 kts with and without the aerodynamic phase lag correction. As may be seen, the on-axes response of the baseline simulation model is quite good. Within the frequency range of interest, the baseline model shows good correlation in both phase and magnitude and the addition of the filter does not degrade the correlation.

Figure 8b depicts the off-axes pitch-rate responses to the same lateral input. The baseline simulation model again exhibits poor prediction of the off-axes response. The mismatch in the phase response correlation is again up to 180 degrees at some frequencies. The results also show that the addition of the 19 degrees of equivalent phase lag significantly improves the phase response correlation while degrading the magnitude correlation somewhat. As in hover, the coherence of the off-axes flight data is low and falls below acceptable values for a portion of the 1 to 10 rad/sec interest region. Again, this may be attributed to low signal magnitude caused by high inertia in pitch.

Figure 9a depicts the on-axes pitch-rate to longitudinal input response of the model at 60 kts with and without the aerodynamic phase lag correction. The figure shows that the on-axes response of the baseline simulation model is quite good. Within the frequency range of interest, the baseline model shows very good correlation in both phase and magnitude and the addition of the correction does not degrade the on-axes correlation.

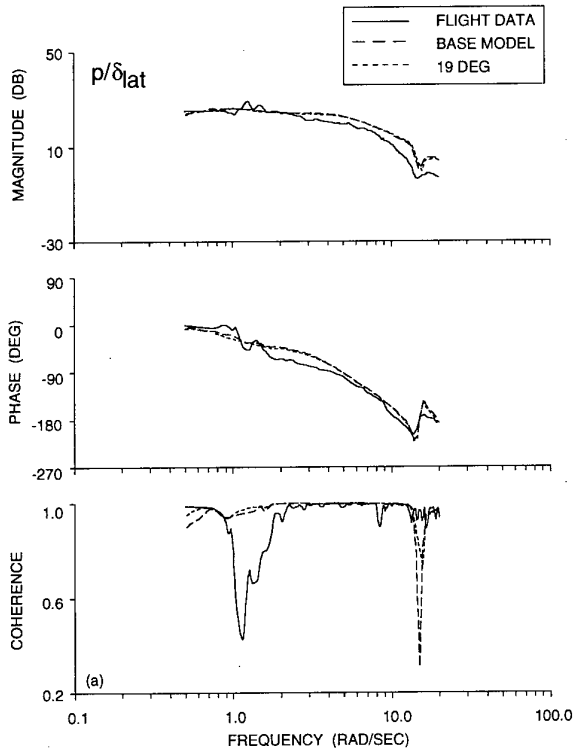

Figure 8a: Roll-rate response to lateral input at 60 kts

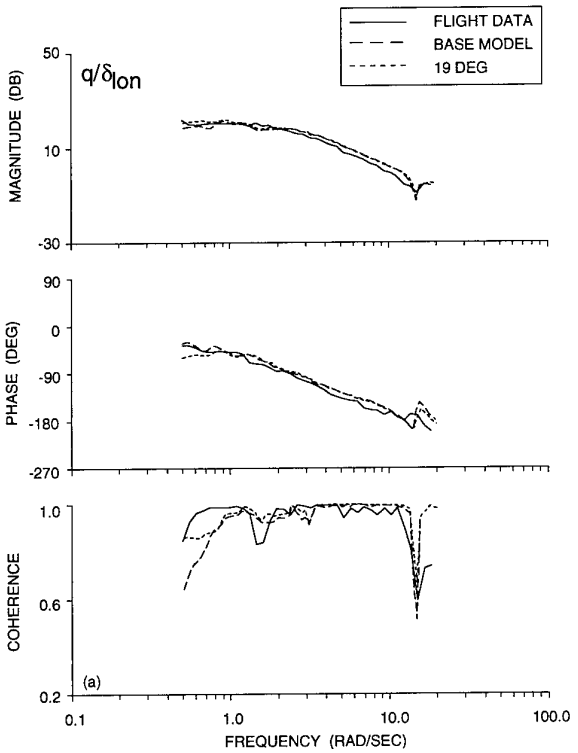

Figure 9a: Pitch-rate response to longitudinal input at 60 kts

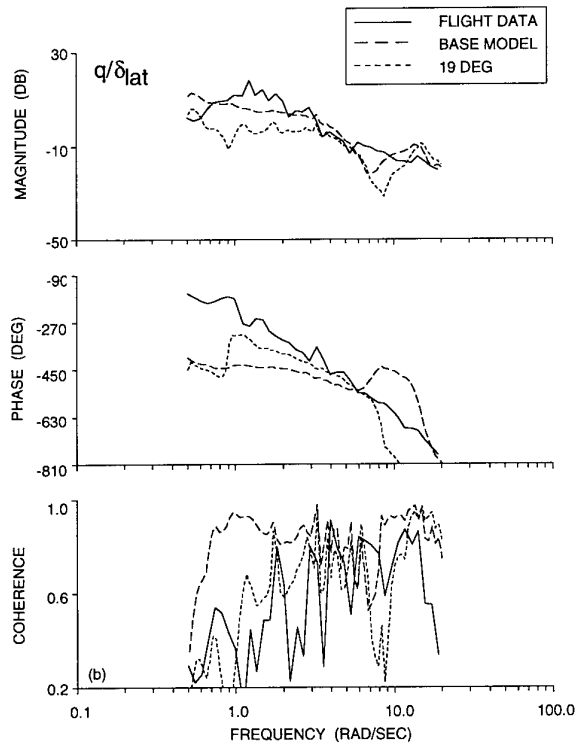

Figure 8b: Pitch-rate response to lateral input at 60 kts

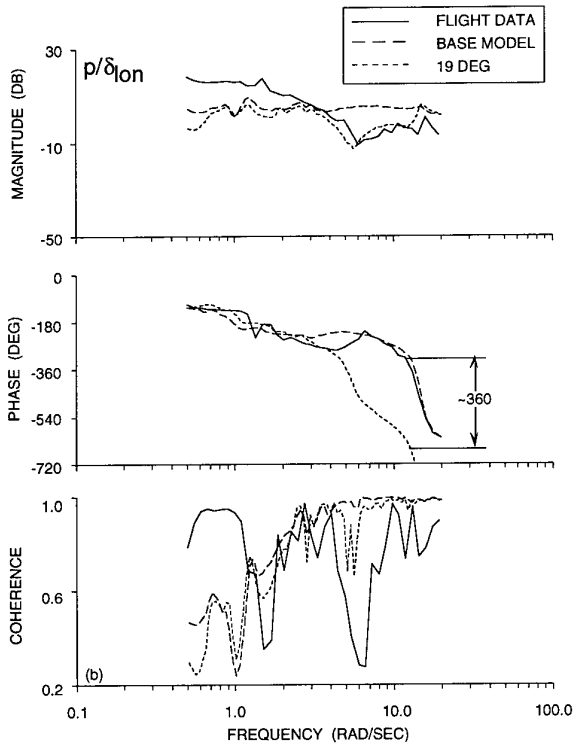

Figure 9b: Roll-rate response to longitudinal input at 60 kts

Figure 9b depicts the off-axes roll-rate responses to the same longitudinal input. As mentioned previously, the baseline simulation model does a good job of duplicating the phase of the response throughout the frequency range of interest. However, the magnitude response correlation is quite poor. Adding 19 degrees of aerodynamic lag degrades the phase correlation above 6 rad/sec while improving the magnitude correlation considerably beyond 2 rad/sec. Note that again, as in hover, the coherence of the flight data in the roll-to-pitch off-axes response is much better than the pitch-to-roll case.

A closer examination of figure 9b indicates that the corrected-model actually matches the off-axes dynamics of the aircraft much better than upon initial examination. Looking at the magnitude plot for the corrected-model, it can be seen that a pair of lightly-damped complex zeroes are indicated at a frequency of about 6 rad/sec. This matches the flight data which also indicates a pair of lightly damped zeroes at about the same frequency. The phase results match at low frequency and are simply offset by 360 deg. at high frequency. The difference indicates that whereas the lightly-damped flight-data-zeros contribute a rapid phase lead, the corrected-model-zeros contribute a rapid phase lag over the same frequency interval. These characteristics indicate that relative to the flight data zeroes, the corrected-model-zeroes have essentially the same natural frequency, but are shifted slightly to the right of the imaginary axis (on the complex plane). This is verified by reversing the phase contribution of the corrected-model zeroes to represent the case of complex zeroes located at the mirror image position (figure 10). This mirror image shift of the zeroes does not affect the magnitude curve.

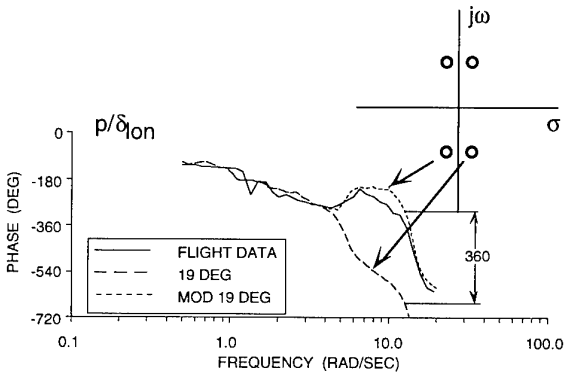

Figure 10: Effect of minimum-phase versus nonminimum-phase zeros

As may be seen from figure 10, the adjusted phase response matches the flight data well, verifying the shift in the real-part of the complex zeroes as the cause of the original discrepancy. Numerical investigations conducted by the authors suggest that a physical source of the discrepancy in the damping of the zeros may be an error in the assumed pitch-flap coupling, δ_3. Though the physical δ_3 angle for the AH-64 rotor is zero, there can be a contribution to the effective δ_3 from control linkage geometry and shaft flexibility. In any case, the influence of a slight error in the predicted damping ratio of the coupling response zeros is probably of little practical significance. Thus overall, the corrected model can be said to match the response of the aircraft better than the original model, and the compromise lag value of 19 degrees is quite satisfactory.

The baseline simulation model results from figure 9b together with the 24 degrees of aerodynamic lag correction results from figure 7 highlight the need for different values of aerodynamic phase lag in each axis to achieve best correlation. One potential solution to this problem might be to implement the aerodynamic phase lag as a 1st harmonic function of the rotor azimuth. This would be consistent with the 1st harmonic nature of dominant inflow dynamics. Note, however, that other effects, such as insufficient modeling of the interaction of the main rotor wake with the tail surfaces (ref. 18), may also contribute to this apparent need for different Aerodynamic Phase lag values for the two coupling responses.

DISCUSSION

The simulation results in this study show that considerable improvement in the AH-64 off-axis response modeling can be achieved with a very simple empirical correction to the blade element aerodynamic calculations. However, the current results were obtained by tuning the aerodynamic phase lag to existing flight test data for this specific helicopter. The broad applicability of this technique to the simulation of new helicopters requires a validated "carpet-plot," that maps the variation of ψ_a for a range of key configuration parameters. In this section, we begin the construction of such a carpet-plot with the incorporation of data from the current study on the AH-64, previous results from UH-60 flight tests, and the SBMR wind-tunnel tests. This combined presentation of results also permits an understanding of the key physical sources for the aerodynamic lag effect.

Collection of Existing Results

The empirical values of ψ_a for the AH-64 obtained in the current study are shown in Figure 11 as a function of non-dimensional advance ratio, $\mu = V_0 / (\Omega R)$. Also shown are the UH-60 results of Fletcher (ref. 7) for hover and 80 kts ($\mu = 0.19$).

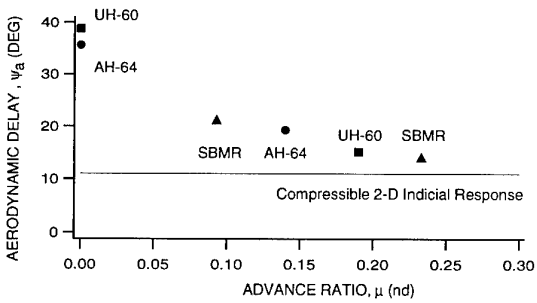

Figure 11: Variation of aerodynamic lag correction with advance ratio from various sources

There is close agreement of the hover results for the AH-64 and the UH-60, which have very close values of hinge off-set. (AH-64: $\varepsilon = 0.038$; UH-60: $\varepsilon = 0.047$). The phase lag values also compare favorably for forward flight when linearly interpolated for the same advance ratio. Clearly, the

aerodynamic phase lag correction washes out with advance ratio, as do the dynamic inflow effects in general.

The initial identification study of the SBMR dynamic response wind-tunnel data (ref. 6) implemented an off-axis correction in terms of an adjustment to the swashplate phasing. These low-speed ($\mu = 0.093$) results were later updated (ref. 19) to account for SBMR feathering axis geometry that actually caused the geometric swashplate rigging to be -14 deg., rather than the design value of -9 deg. indicated in the original study (ref. 6). The SBMR analysis was subsequently broadened to include the forward flight test data at 100 kts ($\mu = 0.233$), and an identification model structure based on aerodynamic phase lag ψ_a, rather than equivalent swashplate phasing. The SBMR aerodynamic phase lag results for the two test conditions analyzed ($\mu = 0.093$ and $\mu = 0.233$) are shown in Figure 11. The SBMR results show the same wash-out trend with advance ratio as seen for the AH-64 and the UH-60. Unfortunately, sufficient data to determine a possible relationship between ψ_a and hinge-offset (SBMR: $\varepsilon = 0.095$) is not currently available.

Physical Sources of Aerodynamic Phase Lag

The test data obtained to date and presented in figure 11 provide a start to the broad carpet-plot needed for general application of the aerodynamic phase lag technique. However, an understanding of the physical sources for the lag is important for the development of theoretical models for correlation with the test data and to fill in the carpet-plot over a detailed grid of helicopter configuration parameters.

While the results display a strong sensitivity of aerodynamic lag with advance ratio for low speed conditions, the correction values clearly wash-out with higher advance ratios. The data suggest that the phase lag reaches a high-speed asymptotic value of about $\psi_a = 13$ degrees. Since dynamic inflow effects also wash-out with advance ratio, and are essentially negligible beyond $\mu = 0.15 - 0.2$, this residual 13 degrees aerodynamic lag is not caused by the geometric distortion of the dynamic wake as modeled by Rosen and Keller (refs. 5 and 8). The source of the residual delay is rather an additional aerodynamic effect which is not currently included in flight mechanics simulation models.

One possible source of the residual aerodynamic phase lag is the 2D unsteady aerodynamic indicial response, which was not included in the AH-64 or UH-60 simulation models, and is generally neglected for helicopter flight mechanics since the 1/rev incompressible contribution is very small. For example, the classical Theodorsen delay for a reduced frequency equivalent to 1/rev motion is about 5 deg. based on tip speed and about 9 deg. based on the speed at the 3/4 radius location (ref. 20). Leishman has shown (ref. 9) a strong dependency of the effective indicial delay on Mach number, although the database of experimental test results presented for low reduced frequency is quite limited. Linear interpolation of the reference 9 data based on flow conditions at the 3/4R indicate an indicial lag of about 11 deg. This corresponds well with the residual (asymptotic) aerodynamic phase lag indicated in figure 11.

If we accept the 2D indicial contribution to the total aerodynamic phase lag to be 11 degrees independent of advance ratio, the contribution to the delay by wake distortion effects at hover is about 25 deg. (average of the AH-64 and UH-60 hover results). The simple theoretical model by Arnold et al (reference 3) of the dynamic wake distortion for the UH-60 in hover yields an equivalent phase lag contribution of 26.5 deg., which is now in very good agreement with the experimental results.

This discussion suggests that the dominant physical sources of aerodynamic phase lag are the dynamic wake distortion due to rotor cyclic flapping, and the 2D compressible indicial response. It would be very interesting to correlate theoretical models of wake distortion at forward flight conditions, and for rotors with higher effective hinge-offsets for comparison with the results shown in figure 11. Additional test data at intermediate values of hinge-offset and advance ratio are also needed to fill in and validate the small sample of experimental results currently available. The goal is a validated carpet plot of aerodynamic phase lag for use in future simulation models of new helicopter configurations.

CONCLUSIONS

1. A significant improvement in the roll response to longitudinal input and pitch response to lateral input modeling accuracy of a blade-element simulation model of the AH-64 was achieved by incorporating a simple aerodynamic phase lag correction. Including this correction did not degrade the satisfactory on-axis response correlation.

2. At hover, a single value of the aerodynamic lag corrected both the roll response to longitudinal input and pitch response to lateral input coupled responses. At 60 kts, the optimum phase lag value is different for the two coupled responses, and a single value selected as a compromise to yield the best overall result. This characteristic suggests a possible refinement based on a 1st harmonic variation of phase lag with azimuth, which would be consistent with the 1st harmonic nature of dominant inflow dynamics.

3. The AH-64 results show a wash-out in the required aerodynamic phase lag value with advance ratio. There is close agreement with identification results for the UH-60, which has comparable hinge-offset. Sikorsky Bearingless Main Rotor (SBMR) results also exhibit this trend.

4. The primary physical sources of aerodynamic phase lag are considered to be: (1) dynamic wake distortion due to angular velocity motion of the tip-path plane, and; (2) compressible two-dimensional unsteady indicial response. The theoretical values for these two contributions match the available test data well.

5. Future efforts should focus on determining and validating a comprehensive carpet-plot of aerodynamic phase lag for use in future simulation models of new helicopter configurations.

REFERENCES

1) Takahashi, M. D., Fletcher, J. W., Tischler, M. B., "Development of a Model Following Control Law for Inflight Simulation Using Analytical and Identified Models", presented at the AHS 51st Annual Forum, Fort Worth, TX, May 1995.

2) Von Grunhagen, W., "Dynamic Inflow Modeling for Helicopter Rotors and Its Influence on the Prediction of Crosscoupling", Presented at the AHS Aeromechanics Specialists Conference, Fairfield County, CT, October 11-13, 1995.

3) Arnold, U. T. P., Keller, J. D., Curtiss, H. C., and Reichert, G., "The Effect of Inflow Models on the Dynamic Response of Helicopters", 21st European Rotorcraft Forum, Saint-Petersburg, Russia, Aug.-Sep. 1995.

4) Curtiss, H. C., Jr., "On the Calculation of the Response of Helicopters to Control Inputs", 18th European Rotorcraft Forum, Avignon, France, September 1992.

5) Rosen, Aviv, and Isser, Aharon, "A New Model of Rotor Dynamics During Pitch and Roll of a Hovering Helicopter", presented at the AHS 50th Annual Forum, Washington, DC, May 1994.

6) Tischler, M. B., Driscoll, J. T., Cauffman, M. G., Freedman, C. J., "Study of Bearingless Main Rotor Dynamics from Frequency-Response Wind Tunnel Test Data", presented at the American Helicopter Society Aeromechanics Specialists Conference, San Francisco, CA, January 1994.

7) Fletcher, J. W., "Identification of Linear Models of the UH-60 in Hover and Forward Flight," presented at the 21st European Rotorcraft Forum, Saint Petersburg, Russia, 29 August - 1 September, 1995.

8) Keller, Jeffrey D., "An Investigation of Helicopter Dynamic Coupling Using an Analytical Model", presented at the 21st European Rotorcraft Forum, St. Petersburg, Russia, August 1995.

9) Leishman, J. G., "Modeling of Subsonic Unsteady Aerodynamics for Rotary Wing Applications," Journal of the American Helicopter Society, vol. 35, no. 1, January 1990, pp. 29-38.

10) Mansur, M. H., "Development and Validation of a Blade-Element Mathematical Model for the AH-64A Apache Helicopter", USAATCOM Technical Report 94-A-022, NASA Technical Memorandum 108863, April 1995.

11) Harding J. W., Bass, S. M., "Validation of a Flight Simulation Model of the AH-64 Apache Attack Helicopter Against Flight Test Data," American Helicopter Society 46th Annual Forum, Washington D.C., May 1990.

12) Howlett, J. J., "UH-60A Black Hawk Engineering Simulation Program: Volume I -- Mathematical Model", NASA CR-166309, Dec. 1981.

13) "MACSYMA Reference Manual", The Mathlab Group. Laboratory for Computer Science, Massachusetts Institute of Technology, Version 10, January 1983.

14) Chen, Robert T. N., "Flap-Lag Equations of Motion of Rigid, Articulated Rotor Blades with Three Hinge Sequences", NASA TM-100023, Nov. 1987.

15) Peters, D. A., and Ha Quang, N., "Dynamic Inflow for Practical Applications", Journal of the American Helicopter Society, vol. 33, no. 4, 1988, pp. 64-68.

16) Ballin, M. G., and Dalang-Secretan, M. A., "Validation of the Dynamic Response of a Blade-Element UH-60 Simulation Model in Hovering Flight," American Helicopter Society 46th Annual Forum, Washington D.C., May 1990.

17) Tischler, M. B., and Cauffman, M. G., "Frequency-Response Method for Rotorcraft System Identification: Flight Application to BO-105 Coupled Rotor/Fuselage Dynamics", Journal of the American Helicopter Society, vol. 37, no. 3, July 1992, pp. 3-17.

18) Curtiss, H. C., Quackenbush, T.R. , "Influence of the Rotor Wake on Rotorcraft Stability and Control," Paper No. 70, 15th European Rotorcraft Forum, Amsterdam, The Netherlands, September 12-15, 1989.

19) Tischler, M. B., "System Identification Methods for Aircraft Flight Control Development and Validation," NASA TM110369, Army TR-95-A-007, Oct. 1995.

20) Johnson, W., Helicopter Theory, Princeton University Press, Princeton, New Jersey, 1980.

Effect of Propulsion System Dynamics on Rotorcraft Aeromechanical Stability in Straight and Turning Flight

Giorgio Guglieri
Politecnico di Torino
Dipartimento di Ingegneria Aeronautica e Spaziale
Corso Duca degli Abruzzi, 24, 10129 Torino (Italy)

Roberto Celi
University of Maryland
Department of Aerospace Engineering
College Park, MD 20742 (USA)

Fulvia Quagliotti
Politecnico di Torino
Dipartimento di Ingegneria Aeronautica e Spaziale
Corso Duca degli Abruzzi, 24, 10129 Torino (Italy)

Notation

a	Real part of eigenvalue (rad/s)
b	Imaginary part of eigenvalue (rad/s)
C_T	Thrust coefficient
B_1	Engine damping (Nm s / rad)
e	Hinge offset (m)
F	Flap (subscript)
I_{eq}	Moment of inertia of propulsion system, referred to rotor speed (Kg m^2)
K_s	Torsional stiffness of the rotor shaft (Nm /rad)
K_θ	Proportional gain (pitch control)
L	Lag (subscript)
n	Load factor
N_b	Number of blades
r_g	Engine/rotor nominal rpm ratio
Q_E	Engine torque (Nm)
R_{2k}	Blade lag reaction acting on the hinge (N)
I_{hub}	Moment of inertia of the hub (Kg m^2)
ϕ	Roll attitude (rad)
θ	Pitch attitude (rad)
θ_{1s}	Longitudinal cyclic (rad)
θ_{1c}	Lateral cyclic (rad)
μ	Advance ratio
ψ	Shaft angular displacement at the hub (rad)
ψ_1	Shaft angular displacement at the exit of the gearbox (rad)
σ	Rotor solidity
τ_p	Delay (s)
ζ	Damping ratio ($-a/\omega_n$)
ω_n	Natural frequency $(a^2+b^2)^{1/2}$
ω_{BW}	Bandwidth

Introduction

In recent years there has been growing interest in improving the fidelity of mathematical models of helicopter flight dynamics through a more accurate representation of the main rotor dynamics.

The main objective of this paper is to study the effect of several parameters of the propulsion system on the aeromechanical characteristics of a hingeless rotor helicopter, both in straight flight and in coordinated turns. The effects of these parameters on the handling qualities of the aircraft will also be examined (pitch and roll frequency response).

Mathematical Model

The mathematical model of the helicopter used in this study is a nonlinear blade element type model that includes fuselage, rotor, main rotor inflow and propulsion system dynamics. The response to pilot inputs is obtained from direct numerical integration of the equations of motion. A system of small perturbation equations of motion is obtained by numerical linearization of the nonlinear equations about a trimmed equilibrium position. The trim procedure is the same as in Ref. [1]. Thus, the rotor equations of motion are transformed into a system of nonlinear algebraic equations using a Galerkin method. The algebraic equations enforcing force and moment equilibrium, and additional kinematic equations that must be satisfied in a turn, are added to the rotor equations, and the combined system is solved simultaneously. The solution yields the harmonics of a Fourier series expansion of the rotor degrees of freedom, the pitch control settings, trim attitudes and rates of the entire helicopter, and main and tail rotor inflow.

The propulsion system is not included in the trim process. This implies two assumptions. The first is that the engine can generate a sufficient torque in any flight

Paper presented at the FVP Symposium on "Advances in Rotorcraft Technology", held in Ottawa, Canada, 27-30 May 1996, and published in CP-592.

condition. The second is that the small fluctuations of rotor speed associated with the lag dynamics of the rotor do not affect the engine torque.

The 6 degrees of freedom rigid body motion of the aircraft is modeled using nonlinear Euler equations. Linear aerodynamics is assumed for fuselage and empennage, and aerodynamic interference effects are neglected.

The blades are assumed to be rigid, with offset hinges and root springs selected so as to achieve fundamental natural frequencies in flap and lag of 1.125/rev and 0.7/rev respectively. The coupled flap-lag dynamics of each blade is modeled. The main rotor has four blades.

Unsteady aerodynamic effects are modeled using a 3-state dynamic inflow model [2].

The modeling of the propulsion system is similar to that used by Chen [3]. Thus, the equation for engine/drive train torque equilibrium is:

$$I_{eq}\ddot{\psi}_1+K_S(\psi_1-\psi)+B_1r_g^2\dot{\psi}_1=r_gQ_E \qquad (1)$$

and the equation for shaft equilibrium is:

$$K_S(\psi_1-\psi)+\sum_{k=1}^{N_b} e\,R_{2k}=I_{hub}\ddot{\psi} \qquad (2)$$

Eq. 2 is more general than the corresponding equation in Ref. [3], which focused on specific rotor modes in which the blades moved in lag only, and with identical angular displacements. The forcing torque is obtained by summing the force contributions R_{2k} of each blade in the hub plane, multiplied by the hinge offset moment arm e.

Numerical solution

The coupled rotor-fuselage trim in steady turn is solved converting the rotor ODE into AE using the Galerkin method (10 eqns.). The aircraft trim equations (11 eqns.) and the momentum inflow equations for both main and tail rotor (2 eqns.) are also included. The influence of propulsion system on trim conditions is neglected. The 23 unknowns are determined simultaneously by means of a nonlinear numerical solver.

A complete set of small perturbation equations is extracted through numerical linearization about trim. This linearized system (32 states and 4 controls) is used for poles and frequency response. The effects of propulsion system dynamics are obviously included.

Free flight responses are obtained from numerical integration of equations of motion.

Results

The general characteristics of the basic hingeless helicopter adopted for computations are presented in Tab. 1. The reference torsional stiffness and moments of inertia of the flexible drive train are given in Tab. 2. One component of the proportional control system (Tab.3) is active for pitch attitude stabilization. Two sets of computations (Tab. 4) were performed in order to investigate the combined effects of turn rate, advance ratio and propulsion system design.

Rotor speed	22 rad/s
Rotor disc radius R	9 m
Blade m.a.c.	0.6 m
Rotor hinge offset	1.125 m 12.5 %
I_{XX}	10000 Kg m^2
I_{YY}	54000 Kg m^2
I_{ZZ}	47000 Kg m^2
I_{XZ}	2500 Kg m^2
Mass	9075 Kg
Rotor solidity	0.084
C_T/σ (hover)	0.084
Lock number	7.78916
Blade mass per unit length	16 Kg/m
Number of blades (MR)	4
Blade twist	0 rad
Horizontal dist. between CG and rotor	0 m
Vertical dist. between CG and rotor	2.25 m
Horizontal tail surface	4.15 m^2
Horizontal dist. between CG and HT	9.9 m
Vertical dist. between CG and HT	-0.45 m
Vertical tail surface	3.04 m^2
Horizontal dist. between CG and VT	10.66 m
Vertical dist. between CG and VT	0.91 m
Horizontal dist. between CG and TR	11.1 m
Vertical dist. between CG and TR	1.8 m
Number of blades (TR)	3
Tail rotor radius	1.95 m
Tail rotor speed	100 rad/s
Tail rotor m.a.c.	0.3 m
Flap frequency ratio $\lambda 1$	1.125 /rev
Lag frequency ratio $\lambda 2$	0.7 /rev

Tab. 1 - The basic helicopter

Shaft stiffness	541065 Nm/rad
Engine-drive train inertia	1673 Kg m^2
Hub inertia	164 Kg m^2
Damping of propulsion system	0 Nm s / rad

Tab. 2 - Propulsion system

K_θ	- 0.2
K_q	0
K_ϕ	0
K_p	0
K_Ω	0

Tab. 3 - The proportional control system

Flight condition	Advance ratio	Load factor / Turn rate
1	0.0	1.0 / 0 rad/s
2	0.1	1.0 / 0 rad/s
3	0.1	1.5 / 0.555 rad/s
4	0.2	1.0 / 0 rad/s
5	0.2	1.5 / 0.2775 rad/s

Design	I_{EQ}/I_{EQ_0}	K_S/K_{S_0}	Ω/Ω_0
A	1.0	1.0	1.0
B	1.5	1.0	1.0
C	1.0	1.5	1.0
D	1.0	1.0	0.9

Tab. 4.a - Test matrix

μ	K_S/K_{S_0}	I_{EQ}/I_{EQ_0}	$d\psi/dt$ (rad/s)
0.1	1	1	0-0.3
0.2	1	1	0-0.125
0.2	1-10	1	0
0.2	1	1-10	0
0.2	1-10	1	0.1
0.2	1	1-10	0.1

Tab. 4.b - Test matrix

Re (rad/s)	Im (rad/s)	Mode	ζ (rad/s)	ω_n (rad/s)	ω_n (1/rev)
-24.131	3.5964	inflow	0.98908	24.398	1.1090
-12.230	0.0000	inflow	1.0000	12.230	0.55591
-11.018	21.509	ω_F	0.45593	24.167	1.0985
-9.6519	20.151	ω_F	0.43199	22.343	1.0156
-9.5994	42.377	$1+\omega_F$	0.22093	43.450	1.9750
-3.6516	8.4506	$(1-\omega_F)$ / roll	0.39666	9.2058	0.41845
-2.4330	0.0000	pitch	1.0000	2.4330	0.11059
-1.7977	2.3315	$(1-\omega_L)$	0.61061	2.9441	0.13382
-0.42022	0.0000	heave	1.0000	0.42022	0.019101
-0.33234	0.11740	dutch roll	0.94290	0.35247	0.016021
-0.25778	15.389	ω_L	0.016748	15.391	0.69960
-0.18459	0.0000	spiral	1.0000	0.18459	0.0083905
-0.086130	115.00	hub mode	0.00074895	115.00	5.2273
-0.031680	17.673	shaft mode	0.0017925	17.673	0.80333
-0.024580	37.500	$1+\omega_L$	0.00065546	37.500	1.7046
-0.012220	6.8440	$1-\omega_L$	0.0017855	6.8440	0.31109
-0.010070	0.33522	phugoid	0.030026	0.33537	0.015244
0.0000	0.0000	heading	0.0000	0.0000	0.0000
1.0000e-05	0.0000	heading / eng.	-1.0000	1.0000e-05	4.5455e-07

Tab. 5 - Poles in hover

Poles were identified by comparing frequencies and eigenvectors. An example is given in Tab. 5 (basic configuration in hover). Real and imaginary parts of the 32 eigenvalues are presented. Damping ratios and natural frequencies were also computed.
The following modes were classified:

- main rotor inflow, highly damped and stable;
- collective flap ($\omega_F \approx \lambda_1 = 1.125$ /rev);
- progressive flap ($\omega_n \approx 1+\omega_F$);
- regressive flap / roll mode ($\omega_n \approx 1-\omega_F$ and $a \approx L_p$);
- pitch mode ($a \approx M_q$);
- collective lag ($\omega_L \approx \lambda_2 = 0.7$ /rev);
- progressive lag ($\omega_n \approx 1+\omega_L$);
- regressive lag ($\omega_n \approx 1-\omega_L$);
- heave mode ($a \approx Z_w$);
- dutch roll, spiral and phugoid;
- heading mode (a=b=0);
- hub/engine rigid body mode, marginally unstable;
- first torsional mode (shaft mode);
- second torsional mode (hub mode);

Note that the last three modes are related with engine dynamics [3]. Furthermore, propulsion system introduces intermodal couplings that complicate the identification of poles and normal modes.

Response to positive step collective input was also analyzed for different advance ratios and turn rates. The rpm responses (Fig. 1 and 2) are characterized by a sharp deceleration of engine/drive train system, that can be mitigated acting on the rpm governor in the control system ($K_\Omega \neq 0$).

The oscillatory behaviour of the shaft angular speed Ω_1 demonstrates that the first torsional mode is excited by the command input.

The effect of advance ratio in forward flight on longitudinal and lateral bandwidth and delay is presented

in Fig. 3 and 4. The behaviour of the basic helicopter meets ADS33 requirements for higher level handling qualities.

Differently, the progressive increase of turn rate may produce significant modifications of longitudinal handling qualities. Anyway, bandwith and delay still remain acceptable when low load factors are considered (Fig. 5 and 6). On the contrary, faster turns exhibit a sudden switch to lower levels for longitudinal handling qualities.

This result can be explained by the comparison of the longitudinal transfer functions θ/θ_{1S} for level flight and fast turn. This analysis is presented in Fig. 9 and 10. A noticeable bandwidth reduction is observed for n=1.5 due to the combined effect of ω_{180} decrease and low frequency flat response. As a consequence, the system becomes gain limited instead of phase limited. Moreover, the phase drops abruptly with the dual impact of reducing ω_{180} and increasing delay $\tau_{p\theta}$.

Lateral handling qualities are substantially unaffected (Fig. 7, 8, 11 and 12) by the increase of turn rate.

A complete parametric analysis was also conducted in order to investigate the influence of propulsion system design on engine/drive train modes in forward flight.

The increase of shaft stiffness and equivalent engine inertia alters the imaginary parts of the two torsional poles (Fig. 13 and 14). The presence of inertial coupling is also demonstrated by the comparison between numerical and analytical results for the low frequency mode (shaft mode). The high frequency mode is less sensitive to any alteration of K_S and I_{eq}.

A degradation of the system stability is found for the first torsional mode when the shaft stiffness is substantially increased (Fig. 15). An opposite stabilizing trend is found for large engine moments of inertia.

Finally, it was also determined that pitch and roll handling qualities of the basic helicopter are largely unaffected by propulsion system design. On the contrary, important changes in heave response are expected.

Conclusions

The present analysis demonstrated that:

- A significant bandwidth decrease in turning flight is observed. The mechanism is related to the decrease in ω_{180}. The system becomes gain limited.
- The increase in drive system stiffness may trigger instabilities.
- The propulsion system introduces intermodal couplings that complicate the identification of poles and normal modes.
- Pitch and roll handling qualities are largely unaffected by propulsion system design.

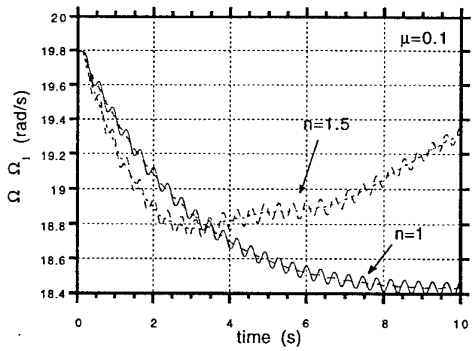

Fig. 1 - The effect of turn rate on rpm response to step (1 deg) collective input

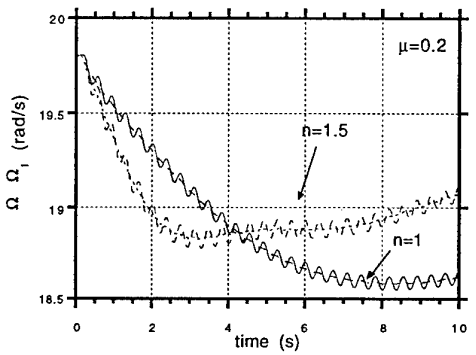

Fig. 2 - The effect of turn rate on rpm response to step (1 deg) collective input

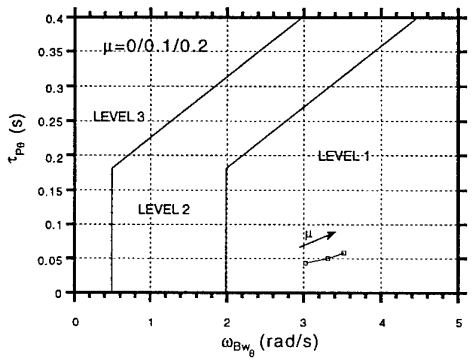

Fig. 3 - The effect of advance ratio on bandwidth and phase delay for baseline configuration (longitudinal response - target acquisition and tracking)

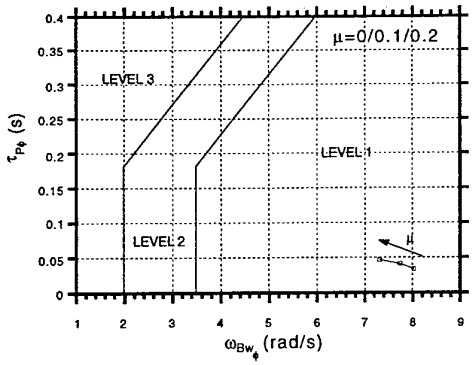

Fig. 4 - The effect of advance ratio on bandwidth and phase delay for baseline configuration (lateral response - target acquisition and tracking)

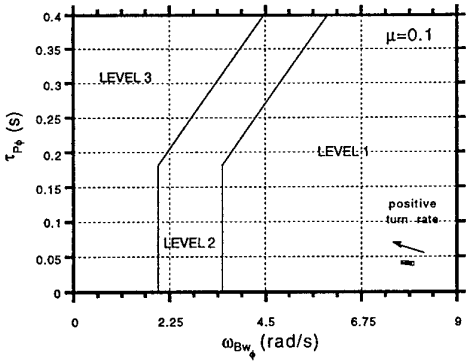

Fig. 7 - The effect of turn rate on bandwidth and phase delay for baseline configuration (lateral response - target acquisition and tracking)

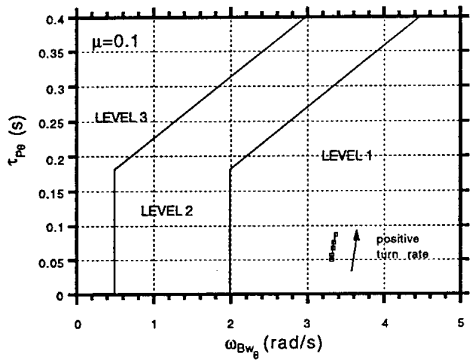

Fig. 5 - The effect of turn rate on bandwidth and phase delay for baseline configuration (longitudinal response - target acquisition and tracking)

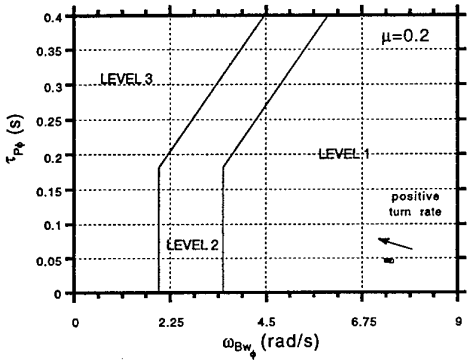

Fig. 8 - The effect of turn rate on bandwidth and phase delay for baseline configuration (lateral response - target acquisition and tracking)

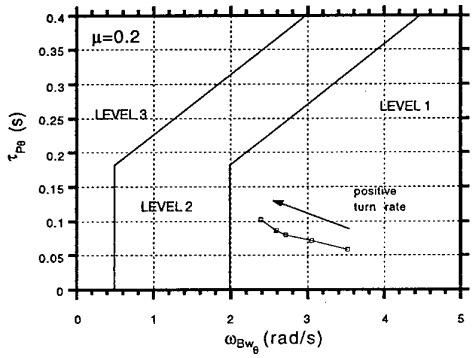

Fig. 6 - The effect of turn rate on bandwidth and phase delay for baseline configuration (longitudinal response - target acquisition and tracking)

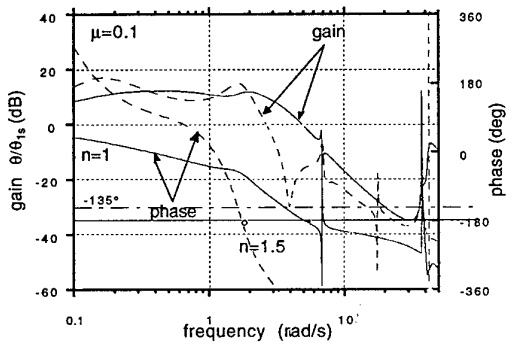

Fig. 9 - The effect of turn rate on pitch frequency response

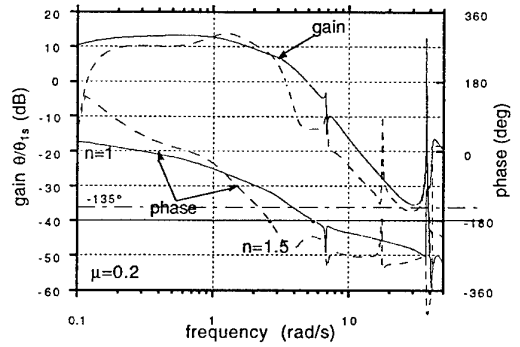

Fig. 10 - The effect of turn rate on pitch frequency response

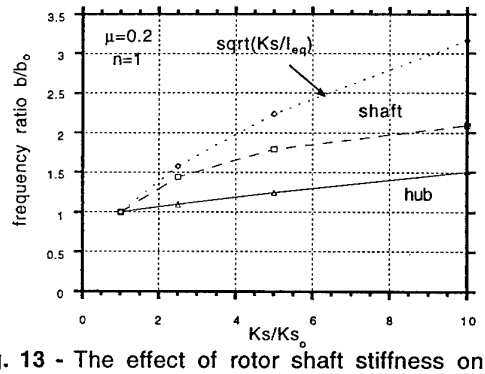

Fig. 13 - The effect of rotor shaft stiffness on the frequency of the engine/drive train/rotor torsional modes

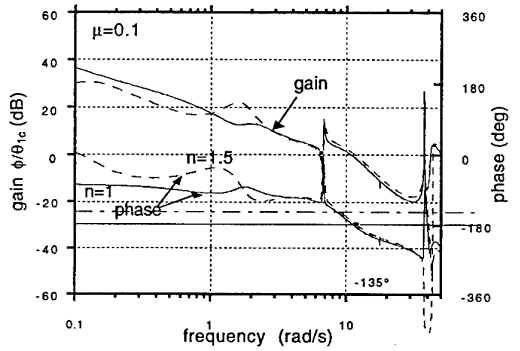

Fig. 11 - The effect of turn rate on roll frequency response

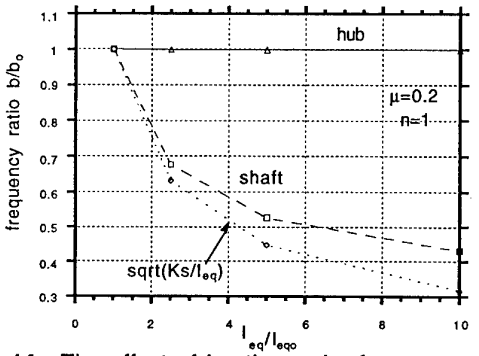

Fig. 14 - The effect of inertia on the frequency of the engine/drive train/rotor torsional modes

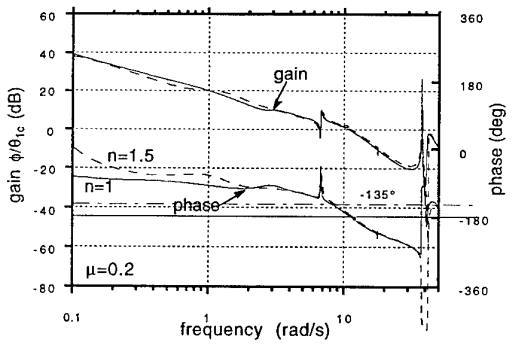

Fig. 12 - The effect of turn rate on roll frequency response

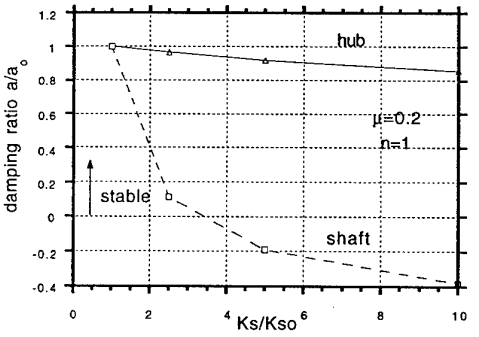

Fig. 15 - The effect of rotor shaft stiffness on the damping of the engine/drive train/rotor torsional modes

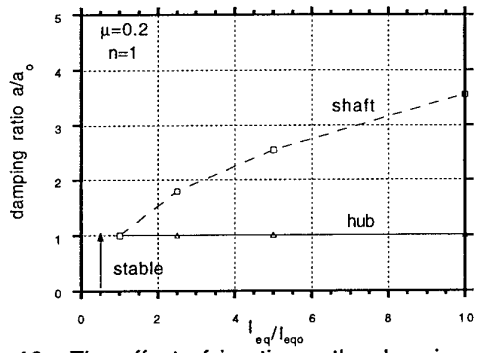

Fig. 16 - The effect of inertia on the damping of the engine/drive train/rotor torsional modes

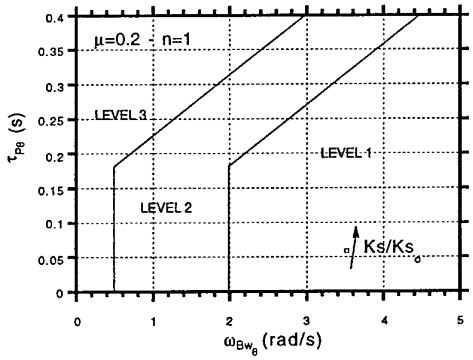

Fig. 17 - The effect of rotor shaft stiffness on bandwidth and phase delay for baseline configuration (longitudinal response - target acquisition and tracking)

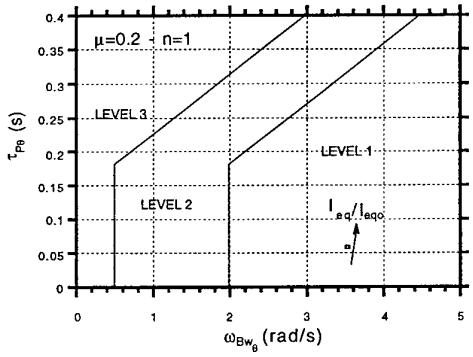

Fig. 18 - The effect of inertia on bandwidth and phase delay for baseline configuration (longitudinal response - target acquisition and tracking)

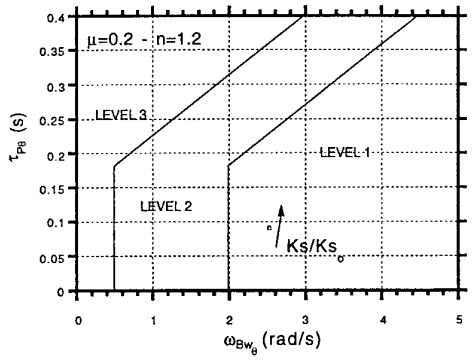

Fig. 19 - The effect of rotor shaft stiffness on bandwidth and phase delay for baseline configuration (longitudinal response - target acquisition and tracking)

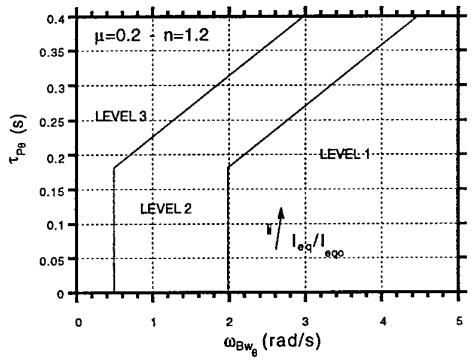

Fig. 20 - The effect of inertia on bandwidth and phase delay for baseline configuration (longitudinal response - target acquisition and tracking)

References

1) Celi, R., "Hingeless Rotor Dynamics in Coordinated Turns", *Journal of the American Helicopter Society*, Vol. 36, No. 4, Oct. 1991, pp. 39-47

2) Peters, D.A., HaQuang, N., "Dynamic Inflow for Practical Applications", *Journal of the American Helicopter Society*, Vol. 33, No. 4, Oct. 1988, pp. 64-68

3) Chen, R.T.N., "An Exploratory Investigation of the Flight Dynamic Effects of Rotor RPM Variations and Rotor State Feedback in Hover", *18th European Rotorcraft Forum*, Avignon, France, Sept. 1992

Aerodynamic and Acoustics of Rotorcraft
A Survey of the 75th Fluid Dynamics Panel Symposium - Berlin

H. Körner,
K. Pahlke

DLR, Institute of Design Aerodynamics
SM-EA, Postfach 3267, 38022 Brauschweig
Germany

Summary:

A survey of the 75th Fluid Dynamics Panel Symposium is given. The paper concentrates on dynamic stall, experimental investigations on helicopter rotors, 3D aerodynamic prediction methods and acoustic prediction methods.

CFD methods were applied to dynamic stall on oscillating airfoils. The agreement with experimental data is acceptable for light and medium stall if appropriate turbulence models are used and the transition is fixed. None of the methods was able to accurately predict deep dynamic stall.

A large effort was spent for the investigation of the blade vortex interaction (BVI) noise. New national and multi-national experimental campaigns were conducted. Several researchers worked on the development and validation of aerodynamic and acoustic prediction methods for BVI. The efficiency of Higher Harmonic Control and of Individual Blade Control inputs for the reduction of BVI noise were investigated. The blade vortex miss distance was found to be the most important parameter for BVI noise. Methods for the prediction of high speed impulsive noise have been developed and encouraging results were presented.

Symbols:

c	chord
c_p	pressure coefficient: $c_p = \dfrac{p - p_\infty}{\frac{1}{2}\rho_\infty (\omega \cdot r)^2}$
k	reduced frequency $k = \dfrac{\omega \cdot \frac{c}{2}}{V_\infty}$
M	Mach number
$M_{\omega R}$	Mach number at blade tip due to rotation $M_{\omega R} = \dfrac{\omega \cdot R}{(\text{speed of sound})_\infty}$
p	pressure
r	radial position of a rotor section
$\vec{r}$	$= (x, y, z)^T$ coordinate vector
R	rotor radius
t	time
T	time for one revolution
u, v, w	Cartesian velocity components
V_∞	free stream velocity
x, y, z	Cartesian coordinates: x: direction of the free stream, y: spanwise (radial) direction, z: normal to x and y direction, positive up
α	angle of attack
α_{TPP}	incidence of tip path plane
θ	rotor blade pitching angle
μ	advance ratio: $\mu = V_\infty / (\omega R)$
ρ	density
σ	solidity of the rotor
ψ	azimuth angle
ω	angular velocity
Subscript:	
∞	free stream value

1. Introduction

The AGARD Fluid Dynamics Panel's Symposium on Aerodynamics and Aeroacoustics of Rotorcraft was held in Berlin, Germany, 10-13 October 1994. The Symposium addressed recent analytical/ numerical developments of the aerodynamic and aeroacoustic design of rotorcraft. Thirty-four papers were given and they have been published in Con-

Paper presented at the FVP Symposium on "Advances in Rotorcraft Technology", held in Ottawa, Canada, 27-30 May 1996, and published in CP-592.

ference Proceedings AGARD-CP-552 [37]. A Technical evaluation report by L. Dadone which provides a summary of each paper followed by general comments can also be found in [37].

Six topics were addressed in the symposium:

- Dynamic stall
- Wind Turbines
- Three-Dimensional Aerodynamic Prediction Methods
- Experimental Investigations on Helicopter Rotors
- Acoustic Prediction Methods
- Interference Problems.

The authors try to give a synthesis of the symposium. We will concentrate on four topics: Dynamic Stall, Experimental Investigations on Helicopter Rotors, 3D Aerodynamic Prediction Methods and Acoustic Prediction Methods. These topics which will serve as headers for the following four chapters. In chapter 6 the paper will be concluded.

2. Dynamic Stall

The term "dynamic stall" usually refers to the unsteady separation and stall phenomena of aerodynamic bodies that are forced to execute time-dependent ramp or oscillatory motions. It is a complex fluid dynamic phenomenon of practical importance and occurs on retreating blades of helicopter rotors, maneuvering aircraft wings, wind turbine blades, and compressor cascades [2].

Experimental results from an ongoing study of the effects of compressibility on dynamic stall of an oscillating NACA 0012 airfoil were presented by Chandrasekhara and Carr [3]. A special experimental facility has been developed which provides unobstructed optical access to the complete airfoil contour (including the leading edge). Stroboscopic Schlieren flow visualization pictures and PDI interferograms were presented. In Figure 1 the vortex release angle $\alpha_{release}$ is plotted versus the reduced frequency k for M = 0.20, 0.25,..., 0.45 and an angle of attack variation given by

$$\alpha = \alpha_0 + \alpha_1 \sin(\omega \cdot t)$$

with $\alpha_0 = 10°$ and $\alpha_1 = 10°$.

The curves for M ≤ 0.3 are almost identical indicating that compressibility effects become important only for M ≥ 0.3. The dynamic stall angle increases for all Mach numbers with increasing reduced frequency k. It is reported that for untripped airfoils a small laminar separation bubble is generated. As the angle of attack is increased the bubble breaks down and a vortical structure appears. For M = 0.45, k = 0.05, α = 10° a supersonic region was detected. In this region up to 5 shocks were visible which terminated in the sonic line. The dynamic stall vortex appeared at the foot of the last shock. It was pointed out that proper tripping is necessary if higher Reynolds number flow are to be simulated in the wind tunnel. Improper tripping may lead to even false tendencies, i.e. in accelerating the stall process compared to the untripped airfoil.

Four papers dealt with the application of 2D CFD codes based on the Reynolds-averaged Navier-Stokes (RANS) equations (Ekaterinaris et. al. [2], Dindar and Kaynak [4], Geissler and Sobieczky [6], Tchon et. al. [8]) to dynamic stall problems. Most of the codes in practical applications use a prescribed transition which is fixed for the whole computation.

Ekaterinaris et. al. [2] give a systematic investigation of several turbulence models (Baldwin-Lomax algebraic model, Renormalization Group based algebraic model, half-equation Johnson-King model, one-equation Baldwin-Barth model, one-equation Spalart-Allmaras model, modified two equation κ-ε model, modified two equation κ-ω model) for a NACA 0015 airfoil undergoing harmonic oscillations in a uniform free stream of M_∞ = 0.3 and $Re_c = 2 \times 10^6$. The airfoil oscillates with an amplitude of $\alpha_1 = 4{,}2°$, and a reduced frequency k = 0.1. In the experiment the airfoil was tripped at the leading edge. Therefore all computations were carried out with a fully turbulent boundary layer. None of the turbulence models was able to accurately predict the quantitative behaviour for c_l, c_d and c_m although the qualitative behaviour was correct for some of the models. The largest differences between computation and experiment were reported for the algebraic turbulence models which

should not be used for cases with considerable separation.

The comparison of the results produced by the one-and-two-equation models showed no clear trend which is the best model. The overall agreement was acceptable for the mainly attached flow (α_0 = 4°). Larger differences occurred for light stall (α_0 = 11°) and the largest differences for deep stall (α_0 = 15°).

The comparison with a similar experiment with an untripped airfoil showed that it is essential to model transition in order to predict correctly the stall behaviour.

Finally the numerical results showed some sensitivity to the numerical algorithm (central-difference, upwind-difference) in spite of using reasonable fine grids.

Tchon et. al. [8] apply a 2D RANS method with the κ–ω turbulence model according to Wilcox is to a section of a Darrieus type vertical axis wind turbine. Again the results do agree qualitatively with the experiment but the quantitative agreement is poor.

The effect of a time-dependent deformation of a NACA 23012 airfoil on the deep dynamic stall behaviour was investigated by Geissler and Sobieczky [6] using a 2D RANS method with a Baldwin-Lomax turbulence model. It was shown that with a nose drooping the shedding of the dynamic stall vortex can be strongly reduced.

A semi-empirical method was presented by Ivtchin [5] for the computation of the rotor shaft power on the basis of given experiments for oscillating airfoils with accounting for the instantaneous effects on the airfoil's lift, movement and drag.

3. Experimental Investigations of Helicopter Rotors

Two papers dealt with flight tests (Samokhin and Rozhdestvensky [21], Tarttelin and Martyn [22]) and five papers (Niesl et. al. [19], Kataplioglu and Caradonna [20], Seelhorst et. al. [23], Berton et. al. [24], Kube et. al. [25]) with wind tunnel experiments. It is interesting to see that all experimental papers present results of direct acoustic measurements or of flow field data like velocity or vorticity fields which are closely connected to the generation of noise (especially BVI noise). This strong interest shows the need of new civil helicopters to meet future strict noise regulations. The descending flight for the approach to a heliport (BVI noise) plays an important role in this context.

Samokhin and Rozhdestvensky [21] present measurements of the overall noise containing the acoustic fields of the main and tail rotor, the contributions of the engine, the gearbox and the transmission for the MI-24 and MI-28 helicopters in level flight for a range of advance ratios. It is pointed out that the main rotor is an important acoustic source which dominates the overall noise level for several flight conditions. The comparison of a MI-28 helicopter with a production type 3-bladed tail rotor and with an x-shape 4-bladed tail rotor showed a reduction in the overall noise level heard on ground by 3-5 dB.

Tarttelin and Martyn [22] describe key results from an on-going research program carried out by the DRA on the Aeromechanics Lynx Control and Agility Testbed (ALYCAT).The Lynx helicopter used in this program was equipped with instrumented main and tail rotor blades. The objective of this test program is to obtain a large data base for advanced flight simulation.

Papers [19], [20], [23] and [25] are devoted to investigations for the reduction of BVI noise. The effects of new control laws for the rotor like higher harmonic control (HHC) or individual blade control (IBC) on BVI and vibrations are described by Niesl et. al. [19] and Kube et. al. [25]. Both approaches are based on the following effects for the reduction of the BVI noise (see Figure 2):

1. Reduction of the blade pitch angle at the position where blade vortex collision happens.

2. Reduction of the vortex strength at the position where the tip vortex is generated.

3. Increase of the miss-distance between vortex and blade.

The basic idea is to achieve these effects by higher harmonic control inputs. With higher harmonic inputs at the blade root, it is important that the desired harmonic function is obtained also along the blade and especially at the blade tip. Figure 3

shows measured BVI locations similar to a $6°$ descending flight of a BO105 helicopter. The noise is radiated from about $60°$ azimuth position. Consequently, the corresponding tip vortex is then generated at $120°$ azimuth. On these positions the highest noise reductions are expected. Furthermore, effects number 1 and 2 are presuming a reduction o the blade pitch. Therefore, it seems to be most promising to position the first negative wave at about $60°$ (see Figure 4).

Paper [25] presents first results from the Higher Harmonic Control Aeroacoustic Rotor Test (HART) in the DNW a joint approach of the Aeroflightdynamics Directorate (AFDD, Ames Research Center), NASA (Langley Research Center), ONERA, DLR and DNW. For this test different measurement techniques like laser light sheet (LLS), laser doppler velocimetry (LDV), acoustic and non-intrusive blade deflection measurements were applied to a highly instrumented hingeless Mach scaled model of the BO105 main rotor. Figure 5 shows the DLR Rotor Test Rig in the DNW. The BVI noise pattern below the rotor is presented in Figure 6 for an HHC control input of a 3/ref blade pitch angle of $0.85°$ amplitude and a phase shift of $300°$ measured with the movable microphone array. The maximum BVI noise level occurring between $60°$ and $100°$ rotor azimuth approximately could be reduced by more than 6dB. Tip vortices in different cross sections could be visualized using the LLS technique with a remotely controlled smoke probe. The corresponding vortex lines, constructed from the successive laser cross sections, are shown in Figure 7 exemplarily for the baseline case without HHC and the minimum noise case. The figure shows the increased miss distance occurring in the minimum noise case which explains the reason for the BVI noise reduction.

The control inputs for HHC were conducted with actuators in the non-rotating system under the swash-plate. The shortcoming of HHC in the fixed system is that the pitch angle of one blade cannot be changed without changing the blade pitch of the other blades. Therefore, in the case of the 4-bladed rotor, only 3/rev, 4/rev and 5/rev input modes are possible. This limitation can be overcome by introducing actuators in the rotating system. For the Individual Blade Control (IBC) system, the conventional blade pitch links are replaced by servo-hydraulic actuators. Such an IBC experiment was described by Niesl et. al. [19]. It was carried out in the 40x80 ft wind tunnel at NASA Ames Research Center, utilizing a full scale MBB-BO105 four bladed rotor system. Acoustic data was measured with fixed microphones and with a movable microphone traverse. Total forces were measured. Accelerometers in the blade tip gave informations about the blade motion. With the IBC system different frequency functions can be used. The case of a single input frequency (see Figure 4) reproduces the results of the HHC. Very similar results were obtained with respect to noise or vibration. The major advantage of the IBC system is seen in the capability to introduce combinations of harmonics, thus generating a pulse (wavelet) which changes the blade pitch over a small azimuth range whereas the blade pitch over the rest of the rotor disc is not affected. Figure 8 shows such a pulse as input at the blade root and the answer of the blade at the tip. There is not only a time lag between the root input and the pitch at the tip but also some significant overshoots with opposite sign. Figure 9 gives the noise reduction versus azimuth for pulses of a length of $60°$ and $90°$. The noise is reduced for $60°$ azimuth but less than expected and there are some regions were the noise is increased due to the high pitch overshoots at the blade tip. Due to this problem the advantages of the IBC system compared to the HHC system could not be demonstrated in this paper.

LDV measurements for a 4-bladed model rotor (diameter=1.02m) were carried in the open test section of the ILR Aachen low-speed wind tunnel (see Seelhorst et. al. [23]). Two different blade geometries were tested: a rectangular blade with a NACA 0015 section and a blade with a swept back tip with a winglet. The miss distance between vortex and blade was increased for one specific low speed flight condition. Therefore the BVI intensity was decreased.

Kataplioglu and Caradonna [20] present results of an experiment with a nominally non-lifting rotor and a vortex generator in the 80 by 120 ft NASA Ames wind tunnel. A small scale (7 ft diameter) 2-bladed teetering rotor was used. The blades were

untwisted and have a rectangular planform with NACA 0012 airfoil sections of 6 inch chord. The vortex was generated separately by a wing tip, placed upstream of the rotor and set at an angle of attack. Blade pressures were measured with 60 transducers. A movable array of microphones was used to obtain a survey of the acoustic farfield. This setup (see Figure 10) should allow to systematically vary the important parameters of BVI, i.e. vortex/blade miss distance, vortex strength or vortex sense. Thus producing benchmark test cases for CFD methods. The externally generated vortex does have a global effect on the rotor behaviour through its effect on the trim state. The rotor is trimmed to zero flapping in order to consistently locate the blade and vortex with respect to each other. This generates a varying rotor lift together with a wake. Due to these effects the whole flow field is much more complicate than expected. In Figure 11 the sound pressure is plotted. The change of the pressure from the initial rise to the minimum peak is a measure of the BVI acoustic event (BVI acoustic amplitude). This amplitude is plotted as a function of nominal vortex miss distance in Figure 12. The asymmetry with respect to the results for the angle of attack of the vortex generator α_V is not fully understood. Nevertheless this kind of data provides a good set of test cases for CFD methods.

4. Aerodynamic 3D Prediction Methods

Six papers were devoted to Aerodynamic 3D Prediction Methods: Landgrebe [1], Costes et. al. [12], Raddatz and Pahlke [13], Berezin and Sankar, [14], Narramore [15], Röttgermann and Wagner [16] and Bessone and Petot [17].

Costes et. al. [12] present a detailed survey of the aerodynamic methods which are currently used at the Applied Aerodynamics Department of ONERA for the aerodynamic analysis for helicopter rotors in hover and forward flight. For the trim the code R85 is used. This code uses an aerodynamic based on blade element theory using steady 2D airfoil tables. Several empirical correction techniques are available in order to account for 3D effects close to the blade tip. Three wake models have been implemented: a linear half-empirical prescribed wake model of Meijer-Drees, a vortex lattice method with prescribed wake (METAR) and a free wake model (MESIR). For flight conditions with BVI the use of a free wake model is necessary in order to get good results. This is typically the case for low advance ratios $\mu < 0.25$. The blade is modelled as a beam undergoing flap, lag and torsion with linear terms only. Rotational fully coupled modes are computed to model flexibility. R85 is able to compute the trim and the rotor performance for a given flight condition. The overall agreement of the performance prediction was reported to be acceptable for several rotors. A main problem of this kind of simulation is the prediction of the 3D effects at the tip of non-rectangular blades. Therefore a 3D full potential method with entropy corrections (FP3D) is applied. ONERA developed a coupling procedure for R85 and FP3D which allows to obtain fully trimmed FP3D results. Figure 13 compares a R85 computation based on 2D airfoil tables only with a coupled R85/FP3D computation showing an improved thrust versus azimuth prediction for the coupled computation. For hover a lifting line method and a full potential method with a Lagrange model of the vortex wake (Steinhoff approach) are applied. For optimization purposes the existing aerodynamic codes can be coupled with an optimizer. Only results of an optimization with the R85 code with prescribed wake were shown.

An improved procedure for coupling existing aerodynamic, dynamic and wake models is presented by Bessone and Petot [17].

Narramore [15] reviews how CFD is put to use in industry at Bell Helicopters Textron in support of rotorcraft design. Due to recent developments in workstation technologies and inverse design methods it is possible to design airfoils for transonic flows based on the 2D compressible RANS equations interactively. Figure 14 compares pretest computations with the measured polar. The transition was fixed at 4% chord. The drag level compares well. It is pointed out that at the present time 2D computational results can be used to determine the best airfoil configuration, but that wind tunnel data is still required to assess the final performance characteristics. Mature 3D methods in industrial use for subsonic attached flows are 3D panel methods coupled with boundary layer codes. At Bell VSAERO is used in order to provide the pressure loads on the surface of fuselages as an input for a finite element model (NASTRAN) for the prediction of surface deformations. Such a model cannot be

applied for transonic flows, for the evaluation of the drag or the analysis of separation. Therefore 3D CFD methods have been developed. Although a 3D full potential method was applied successfully to main rotors, a decision was made to concentrate on RANS algorithms for use in rotorcraft problems (main rotor as well as fuselage). The RANS codes are still in a phase of validation and improvement. Today they are used for the investigation of flow details parallel to wind tunnel experiments and for parametric investigations a priori to wind tunnel experiments. Figure 15 shows computational particle traces on the upper surface of a nonrotating rotor blade. The flow is dominated by an inboard separation bubble and a large tip vortex with a region of fully attached flow at the beginning of the hyperbolic tip.

An extension of an existing panel method to flows containing weak shocks is described by Röttgermann and Wagner [16]. The method consists of three modules: a boundary element method using a surface grid, a field panel method using a cartesian field grid and a vortex lattice method for the computation of a free wake. The Cartesian field grid may penetrate the solid surface arbitrarily. By simplifying the resulting matrix equations the computational costs with respect to CPU time and memory could be reduced to 30% of the original method. First results of this method for the Caradonna-Tung rotor[40] are given in Figure 16. When extended to unsteady flows, this method seems to be very promising for rotor/fuselage interference investigations for low and medium advance ratios.

Results of a 3D CFD code based on the Euler equations are presented by Raddatz and Pahlke [13] for the Caradonna-Tung rotor in hover. The paper is focused on the inherent wake capturing properties of the Euler solver. Calculated wake geometry features and pressure distributions were compared to test results by Caradonna and Tung. A grid refinement study with a coarse, a medium and a fine grid was carried out. The study shows that the wake resolution was strongly improved going from the coarse to the medium and going from the medium to the fine grid (see Figure 17). The improved wake resolution for the fine grid has only a very small effect on the surface pressures compared to the medium grid (see Figure 18). The surface pressures can be accepted for the medium grid. The investigation of boundary treatments (including chimera boundaries for overlapping grids) shows that a spatially second.order boundary treatment is necessary in order to avoid a smearing of the vortices. Otherwise the grid points have to be clustered at inner block boundaries.

Due to the high cpu time for time-accurate RANS computations for rotors in forward flight a hybrid RANS/Full Potential method is proposed by Berezin [14]. The use of the full potential solver in those regions of the flow, where the viscous effects can be neglected saved about 40% of the overall cpu time. First results were presented which showed some disagreements between the original RANS method and the hybrid method for certain azimuth regions.

The keynote paper by Landgrebe [1] gives an overview of the ongoing CFD research for rotorcrafts in the U.S. Since this overview cannot be summarized within a few lines the authors kindly ask the reader to refer to the paper. The most important issue of the paper is the accurate modelling of the vortex wake of the main rotor. Most CFD methods are based on a Finite Volume or a Finite Difference discretization of the Euler or the RANS equations with the vortex wake being part of the solution. These codes suffer from numerical dissipation. Different approaches to improve the situation have been published:

- grid refinement in structured grids at the position of the vortices,
- overlapping structured grids with additional refined grids at the vortices,
- unstructured grids which are solution (vortex) adapted,
- combination of unstructured and overlapping structured grids,
- use of higher order schemes (4th and 5th order).

5. Acoustic Prediction Methods

Beaumier et. al. [26], Ianniello and De Bernadis [27], Gennaretti et. al. [28], Schultz et. al. [29], Toulmay et. al. [30], Baeder [33], Lyrintzis [34] deal with acoustic predictions for isolated rotors or the complete helicopter.

A unified aerodynamic and aeroacoustic analysis for transonic hovering rotors based on a boundary

integral method is presented by Gennaretti et. al. [28]. With this approach a field grid is necessary only in those regions of the flow which contain non-linear terms. Although the first aerodynamic results for non-lifting hovering rotors show some discrepancies compared to CFD full potential or Euler solvers the acoustic predictions compare well with existing experimental data for the non-lifting UH-1H rotor in hover ($M_{\omega R} = 0.85$). Further validation is necessary for this method.

De Bernadis [27] and Schultz et. al. [29] deal with acoustic predictions based on the Ffowcs-Williams/ Hawkings (FHW)-equation in Farassats formulation 1 and 1A. Aerodynamic input data like the blade pressures and the perturbation velocity field around the blade are required. In paper [29] prediction methods for both the BVI and the highspeed impulsive (HSI) noise are presented. Since BVI typically occurs for low speed flight conditions a Lifting Body Surface method based on linear potential theory is used for the aerodynamic prediction with the assumption of rigid rotor blades. This method is coupled with a fixed wake model. Although the predicted aerodynamic pressures show only a fair agreement with the experimental data the acoustic predictions agree relatively well with measured sound pressures. The main part of [29] is devoted to HSI noise. A Finite Volume Euler method was used for the aerodynamic prediction with the Beddoes fixed wake model for forward flight cases. Four approximations for the quadrupolterm are presented and applied to a non-lifting hover and a lifting forward flight test case. Figure 19 compares the different approximations for the UH-1H rotor in non-lifting hover ($M_{\omega R} = 0.90$). The basic idea for all the approximations is to reduce the computational effort by reducing the volume integral for the quadrupolterm to sum of a number of line integrals (approximations c) and d)) or to a pure surface integral (e)).Approximation d) is reported to be a good compromise between accuracy and computational effort. Figure 20 compares predicted sound pressures with approximation d) for different microphone positions for Ah1/OLS rotor in highspeed forward flight. For the in-plane results (mic 6, 2 and 8) the agreement is quite good while the pressures are underpredicted for the out of plane positions.

Baeder [33] presents HSI noise predictions based on direct Euler computations or on a coupled Euler/ Kirchhoff method. The advantage of a Kirchhoff method for HSI noise compared to the evaluation of the quadrupolterm is that the Kirchhoff method needs the aerodynamic data on a closed surface which contains the non-linearities of the flow field. Therefore only a surface has to be evaluated which reduces the amount of data (storage) and the computational effort compared to the volume integration for the quadrupolterm. Figure 21 compares three methods for the prediction of the sound pressure for the non-lifting UH-1H rotor ($M_{\omega R} = 0.90$): direct Euler, Euler/Kirchhoff and the thickness+drag contribution of the FWH equation. The direct Euler and the Euler/Kirchhoff method are in good agreement with each other and with the experimental data. For a rotor in non-lifting forward flight HSI noise results with similar agreement to experimental data were obtained. In a second part Euler computations for simplified BVI cases are presented. An isolated vortex is prescribed. The vortex is preserved in the Euler solution through the use of a non-linear perturbation technique. This vortex travels with the free stream and interacts with a nominally non-lifting rotor such that parallel interaction takes place at 180 degree azimuth (see [20]). First qualitative results are presented indicating that an Euler method can handle such problems with respect to acoustic investigations. In addition 2D computations for this setup were carried out in order to evaluate the possible BVI reductions by an appropriate blade motion. Lyrintzis [34] presents a comprehensive review of the use of Kirchhoff's method in rotorcraft aeroacoustics.

The results of the HART prediction team for the prediction of BVI cases with HHC are discussed by Beaumier et. al. [26]. The following partners were involved: AFDD, DLR, NASA and ONERA. AFDD and NASA use versions of CAMRAD for trim and wake computations and a full potential rotor code for the computation of surface pressures. The acoustic data is computed on the basis of the surface pressures. At NASA a second method is used which takes the blade loadings directly out of CAMRAD and computes the acoustic on the basis of the blade loading. DLR uses a lifting line method (S4) for the trim which is coupled with a fixed wake model according to Beddoes. The loading is used

as input for the acoustic code AKUROT which includes the thickness and the loading term for BVI computations. ONERA uses R85/METAR for the trim and the computation of a prescribed wake. This wake is distorted by MESIR. The free wake is used as an input for MENTHE (Modelling of the Roll up of the Vortex Sheet of a Helicopter Rotor) which computes the roll up of the vortex wake. With this data available surface pressures are computed with a 2D panel method with corrections for 3D effects. The acoustic signals are computed with the PARIS code using these surface pressures. Results for four test cases were selected: one test case without HHC and three test cases with an HHC control amplitude of 1.2 degree which differ in the settings for the HHC phase (Run 178: phase of 124 degree). The onflow conditions are given by

$$\mu = 0.15, M_{\omega R} = 0.641, \alpha_{TPP} = 3.8°.$$

Figure 22 compares the computed blade torsion for the case without HHC and with HHC. The elastic torsion show differences of up to $3°$ between the predictions of the different partners. The comparison of the sound pressure levels in Figure 23 shows similar differences. The quantitative agreement is not satisfying between the predictions and the experimental data. These results show the need for further improvements of the prediction tools. The importance of a correct simulation of the blade dynamics and of the wake are pointed out in the conclusions of [26].

Toulmay et. al. [30] describe the methods available to predict exterior noise from the French helicopters manufacturer's point of view. The requirements are divided into four different noise assessment categories: 1) Overall rotor noise, 2) Blade Vortex Interaction, 3)Fan-in-fin (fenestron) and 4) Complete helicopter in flight. It is pointed out that the most important step in the prediction is the correct prediction of the airloads. The paper discusses in detail the different methods of analysis and shows several examples of test/theory correlation with wind tunnel and flight test data. In some instances, as with engine noise and complete helicopter configurations, there is no substitute for tests.

6. Conclusion

Dynamic Stall: Although a large amount of experimental data is available the assessment of CFD simulations is still difficult due to uncertainties in the repeatability of measured dynamic stall. The details of the dynamic stall phenomenon are still not fully understood. Hence there is a need for further tests with detailed flow analysis like [3]. The agreement of CFD simulations with experimental data is acceptable for light and medium stall if appropriate turbulence models are used and the transition is fixed. None of the methods was able to accurately predict deep dynamic stall. Transition prediction is important for the prediction of stall on real helicopter rotor blades.

Experimental Investigations of Helicopter Rotors: Several experiments were devoted to the investigation of rotor noise (BVI and HSI noise). Most wind tunnel experiments concentrated on the BVI topic. The Higher Harmonic Control Aeroacoustic Rotor Test (HART) in the DNW was successfully conducted and a large amount of aerodynamic, acoustic and dynamic data is available. New in-flight test facilities are being developed (e.g. in UK with instrumented main and tail rotor). Such facilities provide necessary informations about the interference between main rotor, fuselage, engine exhausts and tail rotor. Flight tests are still necessary for the assessment of the effects of design changes on the overall performance (aerodynamic and acoustic) of helicopters.

Aerodynamic 3D Prediction Methods: The comprehensive rotor analysis codes used in Europe and US at research centres and industries are very similar. They have reached a certain degree of maturity although the test-theory correlation is not fully satisfying. It was interesting to see that the codes predict similar overall aerodynamic performances but quite different blade movements (flapping and torsion) for the same test cases. A huge effort was spend for the development of more accurate and more reliable CFD methods for main rotors. The results are very promising but the codes are still far away from an industrial use. The main problems are the efficiency of the flow solvers, the high manpower needed for grid generation, turbulence modelling and numerical diffusion of the vortical wake.

Acoustic Prediction Methods:

Several researchers worked on the development and validation of aerodynamic and acoustic prediction methods for BVI. The efficiency of Higher Harmonic Control and of Individual Blade Control inputs for the reduction of BVI noise were investigated. The blade vortex miss distance was found to be the most important parameter for BVI noise. Methods for the prediction of high speed impulsive noise have been developed and encouraging results were presented. The weakest point in the aeroacoustic prediction seems to be the prediction of the aerodynamic flow field (position and strength of vortices, shock strength and disturbance velocities for transonic flows).

7. Bibliography

References [1] to [35] list the papers of the 75th Fluid Dynamics Symposium in order of presentation. These papers were published in the AGARD Conference Proceedings [37].

[1] Landgrebe, A.J.: *New Directions in Rotorcraft Computational Aerodynamics. Research in the U.S.* AGARD-CP-552, August 1995.

[2] Ekaterinaris, J.A.; Srinivasan, G.R.; McCrosky, W.J.: *Present Capabilities of Predicting Two-Dimensional Dynamic Stall.* AGARD-CP-552, August 1995.

[3] Chandrasekhara, M.S.; Carr, L.W. : *Compressibility Effects on Dynamic Stall of Oscillating Airfoils.* AGARD-CP-552, August 1995.

[4] Dindar, M.; Kaynak, Ü.: Effect of Turbulence Modeling on Dynamic Stall Computations. AGARD-CP-552, August 1995.

[5] Ivtchin, V.A. *Investigation into Effect Produced by Blade Airfoil Unsteady Airflow on Helicopter Main Rotor Power Required.* AGARD-CP-552, August 1995.

[6] Geissler, W.; Sobieczky, H.: *Dynamic Stall Control by Variable Airfoil Camber.* AGARD-CP-552, August 1995.

[7] Snel, H.; van Holten, Th. : *Review of Recent Aerodynamic Research on Wind Turbines with Relevance to Rotorcraft.* AGARD-CP-552, August 1995.

[8] Tchon, K.F.; Hallé, S.; Paraschivoiu, I.: *Dynamic Stall Simulation Applied to Vertical Axis Wind Turbines.* AGARD-CP-552, August 1995.

[9] Madsen, H.A.; Rasmussen, F.: *Stall Hysteresis and 3D Effects on Stall Regulated Wind Turbines: Experiment and Modelling.* AGARD-CP-552, August 1995.

[10] Filippone, A.; Sørensen, J.N.: A Viscous-*Inviscid Interaction Model for Rotor Aerodynamics.* AGARD-CP-552, August 1995.

[11] Voutsinas, S.G.; Belessis, M.A.; Rados, K.G.: *Investigation of the Yawed Operation of Wind Turbines by Means of a Vortex Particle Method.* AGARD-CP-552, August 1995.

[12] Costes, M.; Beaumier, P.; Gardarein, P.; Zibi, J. : *Méthodes de Calcul Aérodynamique Appliquées aux Rotors d'Hélicoptères à l'ONERA.* AGARD-CP-552, August 1995.

[13] Raddatz, J.; Pahlke, K. : *3D Euler Calculations of Multibladed Rotors in Hover: Investigation of the Wake Capturing Properties.* AGARD-CP-552, August 1995.

[14] Berezin, C.; Sankar, L. : *Forward Flight Rotor Airloads Predictions Using a Coupled Navier-Stokes / Full-Potential Analysis.* AGARD-CP-552, August 1995.

[15] Narramore, J.C.: *Computational Fluid Dynamics Development and Validation at Bell Helicopter.* AGARD-CP-552, August 1995.

[16] Röttgermann, A.; Wagner, S. : *Cost Efficient Calculation of Compressible Potential Flow around a Helicopter Including Free Vortex Sheet by a Field Panel Method.* AGARD-CP-552, August 1995.

[17] Bessone, J.; Petot, D.: *Evaluation de Modèles Aérodynamiques et Dynamiques des Rotors d' Hélicoptères par Confrontation a l' Expérience.* AGARD-CP-552, August 1995.

[18] Hamel, P.G.; Kaletka, J.: *Rotorcraft System Identification - An Overview of AGARD FVP Working Group 18.* AGARD-CP-552, August 1995.

[19] Niesl, G.; Swanson, S.M.; Jacklin; S.A.; Blaas, A.; Kube, R.: *Effect of Individual Blade Control on Noise Radiation.* AGARD-CP-552, August 1995.

[20] Kataplioglu, C.; Caradonna, F.X.: *A Study of Blade-Vortex Interaction Aeroacoustics Utilizing an Independently Generated Vortex.* AGARD-CP-552, August 1995.

[21] Samokhin, V.F.; Rozhdestvensky, M.G.: *External Noise of Single Rotor Helicopters.* AGARD-CP-552, August 1995.

[22] Tarttelin, P.C.; Martyn, A.W.: *In Flight Research with Instrumented Main and Tail Rotor Blades Using the DRA Bedford Aeromechanics Research Lynx Helicopter.* AGARD-CP-552, August 1995.

[23] Seelhorst, U.; Beesten, B.M.J.; Bütefisch, K.A. : *Flow Field Investigation of a Rotating Helicopter Rotor Blade by Three-Component Laser-Doppler-Velocimetry.* AGARD-CP-552, August 1995.

[24] Berton, E.; Favier, D.; Maresca, C.; Nsi Mba, M. : *Determination des Charges Aérodynamiques du Rotor en Vol Stationnaire, a l'Aide d'une Technique de Vélocimétrie Laser.* AGARD-CP-552, August 1995.

[25] Kube, R.; Splettstößer, W.R.; Seelhorst, U.; Yu, Y.H.; Boutier, A.; Micheli, F.; Merker, M.: *Initial Results from the Higher Harmonic Control Aeroacoustic Rotor Test (HART) in the German-Dutch Wind Tunnel.* AGARD-CP-552, August 1995.

[26] Beaumier, P.; Prieur, J.; Rahier, G.; Spiegel, P.; Demargne, A.; Tung, C.; Gallman, J.M.; Yu, Y.H.; Kube, R.; van der Wall; B.G.; Schultz, K.J.; Splettstößer, W.R.; Brooks, T.F.; Burley, C.L.; Boyd, D.D. Jr.: *Effect of Higher Harmonic Control on Helicopter Rotor Blade-Vortex Interaction Noise: Prediction and Initial Validation.* AGARD-CP-552, August 1995.

[27] Ianniello, S.; De Bernadis, E.: *Calculation of High-Speed Noise from Helicopter Rotor Using Different Descriptions of Quadrupole Source.* AGARD-CP-552, August 1995.

[28] Gennaretti, M.; Iemma, U.; Morino, L. A: *Boundary Integral Method for Unified Transonic Aerodynamic and Aeroacoustic Analysis of Hovering Rotors.* AGARD-CP-552, August 1995.

[29] Schultz, K.-J.; Lohmann, D.; Lieser, J.A.; Pahlke, K.: *Aeroacoustic Calculation of Helicopter Rotors at DLR.* AGARD-CP-552, August 1995.

[30] Toulmay, F.; Falchero, D.; Arnaud, G.: Prévision du Bruit Externe des Hélicoptères: *Les Méthodes Numériques Vues par un Industriel.* AGARD-CP-552, August 1995.

[31] Syms, G.; Zan, S.J. : *The Role and Status of Euler Solvers in Impulsive Rotor Noise Computations.* AGARD-CP-552, August 1995.

[32] Newman, S.J.: *A Theoretical and Experimental Investigation into the Rotor Blade Aeroelastic Behaviour of a Shipborne Helicopter during Rotor Engagement and Braking.* AGARD-CP-552, August 1995.

[33] Baeder, J.D. : *The Role and Status of Euler Solvers in Impulsive Rotor Noise Computations.* AGARD-CP-552, August 1995.

[34] Lyrintzis, A.S.: *The Use of Kirchhoff's Method in Rotorcraft Aeroacoustics.* AGARD-CP-552, August 1995.

[35] Wells, V.L.; Han, A.Y.; Crossley, W.A.: *Acoustic Design of Rotor Blades Using a Genetic Algorithm.* AGARD-CP-552, August 1995.

[36] Hamel, P.G. (editor) : *Rotorcraft System Identification* AGARD AR-280, 1991.

[37] *Aerodynamics and Aeroacoustics of Rotorcraft.* Papers presented at the 75th Fluid Dynamics Symposium, Berlin, Germany, 10-13 October, 1994. AGARD-CP-552, August 1995.

[38] *Prediction of Aerodynamic Loads on Rotorcraft.* AGARD Conference Proceedings No. 334. Fluid Dynamics Panel Specialists' Meeting held at Church House, London, United Kingdom, 17-18 May, 1982.

[39] Hamel, P.G. (editor) : *Rotorcraft System Identification* AGARD LS-178, 1991.

[40] Caradonna, F. X. and Tung, C.: *'Experimental and Analytical Studies of a Model Helicopter Rotor in Hover',* NASA TM-81232, September 1981.

8. Figures

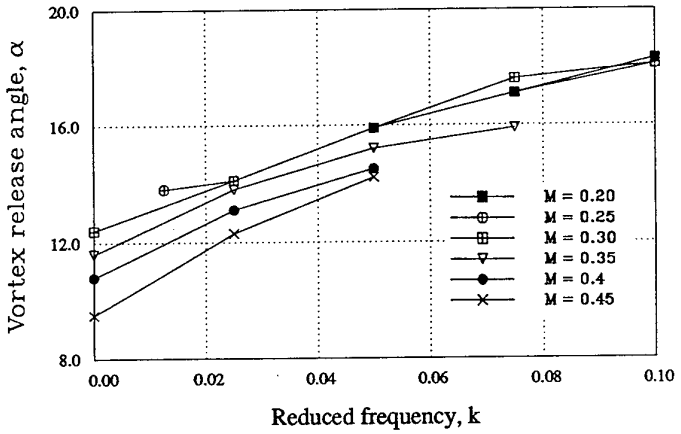

Figure 1: Quantitative Effects of Reduced Frequency on Dynamic Stall process [3]

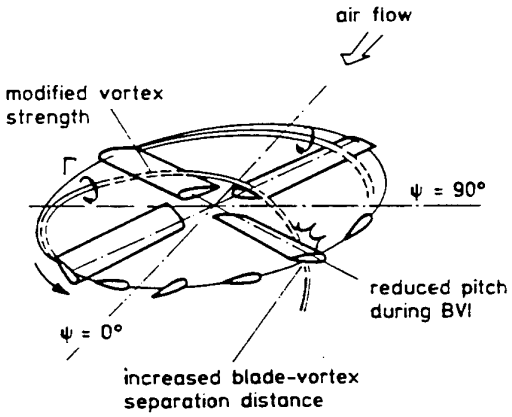

Figure 2: Noise Reduction Mechanism by Higher Harmonic Rotor control [19]

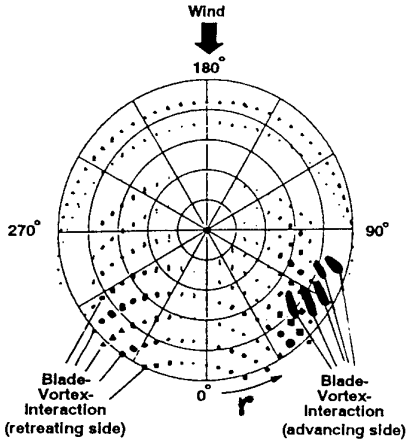

Figure 3: Measured BVI Locations in the Rotor Disc at 4° Tip Path Plane [19]

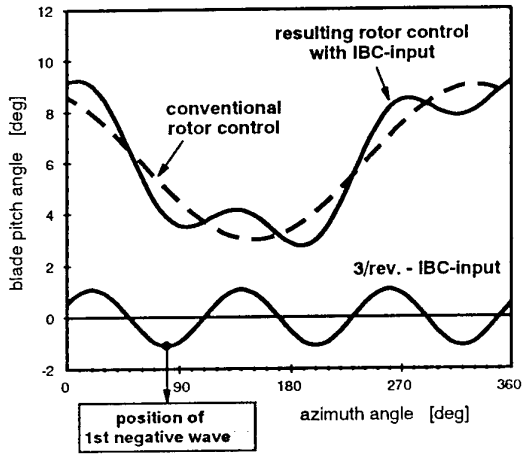

Figure 4: Blade Root Pitch Angle vs. ψ for Conventional Rotor Control and a 3/rev Higher Harmonic Signal [19]

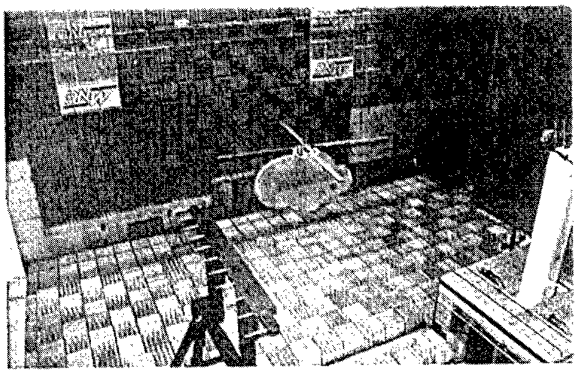

Figure 5: DLR Rotor Test Rig in DNW [25]

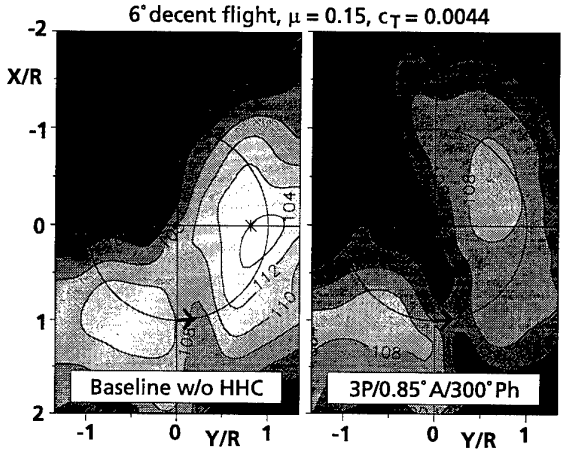

Figure 6: BVI Noise Pattern Below the Rotor (see [25])

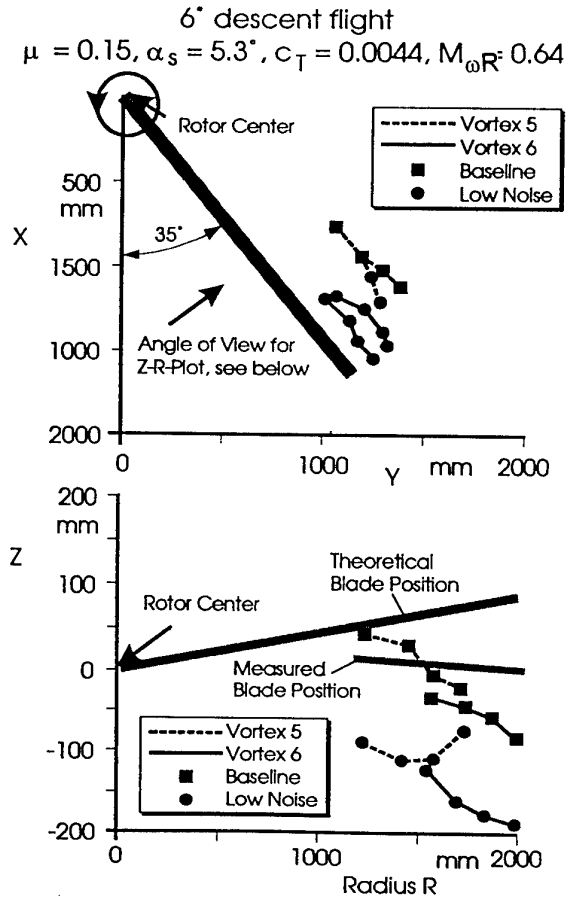

Figure 7: Vortex Trajectories Determined by LLS [25]

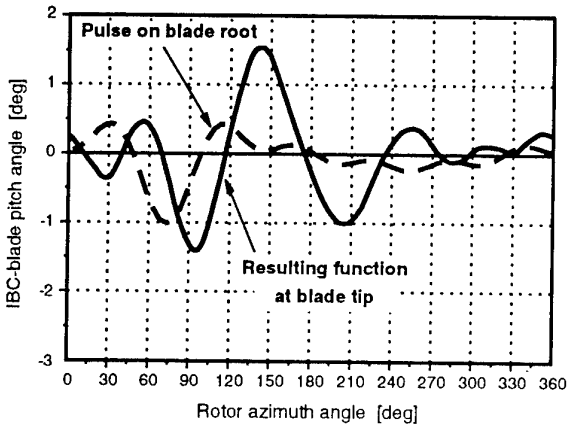

Figure 8: Blade Pitch Curve at Blade Root and Blade Tip for a Pulse Input at $\psi = 70°$ [19]

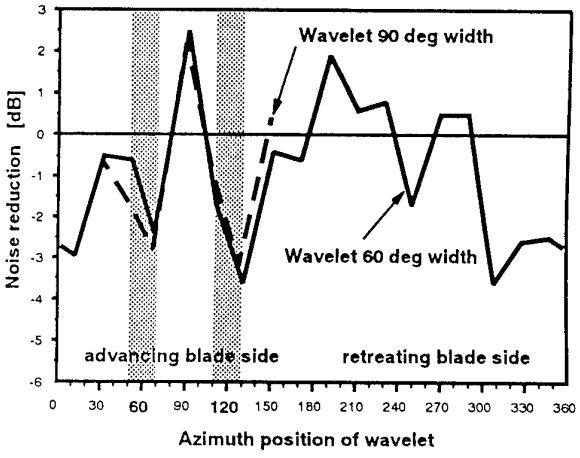

Figure 9: Noise Results by Input of a Wavelet at Blade Tip [19]

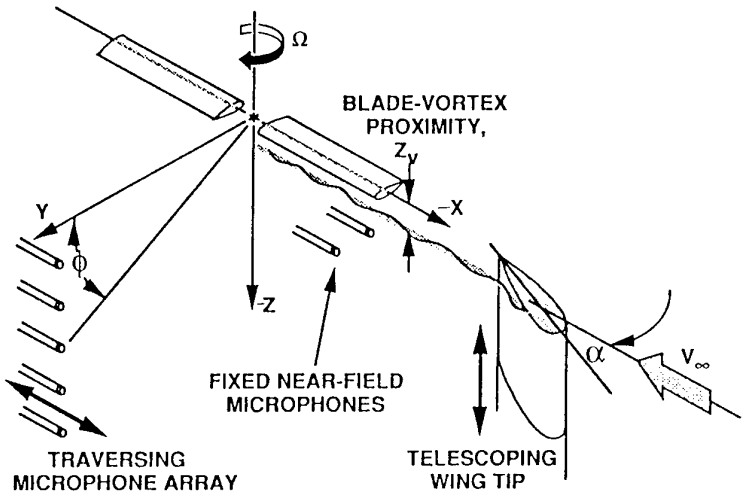

Figure 10: Sketch of BVI Test Set-Up and Definition of Parameters [20]

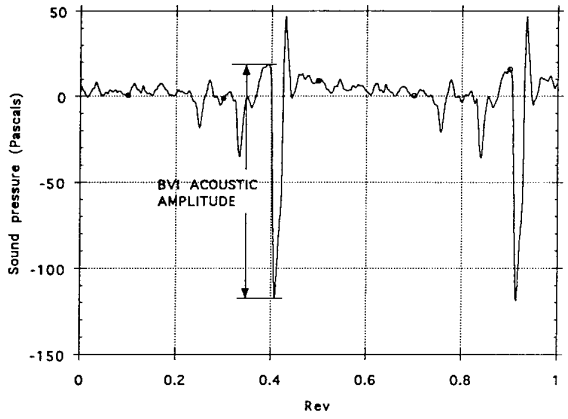

Figure 11: Typical Far-Field Acoustic Time History for Parallel BVI [20]

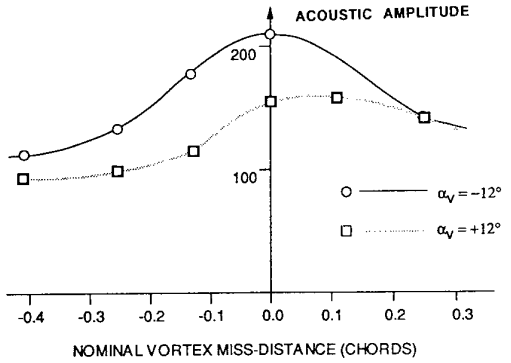

Figure 12: The Effect of Vortex Proximity on the BVI Acoustic Amplitude [20]

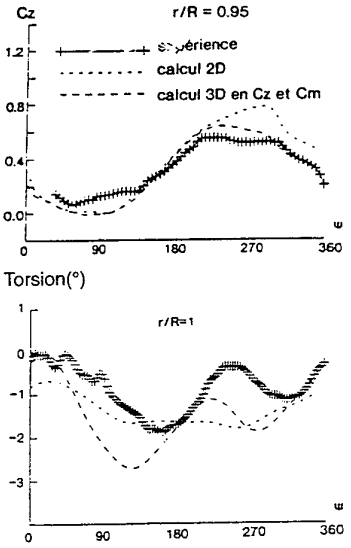

Figure 13: Effect of Coupling R85 with FP3D [12]

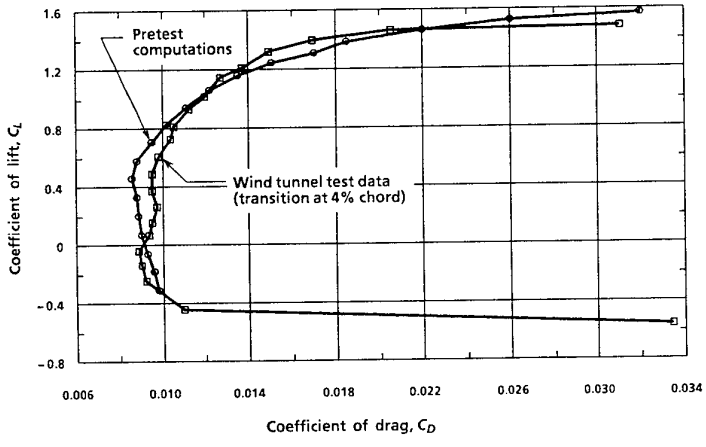

Figure 14: Drag Levels with Transition Fixed were Predicted Prior to the Wind Tunnel Test [15]

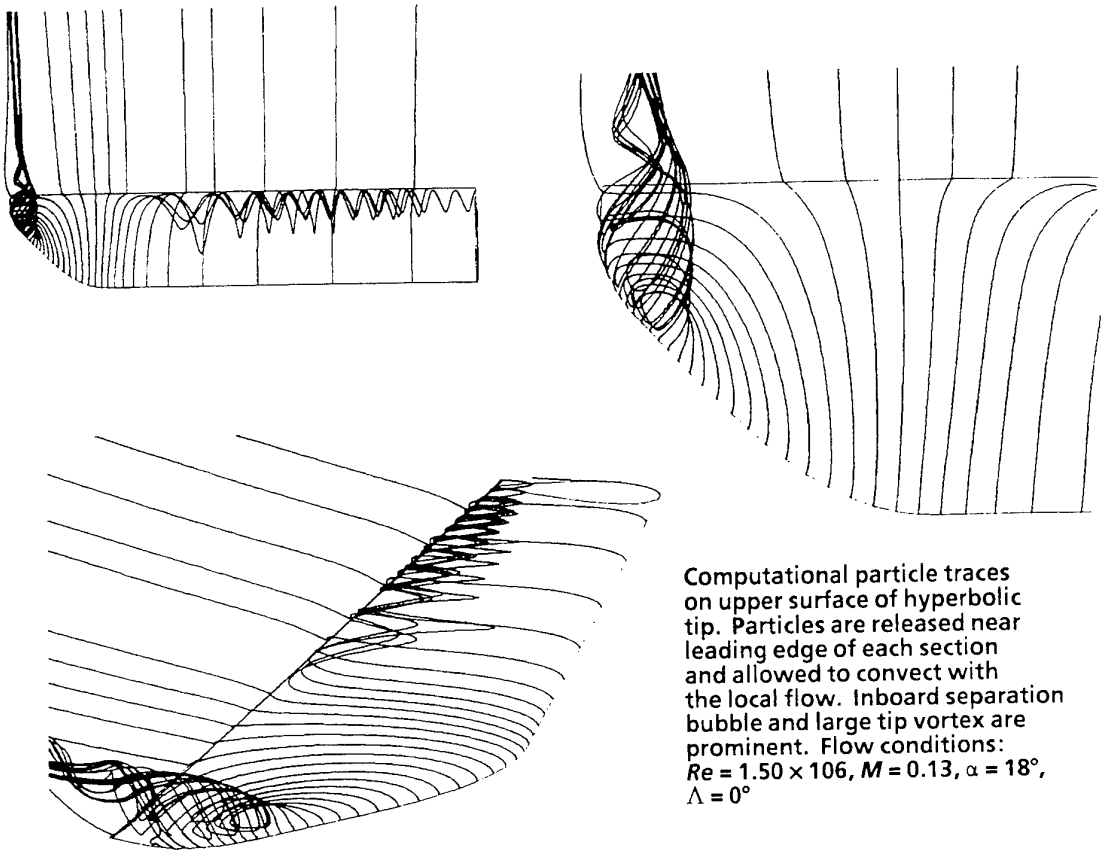

Computational particle traces on upper surface of hyperbolic tip. Particles are released near leading edge of each section and allowed to convect with the local flow. Inboard separation bubble and large tip vortex are prominent. Flow conditions: $Re = 1.50 \times 106$, $M = 0.13$, $\alpha = 18°$, $\Lambda = 0°$

Figure 15: RANS Results were Used to Interpret Wind tunnel Flow Patterns [15]

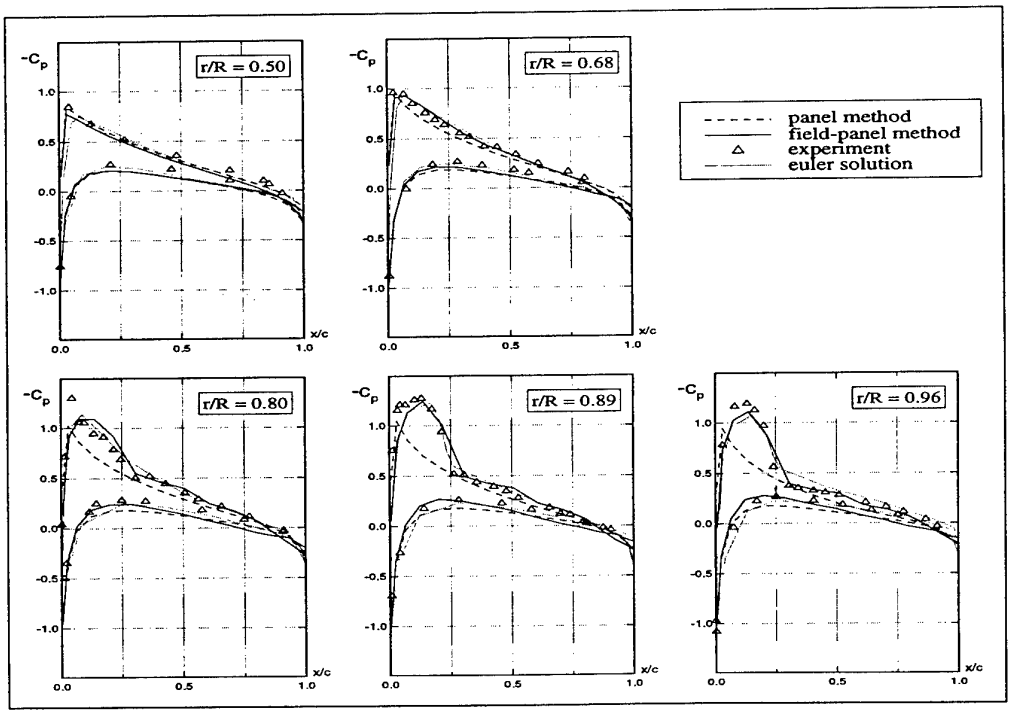

Figure 16: c_p-Distribution for the Caradonna-Tung Rotor $\theta = 8°$, $M_{\omega R} = 0.794$ [16]

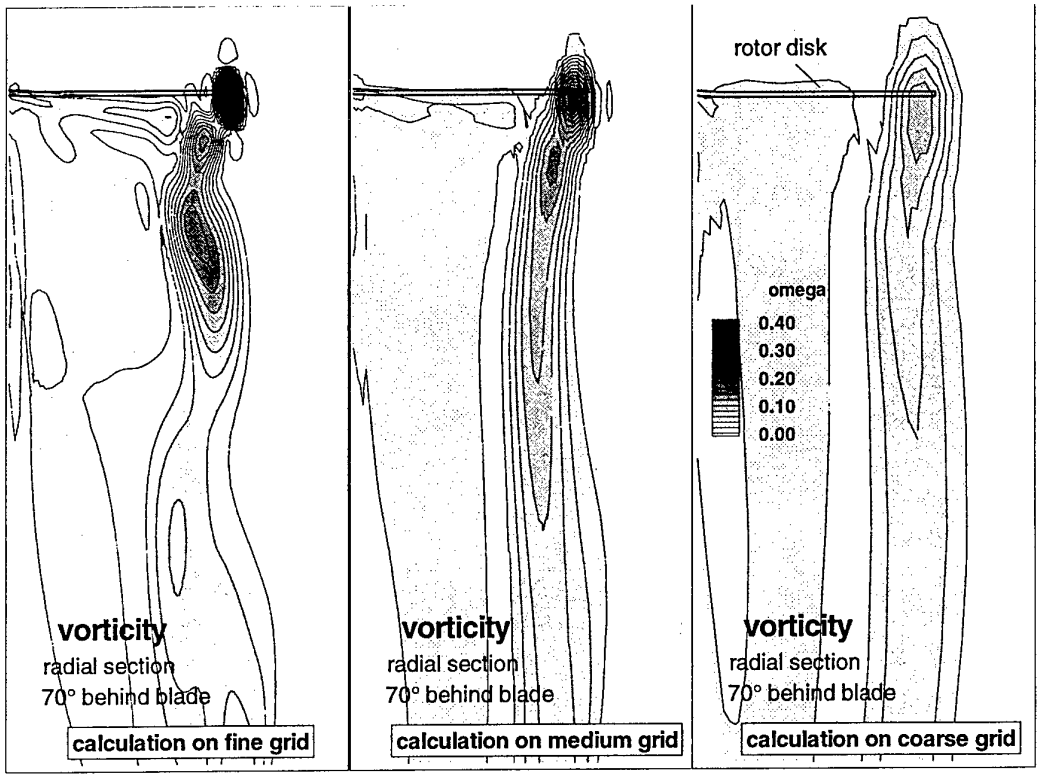

Figure 17: Grid Refinement Study at a radial Position $70°$ Behind the Rotor Blade [13], Caradonna-Tung Model Rotor in Hover $\theta = 8°$, $M_{\omega R} = 0.794$, Coarse: 57x21x33 Points, Medium: 113x41x65 Points, Fine: 225x81x129 Points

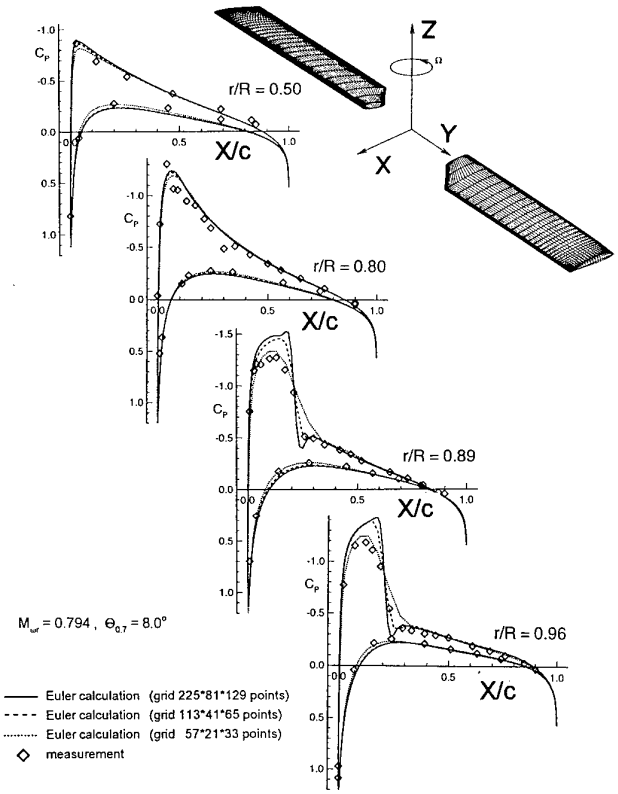

Figure 18: Pressure Distributions of 2-Bladed Caradonna-Tung Model Rotor in Hover [13]

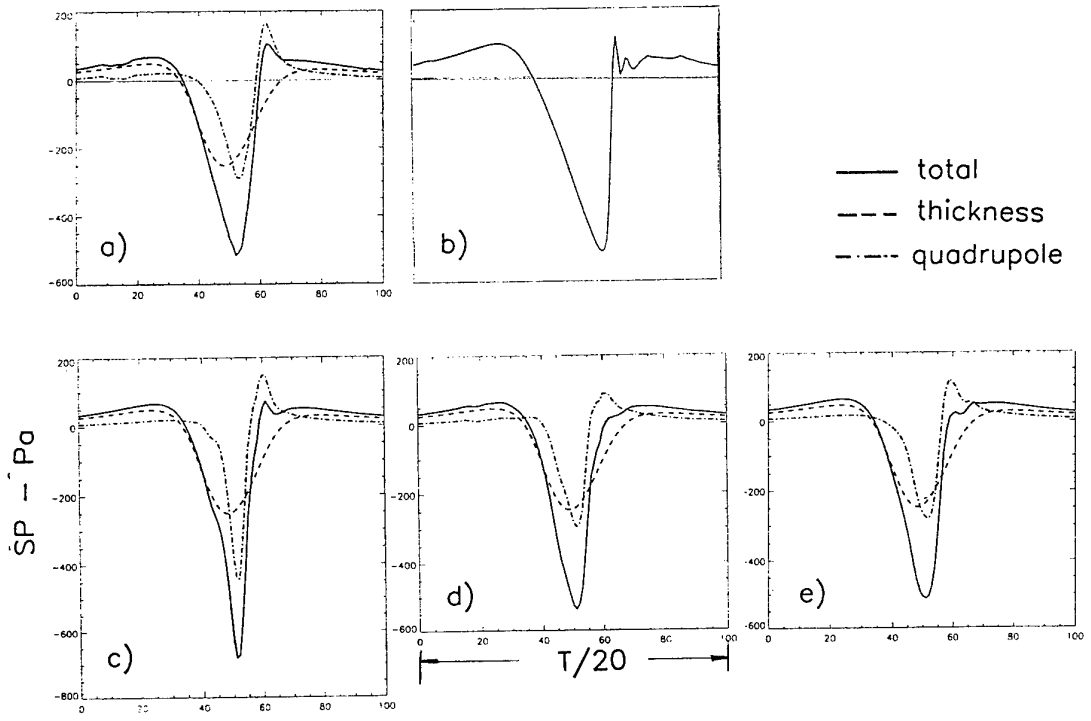

a) Volume Integration
b) Experiment
c) Pre-Integration in the Original Grid System
d) Pre-Integration after Coordinate Transformation
e) Approximation Using the Surface Values

Figure 19: In-Plane Sound Pressure Signatures Compared with Experiment for Different Quadrupolterm Approximations and a Microphone Position of $r/R = 3.09$ (Twisted UH-1H Rotor in Hover, $M_{\omega R} = 0.9$) [29]

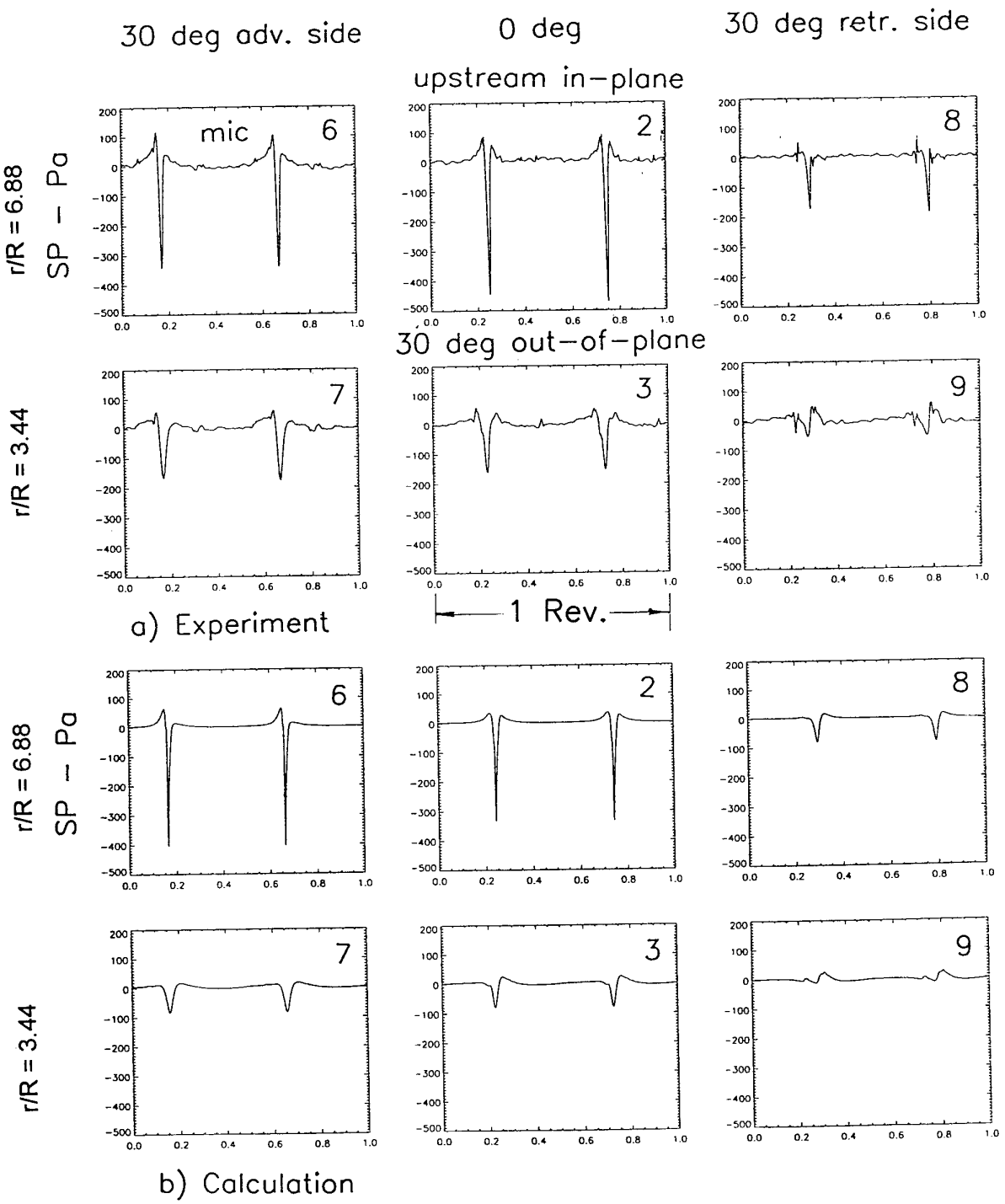

Figure 20: Comparison of Calculated and Measured Sound Pressure Time Histories for Different Microphone Positions (AH1-OLS Model Rotor $\mu = 0.345$) [29]

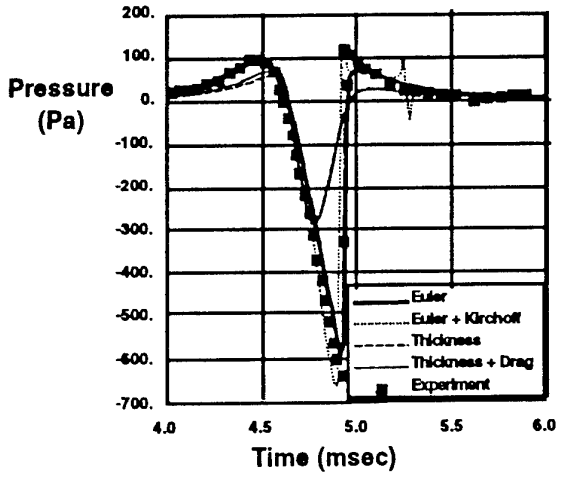

Figure 21: Comparison of the Predicted Pressure Time Histories in the Plane of the Rotor at $r/R = 3.09$ for Untwisted UH-1H Rotor for Three Methods at $M_{\omega R} = 0.9$ [33]

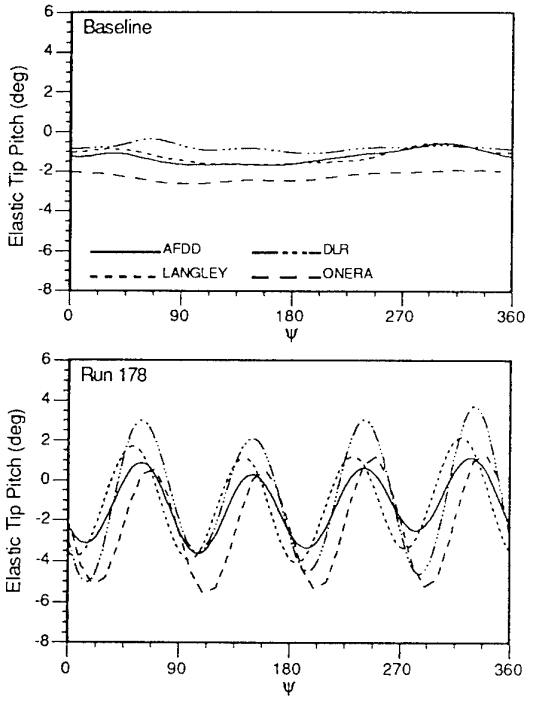

Figure 22: Predicted Elastic Pitch Angle at the Blade tip as a Function of Azimuth [26]

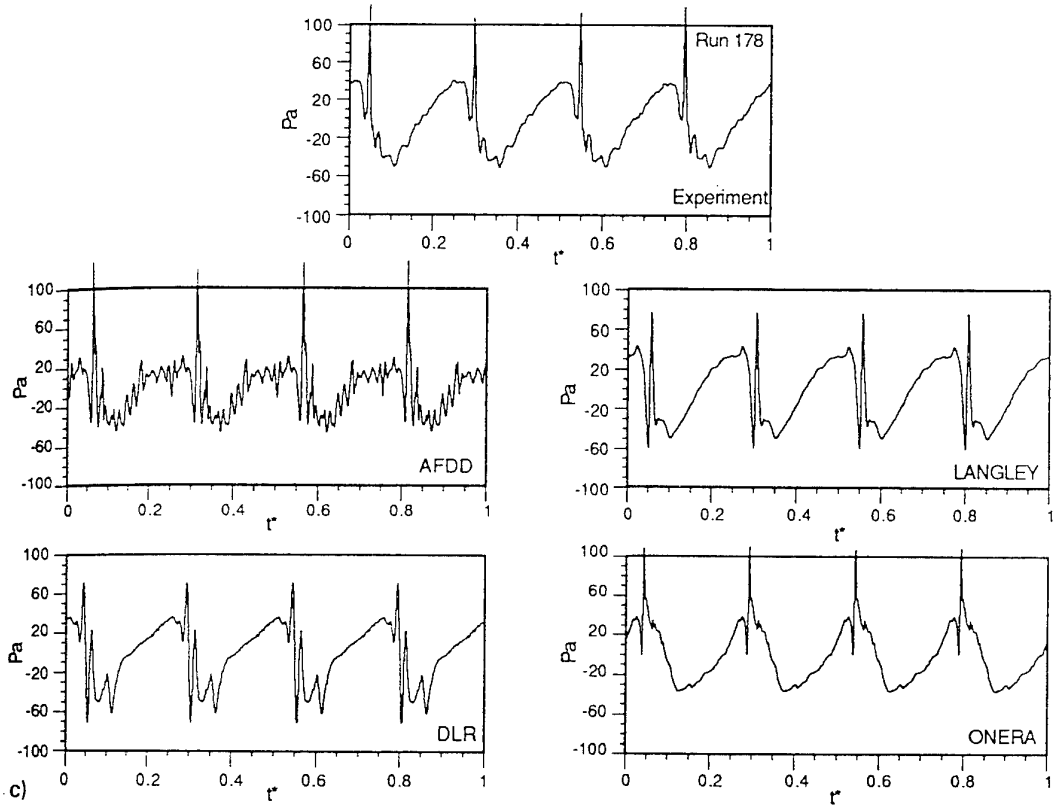

Figure 23: Typical Acoustic Signatures: Theory/Experiment Correlation for Single BVI [26]

The Integrated Development of a Medium Lift Military/Civil Helicopter

J P Graham - Deputy Chief Designer (Support Helicopter)
GKN Westland Helicopters Limited, EH101 Engineering
Box 226, GKN WHL, Yeovil
Somerset BA20 2YB, UK

1. INTRODUCTION

The EH Industries EH101 medium sized rotorcraft is the first of its kind to achieve production status that has been designed from the outset as a vehicle able to meet, without significant compromise, all appropriate civil and military regulatory requirements.

Now that the design and development programme is nearing completion it is an appropriate time to review the success of the joint civil/military programme strategies which were implemented by EH Industries from the outset and which have significantly shaped both the product of the programme (EH101) and the programme design process.

2. BACKGROUND

During the mid 1970's the UK Ministry of Defence (MoD) began to investigate how best to replace the in-service Anti-Submarine Warfare Mk 1 Sea King (HAS-1) which had been accepted into service during 1969. That a Sea King replacement (SKR) was being actively planned within only 5 years of entry into service of its predecessor reflects the seemingly inevitable gestation period for a modern aerospace project.

Two lines of development were originally investigated by both GKN WHL (then Westland Helicopters Ltd) and MoD Research Agencies under the auspices of feasibility and project definition studies; a significant development of the HAS Mk 1 Sea King and an all new design. The eventual result of this early work was published in 1976 and clearly demonstrated that there was a significant performance improvement between the 1950s technology Sea King derivative and the prospect of an all new design.

At this time the all new option was targeted closely at the Naval roles of anti-submarine, anti-surface vessel, and deep water search and rescue roles. The multi-role fleet helicopter, project WG27, featured buried weapon carriage, a fuselage just large enough to carry the mission fit, "rubber" engines of indeterminate origin, and various novel configuration aspects aimed at minimising its folded dimension.

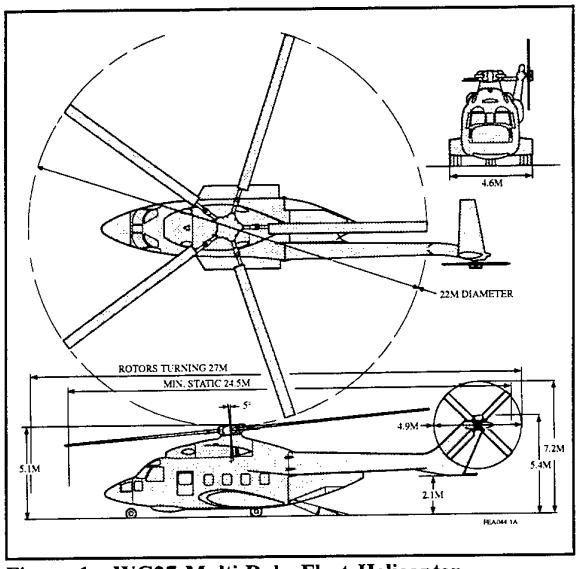

Figure 1 - WG27 Multi-Role Fleet Helicopter

It was immediately clear that the Navy preferred the all new approach so as to "leap frog" the technology of SKR beyond some of the more modern designs available or in prospect, such as HAS 1 Lynx, Dauphin, and LAMPS III. However, the estimated costs for such a programme were inevitably large and there was no clear way in which a full scale programme could be launched in isolation from a partner with whom to share costs. The initial solution was to initiate further studies to refine the design with particular reference to reducing risk and cost; it was now that a solution using 3 available engines emerged under the designation WG34. Additionally, a technology demonstration programme (known as WG34A) was launched and alliances sought with other Sea King operators, most notably the Italian MoD, where its Naval service, the Marina Militare Italiana (MMI), had a similar operational need to replace SH-3D.

Paper presented at the FVP Symposium on "Advances in Rotorcraft Technology", held in Ottawa, Canada, 27-30 May 1996, and published in CP-592.

Government level collaboration was quickly matched by Industry and a collaborative engineering team was established by Agusta and GKN WHL followed shortly afterwards by the formation of a jointly owned management company, EH Industries, in June 1980.

All participants were keenly aware that overall programme viability was inexorably linked to both cost and market share. Final project definition studies included a major market survey as an integral feature whose aim was to identify the widest possible market place comprising both military and civil operators. The end result was the configuration now known as EH101 which had a gross take-off mass increased by 17% over WG34 but was otherwise broadly similar. From a programmatic perspective, industry agreed to fund some 30% of the development costs. In 1984 the full scale Integrated Development Programme (IDP) was finally launched for the design and build of 9 pre-production aircraft systems plus a range of ground based facilities.

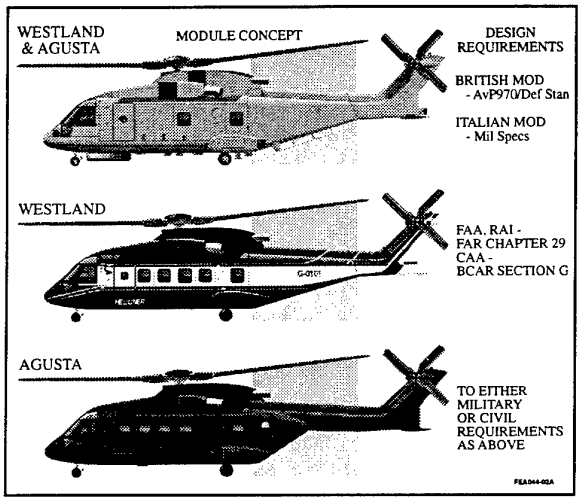

Figure 2 - EH101 Basic Variants

Today, in 1996 the basic programme is virtually complete; the nine pre-production aircraft, comprising both military and civil variants, have accumulated over 3800 flying hours, civil type certification has been achieved, and the first military production aircraft delivered. The basic configuration today is identical to that defined during final joint project definition in 1982 except for the gross take-off mass which has grown by a further 2%, to 14.6 tonnes. The UK Navy has elected to name their Variant 'Merlin'; as yet no name has been assigned to the MMI Variant.

Late in the programme the UK MoD(PE) determined that it would procure production aircraft systems through a Prime Contractor, and after a competition in 1991 selected IBM ASIC (now Loral ASIC), in preference to a bid from BAe and GEC, for the supply of 44 Merlin weapon systems. The MMI Prime Contract is let via Agusta.

During 1995 the UK MoD(PE) ordered 22 Support Helicopter (SH) Variants of EH101 Utility through GKN WHL as Prime Contractor. An Export Variant has been launched under the name Cormorant.

The overall programme aims have been met with only customerisation work for Merlin, MMI, Civil, the SH, and future customers remaining to be completed.

Figure 3 - The Result of the IDP

3. DESIGN REQUIREMENTS - ORIGIN AND DEFINITION

A traditional national military programme would be expected to have design requirements derived directly from the statement of operational requirement and national design regulations. Similarly, a civil programme must meet both market requirements and appropriate civil regulatory Authority design standards.

For EH101, EH Industries had to merge two military operational requirements, plot the worst case envelope of background military and civil design regulations, and also determine how best to achieve simultaneous FAA/CAA/RAI certification. The former was resolved by the publication of a single operational requirement by the joint Italian/UK International Project Team (IPT), set up in London during mid 1981.

Plotting of the appropriate boundary of regulatory design requirements was an equally onerous task, but one which was undertaken predominantly by Industry, although a number of trade-offs could not be determined without support from the IPT.

Overall, the major regulatory standards applicable to the EH101 IDP are:

US Mil Specs/Mil Stds (Italian MoD)
AvP 970 (UK MoD)
FAR Part 29 (Italian RAI and US FAA)
BCAR Section G (UK CAA)
RTCA-D0178A (Software)
JSP 188 (Software)
RTCA-D0160 (EMC)
STANAG 4234 (EMC)

These requirements were set out in the early 1980's and were further supported by in-house standards governing design practice, materiel selection, electrical installation, inter-LRU wiring strategy, supportability requirements, and many other aspects.

Looking beyond the requirements of the IDP it can be expected that new customers may wish to impose alternative regulatory requirements. This may simply reflect the 12 year gap between the baseline standards imposed from the outset and now, or that a new customer might have a different perspective on what constitutes acceptable standards. Such a position has been taken by the UK MoD(PE) in respect of the UK MoD order for the SH. Here, all specific airframe design is being carried out against Def Stan 00-970 (rather than AvP 970), inter-LRU EMC is to Def Stan 59-41, and software is controlled by the latest GKN WHL in-house standard.

To date, the very broad base of regulatory requirements imposed directly by the nature of a joint civil/military programme has proven to be able to robustly satisfy requirements for new standards either by demonstrating equivalence or supporting the argument that their imposition is not value added for EH101.

4. THE INFLUENCE OF MARKET REQUIREMENTS ON DESIGN

The detailed influence of customer requirements, whether they be military operational, commercial or civil aspects based, is vastly complex and well beyond the scope of this paper. Typically these influences would include operational performance/ utility, mass, cost, risk, supportability aspects, preferred materials/suppliers, preferred technology and safety. However, it is both practicable and useful to highlight the key influences which have shaped EH101.

4.1 Rotor Sizing

Critical to the needs of the primary Naval sponsors was, and remains, operation from small ships. This imperative dictated that the rotor could be no larger in diameter than HAS Mk 1 Sea King/SH-3D, or 18.6 m. With the maximum gross take-off mass already targeted at 14+ tonnes, and cruise speeds at, or above, 150 kts this rotor radius constraint was a key design driver. In addition, tip speed had to be kept low to meet future civil noise requirements and fatigue lives needed to be better than 10000 hrs.

The solution has been to use the UK British Experimental Rotor Programme (BERP) blade technology which was able to significantly improve on the HAS 1 Sea King/SH-3D but at a minimum overall mass impact. The production blade is directly derived from the demonstrator programme which concluded with GKN WHL capturing the absolute world speed record for rotorcraft. Without access to this level of performance the rotor would have needed a substantial increase in blade area and attracted a significant mass penalty.

Figure 4 - The BERP Main Rotor Planform

4.2 Anti-torque Device

After consideration of a range of possible alternatives EH101 was configured with a traditional tail rotor but one having exceptional control power in order that the aircraft would have appropriate handling qualities in the vicinity of a small ship in bad weather.

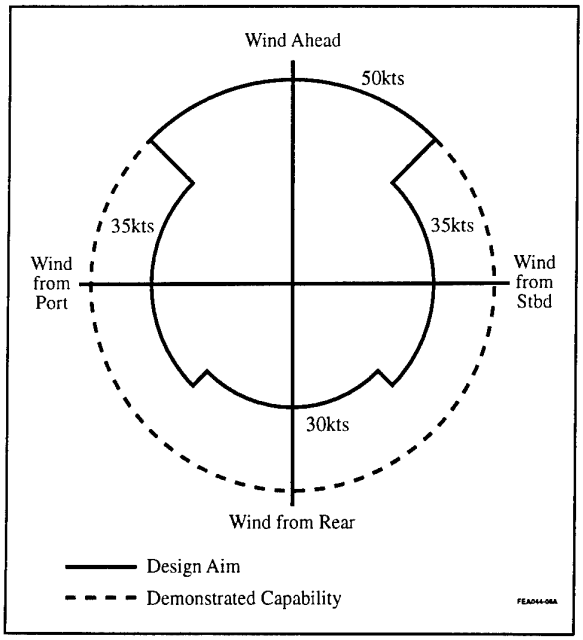

Figure 5 - Wind Envelopes

The tail rotor has a diameter of 4 m and is designed to a maximum transient mast torque equivalent to 1300 HP. The low speed envelope has been flown up to the maximum gross take-off mass of 14.6 tonnes.

4.3 Structural Aspects

At the outset of EH101 design, most rotorcraft experience was with the safe-life principle, where a finite service life is declared for primary structure/dynamics.

Agusta and GKN WHL decided to substantially embrace damage tolerant design for EH101. This technique has been predominantly targeted at a dramatic improvement in safety and mission reliability but these same techniques will also contribute to battle damage tolerance.

The features embodied in EH101 include multiple load paths in the blade attachment and rotor head, widely spaced engines, multiple services powered by separate drives, multiple load paths for transmission attachment, and multiple lift load paths in the main structure. These are perhaps the main areas of damage tolerant design, less obvious are the proven tree strike/ballistic tolerance of the composite main blade, integrated health and usage monitoring system (HUMS), redundant core avionics processing, and the graceful degradation philosophy designed into much of the avionics system.

It is of interest to note that the UK MoD customer has recently embraced the concept of safety assessment which is being retrospectively applied to Merlin and is a requirement for SH. Since the EH101 was already designed to conform with the civil authorities safety case requirements the late imposition of this requirement from the military Authorities has proven to be a straightforward, process.

Definitive low and high cycle fatigue testing of the main load paths has now been completed for EH101, confirming that a safe life of 10000 hrs has been achieved against the military spectrum and a 40000 hrs service life for civil useage is expected.

4.4 Undercarriage

The key requirements for undercarriage design are those deriving from small ships operation. In particular the maximum non-damaging sink rate at maximum gross mass is 11.5 ft/sec and dominates the static strength. Long periods lashed to a heaving, rolling, pitching ships' deck produces a very severe fatigue case. In respect of the civil design cases the undercarriage is significantly overdesigned.

Recognising that the aircraft must have a broad appeal it was determined that the single main wheel arrangement, which suited Merlin operations from hard surfaces, would not be well matched to operations from unprepared sites. Accordingly, the basic design can incorporate a second main wheel if the customer desires. A twin main wheel/balloon type nose wheel solution is adopted for the SH providing a soft field performance significantly better than other similarly roled aircraft.

A/c Type	No of A/c Passes		
	CBR9	CBR5	CBR3
EH101 (SH)	6049	178	8
Mk 4 Sea King	3894	114	5
Chinook HC-1	3156	93	4

Table 1 - Relative Soft Field Performance

4.5 Avionics Systems

The Naval avionics requirements for a highly complex ASW/ASV role are not obviously well matched to civil operators or a battlefield support role. However, some common threads do exist and these have been rigorously followed through in the implementation of EH101.

Both military and civil aircraft require an automatic flight control system, cockpit instruments, and navigation features. Both aircraft also have a requirement to collect and condense sensor/discrete signals. One key difference is that the accepted civil standard data bus is ARINC 429 but the military preference would be Mil-Std-1553B.

For EH101 the chosen implementation has been to utilise ARINC 429 or discrete connections for all common avionic systems and to then marry this to Mil-Std-1553B for the complex military mission fit. Whilst this approach has added some complexity it is considered to be the most effective solution for EH101 given that, to be successful, the aircraft had to appeal to a wide variety of potential customers without recourse to major re-design or significant implementation divergence.

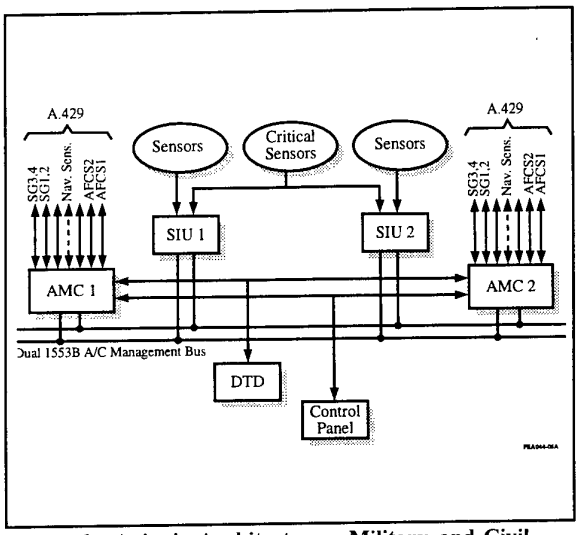

Figure 6 - Avionic Architecture - Military and Civil

Both military and civil customers are particularly concerned by reliability and availability. The EH101 avionic architecture deliberately uses technology to reduce piece part count, assign many functions to software, and promote integration to reduce crew (and maintainer) workload.

Cockpit instrumentation is dominated by an integrated electronic instrument system, comprising 12 key LRUs compared with perhaps 50-60 discrete instruments in HAS 1 Sea King. The AFCS is a fully digital, four axis/four lane, implementation, designed to meet demanding requirements of reliability, integrity, and extended pilot intervention times. Navigation is an integrated combination of inertial, GPS NAVSTAR, radar/radio aids, and air data. This basic core is available for both military and civil implementations. Additional functionality related to aircraft performance, route management, mass/cg management, maintenance management, HUM and data fusion can then be added by either a Flight Management System (FMS) for civil application or dual redundant AN/AYK 204 Aircraft Management Computers (AMCs) for the military architecture. Software has been written in the PASCAL high order language.

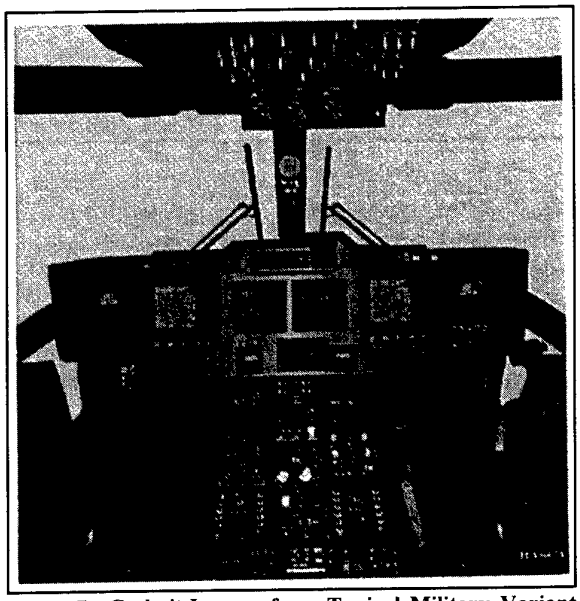

Figure 7 - Cockpit Layour for a Typical Military Variant

The UK Naval Operational Requirement was predicated on the concept of single pilot operation. Whilst this is not directly applicable to civil operations substantial effort has been expended to achieve this goal and the result is that the EH101 cockpit is low workload, with all key functionality available to the right hand seat.

4.6 Cabin Volume

The primary dictate for cabin volume resulted from the market survey undertaken by EH Industries during the early 1980s. It became clear that a 30-32 seat configuration was most appropriate for civil operations and 24-30 seat for battlefield support missions. These requirements were in excess of the minimum acceptable cabin volume required to meet the strict Naval missions. The result for EH101 is a very spacious main cabin of 6.5m long, 2.3 wide and 1.8m high with no obstructions.

4.7 Fuel Volume

All fuel is located below the main cabin floor based on a minimum arrangement of three feed tanks. The option of side pod mounted tanks was rejected at an early stage because this approach was not readily compatible with external weapon carriage and significantly impacted the lower vision plot available from the cabin windows, an important feature of both search and rescue (SAR) and battlefield support missions.

A fuel system installation concept was developed to provide up to six essentially identical fuel bays below the floor, each able to carry some 800 kg of fuel in bag tanks that could be crashworthy and self-sealing as required. Fuel gauging was integrated by a fuel gauging computer which is pin selectable to recognise all likely alternative arrangements. Thus, whilst the EH101 fuel system can be configured to accommodate almost 5000 kg of internal fuel, other configurations can be readily accommodated such that the shorter range operator need not be burdened by the hardware mass, and cost, associated with a 700 nm plus range that may be required by a SAR operator. Ferry tanks can be carried internally to extend the capacity of the fuel system and the configuration of the system fuel gallery is such as to make this an easy role fit.

5. THE INFLUENCE OF REGULATIONS ON DESIGN

During the formative period of the design of EH101, it became clear that a unified and formalised definition of the appropriate civil and military design regulations would need to be prepared. At the same time a similar process was initiated to ensure that the 'in-house' design regulation applied by Agusta and GKN WHL were brought into alignment.

This pro-active approach has meant that the most demanding boundary of regulations were built into the design from the outset. In some cases the differences between civil and military requirements were so significant that a dual track approach was adopted and the configuration allowed to diverge as the most cost or mass effective solution. However, these examples are few in number such that the majority of the EH101 design is entirely common between civil and military versions. The most significant difference is in respect of the certification standard where the regulatory Authorities retain their independence and demand proof of compliance with their own stated requirements.

5.1 Safety Case

Both civil and military requirements have long recognised airworthiness as a key feature of a successful design, and have developed a regulatory approach to ensure that an appropriate design is implemented. However, this approach is further underpinned by civil regulations where numerical safety targets are defined as a key means by which a design audit can be accomplished and reported.

For the civil variant of EH101 it was always clear that a detailed safety assessment would be required to meet the requirements of FAR and BCAR. Lately, military operators have begun to impose requirements for safety analyses to be undertaken, and Merlin initiated this action for EH101 by imposing the requirements of Mil-Std-882, or "equivalent". The actual safety analysis programme implemented is as per the civil regulatory approach for the safety of the aircraft and its crew, combined with a Mil-Std-882 approach to third party safety. Thus, the safety case for Merlin is dominated by a process which identifies safety as a numerical value. The SH programme employs this same approach and the UK MoD has now defined that the report which concludes the safety analysis must be in place prior to first flight and not entry into service.

Once the civil safety assessment was completed in 1994 the Merlin and SH programmes were effectively derivatives which introduced differences in use and equipment fit; both programmes require their own unique reporting but significant savings are expected to be made by basing the work on that previously reported to the civil Authorities.

5.2 Transmission

Generally the civil requirements of BCAR Section G and FAR Part 29 are more comprehensive than the equivalent AvP and Mil-Stds, although the UK military requirement for a factored load test to establish fatigue limitations are much more demanding than the endurance tests identified by FAR and Mil Std requirements. This requirement alone has required the EH101 main transmission to be run at 7000 HP, compared with the 5305 HP take-off placard limit for Merlin.

One specific area of regulation that is better defined by civil requirements is oil loss tolerance where a 10 minute duration is specified. Military requirements are less clear but Agusta determined that the civil requirements should be regarded as a bare minimum and the design has been proven to 30 minutes without modification.

5.3 Main Rotor

The only civil regulation deemed to have influenced the rotor configuration was that relating to noise. EH101 was originally constrained to a tip speed of 670 ft/sec at 100% N_R; during development the nominal rotor speed has been increased to 102% N_R with a subsequent increase in tip speed to 683 ft/sec. The aircraft has been certified as meeting the CAN 7 regulations and has been demonstrated to meet the much more demanding CAN 6 requirements as well. Fly-over noise levels are particularly low, with a margin of over 7 EPN dB against the CAN 7 regulations having been regularly demonstrated.

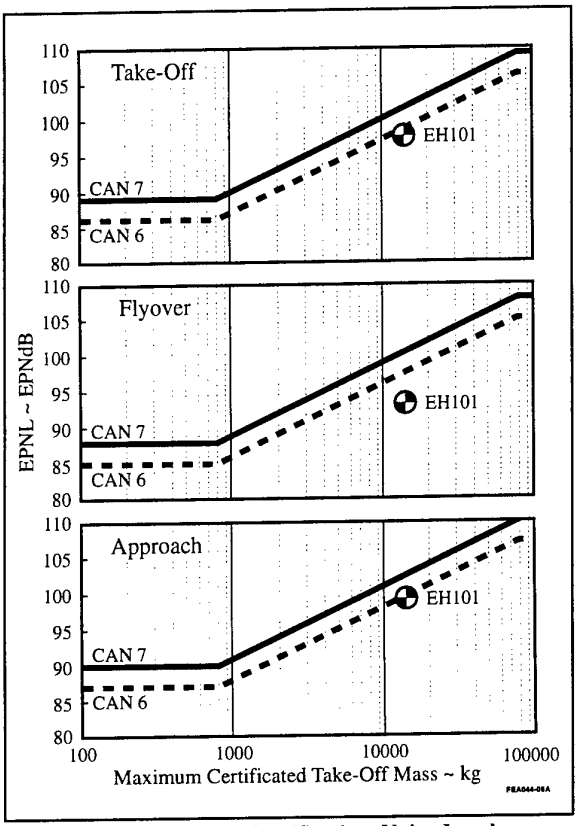

Figure 8 - EH101 Type Certification Noise Levels

5.4 Tail Rotor

The large tail rotor control power demanded by Naval operations has required EH101 to be equipped with a speed sensitive switched yaw pedal limiter so as to pass the demanding civil yaw manoeuvre structural strength requirements. By this means the design case has been reduced from 40° side slip angle at 145 kts to 40° at 120 kts.

5.5 Bird Strike

The worst case requirement was clearly represented by the BCAR requirements for a 1.8 kg bird at 160 kts. Tests have been carried out and the EH101 canopy and associated structure has been certified as compliant with this requirement. To our knowledge this is the most demanding test ever applied to a rotorcraft canopy.

5.6 Ice Protection

A vital operational requirement for North Atlantic Naval operations was to be able to operate in stringent icing conditions. The definition of icing environments is not straightforward and is typically differently described by civil regulations, military airframe regulations, and military engine regulations.

At the time when system design was in-hand the best understood definition was that developed by the UK military Authorities, defined in AvP 970 Chapter 714. The key condition was to be maximum continuous icing whereby EH101 would be designed to operate without a time limit in icing which was the worst likely to be encountered anywhere in the world. This condition is broadly equivalent to FAR 29 App C and BCAR paper G610.

To achieve the required performance EH101 has electro-thermal de-icing of the main blades and anti-icing of the engine intakes, tail rotor, windscreens and pitot/statics. Sufficient electrical power is available to maintain full performance after a single generator failure. Testing in Denmark and Canada has established good confidence that full compliance will be demonstrated.

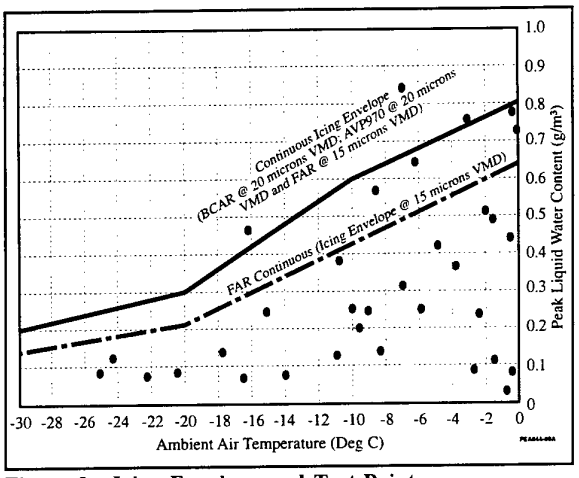

Figure 9 - Icing Envelope and Test Points

5.6 Electromagnetic Compatibility (EMC)

Both civil and military regulations impose severe EMC requirements, pertinent both to the external and inter-LRU environments. From the outset EH Industries determined that it would impose not only the most stringent of the available standards but would also initiate design process controls to impose consistent rigour to the layout of LRUs, the routing of cables, and the establishment/maintenance of inherent screening available from the airframe, even though substantial use is made of composites.

Development of a robust EMC implementation has been taken extremely seriously, to the extent that a non-flightworthy pre-production aircraft was built to provide a fully representative EMC rig as an alternative to the traditional EMC laboratory rig.

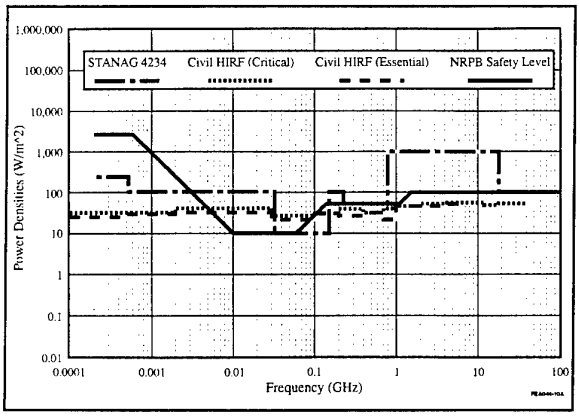

Figure 10 - External EMC Environment

Type certification testing for EMC was successfully completed in 1994. Military testing has placed the pre-production Merlin in the UK Radio-Frequency Environmental Generator (REG) rig at DTEO Boscombe Down to illuminate the aircraft to STANAG 4234 levels, with very good success. In fact the main difficulty experienced was in respect of limiting crew exposure to excessive radiation levels.

Figure 11 - Merlin under test at the REG (Crown Copyright DTEO Boscombe Down)

Overall, EH101 is easily the most EMC hard aircraft ever designed by Agusta and GKN WHL. Testing has demonstrated that the design rigour has succeeded and the required hardness has been achieved with only minor recourse to post design palliative measures. Remaining tests only apply to configuration changes between pre-production and production aircraft.

5.7 Lightning Protection

Requirements for survival of primary effects of lightning strike are similar for both military and civil variants but the civil authorities also demand clearance to indirect effects. Testing has been undertaken using both the EMC "rig" aircraft and flying pre-production assets. Very few problems have been encountered with perhaps the most significant being the traditionally difficult balance between lightning protection and radar frequency transparency of the weather radar radome.

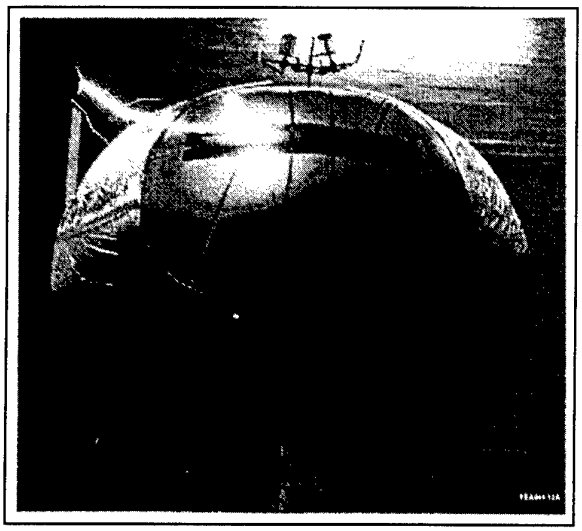

Figure 12 - Lightning Strike Testing of the Civil Nose Radome

6. MANAGEMENT CHALLENGE

The challenges associated with achieving the goal of a joint civil/military design represented only one of many faced by EH Industries as they established a joint Agusta/ GKN WHL programme to implement the £1B full development activity initiated in 1984.

Certain key tasks related to design were established:

a) a joint definition of the appropriate regulatory boundary was established and imposed upon the design from the beginning.

b) the detailed impact of these regulation based requirements on design/test were established by a single partner (according to workshare) but only promulgated after joint agreement.

c) a certification/qualification programme was established specifically aimed at the requirements of the civil/military authorities.

d) close liaison with the certification/qualification bodies was established early and maintained rigorously throughout the programme.

During the latter period of civil certification a substantial joint Agusta/GKN WHL effort was established and managed by EH Industries to ensure that design/test data were presented to the Authorities in a complete and timely manner. A similar task is currently nearing completion for the IDP military qualification.

The lessons learnt during this process can be summarised as a need to be ruthless in the flow down of requirements into design, to explicitly target testing at well defined goals, and to involve the Authority early to the overall process. All of these aspects have featured in the programme to date but further emphasis would do no harm.

Use of modern IT, such as in the form of computer aided systems engineering (CASE) tools, will help in the future to plan and manage the extensive design/certification/qualification task demanded by the civil and military Authorities and to manage design change. This has been adopted from the outset for the SH, is partially adopted (for the core software functionality) for Merlin, but was not grasped sufficiently for IDP except in that the management of certification/qualification data makes extensive use of distributed relational data bases.

IDP military qualification requires proof of compliance to be established for some 9500 line items; civil certification demanded attention to 7000 line items and the SH will have 2500 line items.

Closely associated with achieving a certified/qualified design is the actual as-built standard of the aircraft and its systems. All of the pre-production fleet were designed and built using a form of configuration control which was flexible but which ensured that the build standard of any aircraft could be established at any time. For production, EH Industries initiated a configuration management system (CMS) in accordance with STANAG 4159, Def Stan 05-57 and AER00-00-5/-6; the resulting process adopted is broadly equivalent to Mil-Std-973. The purpose of CMS is to ensure that changes to the functional baseline can only be introduced with deliberate effort such that all impacts are rigorously understood before a change is initiated and the build standard remains well defined at all stages. With hindsight this process has proved to be a significant burden in respect of the build of the initial production aircraft and would perhaps be better suited to the stable long term product. The main difficulties have been with the process time necessary to agree even minor change, much of which has proven essential and not just a design enhancement. However, overall the key statistics look encouraging in that the first production aircraft flew 9 days early and that the number of changes per issued drawing is around 2.4 compared with an accepted industry norm of perhaps over 3 at this stage.

7. IMPACT OF COMMON CIVIL/MILITARY DESIGN

The overall impact to the EH101 programme of achieving its goal of an integrated civil/military design and development programme is to some extent speculative but it is possible to identify the order of mass burden that has resulted.

Considering the key configuration impacts discussed above then the following can be concluded:

a) The rotor system already achieves a minimum mass solution but can only provide the required performance by application of the sophisticated BERP aerodynamic technology. Using a more traditional level of technology a rotor of the same radius would need additional blade area and that would have dramatically driven the rotor mass upwards.

b) Meeting the civil noise regulations demanded a slow tip speed, although BERP already exhibits the useful planform characteristics of swept thin tips. Extrapolation of the BERP performance by reference to the Lynx fit, including the world speed record experience, would indicate that a tip speed some 800 ft/sec is practicable (if noisy) and if implemented could have saved over 200 kg of vehicle mass.

c) The fuselage structure meets all of the appropriate civil requirements for crash, bird strike, fatigue, flotation and fire proofing. Generally, these requirements are similar to or more severe than the military equivalent and a mass penalty of some 200 kg can be assigned to these aspects.

d) Achieving a true damage tolerant design is somewhat more difficult to assess in that this approach pervades the main structural load paths and all key services. It has been estimated that the penalty of damage tolerance is as high as 300 kg.

Thus, overall EH101 is carrying some 700 kg of mass penalty in comparison with a purely military design using design regulations extant in 1980. If a military design were to be initiated today then it is certain that many of the safety features previously ascribed to civil requirements only would have to be accommodated.

In addition to the penalties of meeting civil regulatory standards, EH101 is designed to achieve significant improvements in overall vehicle performance when compared with previous generation helicopters. The increase in useful speed to above 150 kts, non-damaging descent speeds of up to 11.5 ft/sec, and the achievement of a full 3g manoeuvre case have all added to the structural mass. When compared with Sea King/SH-3D it has been established that improvements to performance of this nature have directly resulted in a mass increase of some 1400 kg.

Thus, overall EH101 suffers a mass penalty of around 2000 kg plus so as to meet the contempory performance and regulatory demands of both military and civil operators. The maximum gross take-off mass for EH101 is (initially) 14.6 tonnes; a fully equipped para-military/military Utility Variant would have an aircraft empty mass of between 9000 and 9500 kg depending on mission fit; the payload fraction can be expected to range from 40% to 35%. A similar payload fraction range is evident for NH90 and S92 on the basis of data available in the public domain.

Whilst EH101 is the first large rotorcraft to be designed to meet combined civil and military regulatory requirements it will not be the last. The attraction of inherent safety, improved performance and cost effectiveness is probably irresistable to operators, procurement agencies and Industry alike.

8. THE PRINCIPLE OF CUSTOMERISATION

The EH101 has been granted a joint FAA/CAA/RAI certification and the military qualification is progressing to plan. In every sense the realisation of a common civil/ military design has been achieved. However, it has always been recognised that not all mission specific features could be sensibly incorporated into a truly common airframe. The ramp door of the Utility Variant is a good example where the value of this feature to the Naval ASW/ASV role would not compensate for its mass penalty.

EH101 is available in four basic variants resulting from the IDP; military ramped and non-ramped (nominally Naval) and an equivalent civil pairing. This variation is not sufficient to define the full range of possible customer specific requirements and it is expected that the military customer in particular may well have substantial need for avionic and defensive aids specifics.

It is useful to review the most recent customerisation tasks undertaken, associated with the SH Variant which is configured to suit the RAF requirements of battlefield support, special forces operations, SAR, and other duties.

SH specific configuration aspects include the following:

a) integrated underslung load (USL) hook, rated at 5400 kg.

b) strengthened floor to permit internal loading of high density cargo.

c) four tank fuel system, configured to have minimal impact on longitudinal CG as fuel is used and integrated with a probe/drogue style of air-to-air refuelling.

d) crashworthy troop and crew seats, total cabin seating is 26.

e) a sophisticated, secure, communications fit having integrated electronic counter measures (ECCM), and coverage between 2 MHz and 400 MHz operating frequency.

f) a comprehensive defensive aids suite (DAS) fit.

g) enhanced HUM able to monitor the health of all transmission gears/bearings/ shafts, the status of engine vibration, and the full time assessment of rotor track and balance; data capture is fully automatic, with a manual override capability.

h) a full NVG compatible lighting fit.

i) a role fit forward looking infra red stabilised sensor.

All of these specific features require design and development action but the basic core vehicle and system design is proving sufficiently robust such that the changes can be accommodated with relative ease.

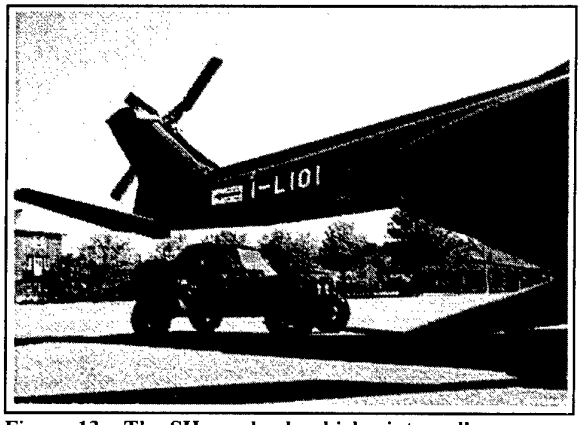

Figure 13 - The SH can load vehicles internally

Avionic system changes require integration of the all new (to EH101) communications via the Mil-Std-1553B data bus, an all new digital secure intercomm and revision of certain core management software. Whilst these tasks include some significant EMC/TEMPEST installation aspects, the EH101 design standards developed at the outset of the IDP have established a proven basis for a low risk solution. Functional integration requires software modifications which are being introduced in concert with other management function changes, integrated into a single core software release. To meet a set of demanding computer resource requirements an updated AN/AYK 204 computer will be utilised having a 486 processor to give enhanced throughput and memory allocation; this change impacts the processor card only, allowing the basic LRU structure and qualification standard to be retained.

Aircraft systems are not being modified except that load shedding arrangements in the face of a generator failure, whilst operating in icing, will be less restrictive than Merlin because either of the two 90 KVA generators can easily supply all of the electrical demand for the simplified avionic fit demanded by the SH.

To meet the RAF requirements for hot and high take-off, fully equipped, with an out of ground effect (OGE) thrust margin of 5%, two further significant specific features have been introduced. Firstly the main transmission placarded take-off rating has been lifted to 112% torque, or 5520 HP, and secondly a derivative of the RTM 322 is being implemented, configured to provide both an enhanced take-off rating and a 20 second emergency rating. The former will be qualified by testing alone, since the overall SH usage is similar to Merlin and the transmission has already successfully completed basic testing including running at over 7000 HP. For the engine, design effort is required to allow the power turbine inlet temperature to be increased but these changes are not technologically challenging as demonstrated by the first major engine chamber test occurring within 9 months of contract effective date.

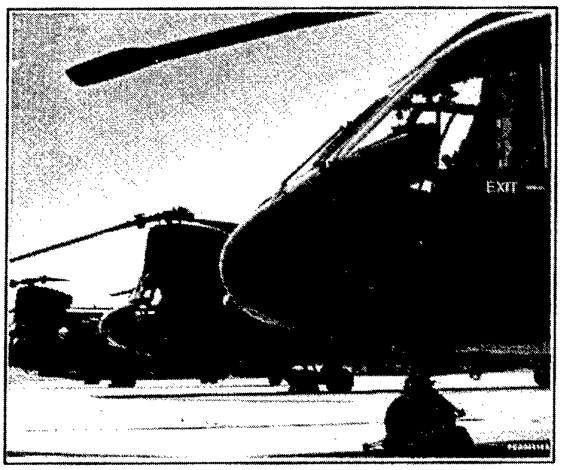

Figure 14 - The changing shape of the RAF SH Fleet

9. CONCLUSION

One of the most significant precepts of the EH101 programme was the deliberate intent to produce a single aircraft and system design able to satisfy the operational and regulatory requirements of both civil and military customers. The aim of a totally common approach has not been achieved mainly for reasons of cost or mass effectiveness, but there is an essential and substantive core which is common.

Joint FAA/CAA/RAI certification was achieved in 1994 which was the culmination of a process started ten years earlier with preliminary design and as yet stands as a unique achievement amongst rotorcraft. Military qualification will be completed in respect of the IDP in the immediate future leaving only customerisation changes for Merlin, MMI and SH derivatives to be undertaken separately.

The first production aircraft, Merlin, flew in December 1995 and was formally delivered on 6th March 1996 having completed its basic test flying. The first production civil aircraft will be granted type certification in 1997 and delivered to its customer in 1998.

EH101 has vindicated the principle that it is feasible, cost effective, and operationally valuable to merge the civil and military regulatory requirements into a basic common rotorcraft design. With the recent moves by the military customer towards civil standards of safety this process is probably inevitable for future rotorcraft.

The approach is not without penalty, and payload fraction will tend to decline with the next generation of general purpose helicopters until improved rotor, engine, transmission and avionic technologies can be assimilated into the product.

From a programmatic sense, the biggest improvement that could be established over current practice would be for the civil and military regulatory authorities to merge their effort. In this way it would be possible to envisage that a common design could be assessed against a common set of certification/qualification rules by a common civil/military Authority. Such an approach would dramatically simplify the task faced by Industry, reducing costs and programme timescales significantly, and also present a much reduced overall burden to the Authorities.

10. ACKNOWLEDGEMENTS

The author would like to acknowledge the assistance of EH Industries, Agusta Spa, and the MoD(PE) Project Offices for Merlin and Support Helicopter in the prepartion of this paper.

COMPOUND INTEREST - A DIVIDEND FOR THE FUTURE?

D V HUMPHERSON
HEAD OF ADVANCED PROJECTS DEPARTMENT
GKN WESTLAND HELICOPTERS LIMITED
Box 255, YEOVIL SOMERSET BA20 2YB, UK

1. SUMMARY

This paper seeks to explore the application of thrust and lift compounding as a cost efficient development of the traditional helicopter.

The principal deficiencies of the edgewise rotor are examined and the use of compounding to overcome these limitations and enhance rotorcraft capabilities, is developed.

Potential missions suitable for the various types of compounding and the concept of a family of vehicles to cover a wide variety of applications are discussed.

A possible technology demonstrator, based on a Lynx airframe and its build standard are described. Finally a list of overall conclusions are drawn.

2. LIST OF ABBREVIATIONS

ACH	Advanced Compound Helicopter
AWACS	Airborne Warning and Control System
BVI	Blade Vortex Interaction
LCC	Lift Cycle Costs
MoD	Ministry of Defence
NoE	Nap of the Earth
OA	Operational Analysis
PV	Private Venture
SAM	Surface to Air Missile
SAR	Search and Rescue
SOT	Stator Outlet Temperature
TAS	True Air Speed

3. INTRODUCTION

It is widely held that before a problem can be solved, it must be defined. Experience has similarly confirmed that it is advisable to define the term compounding at the earliest opportunity in any discussion on the topic. Therefore, as used in this paper,

- Lift compounding involves the addition of a second, separate source of lift in addition to the main rotor.

and,

- Thrust compounding involves the addition of a second, separate source of thrust in addition to the main rotor.

There have been many attempts, over the years, to produce a viable compound helicopter and a number of designs have flown; some with considerable success. Despite this, apart from a few Soviet types which appeal to a degree of lift compounding (eg. MIL24), the technique has yet to be embraced for an operational helicopter. It is almost certain that there is no one single cause for this, but that in practice the reasons are numerous and some of the technical ones are identified later.

The principle of compounding may be traced back to the earliest days of rotorcraft, when pioneer autogyros and helicopters were frequently equipped with wings and propellers. By definition, an autogyro requires a source of propulsive thrust to complement its lifting rotor and hence will always be thrust compounded. Although this form of rotorcraft was superseded by the more versatile helicopter, there is some evidence to suggest that the autorotating or partially offloaded rotor offers improvements in the equivalent lift to drag ratio. It is the promise of superior values of airframe efficiency, from this and other sources, that is at the heart of the benefits of compounding. To consolidate this there would also appear to be further advantages, including reduced vibration and lower noise signatures, that will be explored later in the paper.

Whilst the basic physics of compounding have always been open to exploitation, the details of the process are still imperfectly understood. In addition to this, it is only as the understanding grows that it is becoming apparent the enabling technologies have always been lacking or incomplete.

Clearly these two considerations are interdependent and it is only now that a path is emerging whereby, on the one hand we believe we are starting to understand the process and its application sufficiently well, whilst on the other hand the necessary technologies to fully exploit compounding are in sight of maturity.

It would thus appear that a significant opportunity to progress the cause of rotorcraft is about to present itself, should we care to grasp it.

4. BACKGROUND

The interest in compounding at GKN Westland Helicopters Limited emerged in the early 1980's when attention turned to researching future rotorcraft designs that would offer substantially enhanced performance. The exercise was not initially couched in terms of specific applications but was more concerned with a debate into the fundamental issues.

Overlying the technical arguments has been an acceptance that any future research programme, whilst being adventurous conceptually, could not be adventurous financially. This was especially true for a relatively small organisation such as the then Westland Helicopters and was influential in the choice of lift and thrust compounding as the way forward. There was also a powerful argument that said that we should build on what we knew; evolution not revolution.

Although it is not believed to have been directly linked, since its evolution had different roots, the emergence of the BERP blade has very ably complemented the compound concept, in that it has generated a very capable rotor over the entire flight envelope, especially at high forward speeds.

It is important that the rotor remains aerodynamically efficient over the extended flight envelope, despite being offloaded, if the fundamental advantages of the technique of compounding are not to be squandered.

Paper presented at the FVP Symposium on "Advances in Rotorcraft Technology", held in Ottawa, Canada, 27-30 May 1996, and published in CP-592.

The concern for improvements in platform performance was underlined by a belief that this aspect of rotorcraft development had largely stagnated (with the exception of a few initiatives such as BERP). The helicopter appears to have been regarded as essentially an air vehicle geared to hover/low speed flight since it accomplishes this in a more versatile manner than any alternative. There has been a great deal of attention paid to the systems elements of helicopter projects over the last two decades to the point that it may now be argued that platform performance is inadequate to fully exploit the real potential of the total weapons system in some circumstances.

In addition to this it was becoming clear that rotorcraft applications were likely to broaden and more emphasis would be laid on quantities such as productivity and timeliness of response. Such issues were believed to be of relevance to both civil and military roles even though the exact character of these roles might differ.

Overall it may be concluded therefore, that compounding should be examined as a serious candidate for future rotorcraft development.

5. LIMITATIONS OF THE TRADITIONAL EDGEWISE ROTOR

Many of the deficiencies associated with the edgewise rotor stem from the asymmetry inherent during forward flight, as illustrated in Figure 1.

Whilst many palliative measures have been adopted in attempts to ameliorate the consequences, the underlying mechanism remains.

One consequence is the need to preserve rotor trim in forward flight. This in turn leads to the falling rotor thrust characteristic, as forward speed rises and is illustrated in Figure 2.

The situation is exacerbated by the need to generate a propulsive component of thrust in a conventional helicopter, by tilting the rotor disc nose down. This further complicates the local flow field round the blade in addition to the azimuthal variations noted above.

A range of vehicle limitations follow from the constraints imposed by the rotor. Perhaps the most prominent of these limitations emerge as,

- Poor lift to drag ratios.
- Limited forward speed capability.
- High vibration.
- Poor high speed agility.
- Uncompetitive productivity.

6. ADVANTAGES OF COMPOUNDING

It is to these problems that compounding is addressed with a view to enhancing fundamental vehicle characteristics. Although at the present time data is limited there is reason to believe that the rotor lift to drag ratio, ie. its intrinsic aerodynamic efficiency as a lifting device, may be significantly enhanced by operating with thrust and/or lift compounding.

The optimum rotor operating condition would appear to be in partial autorotation, as illustrated in Figure 3. This does imply the need for thrust compounding to supply the propulsion deficit. A further contribution arises from considerations of safety. When offloaded, the rotor may be operating outside its conventional, 'lg', flight envelope. In the event of rotor power failure then it is conceivable that successful autorotation entry, from these flight conditions, may not be possible. This is especially true for a vehicle with a good lift to drag ratio and measures are likely to be necessary to degrade this temporarily eg. by the use of speed brakes.

The dilemma is avoided however, if the rotor is in autorotation in normal cruise flight. In this situation engine failure becomes an inconvenience and not a threat to continued safe flight.

The data in Figure 3 is the result of some recent investigations into high speed autorotation undertaken at GKN Westland Helicopters, as part of an MoD funded study.

It is interesting that the benefits emerge as a power saving and become most apparent at high forward speeds when the propulsive efficiency of the rotor is also much reduced. At low forward speeds the rotor generates propulsion very efficiently, but this clearly reduces as speed rises.

At speeds approaching the upper edge of the conventional helicopter flight envelope (circa 200 + knots), it may be seen that the effective rotor propulsive efficiency is about the same as might be expected from a typical fan or propeller auxiliary propulsion device. Hence such a device becomes competitive in terms of power consumption. As the forward speed rises still further the situation becomes more advantageous and significant total power savings are indicated, such that thrust compounding would appear to be the best solution for helicopter flight under these conditions.

A similar situation arises from the application of lift compounding, although here the details are slightly different.

In essence the rotor may again be offloaded, by for example a wing, with gains in reduced vibration and an expanded flight envelope.

Studies have identified high altitude, low speed missions as reaping particular benefit. In this flight condition the rotor can supply propulsive thrust efficiently and without excessive disc tilt, so that lift only compounding may prove appropriate.

At other flight conditions lift compounding is best combined with thrust compounding and offers great potential for applications where excellent high speed agility is demanded.

In continuous high speed cruise it is also possible to take advantage of the superior lift to drag ratio of a suitably designed wing to enhance the overall aerodynamic efficiency of the total vehicle. Experience has shown, though, that great care is required in design to extract full advantage from this process.

Offloading the rotor, both in terms of lift and propulsion will also extend the forward speed capability by relieving the retreating stall boundary.

Typical trends of aircraft mass with forward speed to accomplish a given mission, for conventional and compound helicopters are shown in Figure 4 where speed and mass advantages are apparent for the compound.

For a given flight condition, the level of vibration may be expected to reduce as the rotor is offloaded and operated at a less nose down disc attitude. This arises at least in part from the reduced aerodynamic forcing associated with lower thrust levels and more benign local flow conditions.

It is anticipated that reductions in vibration will lead to significant improvements in mission effectiveness due to reduced crew fatigue and much enhanced reliability of both airframe and equipment. In the course of recent studies, efforts have been made to quantify these benefits.

A credible methodology has been evolved and this has identified Life Cycle Cost savings via maintenance reductions. Little success has been achieved to date, however in linking actual levels of vibration to actual levels of unreliability. Whilst data exists in service records, when a detailed reduction of the information was attempted it was apparent that the data was too sparse to draw definite conclusions. It is clear that further work is necessary in this area, although even at this stage it can be predicted with a measure of confidence that the technique of compounding can lead to reductions in Life Cycle Costs.

The combination of improved lift to drag ratio and the potential for higher cruise speeds offer the prospect of significant gains in productivity so that fleet sizes to achieve a given objective are much reduced. In this connection, the drive for improved lift to drag ratios should also encompass classical drag reduction measures that would apply to any rotorcraft. The benefits associated with compounding are available in addition to this. The higher speed potential of compounded helicopters means that total drag reduction is of greater benefit than for their less speedy conventional counterparts in arriving at fuel efficient, productive designs.

The redundancy of forces and moments available in a compounded rotorcraft offer the ability to trim the vehicle to a given attitude over a wide range of flight conditions. This has several advantageous consequences for both civil and military operations.

Perceived noise levels in both cruise and approach phases of flight may be managed to reduce nuisance and obtrusiveness. The reduced disc tilt in cruise flight means that the acoustic signal travels further and hence suffers more atmospheric absorption, before reaching an observer on the ground. For situations where the vehicle is cruising at medium altitude, then flight test experience has indicated that the noise nuisance is extremely low.

During the approach to land, the vehicle trim may be managed to avoid BVI (blade slap) over a wide range of approach angles. Hence this most intrusive form of helicopter noise may be minimised.

Both passenger and crew comfort may be maximised by maintaining a horizontal fuselage attitude throughout the flight. In the military context the ability to trim the fuselage axis also has great significance in terms of target acquisition, target tracking, weapons release and NOE flight. The total impact of these latter capabilities has yet to be fully investigated.

7. AVAILABLE EVIDENCE

A limited amount of data exists to support the above beliefs and some flight test evidence is shown in Figure 5. This was recorded during the World Speed Record Flights of G-Lynx. The much reduced vibration levels are also associated with the very low value of aircraft drag and hence much improved aircraft lift to drag ratio. Although this process could apply to all conventional rotorcraft there are limits associated with practicality. The introduction of compounding would extend any benefits yet further. Depending on how the force accounting is performed, it may be convenient to regard thrust compounding as a very effective form of drag reduction.

Although a number of compound helicopters have flown, there is not a large body of supporting evidence readily available to underwrite future applications. In part this may have been due to the nature of flight test experimentation and equipment procurement at the time of the relevant research programmes.

Latterly, as part of funded studies sponsored by the UK MoD and PV work by GKN-WHL, efforts have been made to establish data relevant to the application of compound helicopters to a wide range of missions. This work is furnishing mounting evidence to guide the best use of those enhancements offered by the technique of compounding.

During the course of these studies it has become increasingly clear that the benefits available range over a wide spectrum and need thoughtful implementation to fully exploit this major opportunity for rotorcraft technological development.

In addition to the improvements in fundamental vehicle qualities sought at the outset, which ultimately find expression in operational analysis studies, there are also advantages to be gained from other beneficial characteristics, as outlined earlier.

It is interesting that the OA studies also suggested that for many missions, while direct combat is not necessarily sought, escape and hence survival, from an encounter with the opposition is heavily influenced by superior capability in the area of combat flight performance.

A wide range of roles have been investigated to date, with encouraging results.

8. FUTURE APPLICATIONS

Whilst helicopters have already been adopted for roles, such as anti-armour that could be labelled as aggressive, the general tenor of their operations has tended to reflect a measure of vulnerability and/or limitation.

Technological development in general and compounding in particular are lifting the helicopter to the point where it might conceivably become regarded as amongst the more aggressive elements in the military inventory.

Modern weapons and sensors are extremely effective and confer great accuracy and destructive power. It is no longer necessary for a vehicle to weigh tens of tons in order to transport powerful weaponry.

In addition, the enhanced platform speed, productivity and agility of the ACH mean that maximum use may be made of this

burgeoning lethality. It is now possible to position a weapon system of fearsome power and possessing great speed of response in otherwise inaccessible situations. At the same time it does have to be acknowledged that no rotorcraft will ever be totally invulnerable to counter attack, but the ability of the ACH to rapidly seek available cover via agility and minimise exposure to danger via speed represent a unique combination of qualities that contributes to a maximum chance of survival in hostile conditions.

In addition to the OA results themselves, the studies also confirmed that the application of compounding to a given role is an iterative process. Not only does the vehicle need to be appropriately configured, but there is also a corresponding optimum mission profile. Clearly these two processes are not necessarily independent and to date only existing mission profiles have been employed. The next phase of study will endeavour to identify mission profiles appropriate to compounds and further optimise the vehicle configurations.

It is likely that the type of compounding and possibly its implementation will be matched to specific roles (or groups of roles). High altitude, low speed missions, which as noted earlier favour lift compounding, are an example of this process.

In contrast, hover dominated missions, are not best served by lift compounded vehicles, due to the penalty of wing download.

Those roles that combine low speed/hover and high speed dash requirements, such as SAR, etc. are well suited to thrust only compounding.

For cruise dominated applications such as off-shore oil support, then the improved lift to drag ratio of a wing and superior high speed propulsive efficiency of a dedicated propulsor can combine to mean that a lift and thrust compounded solution offers very worthwhile overall benefits. This configuration may also be well matched to applications, such as escort, where it may be speculated that at some time in the future high speed agility and sufficient speed to regain the convoy after an engagement, will become crucial.

As presently conducted, reconnaissance involves a great deal of hover/low speed flight and is well suited to a conventional helicopter though requirements for increased speed of response or higher productivity could modify this finding.

It is also clear that the enhanced capabilities afforded by compounding offer the opportunities to expand the range of roles that may be undertaken by rotorcraft. This reinforces the concept of a family of helicopters, eg. conventional variants, lift compounded variants, thrust compounded variants, etc., with a high degree of commonality, but offering a great overall range of versatility.

The aim will be to achieve a level of this commonality such as to generate considerable savings in design, manufacture, logistics, maintenance and training. At the same time the total asset, ie. the complete range of vehicles and systems would represent a large increase in capability over and above that available today. A further extension of this process arises from the ever increasing capabilities of the subsystems, ie. weapons, sensors, flight control systems, etc. The combined effect is to confer significant improvements in total system performance such that appropriately equipped rotorcraft can now be considered for applications for which they were not previously believed to be adequate. The nett result is that rotorcraft could be applied to a greatly expanded spectrum of roles and offer unrivalled effectiveness in accomplishing them. It is felt that this family concept is ideally suited to the evolving philosophy of regarding low level airspace as the third dimension of all aspects of the ground battle. This is helicopter territory; in particular it is compound helicopter territory.

In the course of the operational analysis studies certain novel roles for the ACH suggested themselves though none of these have been followed up in detail nor do they reflect official interest. One, possibly contentious thought involves a mission denying airspace over the battlefield to fixed wing combat aircraft. It may be possible to conceive of circumstances in which the initiative lies firmly with the helicopter. Dissemination of information about the digital battlefield will be extensive and rapid. It follows therefore that details of incoming fast jet flight paths could be made available to air combat ACH's from a multitude of sources including AWACS. Suitably placed ACH's could then select covert launch positions for air to air weapons in much the same way that current SAM systems operate, albeit with much greater flexibility than the ground based units. The expanded flight envelope of the ACH means that the opportunities to successfully deploy in the manner outlined above are much increased.

Whilst the above may be regarded as provocative and will hopefully act as a stimulus for debate, it is a good example of the mechanism whereby enhanced platform capability may make available a new dimension in vehicle applications, which the relevant military specialists can then exploit.

The real challenge here is to understand how to use this new total capability most efficaciously, since clearly there is again some feedback into vehicle design.

Studies to date have also indicated that compounding can represent the simplest (and probably the cheapest) development route to a given level of system performance.

A final advantage of the underlying philosophy arises from the robustness of the total family approach. The specification of new vehicle and system requirements has always been challenging particularly with the need to retain competitiveness over a long period of time. Today with the prospect of greatly extended service lives for the platform, the speedy evolution of systems technology and the rapidly changing nature of both military and civil needs, the problem is doubly difficult. Hence the increasing requirement is for new equipment to be adaptable and conceptually robust. In this regard the technique of compounding allied to the idea of a family of helicopters offers the prospect of addressing this challenge in an elegant and cost effective manner.

9. PLANNED DEMONSTRATOR

Much effort is currently being channelled into studies to examine the need for the construction of a Technology Demonstrator, based on a Lynx Airframe.

The Lynx was chosen as being an eminently suitable candidate aircraft on several counts, including the fact that it had already flown at speeds approaching 220 knots. As a result of this flight test experience it was known that the behaviour of the aircraft under these conditions was very satisfactory and the risks associated with further expansion of the flight envelope were minimised. Indeed it was initially planned to use G-Lynx, the aircraft which gained the World Speed Record in August 1986, since considerable preparatory work had already been implemented on this vehicle, especially in terms of drag reduction. This plan, however, has been overtaken by events and the aircraft now languishes in a museum.

To improve the speed of a Lynx by something of the order of 50% over and above service release clearly implies a substantial increase in installed power.

Rolls Royce plc have been partners in this ACH study from the very early stages and the RTM 322 engine, which they manufacture in conjunction with Turbomeca of France, offers the required level of installed power.

A happy chain of circumstances has conspired to make the installation of these much more powerful engines a relatively simple and straightforward matter.

The Lynx gearbox was developed for installation in the W30 series of aircraft and the 30-200 variant flew with General Electric T700 engines. Fortunately for the demonstrator project, the RTM322 has been designed to the same interface criteria as the T700. Hence it is possible to mount the W30-200 transmission straight onto the Lynx airframe and install RTM322 engines with a minimum of re-engineering.

For the purposes of demonstration a simple, light, low cost and low risk solution was sought to the provision of propulsive thrust.

To meet this requirement, Rolls Royce has designed a variable area nozzle to fit onto the back of the RTM322 engine. Since the RTM322 generates shaft horsepower in excess of the Lynx rotor requirements, the variable area nozzle serve to extract excess gas energy in the form of jet thrust.

By manipulating final jet area and SOT, ie. throttle setting, it is possible to generate a wide range of combinations of jet thrust and shaft horsepower throughout the flight envelope. Thus it is possible to implement various degrees of thrust compounding.

Similarly, the installation of a wing equipped with trailing edge flaps, would provide for lift compounding. The optimum balance of lift between the rotor and the wing will vary with the required flight condition. For example maximum 'g' manoeuvres and cruise at best specific range will demand greatly differing strategies. The wing contribution can be provided by an appropriate combination of incidence and camber (ie. flap setting). Indeed we would expect these quantities to vary even in a given flight regime. For example, as fuel is burned during cruise, the aircraft weight reduces and the optimum lift balance will change.

The initial view of the demonstrator is that the vehicle will not be fitted with a comprehensive flight and engine control system to manage these strategies such as will be demanded for efficient operation of a production aircraft. Indeed one element of the demonstrator programme will entail the acquisition of data to enable the design of exactly such a future control system. It is likely that the wing will be also complemented by a trimming tailplane to react the powerful pitching moment arising from the flaps and a trimming rudder will offload the tail rotor in trim.

The overall configuration of a possible Lynx demonstrator is shown in Figure 6.

Initial studies have indicated that adequate control of both engine and airframe, for demonstration purposes, can be achieved by modification of the existing systems. Considerable thought has been applied to the nature of such changes both to understand failure modes and to minimise the requalification of flight critical systems. For example, extra hydraulically powered controls will not be used. This avoids breaking into the existing hydraulics circuit supplying the flight controls, which are preserved unchanged. Adequate control power is available in all three axes from the existing controls, though as indicated earlier pitch and yaw trim via aerodynamic surfaces will be added.

10. ACKNOWLEDGEMENTS

This work has been carried out with the support of the Directorate of Future Systems (DFS(Air)) at the UK MoD(PE). The Author would also like to acknowledge the help and advice offered by colleagues at DFS(Air), Rolls Royce plc and the GKN Westland Group in the preparation of this paper.

11. CONCLUSIONS

- Compounding offers a route to improving the fundamental platform characteristics of the helicopter, for example,
  - Lift to drag ratio
  - Propulsive efficiency
  - Noise
  - Vibration
  - Vehicle attitude
- These improvements are available at low cost and low risk, via a process that builds on what is known,
  - Evolution not revolution
- Compounding provides a more versatile vehicle applicable to a wider range of missions, including tasks for which the helicopter was previously judged ineligible.
- The overall result should be
  - Better productivity
  - Better LCC
  - Wider flight envelope
  - Larger market

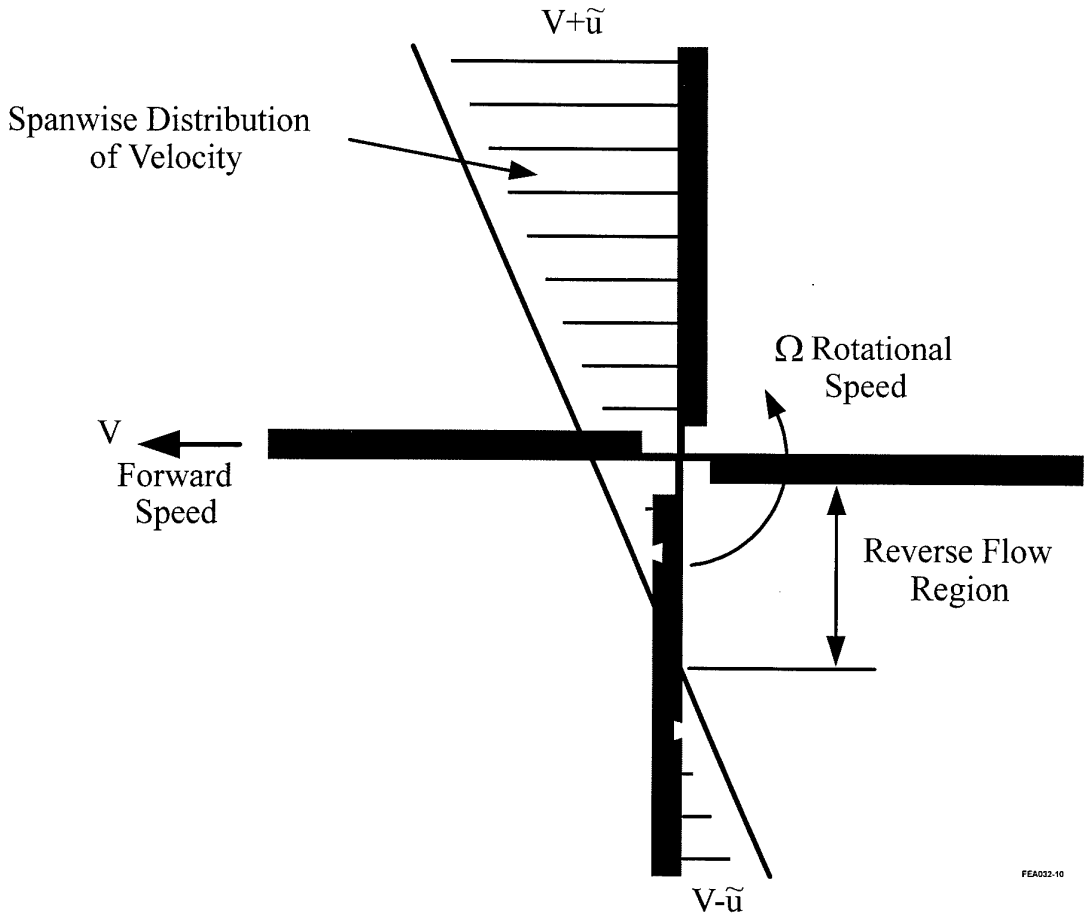

FIGURE 1

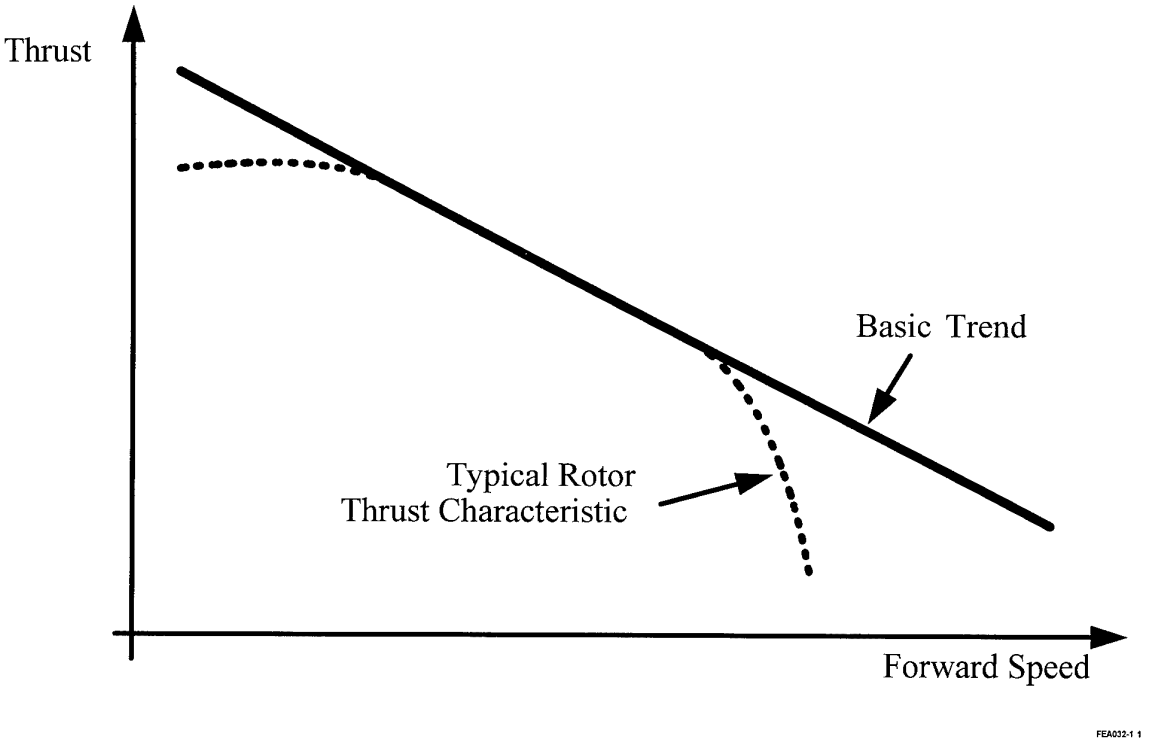

FIGURE 2

FIGURE 3

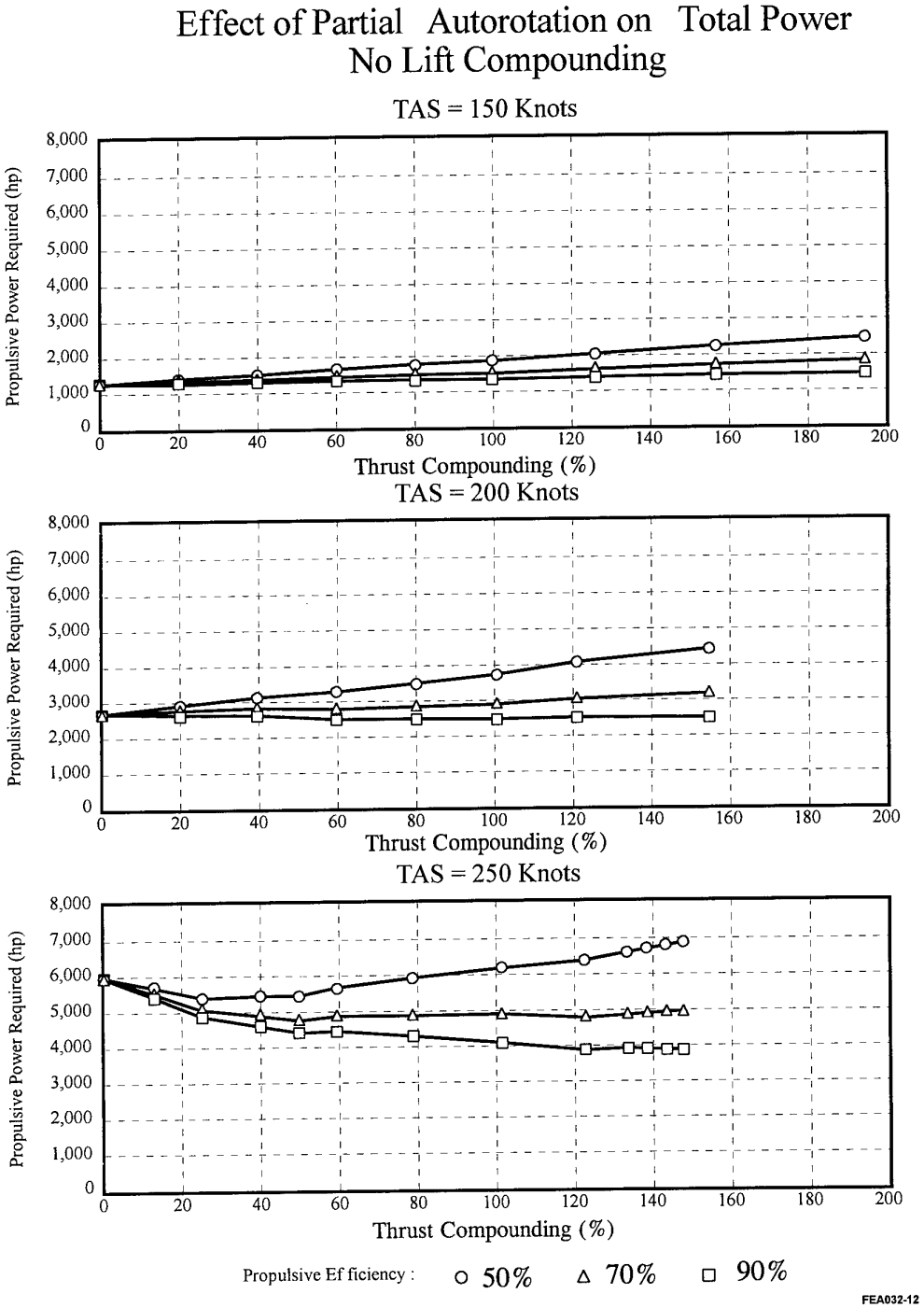
Effect of Partial Autorotation on Total Power
No Lift Compounding
TAS = 150 Knots
Propulsive Power Required (hp)
8,000
7,000
6,000
5,000
4,000
3,000
2,000
1,000
0
0 20 40 60 80 100 120 140 160 180 200
Thrust Compounding (%)
TAS = 200 Knots
Propulsive Power Required (hp)
Thrust Compounding (%)
TAS = 250 Knots
Propulsive Power Required (hp)
Thrust Compounding (%)
Propulsive Ef ficiency : ○ 50% △ 70% □ 90%
FEA032-12

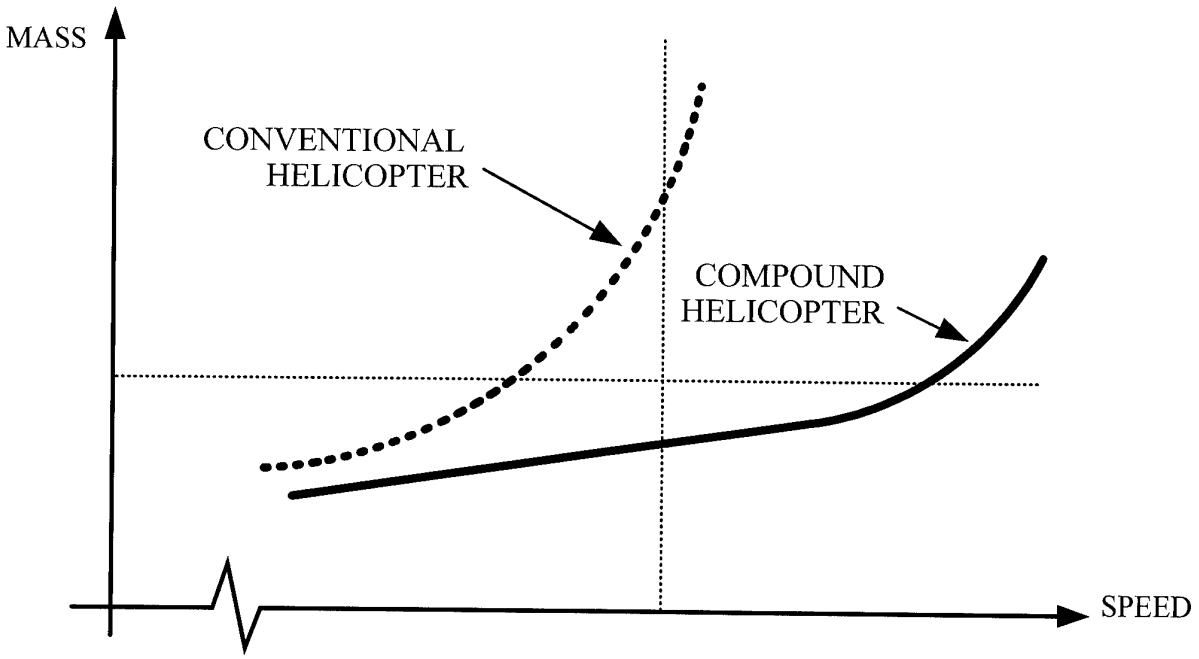

Comparison of all up mass to perform a given mission

FEA032-13

FIGURE 4

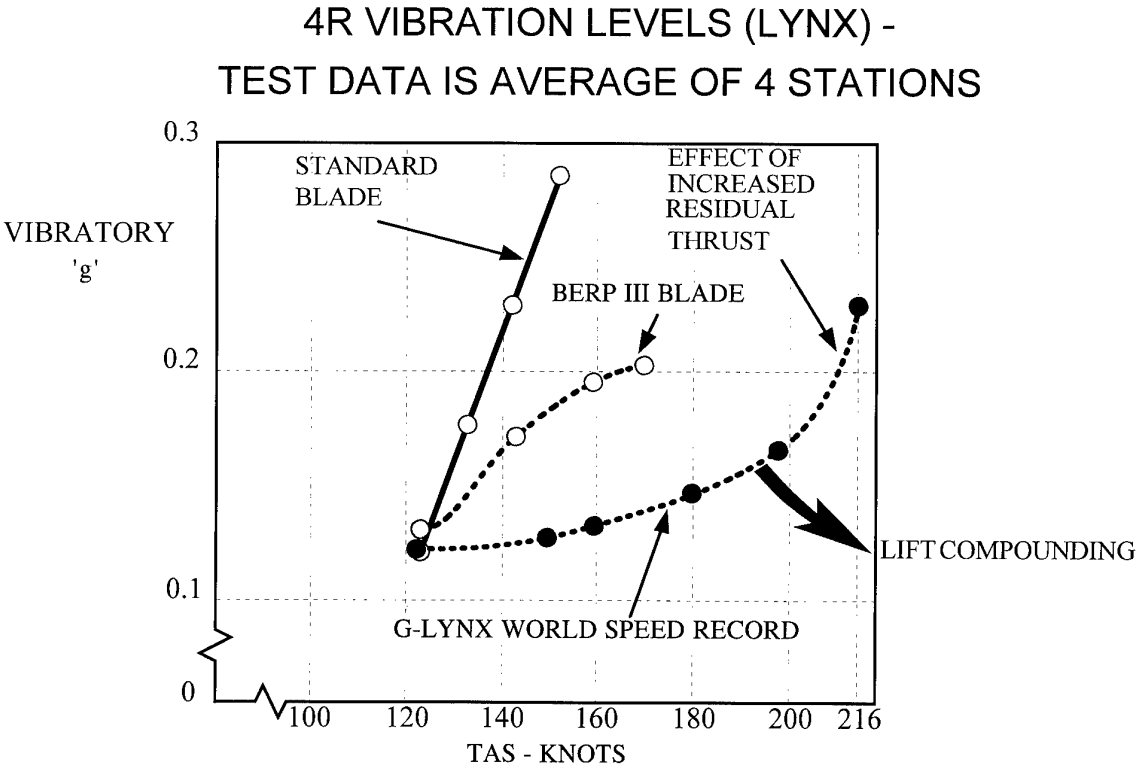

FIGURE 5

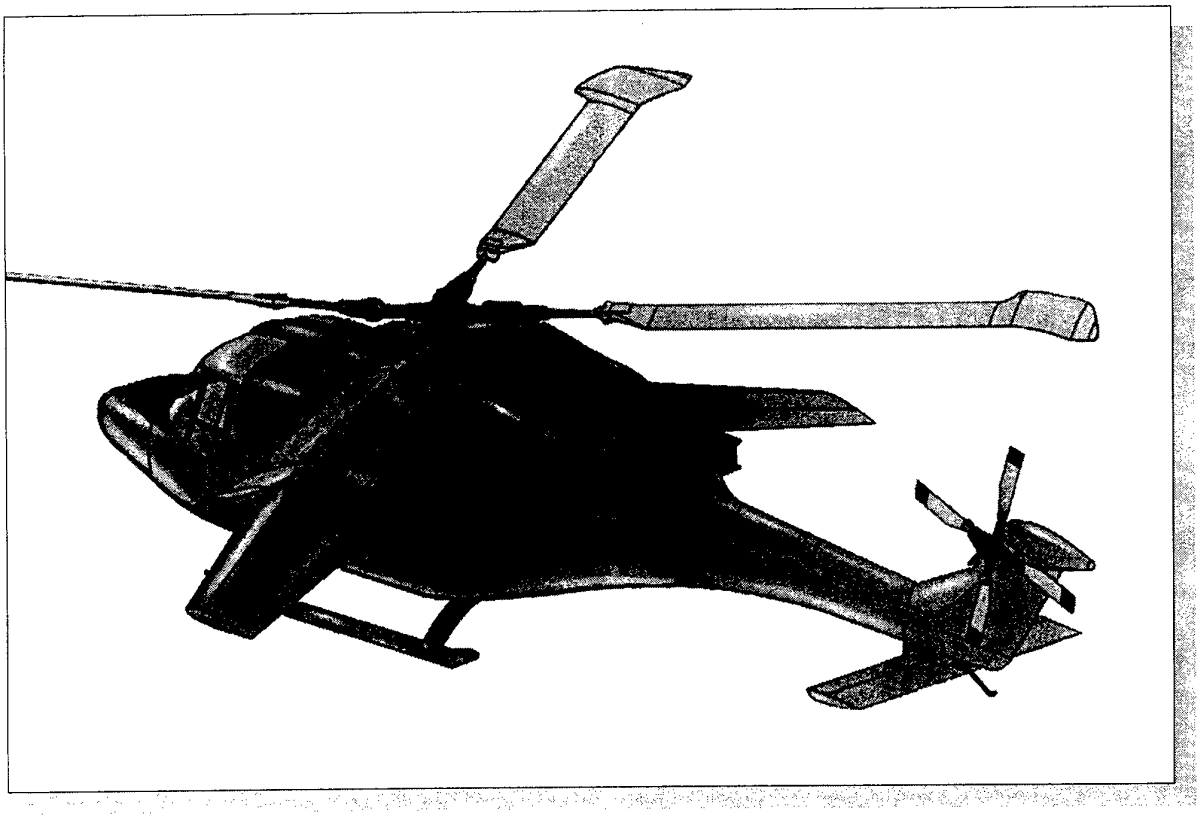

FEA032-05

FIGURE 6

RAH-66 COMANCHE PROGRAM STATUS

Mr. Arthur W. Linden
Director Boeing Sikorsky Joint Program Office RAH-66
Mr. Martin H. Stieglitz
Deputy Director Boeing Sikorsky Joint Program Office RAH-66
Sikorsky (Trumbull One Facility)
35 Nutmeg Drive (M/S ZII5A)
Trumbull, CT 06611, USA

SECTION 1. INTRODUCTION

In an era of ever changing threats and declining defense budgets, the U. S. Army strategy is to procure systems that incorporate new technology and that leverage existing battlefield systems to fix war fighting deficiencies. The RAH-66 Comanche exemplifies this strategy. Developed through an evolutionary series of analyses, simulations, tests and demonstrations, the Comanche weapon system integrates war fighting capability to provide battlefield overmatch, while minimizing the cost of ownership to the Army.

Comanche is an integrated advanced weapons system designed to operate and survive on the combined arms digital battlefield. Its low-observable (LO) characteristics protect the element of surprise and reduce the detectability of the aircraft, thus increasing survivability. Comanche's advanced sensor suite provides the aircraft effective standoff while allowing it to remain undetected by the enemy and still operate within onboard armament system range. This capability allows the pilot to correctly identify targets and can effectively reduce fratricide under nonlinear operations. The Comanche's advanced digital communication system makes Comanche the targeting element for the Army's long-range advanced shooters like the Multiple Launch Rocket System (MLRS) and the Army Tactical Missile System (ATACMS).

This paper provides an update to the development status of the RAH-66 Comanche helicopter. Section 2 reviews key technologies that form the heart of Comanche. Section 3 explains the Comanche design affords rapid deployability and low-cost supportability. The extensive use of simulation throughout Comanche development is described in Section 4. The success of the Comanche program rests in large part on the successful teamwork that is integral to all program activities. Section 5 explains the Team Comanche approach. Finally, Section 6 describes the plan to field the Army's 21st century reconnaissance attack helicopter in 2006.

SECTION 2. COMANCHE TECHNOLOGY

Comanche Overview

The RAH-66 is a twin 1,380 hp turboshaft engine, two-seat (tandem) helicopter design. Its mission is to perform armed reconnaissance for cavalry units, and attack missions for light divisions. The T-800 engines provide power to an advanced technology, split-torque main gearbox, which drives a five-bladed, bearingless, composite main rotor and a FANTAIL™ anti-torque system. Significant systems and key design features for the Comanche include: low signature (radar, visual, infrared, acoustic); improved target acquisition sensors; increased maneuverability, agility and speed; increased survivability; significantly reduced operation and support costs; and reduced supportability requirements, including a simple remove-and-replace maintenance concept.

As indicated in Figure 27-1, the RAH -66 has five durable all-composite rotor blades; a highly reliable bearingless main rotor head; a compact transmission; multiservice communications and datalink antennas; a shrouded high-thrust tail rotor; engine exhaust infrared signature suppression; low-observable composite structure; easy access aft electronics bay; internal weapons carriage for low detectability; retractable landing gear for low detectability; high reliability electronics in easily accessible bays; computer driven battle management; a 20 mm turreted gun; long-range infrared/TV targeting sensors; infrared piloting sensor/low visibility image intensifier; and helmet-mounted displays for head-up flying.

Airframe Materials

In the airframe, shown in Figure 27-2, composites are used in the skins, doors, frames, bulkheads, internal center keelbeam box structure, main rotor pylon fairing,

Paper presented at the FVP Symposium on "Advances in Rotorcraft Technology", held in Ottawa, Canada, 27-30 May 1996, and published in CP-592.

FANTAIL shroud, vertical pylon, and horizontal stabilizer. The major composite material systems used include new toughened epoxy resins, bismaleimide resins, and graphite fibers with improved stiffness and strain allowables. Figure 27-3 shows Comanche's dramatic shift in usage away from aluminum and towards composites.

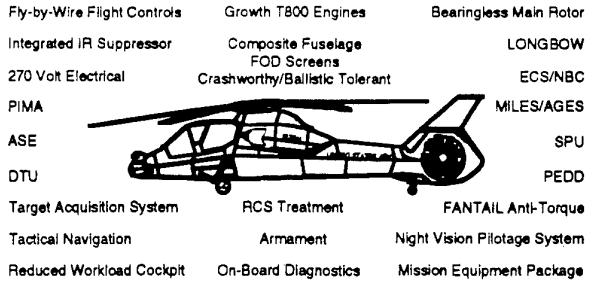

Figure 27-1. Comanche Functionality

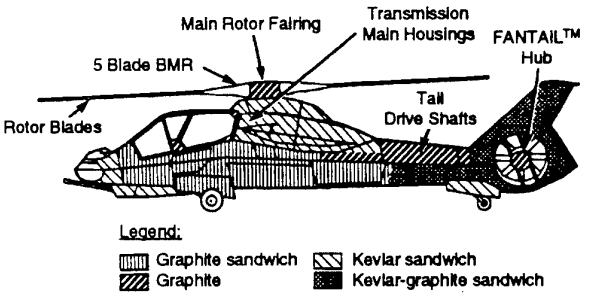

Figure 27-2. Comanche Airframe Design

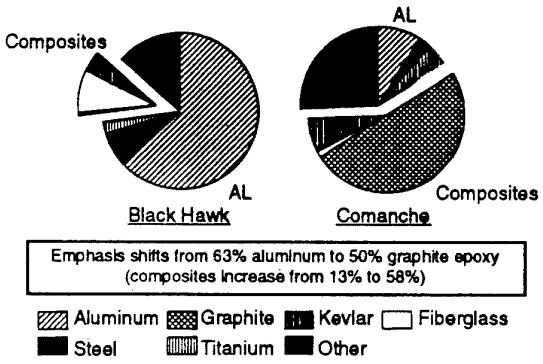

Figure 27-3. Comanche Airframe Material Usage

Dynamic Systems

Main Rotor

The Comanche main rotor system employs a five-bladed bearingless main rotor (BMR) with a 10.4 percent equivalent hinge offset. This simple, easily maintainable design reduces the rotor's acoustic signature and still meets high maneuverability, performance, and survivability requirements for both air-to-air and air-to-ground combat and terrain avoidance. The Comanche main rotor design also meets current standardized military specification ride comfort requirements.

In a bearingless design, the composite flexbeam is tailored to accommodate flapping, lead-lag, and pitch motions of the blade. The flexbeam connects the rotor blade to the hub, and control inputs are transmitted to the blade through a torsionally stiff torque tube that surrounds the flexbeam. Each blade has a single flexbeam that bolts to the titanium hub at the root end, and is bolted to the blade at the outboard end. Graphite cross-plies provide local reinforcing where the flex beam attaches to the hub.

The Comanche main rotor blades, torque tube, flexbeam, and quill shaft are all made of composite materials, as shown in Table 27-1. The rotor system also uses viscoelastic lag dampers and elastomeric bearings at the ends of the control rods. This carefully selected mix of materials results in a damage-tolerant design with benign failure mechanisms, making this rotor particularly survivable after combat damage.

Table 27-1. Comanche Main Rotor Composite Materials Usage

Component	Fiber System	Resin System
Blades	Graphite and Fiberglass	Epoxy
Quill Shaft	Graphite tows and unidirectional broadgoods	Bismaleimide Resin
Torque Tube	Graphite tows and unidirectional broadgoods	Epoxy
Flexbeam	Fiberglass and Graphite	Epoxy

FANTAIL™

The FANTAIL anti-torque system was chosen for Comanche for its superior maneuverability and signature characteristics. The 13° canted design incorporates features that reduce the aircraft's acoustic signature.

Designed with eight high-aspect-ratio blades operating at a low tip speed of 646 feet per second (197 meters per second), the system also incorporates a relatively large spacing between the fan blades and their support structure that virtually eliminates interaction tones.

The helicopter is also capable of completing a 180° turn-to- target maneuver in less than 5 seconds with winds up to 45 knots from any direction.

A full-scale prototype of the Comanche FANTAIL was built and tested on an S-76 aircraft (Figure 27-4) with impressive results. This aircraft achieved sideward and rearward flight speeds of 70 knots, and demonstrated a hover yaw acceleration of 0.86 radians/second/second to meet the Comanche 180° turn-to-target maneuver, with power consumption very close to that of a conventional tail rotor.

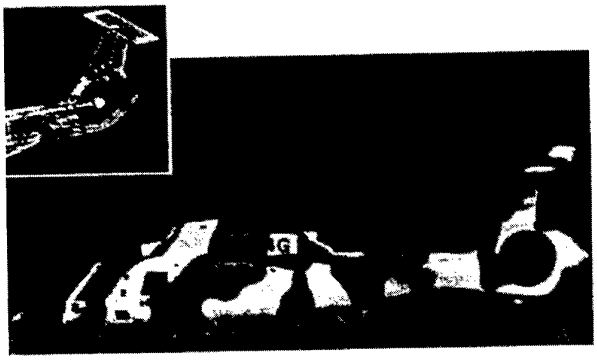

Figure 27-4. S-76 FANTAIL Demonstrator Aircraft

Drive Train Technology

The split torque main gearbox, shown in Figure 27-5, is a compact, simple, low-maintenance, lightweight design. The main gearbox has a dual engine rating of 2,198 HP and a single engine rating of 1,430 HP. The split torque concept provides two load paths from each engine to the final bull gear stage, thereby retaining a high RPM and low torque until this final stage. Taking an 11-to-1 reduction at the final stage results in a lower weight and very compact size for such a high-power gearbox. Fabrication of gears from high-hot-hardness steels also reduced gearbox weight. The split torque design also permits the use of plug-in, direct drive accessories that further reduce weight, cost, and complexity.

Current production over-running clutches generally operate at speeds under 12,000 RPM, well below the optimum speed for achieving the lowest weight, most compact design. Comanche uses a spring clutch with a helical coil that expands against a bore to provide frictional drive. Operating at 23,000 RPM, this clutch design resulted in a 3 percent reduction in main gearbox weight, due to the lower torque operation at this high RPM. Costs associated with this design are also lower, since the spring clutch consists of only 8 parts, in contrast to the 33 parts that comprise a comparable ramp roller clutch.

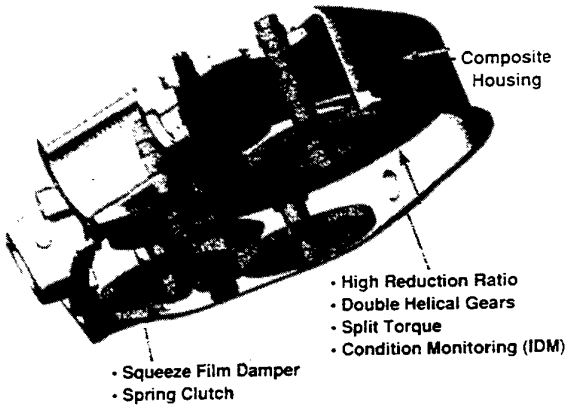

Figure 27-5. Comanche Drive Train Technologies

T800 Engines

The Comanche is powered by two LHTEC T800-LHT-801 engines, each providing 1,037 HP at intermediate rated power (30 minute IRP rating) and 1,123 HP at maximum rated power (10 minute MRP rating) at an altitude of 4,000 feet (1,220 meters) and an ambient temperature of 95°F (35°C). The engine design is modular and incorporates two centrifugal compressors with integral lubrication system and inlet particle separators.

The Comanche engine control system is coupled to the flight control system in order to provide better anticipation of rotor load demands and to control rotor speed under varying load conditions. The integrated fuel and flight control systems provides the following major features:

(1) collective pitch control anticipation to enhance main rotor speed control;
(2) a lateral control rate anticipator to anticipate power changes and reduce transient torque spikes;

(3) a yaw command rate anticipator to anticipate large anti-torque system loading and minimize rotor speed decay, and;
(4) load factor enhancement that increases reference rotor speed when load factor is demanded, to allow more maneuvering capability at reduced rotor loads.

Manufacturing Technologies

The extensive use of advanced technology in the Comanche design was contingent upon developing a producible system that meets stringent design-to-cost goals. The air vehicle design, manufacturing, and producibility concepts were developed concurrently through the use of integrated product development teams. The major enabling technologies that have produced these advances include the extensively used 3-D CATIA and PRO-E models for engineering design; Rule Based Technology (RBT); process control; numerically controlled programming; and tool design. A common 3-D electronic database used by all members of the product development teams resulted in a seamless transfer of data from design to manufacturing.

Under the Comanche program, airframe engineering master drawings are replaced with electronically dimensioned, toleranced drawings with datums at key part features to allow coordination of the tooling, assembly, and inspection of parts through final assembly. Electronic data, created by a three-dimensional computer-aided design system (CAD) replace the physical master model. This 3-D database allows the manufacturing engineer to develop pictorial process plans, numerically controlled machining programs, and "masterless tooling" by working directly from the same database that the designer created to design the part. A comprehensive and detailed building-block approach to design, analysis, and test was mandatory to reduce program risks associated with the integration of new technologies with new manufacturing approaches.

The airframe design focused on the modular assembly. An approximately 24 foot (7.3 meter) long keelbeam box structure was manufactured using two linear co-cured keel beams assembled to a lower skin panel by various cross-frame and bulkhead subassemblies. The keelbeam takes all the airframe loads. As a result, airframe skins are secondary structures and can therefore accommodate the large number of fuselage cut-outs without the weight penalties that would occur in a semi-monocoque construction.

Comanche has pioneered the use of a lightweight honeycomb core that is only 60 percent as dense as the core found in older designs. This is made possible through the use new techniques that eliminate the crushing of low-density core when it is cured in an autoclave. The result is a lower-weight airframe.

Flight Controls

The Comanche flight control system is a triply redundant, functionally partitioned, fly-by-wire system that receives its sensor data from a digital data bus. In the cockpit, the pilot has a sidearm controller and a displacement collective pitch control. The sidearm controller provides pitch, roll, and yaw control, and has limited control authority in the vertical axis that acts like a collective pitch "beeper." When the pilot pulls up on the sidearm controller, the aircraft rises slowly; when he pushes down on it, the aircraft stops climbing. All actuators are jam-resistant, dual hydraulic actuators with redundant control valves. Electrical and hydraulic power sources are redundant as well, and all critical components are strategically separated from each other to enhance ballistic protection. The system is also shielded to provide hardening against electromagnetic interference, lightning, and nuclear radiation. A two-level maintenance diagnostic system has been demonstrated to have 99 percent accuracy in fault detection, and 98 percent accuracy in fault isolation. Predicted flight safety reliability and mission reliability greatly exceed their respective requirement allocations.

A schematic of the flight control system is shown in Figure 27-6, and its functional partitioning is depicted in Figure 27-7.

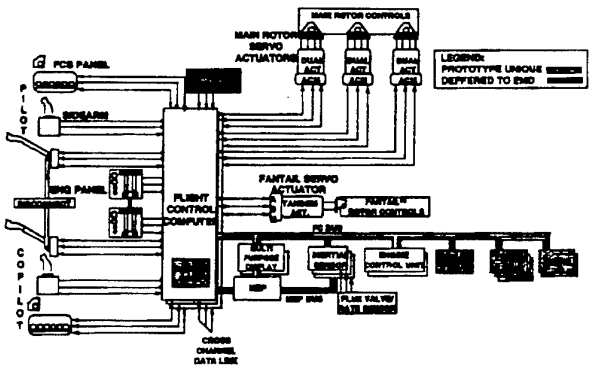

Figure 27-6. Comanche FCS Schematic

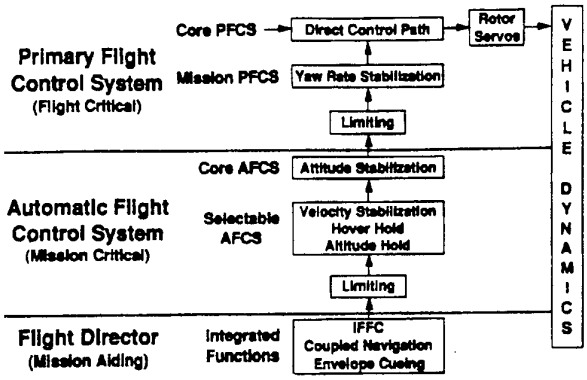

Figure 27-7. Comanche Flight Control System Partitioning

Mission Equipment Package

The Comanche Mission Equipment Package (MEP) architecture is shown in Figure 27-8.

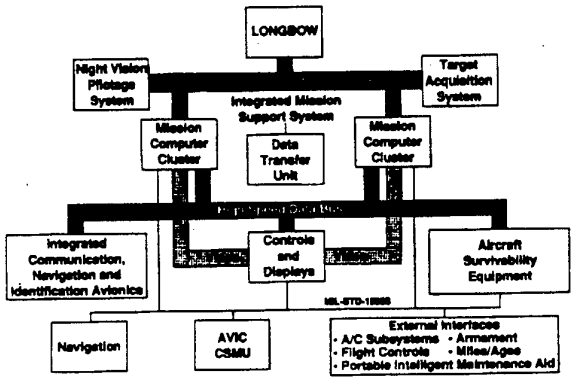

Figure 27-8. Comanche MEP Architecture

By combining very high speed integrated circuit (VHSIC) technology with parallel processor technology, Comanche achieves a data processing throughput capability of 150 million instructions per second (MIPS).

Comanche's sensors are its eyes and ears. The second generation focal plane array forward looking infrared (FLIR) technology embodied in Comanche has a greater than 40 percent better range performance than earlier FLIRs, providing for increased operational standoff range and survivability.

The Electro-Optical Sensor System (EOSS) is located in the nose of the aircraft. The EOSS consists of the Electro-Optical Target Acquisition and Designation System (EOTADS) and the Night Vision Pilotage System.

The EOTADS is an on-turret, stabilized, multifunction electro-optical system containing a day/night thermal imaging FLIR sensor, a solid state television camera, and a laser range finder/designator. The EOTADS enables the crew to detect, classify, recognize, track, and engage targets using manual and aided search modes.

The FLIR uses state-of-the-art, second generation, time delay integration detectors for thermal imaging in the 8 to 12 micron wavelength region. The EOTADS is integrated with the Aided Target Detection/Classification and Automated Target Tracker to provide the capability of performing automated wide-area searches, then storing the imagery for recall by the crew or for automated target detection and classification. The EOTADS has three fields of views, two for targeting and one wide field of view with unity magnification for backup pilotage.

The Night Vision Pilotage System consists of a second generation FLIR that is similar to that in the EOTADS and a solid state Image Intensified Television (IITV) to provide complementary night vision capability. The FLIR and IITV sensors are located in a helmet-slewable stabilized turret located on top of the EOTADS.

Nap-of-the-earth flight in a combat environment is extremely dangerous and demanding of pilot skills. The pilot must have his eyes out of the cockpit, yet still have access to important flight instrument and MEP sensor data. Comanche's systems accommodate these requirements through the Helmet Integrated Display and Sighting System (HIDSS). The HIDSS is a biocular, helmet-mounted display that provides the Comanche crew members with a heads-up, eyes-out capability for pilotage and weapon sighting activities. The FLIR, IITV, and 20 mm Gatling gun are slaved to the HIDSS, pointing wherever the pilot looks.

Cockpit Displays

A layout of the two Comanche multifunction cockpit displays is shown in Figure 27-9. The right multifunction display is a 6 by 8 inch (150 mm by 200 mm) high-resolution, color, active matrix liquid crystal display unit used primarily for instrument graphics and map displays.

The left multifunction display is a 6 by 8 inch (150 mm by 200 mm), high-resolution, monochrome, active matrix liquid crystal display unit for textual menus and video from the sensors.

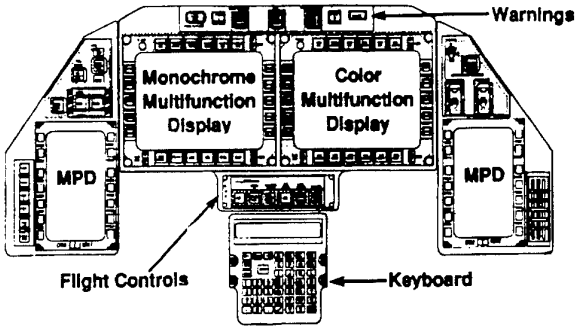

Figure 27-9. Comanche Cockpit Displays

Navigation and Communication Capabilities
Comanche is the first helicopter to use the joint service integrated communication, navigation, and identification avionics (ICNIA) system. For navigation, Comanche utilizes an inertial navigation system and a Global Positioning System. The fly-by-wire control system receives aircraft state variables from the doppler velocity system and a blade-mounted air data system. A radar altimeter and a digital map interface complete the navigation suite.

For communications, ICNIA provides two Single Channel Ground Airborne Radio System (SINCGARS) VHF-FM radios, one VHF-AM radio, one UHF-AM HAVE QUICK radio, an MK XII Identification Friend or Foe (IFF) transponder, voice security system, and automated data modem hardware.

Weapons and Fire Control
Although small, the Comanche is heavily armed. The Comanche carries a 20 mm, turreted Gatling gun with 500 rounds of ammunition. In addition, the Integrated Retractable Aircraft Munitions Subsystems (IRAMS) carried inside internal bays on each side of the aircraft each have three weapon stations capable of carrying one Hellfire or two Stingers, or four 2.75-inch rockets per station. Installation of the External Fuel/Armament Management System (EFAMS) provides an additional four weapon stations per side. These EFAMS stations can each carry the same mix of weapons carried by the IRAMS. With the EFAMS installed, the aircraft has a total of 14 weapons stations that can be loaded with any combination of Hellfires, Stingers, or rockets. The EFAMS is also capable of carrying external fuel tanks in place of weapons.

Survivability
. .The Comanche uses radar, acoustic, and infrared signature reduction technologies, along with lightweight armor, integrated airborne survivability equipment, and a regenerative nuclear-biological-chemical (NBC) filtration system to improve the aircraft's survivability on the battlefield of the future.

Low Observables
Through a combination of shaping and radar-absorbent materials, the radar signature of the Comanche has been reduced by a factor of 600 below that of a typical heavy attack helicopter and by a factor of 200 below that of a typical scout helicopter.

Comanche uses a high aspect ratio infrared emission suppressor, with lobed ejectors that permit efficient mixing of exhaust and ambient air within a very short distance. The mixed air is ejected through a slot running along the length of the aircraft's tailcone. This ribbon exhaust provides low plume and surface temperatures, as well as line-of-sight blockage of internal engine components. In conjunction with careful management of all internal airflows, the Comanche infrared suppression system reduces its signature by a factor or 4.5 below that of a typical heavy attack helicopter and by a factor of 2.0 below a typical scout helicopter.

Selection of a five-bladed, swept tip, low tip speed main rotor, combined with the FANTAIL, has succeeded in drastically reducing the Comanche's acoustic signature. Comanche's aural signature has been reduced by a factor of 1.6 below that of a typical heavy attack helicopter and by a factor of 1.4 below that of a typical scout helicopter. Comanche's electronic acoustic signature, which acoustic detectors and acoustic mines listen for, has been reduced by a factor of 5.0 below that of a typical heavy attack helicopter and by a factor of 2.5 below that of a typical scout helicopter. These impressive signature reductions significantly reduce Comanche's detectability against current and projected threat weapons.

Ballistic Protection
Ballistic protection in Comanche is provided by armor, hardening, shielding, and redundancy.

Comanche uses an innovative lightweight armor technology to protect the crew members. This armor uses Spectra- or Kevlar-wrapped silicon carbide and boron carbide tiles.

Nuclear, Chemical, and Biological Contaminant Filtration
Comanche uses an innovative NBC filtration system that removes all known particulate, liquid, and gaseous contaminants. The system uses a pressure swing adsorber, a water separator and coalescer, and a high-

efficiency particulate air filter. It is regenerable and self-cleaning, has a built-in-test system, and an indefinite operational life.

SECTION 3. SUPPORTABILITY

The most significant Supportability feature of the Comanche is its design for support in a two-level maintenance system. The significance of this design feature is related to the operating and support cost savings realized from the elimination of the need for intermediate level maintenance resources, such as manpower, facilities, test measurement and diagnostic equipment (TMDE), and other intermediate-level peculiar support equipment.

Supportability Design Influence

From the start of the Comanche design, every effort was made to identify and eliminate design characteristics that would require an intermediate level of maintenance. This process highlighted two significant features that are critical to achieving two-level maintenance:

Partitioning: Eliminates the need to dissemble expensive subsystems in order to replace inexpensive components in those systems.

Diagnostics: Need for expensive TMDE to fault isolate so that the correct components would be replaced.

Comanche components have been partitioned so that parts with different cost and reliability have been segregated for ease of removal and replacement. Diagnostics have been incorporated into the design through an integrated architecture so that expensive TMDE is not required. The Comanche's extensive on-board integrated diagnostics incorporates prognostic capability. The prognostic capability includes the application of regime recognition in a structural life usage program and the tracking of flight safety critical dynamic components.

The resulting design philosophy prohibited the layering of components, limited the number of fastener sizes used in the design, and emphasized Manpower and Personnel Integration (MANPRINT) features associated with accessibility, anthropometric requirements, and task complexity. This influence was accomplished through:

- Supportability membership in design-related inte grated product teams.
- Continuous testability analyses and maintainability assessments.
- Validation of two-level maintenance cost effectiveness through repair-level analysis.

By adhering to this process, intermediate-level tasks have been successfully eliminated, and the remaining aviation unit maintenance (AVUM) and depot tasks have been reduced. AVUM tasks comprise remove-and-replace, on-aircraft repairs, and minor off-aircraft repairs that can be accomplished next to the aircraft. Depot tasks include component repair in support of the supply system and major structural airframe repairs and overhaul/rebuild.

Comanche Flight Line Tools

As a result of the process outlined above, Comanche requires a flight line tool box that contains fewer than 50 tools. Additionally, over 50 percent of the airframe surface is comprised of access panels and maintenance platforms. The needs for torque wrenches, safety wire and cotter pins has been reduced to a very few applications, significantly fewer than any other helicopter. Time line analysis, validated by the Army, indicates that the Comanche can be rearmed and refueled in less than 15 minutes.

The Comanche also incorporates a small Portable Maintenance Aid (PMA) which serves as the digital automated logbook, the delivery for the interactive electronic technical manuals, and an off-board diagnostics aid that interfaces directly with the aircraft's MIL-STD-1553B data bus, and from the data bus all fault data for every subsystem down to the line-replaceable-unit or line-replaceable-module level.

Comanche vs. Current Light Helicopter Fleet

The result of this approach has been a revolutionary Comanche design compared to the current light helicopter fleet:

- Manpower needs are reduced by 32 percent
- Required maintainer specialties are reduced from 9 to 4
- Tools and support equipment are reduced by 83 percent
- Number of parts reduced by 34 percent
- Training costs are reduced by 50 percent
- Maintenance levels are reduced from 3 to 2.

Additionally, as shown in Figure 27-10, the operating and support costs for Comanche are dramatically lower than any other Army reconnaissance or attack helicopter. The bottom line is that Comanche requires only 25 percent of the per-flight-hour maintenance time required by current helicopters.

SECTION 4. SIMULATION

The demanding environment and missions in which new weapons systems must perform present the helicopter manufacturer with a truly formidable challenge. The

complex nature of the technologies involved, coupled with limited budgets and ambitious schedules, make validation of design and implementation particularly challenging. To mitigate these risks, simulation has become increasingly important in the design and operational employment of new weapons systems.

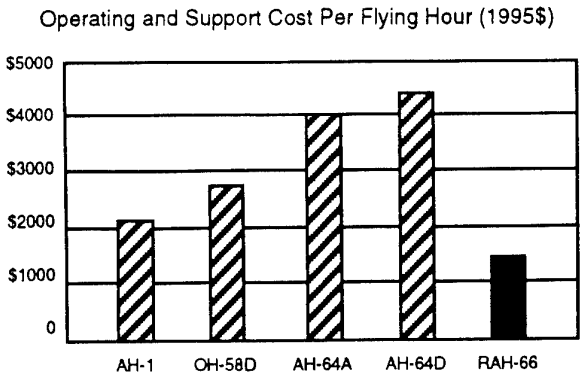

Figure 27-10. Comanche O&S Costs Are Real and Achievable

Simulation within the DOD normally has three major categories: constructive, virtual and live. Constructive simulation includes war games and math models used as analytical tools to predict system or subsystem performance. Performance evaluation consists of mission effectiveness, detectability, and survivability. Virtual simulation is a virtual reality environment for human interaction. Flight simulators fall into this category. Live simulation is exactly what the word implies. It includes evaluation of hardware on instrumented ranges. For the purpose of this paper, Comanche simulation will focus on the constructive and virtual categories.

In the very early phases of the Comanche's definition and development, virtual simulation was used extensively both at Boeing and Sikorsky. The exploratory phases of the Comanche program (the Advanced Rotorcraft Technology Integration (ARTI) program, Light Helicopter Experimental (LHX), program and the Light Helicopter (LH) program) were largely a series of trade studies and evaluations to demonstrate proof of concept and reduce the number of competing contractors. The ARTI program identified the required level of automation and advanced crew interface concepts. The LHX program focused on advancing and demonstrating critical technologies necessary for Comanche development. The LH request for proposal included all of the lessons learned from ARTI and LHX and culminated in contract award to Boeing Sikorsky in April of 1991. All of these precursors to the RAH-66 Comanche depended heavily on the results of trade studies, demonstrations, and analyses conducted primarily through the use of simulation.

The cockpit layout and operation are prime examples of the importance of simulation. Boeing and Sikorsky developed a Pilot-Vehicle Interface Mechanization Specification (PVIMS) to identify the operational requirements of the cockpit. The PVIMS specifies the step-by-step controls and displays operation of any task to be performed in the cockpit. The mechanization requirements derived form the specification were simulated in the Comanche Full Mission Simulation Facility to validate weapon system performance and crewmember operation. This process allowed contractor and military pilots to evaluate cockpit operation and Comanche employment early in the development cycle, when cost were schedule impacts are less dramatic.

The Comanche full mission simulation facility consists of a six-degree-of-freedom moving base platform with a 20-foot tall composite dome rigidly attached to the platform.

The Comanche simulation cockpit contains a seat shaker that simulates high frequency cues to the pilots in flight regimes such as transitional lift, rotor stall, weapons delivery, and high load-factor maneuvers. The facility also has aural cueing capability to simulate sounds typically associated with operational flight, such as rotor noise, transmission noise, and landing gear extension noise.

Constructive simulation proved to be very effective in the design optimization of the Comanche. Some of the constructive simulation activities performed on Comanche included: evaluation of aircraft survivability and mission effectiveness; engineering trade and cost effectiveness studies; comparative analyses; and new technology evaluation. These were accomplished using mathematical models generally concerned with aircraft susceptibility, aircraft survivability, and battlefield effectiveness. The aircraft susceptibility models considered radar detection, radar clutter, RF propagation, RF signal strength, infrared detection, electro-optical detection and canopy glint. Aircraft survivability encompassed anti-aircraft artillery and surface-to-air missiles. Battlefield effectiveness dealt with battalion-size to brigade-size forces and air-to-air engagements.

One of the models used extensively for the development of Comanche was the Advanced Tactical Combat (ATCOM) model. ATCOM is a force-on-force, player interactive, Monte Carlo, battlefield effectiveness model. It is capable of simulating combat systems and the

environments they operate within. One of the features of ATCOM is its ability to graphically portray the tactical situation and provide terrain information and data.

By combining ATCOM's Defense Mapping Agency digital terrain data, Comanche signature data, vulnerability data, Comanche mission scenarios, and battlefield simulation, cost-effective trade studies were conducted to influence the design of the aircraft. The output of these trades included data concerning the probability of being detected, the probability of survival given detection, and battlefield survivability and effectiveness.

The Comanche methodology of simulation before design (hardware or software) is used for both the operators and maintainers. Operational suitability of systems, as well as maintenance accessibility, are vital areas in which Comanche simulation has provided decision making criteria in a timely and cost-effective manner. Simulation has been and will continue to be used to evaluate: cockpit design; layout of controls and displays and crew system interfaces; design of the flight control system; evaluation of air vehicle handling qualities; sensor location and performance; mission tactics; susceptibility to enemy threats; mission effectiveness; operational suitability; and pilot workload.

SECTION 5. TEAM COMANCHE

The Comanche program has been built on a foundation of teamwork. From the formation of the Comanche First Team, led by Boeing Sikorsky to compete and win the contract, to the forging of Team Comanche with the Army following contract award, the program has used teamwork to plan and conduct all the facets of the activity and to resolve all issues that have arisen.

Team Comanche refers to the hierarchical structure of teams, from the Integrated Product Team (IPT) level all the way up to an Executive Steering Group (see Figure 27-11). Each team at each level has Government and contractor focal points. Issues that cannot be resolved at a particular team level are brought to the next-higher level for resolution.

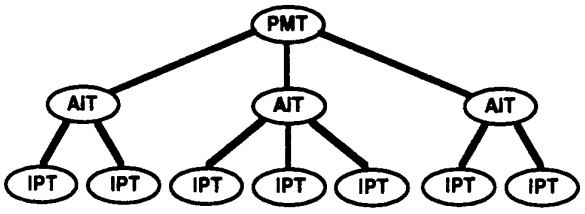

Figure 27-11. Team Comanche - Integrated Product Teams

The IPTs have responsibility for product design, manufacture, test, and support. Analysis and Integration Teams (AITs) coordinate the interfaces and interactions among several IPTs. The Program Management Team (PMT) consists of the Boeing Sikorsky Joint Program Office Directors, the company program managers, and Government Program Office leadership. This group meets weekly by way of video teleconference to review program schedules and key issues.

One of the best examples of the power of Team Comanche is the manner in which the program has responded to DOD acquisition reform. Starting with performance based specifications, revised Statements of Work, and a fresh look at data and quality requirements, the Army Program Office developed a new contract structure. This approach will give the user the weapons system they need, while promoting the collective ingenuity of the First Team in its effort to find the lowest cost/least risk approach.

The Comanche First Team refers to the successful relationship developed between Boeing Sikorsky and several key subcontractors that work together to further program objectives. Subcontract management teams were created with each subcontractor and consist of the subcontractor program manager, the prime contractor material buyer, and the cognizant prime contractor technical manager. These three team personnel are held collectively accountable for meeting all subcontract objectives.

Two cross-company team activities complete the First Team approach. The First Team President's meeting is held approximately once a year and provides an opportunity for top company executives to communicate on key Comanche program issues. The First Team Program Managers' meeting is held on a six-week rotation schedule. Each program manager presents program status and issues, and the Joint Program Office present topics of general interest. Appropriate Government personnel participate in each of the above activities.

SECTION 6. PROGRAM UPDATE

The first Comanche prototype was rolled out on May 25, 1995. Nineteen ninety-five also saw the successful completion of an extensive preflight qualification program, and the 50-hour preflight acceptance test on the tie-down Propulsion System Test Bed (PSTB) that demonstrated the successful integration of all dynamic system components. First flight occurred on January 4, 1996 and featured 36 minutes of flight, including two takeoffs and landings, hover turns, and forward flight. This event marked the beginning of an extensive envelope expansion program. While all aircraft systems operated extremely well, the performance of the flight control

system and the infrared (IR) suppression system were particularly impressive.

The flight control system (FCS) is developed incrementally for the flight test program. In the full-up configuration the FCS has three modules of functionality, the lowest of which is the mission Primary Flight Control System (PFCS). This was the only module available for first flight and it provides only yaw rate stabilization. Even at this capability level, the pilots were able to trim the aircraft for hands-off flight for approximately 5 to 8 seconds. Additionally, the rotor system was extremely smooth and stable throughout the flight and the rotor track was within one-quarter inch.

The IR suppressor system is designed to reduce the aircraft's observability to IR threats. Measurements during first flight confirmed that the system indeed reduces these emissions to less than one-ninth of emissions produced by that of a UH-60 Black Hawk equipped with IR suppressors.

Comanche is currently embarked on a program with a two-fold objective: 1) Develop a production weapon system to support Initial Operational Capability (IOC) in 2006; and 2) Produce six early prototypes with reconnaissance only capability for Army "green suit" evaluation starting in 2002.

Two prototypes (Aircraft 1 and 2) will support the first years of development testing. Aircraft 1 will serve primarily as the structural/mechanical and flight control evaluation vehicle. Aircraft 2 will be used for avionics (MEP) development with increased avionics capability at programmed intervals. When reconnaissance capability has been demonstrated, six additional prototypes will be built to the Aircraft 2 configuration. These six aircraft will be used by the Army for the development of tactics and training procedures.

In the meantime, additional functionality, principally armament related, will be incorporated and tested on Aircraft 2. When full reconnaissance attack capability has been developed, the six prototypes will be upgraded for further Army evaluation. Current planning is for contractor logistics support of the six prototypes during Army usage, and of the first several production lot aircraft.

The final development step is the incorporation of the LONGBOW radar system currently planned for production lot 6.

SECTION 7. SUMMARY

Comanche is on track to address the reconnaissance role on the Army battlefield and to be the attack helicopter of the 21st century. Innovative technology and extensive use of simulation are two of the approaches that are producing the Comanche that will save lives, increase mission effectiveness, and save cost.

Management techniques such as Team Comanche and performance based management have enabled the program to continue to forge ahead even in the uncertain environment of Department of Defense funding.

Acknowledgments

The authors borrowed heavily from reference 1, an excellent comprehensive description on all key technology aspects of the Comanche helicopter. We are indebted to Dr. Kenneth Rosen and Mr. Gary deSimone for their permission and assistance. We also want to thank Mr. William Harper, Mr. Mark Rowland and Mr. William Miller for their contributions to this paper.

References:

1. "An Overview of Technologies Enbodied in the Comanche Program;" Rosen, Kenneth M.; Sikorsky internal document.

THE APPLICATION OF HELICOPTER MISSION SIMULATION TO SYSTEM TRADE-OFF ISSUES

N. Tatlock, C. Silvester and P. Birkett
Systems Integration Department
Defence Research Agency
Building Q153
Farnborough, Hants GU14 6TD, UK

Abstract

This paper discusses the use of simulation for understanding some of the system trade-offs and integration issues associated with the next generation of battlefield helicopters. The HOVERS helicopter mission simulator at DRA Farnborough is discussed and examples of the types of benefits provided by its use are described.

Introduction

Recent world-wide political changes combined with advances in technology have contributed to the rapid development of the role of the military helicopter. In the future, it is likely that helicopters will be increasingly deployed not only in high intensity conflict, but also in low intensity operations such as those associated with UN peace keeping and peace enforcement. Having the capability to deploy and operate to maximum effect, will be largely dependent on the integrated operation of on-board sensors, mission systems, defensive and offensive weapons, platform and the aircrew. It is therefore important to consider the operational impact of the total helicopter system, and to establish an understanding of how the various sub-systems contribute to the overall effectiveness of the aircraft as an integrated weapon system.

In this paper, the trade-offs concerned with the principal components of the fighting helicopter are discussed. The use of "man-in-the-loop" mission simulation to address these issues is presented, together with appropriate examples. The DRA Farnborough mission simulator, HOVERS, which has been developed specifically for study of system trade-offs in low-level helicopter operations, is described.

Trade-off issues

The role of aircrew In a modern military helicopter, the aircrew play a fundamental part in the operation of the aircraft as an effective total mission system. Their tasks fall broadly into two categories:

- piloting;
- tactical management.

Although traditional piloting tasks are vital, particularly in the NOE regime, it is important to emphasise the latter role in view of the complexity of the systems likely to be on board future helicopters. The aircrew represent the natural focus for the information flow within the aircraft, and will build up a tactical picture of the military situation as it affects them. This may require interpretation of information available over a tactical data network, aircraft/weapon status indicators, sensor and navigation displays not neglecting the view out of the aircraft window. The level and extent of the situational awareness of the crew is of primary importance not only to the effectiveness of the helicopter in fulfilling its role but also in ensuring its continued survivability. The timely provision of relevant information displayed to the crew both factually correct and easily assimilated will be an important factor in enabling the crew to make sound decisions concerning target acquisition, engagement, threat evasion, tactical route selection and signature minimisation.

The aircrew also have an important role in operating weapon systems. This is particularly true of the aiming process, which may require precise manoeuvring of the helicopter, together with target designation using manual systems or, in the future, head or eye-pointing systems.

Communication is another important element in the management of the helicopter. In general, the crew in an aircraft will communicate with:

- one another, ensuring that (in a multiple crew aircraft) they operate as a cohesive team.
- other helicopters in the group, enabling effective co-operative operations to be performed. This may also include aircraft of differing nationality on joint operations.
- other forces, for example ensuring route clearance and providing situation reports to the command base.

In general, the aircrew represent a vital component of the total system, enabling the considerable potency of military helicopters to be exploited optimally by the use of effective tactics.

Information Management Over the next decade, the provision of tactical information is likely to be of critical importance for helicopters operating in various battlefield roles. As discussed in the previous section, ready access to current tactical information is likely to result in enhanced situational awareness and thus improve mission effectiveness and survivability.

The introduction of a tactical data network into the cockpit of a battlefield helicopter raises several important integration issues. The aircrew have a considerable workload when priorities are constantly changing in relation to the situation. It is therefore important that information from various sources is brought together and fused to present a single reliable up-to-date picture of the battle situation as relevant to the helicopter. This requires that any spatial and temporal ambiguities between information from the different sources are resolved to avoid confusion. A classic example would be the sighting and reporting of the same targets by observers at different points. In such instances there is ample scope for mis-reporting or inaccurate position reports being fed into the system and transmitted over the data network causing confusion.

The presentation of all this information to the aircrew, requiring them to determine which data are of direct importance to them, imposes an unacceptable additional workload. It is therefore highly desirable that a degree of

Paper presented at the FVP Symposium on "Advances in Rotorcraft Technology", held in Ottawa, Canada, 27-30 May 1996, and published in CP-592.

automation in relation to the priority of threat information be incorporated into the system. Such information could be prioritised based on its threat potential, weapons engagement zone or its location. This would ensure that aircrew are only furnished with that information which is currently relevant to the mission. The ability to call upon all other information would enable them to increase their overall perception and enhance their tactical and situational awareness as and when required. This may also enable re-tasking to another area without the need for a return-to-base briefing.

Finally, it is vital that information is displayed to the crew in a manner which can be easily assimilated. In a battlefield situation when operating NOE, helicopter crews require the capability to operate as much as possible with their heads-up and eyes-out. Helmet-mounted displays (HMD), which, for example, offer the capability to present threat information overlaid conformally on the real world, support this "head-up, eyes-out" philosophy. However, the HMD is limited in the amount and type of information that can be effectively presented. The conventional multi-function head-down display provides a complementary medium, which enables such information as route plans,
safe lanes, air defence areas and long range data to be shown as terrain-referenced overlays.

Weapons In the future, a wide range of weapons, including cannon, free flight aerial rockets (FFAR), high velocity missiles and laser weapons, will be available for use by a helicopter both in an offensive role and in response to attack by a threat. The threats most likely to be encountered are ground-based mobile air defence units, shoulder-launched surface-to-air missiles (SAM), guns and other aircraft.

In many engagements the ability to quickly and safely manoeuvre the aircraft and thus bring the threat within the weapon envelope is likely to be a critical factor. For bore-sighted weapons, the agility of the helicopter will be of greater importance than for turreted weapons, which have an inherent off-bore-sight capability and therefore require a combination of aircraft and turret manoeuvring to perform the aiming process. The use of off-bore-sight targeting systems (steerable sights, head or eye-pointing systems) will also contribute to the speed of response to a threat.

The time-of-flight of a weapon is also an important factor. The laser weapon, with an effective zero flight time, has a considerable advantage in this respect, alleviating the need for complex fire-control calculations. Furthermore, its inherent agility and lack of recoil give it great potential for rapid deployment. However, when operated from a platform with intrinsically high vibration levels, the problems of aiming such a system with the required precision to achieve appropriate terminal effectiveness are considerable.

For beam-rider, wire-guided, laser-guided or semi-active radar-guided missiles, time-of-flight is also important since it directly influences the period for which the helicopter must maintain line-of-sight to the target after firing. From an operational perspective, this affects the vulnerability of the aircraft to enemy weapons. Although autonomous, lock-before-launch, fire-and-forget missiles overcome this problem, the need to establish line-of-sight between missiles positioned on the weapon pylons and the targets leads to exposure of the helicopter during the lock-on and launch phases of an engagement. Again this can compromise the covertness and tactical security of the aircraft.

From this brief discussion, it is evident that the effectiveness of different weapon systems will vary considerably with range, the degree of manoeuvre required and the circumstances of the engagement. Different weapons are likely to be optimal for different situations.

Other Sub-systems Various other sub-systems contribute to the effectiveness of the helicopter as a weapon system. Of these, sensors, such as a thermal imager (TI), are one of the most important since they are employed for three primary purposes:

- As a reconnaissance sight;
- As a weapon aiming sight;
- As an integral component of a visually coupled system (VCS).

As a sighting system, the TI would be located high on the airframe, preferably in a mast-mounted configuration enabling the helicopter to maximise the use of available cover whilst utilising a 360° field-of-regard. Used in conjunction with the armaments, the infra-red sensor potentially provides a means of aiming turreted weapons and has an inherent target acquisition capability, enabling designation of targets for guided missiles. For laser systems operating at IR wavelengths, the TI also affords the feedback for directing the beam onto the target.

Modern attack helicopters are increasingly using visually coupled systems (VCS) to give a day/night, all weather capability in the NOE environment. The basic system comprises a head-position sensor, a helmet-mounted display and an electro-optic imaging sensor (frequently a TI) mounted on a gimbal system. In operation, the imager is automatically pointed in the direction of the crewman's head and the image projected onto his HMD. On the Apache, VCSs are provided for both crew in the tandem seat aircraft, the imaging sensors being positioned in the nose. When flown operationally, the system has proved valuable in extending the conditions when helicopters can be employed.

Another important class of sub-system is the Defensive Aids Suite (DAS), which assumes major significance in the survivability of the helicopter. Future systems are likely to consist of a series of sensors, including laser and radar warning receivers and hostile fire and missile approach warners, together with countermeasures, which may include IR and radar jammers, chaff and decoy flares. In principle, on detecting a threat, it is possible to deploy appropriate countermeasures automatically, although crew intervention may be preferable in tactically sensitive situations. Furthermore, in a fully integrated system, the defensive weapon systems might also be aimed and activated automatically in response to threat warnings.

Studying helicopter systems integration

In approaching the study of complex systems with multiple interactions, it is important to understand not only the technology issues but also the trade-offs at the total system level. A technique, well proven at the Defence Research Agency (DRA), is the use of mission simulators, based on graphics workstations, to provide an environment in which the platform, aircrew, mission systems and weapons can be assessed in a realistic operational context. To this end the HOVERS helicopter mission simulator was developed.

The HOVERS mission simulator

The HOVERS mission simulation facility is designed to allow detailed modelling of helicopter operational scenarios using high fidelity representations of aircraft systems. It enables realistic man-in-the-loop simulation of helicopter missions and uses state-of-the-art graphics workstations to bring together representations of sensors, instruments and the outside world with the man-in-the-loop.

The current configuration comprises 3 manned helicopters, each having 2 crew who can be seated either side-by-side or in a tandem arrangement. Additional computer-controlled forces (friendly and enemy) including other helicopters, main battle tanks, mobile air defence units, APC's, dismounted infantry with MANPADS and artillery, are also available to create a realistic battlefield environment.
Overall control and monitoring is achieved using additional workstations which provide reports of significant events such as missile firings and a master display.

The master display provides a 3-dimensional view of the battlefield, with the facility to show all combatants, missiles and terrain features in real time. Controls to vary the view and track specific combatants are also included, together with a logging facility which enables subsequent replay for tactical debriefing.

Each individual HOVERS station is configured with a position for a pilot and aircraft commander. The pilot flies the helicopter using conventional flight controls. His view of the outside world is provided by 3 graphics workstations. In a head-down location, an instrument panel provides him with all necessary flight and mission information. The aircraft commander currently has a head-down display from a stabilised infra-red sight, which he can control using a joystick and pistol grip. The sight also enables him to fire command-to-line-of-sight or fire-and-forget missiles and operate a laser rangefinder which also includes the grid reference of and range to the object being lased. He is also equipped with a colour digitised moving map display with the ability to reference the map to either north, or the track of the aircraft. It is also possible to overlay the footprint of the thermal image sight and a line on the map indicating the path of the laser beam.

Special features of the HOVERS simulation include dynamic modelling of IR and radar signatures in real-time, a comprehensive Defensive Aids Suite (DAS) and a realistic threat environment.

The multiple man-in-the-loop approach allows the important areas of crew communication, tactical interaction and co-operative operations to be addressed effectively. Perhaps even more significantly, it provides an environment in which tactics and new capabilities derived from emerging technologies can be developed together.

Previous HOVERS trials Over the past three years the HOVERS facility has been used for a total of 7 trials, examining a number of different issues:

- Optimal positioning of sensors;
- Effectiveness of defensive aids;
- Benefits provided by HMD symbology;
- Importance of tactical information.

Tactical information trial One of the most recent trials, examining the impact of the provision of tactical information in the helicopter cockpit, will be used to illustrate the types of study that can be performed using the HOVERS simulator.

It is envisaged that, on the future battlefield, tactical data will be continually received from various sources, integrated and then transmitted automatically to platforms and command units across the battlefield. Each platform will require an information management system (IMS) which will process and present the tactical data in a form that can be readily assimilated by the user. For the battlefield helicopter, this should provide regularly updated tactical information in the cockpit, offering potential improvements in situational awareness, mission effectiveness and survivability.

In order to examine the issues associated with the provision of a tactical information management system in the helicopter cockpit, a man-in-the-loop HOVERS simulator trial was performed. There were three primary objectives of this trial:

- To determine how the provision of automatically updated tactical information in the cockpit would influence operational effectiveness compared with that obtained when the only tactical information available was supplied over combat net radio.
- To investigate methods by which tactical information might be integrated with a display based on a cockpit mission planning system and how information from on-board sensors could be integrated with this display.
- To investigate how staleness in the updated tactical information might influence operational effectiveness.

A series of missions was designed and modelled using the HOVERS simulator. In this trial, a pair of generic attack helicopters was tasked to seek and destroy an enemy advance represented by computer-controlled ground forces and attack helicopters. Both man-in-the-loop simulated helicopters were operated by combat ready Army Air Corps personnel drawn from line regiments. In total, six crews, each comprising a commander and a pilot, flew 90 missions during the course of the three week trial.

Measures of effectiveness were used, together with situational awareness indices, workload measures and comments from the aircrew, to compare the operational impact of the tactical display configurations.

A number of significant results were found:

- The provision of tactical information significantly increased the survivability.
- When equipped with a tactical display providing automatic updates of information, there were *no* cases of fratricide, despite the extremely high threat environment. This was compared with an average of more than one case in every three missions run without a tactical display.
- The availability of tactical information allowed the crews to plan more effective missions. For example, they were

able to prioritise the threats, targeting the highest threat ground vehicles first.

- The provision of tactical information improved the situational awareness and reduced the work load of both pilots and commanders.

- Incorporation of the on-board sensor data into the tactical display provided further improvements in mission effectiveness and survivability.
- The tactical display developed for the trial was highly regarded by the aircrew. Many useful comments were made by the crews concerning improvements and additional information required.

The major conclusion to be drawn from this trial was that information management systems are potentially of great value, improving mission effectiveness, survivability, situational awareness and reducing instances of fratricide.

The results of the trial will be used to help to define future requirements for tactical information provision in the helicopter cockpit.

In addition to the benefits provided to the DRA and the MoD in terms of the increase in knowledge about tactical information systems, the Army Air Corps themselves benefited from the trial from the tactical training afforded by running 30 battlefield missions with technology appropriate to 10-15 years in the future.

Concluding remarks

This paper has described some of the system trade-offs and integration issues associated with the next generation of military helicopters operating NOE in the battlefield. The interactions between weapons, sensors, aircrew and the platform itself are complex and it is important to address not only the technology issues but also the trade-offs at the total system level in appropriate operational contexts. An example of one of the trade-off studies performed at DRA Farnborough was described as an illustration. This used a "multiple-man-in-the-loop" workstation-based approach to the study of helicopter systems integration. This technique has proved a significant step towards gaining an insight into the potential of the future battlefield helicopter

Glossary

AH	Attack helicopter
APC	Armoured Personnel Carrier
DAS	Defensive Aids Suite
DRA	Defence Research Agency
FFAR	Free Flight Aerial Rockets
HMD	Helmet-Mounted Display
IMS	Information Management System
IR	Infra-Red
MANPADS	Manportable Air Defence System
MoD	Ministry of Defence
NOE	Nap-Of-the-Earth
SAM	Surface-to-Air Missile
TI	Thermal Imager
UN	United Nations
VCS	Visually-Coupled System

© British Crown Copyright 1996/DERA. Published with the permission of the Controller of Her Britannic Majesty's Stationery Office.

V-22 Technical Challenges

Steven I. Glusman
V-22 Technology Manager

Robert A. Hyland
V-22 Assistant Technology Manager
Boeing Defense & Space Group, Helicopters Division
P.O. Box 16858, Mail Stop P10-71
Philadelphia, PA 19142, USA

Roger L. Marr
V-22 ITT Contractor Flight Test Director
Cedar Point Road, Hanger 109, P.O. Box 220
Patuxent River, MD 20670, USA

Summary - The Bell-Boeing V-22 Osprey Tiltrotor is an unique aircraft capable of landing vertically like a helicopter, flying at speeds in excess of 300 KTAS like a turboprop, with the added feature of folding the rotor/wing for deployment from shipboard for U.S. Navy/Marines operations. During the development of the V-22 and subsequent 1000+ hours of flight testing, many technical challenges were encountered and overcome. These challenges included: aerodynamic characteristics of the wing, tail buffet, hover performance, hover downwash, structural loads limiting, vibration reduction, landing gear fatigue life, and control law design/Handling Qualities. This paper presents an overview of many of these challenges, discusses the techniques used to perform analysis and flight test, and presents results of the relevant portions of the test program.

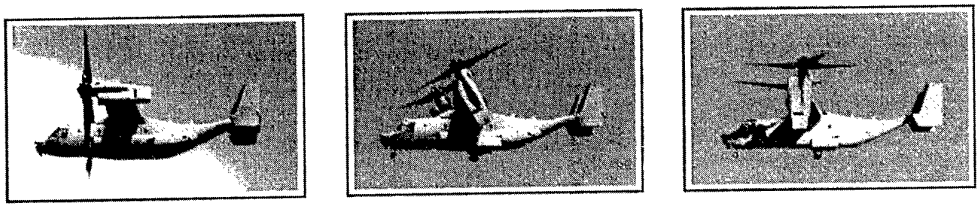

Figure 1. Bell-Boeing V-22 Osprey Tiltrotor Operating Modes

List of Symbols and Acronyms

AFCS	Automatic Flight Control System
CDU/EICAS	Control Display Unit/Engine Indicating and Caution Advisory System
C_L	Lift Coefficient
C_M	Moment Coefficient
DCP	Differential Collective Pitch
EMD	Engineering Manufacturing Development
FBW	Fly By Wire
FCS	Flight Control System
FFS	Force Feel System
FSD	Full Scale Development
HQR	Handling Qualities Rating
ICDS	Interconnect Drive Shaft
IRS	Infrared Suppressor
KTAS	True Airspeed, Knots
LFL	Longitudinal Flapping Limiter
LHA	Landing Helicopter Assault
LHD	Landing Helicopter Dock
LPH	Landing Platform, Helicopter
LRIP	Low Rate Initial Production
LSG	Lateral Swashplate Gearing
OARF	Outdoor Aerodynamic Research Facility
OLC	Opposed Lateral Cyclic
PAO	Pilot Augmented Oscillation
PFCS	Primary Flight Control System
RHP	Rotor Horsepower
RPM	Rotor Speed, Revolutions Per Minute
SHP	Shaft Horsepower
SLL	Structural Loads Limiting
SWC	Symmetric Wing Chord
TCL	Thrust Control Lever
VTOL	Vertical Takeoff and Landing

Presented at the AGARD Advances in Rotorcraft Technologies Symposium, Ottawa, Canada, May 1996

1.0 INTRODUCTION

1.1 Background

The V-22 tiltrotor is a unique rotorcraft in that it can efficiently hover like a conventional helicopter as well as cruise at speeds up to 275 knots with the efficiency and comfort of a turboprop airplane (Figure 1). Designed by the Bell-Boeing team for the U.S. Marines and Navy, this aircraft has completed over 1000 hours of Full Scale Developmental (FSD) flight testing and is currently in the Engineering Manufacturing Develop-

Paper presented at the FVP Symposium on "Advances in Rotorcraft Technology", held in Ottawa, Canada, 27-30 May 1996, and published in CP-592.

ment (EMD) stage where four production representative airframes are being produced. While one FSD vintage aircraft is completing risk reduction flight testing and pilot training, the first EMD V-22 is scheduled to fly in late 1996. The plan for the overall development program is presented in Figure 2.

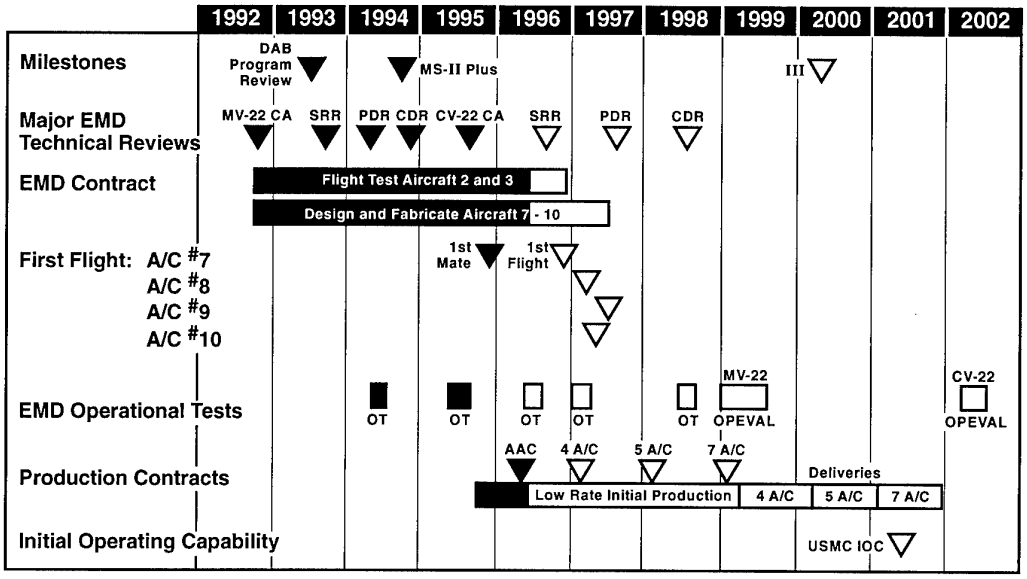

Figure 2. V-22 EMD / LRIP Program Schedule

The V-22 obtains its unique capabilities through its tilting proprotor, specially designed high twist rotors (47.5 degrees twist), and reconfigurable fly by wire (FBW) flight control system. In the VTOL mode (80-95 deg nacelle), Figure 1, the tiltrotor is controlled much like a helicopter using rotor cyclic and collective forces for longitudinal and lateral control. In airplane mode (0 deg nacelle), rotor controls are phased out except for use as trim devices. Standard airplane control surfaces are used to control the aircraft in this flight regime. In conversion or STOL mode (between VTOL and airplane modes), a combination of rotor and airframe forces are used to provide control. The triply redundant FBW flight control system facilitates the phasing and scheduling of these controls and allows for complex control law scheduling with a variety of parameters including nacelle angle and airspeed.

Some of the salient design features of the V-22 are shown in Figure 3. The aircraft has 38-foot diameter rotors and 6150 SHP engines installed in nacelles on each wing tip which can be tilted from 97.5 to 0 degrees. The fuselage, wing, and H-tail were sized primarily by shipboard compatibility and spotting on

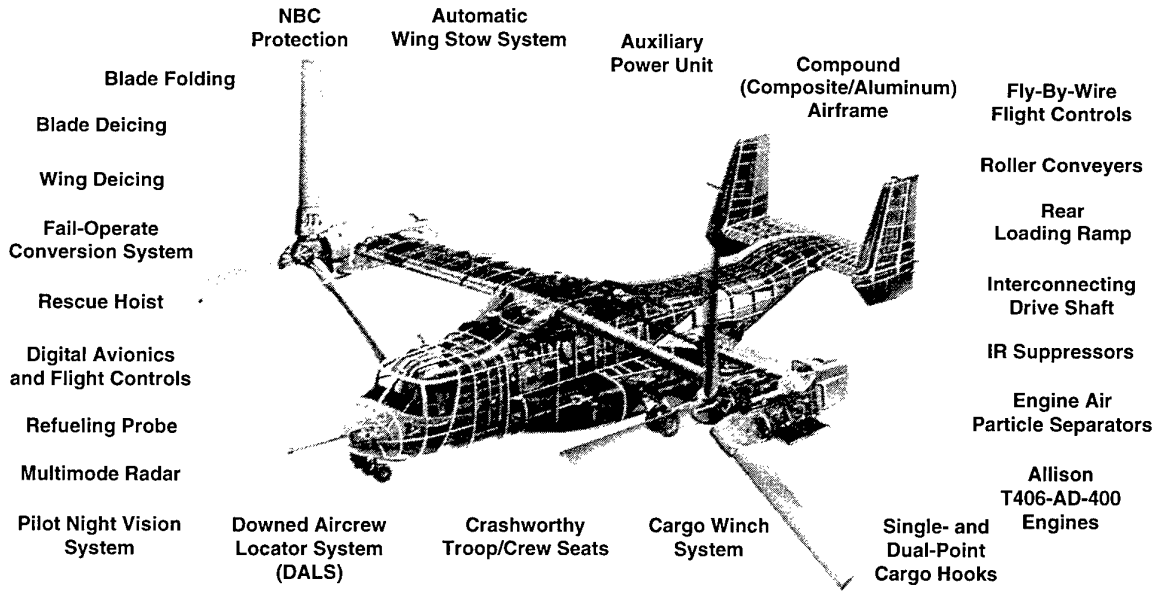

Figure 3. V-22 Multi-Mission Features

the flight and hanger decks of LPH, LHA, and LHD ships. The V-22 has capability for seating 24 combat troops, carrying external cargo up to 15,000 pounds, loading/unloading internal cargo through an aft ramp, folding of the rotor blades and wing for stowage aboard ship, all weather instrument flight, day or night, and continuous operation in moderate icing conditions at weights up to 60,500 pounds for self-deployment. The V-22 structure makes use of the latest in composite materials and manufacturing processes. A synergistic combination of precision machined aluminum, fiber-placed graphite, and titanium makes up the under-spec weight V-22. The cockpit, which includes conventional controls and digital avionics displayed on four MFDs and one Control Display Unit/Engine Indicating and Caution Advisory System (CDU/EICAS). Cockpit displays architecture was redesigned from that used in FSD to enhance crew station effectiveness, provide additional systems information, and reduce overall workload.

1.2 Technical Challenges

During the development of the aircraft and FSD flight testing, several technical challenges were encountered and resolved. Resolution for many of the challenges resulted in enhancements to the overall characteristics of the aircraft. Some were addressed during pre-test design and only required verification in flight test while others were "unknown" until found during flight test. Each presented unique challenges to the design/test team. The following paragraphs describe some of the significant challenges and the techniques used to resolve them.

2.0 HANDLING QUALITIES

The multiple control surfaces of the V-22 enable the Handling Qualities of the aircraft to be tailored for its many flight regimes. The control methodologies employed are illustrated in Figure 4 (Ref. 1). As shown, the pilot interfaces with the control system through a conventional center stick, pedals, and a thrust control lever (TCL). In helicopter mode, control moments are generated by fore/aft longitudinal cyclic pitch (longitudinal stick), a combination of lateral cyclic pitch and differential collective pitch (lateral stick), differential longitudinal cyclic (pedals), and indirectly controlled collective pitch (TCL). In airplane mode, control forces are generated by elevator (longitudinal stick), flaperons (lateral stick), rudders (pedals), and power (TCL).

The Primary Flight Control System (PFCS) provides the flight critical functionality of the unaugmented control system. The Automatic Flight Control System (AFCS) enhances the Handling Qualities through forward control shaping, increased damping, and automatic Hold mode features. V-22 design requirements were to achieve Level 2 Handling Qualities for PFCS

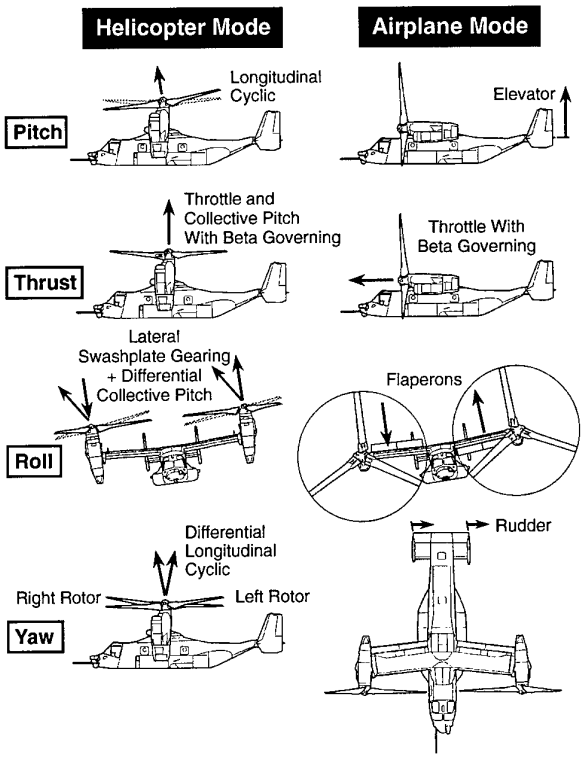

Figure 4. V-22 Helicopter and Airplane Mode Control Characteristics

and Level 1 for AFCS. The AFCS provides high command/response augmentation to improve Handling Qualities for mission oriented tasks. The AFCS is based on a modified explicit model following architecture whereby desired response characteristics are defined within the AFCS control laws. In the longitudinal axis, the pilot is provided an attitude command system. A rate/attitude hold system is provided in the roll axis with the directional axis being a rate command system with heading hold. Unlike a conventional helicopter, the V-22 pilot actually commands engine power not collective pitch (Ref. 2). The V-22 rotor speed governor modulates collective pitch to maintain RPM. In the airplane mode, an angle of attack command system is provided. Automatic turn coordination augments a roll rate/attitude hold system with "feet on floor" capability. In airplane mode, the throttle modules power while the rotor governor maintains RPM. Typically 84% RPM is used in airplane mode to improve performance and reduce vibration and cockpit noise. In helicopter and conversion mode, 100% RPM is used to maximize performance. Interim rated power is available at low speeds utilizing 103.8% RPM to further boost power available for takeoff and landing maneuvers.

Handling Qualities of the V-22 have been extensively evaluated both for the PFCS and for the AFCS (Ref. 3 and 4). Handling qualities evaluations were accomplished using a series of mission task element type

maneuvers, first in simulation, and then in flight test. The results of these evaluations are presented in Figure 5. Overall, Level 2 Handling Qualities have been demonstrated with the PFCS and Level 1 with the AFCS. Some areas found deficient during FSD have been corrected, but remain to be evaluated during EMD. One example, the mechanical design of the Force Feel System (FFS), which exhibited an unacceptable force 'dead-band' in the FSD aircraft has been redesigned for EMD to be within force 'dead-band' tolerances.

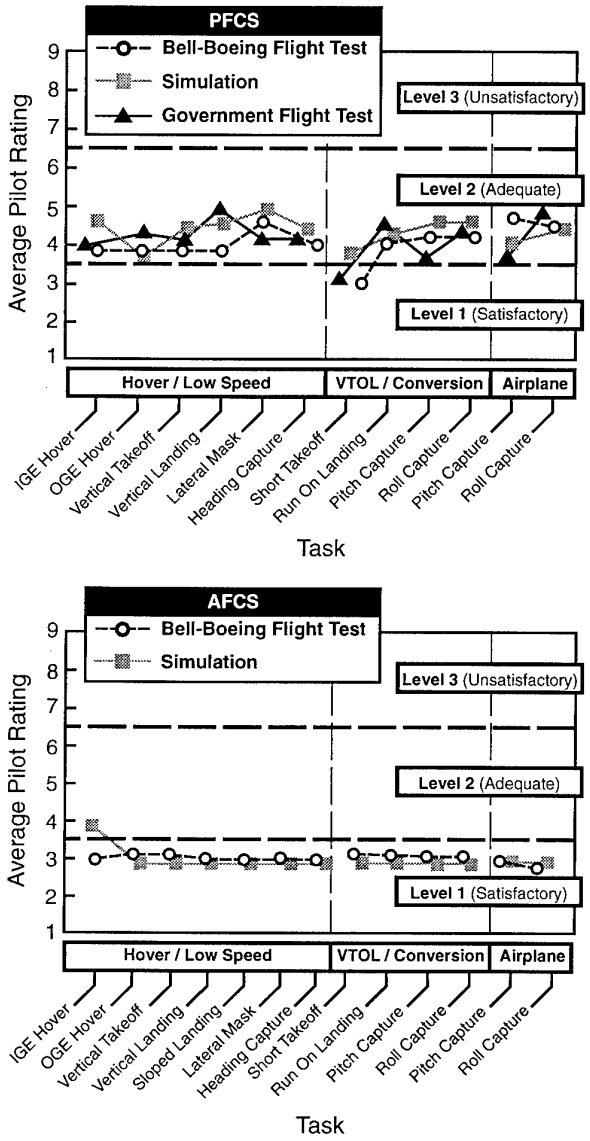

Figure 5. Handling Qualities Summary

3.0 AEROSERVOELASTICS

Aeroservoelastic stability is where the airframe modes couple with the pilot and/or the flight control system. Because of the size and relatively unusual mass distribution of the V-22 (engine/transmission located in nacelles at the wing tips, H-tail), airframe flexibility played a key role in development of the overall Flight Control System (FCS). This drove the initial requirement for numerous notch and low-pass filters throughout the flight control system. The filters were carefully designed to attenuate undesirable coupling with imposing degrading phase delays in the pilot or feedback control paths. At the center of this design effort was a full-state 26th order model (Ref. 5) which provided the design/analysis tool to develop and analyse the filtering. The referenced model includes aircraft rigid body dynamics, the first 10 structural modes, the flight control system, and low-order pilot models. Pilot models were developed through ground shake tests and in-flight Pilot Augmented Oscillations (PAO). The result has been a successful demonstration of required phase and gain margins throughout the flight envelope.

Three significant control system/airframe coupling challenges were identified early in the initial envelope expansion flight testing. The first was a PAO which occurred prior to first flight during unrestrained ground runs. Lateral aircraft oscillations occurred at a frequency of approximately 1.5 Hz when the pilot tightly gripped the control stick as shown in Figure 6. The oscillation had a damping ratio of -4.0% critical. When the pilots' hand was removed from the stick, the oscillation became positively damped with a damping ratio of +3.0%. This was not a classical ground resonance, but the aircraft upper focus rigid body roll mode coupling with the pilots' anthropometric input. The lateral acceleration of the pilot's seat produced an inertial input to the pilots' arm, moving the lateral stick which was, at that time, unbalanced laterally.

Various solutions were considered, including mass balancing the lateral stick, altering the lateral stiffness characteristics of the tires and landing gear oleos, and desensitizing the lateral control axis through software. Lateral stick mass balancing was selected as the solution since simulation showed the other two alternatives either degraded Handling Qualities to unacceptable levels or did not contribute significantly to the cause of the oscillation. With the lateral stick balanced, the mode was shown to be well damped (+8.5%) and there was no oscillations with the pilots' hand on the controls.

The second flight control system/airframe coupling occurred during airplane mode envelope expansion at 250 KCAS. An uncommanded, unstable lateral oscillation at approximately 3.0 Hz occurred again due to the pilot coupling with the asymmetric wing chord bending natural frequency through the lateral stick. Ground based shake tests were accomplished with various pilots to model their inputs and verify control system and airframe natural frequencies. Once the

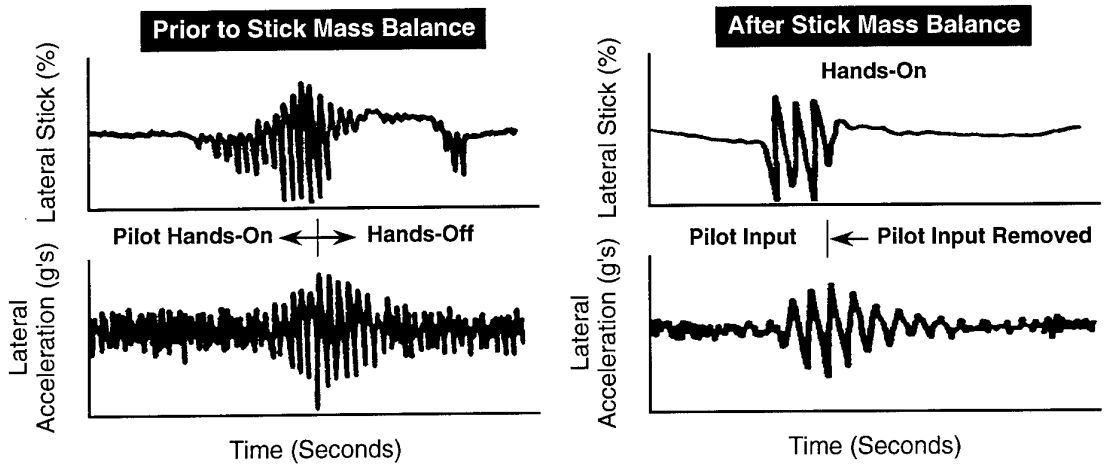

Figure 6. On-Ground Pilot Augmented Oscillation

physics of the oscillation were understood, a notch filter was incorporated in the lateral control axis to reduce the pilots' gain at that frequency. The solution was evaluated in piloted simulation and shown to be stable beyond the flight envelope. The aircraft flight control system was then modified and retested, verifying no instability.

The third involved pilot bio-mechanical coupling, again in airplane mode, with the symmetrical wing chord (SWC) mode. In this instance, pilot coupling occurred through Thrust Control Lever (TCL) motion due to fore/aft acceleration of the cockpit resulting in a significant destabilizing trend above 250 KCAS. During the initial analyses, prior to flight, the model did not predict the destabilizing trend because the pilot coupling was not considered. Based upon pilot in the loop ground-based shake tests, a pilot model was developed and analyses correlated with measured test data. A notch filter was added to correct the coupling.

4.0 STRUCTURAL LOADS LIMITING

The rotor of the V-22 represents a compromise between hover performance requirements, cruise efficiency, and shipboard compatibility concerns. The fuselage structure is designed by stiffness/strength margins to eliminate unnecessary weight while providing required strength for a 4g flight envelope and hard landings typical of those encountered onboard ships. To minimize design loads both in the rotor/drive system and the fuselage, structural loads limiting functionality was an initial criteria designed into the flight control system. The Structural Loads Limiting (SLL) design team, comprised of flight controls, flying qualities, aerodynamic, and structural loads engineers applied a integrated team approach to find a solution which maintained Level 1 Handling Qualities while maintaining loads within design limit thresholds while not unduly penalizing the aircraft maneuver capabilities or the airframe structure. The following are some of the SLL features.

4.1 Drive Shaft Loads, Airplane Mode

In the V-22, the two 38 ft diameter rotors are connected via a composite interconnect drive shaft (ICDS) so that in the event of an engine loss, both rotors receive power from the remaining engine. When both engines are operating however, torque differences between the two rotors, generated in airplane mode maneuvers, manifest themselves as high loads within the ICDS resulting in reduced component life. The V-22 control laws were designed to balance the torque in the rotors using differential collective pitch (DCP). In other words, a helicopter type control input was used during airplane mode to reduce a structure load. Roll rate capability of the V-22 was greatly enhanced by this segment of the control laws as shown in Figure 7. The use of DCP to reduce ICDS loads also provided for enhanced turn coordination; an unexpected but welcomed effect.

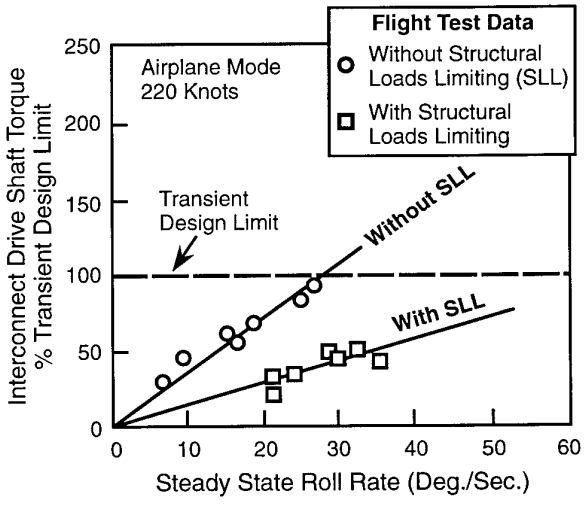

Figure 7. Effect of Structural Loads Limiting On Roll Maneuver Capability

4.2 Drive Shaft Loads, Helicopter Mode

Torque splits in helicopter mode generated by DCP inputs also generate ICDS loading. DCP however forms the primary roll control force posing a challenging resolution. To minimize ICDS loading while improving the lateral axis Handling Qualities, which are influenced by the large roll inertia of the V-22, the SLL team added Lateral Swashplate Gearing (LSG) to the control laws. LSG uses lateral cyclic from the rotors which provides both a rolling moment and a direct sideforce. With the addition of LSG as a lateral control, DCP was reduced leaving only enough to maintain control sensitivity. Pilot opinion of the hybrid lateral control scheme was overwhelmingly positive. Precision lateral control, especially in very low speed flight, was enhanced by the direct sideforce generated by LSG. Loading for large lateral inputs was also reduced as the LSG input did not produce a significant loading through the ICDS.

4.3 Rotor Loads, Airplane Mode

The large rotors of the V-22, as compared to a turboprop airplane, make the rotor susceptible to high in-plane loads during aggressive longitudinal maneuvers especially those associated with high pitch rates. Again, the control laws incorporate SLL considerations to minimize these loads while providing adequate control power for 4g maneuvers. The model following structure within the FCS facilitated this implementation by making commanded rates and accelerations discretely accessible. This system is implemented in a "passive" manner using feed forward limiting and existing feedback paths optimized for loads limiting functions. Careful attention in the design process provided a balance between maneuver requirements to insure Level 1 Handling Qualities while also providing loads limiting functionality. Flight testing of the SLL system has demonstrated the improvement in this area as well. Additionally an active system was investigated, but was not needed to meet required load levels. Active cyclic (Ref. 6) utilized another typical helicopter control, longitudinal cyclic, to actively reduce rotor flapping during aggressive maneuvers and thereby reduce in-plane loads.

4.4 Flapping Limiter, Helicopter Mode

In helicopter and conversion modes, during maneuvering, large rotor flapping of significant duration occurs and results in reduced life of the rotor elastomers. To extend the life of these components, a Longitudinal Flapping Limiter (LFL) was designed using the elevator to "re-trim" the aircraft during a maneuver. The control laws essentially reduce flapping of the rotor by rotating the fuselage relative to the rotor using the moments generated by the elevator. In this case, a typical airplane type control input was used during helicopter mode to reduce a structure load. These control laws increase the rotor components life over a large nacelle/airspeed maneuver envelope by minimizing flapping across the regime automatically.

4.5 Conversion Protection

Conversion protection algorithms provide automatic nacelle movement during conversion (down or forward) as the upper extremes of the conversion corridor is reached, Figure 8. The high speed end of the corridor is set by a combination of power limits and rotor loading. Pilots typically convert (manually) within the center of the conversion corridor by maintaining a level fuselage attitude. However, in the case of an inadvertent conversion outside the "normal" corridor, the conversion protection system will move the nacelles. On the low side of the corridor when conversion rate occurs too fast, nacelle angle changes faster than airspeed increases; conversion is automatically slowed until the appropriate airspeed schedule is achieved, preventing flying below wing stall or "falling out". On the high side of the corridor, nacelles are automatically beeped forward if the aircraft is accelerated to the conversion corridor upper limit. The feature was also favorably received by the pilots in that they could aggressively maneuver the aircraft without exceeding the structural design limits.

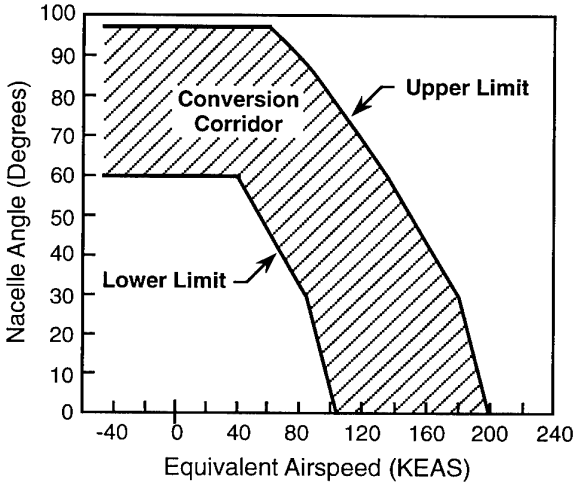

Figure 8. Conversion Corridor

5.0 EMPENNAGE BUFFET

During envelope expansion testing in FSD, large oscillatory loads were observed on the H-tail and aft fuselage. The high loads were associated with wind up turns at moderate speeds (Mach No. = 0.32). Buffet

occurred at angles of attack less than stall angles predicted based on previous wind tunnel tests. In-flight investigations were performed using tufts, aircraft-mounted photographic equipment and various instrumentation to gain insight into the cause of the buffet. In addition, water and wind tunnel tests were conducted to determine the source of the buffet.

A subsonic wind tunnel test was performed in June 1994 using the V-22 0.15-scale model to investigate the source of the buffet and what modifications could be made to reduce or delay buffet onset. The source of the buffet was found to be wing stall emanating from the inboard wing area and the overwing fairing.

Having found the source of the buffet the focus of testing shifted to finding an aerodynamic solution to eliminate, reduce, or delay buffet. Various aerodynamic modifications were attempted including (Ref. 7):

- Gurney flaps on the wing
- Symmetric differential inboard/outboard flaps
- Wing root trailing edge extensions
- Wing vortex generators

None of these modifications were successful at producing a significant reduction of buffet pressures. Two configurations that did produce improvements were conical sponson strakes and forebody strakes. The conical strake improved buffet onset angle of attack and $C_{L_{Max}}$. However, at high post-separation AOA (25°), the tail pressures were high, static margins were significantly reduced, and drag was increased.

The forebody strake configuration (Figure 9) was the most promising configuration. The strake was designed to generate a vortex that added energy to the flow over the mid-wing fairing area thus keeping it

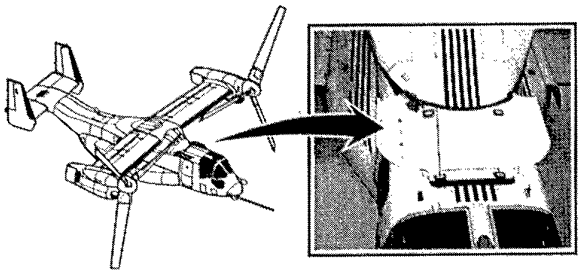

Figure 9. Placement of Forebody Strakes

attached. The effect of the strake on empennage buffet is shown in Figure 10. The strake delays the rise in pressure by about 5° in angle-of-attack on both the horizontal and vertical tails. Additionally, maximum buffet pressures are less with the strake installed. Overwing fairing pressures are also reduced with the strake installed. Pressure changes occur suddenly at approximately 19° alpha without the strake. With the

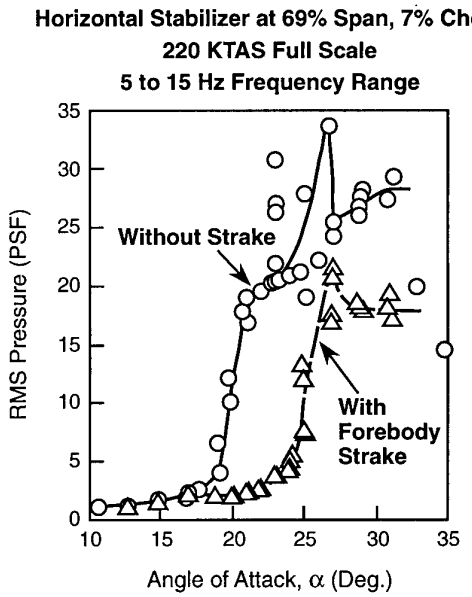

Figure 10. Effect of Forebody Strake On Reduction and Delay of Empennage Buffet Onset

strake, pressure changes occur more gradually at 25° alpha. No effect on drag was noted except at the stall boundary where overall drag decreased.

Having identified a potential solution, the next step was to test the strake on one of the risk-reduction aircraft. Initial flight test results were very positive with up to a 6 deg increase in the angle of attack associated with high buffet loads due to the forebody strake as illustrated in Figure 11. Subsequent testing, however, at higher Mach numbers indicated a less dramatic improvement in buffet angle of attack due to the strake. Further investigation found that the wing leading edge deice boot was malfunctioning resulting in poor aerodynamic performance of the thick V-22 wing. With the leading edge "smoothed" (de-ice boots operating normally), adequate angles of attack were obtained within the required maneuverability without incurring high buffet loads. Flight control system control laws have been modified to incorporate angle of attack limiting algorithms to provide additional protection against inadvertent encounters with tail buffet.

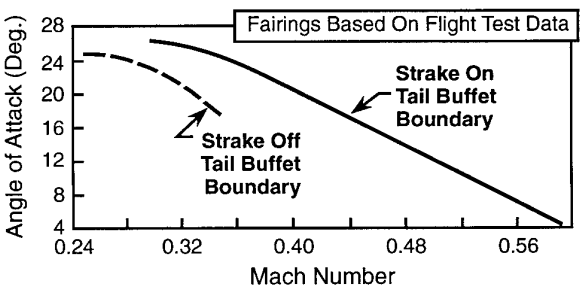

Figure 11. Strake Flight Test Results

6.0 HOVER PERFORMANCE

Hover performance is a critical parameter for all vertical lift aircraft. As a result, a large effort was devoted to understanding and optimizing hover performance for the V-22. In addition to solidity ratio, rotor blade airfoil, rotor radius, and number of blades, design parameters that largely influence hover performance for conventional helicopters; downwash and jet thrust are significant contributors to the hover performance of tiltrotors . Many of the conventional parameters that are optimized to provide improved hover performance were constrained by shipboard compatability requirements imposed on the V-22.

Early analysis and testing shows that rotor wake impingement on the wing causes a large download amounting to up to 10% loss of lift capability. Similar flow patterns have been observed in both large and small scale tests using smoke, surface oil, and tufts. The flow pattern is depicted in Figure 12. As shown, a portion of the impinging downwash travels spanwise inboard until it meets the flow from the opposite rotor. From there the flow rises up in a fountain motion and is reingested by the rotors. This phenomenom is known as the "fountain effect". The large scale rotor test conducted at the NASA Ames Outdoor Aerodynamic Research Facility (OARF) showed that flow recirculation was responsible for reducing rotor thrust (Ref. 8).

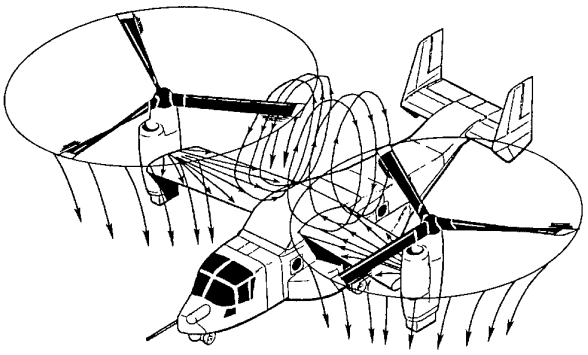

Figure 12. Downwash Flow Pattern

Some of the devices evaluated to reduce the download and re-circulation are discussed in Ref. 9. Tilting of the rotor disk inboard was one approach used. The tilting of the rotor disk inboard is referred to as "opposed lateral cyclic" (OLC). OLC reduces the thrust loss associated with the opposing rotor by reducing the fountain affect and thus the aerodynamic interaction between the two rotors. Reference 9 shows a significant reduction in lost thrust at 5.3° OLC. This reduction provides a 2.8% increase in lift capability. Other promising methods include flaperon deflection, increased rotor speed, and increased engine jet thrust.

Powered wind tunnel model and OARF testing have shown download reductions to be a function of flaperon angle (Figure 13). Based on a variety of test data, the angle for minimum download is estimated to be between 70 and 80 deg. For this reason, the maximum EMD flaperon deflection was increased to 73° from the current FSD maximum of 64°. Early hover performance testing will document the benefit of additional flaperon deflection on the EMD aircraft.

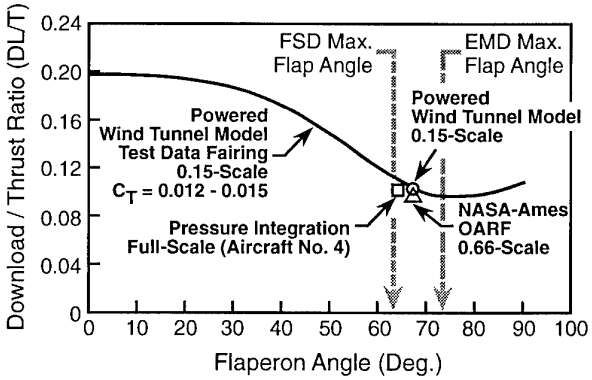

Figure 13. Downwash vs. Flap Angle

7.0 SLING LOADS AND AUTOJETTISON

The V-22 is required to carry a 15,000 pound external load on a dual point hook configuration or up to a 10,000 pound external load from either the forward or aft hook from a single point configuration. A key challenge to meeting this goal, and also proving the ability to carry the load at a relative high airspeed, was in the design and analysis of an autojettison system which protected the aircraft from shock loading in the event of a sling or attachment point failure but also did not result in erroneous autojettisions during normal maneuvering. In attacking this challenge, a thorough understanding of the dynamic interactions between the V-22, the external loads, and the attachment slings connecting the two was required. Again the model described in Ref. 5 was used in this analysis, modified to include the external load configuration. Consideration was given to modifying existing filters to include sling characteristics addressed many of concerns associated with this type analysis. The autojettison requirement was later evaluated during piloted simulation. A schematic of the V-22 autojettison algorithm is presented in Figure 14. The algorithm uses load level sensed from dual redundant cargo hook load cells to determine hook or attachment point failure. Large decreases in one of the two hook loads, with a corresponding increase in the other hook load, is one of the main drivers in the algorithm. Precise timing of change in load is required in addition to jettison the load.

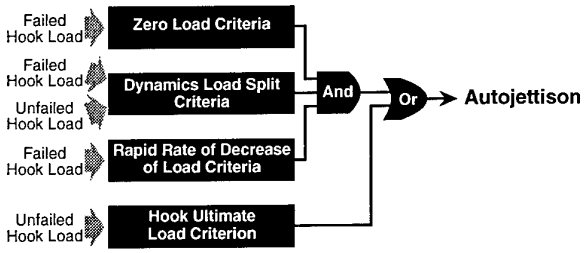

- Autojettison load criteria identifies potential failure and avoids inadvertent jettisons due to large load splits at high 'g' conditions
- Dynamic load split criteria avoids inadvertent jettisons due to gusts or sharp pilot inputs (low g's)
- Rapid rate of decrease of load criteria prevents inadvertent jettisons during sustained zero 'g' flight and during sustained oscillatory inputs with small attachment point separation loads
- Hook ultimate load criterion protects cargo hooks from damaging load levels

Figure 14. Proposed EMD V-22 Autojettison Concept

8.0 VIBRATION

During the initial envelope development flight testing several vibration challenges were encountered and corrected to provide overall an excellent aircraft vibration environment. Items incorporated to the aircraft included empennage fin tuning, hub pendulum absorbers, and wing fences.

The primary sources of excitation for the V-22 are 3/rev hub shears, 3/rev rotor vortices, and broadband wing tip vortices (Ref. 10). Hub shears are more predominate in helicopter and conversion mode due to asymmetric rotor inflow. Blade tip rotor vortices occur in all modes exciting the airframe from impingement on the empennage. Broadband buffeting of the empennage resulting from vortices off the nacelle-wing junction in conversion mode also excited the airframe. In order to control airframe vibration from these sources, the aircraft structure may be tailored, the excitation source may be controlled, or a counteracting excitation may be introduced. Each of these methods were used in meeting the vibration challenges discussed.

8.1 Vertical Fin Tuning

Vertical fin tuning weights were installed to improve airframe vibration in airplane mode based on results obtained during the Ground Vibration Test (GVT) prior to first flight. During the shake test it was found that the Horizontal Stabilizer Torsion (HST) mode was closer to the airplane mode 3/rev forcing frequency then orginally predicted. Incorporation of weight to the top of each vertical fin on the FSD aircraft resulted in lowering the HST mode and reducing cockpit vibration levels 40 to 45%. As a weight reduction measure for the EMD aircraft, the empennage was redesigned by removing the fin weights and tuned by frequency placement to meet the vibration requirement for the fuselage.

8.2 Hub Pendulum Absorber

Analytical predictions of possible pylon and fuselage vibration due to large fixed system inplane 3/rev hub shears were confirmed during initial flight testing. Vibration was predominately the result of rotor yoke chord bending 2/rev inplane shears in the rotating system. The solution identified was to incorporate inplane hub pendulums tuned to reduce the 2/rev shears in the rotating system. Active weights are located on each arm of the pendulum. During level flight, in conversion mode, the addition of the pendulums reduced cockpit and engine vibration 60% and 90% respectively as illustrated in Figure 15. In airplane mode, the reduction to the cockpit was from 30% to 90% dependent on airspeed and 60% for the engine turbine radial. In maneuvering flight, overall cockpit and engine vibration was also improved with pendulums.

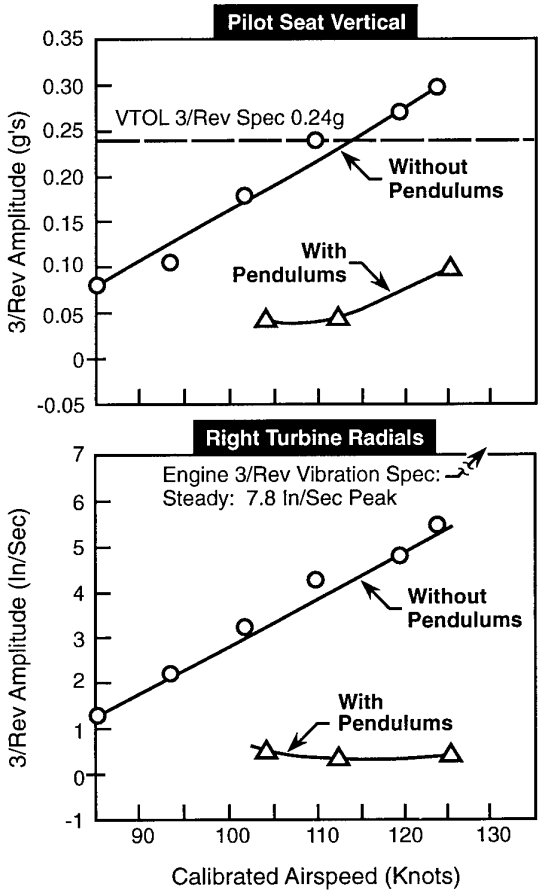

Figure 15. Effect of Pendulum Absorbers On 3/Rev Crew and Engine Vibrations; 60° Nacelle, Steady State Conditions

8.3 Wing Fence

Early in the development of the V-22, wind tunnel tests identified a source of vibration caused by broadband vortices from the wing-nacelle junction, when in conversion mode with the nacelles at 60 degrees, impinging on the empennage. The resulting aperiodic motion, primarily in the lateral direction, produced vibration in the cockpit. A wing fence (Figure 16), located outboard approximately 37 inches from the wing-nacelle junction and extending from the leading edge to the aft closure spar, was installed to alter the direction of the vortices. With the wing fence, overall vibration, particularly in the lateral pilot seat, was decreased by 50%.

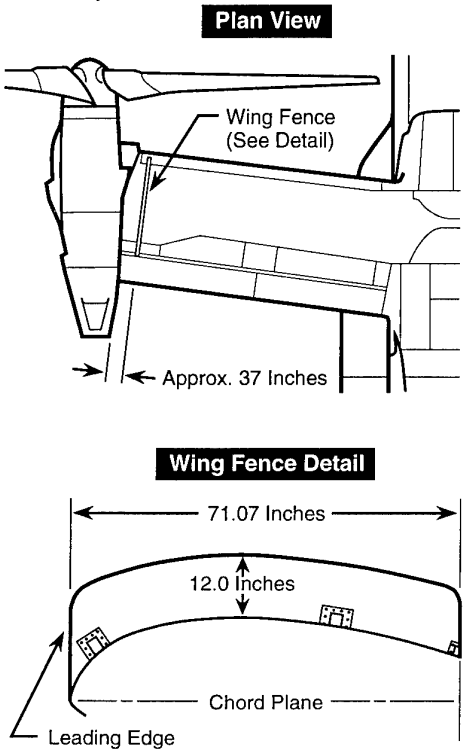

Figure 16. Wing Fence Configuration

9.0 CONCLUSIONS

The V-22 Osprey tiltrotor has demonstrated its unique capabilities in over 1000 hours of flight testing. Extensive analytical modeling analysis completed prior to flight testing, ground vibration tests, and developmental flight tests allowed timely resolution of technical challenges of the V-22 tiltrotor aircraft and provide improved Handling Qualities, performance and vibration. Some of the challenges that were identified prior to flight were verified through flight test wheras others were uncovered during the flight test development program. Analytical models, simulation, wind tunnels, and the flight aircraft were valuable tools available to the engineer to be used in meeting these challenges.

10.0 REFERENCES

1. Landis, K.H., Davis, J.M., Dabundo, C., Keller, J.F.,"Advanced Flight Control Technology Achievements at Boeing Helicopters", International Journal of Control, 59,1, 1994, pp. 263-290.

2. Schaeffer, J., Alwang, R., Joglekar, M., "V-22 Thrust Power Management Control Law Development", 47th Annual Forum of the American Helicopter Society, May 1991.

3. Dabundo, C., White, J., Joglekar, M., "Flying Qualities Evaluation of the V-22 Tiltrotor", 47th Annual Forum of the American Helicopter Society, May 1991.

4. Dabundo, C., Kimball, D., "Initial Flight Test Assessment of V-22 Flying Qualities", 46th Annual Forum of the American Helicopter Society, May 1990.

5. Parham, Jr., T., Miller, D.G., Froebel, A.T., "V-22 Pilot-in-the-Loop Aeroelastic Stability Analysis", 47th Annual Forum of the American Helicopter Society, May 1991.

6. Miller, D.G., Black, T.M., Joglekar, M., "Tiltrotor Control Law Design for Rotor Loads Alleviation Using Modern Control Techniques", American Controls Conference, June 1991.

7. McVeigh, M.A., Lui, J., Wood, T.L., "Aerodynamic Development of a Forebody Strake for the V-22 Osprey", 51st Annual Forum of the American Helicopter Society, May 1995.

8. McVeigh, M.A., "The V-22 Tiltrotor Large-Scale Rotor Performance/Wing Download Test and Comparison with Theory", 11th European Rotorcraft Forum, September 1985.

9. Wood, T.L., Peryea, M.A., "Reduction of Tiltrotor Download", 47th Annual Forum of the American Helicopter Society, May 1991.

10. Rangacharyulu, M.A., Moore, M.J., "Flight Vibration Testing of the V-22 Tiltrotor Aircraft", 47th Annual Forum of the American Helicopter Society, May 1991.

ACKNOWLEDGEMENTS

The authors wish to acknowlege the contribution of all members of the V-22 team to the success of this program. Bell-Boeing and NAVAIR, along with the numerous subcontractor team members, have all integrated their expertise into this unique rotorcraft.

Cockpit Technologies Research at the Flight Research Laboratory of the National Research Council of Canada

J.Murray Morgan and Stewart W Baillie
Flight Research Laboratory
Institute for Aerospace Research
National Research Council of Canada
Ottawa, Ontario, K1A 0R6
Canada

1. ABSTRACT

The Flight Research Laboratory of the Institute for Aerospace Research (FRL) has been involved, under the advice and with the support of the Department of Defense Chief of Research and Development, in examining the use of current and emerging technologies in the helicopter cockpit. The research has followed two general paths, the development of technologies specifically for integration into the helicopter cockpit, and examinations of how these can be used to reduce pilot workload or improve situational awareness for the crew. This paper will describe work at the pilot/machine interface, rather than manipulation of the machine itself. Three on-going segments of this program will be described, Direct Voice Input, Helmet Mounted Displays and advanced Head Down Displays.

2. INTRODUCTION

To put this program in perspective, there is a tendency today to use the term *Cockpit Technologies* to imply new high technology devices or systems implanted at the man/machine interface, with the unstated implication that this is something radical and different. In the history of cockpit development, however, this is far from the truth. Since the time that Sperry first put a gyro horizon in an aircraft, making instrument flight a practical possibility, the cockpit, particularly the military cockpit, has been at the forefront of technical development. How much of the functionality of the F18 cockpit would the Sopwith Camel pilot of 1918 recognize ? What has changed recently, however, is the rate at which new technologies are becoming available. These owe their development to the immense increase in compact computational power that has occurred primarily in the last decade. This has, led to a significant danger in the application of this power to the cockpit, the danger of doing something simply because it is possible, without due consideration of how, or indeed whether, it should be done.

As an independent body, the FRL has for some time been examining the application of computational technologies to the helicopter cockpit. This research has been partially under the auspices of the TTCP (HTP-6) and more recently in cooperation with and with the support of the Department of National Defense (DND) as represented by the office of the Chief of Research and Development (CRAD). This area encompasses three main topics of research:

- Direct Voice Input (DVI)
- Visually Slaved Systems, as exemplified by Helmet Mounted Displays (HMD)
- Advanced Heads-Down Displays (HDD).

The very large body of work into fly-by-wire control systems, including the use of miniature, integrated side-stick controllers, which resulted in a major contribution to the publication for ADS-33 [1] has been deliberately excluded from this presentation for two reasons. Firstly, it is a vital and major topic in its own right and is inherently included in separate discussions, secondly, it concerns the underlying characteristics of the vehicle the pilot is required to fly and as such does not impinge directly on the cockpit environment, except for the controller itself. This paper, therefore, will limit itself to describing our work in the areas of DVI, HMD and HDD.

3. THE TOOLS

3.1 The Airborne Simulator

The Flight Research Laboratory has for over twenty years used an extensively modified Bell 205A-1 helicopter (Figure 1) as a primary research tool in the area of flight mechanics. In particular, the aircraft has been fitted with a full authority, high bandwidth fly-by-wire (FBW) system. The aircraft, dubbed the Airborne Simulator, was acquired in 1969, first flew as a variable stability aircraft in 1972, and since then has been continuously modified to reflect the changing status of computational technology over its lifespan. Even now the evolutionary process that has kept this aircraft at the forefront of flight mechanics research in the Western world continues. The first week of April of this year saw the first flight with a completely new flight control computing system and digitized feel (control loading) system.

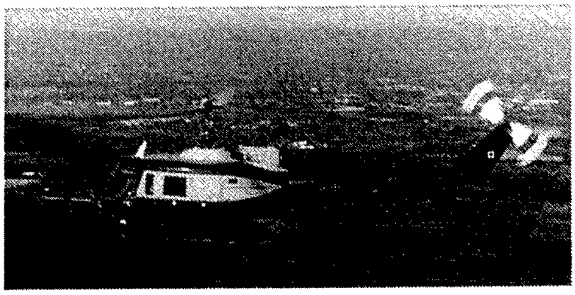

Figure 1 The Airborne Simulator

The aircraft has a full suite of state sensors, high bandwidth dual mode actuators (electrically or mechanically signaled) and the capability of recording a large number of state and control system parameters on a DAT tape. The aircraft is not married to a specific control system architecture: feed forward, state feed-back or model following techniques are used as demanded by the current project.

The majority of the work described here was and is being conducted on this machine.

Paper presented at the FVP Symposium on "Advances in Rotorcraft Technology", held in Ottawa, Canada, 27-30 May 1996, and published in CP-592.

3.2 The Advanced Systems Research Aircraft
Since the Bell 205 is limited in control power and bandwidth by its teetering rotor system, it was decided to build up a new variable stability research platform based on a modern rotor system. In 1993 the laboratory acquired a Bell 412 HP helicopter (Figure 2) to serve this role. This machine is now designated the Advanced Systems Research Aircraft (ASRA). While not yet having a FBW capability (that is scheduled for first flight in November 1996), it has already been modified and used for certain research activities.

ASRA has been fitted with an engineering work-station, based on a ruggedised 486 PC, an inertial reference system (Litton LTN 93), pitot and static pressures and temperature sensors, differential GPS and pilot control sensors. It also has a DAT data recording system, compatible with the FRL data playback and analysis system. Not only can the conventional primary flight instruments be driven from the workstation but the aircraft is currently fitted with a Litton Systems stereoscopic full color flat panel display, which will be described in more detail elsewhere in this paper.

Figure 2 The Bell 412 ASRA

4. DIRECT VOICE INPUT

Research into real-time connected speech recognition at the FRL dates back a little more than ten years. In the early to mid eighties, a speech recognition group, supported by CRAD, the NRC and the Neil Squire Foundation (an organization interested primarily in the provision of aid systems for the disabled) was established at the FRL. The fundamental work of that group, in close collaboration with the Canadian Marconi Company (CMC), resulted in the development of the IMELDA speech recognition technology. The FRL was instrumental in the further development of this technology for application in the helicopter cockpit, a distinctly degraded aural environment.

4.1 The Integration Process.
The first experimental application was made in the FRL Bell 205 Airborne Simulator, which represented a major integration effort. The speech recogniser used was a development unit built by CMC and mounted on a self-contained palette over the central console. It featured an external manual attenuator and certain switches required by the pilot.

The helicopter cockpit is inherently a difficult environment for technology of this type. Problems were encountered in several areas, of which electrical noise and acoustic pollution were the most difficult to overcome.

4.1.1 *Electrical Noise.*
The Bell 205 represented a major challenge from the point of view of electrical noise. Current helicopters commonly have a single source of 400 Hz AC power, either from an engine driven alternator or a DC/AC Invertor. The Airborne Simulator, (to support the extensive project instrumentation system), has a total of six invertors simultaneously active and drawing considerable current. In the aircraft's initial configuration, there was a major electrical spike at 800 Hz (the first harmonic) which appeared to be an insurmountable problem for the DVI system. The original configuration had all six invertors phase locked. Releasing them to run free replaced the single 800 Hz spike, with several close but not identical peaks, which were, therefore, of lower magnitude and less problematical.. A second activity was a major re-work of the aircraft's audio system. This included replacing the standard low output dynamic microphones with a type having built-in pre-amplifiers, thereby increasing the magnitude of the line signal and improving signal to noise ratio into the speech recogniser. These two actions reduced the inductive pick-up problem to negligible proportions.

4.1.2. Audio Pick-up.
The microphones used in the 205, although noise canceling, picked up enough spurious audio to affect system performance. Again this was mainly 400 Hz with its harmonics from such sources as fan or gyro motors. The only alleviation practical was careful adjustment of the microphone position relative to the mouth, attention to head orientation when speaking to the DVI system and manipulation of the manual attenuator.

4.2 Word Recognition Rates.
Eventually, single word recognition rates were increased to levels in excess of 99 % (References 2 and 3) from the 77 to 78% experienced initially. Participation in this study convinced the author categorically that very high recognition rates must be achieved to make these kinds of system acceptable to flight crews. It must be remembered that word recognition rate does not necessarily translate to a phrase recognition rate and it is the phrase that is important, not the single word. Also to gain any significant workload reduction from DVI, feedback to the crew that the DVI system has correctly identified a voice message must be aural, having to examine a visual display for confirmation, as was the case in the development installation, is not acceptable operationally.

4.3 Demonstrations.
In its final and thoroughly functional form, the system was demonstrated widely both nationally and internationally, by application of a fly-by-voice program. For this exercise, the Airborne Simulator was programmed with a series of very advanced control systems, blending one to another as the aircraft state demanded. A front end syntax parser and command interpreter converted DVI phrases into input qualities to the control systems, thus enabling the aircraft. to respond to voice control [4]. It should be noted that the FRL does not advocate voice input as a primary method of aircraft control. The Airborne Simulator is, however, set up in such a way that the internal computers have direct control over the vehicle, and this was the most convenient way of demonstrating the highly successful technology in a catching and dramatic way.

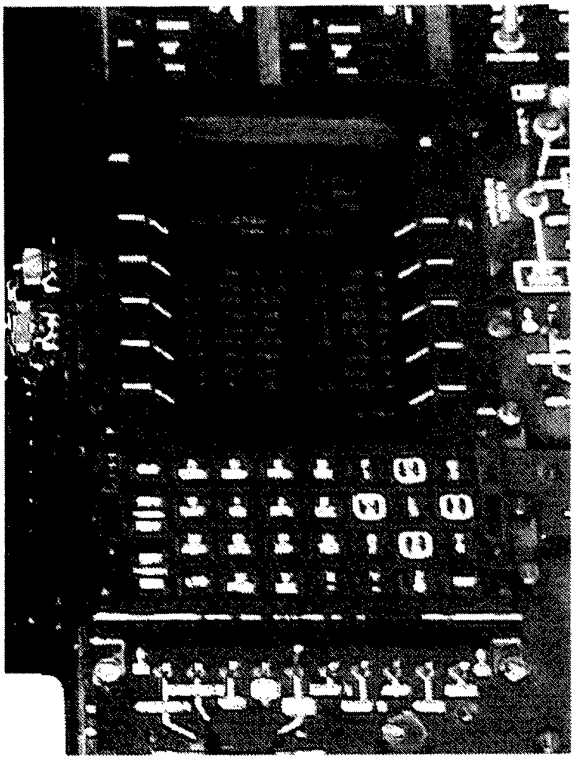

Figure 3 - The CMA2082 in ASRA

4.4 ASRA Installation / CMA 2082
This work is ongoing. The Canadian Marconi Company has now re-developed the hardware into a single card which fits into their CMA 2082 CDU (the unit chosen for the Canadian Griffin helicopter and illustrated in Figure 3). The most recent version of the DVI system features a sophisticated automatic gain control at the input, since the necessity of using a manual attenuator by the pilot was a major drawback in the previous unit. A development copy of this CDU has been installed in the laboratory's Bell 412 HP helicopter, which is the civil version of the Griffin. This installation again required significant integration efforts and it proved necessary, once more, to employ microphones with built-in pre-amplifiers to improve signal to noise ratio sufficiently. At the same time the internal software in the DVI system has been considerably expanded to permit a larger vocabulary and fewer syntactical restrictions.

4.5 Ongoing Activities.
At the time of writing, the aircraft is being prepared for a formal demonstration of this system to the Department of National Defense. Initially FRL pilots will be used as subjects for a pre-demonstration work-up and then Canadian military pilots will be shown the system in pseudo operational scenarios. It is expected that considerable workload relief over the manual operation of the CMA 2028 will be experienced.

5. HELMET MOUNTED DISPLAYS

The FRL has been a partner in the CRAD sponsored Visually Slaved Systems (VSS) program for a number of years. The overall program calls for cooperative research between a group comprising the universities of York and Toronto, CAE Ltd and the NRC. This will enable researchers to examine the use of VSS in the cockpit and at the same time develop an understanding of the human physiology associated with such systems. From the pilot-in-the-loop standpoint, this program hinges on the introduction of two major pieces of research hardware into the research tools available. These are two similar, but not identical, copies of the CAE developed Fibre Optic Helmet Mounted Display (FOHMD). One of these is at the University of Toronto's Institute for Aerospace Studies (UTIAS) for use in ground based research simulator, and one is at the FRL where it is being integrated into the Airborne Simulator.

This section of the paper will describe the equipment and installation as it applies to the Bell 205 Airborne Simulator.

5.1 The Airborne Installation.
The aircraft installation comprises four major sub-systems, these being:

- An Image Generation System
- An articulated Three Axis Sensor Table (TAST)
- The pilot's equipment
- A mechanical head tracker

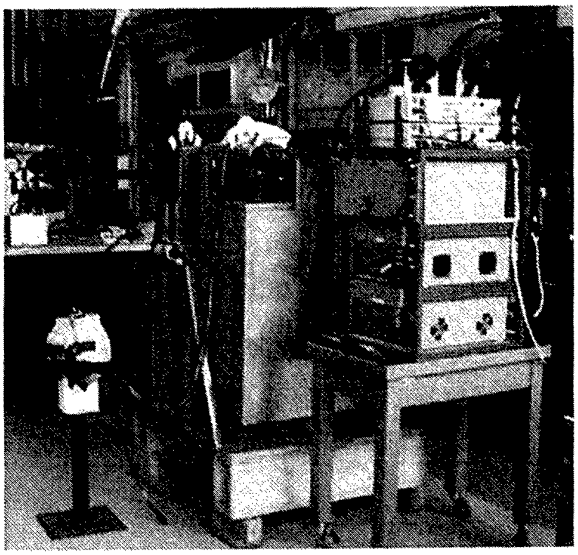

Figure 4 The Image Generation System

5.1.1 *The Image Generation System*
The image generation system (Figure 4) comprises a pair of NTSC standard 3CCD TV cameras, and a pair of re-packaged commercial projection TV systems (PTVS), one per eye and an SGI Indigo graphics generator. Each PTVS takes RGB signals from a single camera and combines them optically into a proprietary telescope, concentrating the light at the input end of a

coherent fibre optic rope which then transmits the full color signal to the pilot's helmet. A fourth projection gun permits the superimposition of symbols from the Indigo on the image. Remote controls in the cockpit give the pilot full control over the set-up and adjustment of the image generation system. Future provision may be made for the replacement of the CCTV sensors with other types of device (Image intensifiers and IR sensors being the most likely candidates).

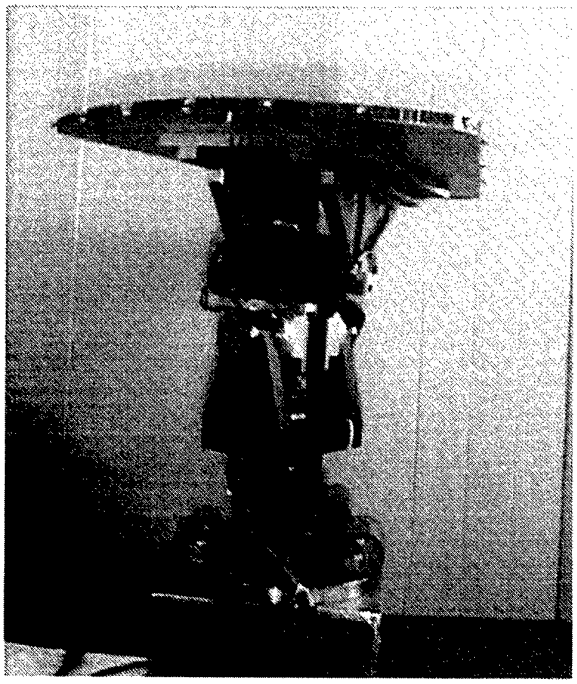

Figure 5 TAST Mk 1

5.1.2 *The Three Axis Sensor Table.*
Early in the program it was decided to develop an hydraulically powered sensor table for the optical sensors. The reason for this was practical. The electrical consumption of the equipment already installed in the Airborne Simulator is such that there is little spare electrical power available for project use, whereas a separate hydraulic system, used to power the control feel system was available and could provide adequate power to produce a high performance table. At this time little is known of the requirements for such a head-slaved table in a helicopter, so the specification was made generous in terms of maximum slew rate and small signal bandwidth. The original unit (TAST Mk 1, Figure 5) was designed and fabricated by Intempco Controls Ltee of Montreal to a FRL specification, but the design, although elegant, was not deemed suitable for actual airborne use. TAST Mk 1 effectively had the sensors, which weigh a total of 28 lb, at the end of a 14 inch stalk. The loads transmitted to the aircraft structure when the sensor package was moved at high bandwidth were deemed unacceptable for structural reasons.
An in-house design, which places the centre of mass of the sensors close to the centre of rotation of the table, with little translational motion, is currently under manufacture. This device, TAST Mk 2 (Figure 6), will employ the rotary hydraulic actuators designed and built for use with TAST Mk 1.

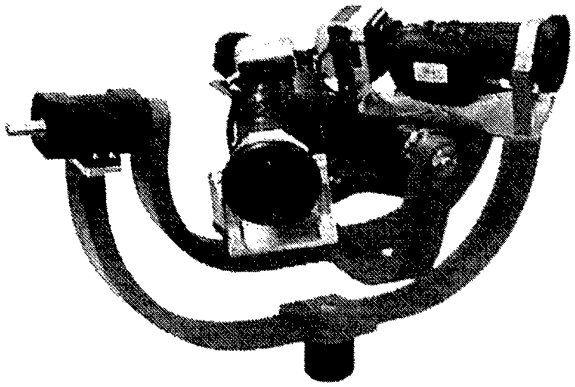

Figure 6 TAST Mk 2

5.1.3 *Pilot's Equipment.*
The pilot's optics and helmet are shown in Figure 7 The helmet features a molded-to- head foam liner, which extends well to the rear of the skull to pick up on the occipital bone, to reduce relative motion between the head and the optic assembly. This is necessary to maintain adjustment of the optics relative to the pilot's eyes, since the exit pupil of the HMD is only 15 mm and picture quality deteriorates quickly if the system is off axis. The optical units, each comprising a telescope, beam splitter and pancake lens, attach to quick release adjustable mounts either side of the helmet. Setting up the helmet assembly for a specific

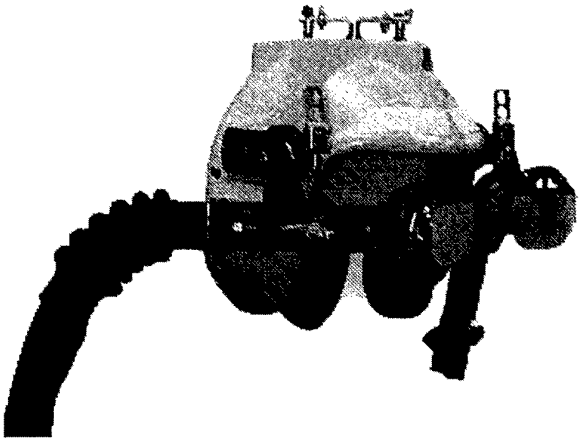

Figure 7 Helmet and Optics for FOHMD

subject requires the use of a special inter-pupillary jig and demands considerable skill on the part of the technician. The top of the helmet carries a mounting plate for the FRL mechanical head tracker (Figure 8). The entire assembly weights some 7.5 lb and results in significant restriction to free head movement due to the drag of the fibre-optic cables. The helmet optics permit a maximum field of view of 62.5 deg per eye for the unit at the FRL and 50 deg/eye in the UTIAS version. These limits determined the lensing of the CCTV cameras. Fixed wedges may

be mounted to the helmet to permit variations in eye to eye overlap. Currently wedges exist for zero, 20 and 40 degrees of overlap. Maximum overlap will always be limited to 40 degrees due to mutual interference between the optical units if greater overlap is attempted.

Figure 8 Helmet/Head Tracker Arrangement

5.1.4 *The Head Tracker*
The mechanical head tracker can also be seen in Figure 8. It is an in-house design, the arrangement being based on the ubiquitous '*Anglepoise* ™' desk lamp. This reflexed arrangement was necessary to overcome the very limited headroom restriction in the Bell 205 cockpit. The tracker permits the observation of three angles, a 'shoulder' yaw angle and three 'wrist' angles. From these four measurements the three helmet orientations relative to the airframe may be computed and the results used to drive the TAST actuators. This device has been used to generate head pointing data in a recent field of view study. It proved stable and capable of providing the required data.

5.2 Work to Date and Current Status.
The problems with TAST Mk 1 have caused significant delays in this program as it affects the FRL. However, some preliminary work has been done. The HMD optical system has been flown, but with fixed, forward facing cameras. This is not, obviously, a desirable configuration, but was deemed necessary to demonstrate that the entire system would survive the helicopter environment. No problems due to vibration or aircraft motion were found. The images remained stable and there were no failures or malfunctions noted. In another exercise, a bench integration of TAST Mk 1 was carried out. Full closed loop operation with the table being driven from head tracker signals via the aircraft's computing system was successful. Subjectively, head pointing and visual scene correlation were good and the visual acquisition of various target objects was easy and natural. This was a useful exercise in that it has given the laboratory experience in end to end closed loop operation which can be applied directly to TAST Mk 2 when it becomes available.

A preliminary experiment to examine the interaction between field of view and overlap, related to the HMD work in general was conducted in house. Some preliminary results are reported in Reference 5.

5.3 Planned Activities.
It is expected that TAST Mk 2 will become available by mid August 1996. At this point it will be mounted on a Bell 205 fuselage, instrumented with strain gauges and integrated with the HMD and head tracker., Skin loads will be measured both in 'normal' operation and under maximum performance test conditions. Provided the loads transferred to the airframe are acceptable, the device will be mounted on the Airborne Simulator for pilot-in-the -loop testing. If the loads are unacceptably high, the bandwidth of the table will be limited by absolute means (eg, flow restrictors in the hydraulic lines) before flight tests are undertaken. The initial flight tests will look at the effects of eye to eye overlap on the pilot's ability to control the aircraft through a variety of typical handling qualities tasks.

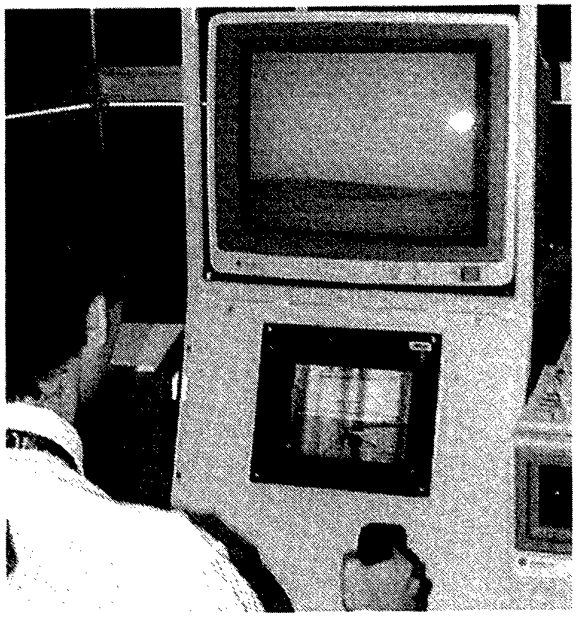

Figure 9 The Ground Based Development Facility

6. ADVANCED HEAD DOWN DISPLAYS

The FRL has an experimental flat panel display, built by Litton Systems of Canada, which uses active liquid crystal technology and has the capability of producing stereoscopic displays without the need for any specialized equipment on the part of the pilot. This is one of two modified versions of a Commanche display panel: the other is presently at the Wright Laboratories. The unit is essentially a blank screen accepting RGB signals, and the FRL is using a SGI Indigo computer to generate various display formats. This display unit has been mounted in ASRA for in-flight evaluation. It can also be mounted in a ground based development facility (Figure 9) for pilot-in-the-loop format evaluations and training, before actual flight trials.

6.1 General Philosophy.
Since the introduction of electronic displays into cockpits, there has been a proliferation of commercially available EFIS systems. All of them have one thing in common, they present the pilot with what is essentially an electronically generated drawing of traditional electro-mechanical instruments. This is understandable since the manufacturers must make what they can sell and their end users are, arguably, one of the most conservative bodies in existence. The available technology, however, lends itself to radically different applications One of these is the 'virtual VFR' or 'Highway in the Sky' presentation for instrument approaches. The FRL is embarking on a major program to investigate the potential benefits, or otherwise, of such pictorial displays. While there have been a number of research programs into the use of pictorial displays, it is believed that this will be the first to actually fly such displays in a helicopter.

The program at the FRL will initially examine how pictorial displays may apply to helicopters performing steep decelerating approaches under IMC. This particular flight regime has been chosen since it is a continuation of the Helicopter IFR program which has been underway at the FRL for over a decade. In this program (Reference 6 presents one of the most recent phases), the Airborne Simulator has been used to develop flight directors to permit helicopter instrument approaches under simulated IMC to decision heights of 50 feet and down to 20 kt ground speed. This program utilised a typical EFIS display. A continuation study using ASRA repeated some of the fundamental experiments using conventional electro-mechanical instruments and accepting the off-the-shelf stability augmentation of the standard Bell 412 HP. This served to provide continuity between the aircraft and to assess the general applicability of the Airborne Simulator results to a standard transport helicopter. It also acted as a lead-in to studies of pictorial displays.

The underlying philosophy for studying pictorial displays is based on the observation that helicopter pilots, at a very early stage in their training, develop the ability to perform accurate and repeatable visual approaches to a limited landing area with no greater reference than the view from the cockpit. At the same time, the ability to perform similar manoeuvres under IMC using conventional instruments requires considerable training, constant practice and sophisticated flight directors, optimized for each aircraft type. If a display can be produced which emulates the visual situation could the future pilot's task be made easier and safer (due to improved situational awareness) while eliminating the need to develop optimized flight director laws for each installation ?

6.2 Display Formats
For the initial study, the SGI Indigo has been programmed to offer:

- A standard EFIS display with a format very close to that in the Airborne Simulator.
- A pictorial display, essentially a limited out-of-the-window picture of a landing pad and one or two vertical features to provide height references. On this is superimposed a partial set of flight parameters, comprising an attitude reference symbol, height and vertical speed, heading, distance to touchdown, ground and airspeed and a slip indicator.

Guidance on the standard EFIS is a full three axis flight director identical to that described in Reference 6. On the pictorial display it is a set of rectangles, representing in height and dimension the standard 2 dots guidance of conventional approach systems. The rectangles are anchored to the surface by single 'posts'. Taken together they form a visual tunnel in the sky, through which the pilot may fly.. Figure 10 shows this display format with the aircraft on the ground on the helipad, facing a guided go-around or missed approach tunnel. On the latter display, guidance may be augmented by a flight path predictor, showing the anticipated aircraft position 1,2,3,4 and 5 seconds ahead of the present. This combination of displays has recently been used for an initial study wherein evaluation pilots were asked to complete simulated steep decelerating approaches using the following combinations of displays:

- Conventional EFIS/Flight Director
- Pictorial display, mono, no predictor
- Pictorial display, stereoscopic, no predictor
- Pictorial display, stereoscopic, with predictor.

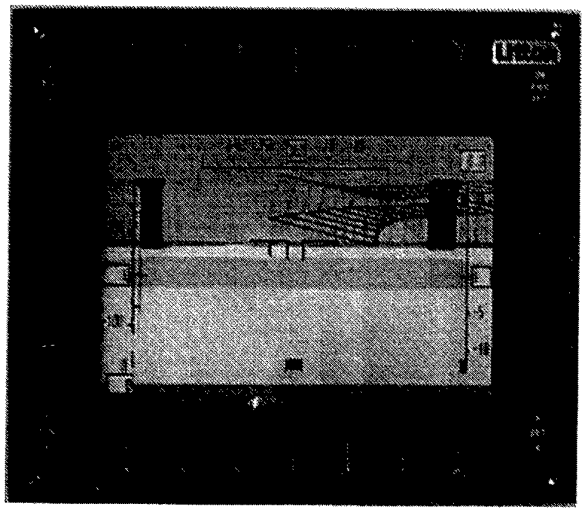

Figure 10 A Typical Pictorial HDD

Three pilots flew a full set of configurations. Performance measurements and Handling Qualities Ratings (using the Cooper-Harper rating scheme, Reference 7) were taken.. Standardised human factors questionnaires were used after each configuration and a final verbal interview was conducted. The flying for this exercise was completed on 23 May 1996 and the data are presently being analyzed. A much larger study is planned for the fall of 1996, the contents of which will depend largely on the results obtained in the initial exercise.

7. PROGRAM SUMMARY
Advanced cockpit technologies are under study at the FRL along three distinct paths, DVI,HMD and HDD. There is a great deal of commonality amongst the persons conducting the research and this should have a great advantage in that the three areas will be seen as an integrated whole and not as individual, unrelated areas of study. Longer term issues, particularly the possible inclusion of less bulky and difficult HMD units into ASRA will permit the

integrated study of all three technologies. It has been learned that these kinds of studies tend to make greater demand on the laboratories resources that was first estimated and that integration of such systems into existing aircraft is by no means a trivial task. However, in the present environment, emerging cockpit technology is the area in which the laboratory believes it can make a most significant contribution to the community as a whole as well as answering to the requirements of our supporters in the Canadian DND.

8. ACKNOWLEDGMENTS

Patently this paper presents a review of a wide ranging program that has drawn heavily on all the resources of the Flight Research Laboratory. Particular notice should be made, though, of the work of

:

- Carl Swail in speech recognition and the integration of DVI systems into the aircraft
- Louis Bolduc in the development of the software suite in ASRA and the for the graphics programming of the HDD.
- Sion Jennings in the initial stereoscopic HDD evaluations
- Gord Burton for technical support of the project instrumentation systems in both the Airborne Simulator and ASRA and
- Brian Bertrand who has shared the safety pilot duties in all three programs.

The authors would like to acknowledge financial contributions and the technical cooperation of the Canadian DND (CRAD), the FAA, CAE Ltd and the US Army AVSCOM.

9. REFERENCES

1. Anon "Handling Qualities Requirements for Military Rotorcraft ", US Army ADS-33 C et seq 1989

2. Zwierzynski, D.A. and Lefebre, C., " Recognition of Degraded Speech with an IMELDA Acoustic Representation: A Helicopter Fly-By-Voice Project. " ESCA Tutorial and Workshop on Speech Processing in Adverse Conditions, Cannes-Mendelieu, France, Nov 1992

3 Starks, D.R. and Morgan J.M., "Integrating Speech Recognition into a Helicopter". Sit.loc. in 2.

4. Morgan, J.M. and Starks, D.R., " Fly-By-Voice, a Technology Demonstration. AGARD-CP-519 ", Chania, Creete,May 1992.

5. Baillie S.W. and Morgan J.M.," Helicopters and Night Vision Goggles, A Synopsis of Current Research on Helicopter Handling Qualities during Flight in Degraded Visual Environments " Presented at the AGARD FVP Symposium on Advances in Rotorcraft Technology, Ottawa, Canada, May 1996

6 Baillie, S.W, Kereliuk, S. and Morgan, J.M., "The Effects of Tailwinds and Control Cross Coupling on Rotorcraft Handling Qualities for Steep, Decelerating Instrument Approaches and Missed Approaches. " NRC Aeronautical Note IAR-AN-77, August 1993

7. Cooper G.W. and Harper R.P., " The Use of Pilot Rating in the Evaluation of Aircraft Handling Qualities ", NASA TND-5153, 1969

Advances in Helicopter Carefree Handling and Control Augmentation

C P Massey
Head of Avionics and Systems Technology
GKN Westland Helicopters
Yeovil
Somerset, BA20 2YB
UK

J Howitt
Senior Handling Qualities and Flight Control Engineer
Flight Dynamics and Simulation Department
Defence Research Agency
Bedford, MK41 6AE
UK

ABSTRACT

This paper describes research being undertaken by GKN Westland Helicopters and the UK Defence Research Agency (DRA) to examine enhanced augmentation of helicopter flight control systems. Current research is targeted at mechanical primary flight control systems with limited authority automatic flight control systems (AFCS) with a view towards early application as a retrofit to in-service helicopters or new versions of existing helicopters.

Recent results from three programmes of research are included. Firstly, research into Integrated Flight and Engine Control (IFEC) undertaken by GKN Westland Helicopters and Rolls-Royce, and supported by the UK MoD. Secondly, research into engine failure/low rotor speed protection systems undertaken by GKN Westland Helicopters, and supported by the UK Civil Aviation Authority. Thirdly, research into Carefree Handling Systems, undertaken collaboratively by GKN Westland Helicopters and DRA, and supported by the UK MoD.

In each case, analytical or piloted simulation results are presented which show the potential benefits in terms of improved performance, reduced workload or enhanced safety.

The paper also describes how each of these separate concepts are compatible and could be brought together in an integrated enhanced augmentation system.

1. INTRODUCTION

The concept of increased augmentation to allow role-related tasks to be conducted with increased agility, safety, and in much reduced visual conditions, is well understood. Examples of such systems include stability and command augmentation systems, flight directors, autopilots, engine/rotor speed governors, head-up/helmet mounted displays, and audio/visual warning systems. However, even with the aid of these systems, the need to respect structural, aerodynamic or control limits can add considerably to pilot workload and can result, *in extremis*, in failure to complete the required task or even loss of the aircraft.

Carefree handling represents the ability of the pilot to manoeuvre throughout the operational flight envelope without concern for exceeding limits. Unlike the "hard" or "never exceed" limits imposed on fixed-wing aircraft to prevent potentially catastrophic loss of control, rotary-wing limits tend to be "soft" and many helicopters can be flown beyond limits in a controlled manner, albeit at the expense of increasing fatigue damage. A practical rotary-wing carefree handling system must therefore balance the sometime conflicting attributes of stability, control, handling qualities and limit protection. Such attributes are difficult to achieve simultaneously with conventional design, but can be realised through the application of advanced control systems.

This paper presents results from three recent research studies led by GKN Westland Helicopters and the Defence Research Agency (DRA). These studies were conducted independently for either the UK Ministry of Defence (MOD) or Civil Aviation Authority (CAA) and addressed a particular aspect of performance and safety enhancement pertinent to each sponsor. The studies fall into the following headline categories:

- Integrated Flight and Engine Control (IFEC)
- Engine Failure/Low Rotor Speed Protection Systems
- Torque Protection Carefree Handling Systems (CFHS)

Although these studies had differing objectives, an obvious relationship links all three, and the experience gained by GKN Westland Helicopters and DRA has provided a strong base from which to explore future integrated systems. The paper will thus conclude with an overview of the potential architecture and functionality of such a system and its application in both military and civil markets.

2. BACKGROUND

2.1. Limitations of Existing Systems

All current production helicopters have flight control systems based around mechanical primary signalling, in many types with a limited authority automatic flight control system (AFCS) to provide stability augmentation and autopilot functions. The flight control system is not functionally integrated with other aircraft systems; integration with the engine control system, if any, is limited to simple feeds from collective lever position into the fuel control.

The systems provided for detecting aircraft or system failures are usually standalone and require the pilot to identify warnings, interpret their meaning, and take appropriate action.

Little assistance is presently given to the pilot in observing the helicopter's limitations, with head-down instruments forming the primary means of respecting the aircraft's limits. The need to be aware of the vehicle's current status and limits, and the need to scan appropriate gauges, inevitably increases the pilot's workload, as does the need to take corrective action when limits are approached. This is particularly true of low-level operations where the pilot cannot afford to be looking into the cockpit and is forced to fly less aggressively so as hopefully to respect the aircraft's limits without referring to the instruments.

It is therefore clear that most current helicopters offer limited assistance to the pilot in performing the primary flying task, reducing the ability to perform that and other secondary mission tasks effectively.

Paper presented at the FVP Symposium on "Advances in Rotorcraft Technology", held in Ottawa, Canada, 27-30 May 1996, and published in CP-592.

2.2 Improved Levels of Augmentation

In striving to improve on current systems, three factors must be considered:

- the need for increased mission effectiveness through improved flying qualities, improved performance and reduced workload,
- the need for improved safety and survivability,
- the need for reduced life cycle costs.

Meeting these requirements and providing optimum flying qualities for all conditions, in the same helicopter, has generally been considered to be possible only with full authority fly-by-wire/active control technology (FBW/ACT), in which the pilot's commands are electrically or optically communicated to a flight control computer, which in turn synthesizes the appropriate collective and cyclic blade pitch demands.

However, for the large number of in-service helicopters, FBW/ACT would be a high risk, high cost mid-life upgrade option. If Level 1 flying qualities are to be conferred on such helicopters, new design concepts based around more conventional control technologies are required. In particular, the conventional architecture of full authority mechanical control linkages between the pilot and the swashplate combined with a limited authority automatic flight control system will have to be retained.

The full potential for flying qualities improvement using this technology has been addressed by GKN Westland Helicopters and DRA in the studies reported herein, and is the focus for ongoing flight control research programmes, whereby similar functionality to a full authority fly-by-wire system is sought within the bounds of current limited authority actuation technology. The research is generic in nature, with the aim of increasing the operational effectiveness of all types of helicopter, especially in adverse environmental conditions, for a full range of roles.

3. INTEGRATED FLIGHT AND ENGINE CONTROL

3.1 Study Background

The basic concept of helicopter engine control has not changed since the introduction of gas turbine engines; a change in rotor load results in a change in free turbine speed, which is sensed by the engine control unit, which in turn adjusts the fuel flow to restore the datum speed condition. Engine control technology has undoubtedly advanced, with additional control parameters and safety features, but even the latest full authority digital engine control (FADEC) systems rely on feedback of the engine power turbine speed. Integration with the flight control system, if any, is limited to simple feedforward from the collective lever to give some anticipation of rotor load change.

Whilst simple engine control systems may be adequate for most non-combat helicopters, the increasingly aggressive manoeuvring required of many modern battlefield helicopters requires a new approach to rotor speed governing and power management.

The following results are presented from a study conducted by GKN Westland Helicopters and Rolls-Royce for the UK MOD investigating the impact of greater integration of helicopter flight and engine control systems on reduced transient rotor speed variation (RTRV). Further details of this study are given in Reference 1.

3.2 Outline RTRV System

The objective of the IFEC/RTRV control system, was to develop a flight/engine control interface which could command engine torque changes more rapidly than a conventional system in response to any change in rotor load requirement, either from changes to the aircraft flight state caused by environmental effects, or from demanded inputs through any of the four primary control channels.

The approach adopted to achieve these objectives, shown in Figure 1, was to derive a torque prediction signal based on easily measured parameters. This signal is compared with the engine output torque to provide a torque error signal which is then fed into the engine control unit as an additional demand.

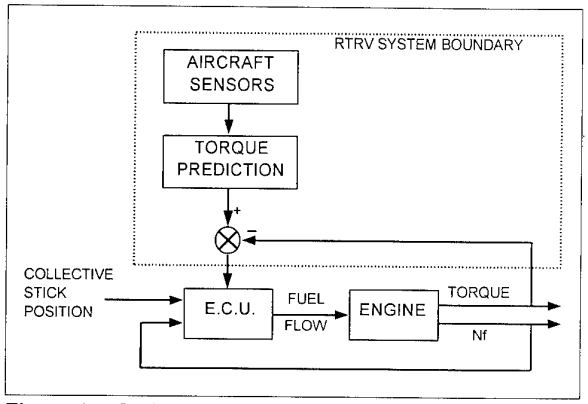

Figure 1 Outline IFEC/RTRV system

In designing the algorithms used to implement all of the IFEC features, care has been taken to ensure that information required by the algorithms was either already available on the aircraft or could be easily measured or generated. There is therefore a high level of confidence that the benefits emerging from these studies are practically realisable.

3.3 Results

Figure 2 shows the results obtained from a Lynx/Gem model by inputting a sinusoidal input into each control channel independently; collective, fore and aft cyclic, lateral cyclic and pedals. (The first column being the input as a function of time, the second the rotor speed and finally the engine output torque).

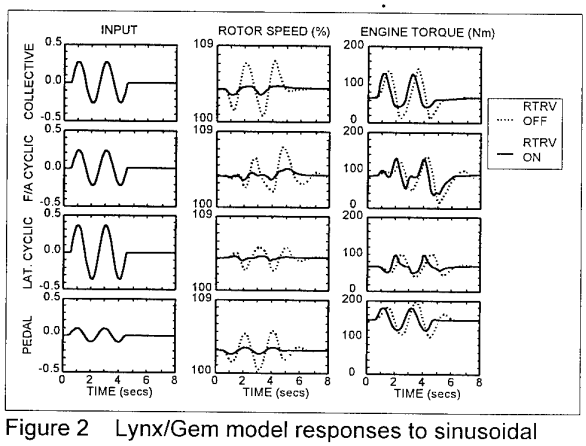

Figure 2 Lynx/Gem model responses to sinusoidal control inputs

It should be noted that pilot inputs into all four control channels can have an influence on the rotor speed. The Gem engine control system has no provision for a collective feed-forward term.

The anticipation signal fed into the engine control system has in all cases quickened the engines' response, thus reducing the phase lag between the required and supplied torque and leading to a substantial reduction in the magnitude of the rotor speed transients.

The capability of this system was also assessed in simulated operational manoeuvres, such as bob-up in hover, banked turns in forward flight, rapid accelerations and spot-turns. Results shown in Figure 3 for a model of an EH101 with RTM322 engines show reductions in rotor speed excursions of up to 80% and corresponding reductions in peak engine torque values, which should benefit engine/transmission system component life.

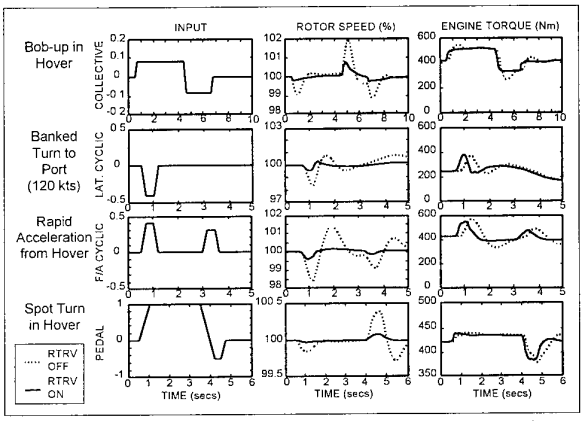

Figure 3 Responses of the EH101/RTM322 model during various manoeuvres

4. ENGINE FAILURE/LOW ROTOR SPEED STUDY

4.1 Origins and Objectives

Another area of potential benefit identified during the IFEC studies was that of providing automatic recovery action in the event of engine or tail rotor drive failures or damage. The engine failure aspects were pursued further by GKN Westland Helicopters in a programme supported by the UK Civil Aviation Authority (Reference 2). The study originated from concern about the number of accidents resulting from failure to conserve rotor speed following engine failure, and specifically from four fatal accidents involving double engine failure in twin engined helicopters.

A study of the UK CAA's accident database identified 87 reportable accidents from 1976 to 1993 where failure to preserve rotor speed was a contributory factor representing 21% of all reported accidents. Ten of these were fatal. Further analysis of these accidents suggested that an additional rotor speed protection system may have helped the pilot retain control in 71 of the 87 accidents including 9 out of 10 of the fatal accidents. It was also noticeable that 8 of the fatal accidents resulted from failures during cruising flight.

The objectives of the programme therefore included establishing techniques for rotor speed protection and evaluating these techniques in piloted simulation.

4.2 Simulation Trials

Techniques selected for assessment included:

- A phase advance filter to provide an earlier indication of loss of rotor speed.
- Enhanced visual warnings to provide more obvious indication of low rotor speed conditions.
- Audible warnings of low rotor speed. This included: multi-tones with different audio tones for different warnings, similar to many production helicopters; tone plus message type warnings; and a modulated tone where the frequency was dependent on the rotor speed and the amplitude dependent on the rotor speed trend.
- Direct intervention using standard series actuators.
- Direct intervention using a rapid collective pull-down actuator (full travel in 2 seconds).

All of these techniques were evaluated against a baseline configuration consisting of a simple low rotor speed audio tone. Trials were undertaken in a fixed based simulator at GKN Westland Helicopters with a projected outside world display and programmable head down instruments. Thirteen pilots from a wide range of backgrounds took part in the trial.

Two failure scenarios were examined:

- Attentive flight, where the helicopter was simulated in trimmed cruise flight at 90 knots with one engine already inoperative. The pilot was therefore fully attentive with his hands on the controls, prior to a second failure occurring, and
- Passive flight, where the helicopter was in cruise at a slightly higher speed of 120 knots, with both engines operating normally. The helicopter was under automatic pilot control with the pilot inattentive, hands-off, performing a secondary task prior to a simultaneous double engine failure.

4.3 Results from Trials

Figures 4 and 5 show averaged results for both failure scenarios and each configuration. The upper part of each figure includes:

- The available intervention time (the time by which the pilot must react to prevent rotor speed from reaching the minimum transient limit).
- The rotorcraft response time (the time for a warning or cue to be given to the pilot). The effect of the phase advance filter can be seen for all configurations compared with the baseline.
- The actual intervention time when the pilot reacts to the failure.
- The system intervention time for the intervention systems.

The lower part of each figure show the corresponding average minimum rotor speed recorded.

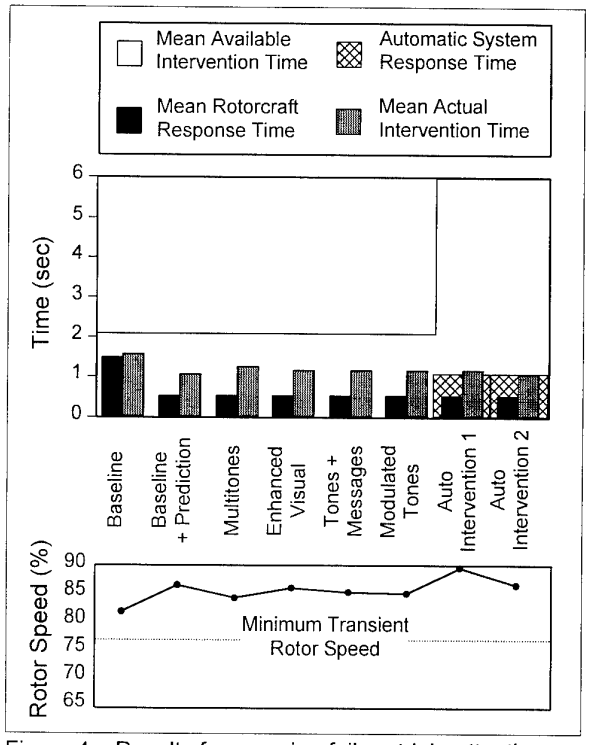

Figure 4 Results from engine failure trial - attentive scenario

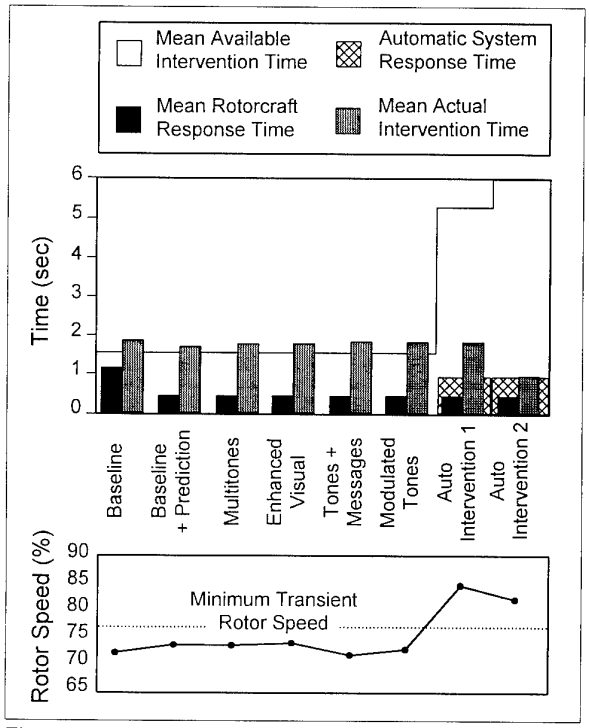

Figure 5 Results from engine failure trial - passive scenario

Key findings from these results were that the phase advance filter led to an earlier pilot reaction to the failure, and that, in hands off inattentive flight, only the automatic intervention systems were able to ensure that all pilots preserved rotor speed above the minimum transient limit.

5. TORQUE PROTECTION CAREFREE HANDLING SYSTEM

5.1 Review of Previous DRA/GKN Westland Helicopters Carefree handling Research

UK MOD Strategic Research on helicopter carefree handling was initiated in the mid 1980's involving a collaborative programme between DRA and GKN Westland Helicopters. This culminated in a series of ground-based piloted simulations using simple conceptual transfer function models of an idealised FBW/ACT helicopter to investigate visual, audio and tactile warning systems together with direct intervention control systems (Reference 3). The value of carefree handling was proved in terms of reduced pilot workload and increased task performance for execution of aggressive, low level mission task elements (MTEs). The lessons learned from the conceptual study were:

- protection of torque limits, and to a lesser extent rotor speed limits, are the primary pilot concerns in terms of increased workload and potential damage to the helicopter,
- a combination of tactile cueing and direct intervention is far more instinctive and effective than audio or visual cueing for limit protection purposes.

5.2 Objectives of Ongoing DRA/GKN Westland Helicopters Carefree Handling Research

Focusing on the need for improved heave-axis augmentation, the most recent study conducted by DRA and GKN Westland Helicopters for UK MOD has concerned the development and ground-based piloted simulation assessment of a limited authority Torque Protection Carefree Handling System for the Lynx helicopter. The study was not intended to demonstrate a Lynx-specific capability, but rather the potential for performance improvement and pilot workload reduction that could be attained using only current limited authority flight control systems technology and hence could form part of a in-service upgrade for many different types.

5.3 Overview of the Torque Protection Carefree Handling System

The system aims to assist the pilot in respecting the maximum continuous and maximum transient engine torque limits via a combination of a programmable active collective soft-stop and control intervention via the heave axis of the limited authority AFCS. A schematic of the system architecture is shown in Figure 6.

The soft-stop provides a very positive tactile cue that a limit is being approached, or has been exceeded, and is similar in character to the precompressed spring stops currently used on the Gazelle. Experience with the collective pitch stops in the Gazelle indicates that a level of pseudo-carefree handling can be achieved, although the system is not adaptive to flight conditions and is helped by the Gazelle's excellent engine acceleration. Nevertheless, it is a proven example of the effective use of tactile cueing which can be exploited in the implementation of a limited authority carefree handling system. Hence, the primary task was to develop a soft-stop similar to the Gazelle intermediate pitch stop which could (i) provide a positive tactile cue, (ii) be overridden to exploit the emergency manoeuvring capability, and (iii) be adaptive to flight conditions.

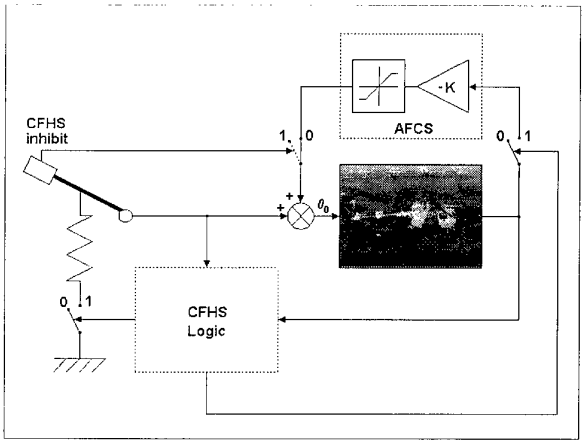

Figure 6 Schematic of the torque protection carefree handling system architecture

The soft-stop was developed to delineate the maximum continuous limit (Figure 7), but the pilot can exercise the transient manoeuvre capability by pulling through the stop against an increasing spring force that will return the torque to the maximum continuous limit should the pilot release the collective lever. If, in an emergency, the pilot wishes to exceed the transient limit, then he can do so by pressing the CFHS inhibit button on the collective grip. This disengages the intervention control law, allowing the pilot to exploit the full power capability. However, the tactile cue of the soft-stop remains enabled as a reminder to the pilot.

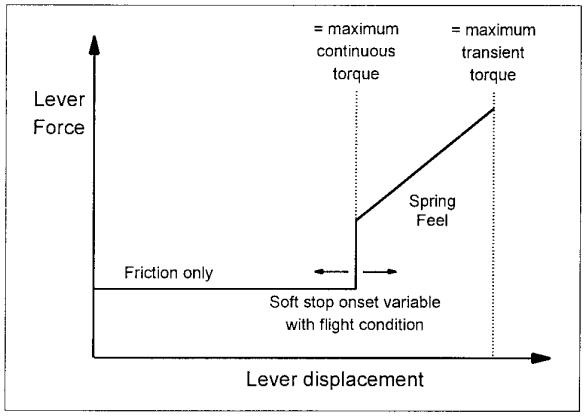

Figure 7 Collective soft stop force-feel characteristics

5.4 Ground-Based Piloted Simulation Trial

A piloted simulation assessment of the limited authority heave-axis carefree handling system was conducted on the Advanced Flight Simulator (AFS) at DRA Bedford. Core to this facility is the large motion system which provides $\pm 30°$ of pitch, roll and yaw, ± 4 metres of sway and ± 5 metres of heave motion (Figures 8 and 9). These displacements can all be achieved simultaneously, allowing significant acceleration cueing to be achieved. In addition, the pilot's seat is dynamically driven to give vibration cues.

The assessment took the form of a back-to-back comparison between a standard Lynx and one retrofitted with the limited authority torque protection carefree handling system. The assessment covered a number of hover, low speed and high speed mission task elements and similar trends in limit

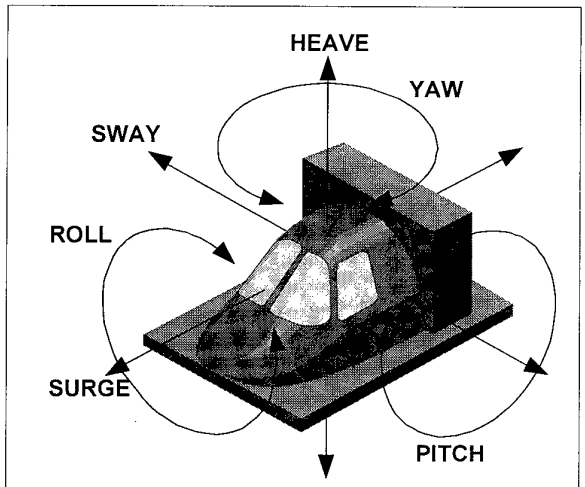

PERFORMANCE ENVELOPE

Axis	Displacement	Acceleration
Pitch	+/- 0.5 rad	+/- 2 rad/s^2
Roll	+/- 0.5 rad	+/- 3 rad/s^2
Yaw	+/- 0.5 rad	+/- 1.5 rad/s^2
Sway	+/- 4 m	+/- 5 m/s^2
Heave	+/- 5 m	+/- 10 m/s^2

Figure 8 DRA Bedford Advanced Flight Simulator; motion system performance capabilities

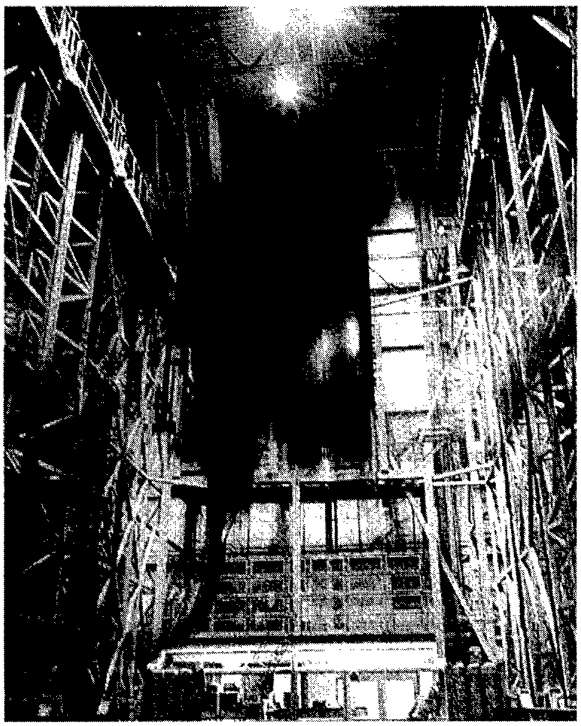

Figure 9 DRA Bedford Advanced Flight Simulator; the Large Motion System in operation

observance and task performance were seen in all tasks. However, for brevity, only a bob-up/bob-down and a turn-to-

target air combat task will be discussed in this paper.

With reference to Figure 10, a transparent vertical grid structure was used as a line-of-sight reference for an aggressive bob-up/down manoeuvre. From an initial stabilised hover at 25ft, the pilot was required to bob-up through approximately 50ft and establish a line-of-sight between the top of the grid structure and two marker boards positioned on the ground beyond *as quickly as possible*. Desired performance required that the line-of-sight contact be established with only a single overshoot of ± 5 feet or less, torque be maintained at or below the maximum continuous limit and heading be maintained within $\pm 5°$. Adequate performance required that the line-of-sight contact be established with only a single overshoot of ± 10 feet or less, torque be maintained at or below the maximum transient limit and heading be maintained within $\pm 10°$. For both desired and adequate performance, the pilot was required to stabilise the helicopter in the higher hover position for three seconds before bobbing back down to the original height. The bob-up/bob-down was assessed as one task.

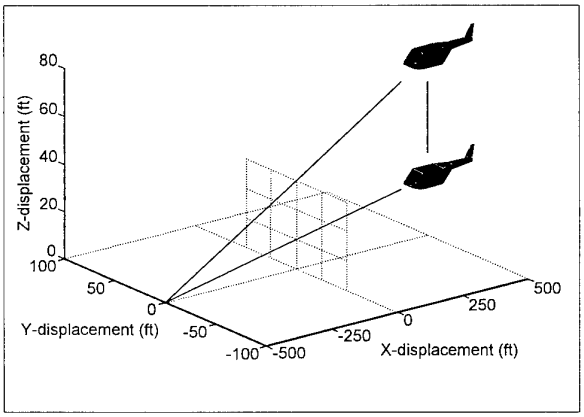

Figure 10 3-D visualisation of the bob-up/bob-down task

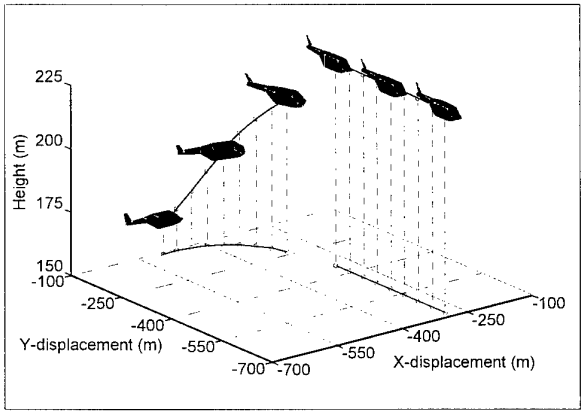

Figure 11 3-D visualisation of the air combat engagement task

The 90° turn-to-target air combat engagement task, shown in Figure 11, demanded higher aggression multi-axis manoeuvring with a high degree of spatial awareness. The task was initiated with the aggressor (Blue) helicopter flown by the subject pilot in straight and level flight at 80 knots on a heading of 0°, whilst the target (Red) helicopter was flying 175 feet higher than Blue on a heading of 090°, also at a speed of 80 knots. As Red crossed Blue's "twelve o'clock", Blue was required to turn and climb to engage Red *as quickly as possible*. It was assumed that Blue was armed only with a forward firing gun aimed via a simple "iron cross" sight that required the pilot to stabilize the helicopter in the target's "six o'clock". The task was deemed to be complete when Blue had attained the same flight level as Red and stabilized in Red's "six o'clock". Desired performance required that the torque be maintained at or below the maximum continuous limit, whereas adequate performance required that the torque be maintained at or below the maximum transient limit.

5.5 Discussion of Results

For all tasks, the pilots commented very favourably on the fact that the carefree handling system obviated the need to monitor the head-down torque gauge in the cockpit, thus enabling them to fly the tasks "eyes out" whilst relying purely on the soft-stop to pull maximum torque. The additional rate information that was available "eyes out" also helped the pilots to adopt a smoother control strategy and fly the tasks more quickly.

Figure 12 shows a comparison of the maximum instantaneous torque exceedance for each of the two configurations in the bob-up/bob-down task. It can be seen that an order of magnitude improvement in limit protection was achieved with the engagement of the carefree handling system.

Figure 13 shows the performance/workload trade-off in the form of a Cooper-Harper Handling Qualities Ratings versus Agility Factor cross-plot. The Agility Factor is calculated as the ratio of the minimum theoretical task time to the actual task time, and hence represents that fraction of the inherent performance that the pilot is able to exploit. Of particular note in the bob-up task, was the fact that without the carefree handling system, increased aggression actually resulted in a less agile response since the pilot was more likely to over-torque and also excite the collective/yaw coupling. This can be seen in the degradation of handling qualities from HQR=4 (moderate compensation) to HQR=6 (extensive compensation). With the carefree handling system engaged, however, there was a more predictable trend with a 10% increase in agility achieved at the expense of slightly increased workload

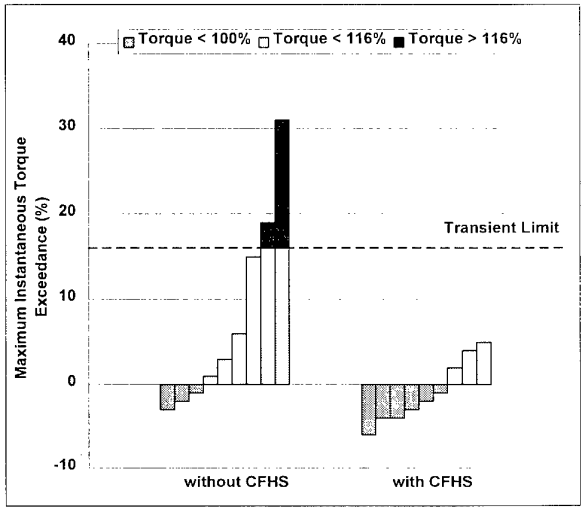

Figure 12 Bob-up/bob-down results: maximum torque exceedance

(HQR=3, minimal compensation, to HQR=4, moderate compensation).

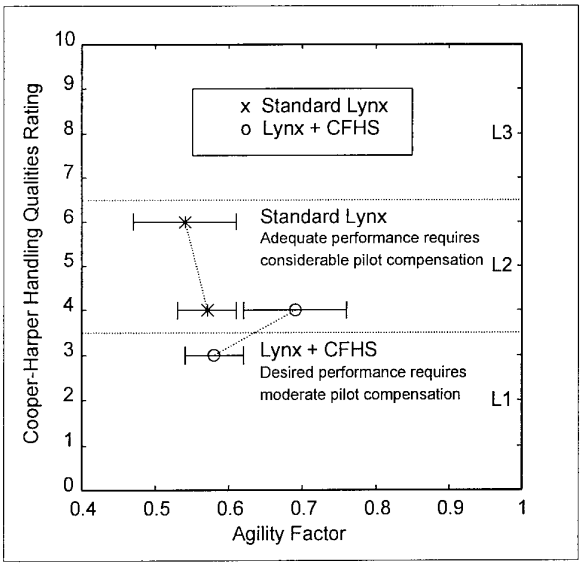

Figure 13 Bob-up/bob-down results: handling qualities rating versus agility factor

For the turn-to-target task, Figure 14 shows the comparison of the maximum instantaneous torque exceedance for each of the two configurations. Once more, it can be seen that a significant improvement in limit observance was achieved with the carefree handling system engaged. The corresponding performance/workload trade-off is again displayed in the Cooper-Harper Handling Qualities Ratings versus Agility Factor format as shown in Figure 15. The increase in performance afforded by the carefree handling system was particularly obvious for the target engagement task. Although the pilots did not perceive a noticeable improvement - possibly due to the high level of attention required to visually acquire the target - they were consistently able to engage the target 1 - 2 seconds quicker with the carefree handling system engaged. Again, this increase in performance was also accompanied by a significant reduction in workload from Level 2 to predominantly Level 1 pilot ratings.

The results showed the following benefits for the limited authority torque protection system.

- The soft-stop is a very valuable tactile cue, effectively eliminating unintentional torque limit transgressions in high aggression, large amplitude manoeuvres.
- Task time can be reduced by up to 20% in such manoeuvres by allowing the pilot to command maximum available performance in a controlled and predictable manner.
- Workload can be reduced by up to two points on the Cooper-Harper scale and situational awareness improved by relieving the pilot of the need to monitor cockpit instruments.

Overall, a limited authority torque protection carefree handling system would appear to offer an effective, lower cost, lower risk alternative to an equivalent full authority fly-by-wire/active control system.

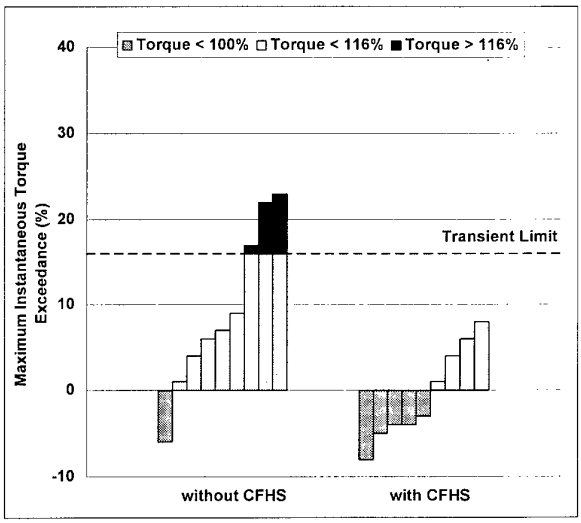

Figure 14 Air combat engagement task: maximum torque exceedance

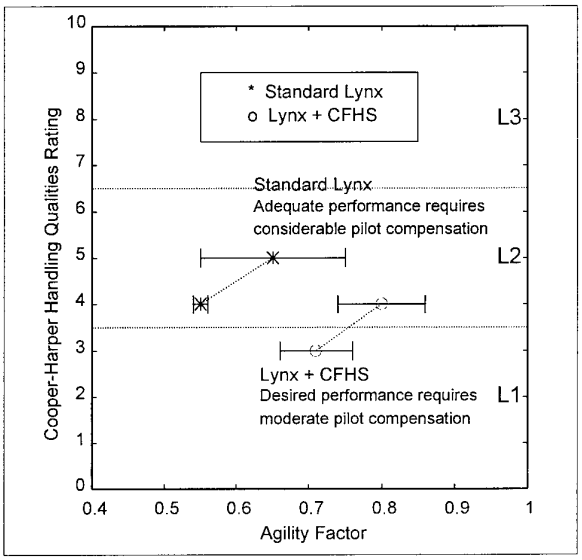

Figure 15 Air combat engagement task: handling qualities rating versus agility factor

6. INTEGRATED FLIGHT AND ENGINE CONTROL CAREFREE HANDLING SYSTEM

Previous sections of this paper have described three separate areas of work aimed at slightly different aspects of control augmentation and pilot assistance. In general these features can all be implemented around a conventional helicopter flight control system with a limited authority AFCS.

It can be seen that many of the features examined are compatible and indeed the further benefits could arise from integration of these features into an upgraded augmentation system. IFEC offers improved torque prediction and engine/rotor damping which in turn will improve the performance of the torque protection features. The automatic intervention features highlighted as being so successful in the engine failure study are an extension of the heave axis carefree handling features into abnormal operating conditions, and require similar hardware and architecture to the existing all engines operating heave axis carefree handling features.

Upgrades of existing helicopter flight control systems can therefore be envisaged featuring comprehensive heave axis augmentation providing very crisp response, carefree torque and rotor speed protection and enhanced safety.

The retrofit of an active collective soft-stop combined with limited authority flight control system intervention and an advanced engine control system into the current generation of military helicopters, offers the potential for significantly extending their combat capability and mission effectiveness. Operational benefits would result from reduced pilot workload, increased pilot capacity and situational awareness, a greater potential for exploiting the full performance of the helicopter, and an associated improvement in survivability. This latter point would also be of significant benefit to the civil market. Also, despite the potential for more aggressive tactical flight, powertrain limit exceedances, and hence life-cycle costs, are likely to be reduced.

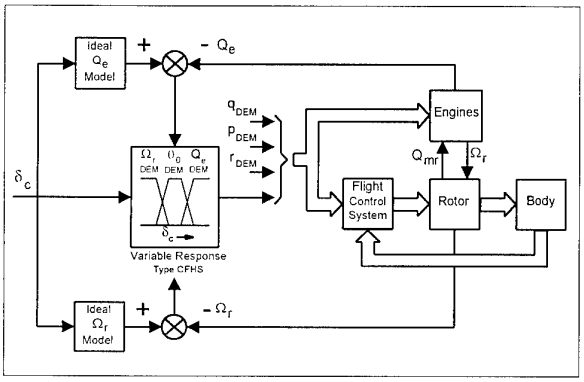

Figure 16 Schematic of an integrated flight and engine control carefree handling system architecture

A schematic of a proposed architecture (Reference 4) for an Integrated Flight and Engine Control Carefree Handling System is given in Figure 16. Note that all four primary flight control inputs may be communicated to the engine control system to achieve improved torque prediction, engine/rotor damping and transient rotor speed response. Superimposed on this inner-loop, it is proposed that the maximum benefit of engine/airframe integration can be achieved via a novel heave-axis carefree handling system (CFHS) mode that blends between collective blade pitch command (θ_0), torque command (Q_e) and rotor speed command (Ω_r) as a function of collective lever position (δ_c).

For small to moderate amplitude inputs around trim, the CFHS would default to the open-loop mechanical mode, with an exact link between collective lever position and main rotor collective pitch giving good handling qualities for precise height control - effectively height rate command. However, for large amplitude manoeuvring, the CFHS would blend to closed-loop control of torque at high collective pitch and closed-loop control of rotor speed at low collective pitch in split-needle/engine-off situations (Figure 17). Flight control system mode blending in the manner proposed allows the pilot to control the most appropriate variable for carefree handling and command directly the full range of available performance.

To reinforce this, the control law would be augmented with tactile cueing in the form of twin collective soft-stops that, in normal operation, would delineate both the maximum continuous multi-engine torque and rotor speed limits, but still allow the pilot to pull or push through to the maximum transient limits for emergency manoeuvring.

A higher level decision-making controller would also be required to prioritise the most appropriate limits to be respected based on the health and status of the helicopter and its operating environment - *e.g.* engine torque limits at sea level versus engine temperature limits in hot/high operations, multi-engine maximum continuous torque limits in normal operation versus single engine maximum contingency torque limit in engine-off emergencies, power-on rotor speed limits in normal operation versus power-off rotor speed limits in autorotation *etc.*

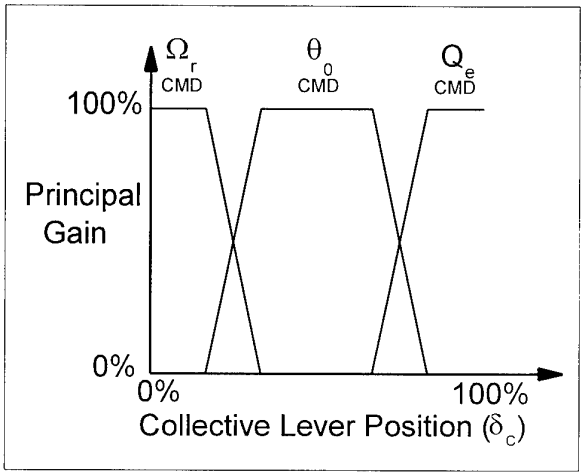

Figure 17 Schematic of an advanced integrated flight and engine control carefree handling mode blend

The collective soft-stop feel characteristics could be easily retrofitted by driving a simple actuated spring feel unit from the torque and rotor speed prediction algorithms, whilst in general, the feedback elements could all be implemented around a conventional mechanical flight control system with a limited authority AFCS. However, it may be necessary to increase the heave-axis authority limit beyond the $\pm 10\%$ typical of many current helicopters in order to achieve true torque and rotor speed command response types - a nominal figure of $\pm 20\%$ is suggested.

7. CONCLUSIONS

Various augmentation features have been developed and evaluated in simulation to improve mission effectiveness through improved task performance and reduced pilot workload, and to improve safety through protection of limits and provision of assistance to the pilot in emergency situations. These features are also expected to benefit life cycle costs through improved reliability, safety, and extended component lives. Recent work has concentrated on enhancing existing limited authority augmentation systems and has shown the potential to reduce task times by up to 20%, reduce workload by up to two points on the Cooper-Harper scale and eliminate unintentional torque limit transgressions in high aggression, large amplitude manoeuvres.

Further improvements to these systems can be expected from integrating flight and engine control to provide better damped engine responses and better prediction of rotor load.

The effectiveness of automatic intervention in the event of engine failure has also been demonstrated and this is a logical extension to the existing carefree handling system.

Future development will concentrate on development of these systems for flight trials and incorporation of features to assist the pilot in observing other aircraft limits.

ACKNOWLEDGEMENT

The authors would like to acknowledge the assistance of Dr G Padfield, Mr I Woodrow, and Mr D Haddon in the preparation of this paper.

REFERENCES

1. Massey C P, Haddon D R, "The Application of Integrated Flight and Engine Control to Helicopters", European Rotorcraft Forum, September 1993.

2. Haddon D R, "The Protection of Rotor Speed Following Power Failure", European Rotorcraft Forum, October 1994.

3. Massey C P, Wells P, "Helicopter Carefree Handling Features", RAeS Conference on Helicopter Handling Qualities and Control, November 1988.

4. Howitt J, "Carefree Manoeuvring in Helicopter Flight Control", American Helicopter Society 51st Annual Forum, May 1995.

© GKN Westland Helicopters 1996
© British Crown Copyright 1996/DERA
Published with the permission of the Controller of Her Britannic Majesty's Stationery Office

ACTIVE CONTROL OF AEROMECHANICAL STABILITY

by

Tomasz KRYSINSKI,
DYNAMICS MANAGER (F/DT.AV)
EUROCOPTER FRANCE
13725 Marignane Cedex
France

SUMMARY

This paper presents the active control of aeromechanical stability as a powerful means of simplifying rotor design in future helicopters.

The mathematical simulation model is presented and the results are compared to flight test data.

The active control of ground resonance was fully validated with flight tests in the Super Puma Mk2 helicopter which behaved in a highly efficient and robust manner.

An active control strategy is suggested for air resonance and drive train stability; a validation with flight tests is forecast in the near future.

The proposed controls are simple and easy to integrate in a conventional Flight Control System (FCS).

The actuators available in the current FCS are sufficient as far bandwidth required for active control of aeromechanical stability is concerned

Notations

b	number of blades
c	eccentricity
h	distance of rotor hub from fuselage mass center
$T_{\gamma R}$	tail rotor torque
u	vector of control inputs
X	vector of coordinates
X_θ	vector of equilibrium position
x	vector of state space
y	vector of output measurements
x, y, z	vertical, longitudinal and lateral translations of the fuselage mass center
αz, αy, αx	yaw, pitch and roll rotations about the helicopter body
βi, δi	flap and lead-lag angle of blade i
θi	pitch angle about the blade i
θ_{MR}, θ_{MGB}, θ_{ENG1}, θ_{ENG2}, θ_{TR}	drive train rotations
Ω	rotor speed

1. INTRODUCTION

Most of the main rotor heads currently in service around the world are "soft in plane" designs.

Designing and developing reliable dampers has always been a particular concern for helicopter manufacturers as they represent a significant share of both the initial and direct operating costs.

Lead-lag dampers increase the maintenance, weight and complexity of rotor systems.

Payload, flight configuration as well as other constraints e.g. reduced weight and hub compactness need to be considered as a result of the wide range of the helicopter's operating conditions.

Lead-lag dampers are fitted to counter aeromechanical rotor/fuselage instabilities since it is difficult for the designer to avoid ground and flight resonances.

These dampers help tailor frequency and damping in the 1st lead-lag mode. Lead-lag dampers fall under two categories:

- visco-elastic dampers (frequency adapters) combining high stiffness and low damping
- hydraulic dampers combining high damping and low stiffness

Visco-elasticity offers more advantages as a technology than hydraulics (Fig. 1).

The aeromechanical rotor / fuselage instabilities impose mixing visco-elastic and hydraulic technologies in some applications (Fig. 2).

Lead-lag dampers can be used with different hub designs in conventional and interblade configurations (Fig. 3).

Paper presented at the FVP Symposium on "Advances in Rotorcraft Technology", held in Ottawa, Canada, 27-30 May 1996, and published in CP-592.

These configurations combine the drawbacks inherent to hydraulic and viscoelastic components and often induce thermal and wear problems.

Interblade damper technology gains are high in terms of space available, higher damper lever arm and reduced hub loads for rotors with a high number of blades. The risks with pure interblade technology are related to the absence of stiffness and damping in the first drive train mode (Fig. 4).

This short review of hub and lead-lag damper technologies underlines the difficulties inherent to the design of simple and reliable dampers meeting the stringent requirements of modern rotors.

The purpose of an active control is to improve the aeromechanical stability of modern rotors as well as simplify the design of lead-lag dampers.

Active control could help designers do away with lead-lag dampers at least in some applications.

2. AEROMECHANICAL ROTOR - FUSELAGE / DRIVE TRAIN STABILITY PROBLEMS

The helicopter's aeromechanical instability also known as air or ground resonance is the result of coupling between the rotor's lead-lag regressive mode and the body's degrees of freedom.

Ground resonance

In ground resonance, the body modes are generated by the structure on the landing gear.
Ground resonance occurs when the frequency of the fuselage on the ground corresponds to the lead-lag frequency in the fixed system (Fig. 5).

The lead-lag motion of the blade then induces loads on the hub that are generated as a result of a lateral and longitudinal shift in the rotor's center of gravity from the center of rotation. These loads excite both the rotor-fuselage mode at its natural frequency, thus inducing displacements in the center of the rotor, and the rotor at its natural frequency.

Unstable ground resonance is highly destructive and has been the cause of early prototype crashes.
Obtaining satisfactory stability margins is one of the prime concerns in current helicopter design.

Hingeless and bearingless rotors in light and medium sized helicopters require less damping than hinged rotors because of the high natural frequency of the first blade lead-lag modes.

Ground resonance stability only requires a small amount of structural damping generally provided by elastomeric or small hydraulic dampers. Additional damping can be obtained, with increased rotor thrust, through aeroelastic coupling of blade pitch and lag motions by proper selection of rotor design parameters

The non linearity of the lead-lag damper and the landing gear characteristics are key parameters of the ground resonance phenomenon.

A helicopter which is stable can, in some cases, become unstable when the pilot excites ground resonance by precessing the cyclic pitch in the rotor's sense of rotation.

This excitation generates through Coriolis forces a lead-lag displacement of the blade, a dynamic deformation of the damper and a reduction of the 1st lead-lag frequency in the rotating system; the body mode frequency is then decreased at the same time (see Fig. 7).

Changing the characacteristics can induce ground resonance (Fig. 7 and 8)

Air resonance

Air resonance is similar to ground resonance and involves coupling the 1st lead-lag, 1st flap and rigid body fuselage mode.
Air resonance stabilities are of two kinds. The first is directly related to rotors with high hinge offset, hingeless and bearingless rotors. It is the result, in this case, of an interaction between the 1st regressive lag mode and the coupled flap and fuselage mode
The second kind is related to articulated rotors in high g manoeuvres. The rigid roll body mode can then be coupled with the 1st lead-lag mode through Coriolis forces. This instability is explained with an example (Fig. 9).

Drive train stability

The helicopter drive train system is composed of rotors, engines and their fuel control laws, shafts and gears. Together, these systems can generate different dynamic problems such as torque oscillations and rotor speed variations that degrade the handling qualities
The helicopter drive train dynamic analysis is mainly focused on suitable tuning of the torsional modes of the system, providing a proper separation from the $b\Omega$ as well as $2b\Omega$ excitation frequencies.

This model designed without any major simplification helps to analyze the torsional dynamics of the whole drive train system.

Some modifications are usually introduced in the main gear box design process to avoid resonances. The main and tail rotor dynamic characteristics are introduced in the model to take the main gear box coupling with the soft blade modes into account. The lead-lag stiffness of the blades is often adjusted to raise this mode over $b\Omega$ and gain a sufficient safety margin with respect to this excitation.

Another significant aspect of the drive train investigation is the low frequency stability analysis. Large collective pitch changes generate high power demands from the engines and since large rotor inertiae cannot be rapidly accelerated or decelerated, high control gains are required in the engine fuel control laws.

On the other hand, these high gains can lead to unstable coupling of the 1st drive train mode with the engine governor. These unstable oscillations are of special concern in interblade lead-lag damper technology. An example of unstable oscillations is given (Fig. 10); these particular oscillations were cancelled with a modification of the engine fuel control laws.

3. AEROMECHANICAL STABILITY MODELING

The basic ground resonance theory was originally developed by Coleman (ref 5).

The 1st lead-lag mode and the hub in plane mode were the only degrees of freedom taken into account in the analysis.

The current models include additional degrees of freedom and aerodynamic efforts are also taken into account.

The model that was used in this study has been developed over a number of years.

The helicopter elements that were taken into consideration are shown (Fig. 11)

The helicopter's body is represented as a rigid fuselage with yaw, pitch and roll rotations identified αz, αy, αx respectively about the center of mass as well as vertical, longitudinal and lateral translations of the center of mass identified x, y and z respectively. The landing gear is assimilated to perfect springs and dampers (Fig. 12)

The rotor having four identical blades is located at a distance *h* directly above the fuselage mass center. The blades are assumed to be rigid.
The helicopter models under study have a hinged rotor. The blade-hub link is modelized with a ball joint. The rotation along the blade's longitudinal axis designated pitch (θi) is determined by the pilot. The other two possible rotations are designated lead-lag movement (δi) and flap movement (βi) respectively (Fig. 13).

The center of the link is, by construction, located at a distance *e* for eccentricity from the hub's axis of rotation.

A lead-lag damper inserted between the hub and the blade introduces stiffness and damping. The interblade configuration can also be modelized.

The rotor / fuselage / drive train coupling is the result of the torsion characteristics of the drive train components.This drive train is modelized with sub-assemblies (Rotor mast, Main Gear Box, Engine 1 and 2, Tail rotor) for which equivalent mass characteristics can be determined individually and set to the rotor mast rotation. The link between the different components is represented with torsion springs (Fig. 14).

The torsion angles between the different components are designated θ_{MR}, θ_{MGB}, θ_{ENG1}, θ_{ENG2}, and θ_{TR}.

The aerodynamic forces applied on the blades are based on classical, two-dimensional quasi-study theory and uniform inflow. A dynamic inflow model is included. Compressibility and unsteady flow are neglected.

The system's equations are expressed by the Lagrange method. The non-linear periodic equations of motion are therefore linearized. The equilibrium position is independent of time and obtained in hover.

The linearized periodic coefficient perturbation equations are converted into a constant coefficient system with Coleman's transformation.

This transformation involves projecting in the trihedron the variables related to the blades (βi, δi, θi) and proceeds as follows (4 bladed rotor) :

(1)

$$\beta_i = \beta_0 + \beta_{1c} \cdot \cos\left(\Omega t + (i-1)\frac{\pi}{2}\right) + \beta_{1s} \cdot \sin\left(\Omega t + (i-1)\frac{\pi}{2}\right)$$

$$\delta_i = \delta_0 + \delta_{1c} \cdot \cos\left(\Omega t + (i-1)\frac{\pi}{2}\right) + \delta_{1s} \cdot \sin\left(\Omega t + (i-1)\frac{\pi}{2}\right)$$

$$\theta_i = \theta_0 + \theta_{1c} \cdot \cos\left(\Omega t + (i-1)\frac{\pi}{2}\right) + \theta_{1s} \cdot \sin\left(\Omega t + (i-1)\frac{\pi}{2}\right)$$

This set of equations is also expressed as follows:

$$M(X_0)\ddot{X} + C(X_0)\dot{X} + K(X_0)X = F(X_0)\theta \quad (2)$$

X is the coordinates vector, X_0 is the equilibrium position vector and Θ is the control inputs where:

$$X^T = [x\ y\ z\ \alpha x\ \alpha y\ \alpha_z\ 0_{Mr}\ 0_{Rip}\ \theta_{arg1}\ \theta_{arg2}\ \theta_{TR}\ \beta_0\ \beta_{1c}\ \beta_{1s}\ \delta_0\ \delta_{1c}\ \delta_{1s}]$$

$$\Theta^T = [\theta_0\ 0_{1c}\ \theta_{1s}\ T_{TR}] \quad (3)$$

The pilot uses the rudders to change T_{TR}, the collective pitch change lever to change θo and the cyclic pitch stick to change $\theta 1c$ or $\theta 1s$. The Automatic Flight Control System also acts on those variables.

The coupled drive train / fuselage / rotor dynamics are then evaluated by transforming the equations into a first order form with Duncan's method.

$$\dot{x} = Ax + Bu$$
$$y = Cx \quad (4)$$

x is the state space variable vector; y is the output measurements vector.

The final form of the equation is also used to compute the time history responses as well as the frequency response of the system.

4. ACTIVE CONTROL OF AEROMECHANICAL STABILITY

The main idea behind active control of aeromechanical stability is being able to use the hardware that is already available in the helicopter. The actuator is a conventional swashplate piloted by a servo-control in the fixed system. The control frequency is very low (less than 1/rev) and compatible with the bandwitdth of actuators, hydraulic or electrical units used in a classical FCS. It can be pointed out that conventional Stability Augmentation Systems installed in many helicopters use body pitch and roll rate feedback to the longitudinal and lateral cyclic controls to stabilize the helicopter's pitch and roll motions.It is well known that improper design of a high bandwidth FCS can destabilize a helicopter air or ground resonance modes (The problem is generally solved with the introduction of a low pass or notch filter in the FCS feedback loop to prevent reinjection of air/ground resonance oscillations into the cyclic control actuators). This means that air/ground resonance stability augmentation can also be achieved provided the proper compensation is introduced in the body state feedback loop.

Further to analytical investigations, Eurocopter France supported by the French Ministry of Defence launched an exploratory development called OSCAR for Optimal Stability and Control of Aircraft Resonance to demonstrate this technology in flight and to evaluate various control strategies.

Control laws were developed with simulations. The rule to follow as far as observation variables were concerned was for the controller to select parameters easily available in the helicopter (accelerations, angular velocities in the fixed system). The helicopter selected for tests was Super Puma Mk2 (Fig. 15).

Helicopter tests were carried out in the laboratory to determine the dynamic characteristics for ground resonance analysis (Fig 16). The data measured was the rigidity of tyres, the landing gear deformations and the global characteristics of the fuselage body modes on the ground. It was noted that the production 332 Mk2 helicopter is perfectly stable on the ground. The experimental visco-elastic damper (Fig. 17) was manufactured according to theoretical predictions to explore instability on the ground. This damper was characterized with dynamic laboratory tests and the stiffness as well as damping constants were derived from theoretical investigations. The theoretical model allowed elaborating the control strategy and the control loop is shown (Fig. 18).

Active control is based on the injection of a cyclic control into the rotor calculated from a parameter measured in the fixed datum. Acceleration was selected and treated. The signal was then fed as a voltage in the AFCS. The swashplate was thus precessed in the rotor's sense of rotation to have the excitation at drag frequency in the rotary datum.

The experimental system developed for the tests is shown (Fig. 19). This system which allows changing the characterisics of the command during tests was validated with simulated signals in the laboratory.

During the first tests the helicopter was in a low weight stable configuration where stable convergent oscillations were noticed even with very high cyclic stick excitations (Fig. 20). The weight was then increased and ground resonance tests were repeated; divergent oscillations were then noted after excitation (Fig. 21). The pilot had to take off as a result of high vibrations and loads. This unstable behaviour in ground resonance was in good agreement with the theoretical calculations. A comparison of calculations and measurements is presented (Fig. 22).

The closed loop was tested with controller gains and phases derived from theoretical calcultions. It is shown that the system is unstable in open loop and perfectly stable in closed loop. The pilot considered the helicopter unacceptable without active control. With active control, it passed the certification tests easily with a time half the amplitude below 2s (Fig. 23). In closed loop, excitation tests were repeated with different control settings and positions on the ground. The system was again shown to be perfectly stable (Fig. 24). Stability margins were determined for the gain with fixed phase and for that with fixed gain. A comparison of calculated and measured margins is presented (Fig. 25) and it can be noted that measurements compare very favourably with theoretical predictions. System integration studies demonstrated that the active control of ground resonance can easily be integrated in a classical FCS.

The second significant step in the active control of aeromechanical stability is air resonance. The very promising results obtained with active stabilization of ground resonance were the decisive factor in the selection of a similar control strategy for air resonance. The observation parameters were angular roll and pitch velocities. Simulations were undertaken with several control laws and results are presented (Fig. 26). The roll rate/roll pitch cyclic input transfer function shows a satisfactory damping increase with different feedback controllers. The difference between controllers is noted at very low frequencies. Simulations were also undertaken in the time domaine presented (Fig. 27). Every controller provides a satisfactory input to the pilot's cyclic stick excitation.

Theoretical studies were also conducted for active stabilization of the 1st drive train mode in interblade rotors, in particular. The objective of this active stabilization is the reduction of high resonance in those areas where engine governor gains are high. The 1st drive mode was identified in flight prior to the active control feedback development. This identification was conducted with the main rotor collective pitch as exciter. The excitation was sinusoid. The parameters measured on the drive train were the main rotor's mast torque and the engine shaft's torque expressed as follows:

$$T_{MAST} = (\Theta_{MR} - \Theta_{MGB}) \cdot K_{MGB}$$

$$T_{ENG} = (\Theta_{ENG} - \Theta_{MGB}) \cdot K_{ENG}$$

K_{MGB} and K_{ENG} are the equivalent torsional stiffnesses of the rotor mast and engine shaft. A comparison is presented, as an example, between the temporal responses of the parameters measured and those derived by simulation (Fig. 28). The correlation between model and tests can be checked graphically. The amplitudes obtained are similar and resonances occur at the same frequencies. The similarity between the highest torque responses both calculated and measured confirm the validity of the model. The closed loop studies were undertaken with engine torque as the observation parameter (Fig. 29); A highly significant damping increase in closed compared to open loop is shown (Fig. 30). The closed loop will be experimented in flight in the near future.

5. CONCLUSION

Active control of aeromechanical stability is surveyed and the following conclusions are drawn:

1 Considering that operating conditions, payload and flight configurations, reduced weight and hub compactness cover quite a wide range, there is a need for active control of aeromechanical stability to simplify the design of main rotor lead-lag dampers.

2. The research work described here helped develop a mathematical model simulating the aeromechanical behaviour of the helicopter in the 0 to 10 Hz range; the model was extensively validated with flight test measurements; the active control feedback was made available based on theoretical calculations for ground resonance, air resonance and drive train stability control

3. The active control of ground resonance was fully validated with flight tests in the Super Puma Mk2 helicopter with a modified, low damping, lead-lag damper. The controller was robust and highly efficient and the correlation with theoretical calculations was very good.

4. An active control strategy is suggested for air resonance and drive train stability; this strategy shall be validated with flight tests in the near future.

5. Every controller that was proposed can easily be integrated in a classical FCS. The current FCS actuators are sufficient as far as the bandwidth required for active control is concerned

6. REFERENCES

1. WALKER W.R.,
« A review of helicopter aeroelastic stability research », La Recherche Aérospatiale,
1995, n° 1, 15-27

2. **STRAUB F.K. and WARMBRODT W.**
« The Use of Active Controls to Augment. Rotor/Fuselage Stability », Journal of the American Helicopter Society,
Vol. 30, n° 3, July, 1985, pp. 13-22

3. NAHAS N,
« Helicopter Ground Resonance » - A Spacial Model Analysis, Aeronautical Journal,
1984, pp. 299-307

4. **JOHNSON W.,**
Helicopter theory,
1980, Princeton University Press

5. **COLEMAN R.P. and FEINGOLD A.M.,**
« Theory of self-excited Mechanical Oscillations of rotors with Hinged Blades »,
NACA report 1351, 1958

6. **ACHACHE M., POLYCRHONIADIS M.**
« Development of an Experimental System for Active Control of Vibration on Helicopters - Development Methodology for an Airborne System » - 12th ERF - Garmisch Partenkirchen, Sept. 86

7. **POLYCHRONIADIS M.**
« Generalized Higher Harmonic Control Ten Years of Aerospatiale Experience »
16th ERF, Glasgow, Sept. 90

8. **Ph. ROESCH, M. ALLONGUE, M. ACHACHE**
« Towards generalized active control of helicopters »
19th European Rotorcraft Forum Italy,
Sept. 1993

9. **M. ALLONGUE, T. KRYSINSKI**
« Validation of New General Aerospatiale Aeroelastic Rotor Model through the wind tunnel and flight test data »
46th AHS Annual Forum,
Washington USA, 1989

10. **B. GUIMBAL**
« Design, evaluation and proof-of-concept flights of a main rotor interblade viscoelastic damping system »
14th European Rotorcraft Forum Italy,
Sept. 1988

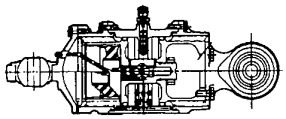

WEIGHT	REFERENCE
NUMBER OF PARTS	61
MAINTENANCE	- VISUAL - OIL CHECK - OVERHAULS
RELIABILITY	REFERENCE

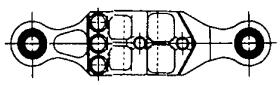

/2
14
- VISUAL - ON CONDITION
MUCH IMPROVED

Fig. 1 : Hydraulic vs visco-elastic

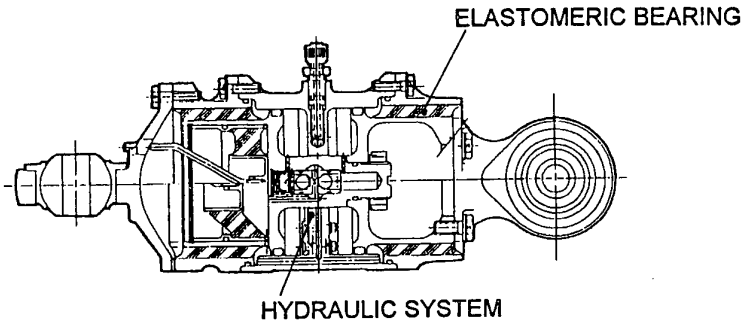

Fig. 2 : Mixed lead-lag damper technology

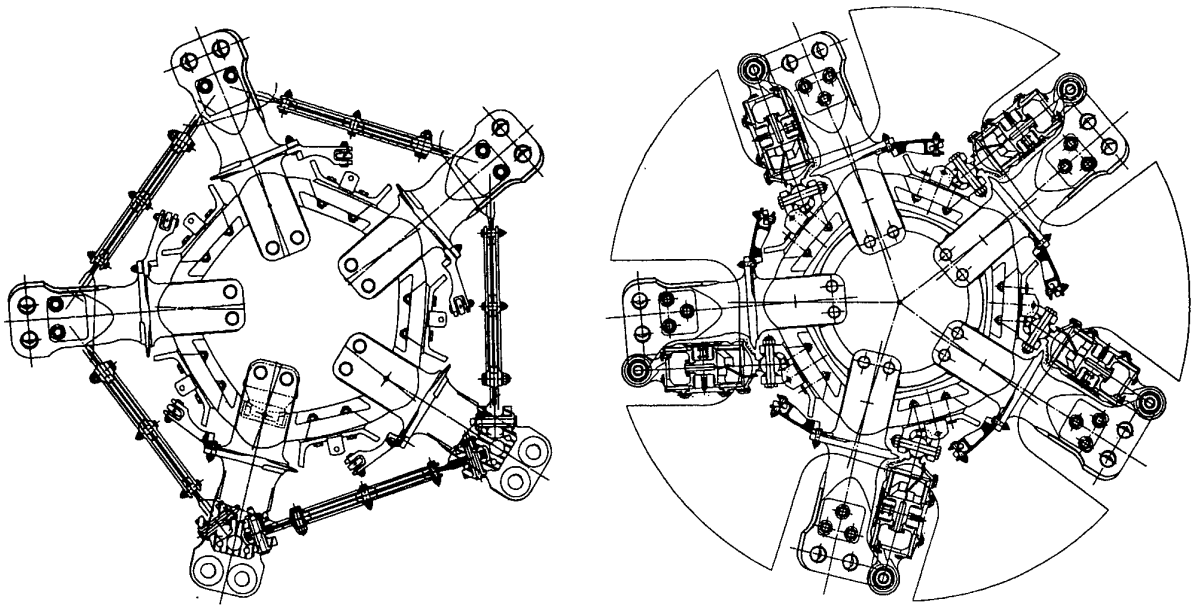

Fig. 3 : Classical and interblade configuration

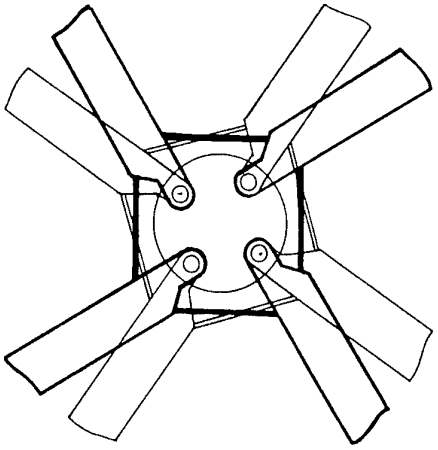

Fig. 4 : 1st lead- lag collective mode

Ground resonance

Body frequency = ωs

Lead-lag frequency = ωδ

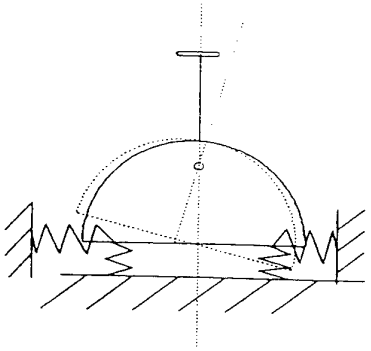

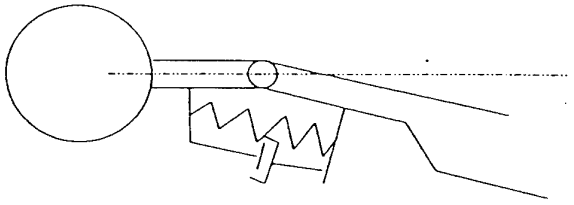

Lead-lag frequency in fixed system Ω-ωδ
Ω - Rotational speed

Ground resonance condition

$$\omega s = \Omega - \omega\delta$$

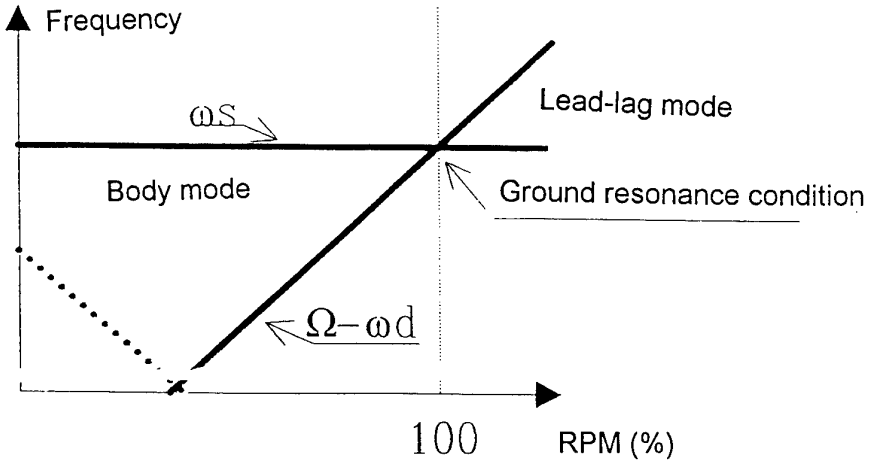

Fig. 5 : Ground resonance mechanism

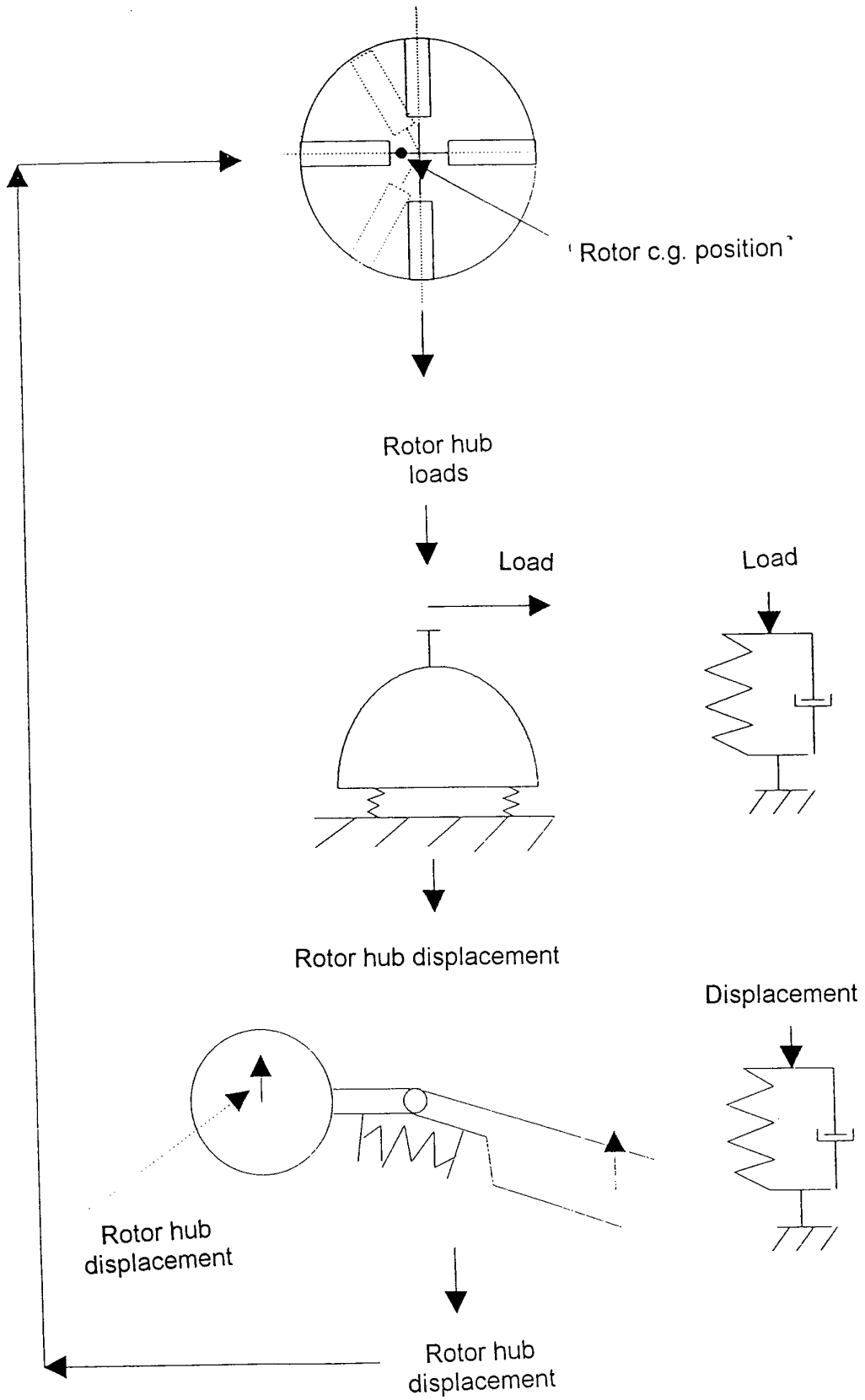

Fig. 6 : Ground resonance mechanism

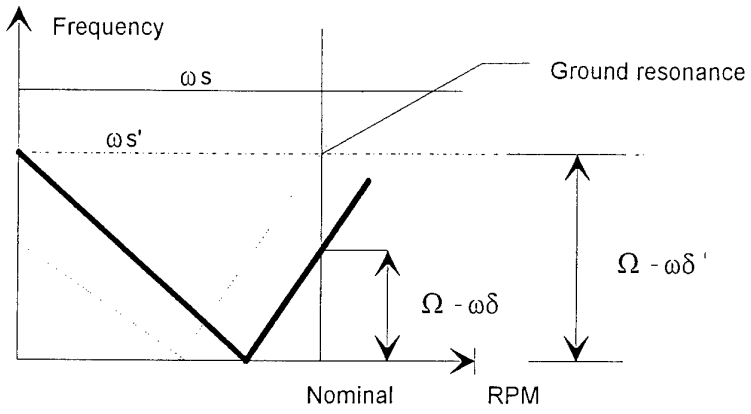

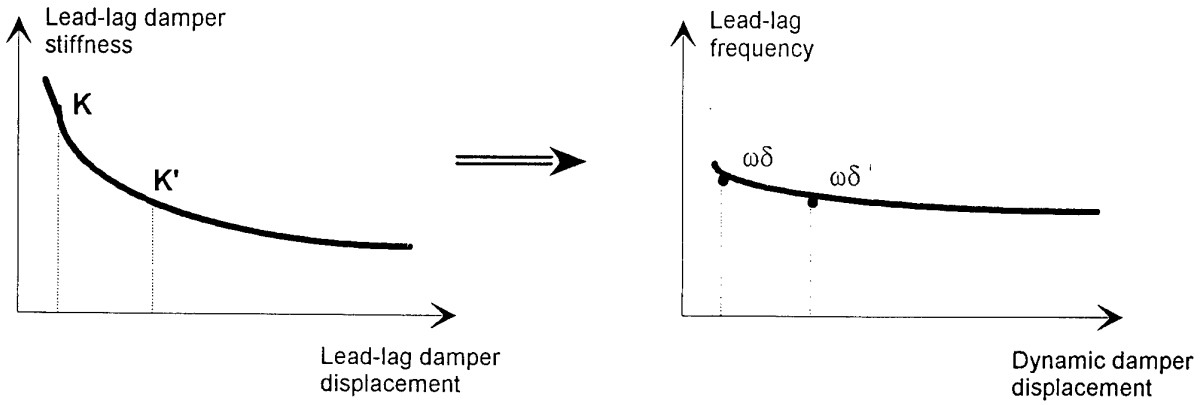

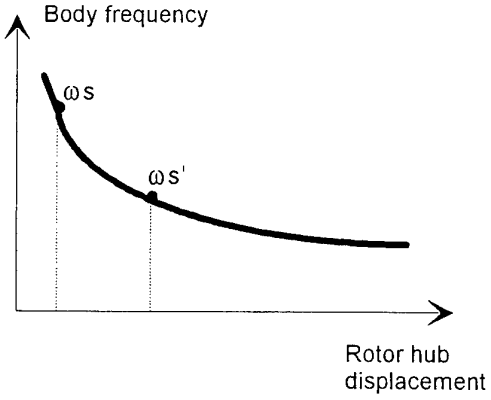

FIG. 7 : Influence of non linearity on ground resonance

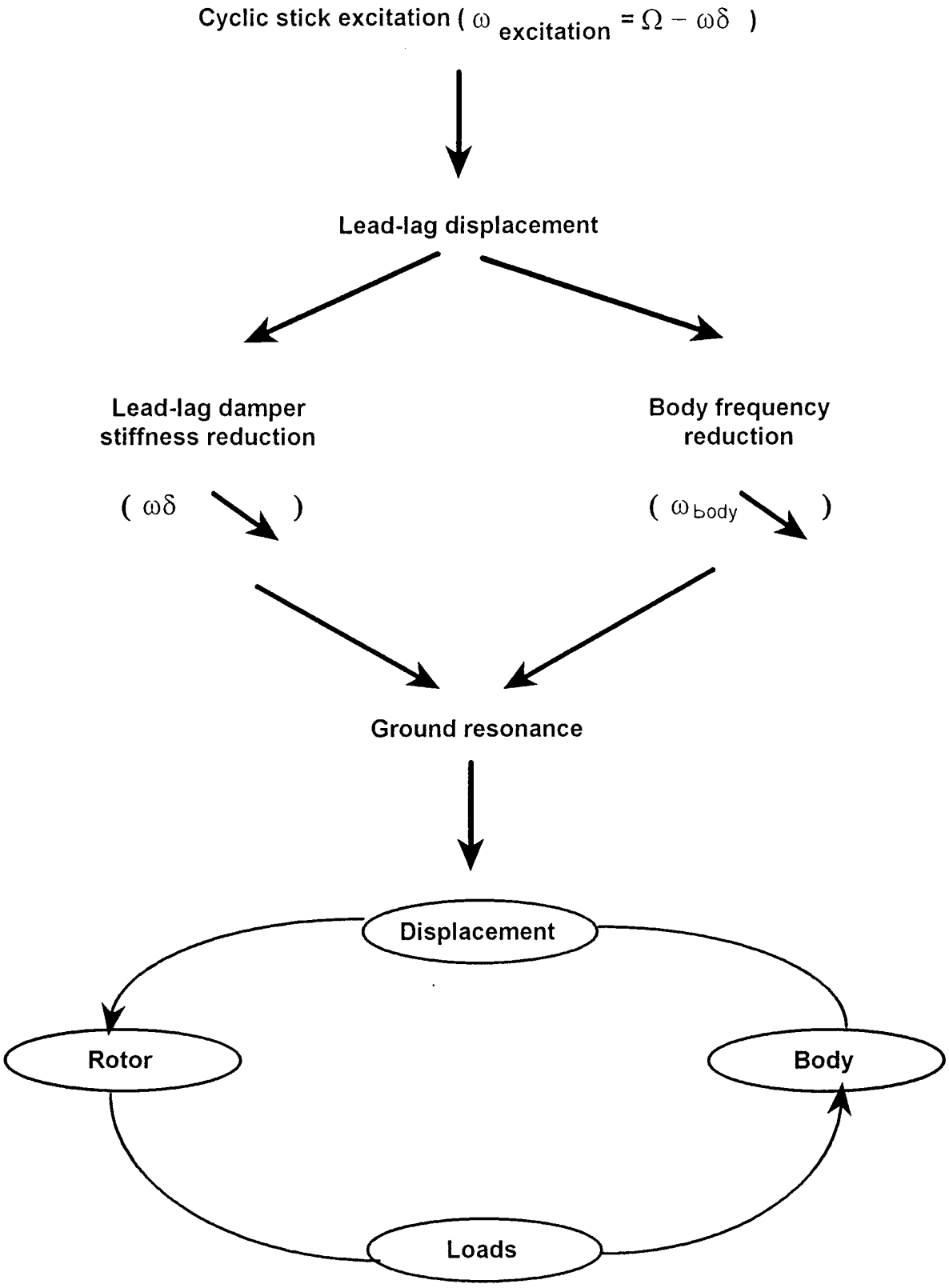

FIG. 8 : Influence of stick excitation on ground resonance

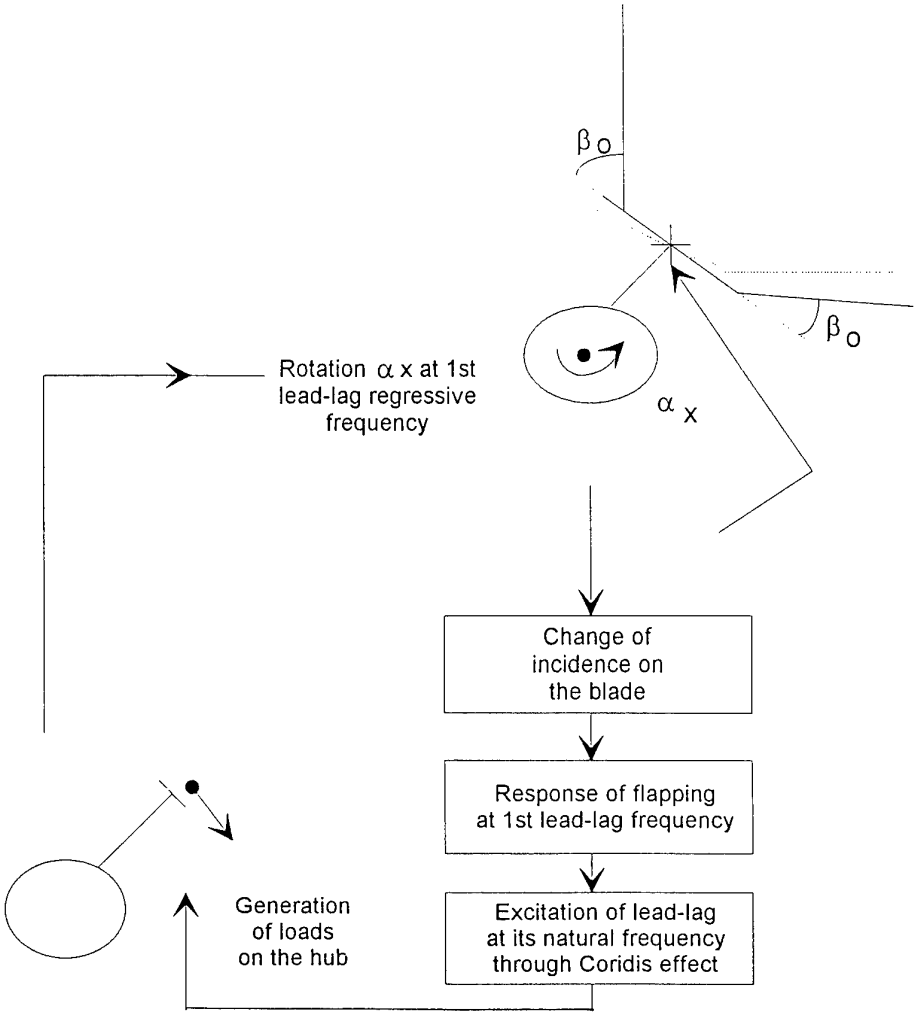

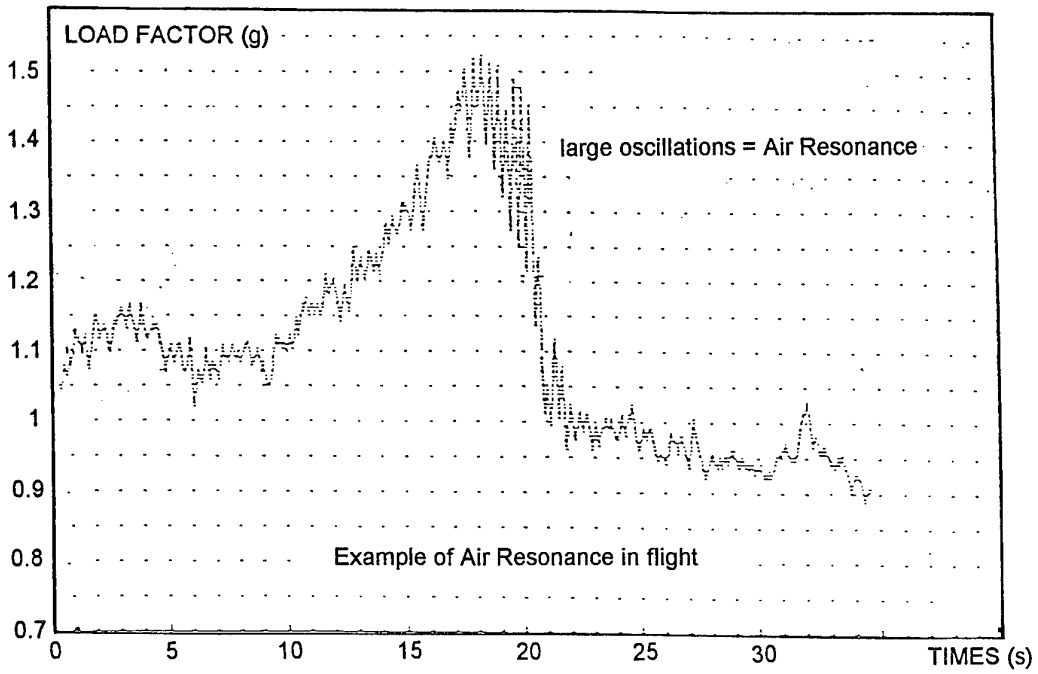

FIG. 9 : Air-resonance mechanism for high loads

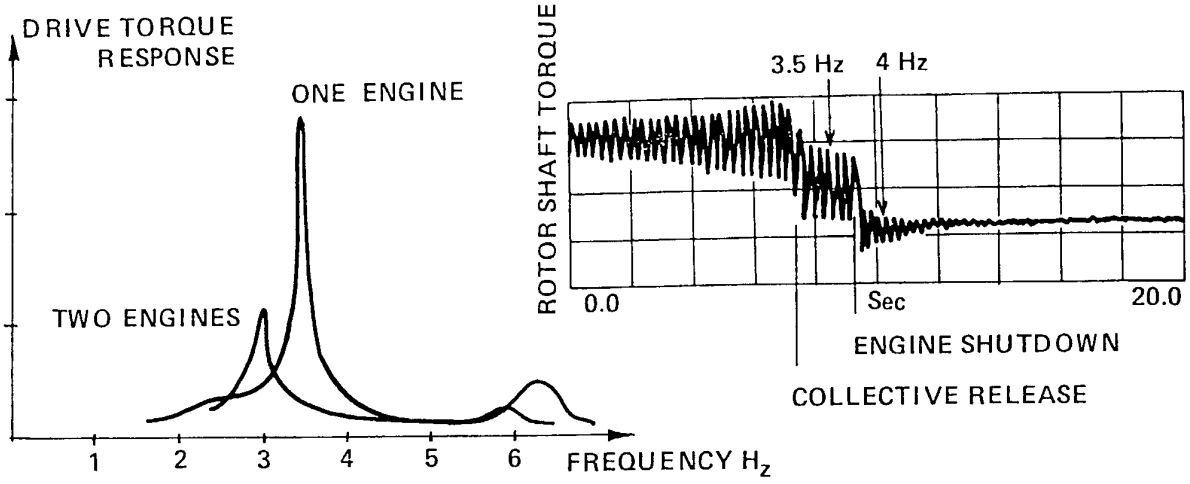

Exemple of drive train response with misadapted governors

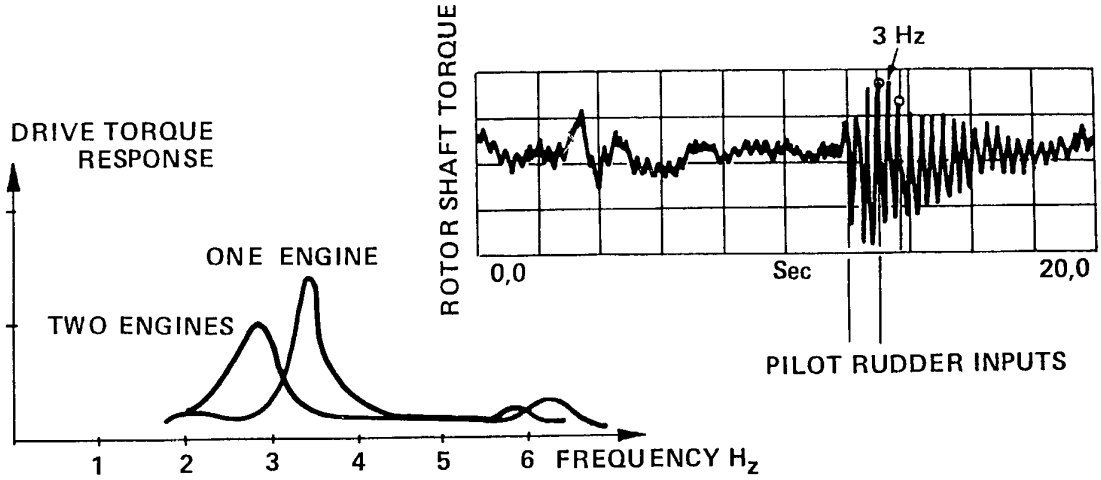

Exemple of drive train response with modified governors

Fig. 10 : Example of drive train response for interblade lead-lag damper

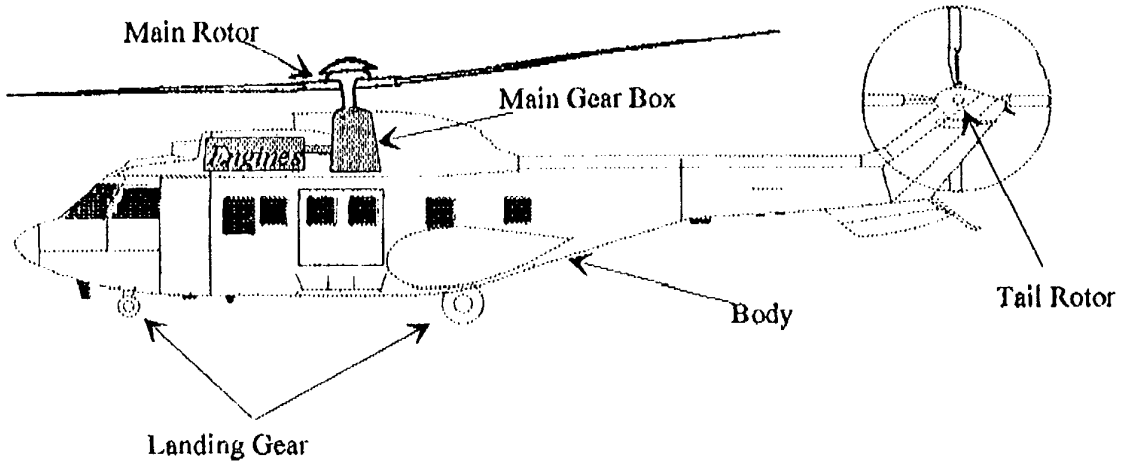

Fig. 11 : Elements used in the modeling

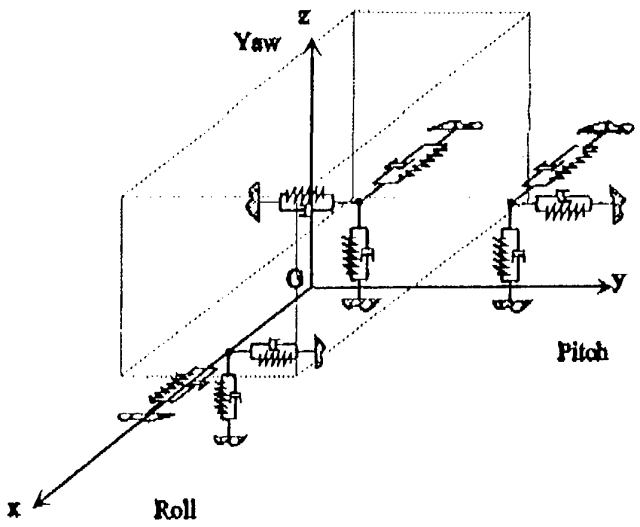

Fig. 12 : Landing gear modelisation

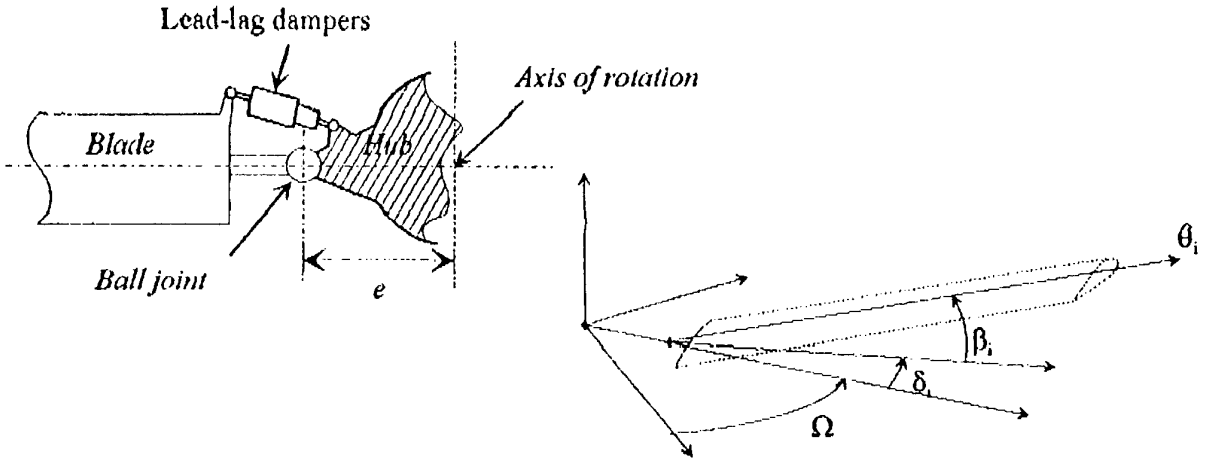

Fig. 13 : Blade modeling

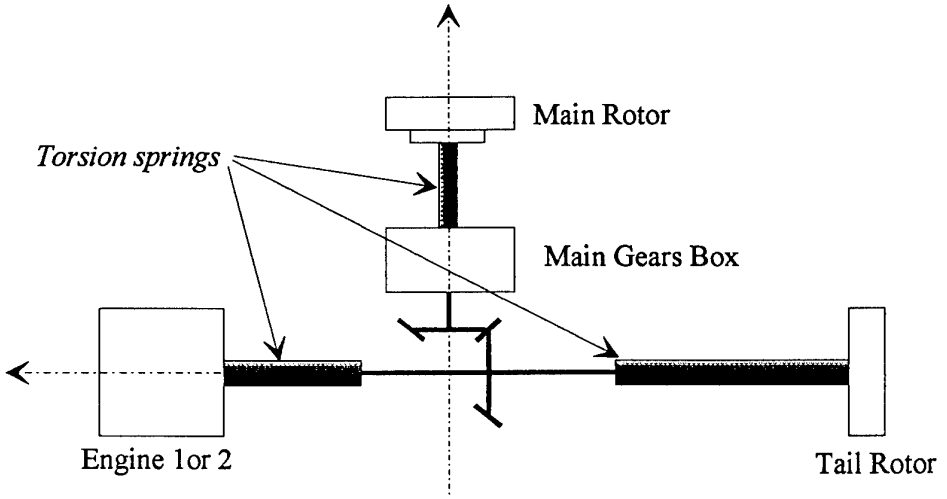

Fig. 14 : Drive train torsional modelisation

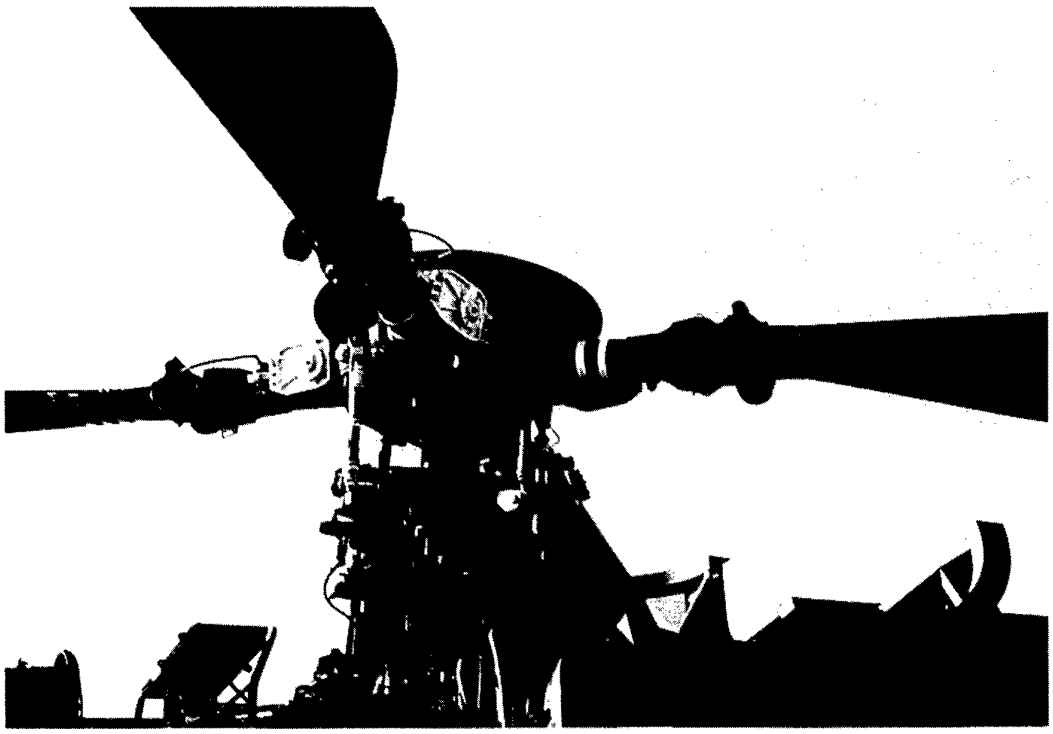

Fig. 15 : 332 MK2 with experimental lead-lag damper

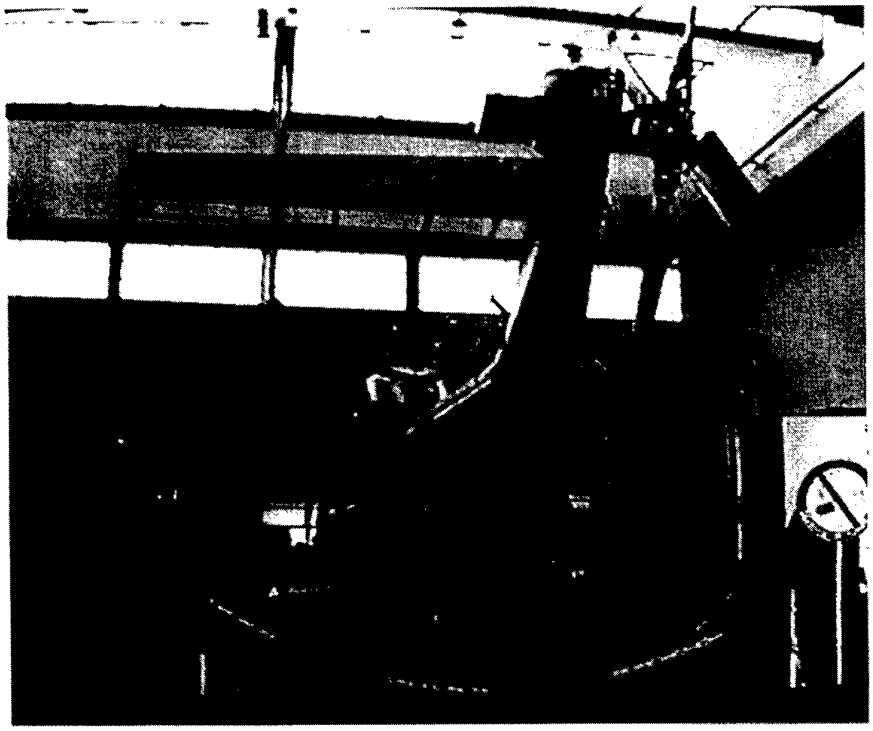

Fig. 16 : 332 MK2 ground resonance shake test in laboratory

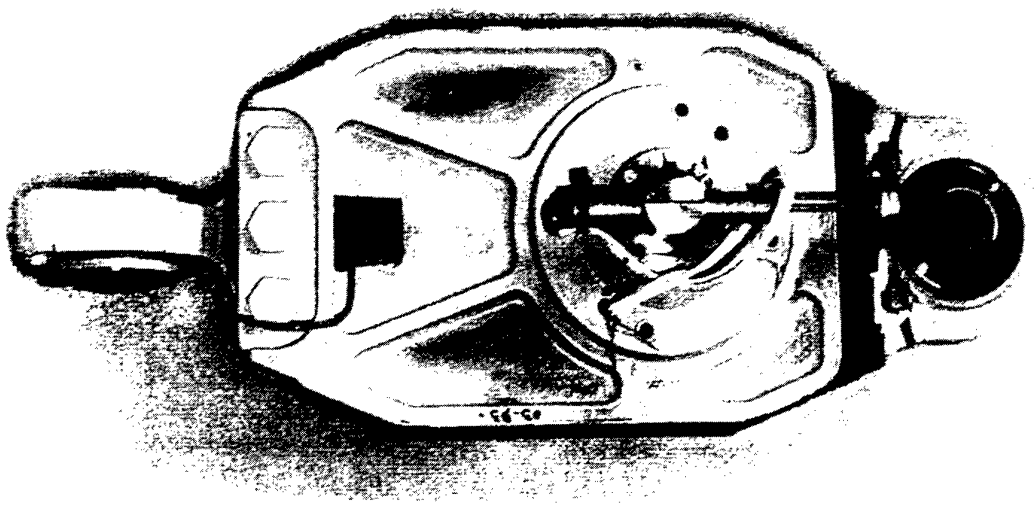

Fig. 17 : 332 MK2 experimental lead-lag damper

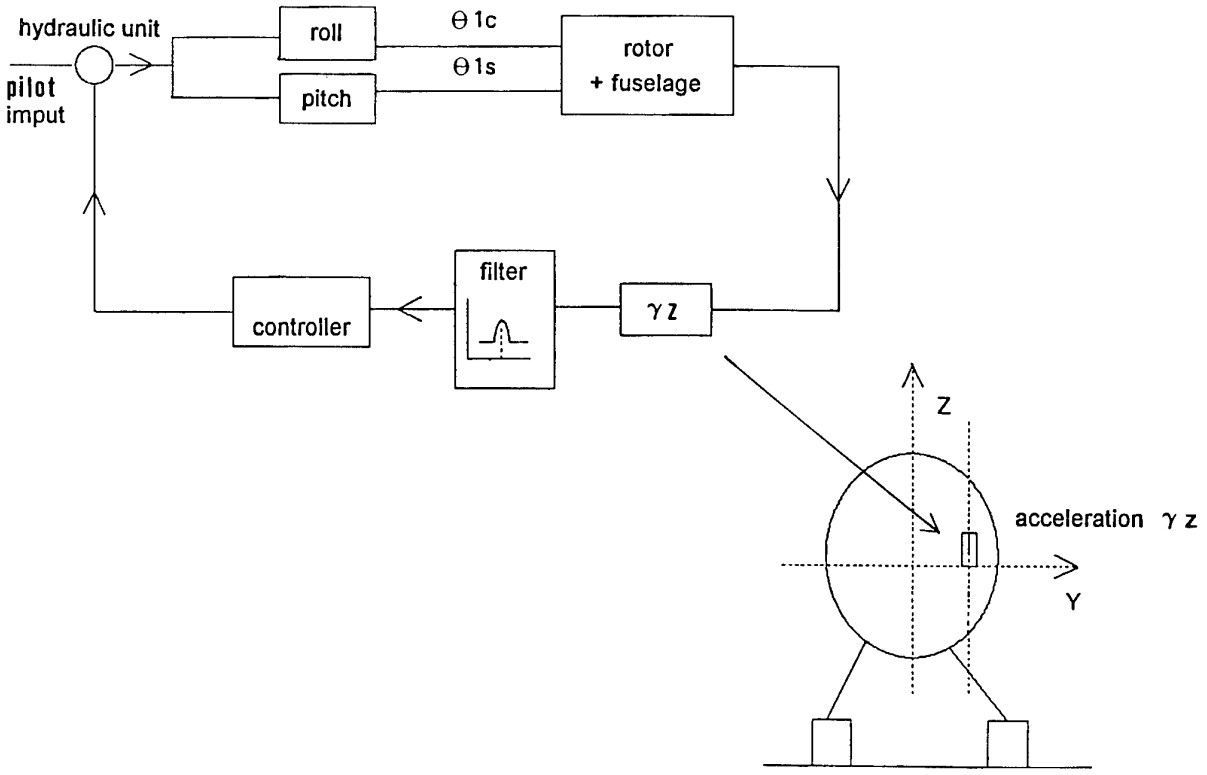

Fig. 18 : Active ground resonance control loop

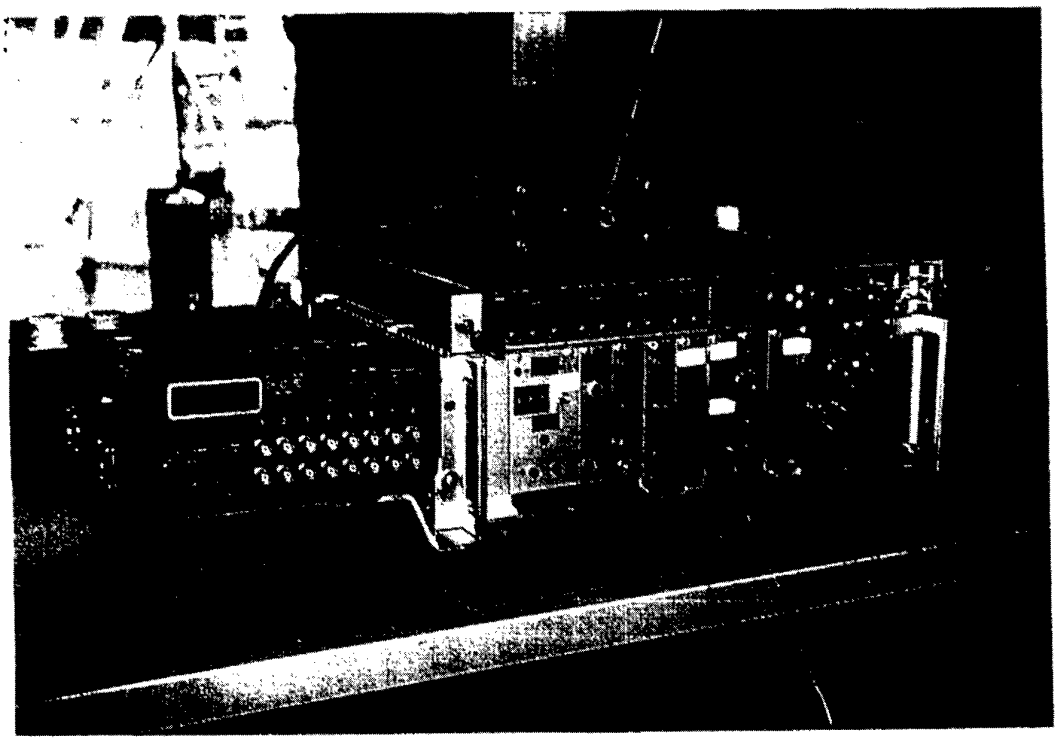

Fig. 19 : Active control system used during tests

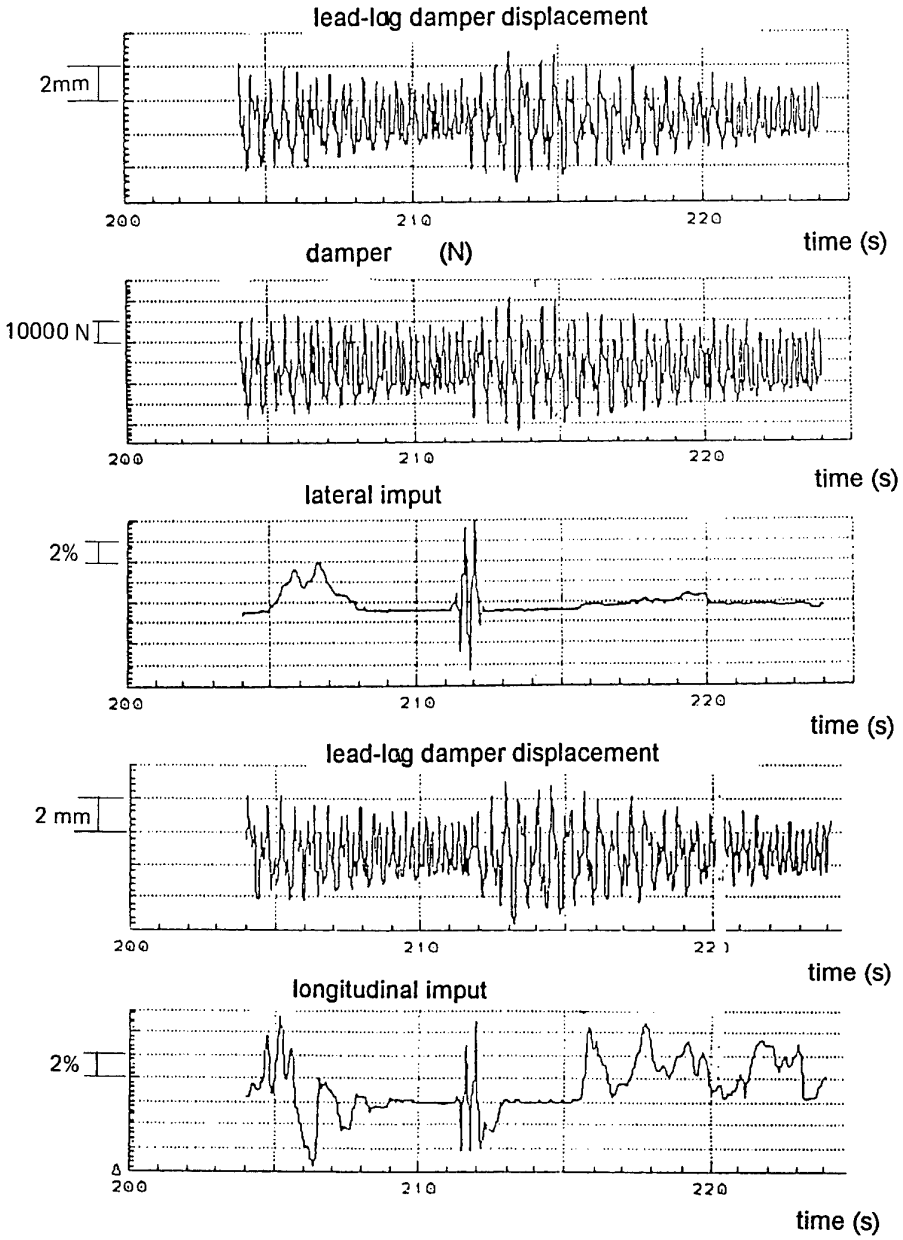

Fig. 20 : Excitation of ground resonance ; low mass stable configuration

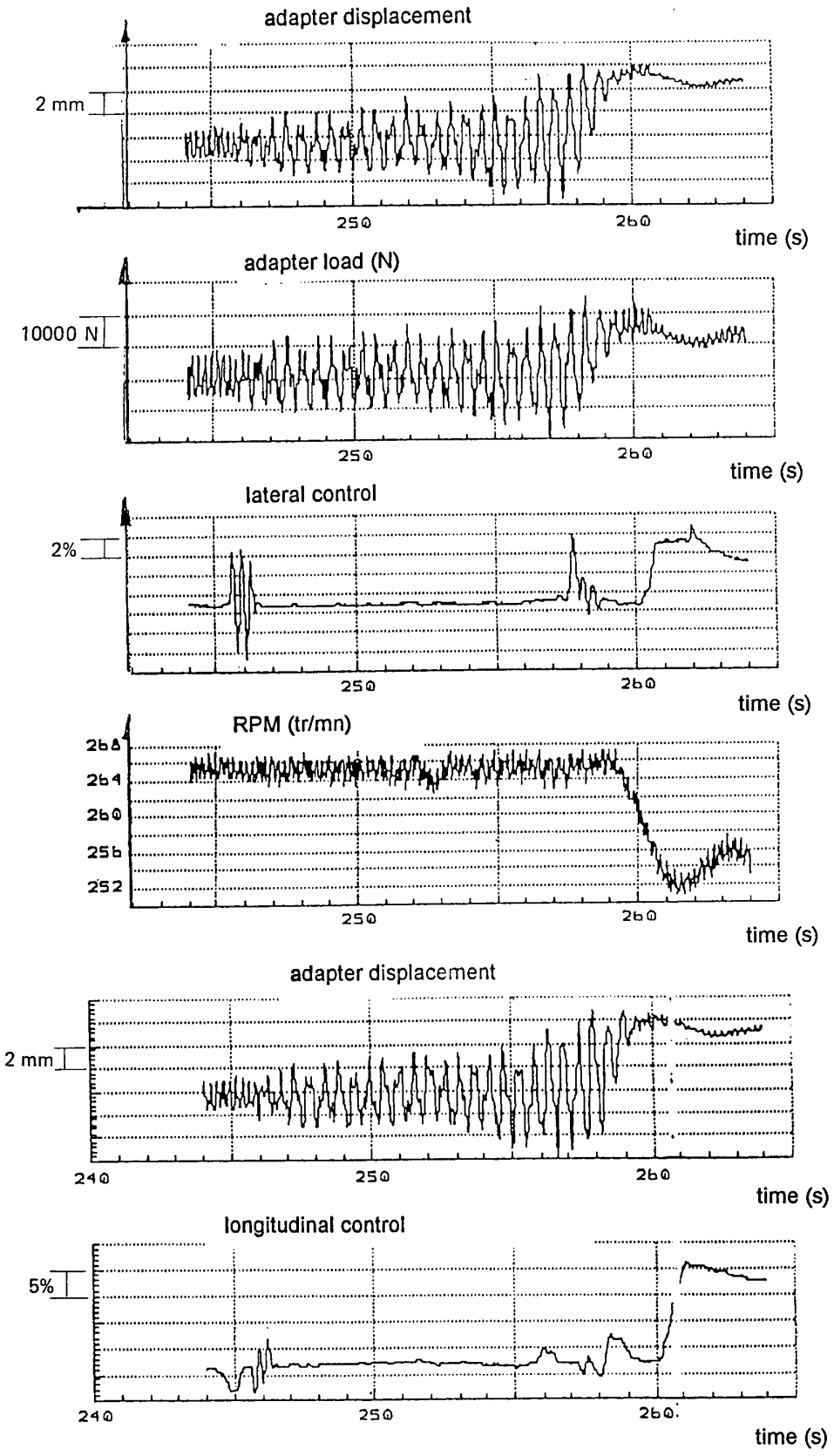

Fig. 21 : Unstable ground resonance behaviour

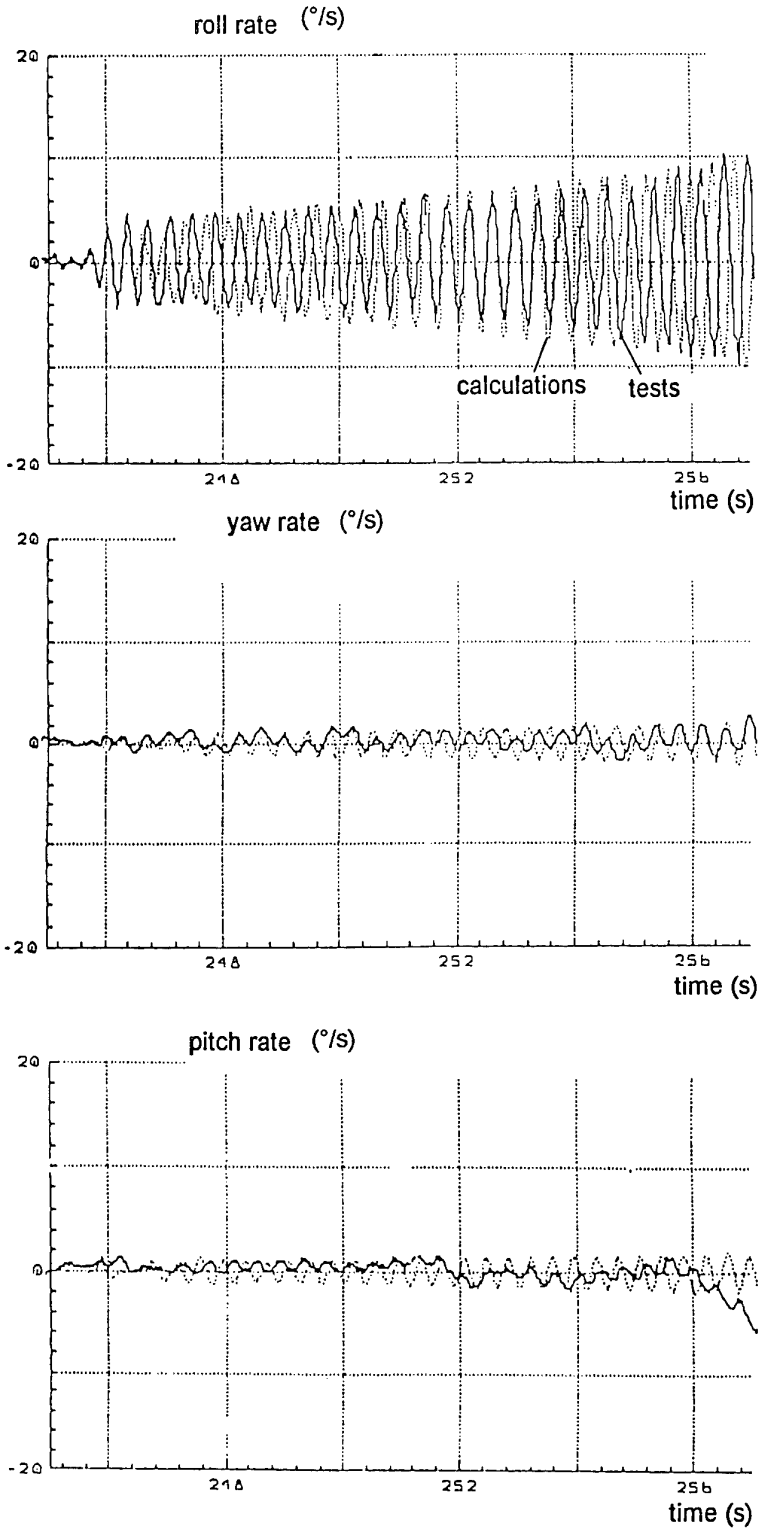

Fig. 22 : Unstable ground resonance oscillations comparison of calculations and measurements

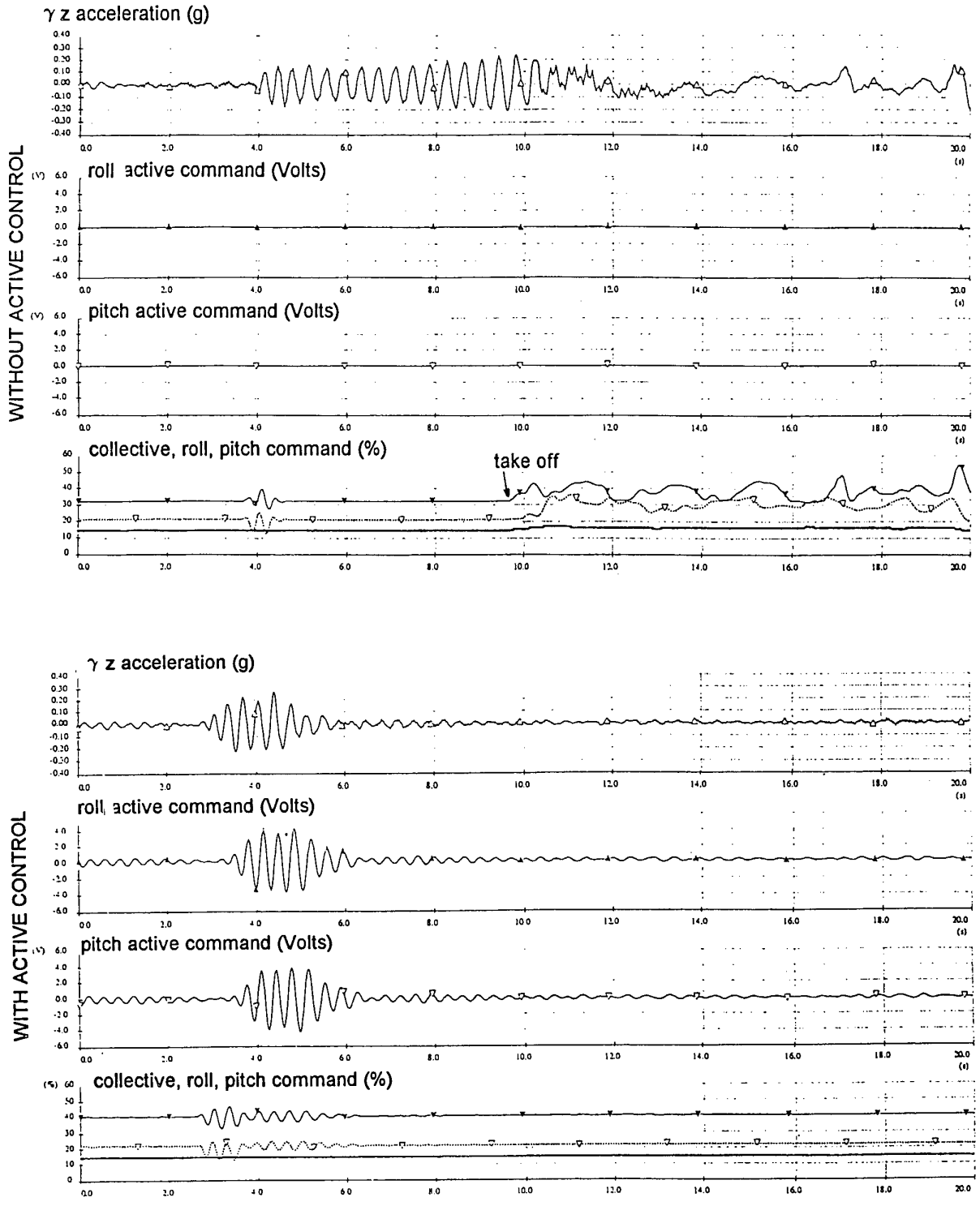

Fig. 23 : Comparison of closed and open loop active control of ground resonance

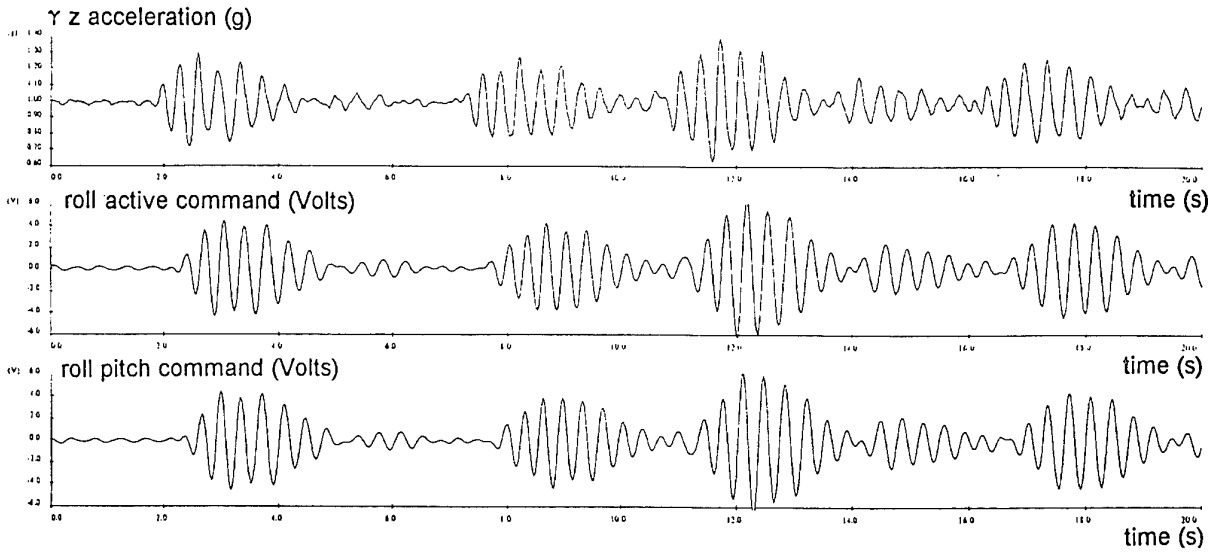

Fig. 24 : Exciation of ground resonance in closed loop

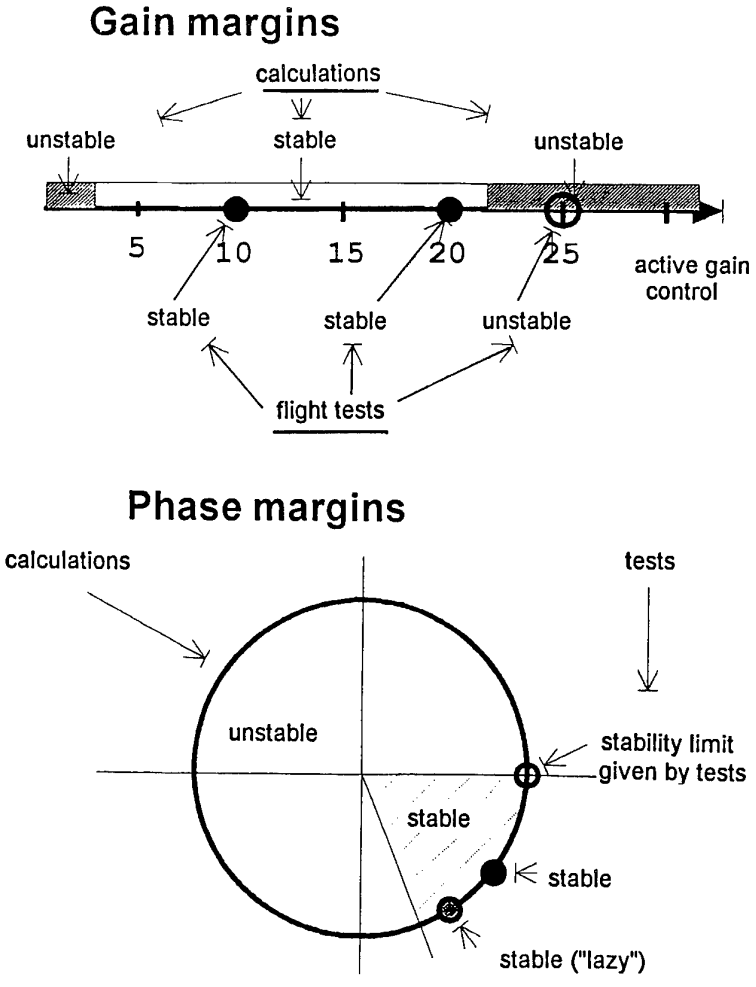

Fig. 25 : Stability margins active control of ground resonance

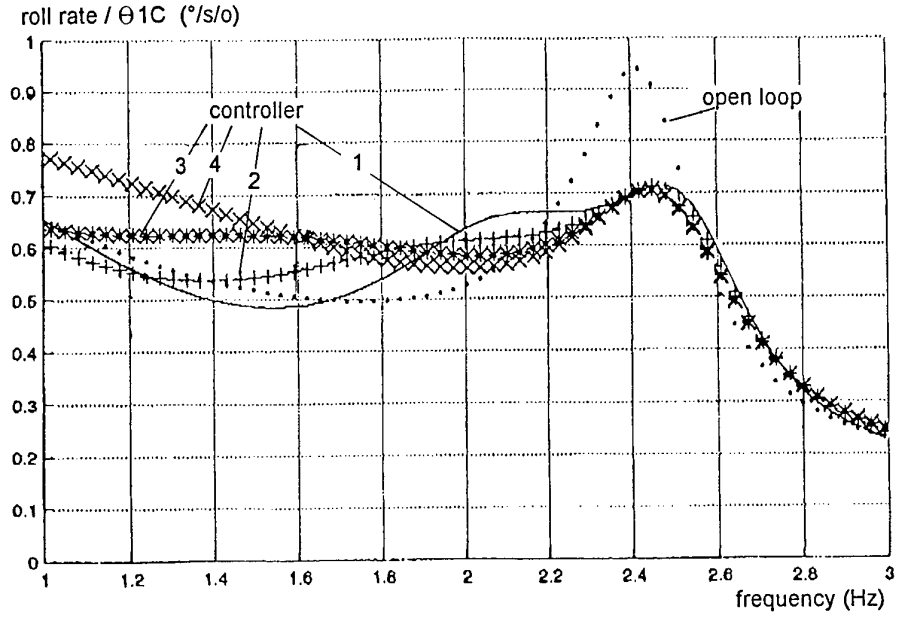

Fig. 26 : Air-resonance transfer function with active feedback loop

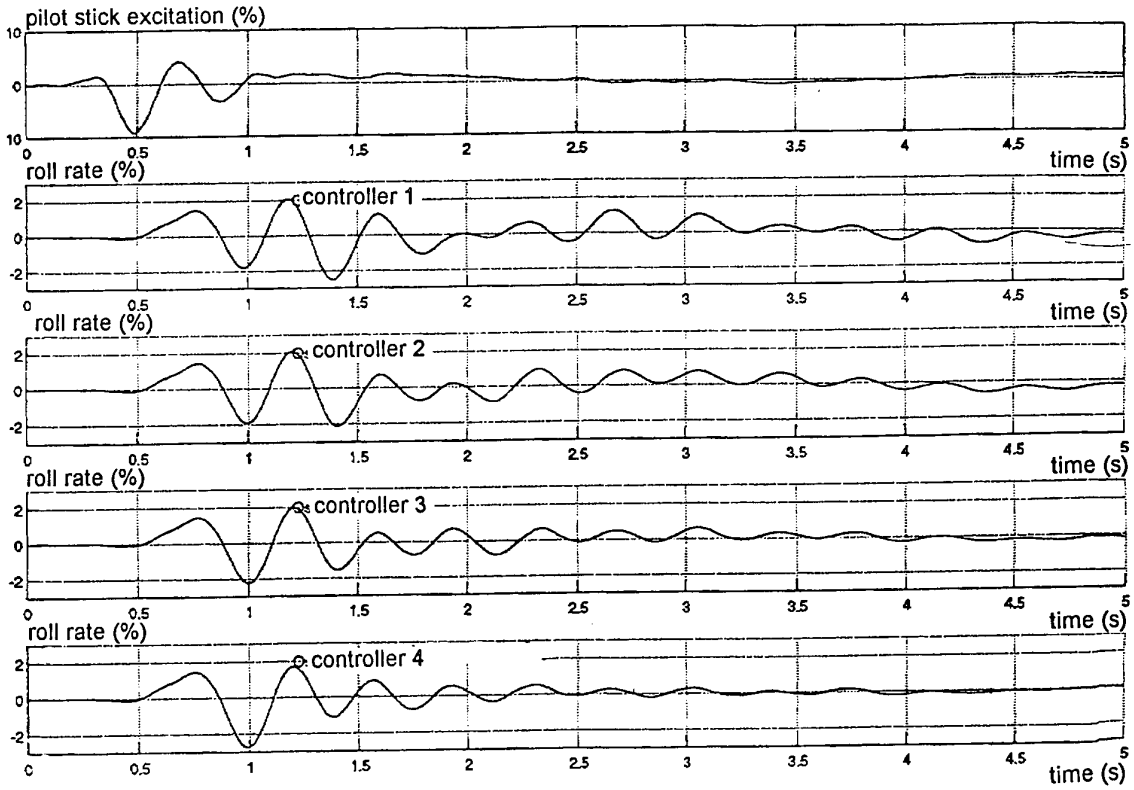

Fig. 27 : Air-resonance time domain response

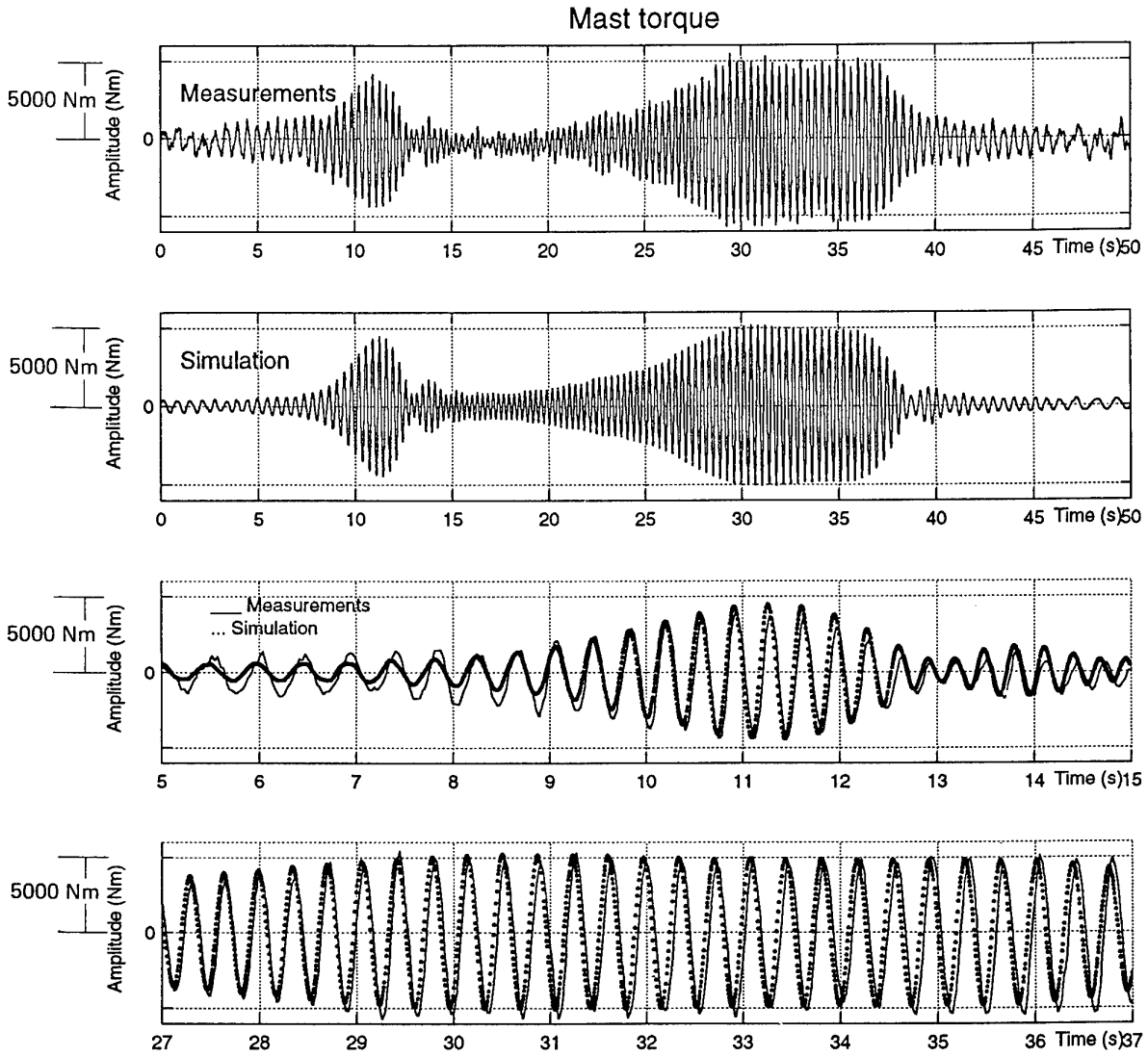

Fig. 28 : Drive train identification, calculations/measurements comparison

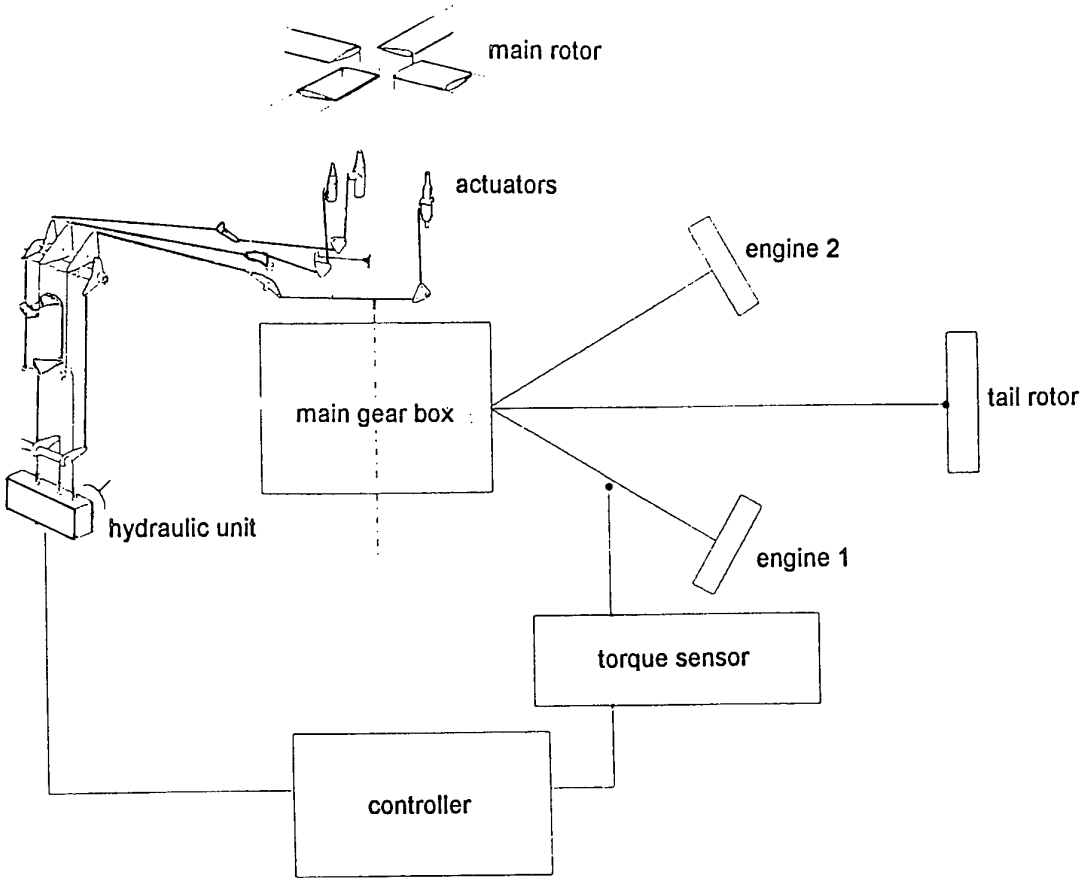

Fig. 29 : Drive train active control loop

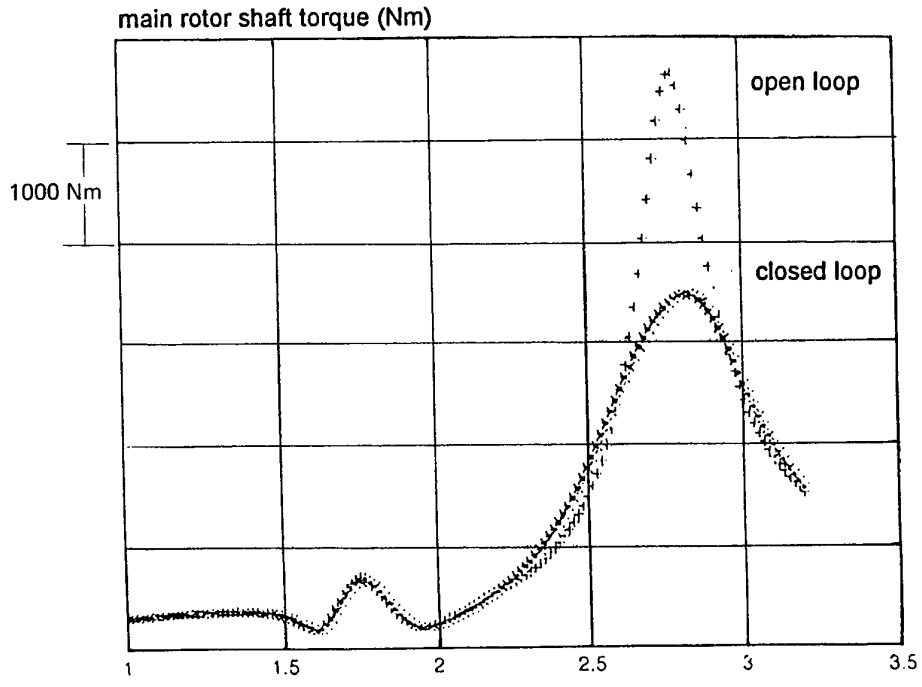

Fig. 30 : Active control of drive train

Helicopters and Night Vision Goggles: A Synopsis of Current Research on Helicopter Handling Qualities during Flight in Degraded Visual Environments

Stewart W. Baillie
J. Murray Morgan
Flight Research Laboratory
National Research Council, Montreal Road
Ottawa, Ontario K1A 0R6
Canada

1.0 INTRODUCTION

The role of the helicopter in military operations often involves flight in adverse weather conditions and the execution of flight manoeuvres designed to maintain minimal exposure to the enemy. This translates into a requirement for helicopters to fly very low level, nap-of-the-earth, at night or in bad weather. This type of flying places a high demand on the pilot to accurately perceive the environment and to precisely control the flight path of the aircraft. To assist the pilot in this task, he is often provided night vision goggles or some type of infra-red or radar-based vision system to augment his visual environment. Unfortunately, even with these vision enhancing aids, the pilot's visual environment often does not possess the quality (in terms of texture, contrast, field of view and other parameters) that is usually available in normal daylight. This poor but operationally important visual environment is now commonly referred to as a degraded visual environment or DVE.

The Flight Research Laboratory of the Institute for Aerospace Research, National Research Council Canada has been conducting research regarding the handling qualities of rotorcraft flying in degraded visual environments since 1987. These efforts have been coordinated with a variety of international partners including the US Army Aeroflight Dynamics Directorate and Hoh Aeronautics under TTCP (The Technical Cooperation Program). The NRC effort has been funded in part, by the Air Vehicle Research Sector, a detachment of the Defence and Civil Institute of Environmental Medicine, Canadian Department of National Defence. The program has focused on studying the practical effects of degrading the pilot's visual environment and on the search for ways to counteract these effects. The program has involved theoretical considerations, pilot-in-the-loop evaluations using ground-based simulators, such as the NASA Ames Vertical Motion Simulator, and in-flight evaluations on the NRC Bell 205 Airborne Simulator (Figure 1).

This paper will summarize the concepts and research results that have been gathered on the topic of the handling qualities of helicopters flown in degraded visual environments. While concentrating on those research efforts performed under the TTCP program, the paper will also incorporate the results of other efforts where appropriate. In particular, the paper will consider four major areas:

1) the concept of the Useable Cue Environment (UCE) and how this concept applies in practical situations and procedures;

2) experimental results describing which qualities of a visual field are important for the helicopter piloting task;

3) experimental results describing the degradation in handling qualities due to a reduction in Useable Cue Environment (a DVE), the rationale behind this degradation and the subsequent handling qualities improvements made possible by augmentation of the helicopter response; and,

4) the improvements in handling qualities for DVE flight that are possible by reprogramming an existing helicopter stability augmentation system into what is known as a limited authority response type.

The paper emphasizes the practical implications of the experimental results and suggests approaches to improve operational capabilities of existing aircraft as well as those yet to be designed.

2.0 THE CONCEPT OF A USEABLE CUE ENVIRONMENT

As a pilot flies a helicopter, he uses a multitude of cues to infer how the helicopter is moving and performing. Based on these cues, the pilot makes inputs to the aircraft controls and stabilizes the helicopter to achieve the desired flight path. The total set of cues available to the pilot is described by the phrase "Useable Cue Environment" or UCE. The UCE is formed from the visual environment outside the aircraft (what is outside to see), what systems are available to view the outside environment (eg. human eye in daylight, night vision goggles or infrared displays at night, etc.), and those systems that present situational information in the cockpit (e.g. head-down hover displays, attitude indicators, airspeed indicators, tactical information and navigation displays). Aircraft motion, vibration and noise are additional elements that may contribute to the UCE, especially if the pilot has extensive experience with the given aircraft and can infer aircraft state from these cues (ie. they are ***useable*** cues).

The concept of UCE, as described above, seems almost trivial. It is only when the piloting task is introduced into the consideration does the concept of UCE allow an increased understanding of the DVE problem. A discussion of this consideration was initially presented in Reference 1 and is summarized below.

Most helicopters, in their purest, unaugmented form at slow speed, are unstable vehicles which require a considerable level of pilot effort to stabilize and control. A typical root locus plot of the attitude and horizontal position dynamics of an unstabilized helicopter has unstable poles, an oscillatory, neutrally stable attitude mode (labelled A on Figure 2), and a slightly divergent position mode (labelled B on Figure 2). As shown in Figure 2, to stabilize these two modes, the pilot must generate lead in both aircraft attitude and position. From a practical point of view, in order to achieve a stable hover in an unaugmented helicopter, the pilot must be able to predict what the aircraft attitude will be in approximately 1/2 second and what the aircraft position will be in

Paper presented at the FVP Symposium on "Advances in Rotorcraft Technology", held in Ottawa, Canada, 27-30 May 1996, and published in CP-592.

approximately 1 second. Needless to say, the above statement describes a condition of continual monitoring and control to maintain a desired flight path.

A trained helicopter pilot is able to generate the required attitude and position "lead" and is able to stabilize unaugmented helicopters without much difficulty in normal daylight conditions. Ab-initio pilots, in the same visual conditions, have a hard time stabilizing the same helicopter in the hover. In this case, the same cues are available but the ab-initio pilot has not learned the ability to use them (the U of UCE!). The typical hover performance of ab-initio pilots can be described as erratic at best. When they use a near field point of regard, such as a reference point on the ground, the helicopter hover is usually oscillatory in attitude and position, and often unstable in either or both of these states. At this point an instructor pilot will usually tell the student to focus his gaze on the horizon, where the attitude of the helicopter is more apparent, and helicopter angular rate can be more easily discerned. This change of focus usually leads to a stabilization of helicopter attitude but, since a focus on the far field does not give good cues regarding absolute position of the helicopter with reference to a given point, the accuracy of position keeping is poor and oscillatory. As pilots learn to infer the attitude and angular rate from visual elements that are closer and closer to the helicopter, the position keeping of the pilot improves since the nearer focus provides better translational rate cues.

Well trained pilots who are new to flying in degraded visual environments have difficulties in stabilizing the attitude and position of the helicopter which are very similar to those of the ab-initio pilot, suggesting that the cues that the pilot uses to stabilize the helicopter in good visual environments have been taken away and that those cues that remain are either insufficient or as yet unusable by the pilot. Like an ab-initio pilot, the new to NVG pilot often has initial trouble in stabilizing attitude but usually overcomes this tendency quickly. A more lasting trait is that of slowly drifting in position and not discerning the error until it becomes large.

Of course pilots, being the adaptable lot that they are, learn to compensate for the reduced set of visual cues available during flight with night vision goggles and there are many operational pilots who are clearly capable of accurately stabilizing a helicopter in this degraded visual environment, especially in the higher night illumination levels such as partial moon conditions. One compensation technique that is prevalent among night vision goggle pilots is the use of a rapid scan of the head from the side to the front to gather more attitude and position information quickly. In a "Night Vision Goggle Primer" to pilots in a recent copy of Flying Safety Magazine (Reference 2) the author advises the reader: "Current goggles have only a 40 degree field of view, and you'll have to learn new scanning techniques to overcome this limitation".

The development and use of piloting techniques to compensate for system characteristics implies an increase in pilot workload and a degradation of aircraft handling qualities. The occurrence of helicopter accidents related to flight in DVE suggests that the level of pilot compensation has a measurable price. In cases where the visual environment degrades quickly, for example flying into a fog bank at night or encountering recirculating snow or sand, the price becomes even more apparent. For this reason the study of the visual cues used by a pilot in hover manoeuvring is very relevant today.

3.0 IMPORTANT QUALITIES OF THE VISUAL ENVIRONMENT

A 1985 study by Hoh described in Reference 3 looked specifically at what pilots use in the visual field to stabilize helicopters in slow speed flight. In this experiment, both the field of view available to the pilot and the amount of detail available for the pilot to see were varied while the pilot performed a series of handling qualities evaluation tasks in a Hughes 500 helicopter. The field of view was varied by blanking off various portions of the wind screen on the evaluator side of the helicopter while the detail was varied by the use of large markers (traffic cones) and IFR training goggles which, by blurring the near field of regard, could prevent the pilot from perceiving the fine detail of the dry lake bed which was the site of the tests.

Back to back evaluations of the handling qualities of the helicopter for different visual environments led to the following conclusions:

- "there is considerable evidence that fine-grained texture is an important cue for hovering and low speed flight"

- "a small field of view (38 deg x 23 deg) is sufficient (for stabilization and control, ed.) if the texture is available"

- "pilots use "microtexture" in the foreground to obtain attitude as well as translational rate cues"

Hoh suggested that the visual information which is important corresponds to the improvement in visual acuity between 20/80 and 20/50. With 20/80 vision, large obstacles are still discernable but the information required to allow a pilot to generate the lead required to stabilize and control helicopters is not evident. With 20/50 vision, on the other hand, no degradation in the ability to manoeuvre or stabilize a helicopter is noticed.

In addition to the fundamental understanding of visual texture that this experiment developed, it also formed the basis for the development of the useable cue environment rating process, described fully in the Aeronautical Design Standard 33 - Helicopter Handling Qualities (Reference 4). The useable cue environment rating process was based on the realization that there is not a detailed enough data base to fully define the handling qualities related effects of the quality of a visual system or to take into account the variety of tradeoffs that can be made. It is also a given that the subjective evaluation of visual scene quality is extremely imprecise. To overcome these deficiencies, the UCE rating process relies on test pilots to evaluate their ability to aggressively make corrections in attitude, translational rate and altitude while flying a "standard" helicopter. The resulting three ratings are combined to form a single number which describes the quality of the visual scene. Experience is now showing that particular devices, such as night vision goggles, in particular environments, such as a starlit night, correspond to standard UCE levels, in this

case, UCE 2.[1]

In another study, Vollmerhausen (Reference 6), used a device to alter the pilots visual acuity and field of view while flying a terrain following mission in an AH-1 COBRA helicopter. The terrain following flight task has significantly fewer stabilization demands than some of the previously considered tasks and the data for this experiment consisted of performance measures, as well as pilot ratings. The results of this evaluation led to the conclusion that a head referenced, 40 degree field of view is sufficient for the terrain following task provided that a minimum visual resolution of 0.6 cycles/mrad was available (approx. 20/60 vision). The report also emphatically stated that visual field of view should only be increased if this minimum resolution can be maintained.

To describe the current capabilities of night vision goggles, the chart in Figure 3, taken from Reference 6, describes the best available resolution of night vision goggles versus the ambient illumination. Note that at an illumination of 0.0005 foot candles, the equivalent of almost a moonless night, the perfect ANVIS - 6 goggles have the minimal resolution of 0.6 cycles/mrad (approx. 20/60).

To further consider the important qualities in a visual environment, a small in-house study was performed at NRC to look specifically at the effects of the reduced field of view imposed by vision aids, such as night vision goggles (Reference 7). In this study three pilots flew the Bell 205 Airborne Simulator configured with a rate command system which was evaluated to possess Level 1 handling qualities in a good visual environment. The pilots flew the aircraft while wearing the field of view restricting goggles shown in Figure 4 which could vary both the size of the field of view and the overlap region between the two eyes. Fields of view were varied between 150 and 20 degrees for both 0 and 100% overlap configurations. Figure 5 shows the handling qualities rating results for the 100% overlap cases. This data shows that for pure stabilization tasks, such as a precision hover and landing, the handling qualities start to degrade at fields of view between 30 and 40 degrees. (for 100% overlap). On tasks such as pirouettes and quickstops, where larger aircraft attitudes and angular rates are encountered, this limit increases slightly to between 40 and 75 degrees. In considering these results, it should be noted that this test was performed with perfect acuity, resolution and texture in the field of view available to the pilot.

The overall significance of this entire discussion is that the visual environment provided by night vision goggles is on the borderline of sufficient in terms of field of view to enable the stabilization and control of helicopters in slow speed and hover manoeuvring flight. Since the representation of what is portrayed in that field of view is also degraded, especially in lower light level conditions, the total combination causes a handling qualities degradation in almost any light condition . The magnitude of this degradation, and approaches to counteract the degraded visual environment have been the focus of considerable effort.

4.0 RELATIONSHIPS BETWEEN USEABLE CUE ENVIRONMENTS, HELICOPTER RESPONSE CHARACTERISTICS AND HANDLING QUALITIES

A number of in-flight evaluations have been conducted at the Flight Research Laboratory to assess the degradation of handling qualities due to degraded visual environments and the handling qualities improvements that can be achieved by changing the stability and control response of the helicopter (References 1 and 8). In each of these experiments, evaluator pilots wore a device to alter the available useable cue environment; IFR training goggles which reduce the texture that can be seen by presenting a variable level of fog through which the pilot sees, night vision goggles with daylight training filters which provide both a reduction in texture and field of view, and a night vision goggle simulator which similarly restricts field of view and reduces texture. The aircraft response type evaluated was subject to a wide range of variations but can be summarized into three major types; rate response, attitude response and translational rate response. The control input response of each of these three response types is shown in Figure 6.

A summary of results of this group of evaluations is shown in Figures 7 and 8. The data in Figure 7 documents the relationship between useable cue environment and handling qualities for a typical, rate response helicopter and typical hover manoeuvring tasks. The degradation of handling qualities from Level 1 in UCE 1 to Level 2 in UCE 2 is clear and unmistakable. It should be noted that the task description used during the gathering of this data did not vary when visual environments changed except for a relaxation in the time allowed for completion of the manoeuvre. The handling qualities degradation documented in these results is a direct consequence of the reduced quality of the angular rate cues that the pilot has available to him, This cue degradation causes the pilot to use more of his capacity in stabilizing the aircraft in attitude, while at the same time reducing the quality of the translational rate stabilization.

The data shown in Figure 8 demonstrates that the degradation in handling qualities with UCE can be overcome by altering the response of the helicopter. The handling qualities ratings for the attitude response type with a height hold option in UCE 2 are clearly an improvement over the rate response ratings for the same visual environment and tasks. Relieving the pilot of the attitude stabilization task by giving him an aircraft that has an attitude response and compensating for the weak vertical rate cues that are provided by NVGs in UCE 2 by adding a vertical rate command/height hold system creates handling qualities to be quite close to the original, "satisfactory level" for the rate response type in UCE 1. Other data, reported in Reference 8, has also demonstrated that as the visual environment degrades further, to UCE 3, satisfactory handling qualities are only attainable through the use of a highly augmented helicopter possessing a translational rate command/hover hold system. In UCE 3, the pilot spends all of his time trying to discern where the aircraft is and therefore all of the stabilization tasks must be done by the aircraft system.

[1]Well adjusted NVGs on a full-moon lit night are considered by some to be borderline UCE 1, although some data suggests that even in the best conditions, NVGs are UCE 2 (Reference 5) (UCE 1 is the best possible level while UCE 3 is the worst)

For all of the evaluations cited thus far, the helicopter response type was full authority, attainable only with a full-authority, fly-by-wire control system. While the handling qualities data for these implementations are important for future helicopter designs, it is impractical to assume that all present-day helicopters will be scrapped for new ones or will be refitted with full-authority fly-by-wire control systems to improve their handling qualities in degraded visual environments. For this reason, and with the existing data as background, studies were undertaken to find a practical solution to the problem for existing aircraft.

5.0 LIMITED AUTHORITY RESPONSE TYPES

Most currently fielded rotorcraft have some form of limited authority stability augmentation system (SAS). These systems usually have a combination of low authority, high frequency actuators which act on the rotor system without feedback to the pilot, and full authority, low frequency trim (or parallel) actuators which act on the rotor system by moving the trim or zero force position of the pilot's cyclic control. This architecture, shown in Figure 9, allows the SAS to be a relatively simple system, usually duplex in nature with some limit to the aircraft envelope when one side of the system is inoperative. This simplicity is acceptable because a failure of any actuator, sensor or computer in the system results in an aircraft response which is small enough or slow enough to be overridden by the pilot prior to loss of control. If these simple systems could be reprogrammed to give the aircraft a response type demonstrated to improve handling qualities in UCE 2 or UCE 3 over a limited envelope, it is possible that a handling qualities improvement would result. Since the actuators of these systems have limited authority, it is apparent that the resulting response type created by reprogramming the actuators would also have limited authority, thus the name Limited Authority Response Type (LART).

Design studies, based on existing aircraft and installed SAS, have shown that the SAS actuators can be reprogrammed to develop an attitude response type in the pitch and roll axes which have the same dynamic characteristics as the full authority systems discussed earlier in this paper. These systems, however, can only be functional over a limited attitude regime close to the aircraft trim attitude and over a limited range of angular rate as well. Outside of this regime the high frequency, low authority series actuators may be on a hard position limit (saturated) while the low frequency parallel actuators may be rate limited. In either case, the resulting aircraft dynamic response is significantly different from that demonstrated by the aircraft when it is kept within the unsaturated regime. Since the handling qualities of the helicopter in DVE when the LART system is unsaturated are already understood (based on full authority studies), more recent studies have concentrated on what happens when the LART saturates and the aircraft reverts to its unaugmented form. These studies were first reported in Reference 9.

The evaluations of LART at NRC were based on the dynamics of a UH-60 helicopter. As such, the Bell 205 was first configured to possess UH-60 like characteristics, around which a simulation of a reprogrammed SAS was placed as shown in Figure 10. In the simulation of the SAS, the size of the actuators was chosen to be a variable so that the effect of the attitude at which the LART saturated could be assessed. All configurations evaluated were developed to possess the same attitude response type when unsaturated and were characterized by the attitude at which the series servo would saturate and the amount of parallel servo used.

The primary results of the two evaluations are summarized in Figures 11 and 12 . Figure 11 shows the average of the handling qualities ratings gathered for the LART configurations using both a series and a parallel servo with the series servo saturating at 2.5 degrees. While the ratings suggest that all versions of the LART that used the parallel servo had reasonable handling qualities, pilot comments highlighted a dislike for parallel servo use since it tended to create the impression that the aircraft was doing something uncommanded. Few pilots liked the sensation of the stick moving around underneath their hand. Based on the data in the figure and pilot comments, the use of a parallel servo for minor trim follow-up is probably the practical limit for a LART architecture (configuration Kp/Ks = 0.37).

Figure 12 shows the average handling qualities ratings gathered for LART systems using only a series servo of variable size. These results show that a system using only the series servos that saturate at 2.5 degrees (from the reference attitude which is trimmable), provides a reasonable improvement in handling qualities in DVE over the original rate response of the aircraft. The system with a 10 degree envelope provides clearly improved handling qualities in DVE. This data also shows that the 10 degree system was rated as possessing better handling qualities than a full authority attitude command system. This improvement of handling qualities, notable for aggressive tasks such as sidesteps and quickstops, suggests that short time periods with actuators saturated may be desirable. Some pilot comment in this regard suggested that a full-authority attitude response type tends to reduce the available agility of the aircraft due to the large cyclic displacements and forces required for large attitude changes while the onset of actuator saturation in the LART configurations provides increased agility by momentarily producing a rate-like response. Once the aggressive manoeuvring is completed the series actuator unsaturates, providing the attitude response required for the stabilization at the end of the manoeuvre. Unfortunately, this opinion was not shared by all evaluators, as some suggested that the aircraft had a tendency to "dig-in" when saturated. This "dig-in" characteristic is the unaugmented response of the helicopter to a constant input, creating an acceleration in helicopter angular rate.

The comments about the aircraft "digging in" led to a second series of tests. In these tests the primary objective was to improve the characteristics of the helicopter when the LART servos were saturated. A secondary objective was to obtain evaluation data in more realistic conditions to more clearly demonstrate the potential of a LART system. For this second series of tests, the Bell 205 was once again configured to represent UH-60 -like dynamics around which a SAS was simulated. Unlike previous tests, however, the manner in which the SAS servos behaved at large attitudes and angular rates was modified. The simple LART system, as previously studied, would saturate at large attitudes or angular rates and would remain saturated until the aircraft attitude or angular rate was reduced. The simple LART servo provided no useful function when saturated and the helicopter response at these conditions was completely unaugmented. In contrast, if the SAS

servos had not been reprogrammed, they would improve the characteristics of the helicopter throughout the aircraft envelope. This improvement may not be as good as that provided by the LART function when unsaturated but it is far better than the unaugmented aircraft response. The concept behind improving the LART system was to continually monitor the aircraft state and, if the resulting LART servo command exceeded the servo limits, a time based blend from the LART command to the original SAS command was initiated. The SAS command would also blend out when the LART command was back inside the servo limits.

If successful, the blended LART system would provide a handling qualities improvement in DVE for attitudes and angular rates that were within the LART authority limits, and provide the standard stability augmentation that the baseline aircraft has for attitudes outside the LART limits. The difficulty, of course, was to determine a blending function that did not introduce its own set of handling qualities problems.

In order to meet the second objective of the test, namely a more realistic evaluation scenario, the night vision goggle simulators were modified so that a command by the safety pilot could cause the image of the NVG simulator to degrade as a function of height, power and forward speed. This modification allowed the safety pilot to command a "brown-out" on demand, which the evaluation pilot had to contend with.

After an extensive period of ad-hoc development trials, a LART blend function was developed which seemed to meet the requirements. Three qualified test pilots evaluated the aircraft in both the standard SAS mode and in the blended LART mode for the series of ADS-33 low speed manoeuvres and random brownouts which occurred during the trials. The overall handling qualities ratings gathered during this short trial showed that the blended LART resulted in a significant handling qualities improvement for tasks such as landing and precision hover over the standard SAS in DVE. The handling qualities ratings for manoeuvring tasks, such as quickstops and sidesteps were the same or better than the SAS as well (Figure 13). For the aggressive tasks the blended LART aircraft was noted to provide some assistance in returning the aircraft to the hover following large amplitude manoeuvres.

The most significant result of this ad-hoc trial was the pilot commentary describing the occasions when the night vision goggle simulators unexpectantly "browned out". Overall, pilots rated the blended LART as superior to a SAS for any brown out event, making the event routinely controllable and making the consideration of executing a "run-on-landing" possible. One pilot commented that the blended LART system was ".... very much of an advantage over the first system...", (the SAS configuration). While the pilots differed in opinion as to whether they had the ability to land in the brown out condition, it was clear that the level of workload required to apply power and depart the brown out condition was much reduced from the ordinary SAS configuration. The height hold feature of the aircraft was also mentioned as essential to gain this handling qualities improvement.

6.0 CONCLUSIONS

The research to date on helicopter handling qualities for flight in degraded visual environments can be summarized in the following fashion.

1) Numerous studies have shown that the visual environment can have dramatic effects on the handling qualities of helicopters, and a practical result of this is the increase in accidents and incidents when pilots are performing difficult tasks and their visual environment rapidly degrades.

2) In-flight evaluations suggest that the absolute minimum field of view for visual systems should be 40 degrees from a handling qualities point of view and when this field of view is coupled with poor resolution (worse than 20/50) the handling qualities of the helicopter become degraded. Rapid onset of a degradation in the visual field(ie. brown-out, white-out, etc.) seems to exacerbate the handling qualities problems.

3) Since the pilot uses visual cues to both stabilize and control the helicopter, the handling qualities deterioration caused by a degradation of visual cues can be reduced by the augmentation of the helicopter to more a stable response type.

4) While full authority response types are not a practical option for retro fit to today's fleet of helicopters, the blended LART concept of reprogramming of existing SAS systems to develop a more stable response type over a limited envelope, coupled with a blend back to the original SAS programming when outside the envelope, has shown significant promise.

7.0 REFERENCES

1 Hoh, Roger, H., Baillie, Stewart W., Morgan, J.M. " *Flight Investigation of the Tradeoff between Augmentation and Displays for NOE Flight In Low Visibility*" American Helicopter Society Specialist Meeting on Flight Controls and Avionics, Cherry Hill N.J. October 1987

2 Fields, Capt. Bruce, " *Night Vision Goggles: A Primer*", Flying Safety Magazine, Volume 51, Number 10, pp 22 - 25, October 1995

3 Hoh, R.H. "*Investigation of Outside Visual Cues Required for Low Speed and Hover*", AIAA 12th Atmospheric Flight Mechanics Conference, AIAA 1808, Snowmass Co, August 1985

4 Anon. " *Aeronautical Design Standard ADS-33D: Handling Qualities Requirements for Military Rotorcraft*", July 1994

5 Hart, Daniel C. " *ADS-33C Flight Test Maneuvers Validation in a Degraded Visual Environment*", American Helicopter Society 50th Annual Forum, Washington D.C. May 1994

6 Vollmerhausen, Richard H., Nash, Carolyn, J., " *Design Criteria for Helicopter Night Pilotage Sensors* ", American Helicopter Society 45th Annual Forum, Boston, Mass., May 1989

7 Srinivasan, Ramesh, Baillie, Stewart, Morgan, Murray, Bertrand, Brian, "*FOVOS - Field of View and Overlap (Tradeoff) Study*", NRC Report in preparation

8 Baillie, Stewart W., Hoh, Roger.H., " *The Effect of Reduced Useable Cue Environments on Helicopter Handling Qualities*", Canadian Aeronautics and Space Journal, Volume 34, Number 3, pp144-150, September 1988.

9 Baillie, Stewart W., Morgan, J. Murray, Mitchell, David, Hoh, Roger, " *The Use of Limited Authority Response Types to Improve Handling Qualities During Flight in Degraded Visual Environments*" American Helicopter Society 51st Annual Forum, Fort Worth Tx, May 1995

Figure 1 The NRC Bell 205 Airborne Simulator

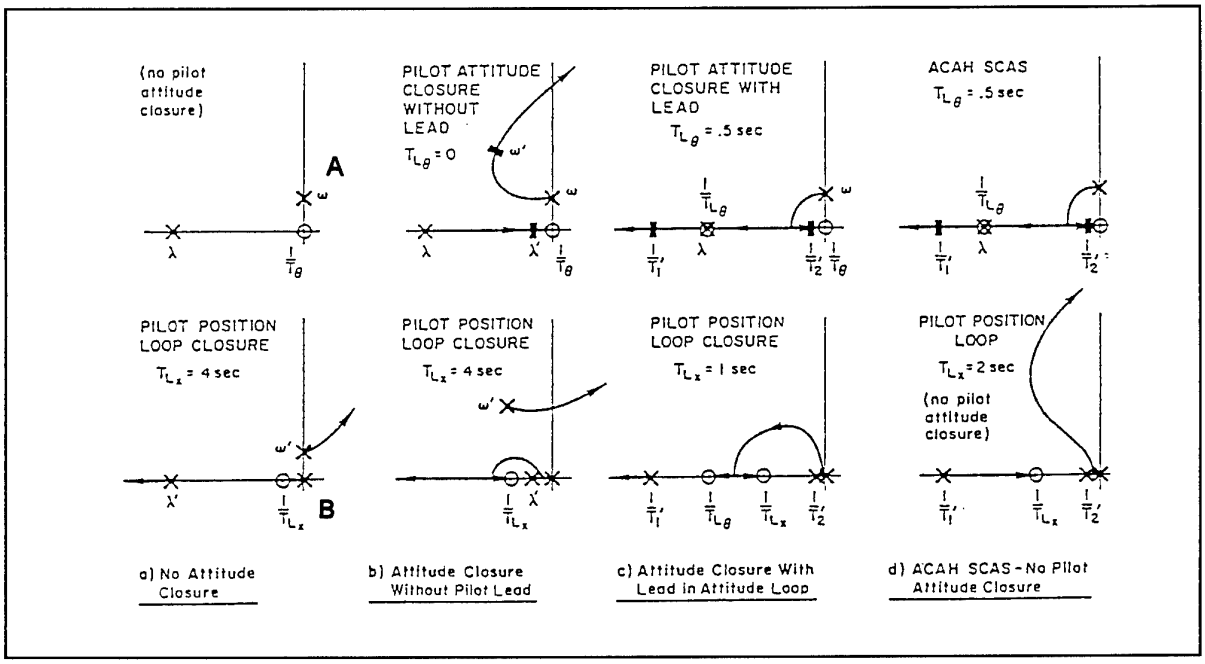

Figure 2 How a Pilot Stabilizes a Typical Helicopter

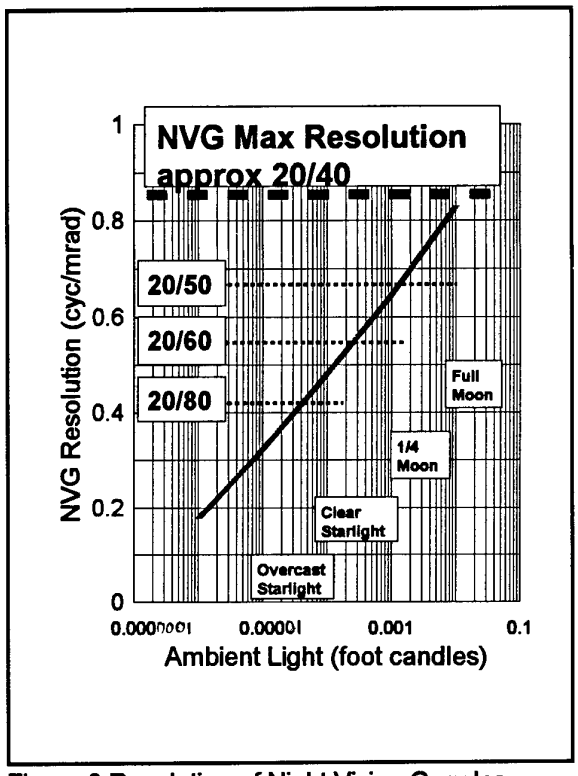

Figure 3 Resolution of Night Vision Goggles

Figure 4 Pilot with Field of View Restrictor Goggles

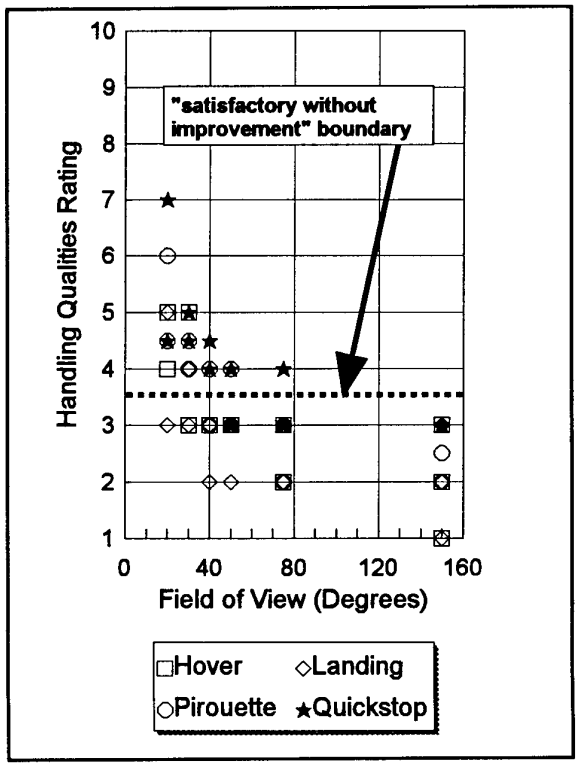

Figure 5 Handling Qualities Degradation due to Field of View Reductions

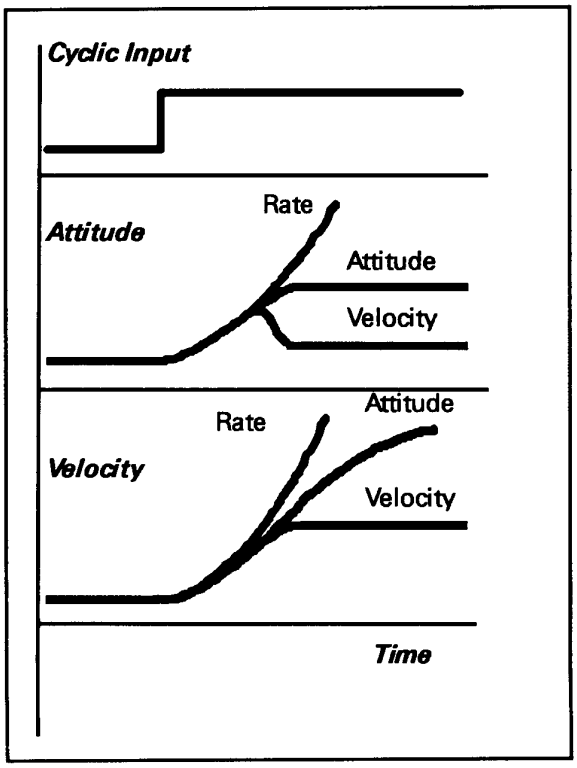

Figure 6 Attitude Response of Advanced Response Type Control Systems

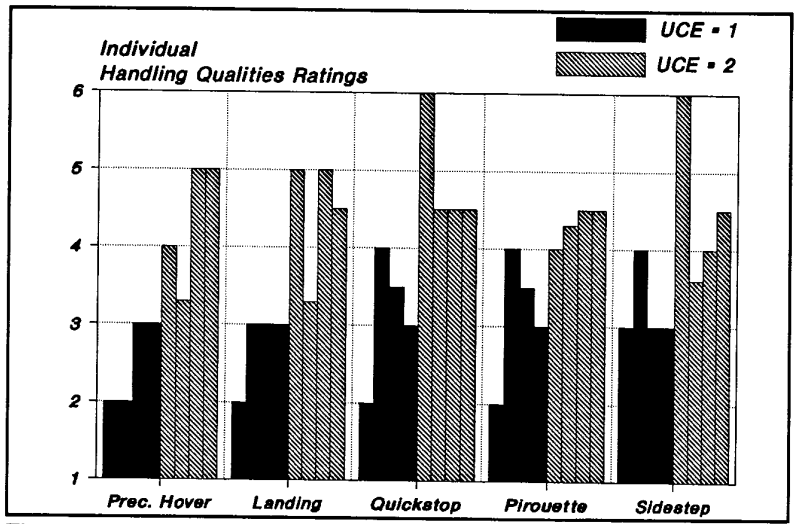

Figure 7 The Deterioration of Handling Qualities for a Rate Response Type with a Degradation in UCE

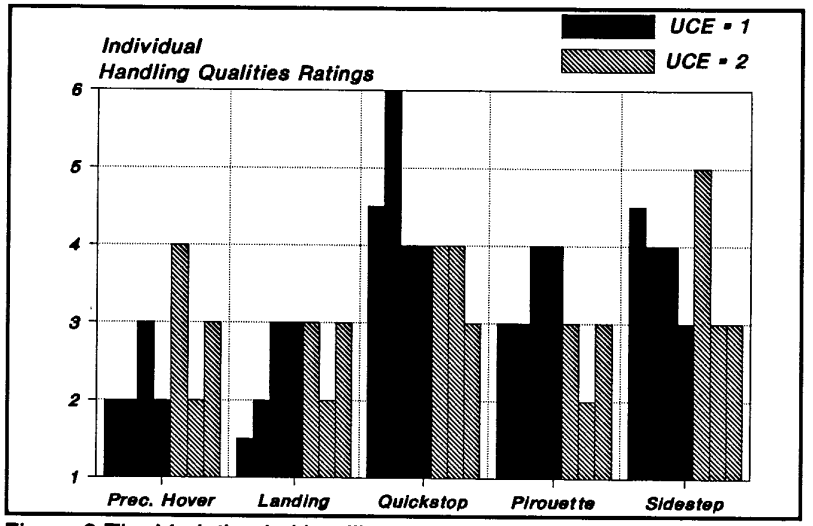

Figure 8 The Variation in Handling Qualities with UCE for a Full Authority Attitude Response Type with Height Hold

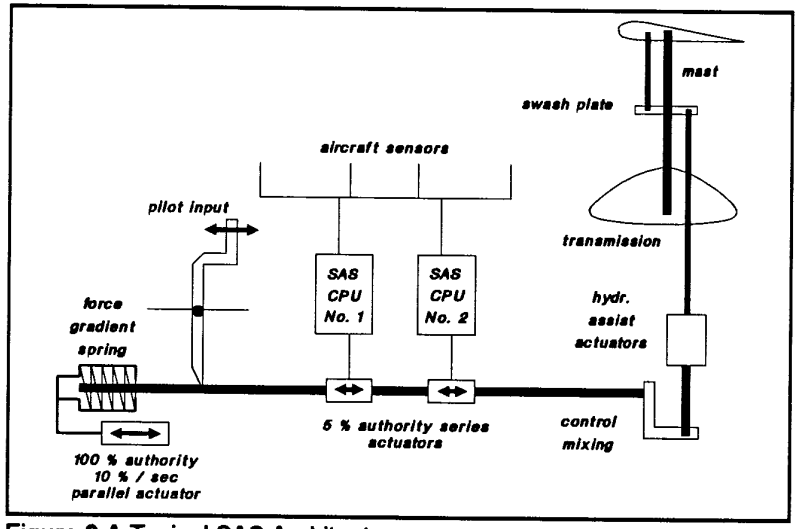

Figure 9 A Typical SAS Architecture

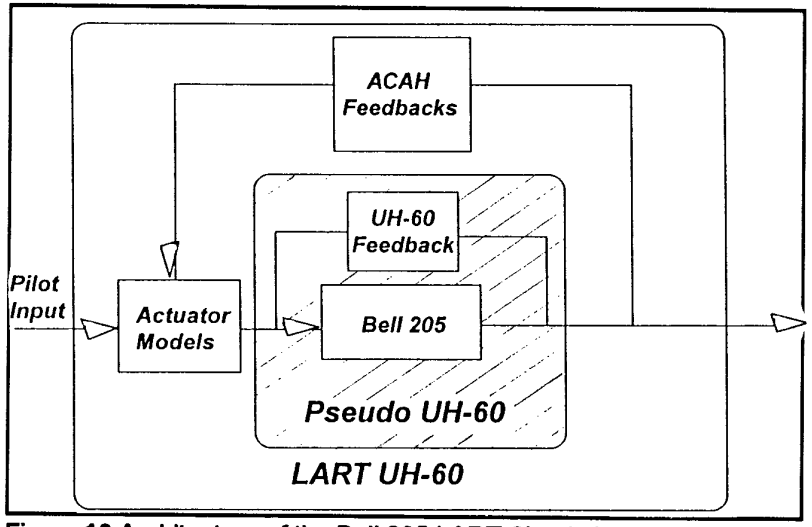

Figure 10 Architecture of the Bell 205 LART Simulation

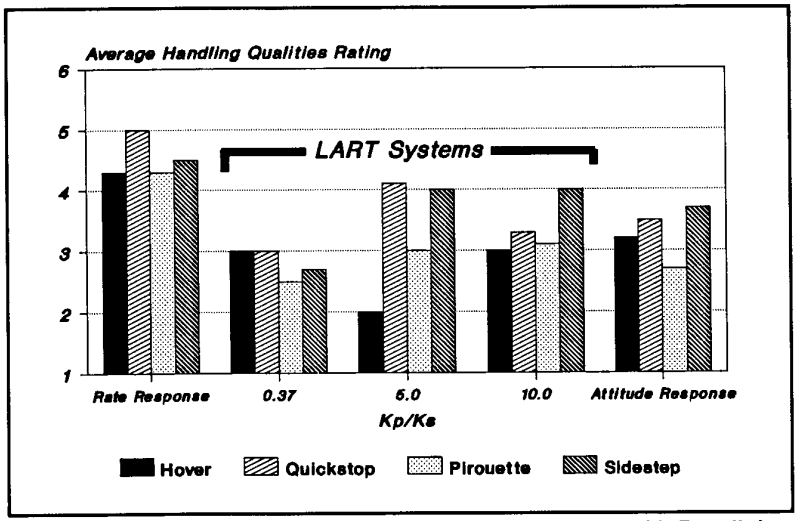

Figure **11** The Handling Qualities of a LART Helicopter with Parallel and Series Servos in UCE 2

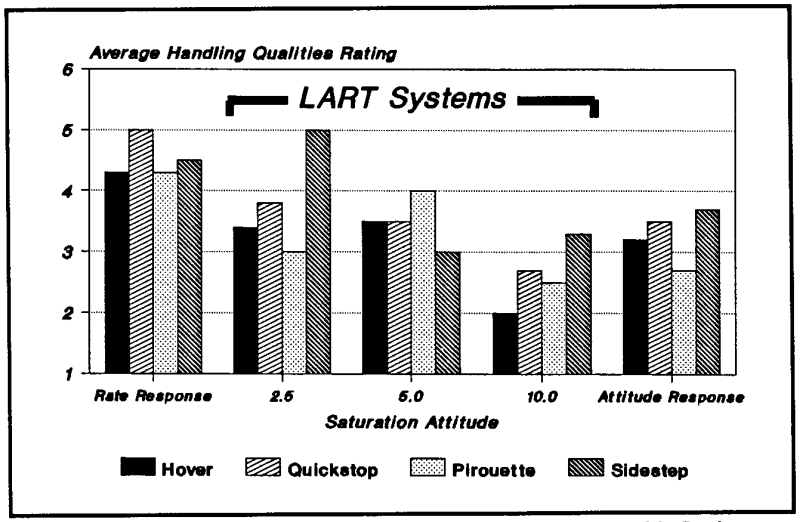

Figure **12** The Handling Qualities of a LART Helicopter with Series Servos only in UCE 2

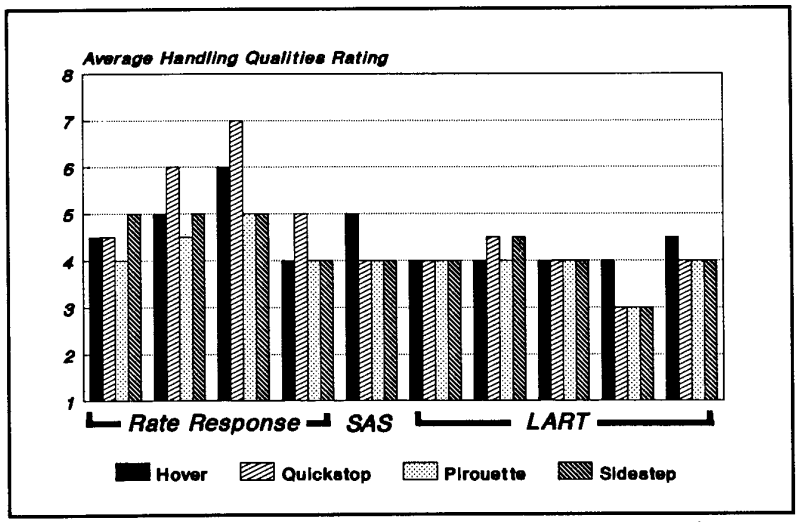

Figure **13** The Handling Qualities of a Blended LART with Series Servos only in UCE 2

The Solid State Adaptive Rotor
Design, Development and Implications for Future Rotorcraft

Ron Barrett
Assistant Professor and Director

James Stutts
Research Assistant

Auburn University, Aerospace Engineering Department, Adaptive Aerostructures Laboratory
211 Aerospace Engineering Building, Auburn, AL 36849-5338

SUMMARY

In recent years, numerous studies have been centered on a novel class of materials which are capable of changing their shapes, imparting forces and generating moments as a function of applied electrical signals. This study is centered on one application of these "adaptive" materials to achieve rotor flight control. A pair of twist-active directionally attached piezoelectric (DAP) torque-plates constructed from PZT-5H piezoceramic sheets laid up on an aluminum substrate were bonded rigidly to a rotor shaft. At the tips of the torque-plates, a pair of rotor blades were mounted on in-plane lag flexures. This two-bladed, 1/12th Froude scaled rotor system was then bench and whirl-stand tested. Because the effective pitch stiffness of the DAP torque-plates was nearly five times greater than the Froude-scaled pitch link stiffness of the full-scale rotor, the first natural frequency of the blade-plate system in pitch was just over 2.5/rev. Pitch angles were commanded from -4° up to +12° as the rotor was spun up to 600 RPM. The thrust coefficient changes peaked at ±0.008 and showed little sensitivity to RPM. Laminated plate theory was used to estimate the pitch deflections as a function of applied electric field and showed good correlation between theory and experiment. The study concludes by illustrating the simple construction of the one-piece rotor which demonstrated all conventional rotor motions – lead/lag, flapping and feathering at up to 2.5/rev with only 194 mW of power consumed per blade.

NOMENCLATURE

A	extensional stiffness matrices	(N/m)
B	coupling stiffness matrices	(N)
D	bending stiffness matrices	(N-m)
C_L	lift coefficient	~
C_T	thrust coefficient	~
E_3	through thickness electric field	(V/mm)
E	element stiffness	(GPa)
L	length	(m)
M	applied moments	(N-m/m)
N	applied forces	(N/m)
OR	orthotropy ratio = E_L/E_T	~
p-p	peak-to-peak	(var.)
t	thickness	(mm)
ΔT	temperature change	(°C)
T	thickness ratio = t_s/t_a	~
z	through thickness dimension	(m)

Greek Symbols

α	coefficient of thermal expansion	(μstrain/°C)
ε	laminate strain	(μstrain)
κ	laminate curvature	(rad/m)
Λ	ith direction actuator free strains	(μstrain)
ν	Poisson's ratio	~
Θ	blade pitch angle	(deg)
σ	stress	(MPa))

Subscripts

1	longitudinal	2	lateral
a	actuator	b	bond
eff	effective	L	longitudinal
s	substrate	T	transverse

Acronyms

CAP	conventionally attached piezoelectric
DAP	directionally attached piezoelectric
HHC	higher harmonic control
IBC	individual blade control
IDE	interdigitated electrode
PFC	piezoelectric fiber composites
RPV	remotely piloted vehicle
SSAR	solid state adaptive rotor

INTRODUCTION AND MOTIVATION

In the past ten years, numerous studies have been presented on the fundamental characteristics, application principles and system designs of adaptive materials and structures. Because these materials are capable of changing their shapes, generating forces and producing moments as a function of external stimuli, they are easily employed as actuators. Some of these external stimuli include electrical and magnetic fields, temperature changes and variations in pH.

Because aircraft flight control actuators generally operate in very demanding environments with stringent specifications on weight, power consumption, volume, reliability and efficiency, application of adaptive materials to this task has been slow in coming. Nonetheless, these materials are well suited to this task as they exhibit superior mass and volume specific energy as well as efficiency when compared to many conventional flight control actuators. Figure 1 illustrates the characteristics of different types of adaptive materials and conventional flight control actuator for a modern U.S. Army missile system.[1-3]

The data in Fig. 1 is representative of the large volume of work which has been performed on adaptive missiles and munitions.[4-9] Studies dating from as far back as 1989 have also been centered on adaptive rotor blades.[10-12]

Paper presented at the FVP Symposium on "Advances in Rotorcraft Technology", held in Ottawa, Canada, 27-30 May 1996, and published in CP-592.

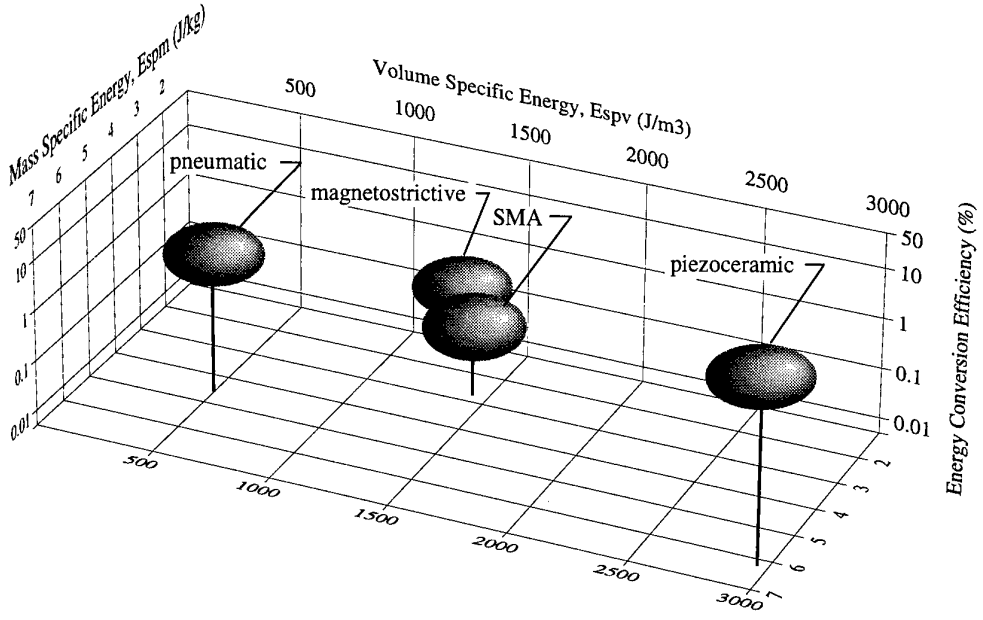

Figure 1 Mass, Volume, Energy and Efficiency Comparison of Conventional and Adaptive Flight Control Actuator Systems over a Simulated 60 Second Flight of a FOG-M Missile (Ref. 1 - 3)

Following early work on twist-active and flapped blades, many others also worked on using adaptive flaps to manipulate blade lift for higher harmonic control (HHC) and individual blade control (IBC).[13 - 16] Because each of these studies demonstrated only very small changes in thrust coefficient at full rotor speeds (generally $\Delta C_T<0.001$), a different approach is needed which is capable of greater levels of lift manipulation. To achieve this higher control authority, a new design using pitch manipulation of the entire blade was conceived, (rather than servoflap control, blade shape shaping, vanes or blowing). To achieve such blade control through a very simple system, a new configuration using adaptive torque-plates was conceived and patented.[11] The design calls for adaptive torque-plates (using directionally attached piezoelectric (DAP) or other twist actuator elements) to be symmetrically bonded to a substrate which is rigidly connected to the rotor shaft. At the ends of each plate, a soft-in-plane lag flexure is integrated along with a rotor blade mount. Through plate bending, the blade is allowed to flap. Lag comes through the soft in-plane lag flexures and feathering is commanded by twist deflections in the plate. Pitch-flap coupling is achieved through a symmetric arrangement of the DAP elements which makes for a bending-twist coupled active laminate. Clearly, this rotor embodies many unique aspects which are a major departure from conventional helicopter flight control system designs. Accordingly, this paper is centered on the basic modeling and experimental evaluation of this rotor.

LAMINATE MODELING

As a preliminary step before modeling the specific actuators to be used on the SSAR, a material selection must be performed. By examining the data of Fig. 1 and the material selection information of References 4 through 9, it is easy to see that piezoceramic or electrostrictive ceramic actuators are well suited to the task of flight control. They possess higher energy densities, greater efficiencies and excellent dynamic characteristics when compared to shape memory alloys, magnetostrictive actuators, piezoelectric polymers or the other classes of adaptive material actuators which are available.

Because piezoelectric ceramics are widely available and commercially used in great quantities (in transducers, tweeters, watch beepers, etc.), they are clearly one of the more economical choices. Although piezoelectric ceramics have been shown to be amenable to flight control of aircraft and munitions, there are many different configurations which are available, including: DAP, conventionally attached piezoelectric (CAP) (Ref. 17 - 19), interdigitated electrode (IDE) (Ref. 20), piezoelectric fiber composites (PFC) (Ref. 21), and combinations of the above types. It has been shown that IDE actuators provide the highest amount and strength of twist actuation by 5 to 20% over all other types of piezoceramic elements.[1] However, DAP elements have some profound benefits over other piezoceramic actuator types which make them extremely attractive as flight control actuators:

i. Inexpensive
(DAP elements are up to two orders of magnitude less expensive than IDE or PFC actuators);

ii. Require no specialized tooling
(DAP elements can easily be made with a piezoelectric sheet, razor blade, flashing tape and sand paper);

iii. Highly orthotropic
(DAP elements can be used with isotropic substrates to form bending-twist coupled plates which are required for induction of pitch-flap coupling);

iv. May be precompressed
(DAP elements may be laminated to a substrate like aluminum and cured at an elevated temperature -- the resulting precompression increases tensile strength by 89% and depoling strain by up to 185%).

Clearly, these advantages over CAP, IDE and PFC actuators make DAP actuators the piezoceramic configuration of choice for control of such a rotor assembly, given the current state of technology. As presented in Ref. 1, however, if directionally attached interdigitated electrode actuators were ever to be manufactured, they would possess more than double the twist performance of conventional DAP elements and would warrant serious consideration as flight control actuators. The primary causes of this disparity is that twist performance is rooted in the actuation strain and stiffness characteristics of the elements. Table 1 illustrates the stiffness and active strain characteristics of several different types of piezoceramic actuator elements.

Table 1 In-plane Properties of Typical from PSI-5A Piezoceramic Actuators at 500 V/mm (Ref. 20 - 24)

	Long. Strain Λ_1 (μstrain)	Lateral Strain Λ_2 (μstrain)	Long. Stiffness E_L (GPa)	Lat. Stiffness E_T (GPa)
CAP Ideal	-211	-211	61	61
CAP Actual	-211	-211	61	61
DAP Ideal	-211	-211	61	0
DAP Actual	-211	-211	60	3
IDE Ideal	423	-211	53	61
IDE Actual	324	-90.8	58 (est.)	61 (est.)
DAIDE Ideal	423	-211	53	0

Because nearly a decade of fairly accurate laminated plate models have been put forth and validated for CAP and DAP elements, only the basics of laminated plate theory modeling techniques will be presented. From Jones (Ref. 25), it can be seen that an active laminate may be represented by the customary stiffness matrix along with externally applied load vectors from external, actuator and thermally induced sources.

$$\begin{Bmatrix} N \\ M \end{Bmatrix}_{ex} + \begin{Bmatrix} N \\ M \end{Bmatrix}_{a} + \begin{Bmatrix} N \\ M \end{Bmatrix}_{t} = \begin{bmatrix} A & B \\ B & D \end{bmatrix}_{l} \begin{Bmatrix} \varepsilon \\ \kappa \end{Bmatrix}_{l} \tag{1}$$

where the applied forces and moments are given by:

$$N = \int \sigma_{dz} \qquad M = \int \sigma z_{dz} \tag{2}$$

Assuming that the elements are symmetrically oriented at 45° which has been shown to be optimal for maximizing twist deflections, then equation 1 may be expanded further, considering the elements are bonded to an isotropic substrate.[8]

$$\begin{bmatrix} A_{11} & A_{12} & 2A_{16} & 0 & 0 & 0 \\ A_{12} & A_{22} & 2A_{26} & 0 & 0 & 0 \\ A_{16} & A_{26} & 2A_{66} & 0 & 0 & 0 \\ 0 & 0 & 0 & B_{11} & B_{12} & 2B_{16} \\ 0 & 0 & 0 & B_{12} & B_{22} & 2B_{26} \\ 0 & 0 & 0 & B_{16} & B_{26} & 2B_{66} \end{bmatrix}_a \begin{Bmatrix} \alpha_a \Delta T \\ \alpha_a \Delta T \\ 0 \\ \frac{\Lambda_1+\Lambda_2}{2} \\ \frac{\Lambda_1+\Lambda_2}{2} \\ \frac{\Lambda_1-\Lambda_2}{2} \end{Bmatrix} +$$

$$\begin{Bmatrix} N_{11} \\ N_{22} \\ N_{12} \\ M_{11} \\ M_{22} \\ M_{12} \end{Bmatrix}_{ex} + \begin{bmatrix} (A_{11}+A_{12})_s \alpha_s \Delta T \\ (A_{11}+A_{12})_s \alpha_s \Delta T \\ 0 \\ 0 \\ 0 \\ 0 \end{bmatrix} =$$

$$\begin{bmatrix} A_{11} & A_{12} & 2A_{16} & B_{11} & B_{12} & 2B_{16} \\ A_{12} & A_{22} & 2A_{26} & B_{12} & B_{22} & 2B_{26} \\ A_{16} & A_{26} & 2A_{66} & B_{16} & B_{26} & 2B_{66} \\ B_{11} & B_{12} & 2B_{16} & D_{11} & D_{12} & 2D_{16} \\ B_{12} & B_{22} & 2B_{26} & D_{12} & D_{22} & 2D_{26} \\ B_{16} & B_{26} & 2B_{66} & D_{16} & D_{26} & 2D_{66} \end{bmatrix}_l \begin{Bmatrix} \varepsilon_{11} \\ \varepsilon_{22} \\ \varepsilon_{12} \\ \kappa_{11} \\ \kappa_{22} \\ \kappa_{12} \end{Bmatrix} \tag{3}$$

The above model has been successfully used for numerous specimens and generally predicts within 5% of experimental values. One of the major sources for deviation from the above model arises from shear lag which is intentionally large in DAP elements. This effect is adequately captured by using the methods outlined in Ref. 7.

One of the most important characteristics of modern piezoceramic actuators which should be captured is the magnitude and direction of precompression. If the actuators are cured at elevated temperatures with a substrate which possesses a coefficient of thermal expansion greater than the piezoceramic, then the element will become compressed upon cooling after the cure. Equation 4 gives a form of Equation 3 which assumes no external forces and in-plane precompression strains only.

$$\varepsilon = \frac{2E_a t_a \alpha_a \Delta T + E_s t_s \alpha_s \Delta T}{2E_a t_a + E_s t_s} \qquad (4)$$

The other very important characteristic of the DAP torque-plate and its constituents is obviously related to the magnitude of laminate twist which may be obtained. By closer examination of Equation 3, it can be seen that externally applied moments can, logically, enhance or degrade the amount of laminate twist deflection. Accordingly, it is imperative that the rotor be balanced so that adverse propeller moments are practically nonexistant. Equation 5 is another degenerate form of equation 3, considering a laminate which is constrained in bending. This is generally a good assumption as centrifugal forces will completely overwhelm the laminate tendency to generate bending deflections during twist activation.

$$\kappa_{12} = \left(E_L(1-\nu_{TL})\Lambda_1 - E_T(1-\nu_{LT})\Lambda_2\right)\left((t_s+2t_b)t_a + t_a^2\right) \div$$

$$\left\{\frac{E_s t_s^3(1-\nu_{LT}\nu_{TL})}{6(1-\nu_s)} + (E_L + E_T - 2E_L\nu_{TL}) \times \right.$$

$$\left.\left(\frac{(t_s+2t_b)^2 t_a}{2} + (t_s+t_b)t_a^2 + \frac{2t_a^3}{3}\right)\right\} \qquad (5)$$

Nondimensionalizing Equation 5 yields a useful expression for comparison of twist-active materials, where the orthotropy ratio, OR = E_L/E_T, and the thickness ratio, T, are the dominant parameters:

$$\frac{\kappa_{12} t_s}{\Lambda_1} = \frac{\left(OR(1-\nu_{TL}) - (1-\nu_{LT})\frac{\Lambda_2}{\Lambda_1}\right)\left(T^2+T\right)}{\frac{OR\,E_s T^3(1-\nu_{LT}\nu_{TL})}{6E_L(1-\nu_s)} + (OR+1-2OR\nu_{TL})\left(\frac{T^2}{2}+T+\frac{2}{3}\right)} \qquad (6)$$

From Equation 6, it is clear that when the orthotropy ratio, OR, and the orthotropic strain ratio, Λ_1/Λ_2, go to one, or the thickness ratio, T, goes to infinity, the laminate becomes inactive in twist. From Equations 5 and 6, it is also clear that the active strains, Λ, play a very important role in determining the amount of twist which is directly related to the amount of unloaded blade pitch by Equation 7.

$$\Theta = \kappa_{12} L_{eff} \qquad (7)$$

Where L_{eff} is the effective length of the DAP actuator elements over the torque-plate.

EXPERIMENTAL MODEL FABRICATION

The SSAR was designed, to match the collective pitch deflection levels of the Boeing ITR rotor. This was primarily accomplished by using the arrangement of Fig. 2 with 0.191mm thick PZT-5H DAP elements laminated to a 0.254mm thick aluminum substrate. The DAP elements were fired, poled and cut to 0.2mm dimensional tolerances, and allowed to age for 1 week after poling. They were then assembled with a 30% attachment contact area and masked off by 5μm Teflon tape as shown in Fig. 3.

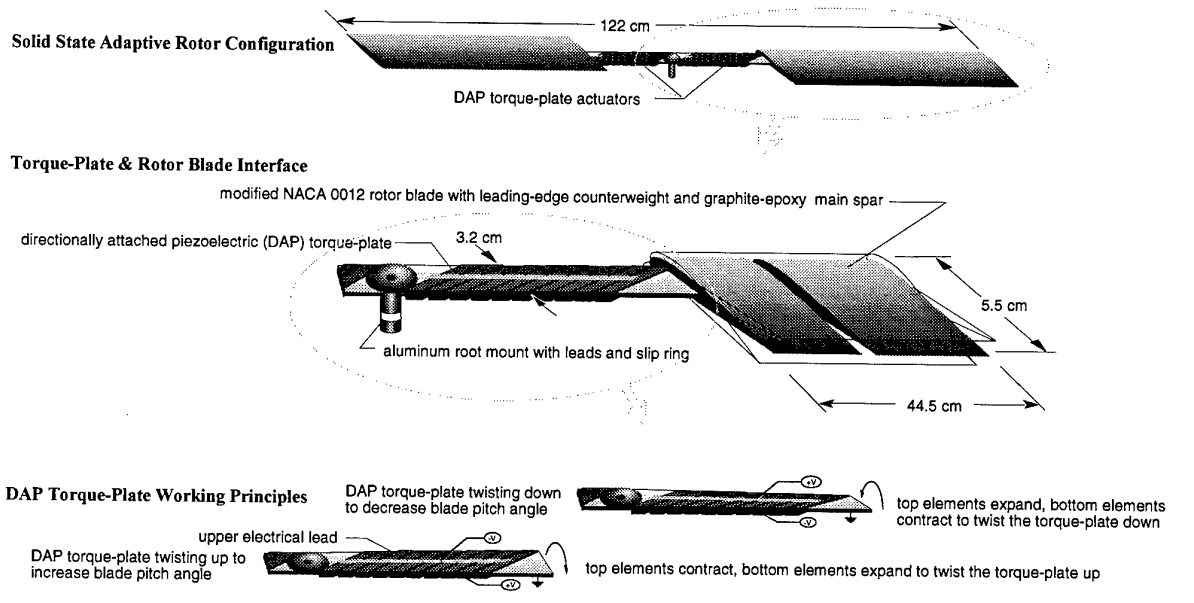

Figure 2 General Arrangement of the Solid State Rotor System and Torque-Plate

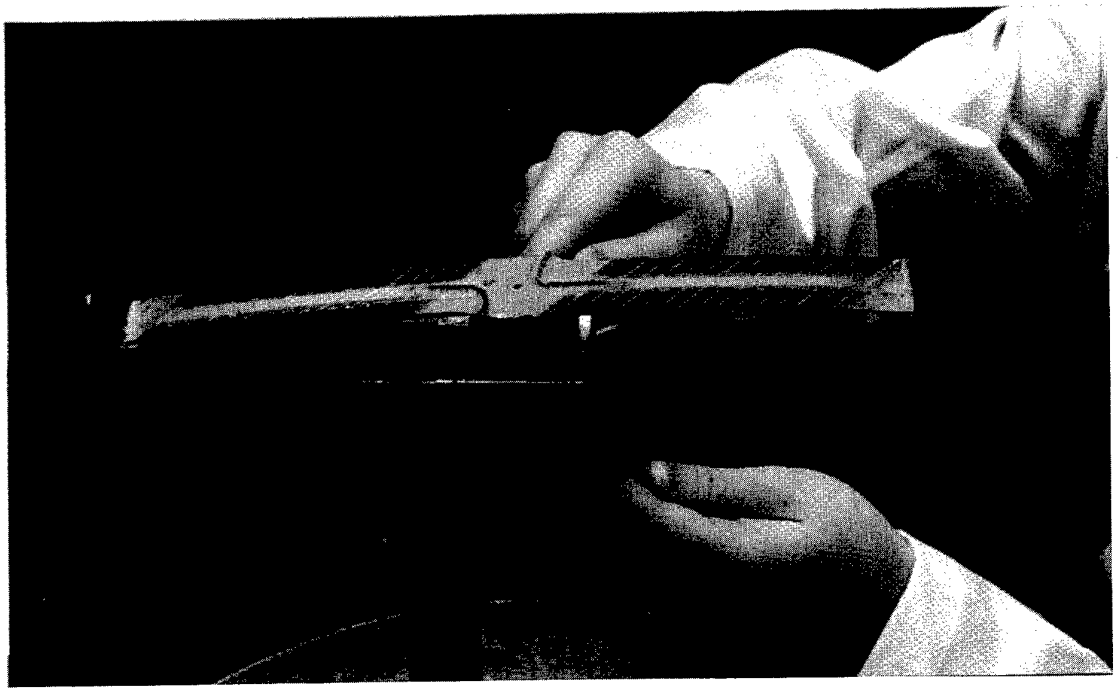

Figure 3 SSAR After Assembly During Continuity Check

Following masking and joining by Teflon tape, the DAP actuator banks were laid on top of Scotchweld™ adhesive tape strips with a 5μm thick, 5mm wide strip of conducting epoxy between the elements and the aluminum substrate. The actuator banks were cured at 177°C for three hours along with a hub fixture. After initial curing, two pairs of 25μm thick, 3mm wide brass strips were added to the DAP actuator banks to act as upper contacts. The brass strips were covered by 8mm wide strips of style #120 fiberglass cloth as a protecting film. Below the rotor, a pair of 0.30mm thick graphite-epoxy strips were added as droop stops. The upper and lower leads were routed on either side of the hub fixture to brass collars which were the inner races of slip rings.

After hub assembly, a pair of 0.25mm thick graphite-epoxy strips were joined to the aluminum sandwiches along the elastic axis and run out to the tips of the blades. A leading-edge counterbalance was added along with a Kevlar trailing-edge stiffener. Electrical testing was conducted on each element individually to verify proper performance, and the rotor was mass balanced to within 0.1 g-cm. Orthogonal balancing weights were added to the rotor at the tips of the torque-plates to eliminate adverse propeller moments.

BENCH AND WHIRL-STAND TESTING

A series of bench tests were first performed to verify actuation capability and deflection range. Both blade actuator banks were driven with a sine signal at 1Hz to check deflection as a function of actuation potential. Following static testing, a frequency sweep was conducted to verify dynamic performance. Deflections were measured by laser-beam reflection techniques as shown in Figures 4 and 5.

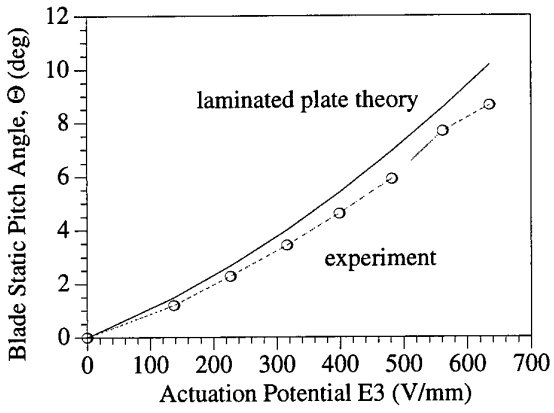

Fig. 4 Static Blade Pitch Angle Change as a Function of Applied Voltage (1/2(p-p))

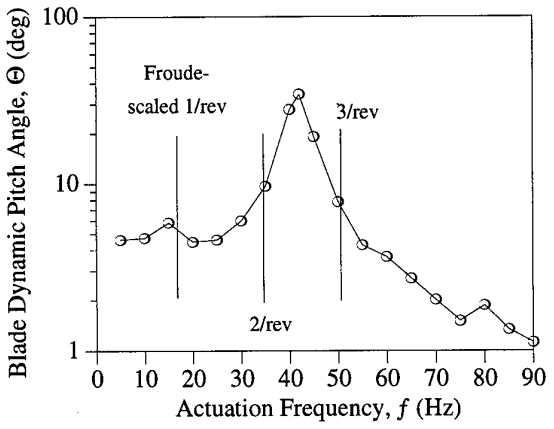

Fig. 5 Dynamic Blade Pitch Angle Change as a Function of Actuation Frequency (1/2(p-p))

Following bench testing, a series of tests were run on the model-scale whirl-stand in the Adaptive Aerostructures Laboratory. Although the Froude-scaled rotational speed was 1001 RPM, the maximum speed of the model-scale rotor was just over 600 RPM. Testing was conducted at 200, 400 and 600 RPM with the coefficient of thrust as the primary variable measured, as shown in Fig. 6.

Because bench testing had uncovered a first natural frequency in torsion of 42 Hz, a frequency sweep was also conducted to determine the rotating blade pitch natural frequency. As expected, it increased less than 4% with increasing RPM to 43.5 Hz. Projecting these results to the full-Froude scaled rotational speed of 1001 RPM, the rotor is clearly capable of large amplitude excitations up to 2.5/rev.

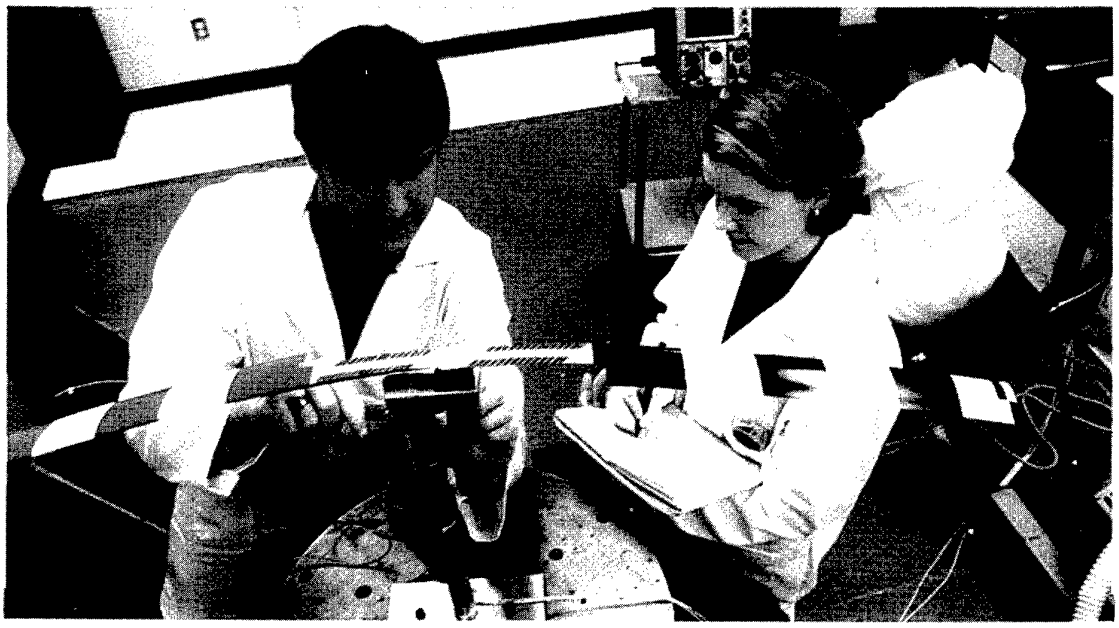

Fig. 6 Solid State Adaptive Rotor Prior to Whirl-Stand Testing

Electrical power was delivered through the ground and the external slip-ring assembly to the DAP actuator banks. Blade pitch deflections were verified by using laser reflection techniques and the rotor thrust was measured by a balance assembly. Fig. 7 shows the thrust variation as a function of rotor speed which was nearly identical for each test condition. Because the blade pitch angles did not degrade with increasing RPM, the thrust coefficients and coning angles also matched.

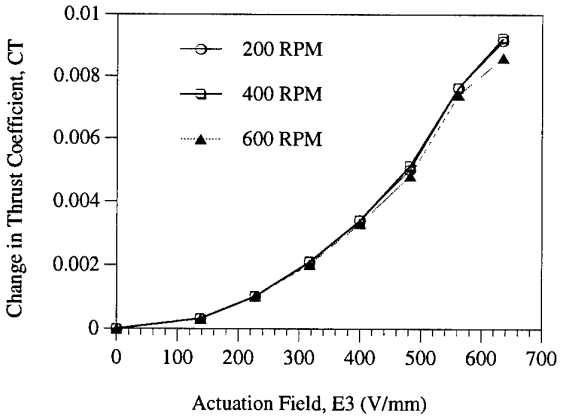

Fig. 7 Virgin Thrust Coefficient as a Function of Rotational Speed and Actuation Field

If an HHC system designer can tolerate an amplitude loss of 30% and a phase lag approaching 180°, then the rotor may be excited up to its break frequency of 63 Hz, or 3.8/rev. Testing was also conducted with excitation frequencies at 1/rev. From simply changing the phase of the signal, the tip-path-plane was observed to tilt fore and aft, left and right up to ±5.6°, thereby mimicking the longitudinal and lateral cyclic functions of conventional helicopters. The most important parameter, however, was the variation in steady pitch angle, Θ, which achieved its full range of deflections at all rotor speeds tested. Table 3 summarizes the results of rotor testing.

Table 2 Summary of Solid State Rotor System Testing, 650 V/mm Maximum Condition

	max	min	nominal setting
Collective Pitch Angle, Θ (deg)	12°	-4°	4°
Thrust Coefficient, C_T	0.014	-.0046	.0046~
Longitudinal and Lateral Cyclic	+8°	-8°	0°

CONCLUSIONS

This study has presented the results of a new type of rotor blade control system which uses directionally attached piezoelectric (DAP) torque plates to pitch 1/12th Froude-scaled rotor blades from -4° to +12° at rates up to 2.5/rev while maintaining ±8° longitudinal and lateral cyclic control. Laminated plate models were derived which predicted unloaded, steady blade pitch deflections to within 8%. Changes in thrust coefficient levels were measured from -0.0046 to +0.014. Pitch deflections and thrust coefficient levels demonstrated little sensitivity to increasing rotor speed. Power consumption was measured at a maximum 194 mW during maximum speed, maximum deflection excitation.

IMPLICATIONS

Because this study is a radical departure from the mechanical swash-plate and pitch link helicopter flight control system which was pioneered in the 1930's, some words on implications and cautions for future rotorcraft are warranted.

The cautions are, of course, rooted in unknowns. Currently, the adaptive structures community has no good data base on high cycle fatigue of adaptive materials. Precompression will help ameliorate the adverse effects of fatigue, but to what extent is still unknown. Further, there are no specifications or mil-specifications written or envisioned for aerospace adaptive materials. Accordingly, it is easy to see that, at least for the commercial sector a hurdle like certification is a long way away, perhaps 10 or 20 years, even if everything went perfectly. Another compounding factor is that the effects of lightning strike are also unknown. Lightning strike tests are slated for a USAF weapon system which uses adaptive canards in 1998. Only after completion of those tests will the community have an idea of the susceptibility of piezoceramics to large electromagnetic pulses.

Although the cautions may seem daunting, the potential positive implications for rotorcraft are profound. Preliminary testing of the hub assembly has indicated that the new, clean lines have dropped the parasite drag by nearly 30%. The simplification of the flight control assembly has led to a drop in system weight by 40% and cut the part count by two orders of magnitude over the conventional hydraulic actuators. Because the torque-plate is a smooth, continuous strip with no gaps or excresecences, the radar cross-section will be significantly lower than that of a conventional rotor hub. Higher harmonic control (HHC) and individual blade control (IBC) may also become a reality. Although flight control is the major function of the SSAR, vibration reduction through HHC and IBC is a synergetic spin-off capability, especially given the 2.5/rev. actuation capability which can be easily expanded to more than 5/rev, given more advanced actuators. Because piezoelectric ceramics are self-sensing, these advanced actuators may be electronically queried about their stress state, temperature and mechanical condition. They may also be used to compensate for battle damage, re-balance an unbalanced rotor or even automatically track the blades. The coup de grace comes in potential cost savings. It is entirely possible that such a system may cost but a fraction of current flight control assemblies. Conventional composites manufacturing techniques are currently used to lay-up the DAP torque-plates and by applying Froude-scaling, the full-scale rotor blade would have only $6,000 worth of piezoceramic elements embedded in a root torque-plate. Given these potential advantages over conventional rotor blade actuation systems, it is possible that we are on the verge of a new era in rotorcraft technology.

ACKNOWLEDGMENTS

The authors wish to acknowledge the support of the National Science Foundation which supported this work through the Alabama EPSCoR Program. The authors are also indebted to Mr. Brett Blazer and David Anderson of the Auburn University Materials Engineering Program for helping with the construction of the solid state rotor. The authors are also grateful for the consistent support, advice and encouragement of Dr. Brian Chin and the rest of the AU Materials Engineering Faculty.

REFERENCES

1. Barrett, R., and Brozoski, F., "Adaptive Flight Control Surfaces, Wings Rotors and Adaptive Aerodynamics," *proceedings of the SPIE Smart Structures and Materials Conference,* San Diego, CA, 26 - 29 February 1996, Vol. 2717, pp. 178 - 198.

2. Berry, Roger P., "Development and Testing of an Open-Center Valve (OCV) Pneumatic Actuator for the Fiber Optic Guided Missile (FOG-M), U.S. Army Missile Command Technical Report RD-GC-89-15, May, 1989.

3. Berry, Roger P., "Design and Development of a Closed Center Valve Pneumatic Actuator for the Fiber Optic Guided Missile (FOG-M),), U.S. Army Missile Command Technical RG-85-1, May, 1985.

4. Barrett, R. M., "Advanced Low-Cost Smart Missile Fin Technology Evaluation," *Final Report to the USAF Armament Directorate, WL/MNAV, Eglin AFB, FL,* by Barrett Aerospace Technologies, Auburn, AL, under contract no. F08630-93-C-0039, December, 1993.

5. Barrett, R. M., "Design and Manufacturing of Adaptive Composites for Active Flight Control Surfaces," *Proceedings of the Second International Conference on Composites Engineering, New Orleans, LA, August 1995, pp. 53 - 54.*

6. Barrett, R., Gross, R. S., and Brozoski, F. T., "Design and Testing of Subsonic All-Moving Smart Flight Control Surfaces," proceedings of the *36th AIAA Structures, Structural Dynamics*

and Control Conference, New Orleans, LA, April, 1995, pp. 2289 - 2296, AIAA paper no. AIAA-95-1081.

7. Barrett, R., "Active Plate and Missile Wing Development Using EDAP Elements," *Journal of Smart Materials and Structures*, Institute of Physics Publishing, Ltd., Techno House, Bristol, UK, Vol.1, No. 3, September 1992, pp. 214-226.

8. Barrett, R., "Aeroservoelastic DAP Missile Fin Development," *Journal of Smart Materials and Structures*, Institute of Physics Publishing, Ltd., Techno House, Bristol, UK, Vol. 2, No. 2, June 1993, pp. 55-65

9. Barrett, R., Gross, R. S., and Brozoski, F., "Missile Flight Control using Active Flexspar Actuators," *Journal of Smart Materials and Structures*, Institute of Physics Publishing, Ltd., Techno House, Bristol, UK, Vol. 5, No. 2, June 1996, pp. 121 - 128.

10. Barrett, R. M., "Intelligent Rotor Blade Actuation through Directionally Attached Piezoelectric Crystals," paper presented at the *AHS National Forum, Washington, D.C. , May 1990.*

11. Barrett, R. M., "Method and Apparatus for Structural Actuation and Sensing in a Desired Direction," *U. S. Patent 5,440,193, invention disclosure: November, 1989, patent issuance: August 1995.*

12. Spangler, R. L., and Hall, S. R., "Piezoelectric Actuators for Helicopter Rotor Control," *31st Structures, Structural Dynamics and Materials Conference,* Long Beach, California, April, 1990.

13. Been-Zeev, O. and Chopra, I., "Continued Development of a Helicopter Rotor Model Employing Smart Trailing-Edge Flaps for Vibration Suppression, *Proceedings of the SPIE Smart Structures and Materials Conference, Smart Structures and Integrated Systems,* San Diego, CA, 27 February - 3 March, 1995, pp. 2 - 19.

14. Giurgiutiu, V., Chaudhry, Z., and Rogers, C. A., "Engineering Feasibility of Induced-Strain Actuators for Rotor Blade Active Vibration Control," *Smart Structures and Materials 1994,* February, 1994, Orlando Florida, Paper #2190-11, SPIE Volume 2190, pp. 107 - 122.

15. Giurgiutiu, V., Chaudhry, Z., and Rogers, C. A., "Active Control of Helicopter Rotor Blades with Induced Strain Actuators," *35th AIAA/ASME/ASCE/AHS/ASC Structures, Structural Dynamics and Materials Conference and Adaptive Structures Forum,* Hilton Head, SC, April 18 - 22, 1994, pp. 288 - 298.

16. Strauß, F.K., Merkley, D. J., "Design of a Smart Material Actuator for Rotor Control," proceedings of the 1995 SPIE Conference on Smart Structures and Materials, San Diego, CA, February, 1995, pp. 89 - 104.

17. Crawley, E. F. and De Luis, Javier, "Use of Piezoelectric Actuators as Elements of Intelligent Structures," *AIAA Journal,* Vol. 25, No. 10, Oct. 1987, pp. 987-997.

18. Crawley, E. F, Lazarus, K. B., and Warkentin, D. J., "Embedded Actuation and Processing in Intelligent Materials," *Paper presented at the 2nd International Workshop on Composite Materials and Structures for Rotorcraft*, Troy, New York, September, 1989.

19. Crawley, E. F., and Anderson, E. H., "Detailed Models of Piezoceramic Actuation of Beams," *Paper presented at the 30th Structures, Structural Dynamics and Materials Conference*, Mobile, Alabama, April 1989.

20. Hagood, N. W., Kindel, R., Ghandi, K., and Gaudenzi, P., "Increasing transverse actuation of electroceramics using interdigitated surface electrodes" *Proceedings of the North American Conference on Smart Materials and Structures,* Albuquerque, NM, pp. 341-352, 1993.

21. Bent, A. A., Hagood, N. W., and Rodgers, J. P., "Anisotropic Actuation with Piezoelectric Fiber Composites," *Proceedings of the Fourth International Conference on Adaptive Structures,* Cologne, Germany, November, 1993.

22. Anon., *Piezo Systems Product Catalog,* Piezo Systems, Inc., Cambridge, Mass, 1990.

23. Anon., "A Guide to Modern Piezoelectric Ceramics," *Morgan Matroc, Inc.,* Bedford, Ohio 1991.

24. Barrett, R., "All-Moving Active Aerodynamic Surface Research," *Journal of Smart Materials and Structures*, Institute of Physics Publishing, Ltd., Techno House, Bristol, UK, Vol. 4, No. 4, June 1995, pp. 65 - 74.

25. Jones, R. M. Micromechanical Behavior of a Lamina. In *Mechanics of Composite Materials*, Hemisphere Publishing Corporation, New York, 1975.

REPORT DOCUMENTATION PAGE

1. Recipient's Reference	2. Originator's Reference	3. Further Reference	4. Security Classification of Document
	AGARD-CP-592	ISBN 92-836-0038-X	UNCLASSIFIED/ UNLIMITED

5. Originator Advisory Group for Aerospace Research and Development
North Atlantic Treaty Organization
7 rue Ancelle, 92200 Neuilly-sur-Seine, France

6. Title
Advances in Rotorcraft Technology

7. Presented at/sponsored by
The Flight Vehicle Integration Panel Symposium
held in Ottawa, Canada, 27-30 May 1996.

8. Author(s)/Editor(s)	9. Date
Multiple	April 1997
10. Author's/Editor's Address	**11. Pages**
Multiple	392

12. Distribution Statement There are no restrictions on the distribution of this document. Information about the availability of this and other AGARD unclassified publications is given on the back cover.

13. Keywords/Descriptors

Rotary wing aircraft	Military aircraft
Design	Aviation safety
Specifications	Design criteria
Research projects	Simulation
Flight characteristics	Flight control
Performance	Maintenance

14. Abstract

This conference proceedings contains papers presented at a Symposium held in Ottawa, Canada in May 1996. The meeting was entitled "Advances in Rotorcraft Technology." Rotorcraft will continue to provide essential military capabilities for the Alliance well into the next century.

The objective of this symposium was to capture the current situation in the rapidly changing field of rotorcraft technology. Special emphasis in the programme was placed upon the following subjects:

- the impact of the increasing use of commercial off-the-shelf technology in military helicopter development and use;
- the increasing acceptance and expanded use of Aeronautical Design Standard ADS-33;
- the issue of rotorcraft flight safety.

It specifically provided information on the Bell 230, the Tiger, Eurocopter EC 135, the V-22 and the RAH Comanche.

AGARD

NATO OTAN

7 RUE ANCELLE • 92200 NEUILLY-SUR-SEINE

FRANCE

Telefax 0(1)55.61.22.99 • Telex 610 176

DISTRIBUTION OF UNCLASSIFIED

AGARD PUBLICATIONS

AGARD holds limited quantities of the publications that accompanied Lecture Series and Special Courses held in 1993 or later, and of AGARDographs and Working Group reports published from 1993 onward. For details, write or send a telefax to the address given above. *Please do not telephone.*

AGARD does not hold stocks of publications that accompanied earlier Lecture Series or Courses or of any other publications. Initial distribution of all AGARD publications is made to NATO nations through the National Distribution Centres listed below. Further copies are sometimes available from these centres (except in the United States). If you have a need to receive all AGARD publications, or just those relating to one or more specific AGARD Panels, they may be willing to include you (or your organisation) on their distribution list. AGARD publications may be purchased from the Sales Agencies listed below, in photocopy or microfiche form.

NATIONAL DISTRIBUTION CENTRES

BELGIUM
Coordonnateur AGARD — VSL
Etat-major de la Force aérienne
Quartier Reine Elisabeth
Rue d'Evere, 1140 Bruxelles

CANADA
Director Research & Development
Information Management - DRDIM 3
Dept of National Defence
Ottawa, Ontario K1A 0K2

DENMARK
Danish Defence Research Establishment
Ryvangs Allé 1
P.O. Box 2715
DK-2100 Copenhagen Ø

FRANCE
O.N.E.R.A. (Direction)
29 Avenue de la Division Leclerc
92322 Châtillon Cedex

GERMANY
Fachinformationszentrum Karlsruhe
D-76344 Eggenstein-Leopoldshafen 2

GREECE
Hellenic Air Force
Air War College
Scientific and Technical Library
Dekelia Air Force Base
Dekelia, Athens TGA 1010

ICELAND
Director of Aviation
c/o Flugrad
Reykjavik

ITALY
Aeronautica Militare
Ufficio del Delegato Nazionale all'AGARD
Aeroporto Pratica di Mare
00040 Pomezia (Roma)

LUXEMBOURG
See Belgium

NETHERLANDS
Netherlands Delegation to AGARD
National Aerospace Laboratory, NLR
P.O. Box 90502
1006 BM Amsterdam

NORWAY
Norwegian Defence Research Establishment
Attn: Biblioteket
P.O. Box 25
N-2007 Kjeller

PORTUGAL
Estado Maior da Força Aérea
SDFA - Centro de Documentaçao
Alfragide
2700 Amadora

SPAIN
INTA (AGARD Publications)
Carretera de Torrejón a Ajalvir, Pk.4
28850 Torrejón de Ardoz - Madrid

TURKEY
Millî Savunma Başkanliği (MSB)
ARGE Dairesi Başkanliği (MSB)
06650 Bakanliklar-Ankara

UNITED KINGDOM
Defence Research Information Centre
Kentigern House
65 Brown Street
Glasgow G2 8EX

UNITED STATES
NASA Goddard Space Flight Center
Code 230
Greenbelt, Maryland 20771

The United States National Distribution Centre does NOT hold stocks of AGARD publications.
Applications for copies should be made direct to the NASA Center for AeroSpace Information (CASI) at the address below.
Change of address requests should also go to CASI.

SALES AGENCIES

NASA Center for AeroSpace Information
(CASI)
800 Elkridge Landing Road
Linthicum Heights, MD 21090-2934
United States

The British Library
Document Supply Centre
Boston Spa, Wetherby
West Yorkshire LS23 7BQ
United Kingdom

Requests for microfiches or photocopies of AGARD documents (including requests to CASI) should include the word 'AGARD' and the AGARD serial number (for example AGARD-AG-315). Collateral information such as title and publication date is desirable. Note that AGARD Reports and Advisory Reports should be specified as AGARD-R-nnn and AGARD-AR-nnn, respectively. Full bibliographical references and abstracts of AGARD publications are given in the following journals:

Scientific and Technical Aerospace Reports (STAR)
published by NASA Scientific and Technical
Information Division
NASA Langley Research Center
Hampton, Virginia 23681-0001
United States

Government Reports Announcements and Index (GRA&I)
published by the National Technical Information Service
Springfield
Virginia 22161
United States
(also available online in the NTIS Bibliographic
Database or on CD-ROM)

Printed by Canada Communication Group
45 Sacré-Cœur Blvd., Hull (Québec), Canada K1A 0S7

ISBN 92-836-0038-X